

# **Simulation and Evaluation of Regional Air Quality in the UK**

Ailish Melissa Graham

Submitted in accordance with the requirements for the degree of Doctor of Philosophy

School of Earth and Environment

The University of Leeds

January 2021

## **Author Contributions**

### **Paper 1:**

Ailish Graham – conceptualization, methodology, software, formal analysis, data curation and writing (original and review), visualisation and investigation, with help and guidance from Stephen Arnold, Richard Pope, Kirsty Pringle and James McQuaid.

Supervision - Stephen Arnold, Richard Pope, Kirsty Pringle and James McQuaid.

Funding acquisition - James McQuaid.

Back trajectory methodology - Ellen Stirling, Richard Pope and Ailish Graham.

EMEP4UK model data - Massimo Vieno.

Paper comments and advice - Ed Butt and Luke Conibear

### **Paper 2:**

Ailish Graham – conceptualization, methodology, software, formal analysis and writing (original and review), visualisation and investigation, with help and guidance from Stephen Arnold, Richard Pope, Kirsty Pringle and James McQuaid.

Supervision - Stephen Arnold, Richard Pope, Kirsty Pringle and James McQuaid.

Funding acquisition - James McQuaid.

Comments and advice – Martyn Chipperfield.

### ***Ground-based observations***

Data curation, code, analysis – Ailish Graham.

Visualisation advice – Richard Pope.

### *Satellite data*

Data processing, gridding and calculation of uncertainties and averaging kernels –

TROPOMI – Richard Pope, Antonio Bruno Giovanni, David Moore and Jeremy Harrison.

Data processing, gridding and calculation of uncertainties –

IASI – Richard Siddans, Brian Kerridge, Lucy Ventress and Barry Latter.

Visualisation and analysis advice and provision of IDL code – Richard Pope.

### *Aircraft data*

Collection of data, processing and calculation of uncertainties – (NO<sub>2</sub>) James Lee and Shona Wilde (PM<sub>2.5</sub>) Alberto Sanchez-Marroquin.

Visualisation advice, provision of IDL code and advice on method for O<sub>3</sub>:CO relationship analysis – Richard Pope.

### *MODIS Visible Images*

Provided by David Moore.

### **Paper 3:**

Ailish Graham – conceptualization, methodology, software, formal analysis, data curation and writing (original and review), visualisation and investigation with help and guidance from Stephen Arnold, Richard Pope, Kirsty Pringle, James McQuaid and Martyn Chipperfield.

Supervision - Stephen Arnold, Richard Pope, Kirsty Pringle and James McQuaid.

Funding acquisition - James McQuaid.

Health Impact Assessment advice and review advice - Ed Butt and Luke Conibear.

Scaling of Fire emissions (advice) – Laura Kiely.

WRF-Chem set-up and automation scripts – Christoph Knote.

**Paper 4:**

Ailish Graham – conceptualization, methodology, software, formal analysis, data curation and writing (original and review), visualisation and investigation with help and guidance from Stephen Arnold, Richard Pope, Kirsty Pringle, James McQuaid and Martyn Chipperfield.

Supervision - Stephen Arnold, Richard Pope, Kirsty Pringle, James McQuaid.

Funding acquisition - James McQuaid.

Fire emissions data - Ed Butt.

Post-processing scripts - Luke Conibear.

Fire emissions scaling advice, simulation advice – Laura Kiely, Carly Reddington, Ed Butt, Luke Conibear, Matt Woodhouse and Dominic Spracklen.

Health Impact Assessment advice – Nicolás Borchers Arriagada

WRF-Chem set-up and automation scripts – Christoph Knote

HPC model set-up and model de-bugging – Helen Burns.

## Acknowledgements

I'd like to extend my sincere thanks to my supervisors Jim McQuaid, Kirsty Pringle, Stephen Arnold and Richard Pope for all of their help, guidance and encouragement throughout my PhD. This was especially important during writing up in lockdown. I'd also especially like to thank Richard Pope for his time teaching me to code at the beginning of my PhD, as well as for giving me the opportunity to supervise several summer placements with him.

Alongside this, I'd like to thank Luke Conibear for his patience and time in teaching me how to run WRF-Chem and for sharing his knowledge. I'd also like to thank everyone in my office (back when we used to be able to sit in a room together) for the tea chats that fixed lots of problems and also all of the final year PhD students for all of the Teams Pomodoro sessions which made writing up much less isolating than it would have been otherwise. Also, a big thanks to everyone in BAG and aerosol group for their feedback on my work.

Finally, I'd like to thank all of my friends, family and Sam for their support throughout, especially this past year.

This thesis is copyright material and no quotation may be published without proper acknowledgement.

## Abstract

Air quality is the largest environmental health risk in the UK, contributing to chronic illness. Long-term exposure to ambient PM<sub>2.5</sub> results in more than 29,000 premature deaths each year and leads to a reduction in life-expectancy of 7-8 months. However, throughout the year air pollutant concentrations vary, controlled by the complex interaction between emissions, meteorology, chemistry and topography, leading to short-term high pollution events. The complexity of the relationships between these factors means that it is challenging to untangle the drivers of high air pollutant concentrations. An improved understanding of the drivers and impacts of high air pollution episodes is vital in informing policy to reduce the impact of short-term air pollutant exposure on population health.

The aim of this thesis was to quantify the impact of different sources and processes on short-term changes in ambient PM<sub>2.5</sub> across the UK as epidemiology studies have shown that short-term exposure to PM<sub>2.5</sub> is associated with increased mortality and morbidity. Several studies had previously shown that the varied meteorology the UK experiences plays a large role in controlling the concentrations of nitrogen dioxide and ozone. Therefore, we extend this analysis to ambient PM<sub>2.5</sub> concentrations. Additionally, wildfires are an emerging threat in the UK due to climate change. The impacts of UK wildfires on air quality and health had not previously been studied, since they had been so rare in the past. Quantifying the impacts of wildfires on air quality and health is particularly important as wildfires since projected to continue to occur more often in the future due to climate change. This is likely to result in pollution from wildfires representing a larger fraction of the population's annual exposure to air pollution in the future. Therefore, it is important that the impacts are minimised through effective science-led policy. This thesis is split into two key themes as a result: the impact of

synoptic weather on ambient PM<sub>2.5</sub> concentrations and the impact of wildfires on air quality and health.

Ground-based observations of PM<sub>2.5</sub> concentrations, a back-trajectory model and output from an atmospheric chemistry transport model were used to investigate the impact of synoptic weather on ambient PM<sub>2.5</sub> concentrations. This indicated that synoptic meteorology has a substantial influence on ambient PM<sub>2.5</sub> across the UK. Easterly, south-easterly and southerly winds transport pollutants from continental Europe to the UK, increasing ambient concentrations observed. Alongside this, anticyclonic conditions lead to higher PM<sub>2.5</sub> concentrations due to the build-up of local emissions under slack winds. This indicates that population exposure to ambient PM<sub>2.5</sub> concentrations is closely linked to synoptic weather. Therefore, policies which only consider reductions in local emissions may not yield the greatest reductions in PM<sub>2.5</sub> and international cooperation is also required.

The Saddleworth Moor and Winter Hill fires in 2018 were one of the first large wildfires in the UK to occur close to a large urban population. They were used as a case-study for the potential impacts of a UK wildfire on ambient air pollutant concentrations and human health. A combination of observational data from satellites, ground-based monitoring, an aircraft flight and an atmospheric chemistry transport model (WRF-Chem) were used to investigate the impacts of the fires. Observations showed that concentrations of pollutants close to the fires were high but, in areas downwind (> 80 km away), concentrations were also enhanced above background values, exposing populations to high concentrations far from the fires. Alongside this, secondary pollutants, such as ozone, were formed in the downwind smoke plume. Modelling results indicated that a large proportion of the population in the region to the west of Saddleworth Moor and Winter Hill were exposed to PM<sub>2.5</sub> concentrations above the WHO guideline limit and the moderate DAQI limit. The fires led to increases in the number of deaths

brought forward due to exposure to PM<sub>2.5</sub> compared to if there were no fires and as a result had a large economic impact.

Finally, the impacts of the 2019/2020 Australian bushfires were estimated using WRF-Chem. Fire emissions from FINN indicated PM<sub>2.5</sub> emissions from the fires were unprecedented. The WRF-Chem model was used to quantify the air quality and health impacts of PM<sub>2.5</sub> from the fires. This indicated that large proportions of the population were exposed to dangerous ('Poor', 'V. Poor' and 'Hazardous') air quality levels between September 1<sup>st</sup> 2019 and January 31<sup>st</sup> 2020. The impacts of the bushfires on AQ were concentrated in the cities of Sydney, Newcastle-Maitland and Canberra-Queanbeyan and Melbourne, with Brisbane and Adelaide less severely affected by the fires. Exposure to PM<sub>2.5</sub> from the fires led to an estimated 180 (95% CI: 74, 294) deaths being brought forward between October 1<sup>st</sup> and January 31<sup>st</sup>. The health impacts were largest in New South Wales, Queensland and Victoria. At a city-level the health impacts were concentrated in Sydney, Melbourne and Canberra since they have large populations that were exposed to high PM<sub>2.5</sub> concentrations for prolonged periods during the fires.

Overall, this thesis aimed to quantify the drivers and impacts of short-term air pollution episodes across the UK. Synoptic weather was shown to play an important role in ambient PM<sub>2.5</sub> concentrations through the build-up of local emissions and long-range transport of PM<sub>2.5</sub> to the UK under continental air masses. This highlights the need for continued cooperation to reduce emissions across Europe. The impact of short-term emerging threats, such as wildfires, was also quantified. This indicated that short-term high pollution events have the potential to have a substantial impact on air quality and health. With increased wildfire frequency projected in the future due to climate change, the results of this work highlight that more research is

required to quantify the cost-benefits of public health interventions or changes in land-management practices that may reduce the risk of wildfires in the UK and Australia.

## Table of Contents

<b>Author Contributions</b> .....	<b>ii</b>
<b>Acknowledgements</b> .....	<b>v</b>
<b>Abstract</b> .....	<b>vi</b>
<b>List of Figures</b> .....	<b>xvii</b>
<b>List of Tables</b> .....	<b>xxviii</b>
<b>Chapter 1 - Introduction</b> .....	<b>1</b>
1.1 Air Pollutants .....	3
1.1.1 Atmospheric Particles .....	5
1.1.1.1 Particulate Matter .....	6
1.1.2 Atmospheric Gases .....	8
1.1.2.1 Nitrogen Oxides .....	8
1.1.2.2 Carbon Monoxide .....	11
1.1.2.3 Non-Methane Volatile Organic Compounds (NMVOCs) .	11
1.1.2.4 Ammonia.....	12
1.1.2.5 Secondary PM <sub>2.5</sub> .....	13
1.1.2.5.1 Sulfate PM species .....	13
1.1.2.5.2 Nitrate PM species .....	14
1.1.2.6 Ozone .....	15
1.2 Physical Atmospheric Processes .....	19
1.2.1 Removal of Air Pollutants .....	19
1.2.1.1 Dry Deposition of Air Pollutants .....	19
1.2.1.2 Wet Deposition of Air Pollutants.....	20
1.2.2 Dispersion of Air Pollutants.....	20
1.2.2.1 Impact of Meteorology .....	20
1.2.2.1.1 Atmospheric Stability.....	21
1.2.2.1.2 Wind Flow.....	23
1.2.2.1.3 Long-range transport .....	24
1.2.2.2 Impact of Topography.....	27
1.3 UK PM <sub>2.5</sub> Concentrations .....	28
1.3.1 PM <sub>2.5</sub> Chemical Composition .....	28
1.3.2 PM <sub>2.5</sub> Sources .....	30
1.3.3 Seasonal Cycle in PM <sub>2.5</sub> Concentrations.....	31
1.3.4 Spatial Variations in Air Pollutant Concentrations.....	33

1.4 Pollution Monitoring and Legislation .....	33
1.4.1 Automatic Urban and Rural Network Observations .....	34
1.4.2 Satellite Observations .....	36
1.4.3 Aircraft Observations .....	37
1.4.4 Model Predictions .....	38
1.5 Health Impacts of air pollution .....	38
1.5.1 Attributing exposure to health impacts .....	38
1.5.2 Mechanism for Health Impacts from PM <sub>2.5</sub> .....	43
1.5.3 Epidemiological Studies .....	45
1.5.3.1 Short-Term Exposure .....	46
1.5.3.2 Wildfire pollutant exposure and mortality .....	47
1.5.3.3 Long-Term Exposure .....	49
1.5.3.4 Concentration response function shape .....	49
1.6 Burden of Disease from Air Pollutants .....	51
1.6.1 Global and Regional Burden of Disease from PM <sub>2.5</sub> .....	51
1.6.1.1 Long-Term (Chronic) Exposure .....	52
1.6.1.1.1 Global .....	52
1.6.1.1.2 UK .....	56
1.6.1.2 Short Term Exposure .....	60
1.6.1.2.1 Global .....	60
1.6.1.2.2 UK .....	61
1.7 Thesis Aims .....	63
<b>Chapter 2 - Methods .....</b>	<b>64</b>
2.1 WRF-Chem Model: Paper 3 and 4 .....	69
2.1.1 The WRF-Chem Model System .....	69
2.1.2 Domain and Model Set-up .....	73
2.1.2.1 UK 2018 Saddleworth Moor Wildfire .....	76
2.1.2.2 Australia .....	77
2.1.2.3 Initial Boundary Meteorology .....	78
<b>Meteorological Reanalysis .....</b>	<b>78</b>
<b>UK</b> 78	
<b>Australia</b> 78	
2.1.2.4 Initial Chemical Boundary Conditions .....	78
2.1.2.5 Anthropogenic Emissions .....	79
2.1.2.6 Fire Emissions .....	80

2.1.2.7 Dust Emissions.....	83
2.1.2.8 Land-use.....	84
2.1.3 Model set-up .....	84
2.1.3.1 Land-surface Model .....	84
2.1.3.2 Boundary Layer Scheme.....	84
2.1.3.3 Gas-phase and Aerosol Chemistry Scheme .....	85
2.1.3.3.1 Aerosols.....	86
2.1.3.3.2 Photolysis .....	87
2.1.3.3.3 Dry Deposition .....	88
2.1.3.3.4 Biogenic Emissions .....	88
2.1.3.4 Radiation Scheme .....	88
2.1.3.5 Microphysics Scheme .....	89
2.1.3.6 Convection Parameterisation Scheme.....	89
2.1.4 Model Uncertainties.....	89
2.2 Health Impact Assessment.....	90
2.2.1 Concentration-Response Function .....	90
2.2.2 Premature Mortality Estimate .....	92
2.2.3 Baseline Mortality Data .....	94
2.2.4 Population Data.....	95
<b>Chapter 3 – Paper 1 .....</b>	<b>97</b>
3.1 Abstract .....	97
3.2 Introduction.....	98
3.3 Data and Methods .....	102
3.3.1 Observations .....	103
3.3.1.1 Lamb Weather Types.....	103
3.3.1.2 Automated Urban and Rural Network .....	106
3.4 Back Trajectories and Integrated Emissions.....	106
3.4.1 Emissions .....	107
3.4.2 Reading Offline Trajectory Model (ROTRAJ).....	108
3.4.3 European Modelling and Evaluation Programme for the UK (EMEP4UK) PM <sub>2.5</sub> Data .....	110
3.5 Results.....	111
3.6 AURN PM <sub>2.5</sub> Observations 2010-2016.....	111
3.6.1 Back Trajectories and Integrated Emissions.....	117
3.6.2 EMEP4UK modelled PM <sub>2.5</sub> and LWT .....	119

3.6.3 Contribution of LWTs to the Daily Air Quality Index (DAQI)...	122
3.7 Acknowledgements.....	125
3.8 References.....	126
<b>Chapter 4 – Paper 2 .....</b>	<b>132</b>
4.1 Abstract.....	132
4.2 Introduction.....	133
4.3 Data & Methods.....	136
4.3.1 Automated Urban and Rural Network Observations .....	136
4.3.2 Satellite Observations .....	136
4.3.3 FAAM Aircraft Data.....	137
4.4 Results.....	141
4.4.1 MODIS visible images.....	141
4.4.2 Automated Urban and Rural Network Observations .....	141
144	
4.4.3 TROPOMI Observations .....	145
145	
4.4.4 FAAM Aircraft Observations .....	149
4.4.4.1 Pollutant Concentrations “in-plume” and “out-of-plume” Near- Field and Downwind.....	150
4.4.4.2 “In Plume” Ozone Production Near-Field and Downwind	153
4.4.4.3 Back Trajectories .....	155
4.5 Discussion and Conclusions .....	157
4.6 Acknowledgements.....	159
4.7 References.....	161
<b>Chapter 5 - Paper 3.....</b>	<b>171</b>
5.1 Abstract.....	171
5.2 Introduction.....	172
5.3 Method .....	176
5.3.1 WRF-Chem .....	176
5.3.2 Wildfire emissions .....	178
5.3.3 Model Evaluation.....	179
5.3.4 Health Impact Assessment.....	180
5.3.5 Economic Cost of Fires.....	182
5.4 Results.....	182
5.4.1 AURN Observations .....	182

5.4.2 Model Evaluation.....	185
5.4.3 Impact on Air Quality .....	188
5.4.4 Daily Air Quality Index and WHO guideline .....	188
5.4.5 Health Impact Assessment.....	192
5.4.6 Economic Impact .....	196
5.5 Discussion and Conclusions .....	196
5.6 Acknowledgements.....	198
5.7 Data Availability.....	199
5.8 References.....	200
<b>Chapter 6 – Paper 4 (draft format) .....</b>	<b>211</b>
6.1 Abstract.....	211
6.2 Introduction.....	212
6.3 Method .....	217
6.3.1 Model Description .....	217
6.3.2 Wildfire emissions .....	218
6.3.2.1 Release of Fire Emissions.....	219
6.3.3 Observations .....	221
6.3.3.1 Ground-based monitoring sites.....	221
6.3.4 Health Impact Assessment.....	221
6.3.5 Population and Baseline Mortality Data .....	222
6.4 Results.....	223
6.4.1 Fire Emissions.....	223
6.4.2 Model Evaluation.....	226
6.4.3 Monthly mean PM <sub>2.5</sub> concentration (Supplementary Material) ...	226
228	
6.4.4 Air Quality Impacts.....	228
6.4.5 Health Impacts .....	233
6.5 Conclusions.....	236
6.6 References.....	238
<b>Chapter 7 - Summary .....</b>	<b>247</b>
7.1 Paper 1: Impact of weather types on UK ambient particulate matter concentrations .....	248
7.2 Paper 2: Impact of the June 2018 Saddleworth Moor wildfires on air quality in northern England.....	251

7.3	Paper 3: Impact on air quality and health due to the Saddleworth Moor fire in northern England.....	254
7.4	Paper 4: Impact of the 2019/2020 mega-fires on air quality and health in Australia.....	257
7.5	Uncertainties .....	260
7.5.1	Back-trajectory method.....	260
7.5.2	Satellite Data.....	260
7.5.3	Modelling.....	261
7.5.3.1	Emissions .....	261
7.5.3.1.1	Fire Emissions .....	261
7.5.3.1.2	Anthropogenic Emissions .....	263
7.5.3.2	Modelling.....	264
7.5.3.3	Health Impact Assessment.....	264
7.5.3.3.1	Health Impacts.....	264
7.5.3.3.2	Population Exposure .....	266
7.6	Implications for Future Work .....	268
<b>Chapter 8</b>	<b>- Conclusions .....</b>	<b>272</b>
8.1	References.....	275
<b>Chapter 9</b>	<b>- Appendices A .....</b>	<b>325</b>
9.1	Site Information .....	325
9.2	Emissions .....	327
9.3	Sensitivity of Integrated Back Trajectories to assumed e-folding lifetime.....	329
9.4	EMEP4UK Evaluation.....	331
9.5	References.....	333
<b>Chapter 10</b>	<b>- Appendices B .....</b>	<b>334</b>
10.1	Meteorological Conditions.....	334
10.2	Satellite Visible Images of Saddleworth Moor Fire Development.....	340
10.3	MODIS Fire Radiative Power.....	342
10.4	HYSPLIT Trajectories .....	344
10.5	Satellite Observations of Tropospheric Column Nitrogen Dioxide.....	346
10.6	TROPOMI Total Column Carbon Monoxide Averaging Kernels.....	349
10.7	Aircraft Instrumentation and Cross-section .....	352
10.7.1	Instrumentation .....	353
10.7.2	Cross section .....	358

10.8 Comparison of TROPOMI with IASI (Infrared Atmospheric Sounding Interferometer) .....	360
10.9 AURN PM <sub>2.5</sub> observations .....	362
10.10 References .....	363
<b>Chapter 11 - Appendices C .....</b>	<b>365</b>
11.1 AURN data.....	366
11.2 Wildfire Emissions Scaling.....	367
11.3 Model set-up .....	371
11.3.1 Release of emissions .....	371
11.3.2 Anthropogenic Emissions .....	371
11.4 Model Evaluation.....	372
11.5 Population Exposure to PM <sub>2.5</sub> .....	372
11.6 Economic Cost of the fires.....	382
11.7 References.....	388
<b>Chapter 12 - Appendices D .....</b>	<b>390</b>
12.1 Fire Emissions.....	390
12.2 Model Evaluation.....	393
12.3 Monthly Mean PM <sub>2.5</sub> concentrations .....	401
12.4 Population Exposure .....	404
12.5 Health Impacts .....	413

## List of Figures

- Figure 1. Schematic profile of source contributions to air pollutant concentrations at a given location. Local emissions, which determine the background concentrations, in grey (LOCAL), long-range transport of regional and international emissions, in magenta (LRT), and emissions from events such as fires, in cyan (EVENTS)..... 2**
- Figure 2. UK anthropogenic air pollution sources sectors. The fractional contribution of each pollutant to emissions from each sector are shown as a percentage (white) and the dominant air pollutant of each sector is indicated (orange). (Public Health England, 2018). ..... 4**
- Figure 3. Schematic multi-modal particle size distribution. The four key size modes are labelled – ‘nucleation’, ‘Aitken’ ‘accumulation’ and ‘coarse’. Typical transformations and example particle types within each mode are also shown (Deutscher Wetterdienst, 2017). ..... 5**
- Figure 4. Particulate matter size and penetration into the body (Clean Fuels Development Coalition, 2019) ..... 7**
- Figure 5. Dominant UK primary PM<sub>2.5</sub> emission sources and health impact mechanisms (Department for Environment Food & Rural Affairs, 2019). 8**
- Figure 6. Schematic of the annual tropospheric ozone budget from a global chemistry-transport model. Data is taken from (Denman, et al., 2007). Adapted from (Centre for Ecology and Hydrology, 2016)..... 16**
- Figure 7. Tropospheric ozone mixing ratio (in parts per billion (ppb)) as a function of VOC and NO<sub>x</sub> emissions. Regions of (A) high-NO<sub>x</sub> (O<sub>3</sub> titration), (C) high-VOC (O<sub>3</sub> loss) and (A-C, B-C) efficient conversion of NO-NO<sub>2</sub> to then form tropospheric O<sub>3</sub> with increasing NO<sub>x</sub> and VOC emissions. (Archibald, et al., 2011; Monks, et al., 2015)..... 17**
- Figure 8. Examples of stability and instability in relation to air parcel temperatures (adapted from Nugent *et al.* (2019)). ..... 22**
- Figure 9. (a) Average composition of UK PM<sub>2.5</sub> (2004-2006) and (b) on days where PM<sub>10</sub> > 50 µg m<sup>-3</sup>. From (Air Quality Expert Group, 2012), adapted from (Yin and Harrison, 2008). ..... 30**
- Figure 10. Percentage contributions (%) to total modelled annual mean ambient PM<sub>2.5</sub> concentrations at UK urban background locations (Department for Environment Food and Rural Affairs, 2016). ..... 31**
- Figure 11. 2009 monthly variation in PM<sub>2.5</sub> concentrations (µg m<sup>-3</sup>) at urban background sites at sites in ‘Northern UK’ (n = 8), ‘Central UK’ (n = 17), ‘Southern UK’ (n = 8) and ‘London’ (n = 8). The 95% confidence interval is indicated by shading. (Harrison, et al., 2012). ..... 32**
- Figure 12. Cross-sectional study design and study outcome..... 39**
- Figure 13. Cohort study design and outcome..... 39**
- Figure 14. Evidence that is combined from toxicological and epidemiological studies to infer causal inference (Adami, et al., 2011). ..... 42**

**Figure 15. Schematic indicating how causal inference is inferred combining epidemiological and toxicological evidence (Adami, et al., 2011)..... 43**

**Figure 16. The hypothetical physiological processes that link PM exposure with cardiopulmonary morbidity and mortality (Pope III, and Dockery, 2006).44**

**Figure 17. Total deaths (per 100,000 population) attributable to ambient particulate matter pollution in 2015 globally (GBD Collaborators 2015, 2017; Institute for Health Metrics and Evaluation, 2015). ..... 53**

**Figure 18. Source categories responsible for the largest impact on mortality linked to outdoor air pollution in 2010. Source categories that are colour coded are: IND, industry; TRA, land traffic; RCO, residential and commercial energy use (e.g. heating, cooking); BB, biomass burning; PG, power generation; AGR, agriculture; and NAT, natural. In the white areas, annual mean PM<sub>2.5</sub> is below the concentration–response threshold. (Lelieveld, et al., 2015). . 54**

**Figure 19. Annual average PM<sub>2.5</sub> concentrations due to combustion emissions from (a) power generation; (b) commercial, institutional, residential, and agricultural sources; (c) industry; (d) road transport; (e) other transport; and (f) all UK combustion sources (Yim, and Barrett, 2012)..... 59**

**Figure 20. Flowchart of the WRF-Chem Modelling System (Peckham, et al., 2015). ..... 72**

**Figure 21. WRF-Chem domain for Saddleworth Moor Fires 2018 simulations76**

**Figure 22. WRF-Chem domain for Australia wildfires 2019/2020 simulations 77**

**Figure 23. An overview of the datasets and method used in this study. Lamb weather types (LWT) are combined with observations of PM<sub>2.5</sub> concentrations from the Automated Urban and Rural Network (AURN), back trajectories from the Reading Offline Trajectory Model (ROTRAJ) and a gridded emission dataset. We also compare our results to a chemistry transport model (EMEP4UK). ..... 103**

**Figure 24. Gridded emissions of primary PM<sub>2.5</sub> for 2010 are shown as an example (annual varying emissions were used between 2010 and 2014). For the outer domain (Purple Box), gridded annual EMEP emissions at 0.5° resolution from the Centre for Emission Inventories and Projections (CEIP, www.ceip.at) are used. While for the inner domain (Red Box) gridded annual National Atmospheric Emissions Inventories (NAEI) emissions at 0.01° resolution are aggregated to 0.05° resolution. Emissions outside of Europe are provided by the Emission Database for Global Atmospheric Research with Task Force on Hemispheric Transport of Air Pollution (EDGAR-HTAP) version 2.2 emissions for 2010 at 0.1° resolution (Janssens-Maenhout, et al., 2015). More information in Supplementary Material: Emissions section. .... 108**

**Figure 25. (a) Annual observations and (b) seasonal: (i) spring (ii) summer (iii) autumn (iv) winter observations of PM<sub>2.5</sub> concentrations from 42 UK AURN sites between 2010-2016 under different Lamb Weather Types (LWTs) (µg m<sup>-3</sup>). Mean concentrations are shown in red, with the 10<sup>th</sup>, 25<sup>th</sup>, 75<sup>th</sup> and 90<sup>th</sup> percentiles in blue. The mean of all LWTs, is shown by the green dashed line. The frequency of each LWT (in %) for the 2010-2016 period, annually and seasonally is also indicated. .... 111**

**Figure 26. Multi-annual mean PM<sub>2.5</sub> concentrations from 42 UK AURN monitoring sites (2010-2016 average in  $\mu\text{g m}^{-3}$ ) averaged over all LWT regimes. The mean, 75<sup>th</sup> and 90<sup>th</sup> percentile PM<sub>2.5</sub> concentration calculated from all sites is shown on the top right of each panel. .... 113**

**Figure 27. The multi-annual mean PM<sub>2.5</sub> anomaly relative to annual mean concentration averaged over all LWT regimes (relative to multi-annual mean concentration averaged over all LWT regimes (2010-2016) (in  $\mu\text{g m}^{-3}$ ), shown in Figure 26) under different flows directions is shown in panels (a) to (f). For clarity, we show the three flow directions with the largest positive anomaly ((a) easterly, (b) south-easterly and (c) southerly) and the three flow directions with the largest negative anomaly ((d) northerly, (e) westerly and (f) north-westerly). The mean, 75<sup>th</sup> and 90<sup>th</sup> percentile PM<sub>2.5</sub> concentrations calculated from all sites are shown on the top right of each panel. Sites where the anomaly is statistically significant ( $p < 0.05$ ) are indicated by black contouring and the percentage of sites where anomalies are statistically significant is also indicated in the top right panel (% sig). The frequency of each LWT (in %) for the 2010-2016 period is also indicated. .... 115**

**Figure 28. AURN annual mean PM<sub>2.5</sub> anomalies (relative to multi-annual mean concentration averaged over all LWT regimes (2010-2016) (in  $\mu\text{g m}^{-3}$ ), shown in Figure 26). Concentrations and anomalies sampled under (a) anticyclonic (b) cyclonic and c) unclassified weather types are shown. The mean, 75<sup>th</sup> and 90<sup>th</sup> percentile PM<sub>2.5</sub> concentration calculated from all sites is shown on the top right of each panel. Sites where the anomaly is statistically significant ( $p < 0.05$ ) are indicated by black contouring and the percentage of sites where anomalies are statistically significant is also indicated in the top right panel (% sig). The frequency of each LWT (in %) for the 2010-2016 period is also indicated..... 116**

**Figure 29. Median UK (background AURN sites) integrated PM<sub>2.5</sub> emissions ( $\mu\text{g m}^{-2}$ ) accumulated over the daily (12 UTC, 2010-2014) ROTRAJ back trajectories (4 days – 15-minute time steps), with a 7-day e-folding lifetime, binned by LWT flow directions. Red circles represent the UK fractional contribution to trajectory accumulated PM<sub>2.5</sub> emissions..... 118**

**Figure 30. The multi-annual mean PM<sub>2.5</sub> anomaly relative to annual mean concentration averaged over all LWT regimes (relative to multi-annual mean concentration averaged over all LWT regimes (2010-2016) (in  $\mu\text{g m}^{-3}$ )) under different flow directions from the EMEP4UK model. 10m winds, also from the EMEP4UK model (nudged to 3-hourly GFS analysis), are over plotted. All LWT wind directions and synoptic types are shown..... 121**

**Figure 31. Percentage occurrence (defined as the percentage of occurrences of easterly, south-easterly and southerly (and westerly north-westerly and northerly) LWTs in each bin) of easterly, south-easterly and southerly weather types and westerly, north-westerly and northerly in each DAQI PM<sub>2.5</sub> concentration bin. Bins 1-10 indicate PM<sub>2.5</sub> concentrations of 0-11, 12-23, 24-35, 36-41,42-47,48-53,54-58,59-64,65-70, >71 (all in  $\mu\text{g m}^{-3}$ )..... 123**

**Figure 32. CEISIN population count (2015). Black triangles indicate the locations of Saddleworth Moor (SM) and Winter Hill (WH), the cities of Manchester (Man) and Liverpool are also marked. Black circles indicate AURN observation sites used in Figure 33. The flight path of the FAAM aircraft on 29<sup>th</sup> June 2018 is also shown in grey, with near-field and downwind sections (Figure 35-Figure 37) of the flight highlighted in red and blue..... 140**

**Figure 33. AURN observations of volatile and non-volatile PM<sub>2.5</sub> for 16<sup>th</sup> June – 14<sup>th</sup> July 2018. Non-volatile PM<sub>2.5</sub> is indicated by the red solid line (2018) and pink shading (2013-2017 standard deviation). Volatile PM<sub>2.5</sub> is indicated by the blue solid line (2018) and light blue shading (2013-2017 standard deviation). The total PM<sub>2.5</sub> concentration for 2018 is also indicated by the black dashed line and the fire period in grey. The WHO 24-hour guideline limit is also in green for reference. .... 144**

**Figure 34. TROPOMI total carbon monoxide (TCCO, moles m<sup>-2</sup>) measurements of the Saddleworth Moor wildfire (25<sup>th</sup> – 30<sup>th</sup> June 2018). Black and purple polygon-outlined regions represent the fire plume (>0.03 moles m<sup>-2</sup>) and edge of plume (0.025-0.03 moles m<sup>-2</sup>). Black dots show pixels where MODIS fire radiative power (FRP) is > 50 mW m<sup>-2</sup>. White dots show the location of the Saddleworth Moor and Winter Hill fires. Blue dots show the location of Manchester and Liverpool. The box and whisker schematics represent TROPOMI tropospheric column nitrogen dioxide (TCNO<sub>2</sub>, 10-5 moles m<sup>-2</sup>) sub-sampled “in-plume”, “edge of plume” and “out of plume” TCCO thresholds. TCNO<sub>2</sub> is also sub-sampled under fire pixels (FRP > 50 mW m<sup>-2</sup>) and non-fire pixels (FRP < 50 mW m<sup>-2</sup>). Red, green and blue represent the median, 25<sup>th</sup> and 75<sup>th</sup> percentiles and 10<sup>th</sup> and 90<sup>th</sup> percentiles, respectively. .... 146**

**Figure 35. Facility of Airborne Atmospheric Measurements (FAAM) observations of carbon monoxide (CO, ppbv) and ozone (O<sub>3</sub>, ppbv) from the Saddleworth Moor wildfires on 29<sup>th</sup> June 2018. (a) CO concentration along flight path (b) O<sub>3</sub> concentration along flight path (c) time-altitude CO profile, (d) time-altitude O<sub>3</sub> profile, (e) CO (black) and O<sub>3</sub> (red) time-series. Time stamps for the flight are included in (a) for reference to in (c) and (d). The sections bounded by the red and blue dashed lines in panels (a), (b), (e) and (f) represent the near-field (NF) and downwind (DW) time phases of the flight. The horizontal purple dashed line in (e) indicates the “in-plume” (> 125 ppbv) versus “out of plume” (< 125 ppbv) threshold. .... 150**

**Figure 36. Box and whisker schematic of CO (left, ppbv), O<sub>3</sub> (centre, ppbv) and NO<sub>2</sub> (right, ppbv) “in-” and “out of plume” (CO > 125 ppbv). Red, green and blue represent the median, 25<sup>th</sup> and 75<sup>th</sup> percentiles and minimum and maximum concentrations, respectively. NF and DW represent the near-field and downwind phases of the plume. .... 153**

**Figure 37. CO (ppbv) and O<sub>3</sub> (ppbv) relationship for different Saddleworth Moor fire plume phases (29th June 2018). Black circles represent all data defined as “out of plume” (<125 ppbv CO), red circles are “in plume” near field and blue symbols are “in plume” downwind. Blue crosses, diamonds and circles represent measurements between 0.25-0.5 km, 0.6-0.85 km and above 0.9 km. Dashed lines represent the CO-O<sub>3</sub> regression for different fire plume altitudes where all downwind relationships are significant at the 95% confidence level (\*)...... 155**

**Figure 38. Population count (km<sup>-2</sup>) (2015) in model domain with Automated Urban and Rural Network (AURN) sites used in model evaluation over plotted (Supplementary Material: Table 12). Sites where elevated PM<sub>2.5</sub> was observed are indicated by red stars and those where concentrations remained below 50 µg m<sup>-3</sup> by black circles. The locations of Saddleworth Moor and Winter Hill are indicated by black triangles. Fire emissions, from FINNv1.5 (time-varying scaling), between June 23<sup>rd</sup> and June 30<sup>th</sup> are indicated by red circles – each circle represents a fire hotspot from MODIS, while the size of the circles is relative to the mass of PM<sub>2.5</sub> emitted in kg day<sup>-1</sup> (scale on left). The area over which scaling was applied to the FINN fire emissions is also shown by the blue box. More details on AURN sites can be found in Supplementary Material: Table 12..... 176**

**Figure 39. Hourly observed and simulated surface PM<sub>2.5</sub> between June 16<sup>th</sup> 2018 and July 14<sup>th</sup> 2018. Modelled values are from the time-varying scaling simulation (see Wildfire emissions and Model Evaluation sections and Table 8), in magenta, and observations from AURN sites are in black. Locations where PM<sub>2.5</sub> observations are elevated are shown by red stars and time series site names in red. The period when the Saddleworth Moor and Winter Hill fires occurred is indicated in grey shading..... 185**

**Figure 40. (a) Areas of low ( $\leq 36 \mu\text{g m}^{-3}$ ), moderate ( $36 - \leq 53 \mu\text{g m}^{-3}$ ), high ( $54 - \leq 70 \mu\text{g m}^{-3}$ ) and very high ( $>71 \mu\text{g m}^{-3}$ ) PM<sub>2.5</sub> as defined by the Daily Air Quality Index (DAQI). Coloured numbers correspond to total number of people exposed to each DAQI level on at least one day between June 23<sup>rd</sup> and June 30<sup>th</sup> 2018. See Supplementary Material: Table 13 for more information on the DAQI. (b) Areas where PM<sub>2.5</sub> is above the WHO 24-hour limit of 25 µg m<sup>-3</sup> and total population exposed to PM<sub>2.5</sub> below (green) and above (red) this threshold on at least one day between June 23<sup>rd</sup> – June 30<sup>th</sup>. (c) Mean increase (%) in PM<sub>2.5</sub> due to fires between June 23<sup>rd</sup> and June 30<sup>th</sup> 2018. Calculated as,  $\frac{PM2.5 \text{ Fires} - PM2.5 \text{ No Fires}}{PM2.5 \text{ No Fires}} \times 100$ , where 10 represents a 10% increase in PM<sub>2.5</sub>. Locations of large urban areas and Saddleworth Moor (SM) and Winter Hill (WH) are also indicated for reference. .... 191**

**Figure 41. (a) Total Excess Mortality ( $E_m$ ) across the entire simulation domain from  $PM_{2.5}$  in the fires and no fires simulations. The fraction of mortality due to fires across the model domain between June 16<sup>th</sup> – July 14<sup>th</sup> 2018 is also shown, calculated as  $(E_m \text{ FIRES} - E_m \text{ NO FIRES} / E_m \text{ FIRES} \times 100)$ . 95% confidence intervals, based on uncertainty in the concentration-response function, are indicated by red and blue shading. (b) Percentage increase in excess mortality ( $E_m$ ) due to fires  $(E_m \text{ FIRES} - E_m \text{ NO FIRES} / E_m \text{ NO FIRES} \times 100)$ , with the economic cost of mortality from fires (in millions of pounds (M GBP)) also shown. .... 194**

**Figure 42.  $PM_{2.5}$  fire emissions ( $Tg \text{ day}^{-1}$ ) across Australia between March 2019 and March 2020 from the FINN near-real time fire emission dataset. The timeseries shows the 2010-2018 25<sup>th</sup> and 75<sup>th</sup> percentiles of daily  $PM_{2.5}$  emissions each day (red) and the mean 2019-2020 daily  $PM_{2.5}$  emissions (blue). Inset map: Map of  $PM_{2.5}$  fire emissions ( $Tg \text{ day}^{-1}$ ) across eastern Australia between March 2019 and March 2020. .... 223**

**Figure 43. (a) Observed (black) and simulated (magenta and cyan) daily mean  $PM_{2.5}$  concentrations. Simulations shown are no fires (cyan) and fires (magenta). The mean  $PM_{2.5}$  concentration from all 64 observational sites across eastern-Australia is shown for the model and observations. (b) The same as above but for individual cities. The observed (black) and simulated (magenta and cyan) mean  $PM_{2.5}$  concentrations are shown for each city. The total number of sites in each city is also shown on the left of each panel. .... 225**

**Figure 44. Daily population exposure (in millions) to Australian Air Quality Index Values across eastern-Australia (nudged\_BL\_fires simulation) between September 1<sup>st</sup> and January 31<sup>st</sup>. More information on how the AQI is calculated in Supplementary Material: Table 25. Daily population-weighted bushfire  $PM_{2.5}$  exposure across all states in model domain (red) and regionally for Victoria (green), Australian Capital Territory blue (yellow) and Queensland (purple) (nudged\_BL\_fires-nudged\_BL\_no\_fires simulation) between September 1<sup>st</sup> and January 31<sup>st</sup>. .... 228**

**Figure 45. Daily population exposure (in millions) to Australian Air Quality Index Values in individual cities (Brisbane (Queensland), Sydney (NSW), Newcastle-Maitland (NSW), Canberra-Queanbeyan (ACT) and Melbourne (Victoria)) between September 1<sup>st</sup> and January 31<sup>st</sup>. More information on how the AQI is calculated in Supplementary Material: Table 25. Daily population-weighted bushfire  $PM_{2.5}$  concentration in the cities of Brisbane (blue), Newcastle-Maitland (purple), Sydney (green), Canberra-Queanbeyan (yellow), Melbourne (grey) and Adelaide (orange) (nudged\_BL\_fires-nudged\_BL\_no\_fires simulation) between September 1<sup>st</sup> and January 31<sup>st</sup>. .... 232**

**Figure 46. Estimated increase in the number of deaths brought forward across model domain (red) and the states of Victoria (green), Australia Capital Territory [ACT] (blue), New South Wales [NSW] (yellow) and Queensland (purple) due to PM<sub>2.5</sub> from bushfires (fires only) between October 1<sup>st</sup> and January 31<sup>st</sup>. Shading indicates the 95% confidence intervals of the estimate. The number of deaths brought forward due to bushfire PM<sub>2.5</sub> (fires only) (red) between October 1<sup>st</sup> and January 31<sup>st</sup> is also broken down by city and region and the total number of deaths shown above the bars. The estimated number of deaths brought forward in each state due to bushfire PM<sub>2.5</sub> (fires only) (red) in this study are compared to the Borchers Arriagada *et al.* (2020) estimate (indigo) and Ryan *et al.* (2021) for the same period..... 235**

**Figure 47. Sources of uncertainties within modelling health impacts from wildfire pollutants. .... 261**

**Figure 48. Median UK (background AURN sites) total accumulated PM<sub>2.5</sub> emissions (µg m<sup>-2</sup>) accumulated over the daily (12 UTC, 2010-2014) ROTRAJ back trajectories (4 days – 15-minute time steps), with a (a) 1-day (b) 3-day (c) 7-day and (d) 14-day e-folding lifetime, binned by LWT flow directions. Red circles represent the UK fractional contribution to trajectory accumulated PM<sub>2.5</sub> emissions..... 329**

**Figure 49. 2010-2016 daily modelled (cyan and magenta) and observed (blue and red) PM<sub>2.5</sub> concentrations, binned by LWT. Mean (red/magenta), 10th, 25th, 75th and 90th percentiles are shown. The mean modelled (magenta) and observed (red) PM<sub>2.5</sub> concentration for all LWTs is shown by the dashed line. .... 332**

**Figure 50. Annual mean concentration and anomaly between 2010-2016 for daily modelled (EMEP4UK) and observed PM<sub>2.5</sub> concentrations at AURN observation sites, binned by LWT. The Pearson correlation (r) is shown at the top of each panel. .... 332**

**Figure 51. ERA-Interim 1200Z mean sea level pressure (hPa 0.5° × 0.5° grid)) with ERA5 geopotential height (m) at 850 hPa overplotted in red for June 19<sup>th</sup>-30<sup>th</sup> 2018 over Northern England. The black dots represent the location of Saddleworth Moor and Winter Hill..... 337**

**Figure 52. ECMWF ERA-Interim 2-m temperature (K, 0.5° × 0.5° grid) for June 19<sup>th</sup>-30<sup>th</sup> 2018 over Northern England. The black dots represent the location of Saddleworth Moor and Winter Hill..... 338**

**Figure 53. ECMWF ERA-Interim 10-m wind speed (m s<sup>-1</sup>, 0.5° × 0.5° grid) for June 19<sup>th</sup>-30<sup>th</sup> 2018 over Northern England. The black dots represent the location of Saddleworth Moor and Winter Hill..... 339**

**Figure 54. MODIS visible images, from NASA’s Aura and Terra satellites, of the Saddleworth Moor and Winter Hill fires between June 25<sup>th</sup>-30<sup>th</sup>. The locations of Saddleworth Moor and Winter Hill are indicated in white, while the locations of Manchester and Liverpool are shown in cyan..... 341**

**Figure 55. MODIS fire radiative power (FRP, mW m<sup>-2</sup>, 0.1° × 0.1° grid) for June 19<sup>th</sup>-30<sup>th</sup> 2018 over Northern England. The white dots represent the location of Saddleworth Moor and Winter Hill. .... 343**

- Figure 56. Back trajectories from HYSPLIT for the aircraft flight on June 29<sup>th</sup> 2018. Trajectories are released from various locations at 250-1000m heights based on the aircraft altitude and track during the near-field and downwind sections of the flight. The path of each trajectory is indicated on the map, while the altitude above ground level is indicated on the bottom plot. .... 345**
- Figure 57. TROPOMI tropospheric column nitrogen dioxide (TCNO<sub>2</sub>, 10<sup>-5</sup> moles m<sup>-2</sup>) measurements of the Saddleworth Moor wildfire (June 25<sup>th</sup> – 30<sup>th</sup> 2019). Black and purple polygon-outlined regions represent the TROPOMI total column carbon monoxide (TCCO) fire plume (>0.03 moles m<sup>-2</sup>) and edge of plume (0.025-0.03 moles m<sup>-2</sup>). Black dots show pixels where MODIS fire radiative power (FRP) is > 50 mW m<sup>-2</sup>. White dots show the location of the Saddleworth Moor and Winter Hill fires. Blue dots show the location of Manchester and Liverpool. The box and whisker schematics represent TCNO<sub>2</sub> sub-sampled under the plume, edge of plume and out of the plume TCCO thresholds. TCNO<sub>2</sub> is also sub-sampled under fire pixels (FRP > 50 mW m<sup>-2</sup>) and non-fire pixels (FRP < 50 mW m<sup>-2</sup>). Red, green and blue represent the median, 25<sup>th</sup> & 75<sup>th</sup> percentiles and 10<sup>th</sup> & 90<sup>th</sup> percentiles, respectively. 349**
- Figure 58. Total column averaging kernels reflecting the altitude sensitivity of the CO total column TROPOMI retrieval during the Saddleworth Moor fire days (June 25<sup>th</sup>-30<sup>th</sup> 2018) for three specific location, Manchester, Liverpool and Saddleworth Moor. .... 350**
- Figure 59. Facility of Airborne Atmospheric Measurements (FAAM) aircraft path (hours since 00 UTC) and altitude(m above ground level (AGL)) from the Saddleworth Moor wildfires on June 29<sup>th</sup> 2018. .... 352**
- Figure 60. Facility of Airborne Atmospheric Measurements (FAAM) aircraft measurements of nitrogen dioxide (NO<sub>2</sub>, ppbv) (red) and carbon monoxide (CO, ppbv) (black) from the Saddleworth Moor wildfires on June 29<sup>th</sup> 2018. The sections bounded by the red and blue dashed lines represent the near-field (NF) and downwind (DW) time phases of the flight. The horizontal purple dashed line indicates the “in-plume” (> 125 ppbv) versus “out of plume” (< 125 ppbv) threshold. .... 355**
- Figure 61. Facility of Airborne Atmospheric Measurements (FAAM) time-series observations of carbon monoxide (CO, ppbv) (black) and PM<sub>2.5</sub> concentration (µg m<sup>-3</sup>) (red) from the Saddleworth Moor wildfires on June 29<sup>th</sup> 2018. The sections bounded by the red and blue dashed lines represent the near-field (NF) and downwind (DW) time phases of the flight. The horizontal purple dashed line indicates the “in-plume” (> 125 ppbv) versus “out of plume” (< 125 ppbv) threshold. .... 356**
- Figure 62. Box and whisker schematic of PM<sub>2.5</sub> aerosol concentration (µg m<sup>-3</sup>) and CO (right, ppbv “in-” and “out of plume” (CO > 125 ppbv). Red, green and blue represent the median, 25<sup>th</sup> and 75<sup>th</sup> percentiles and minimum and maximum concentrations, respectively. NF and DW represent the near-field and downwind phases of the plume..... 357**

- Figure 63.** Aircraft transect representing the fire plume the near-field (NF) flight segment. Red crosses represent where the aircraft was sampling “in-plume” air defined as CO concentrations > 125 ppbv. The plume width is approximately 4482 m and the plume thickness is approximately 52 m, representing an approximate rectangular cross-section. .... 359
- Figure 64.** IASI total column carbon monoxide (TCCO, 1018 molecules cm<sup>-2</sup>) for June 25<sup>th</sup> - 30<sup>th</sup> 2018. Daily background concentrations have been subtracted based on the 1-0°W, 55-56°N average sub-region column value. The black circle representations the location of the Saddleworth Moor fires. .... 361
- Figure 65.** Area over which scaling was applied (blue) to FINNv1.5 emissions for use in WRF-Chem simulations over plotted on peat coverage in domain (Xu, et al., 2018)..... 368
- Figure 66.** Hourly observed and simulated surface PM<sub>2.5</sub> between June 16<sup>th</sup> and July 14<sup>th</sup> 2018. Modelled values are from the no fires (green), no scaling (yellow), 10x scaling (cyan) and time-varying scaling simulations (magenta) (see Manuscript: Model Evaluation and Table 8). Observations from AURN sites are indicated in black. .... 369
- Figure 67.** (a) Time-varying scaling, (b) 10x scaling and (c) no scaling simulated and observed hourly PM<sub>2.5</sub> concentrations at all sites. Individual sites are shown in (d-f), with the mean for each observational site between June 16<sup>th</sup> – July 14<sup>th</sup> 2018 indicated by coloured crosses. The 1:1, 0.5:1 and 1:0.5 lines are shown for reference. The mean correlation coefficient (r), mean bias (MB), normalised mean bias (NMB) and root mean squared error (RMSE in µg m<sup>-3</sup>) across all sites for the simulation period (June 16<sup>th</sup> – July 14<sup>th</sup> 2018) are also indicated in (a)-(c). .... 370
- Figure 68.** Areas of low (0-35 µg m<sup>-3</sup>), moderate (36-53 µg m<sup>-3</sup>), high (54-70 µg m<sup>-3</sup>) and very high (>71 µg m<sup>-3</sup>) PM<sub>2.5</sub>, as defined by the Daily Air Quality Index (DAQI). Coloured numbers correspond to total number of people exposed to each DAQI level on each day. Saddleworth Moor (SM) and Winter Hill (WH) are indicated by black triangles, while highly populated urban areas are indicated by black circles and abbreviated in line with definitions in Figure 65. See Table 13 for more information on the DAQI. .... 375
- Figure 69.** Areas where PM<sub>2.5</sub> is above the WHO 24-hour limit of 25 µg m<sup>-3</sup> and total population exposed to PM<sub>2.5</sub> below (green) and above (red) this threshold on each day between June 23<sup>rd</sup> and June 30<sup>th</sup> 2018. Saddleworth Moor (SM) and Winter Hill (WH) are indicated by black triangles, while highly populated urban areas are indicated by black circles and abbreviated in line with definitions in Figure 65..... 376
- Figure 70.** Daily mean percent increase in PM<sub>2.5</sub> due to fires between June 23<sup>rd</sup> and June 30<sup>th</sup> 2018. Calculated as,  $\frac{PM_{2.5} \text{ Fires} - PM_{2.5} \text{ No sFires}}{PM_{2.5} \text{ No Fires}} \times 100$ , where 10% represents a 10% increase in PM<sub>2.5</sub>. Saddleworth Moor (SM) and Winter Hill (WH) are indicated by black triangles, while highly populated urban areas are indicated by black circles and abbreviated in line with definitions in Figure 65. .. 377

- Figure 71.** Areas of low ( $0-35 \mu\text{g m}^{-3}$ ), moderate ( $36-53 \mu\text{g m}^{-3}$ ), high ( $54-70 \mu\text{g m}^{-3}$ ) and very high ( $>71 \mu\text{g m}^{-3}$ )  $\text{PM}_{2.5}$  as defined by the Daily Air Quality Index (DAQI) in the no fires simulation. Saddleworth Moor (SM) and Winter Hill (WH) are indicated by black triangles, while highly populated urban areas are indicated by black circles and abbreviated in line with definitions in Figure 38. See Table 13 for more information on the DAQI. .... 378
- Figure 72.** Comparison of FINNv1.5 and FINN near-real time (NRT). 2010-2019 FINNv1.5  $\text{PM}_{2.5}$  emissions (red) and 2018-2020 FINN near real time (NRT)  $\text{PM}_{2.5}$  emissions are plotted against MODIS hotspots. The linear fit for 2010-2019 FINNv1.5 is shown in blue. .... 392
- Figure 73.** Annual fire  $\text{PM}_{2.5}$  emission estimates for Australia in 2019. The five key fire emissions datasets are shown: GFED, FINN, GFAS, QFED and FEER (Liu, et al., 2020)..... 393
- Figure 74.** Ground-based observational sites used in model evaluation of daily mean  $\text{PM}_{2.5}$  concentrations. .... 394
- Figure 75.** Comparison of  $\text{PM}_{2.5}$  concentrations from model sensitivity simulations with  $\text{PM}_{2.5}$  observations from 80 observational sites across eastern-Australia. The fires, no\_fires, plume\_rise and scaled\_1.5 simulations, in which all meteorological variables above the BL were nudged, while within the BL only horizontal and vertical winds were nudged. In the fires and scaled\_1.5 simulations fire emissions were released evenly through the BL, while in plume\_rise the plume rise module was used. The fires and plume\_rise simulations used FINN NRT emissions and in the scaled\_1.5 simulation these emissions were scaled by 1.5 in Australia. In the nudged\_BL, nudged\_BL\_no\_fires and nudged\_BL\_scaled\_1.5 simulations nudging was performed for all vertical levels and all meteorological variables. The nudged\_BL and nudged\_BL\_1.5 simulations used FINN NRT emissions and in the nudged\_BL\_1.5 simulation these emissions were scaled by 1.5 in Australia and fire emissions were released evenly through the BL. In both the no\_fires and nudged\_BL\_no\_fires simulations no fire emissions were released. .... 397
- Figure 76.** Comparison of daily mean  $\text{PM}_{2.5}$  concentrations from model sensitivity simulations with  $\text{PM}_{2.5}$  observations from 80 observational sites across eastern-Australia. Observations are shown in black, nudged\_BL\_fires in magenta and nudged\_BL\_no\_fires in cyan for each site..... 400
- Figure 77.** Monthly mean modelled  $\text{PM}_{2.5}$  concentrations across eastern-Australia from the fires (nudged\_BL\_fires) simulation. Monthly mean observations are over plotted..... 401
- Figure 78.** Monthly mean percentage of  $\text{PM}_{2.5}$  attributable to fires, calculated as  $\frac{\text{PM}_{2.5} \text{ fires} - \text{PM}_{2.5} \text{ no fires}}{\text{PM}_{2.5} \text{ fires}}$  using the nudged\_BL\_fires and nudged\_BL\_no\_fires simulations. Monthly mean  $\text{PM}_{2.5}$  concentrations from the nudged\_BL\_fires simulation are also over plotted in contours for reference. .... 402
- Figure 79.** Monthly mean percentage increase in  $\text{PM}_{2.5}$  attributable to fires, calculated as  $\frac{\text{PM}_{2.5} \text{ fires} - \text{PM}_{2.5} \text{ no fires}}{\text{PM}_{2.5} \text{ no fires}}$  using the nudged\_BL\_fires and nudged\_BL\_no\_fires simulations. .... 403

**Figure 80. Daily population exposure to Air Quality Index Values across eastern-Australia between September 1<sup>st</sup> and January 31<sup>st</sup> in the nudged\_BL\_no\_fires simulation. More information on how the AQI is calculated in Table 25.404**

## List of Tables

<b>Table 1. Overview of aerosol modes shown in Figure 3 (Willeke, and Whitby, 1975). .....</b>	<b>6</b>
<b>Table 2. EU Directive Limits (European Commission, 2017) and WHO Guidelines (World Health Organization, 2005) for air pollutants. ....</b>	<b>35</b>
<b>Table 3. Change in life expectancy for 2008 UK population following implementation of different policy scenarios (Committee on the Medical Effects of Air Pollutants, 2010). ....</b>	<b>58</b>
<b>Table 4. Overview of datasets used in Papers 1 and 2. These papers focused on the use of observational datasets, using models to support understanding of relationships identified through the observational datasets. ....</b>	<b>67</b>
<b>Table 5. Overview of datasets used in Papers 3 and 4. These papers focused on the application of air quality modelling to quantify the impacts of wildfires on health through population exposure to PM<sub>2.5</sub>. ....</b>	<b>68</b>
<b>Table 6. Model and Domain settings used for Paper 3 and 4. ....</b>	<b>74</b>
<b>Table 7. 27 LWT classifications (Jenkinson, and Collison, 1977), the 11 LWTs used in this study are indicated in bold (NE, E, SE, S, SW, W, NW, N, Anticyclonic, Neutral &amp; Cyclonic). There are 8 wind types (NE, E, SE, S, SW, W, NW &amp; N, shown in the left columns, and 2 circulation types (anticyclonic, cyclonic), in the top row, and unclassified days, where wind speed and shear were too low to allow classification. Following our grouping of LWT into 11 types, LWT index 3 (ASE) would fall under the anticyclonic and south-easterly classifications (see outer column and row of Table 7). There is also one other LWT (-9: non-existent day) not used in this study. ....</b>	<b>105</b>
<b>Table 8. Model evaluation statistics for WRF-Chem simulations with different FINNv1.5 options for daily mean PM<sub>2.5</sub>. Statistics shown are the mean value of Pearson correlation coefficient (r), mean bias (MB), normalised mean bias (NMB), root mean squared error (RMSE), mean absolute error (MAE) and normalised mean absolute error (NMAE) at each AURN site for the entire simulation (June 16<sup>th</sup> 2018 to July 14<sup>th</sup> 2018). Simulations shown are for FINNv1.5 with no alterations (no scaling), FINN v1.5 with factor 10 scaling over Saddleworth Moor (10x scaling), FINN v1.5 with changing scaling to account for the different stages of the fire (time-varying scaling) and simulations with (no fire emissions). See Model Evaluation and Supplementary Material: Figure 65 for more details on time-varying scaling. .....</b>	<b>187</b>

<b>Table 9. (a) The economic cost of fatality during the Saddleworth Moor Fires, calculated using the value of protected fatality (VPF) from the Department for Transport (DfT). The cost is calculated using the lower, mid and upper excess mortality from short-term exposure to PM<sub>2.5</sub> between June 23<sup>rd</sup> and 30<sup>th</sup> 2018 and the VPF for 2018 (£1.9M - see Supplementary Material Table 15 (a) for more details). (b) The cost breakdown is also shown (see Supplementary Material: Table 15 (b) for further details), based on the central excess-mortality estimates.....</b>	<b>195</b>
<b>Table 10. Automated Urban and Rural Network sites used for PM<sub>2.5</sub> analysis. AURN sites and classifications (UB = Urban Background, RB = Rural Background, BS = Background Suburban).....</b>	<b>326</b>
<b>Table 11. Mean daily non-volatile fraction of PM<sub>2.5</sub> for 2013-2017 and 2018 at Manchester Piccadilly, Salford Eccles and Wigan Centre AURN sites..</b>	<b>362</b>
<b>Table 12. shows details of AURN sites used in model evaluation within this study. ....</b>	<b>366</b>
<b>Table 13. Daily Air Quality Index (DAQI) bands for PM<sub>2.5</sub> (µg m<sup>-3</sup>) and associated behaviour advised by the UK government to reduce the population’s risk. Concentrations for each band are also indicated.....</b>	<b>373</b>
<b>Table 14. Sensitivity of short-term exposure excess mortality results between 23<sup>rd</sup> and 30<sup>th</sup> June on theoretical minimum risk exposure level (TMREL) used. Lower confidence level (lcl), medium confidence level (mcl) and upper confidence levels (ucl) are indicated, based on the 95% confidence intervals of the exposure response function.....</b>	<b>381</b>
<b>Table 15. a) Previous studies estimating the Value of Prevented Fatality in the UK and government estimates across the world. The value used for this study from the Department for Transport, UK is highlighted in grey. b) Detailed values of VPF used to calculate cost of mortality during fires – these values were multiplied by the excess mortality from PM<sub>2.5</sub> from fires (i.e. PM<sub>2.5</sub> Fires – PM<sub>2.5</sub> No Fires). Values are taken from Viscusi et al. (2003) and Deolitte (2009). ....</b>	<b>384</b>
<b>Table 16. (a) Number of hours within each DAQI bin (0-24, 24-48, 48-71, 71+ µg m<sup>-3</sup>) in 2018 (2018/01/01-2018/12/31), simulation period (2018/06/16 – 2018/07/14) and fire period (2018/06/23 – 2018/06/30). (b) Percentage of total annual hourly DAQI occurrences that occurred within the simulation or fire period (i.e. for 0-24 µg m<sup>-3</sup> bin: simulation period (5471/65870*100) and fires period (1375/65870*100)). ....</b>	<b>386</b>

**Table 17. Model evaluation statistics for each of the WRF-Chem simulations for daily mean PM<sub>2.5</sub>. Statistics shown are the mean value of Pearson correlation coefficient (r), root mean squared error (RMSE), normalised mean bias (NMB), and normalised mean absolute error (NMAE) at each observational site for the full simulation time period (September 1<sup>st</sup> 2019 to January 31<sup>st</sup> 2020). Simulations shown are: fires, no\_fires, plume\_rise and scaled\_1.5 simulations, in which all meteorological variables were nudged above the BL, while within the BL only horizontal and vertical winds were nudged. In the fires and scaled\_1.5 simulations fire emissions were released evenly through the BL, while in plume\_rise the plume rise module was used. The fires and plume\_rise simulations used FINN NRT emissions and in the scaled\_1.5 simulation these emissions were scaled by 1.5 in Australia. In the nudged\_BL, nudged\_BL\_no\_fires and nudged\_BL\_1.5 simulations nudging was performed for all vertical levels and all meteorological variables. The nudged\_BL and nudged\_BL\_1.5 simulations used FINN NRT emissions and in the nudged\_BL\_1.5 simulation these emissions were scaled by 1.5 in Australia, in both cases fire emissions were released evenly through the BL. In both the no\_fires and nudged\_BL\_no\_fires simulations no fire emissions were released. .... 398**

**Table 18. Monthly population exposure to PM<sub>2.5</sub> AQI values in the nudged\_BL\_fires simulation (calculated as the monthly mean of daily sum population exposure). More information on how the AQI is calculated in Table 25. .... 405**

**Table 19. Monthly population exposure to PM<sub>2.5</sub> AQI values in the nudged\_BL\_no\_fires simulation (calculated as the monthly mean of daily sum population exposure). More information on how the AQI is calculated in Table 25. .... 406**

**Table 20. Monthly population exposure to PM<sub>2.5</sub> AQI in cities (calculated as the monthly mean of daily sum population exposure). More information on how the AQI is calculated in Table 25. .... 407**

**Table 21. Mean and maximum (September 1<sup>st</sup> – January 31<sup>st</sup>) population-weighted PM<sub>2.5</sub> concentrations for states and cities in eastern-Australia. .... 411**

**Table 22. 2018 regional all-cause, all-age mortality rates per 100,000 for Australia (Australian Bureau of Statistics, 2020). .... 412**

**Table 23. The total number of deaths brought forward between October 1<sup>st</sup> and January 31<sup>st</sup> due to short-term exposure to PM<sub>2.5</sub> in the nudged\_BL\_fires and nudged\_BL\_no\_fires simulations. Using the subtraction method, the number of deaths brought forward due to exposure to PM<sub>2.5</sub> from fires has also been estimated (fires only). .... 413**

**Table 24. The total number of deaths brought forward due to fires (nudged\_BL\_fires-nudged\_BL\_no\_fires) between October 1<sup>st</sup> and January 31<sup>st</sup> due to short-term exposure to PM<sub>2.5</sub> in each state and the large cities. Note the entire area of the Northern Territory and South Australia states was not included in the model domain so the total for these states is not included here. .... 414**

**Table 25. Australian Quality Index (AQI) values and description. The 24-hour AQI is calculated based on the relevant Air National Environment Protection Measure (NEPM) standard, or advisory standard, for each pollutant using the equation (AQI = air pollutant concentration/air pollutant standard x 100). The 24-hour standard for PM<sub>2.5</sub> is 25 µg m<sup>-3</sup> ..... 415**



## Chapter 1 - Introduction

### Motivation

Exposure to ambient air pollution has been shown to increase mortality, as well as shorten life expectancy (United States Environmental Protection Agency (US EPA), 2009); World Health Organization, 2005). Within the UK, air quality is the largest environmental health risk, contributing to chronic illness (Department for Environment Food & Rural Affairs, 2019). Health is adversely affected through both exposure to short-term high pollution events, such as long-range transport or a wildfire, and long-term lower-level pollution, from ambient concentrations (Department for Environment Food & Rural Affairs, 2019). Long-term exposure to ambient PM<sub>2.5</sub> in the UK results in more than 29,000 premature deaths each year (Committee on the Medical Effects of Air Pollutants, 2010) and leads to a reduction in life-expectancy of 7-8 months (Department for Environment Food and Rural Affairs, 2007). The main economic cost of air pollution stems from the adverse health impacts of population exposure to PM<sub>2.5</sub> and is estimated to be between £8.5 and £20.2 billion each year (Department for Environment Food and Rural Affairs, 2007). It is estimated that if no additional measures are implemented, on top of current targets, the economic cost will remain high, at £6.2 to £14.7 billion in 2020, and average life expectancy will continue to be reduced, by 5.5 months (Department for Environment Food and Rural Affairs, 2007).

The concentration of air pollutants varies in space and time, meaning that the air pollutant concentrations which a population is exposed to at any one location is affected by several sources (Figure 1):

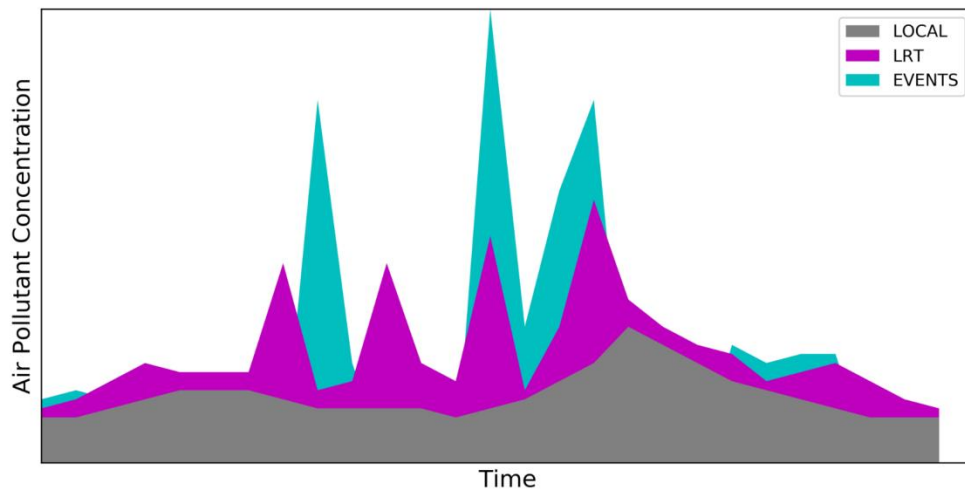


Figure 1. Schematic profile of source contributions to air pollutant concentrations at a given location. Local emissions, which determine the background concentrations, in grey (LOCAL), long-range transport of regional and international emissions, in magenta (LRT), and emissions from events such as fires, in cyan (EVENTS).

- 1) Local emissions, such as those from traffic or power generation.
- 2) Long-range transport of non-local (regional or international) emissions.
- 3) Sporadic events, such as wildfires.

Additionally, other secondary factors can interact with these sources to enhance or decrease air pollutant concentrations, including:

- 1) tropospheric chemistry (through the production of secondary pollutants and the removal of primary and secondary pollutants)
- 2) meteorology (through accumulation and removal processes)
- 3) topography (through accumulation and removal processes)

These secondary factors vary both spatially and temporally (Vallero, 2014). Therefore, their relative contributions vary throughout the year on monthly, daily and hourly timescales, and also vary between different pollutants. This leads to concentrations and population exposure in

a specific location being influenced by a range of sources and factors at different scales and magnitudes (Figure 1). The complexity of the temporal and spatial variability between emissions, secondary factors and concentrations means that it is challenging to untangle the drivers of high air pollutant concentrations. This inhibits effective legislation to reduce population exposure over both short- and long- time scales, since both long-term and short-term exposure to air pollutants have a measurable impact on health. In order to reduce the negative health impacts of air pollution by half the UK Government set stringent emission reduction targets for 2020 and 2030 (Department for Environment Food & Rural Affairs, 2019). However, in order to achieve these targets in 2030, an improved understanding of the sources of pollutants and their relative contribution to concentrations at a given location are vital in providing a robust evidence base.

## **1.1 Air Pollutants**

Air pollution can be defined as any natural or man-made trace constituent that has a measurable effect on humans, animals, materials or the natural environment between emission and removal (Seinfeld, 1986). Pollutants can exist in gaseous, particulate (aerosol) or semi-volatile form. They can either be directly emitted as '*primary pollutants*', or formed through reactions between primary emissions after they have been released into the atmosphere, known as '*secondary pollutants*'. Primary pollutants include sulfur dioxide (SO<sub>2</sub>), nitrogen oxides (NO<sub>x</sub> which includes NO and NO<sub>2</sub>), carbon monoxide (CO), ammonia (NH<sub>3</sub>) and particulate matter (PM) (Figure 2) (Public Health England, 2018). These are emitted from a range of anthropogenic sources, shown in Figure 2, but can also be emitted from natural sources such as deserts and oceans.

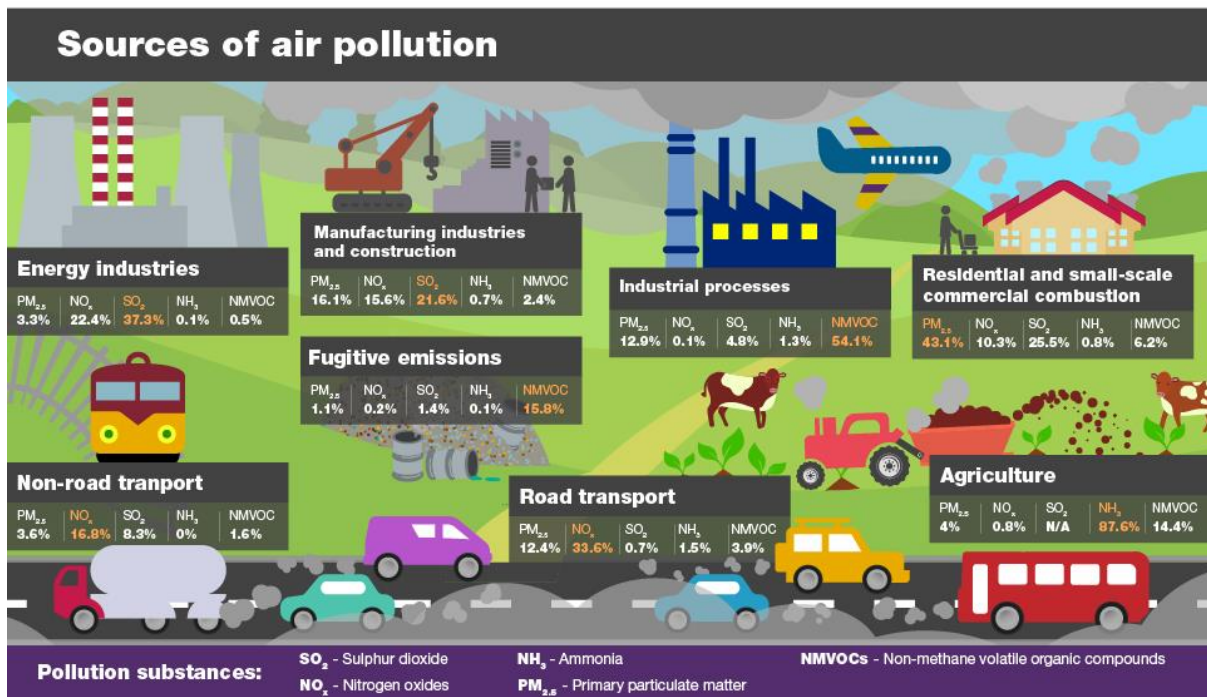


Figure 2. UK anthropogenic air pollution sources sectors. The fractional contribution of each pollutant to emissions from each sector are shown as a percentage (white) and the dominant air pollutant of each sector is indicated (orange). (Public Health England, 2018).

Secondary pollutants include nitrogen dioxide (NO<sub>2</sub>), ozone (O<sub>3</sub>) and several species of PM, including ammonium sulfate (NH<sub>4</sub>NO<sub>3</sub>) and ammonium nitrate (NaNO<sub>3</sub>). Once emitted, pollutants generally exist as trace constituents, however concentrations can vary greatly spatially and temporally depending on emission, chemical transformation, transport and removal processes.

### 1.1.1 Atmospheric Particles

Aerosol particles are suspensions of solid, liquid, or mixed particles (Putaud, et al., 2010). They are very variable in chemical composition and have a wide range of sizes, dependent upon their formation (Figure 3). Particles can be separated into four distinct modes based on their particle diameter: the nucleation, Aitken, accumulation and coarse modes (Figure 3). The particle diameters, sources, formation, growth and removal of each of these particle modes are shown in Figure 3 and Table 1. Table 1 also gives the number/mass concentration and atmospheric lifetime.

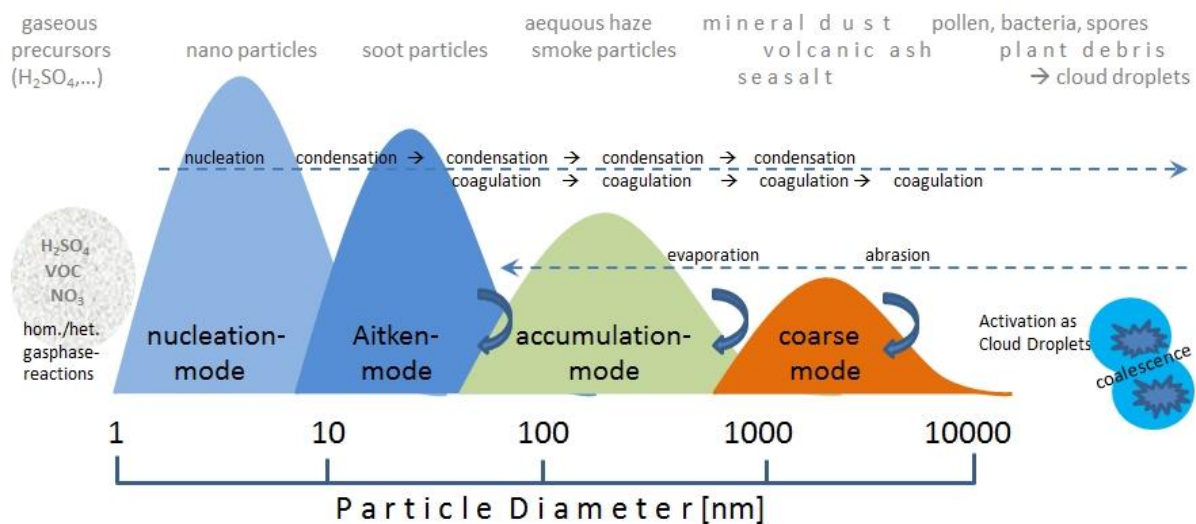


Figure 3. Schematic multi-modal particle size distribution. The four key size modes are labelled – ‘nucleation’, ‘Aitken’, ‘accumulation’ and ‘coarse’. Typical transformations and example particle types within each mode are also shown (Deutscher Wetterdienst, 2017).

Table 1. Overview of aerosol modes shown in Figure 3 (Willeke, and Whitby, 1975).

<b>Aerosol Mode</b>	<b>Particle diameter (<math>\mu\text{m}</math>)</b>	<b>Formation</b>	<b>Growth Processes</b>	<b>Removal Processes</b>	<b>Number Concentration / Mass</b>	<b>Atmospheric Lifetime</b>
<b>Nucleation</b>	< 0.01	Nucleation	Gas to particle conversion (condensation )	Growth to larger modes by condensation and coagulation	High number concentration Low mass	< 1 hour
<b>Aitken</b>	< 0.1	Condensation	Coagulation and coalescence	Growth to larger modes by condensation and coagulation	High number concentration Low mass	A few days
<b>Accumulation</b>	0.1 – 2.5	Condensation/ coagulation	Collision of particles, condensation of gases onto particles	Inefficient removal and slow growth to larger modes	Low number concentration High mass	1-2 weeks
<b>Coarse</b>	2.5 – 10	Condensation/ coagulation	Coagulation	Sedimentation	Low number concentration High mass	Hours to days

#### 1.1.1.1 Particulate Matter

The three largest aerosol modes (Aitken, accumulation and coarse (Figure 3 and Table 1)) are often used to classify particulate matter aerosol (PM), based on particle diameter. PM is split into the ultrafine fraction (diameter  $\leq 0.1 \mu\text{m}$ ), the fine fraction (diameter  $> 0.1 \mu\text{m}$  and  $\leq 2.5 \mu\text{m}$  –  $\text{PM}_{2.5}$ ) and the coarse fraction (diameter  $> 2.5 \mu\text{m}$  but  $\leq 10 \mu\text{m}$  –  $\text{PM}_{10}$ ) (Figure 3 and Table 1). Though PM is generally classified by its size, the composition and shape of PM within each size fraction can vary greatly (Seinfeld, et al., 2016), based on many factors including

emission sources, secondary formation, meteorology and geography (Department for Environment Food & Rural Affairs, 2019).

The size of PM and duration of exposure are key in determining the potential adverse human health effects. Generally,  $PM_{10}$  is too large to be respirable so is deposited in the nose or throat (Figure 4). However,  $PM_{2.5}$  is small enough to be inhaled deep into the lungs, where it can have a negative impact on health (Figure 4, Figure 5).  $PM_1$  can penetrate into the alveoli, through the bronchioles (Figure 4) and  $PM_{0.1}$  can cross through the capillaries in the alveolar walls into the blood (Figure 4).

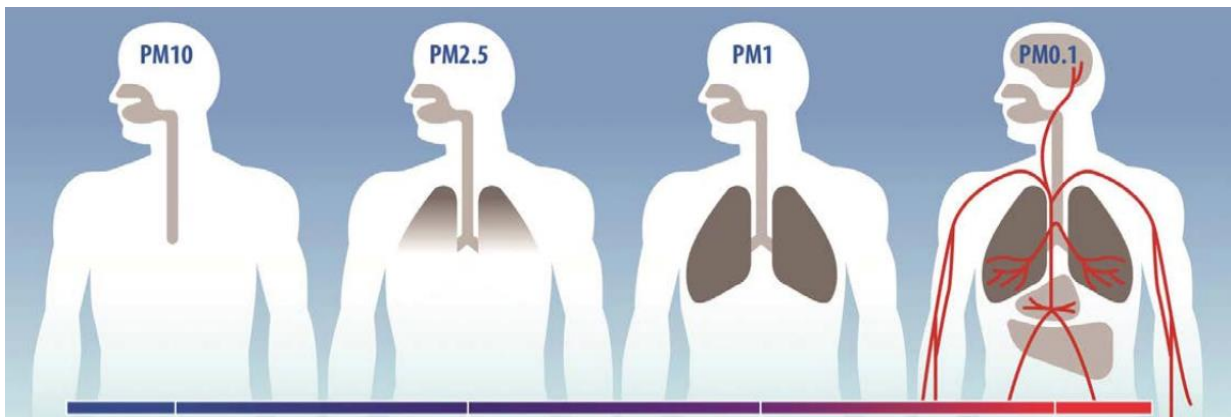


Figure 4. Particulate matter size and penetration into the body (Clean Fuels Development Coalition, 2019)

The strongest epidemiological evidence is associated with exposure to  $PM_{2.5}$  (Harrison, et al., 2004; Pope III, 2007; Pope III, and Dockery, 2006; Public Health England, 2018). Exposure to  $PM_{2.5}$  is associated with increases in morbidity and mortality over short and long-time scales (GBD Collaborators 2015, 2017) (Figure 5). The exacerbation of asthma and respiratory inflammation is shown to be associated with short-term exposure (Public Health England, 2018) (Figure 5). Long-term exposure is associated with increases in heart disease, stroke, lung

cancer and lower respiratory tract infection (GBD Collaborators 2015, 2017; Pope III, and Dockery, 2006).

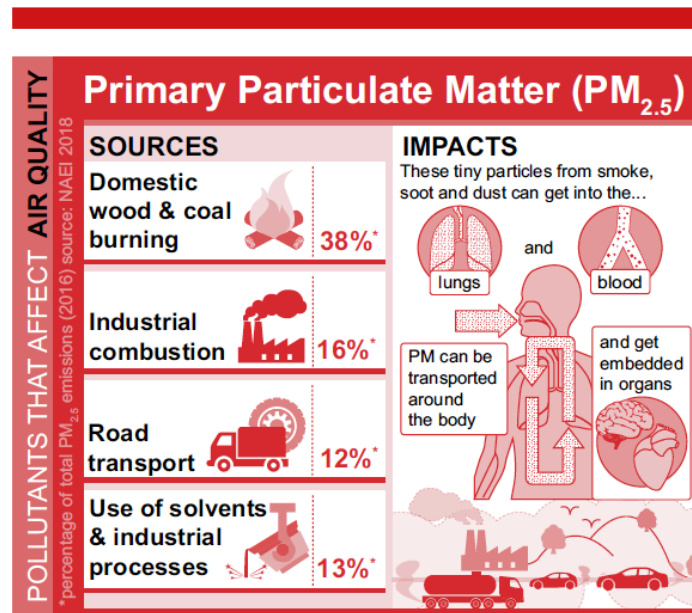


Figure 5. Dominant UK primary PM<sub>2.5</sub> emission sources and health impact mechanisms (Department for Environment Food & Rural Affairs, 2019).

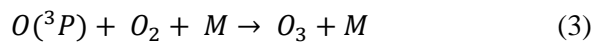
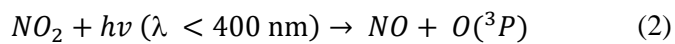
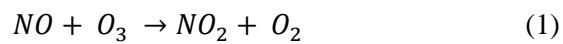
## 1.1.2 Atmospheric Gases

### 1.1.2.1 Nitrogen Oxides

Nitrogen oxide (NO<sub>x</sub>) is formed of two species; Nitric oxide (NO) and nitrogen dioxide (NO<sub>2</sub>) and is produced during the combustion of fossil fuels (in 2017 99% of NO<sub>x</sub> was from the combustion of fuels) (National Atmosphere Emissions Inventory, 2017a). Road transport (~34%), other forms of transport (16.8%) and power/energy production (22%) dominate emissions (Figure 2) (National Atmosphere Emissions Inventory, 2017a; Public Health England, 2018). In the transport sector emissions are largely from diesel vehicles, which emit a larger fraction of NO<sub>2</sub> (between 12% and 70% of total NO<sub>x</sub> emissions) (European

Environment Agency, 2013). Alongside this, total NO<sub>x</sub> emissions are higher for diesel vehicles (European Environment Agency, 2013).

NO<sub>x</sub> emitted as NO, can interconvert to form NO<sub>2</sub> (and back to NO) very quickly (~100s) (Department for Environment Food & Rural Affairs, 2019). This occurs through the reaction with ozone (O<sub>3</sub>) (Equation (1)) and the photolysis of NO<sub>2</sub> by sunlight to return to NO (Equation (2)). This process leads to a net null reaction to re-form O<sub>3</sub> (Equation (3)) (Wood, et al., 2009).



Hydroperoxy radicals (HO<sub>2</sub>) and organic peroxy radicals (RO<sub>2</sub>) can also oxidise NO to NO<sub>2</sub> (through the reactions in Equations (4) and (5)), leading to O<sub>3</sub> formation through NO<sub>2</sub> photolysis in the daytime (Equations (2) and (3)) (Wood, et al., 2009) (Figure 6). Typically > 95% of NO<sub>2</sub> formed (Equations (4) and (5)) undergoes photolysis, leading to the production of O<sub>3</sub> (Wood, et al., 2009).



NO<sub>x</sub> emissions have reduced by 72% since 1990 due to reductions in emissions from all sectors. In the road transport sector the introduction of catalytic converters (77% reduction) and tighter regulations in production of new vehicle engines (Euro standards) have reduced emissions (National Atmosphere Emissions Inventory, 2017a). Though, real-world emissions are higher than in laboratory tests and also higher than emission standards (European Environment Agency, 2017a). In other transport types, emissions have halved due to reductions in emissions from vehicles and changes in fuel types in shipping. Power/energy emissions have also been reduced by >75% due to the combination of better emission control, reduced fuel oil usage and reduced kiln emissions (National Atmosphere Emissions Inventory, 2017a).

Despite reductions in NO<sub>x</sub> emissions, the UK is currently in breach of the EU limit for 24-hour NO<sub>2</sub> concentrations of 200 µg m<sup>-3</sup> in two cities and in breach of the annual mean limit (40 µg m<sup>-3</sup>) in 37 cities. As a result, the UK has been taken to court over failures to meet these targets, which should have been met by 2010. This is as a result of population exposure to NO<sub>2</sub> being shown to cause respiratory irritation and inflammation, which can lead to lower resistance to respiratory infections such as bronchitis (Public Health England, 2018). The Department for Environment Food & Rural Affairs (DEFRA) estimates that in areas exceeding the EU legal limit 80% of NO<sub>x</sub> emissions are from transport (largely diesel cars and vans) (Department for Environment Food and Rural Affairs, 2017).

### 1.1.2.2 Carbon Monoxide

Carbon monoxide (CO) is a tasteless, colourless and odourless gas released during incomplete combustion in vehicles, wildfires and biomass burning, as well as some industrial activities. CO is associated with negative impacts on human health, passing into the bloodstream and replacing oxygen on haemoglobin, thus reducing oxygen uptake. If exposed to high enough CO concentrations (>700 ppmv) this can lead to death through suffocation, however ambient concentrations are much below this at ~2-100 ppmv. CO is also associated with ozone formation in rural areas where NO<sub>x</sub> concentrations are low (Figure 6).

The largest CO source in the UK in 2017 was residential combustion, accounting for 25% of the UK's total emissions (National Atmosphere Emissions Inventory, 2017a). This represents a doubling in contribution since 1990 and is due to much more rapid reductions in emissions from transport (from 65% in 1990 to 16% of emissions in 2017) and industry. These reductions have been driven by the transition from solid fuels to cleaner fuels, such as gas and electricity, and decline in the metal industries. The net effect has been total CO emissions reducing by 79% since 1990. This is in line with the aim of meeting the EU limit on CO concentrations of 10 mg m<sup>-3</sup>, which the UK has met since 2005.

### 1.1.2.3 Non-Methane Volatile Organic Compounds (NMVOCs)

Non-Methane Volatile Organic Compounds (NMVOCs/VOCs) are carbon containing compounds that vary extensively in chemical composition but exhibit very similar behaviour in the atmosphere (National Atmosphere Emissions Inventory, 2017b). VOCs are emitted from a wide range of sources, including combustion and vapours from solvents/petrol. The key sources of VOCs are the industry, transport, fossil fuel extraction, agriculture and residential sectors (National Atmosphere Emissions Inventory, 2017b). However, VOCs can also be

naturally emitted by vegetation (Biogenic VOCs (BVOCs)) (Carlton, et al., 2009; Kroll, and Seinfeld, 2008; Scott, et al., 2014). Once in the atmosphere, VOCs are involved in the formation of secondary air pollutants, such as O<sub>3</sub> and secondary organic aerosols (SOA). SOAs are formed when VOCs are oxidised to form lower volatility products that can partition into the aerosol phase (Scott, et al., 2014). O<sub>3</sub> is formed as a result of photochemical reactions of VOCs in the presence of nitrogen oxides (NO<sub>x</sub>), heat and sunlight (European Environment Agency, 2016). Some VOC species are directly associated with negative health impacts (e.g. benzene) due to being carcinogenic (National Atmosphere Emissions Inventory, 2017b). Other VOCs are associated with negative health impacts due to their role in forming secondary pollutants in the atmosphere (e.g. O<sub>3</sub> and PM<sub>2.5</sub>) (Atkinson, et al., 2016; Jerrett, et al., 2009; Pope III, and Dockery, 2006).

#### 1.1.2.4 Ammonia

Ammonia is a gas that is emitted largely by agricultural processes (e.g. 87% of the total ammonia in 2016) such as manure, slurry and fertilizer storage and spreading (Department for Environment Food & Rural Affairs, 2019) (Figure 2). The remaining 12% of ammonia emissions are split equally between other emissions sources (Figure 2).

Ammonia has an important role in a range of environmental issues such as nitrification, eutrophication, acidification (National Atmosphere Emissions Inventory, 2017a). Alongside this, ammonia is also indirectly linked to the health impacts of exposure to PM<sub>2.5</sub> due to being a precursor species in the formation of secondary PM. The atmospheric lifetime of ammonia increases from a few hours, as a gas, to a few weeks, as a particle, meaning ammonia is important on both local and regional, even national, scales (Department for Environment Food & Rural Affairs, 2019).

In contrast to emissions of primary PM<sub>2.5</sub>, which decreased by 55% between 1990 and 2017, emissions of ammonia only decreased by 13% between 1990 and 2017. However, there has been a trend of increasing emissions from 2015 to present. The increase has been attributed to increased cattle emissions and spreading resulting from the widespread increased use of anaerobic digestion for non-manure waste (National Atmosphere Emissions Inventory, 2017a). As a result, agricultural emissions of ammonia have been identified to be drivers of several of the high PM<sub>2.5</sub> episodes in the UK in recent years (Vieno *et al.*, 2016; Vieno *et al.*, 2016; Public Health England, 2018).

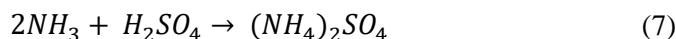
#### 1.1.2.5 Secondary PM<sub>2.5</sub>

Secondary PM<sub>2.5</sub> (ammonium/sodium nitrate (NH<sub>4</sub>NO<sub>3</sub>/NaNO<sub>3</sub>) and ammonium sulfate (NH<sub>4</sub>SO<sub>4</sub>)) contributes to between 50 and 75% of total UK PM<sub>2.5</sub> mass in ambient and high pollution conditions. These secondary PM species are formed from the mixing of precursor emissions of NH<sub>3</sub>, SO<sub>2</sub> and NO<sub>x</sub> in the atmosphere (Air Quality Expert Group, 2005). The reactions involved in PM formation are predominantly inorganic in nature, complex and compete with each other (Sharma, et al., 2007). They depend on solar radiation and meteorological factors such as relative humidity and temperature.

The mechanism forming sulfate and nitrate species of PM<sub>2.5</sub> are described below in Equations (6) - (10) (CENR, 2000).

##### 1.1.2.5.1 Sulfate PM species

Sulfur dioxide (SO<sub>2</sub>) is created during combustion, through the oxidation of sulfur. SO<sub>2</sub> is subsequently oxidised by the hydroxyl radical (OH) to form sulfuric acid (H<sub>2</sub>SO<sub>4</sub>) (Equation (6)). Sulfuric acid can then react with ammonia (NH<sub>3</sub>) to create ammonium sulfate ((NH<sub>4</sub>)<sub>2</sub>SO<sub>4</sub>) (Equation (6)).



#### 1.1.2.5.2 Nitrate PM species

The formation of ammonium nitrate is shown in Equation (8). Nitric acid (HNO<sub>3</sub>) is formed when nitrogen dioxide (NO<sub>2</sub>) reacts with the hydroxyl radical (OH) (Equation (8)). Ammonia (NH<sub>3</sub>) and nitric acid (HNO<sub>3</sub>) can then react on pre-existing particles to form ammonium nitrate (NH<sub>4</sub>NO<sub>3</sub>) (Equation (9)). As a result, ammonium nitrate is associated with an increase in overall PM mass, but not an increase in number density. Ammonium nitrate is a semi-volatile species meaning it can readily transition between the gas (ammonia and nitric acid) and particulate phase (ammonium nitrate). The phase change of ammonium nitrate can occur over minutes to hours, dependent upon atmospheric conditions (Air Quality Expert Group, 2012).

Finally, the formation of sodium nitrate (NaNO<sub>3</sub>) (Equation (10)) requires nitric acid (HNO<sub>3</sub>) and sodium chloride (NaCl) as precursor emissions. This reaction forms sodium nitrate (NaNO<sub>3</sub>) as well as hydrochloric acid (HCl) (Rossi, 2003).





The formation of ammonium sulfate (Equation (6)) is favoured over the formation of ammonium nitrate (Equation (9)). However, where sulfate concentrations are low and nitrogen oxide concentrations are high ammonium nitrate is formed preferentially (CENR, 2000).

#### 1.1.2.6 Ozone

Tropospheric ozone (O<sub>3</sub>) is a gaseous secondary pollutant, formed by photochemical reactions between precursor emissions of carbon monoxide (CO), methane (CH<sub>4</sub>) and Volatile Organic Compounds (VOCs) in the presence of nitrogen oxides (NO<sub>x</sub>), heat and sunlight (Crutzen, et al., 1999). Tropospheric O<sub>3</sub> precursors are largely emitted from the transport, industrial and chemical sectors, though VOCs are also emitted by natural sources (vegetation) (National Atmospheric Emission Inventory, 2016). Although emission sources are predominantly located in urban areas, NO<sub>2</sub> can be transported away from source regions to rural areas, leading to ozone formation downwind.

## O<sub>3</sub> formation

The various mechanisms for tropospheric O<sub>3</sub> formation (Figure 6) will be discussed below.

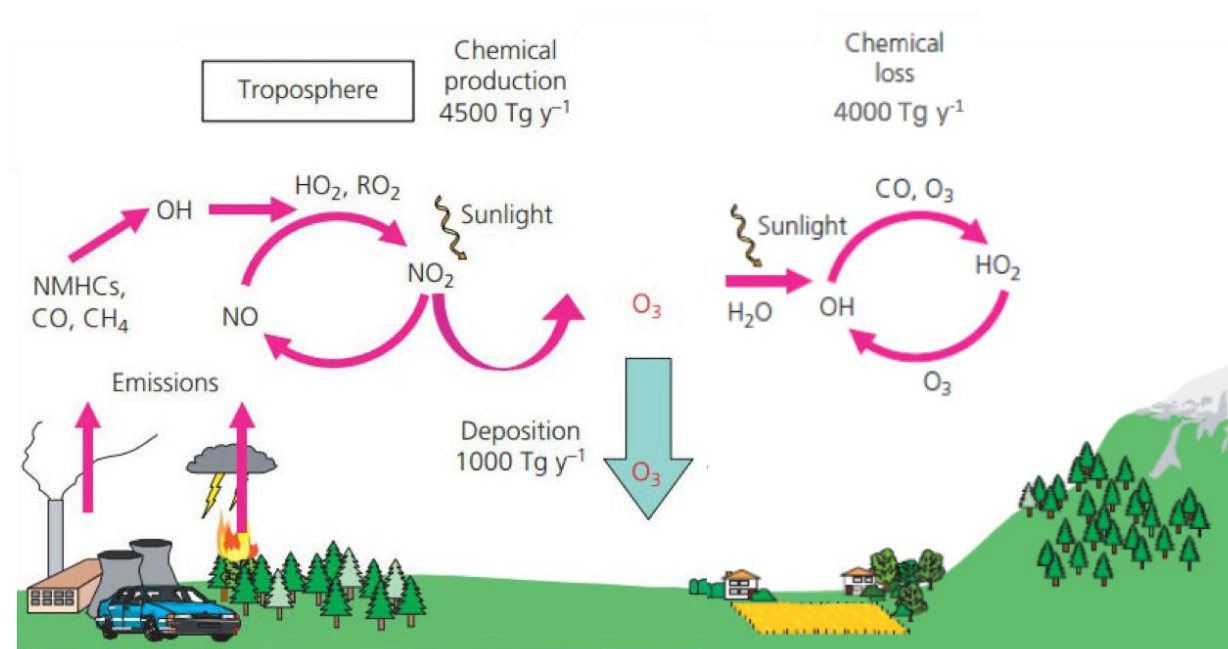


Figure 6. Schematic of the annual tropospheric ozone budget from a global chemistry-transport model. Data is taken from (Denman, et al., 2007). Adapted from (Centre for Ecology and Hydrology, 2016).

Tropospheric O<sub>3</sub> is formed by the oxidation of CO, CH<sub>4</sub> and VOCs (also known as non-methane hydrocarbons (NMHCs)) by the hydroxyl radical (OH) in the presence of nitrogen oxides (NO<sub>x</sub>) (Figure 6). This leads to the formation of hydroperoxyl radicals (HO<sub>2</sub> and RO<sub>2</sub>), which can then react with NO to form NO<sub>2</sub> (Figure 6). Finally, NO<sub>2</sub> is photolysed to form O<sub>3</sub>, leading to net O<sub>3</sub> production (Wood, et al., 2009).

However the formation of tropospheric O<sub>3</sub> is highly non-linear, dependent upon the relative amounts of NO<sub>x</sub> and VOCs in a given location (Monks, et al., 2015).

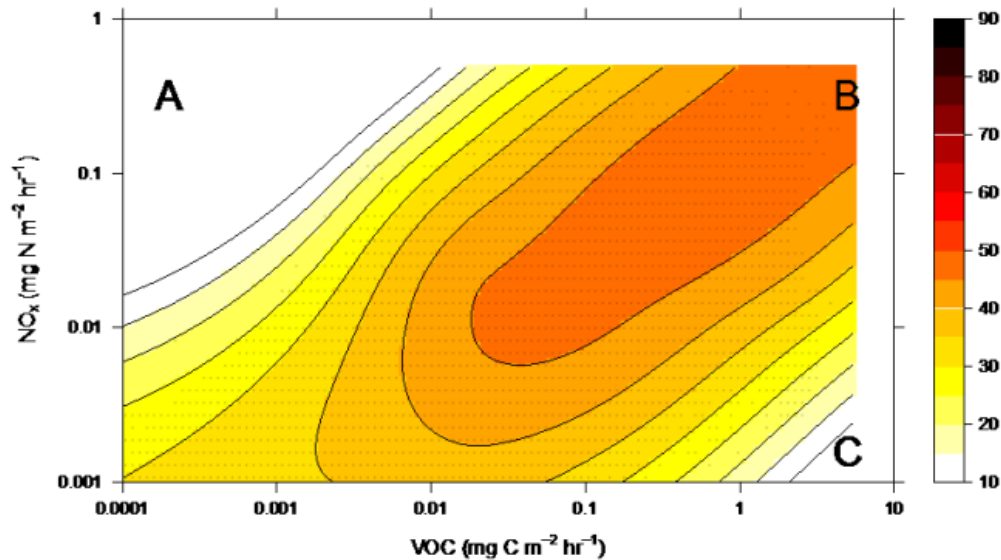


Figure 7. Tropospheric ozone mixing ratio (in parts per billion (ppb)) as a function of VOC and  $\text{NO}_x$  emissions. Regions of (A) high- $\text{NO}_x$  ( $\text{O}_3$  titration), (C) high-VOC ( $\text{O}_3$  loss) and (A-C, B-C) efficient conversion of  $\text{NO}$ - $\text{NO}_2$  to then form tropospheric  $\text{O}_3$  with increasing  $\text{NO}_x$  and VOC emissions. (Archibald, et al., 2011; Monks, et al., 2015).

- 1) In VOC-limited regimes (high  $\text{NO}_x$ , low VOC) (Figure 7 (A))  $\text{O}_3$  formation is inhibited by the availability of VOCs. There is a null  $\text{O}_3$  cycle, due to the titration of  $\text{O}_3$  by high levels of  $\text{NO}_x$ , and therefore  $\text{NO}$ , to form  $\text{NO}_2$ .  $\text{NO}_2$  is then photolysed to form  $\text{O}_3$  (Equation (1)). In this regime,  $\text{NO}_2$  is reduced over time as it is converted to  $\text{HNO}_3$  through the reaction with  $\text{OH}$  and then washed out.
- 2) In  $\text{NO}_x$ -limited regimes (low  $\text{NO}_x$ , high VOC) (Figure 7 (C))  $\text{O}_3$  formation is inhibited by the availability of  $\text{NO}_x$ . Here, net  $\text{O}_3$  loss occurs through the reaction with  $\text{HO}_2$  to form  $\text{OH}$  (Figure 6).
- 3)  $\text{O}_3$  production is most efficient in high  $\text{NO}_x$ , high VOC regimes (Figure 7 (B)) due to an abundance of VOCs and  $\text{NO}_x$  to form hydroperoxyl radicals ( $\text{HO}_2$  and  $\text{RO}_2$ ), which can convert  $\text{NO}$  to  $\text{NO}_2$  (Figure 6). In this regime  $\text{NO}_x$  is a catalyst to  $\text{O}_3$  production.

- 4) In regimes between these, the relative contribution of both VOC and NO<sub>x</sub> emissions must be considered in order to achieve reductions in O<sub>3</sub>. This is because O<sub>3</sub> concentrations do not decrease linearly with VOC and NO<sub>x</sub> emission reductions. For example, reducing VOC emissions in a high NO<sub>x</sub> regime would lead to an increase in O<sub>3</sub> mixing ratios (Figure 7).

The dependence of tropospheric O<sub>3</sub> formation on sunlight and heat means ozone is a spring and summer pollutant. As a result of the complex formation cycles, dependent on the relative amounts of precursor emissions (Figure 7), reductions in O<sub>3</sub> can be difficult to achieve by reducing a single precursor in isolation. This is important because human exposure to O<sub>3</sub> has been shown to be associated with inflammation of the respiratory tract, eyes, nose and throat and long-term, chronic exposure has been linked to increased mortality (Department for Environment Food and Rural Affairs, and Department for Transport, 2017).

Alongside this, O<sub>3</sub> can also cause a wide-range of damage to crops and other vegetation through stomatal conductance during photosynthesis (Emberson, et al., 2018). This can lead to cell damage during respiration and leads to plant leaf damage, visible via discolouration, and subsequent reductions in photosynthesis (US Environmental Protection Agency, 2020). As a result, plant O<sub>3</sub> exposure can lead to reductions in the quality and quantity of crop yields (Emberson, et al., 2018).

### **O<sub>3</sub> removal**

The dominant source of O<sub>3</sub> loss in the troposphere is through photolysis in the presence of water vapour or with the hydroxyl radical (OH) and the hydroperoxyl radical (HO<sub>2</sub>) (Figure 6). O<sub>3</sub> is photolyzed to form molecular oxygen (O<sub>2</sub>) and 'excited oxygen' (O(<sup>1</sup>D)). The excited oxygen atom subsequently reacts with water vapour (H<sub>2</sub>O) to form the hydroxyl radical (2OH).

Tropospheric O<sub>3</sub> can also be removed by OH and HO<sub>2</sub>, though these mechanisms of removal generally account for a much smaller fraction of the total ozone sink (Tadic, et al., 2020). In urban environments where NO<sub>x</sub> concentrations are high, the removal of O<sub>3</sub> by NO dominates. Here, O<sub>3</sub> is quickly removed through titration with NO (Equation (1)). This leads to very low O<sub>3</sub> concentrations and high NO<sub>2</sub> concentrations in urban environments (Figure 7 (A)).

## **1.2 Physical Atmospheric Processes**

### **1.2.1 Removal of Air Pollutants**

The removal of air pollutants has a strong influence on pollutant lifetime and therefore plays a crucial role in determining whether pollutants are subject to long-range transport. Removal occurs through both wet and dry deposition.

#### **1.2.1.1 Dry Deposition of Air Pollutants**

Dry deposition is the removal of gases and particles from the atmosphere in the absence of precipitation (Seinfeld, et al., 2016). Particles and gases are transferred to the Earth's surface by turbulent fluxes toward the surface. The efficiency of dry deposition is determined by the deposition velocity, which is a function of turbulence (Harrison, 2014; Seinfeld, et al., 2016).

The key processes which affect the deposition of particles and gases are:

- The shape and surface and the species reactivity of aerosol particles affects the efficiency of dry deposition (Harrison, 2014; Seinfeld, et al., 2016). Generally, high levels of turbulence and rougher, less spherical particle surfaces lead to increased deposition (Seinfeld, et al., 2016).
- The efficiency of dry deposition of gases is affected by turbulence and species reactivity (Harrison, 2014; Seinfeld, et al., 2016). In general, higher levels of turbulence and higher reactivity of gases lead to increases in deposition (Seinfeld, et al., 2016).

Aerosol particles can also be removed through sedimentation as they grow to larger sizes, causing the mass of particles to increase (Figure 3). Growth reduces the likelihood of the particle remaining airborne and they eventually fall out of the air (sedimentation) (Vallero, 2014). This process occurs continuously in the boundary layer due to turbulent fluxes.

The time taken for different particulate species to be removed through dry deposition varies but for some species, such as sulphate and nitrate, it is large enough (~5 days) to allow for their transport over long distances to occur (Harrison, 2014).

#### **1.2.1.2 Wet Deposition of Air Pollutants**

Wet deposition of air pollution occurs when rain (or snow, hail etc.) removes chemical species from the atmosphere. The process occurs in three steps:

- 1) The species of gas or aerosol comes into contact with precipitation in a cloud or when rain is falling.
- 2) The species is scavenged by a hydrometeor in precipitation or forms a cloud drop.
- 3) The species is deposited at the surface, thus removing it from the atmosphere.

Large, soluble aerosol particles are efficiently scavenged by precipitation meaning wet deposition significantly reduces their atmospheric lifetime (Harrison, 2014). However, this process is episodic in nature.

#### **1.2.2 Dispersion of Air Pollutants**

##### **1.2.2.1 Impact of Meteorology**

Once emitted into the atmosphere, pollutants move away from the emission source in a plume in the direction of the mean wind (Harrison, 2014). As the plume moves away from the source, cleaner air is entrained, leading to an increase in plume size and a decrease in concentrations within the plume over time (and therefore distance). However, the dispersal of pollutants within

the atmosphere varies spatially and temporally. Conditions can vary between the effective dispersal of pollutants (and lower concentrations) and conditions inhibiting dispersion (thus, accumulation and higher concentrations). Several key processes control the dispersion of pollutants in the vertical and horizontal. Atmospheric stability controls the vertical movement, while wind speed and direction control the horizontal movement of pollutants.

#### **1.2.2.1.1 Atmospheric Stability**

The stability of the atmosphere is determined by the vertical temperature gradient (Jacob, 1999). The vertical temperature structure of the atmosphere is controlled by solar heating of the Earth's surface, causing changes in the vertical structure of the atmosphere close to the surface (boundary layer) diurnally and seasonally (Hu, 2015). The boundary layer grows in height during the day due to solar heating of the Earth's surface, and is also higher in summer than winter for the same reason. Since temperature changes with changes in height (and therefore pressure), potential temperature is often used to describe the evolution of the atmosphere with height. Potential temperature ( $\theta$ ) can be defined as the temperature of a parcel of air if it were returned to 1000 hPa without any heat transfer between the parcel and its surroundings (adiabatically), allowing for easy comparison of temperature at different heights. The structure of the boundary layer can be characterised most basically by three states, shown in Figure 8.

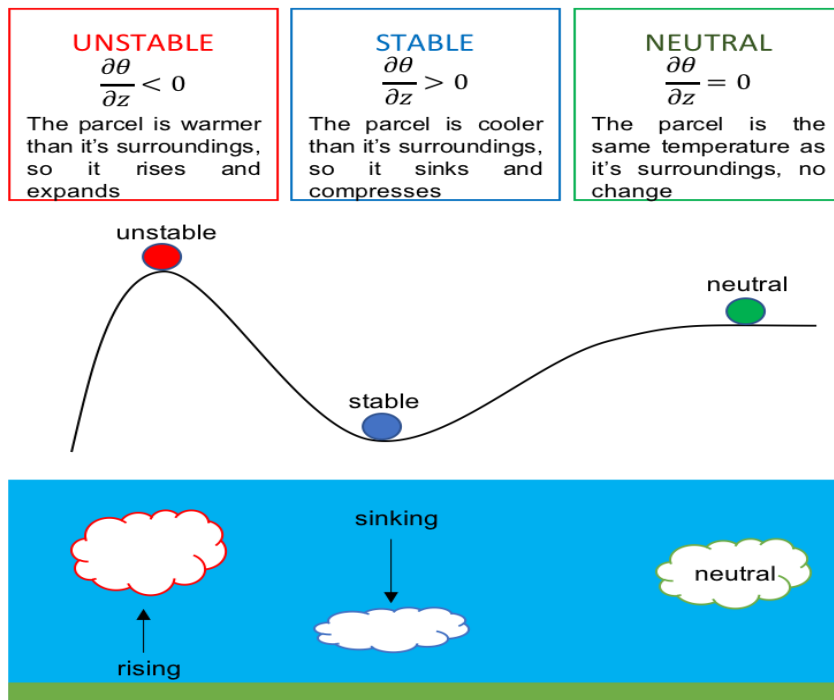


Figure 8. Examples of stability and instability in relation to air parcel temperatures (adapted from Nugent *et al.* (2019)).

Potential temperature can either:

- 1) increase with height (inversion conditions) ( $\frac{\partial \theta}{\partial z} < 0$ )

In an unstable atmosphere, the potential temperature of an air parcel is higher, and density lower, than the surrounding air (due to solar heating). This leads to the air parcel rising until it reaches a region in the atmosphere where it is in equilibrium with the surrounding environment. These conditions promote turbulence and dispersal of pollutants, therefore decreasing concentrations (Department of Environmental Affairs and Tourism, 2018).

2) decrease with height (lapse conditions) ( $\frac{\partial\theta}{\partial z} > 0$ )

In lapse conditions (a stable atmosphere), the potential temperature of an air parcel is the lower, and density higher, than its surroundings. The air parcel therefore remains at the surface, resisting movement upwards. This would lead to pollution accumulation and increased concentrations at the surface (Department of Environmental Affairs and Tourism, 2018).

3) be constant with height (isothermal) ( $\frac{\partial\theta}{\partial z} = 0$ )

Finally, in a neutral atmosphere, an air parcel would remain at the same height it was released because the potential temperature of the air parcel would be in equilibrium with the surrounding environment (Department of Environmental Affairs and Tourism, 2018). If emitted from a stack the parcel would remain at the same pressure/height it was emitted at.

Thus, inversion conditions inhibit stability, while lapse and isothermal conditions generally favour stability. The stability of the atmosphere varies throughout the year and the day, due to seasonal and diurnal variations in solar heating (Hu, 2015). Generally, the boundary layer is more stable in the winter than summer and more stable at night and the early morning than in the middle of the day.

#### **1.2.2.1.2 Wind Flow**

Wind speed and direction govern the horizontal movement of pollutants within air (Jacob, 2000). Increases in wind speed lead to increased dispersion of pollutants, while wind direction controls the course of pollution transport. Large-scale wind is caused by atmospheric pressure gradients and so varies with space and time. At the synoptic scale, pollution dispersion is controlled by high and low-pressure systems.

High-pressure systems are generally associated with:

- the subsidence of air and therefore stable conditions, with generally light winds.
- reduced pollutant dispersal and increased pollutant concentrations locally.

Low-pressure is usually associated with:

- rising air and instability with increased wind speeds due to large pressure gradients.
- improved pollutant dispersal and often wet deposition, leading to lower pollutant concentrations.

Locally, the topography of the Earth's surface can affect wind direction and speed. Examples of this include sea breezes, urban heat islands and mechanical turbulence caused by buildings (Cheremisinoff, 2002). This can have an impact of the concentrations of pollutants at local and regional scales.

#### **1.2.2.1.3 Long-range transport**

The long-range transport of pollutants is linked to both atmospheric stability and wind flow. Usually plumes of pollutants are released just above the surface, within the turbulent boundary layer, so that pollutants are dispersed but do not travel far from the source before being deposited at the surface. However, if the height at which a plume of pollutants is released is above the height of these convective and turbulent processes, it is capable of travel for hundreds of miles in favourable winds and weather conditions (Vallero, 2014).

The long-range transport of air pollutants was not known about until the 1960s when scientists discovered that air pollutants emitted thousands of kilometres away were a significant contributor to acid rain in the northern hemisphere (United Nations Economic Commission for Europe, 1979). This led to the establishment of the Convention on Long-Range Transboundary Air Pollution (CLRTAP), which sought to create understanding that air pollution can cross borders (United Nations Economic Commission for Europe, 1979). The key air pollutants

identified to be subject to long-range transport were SO<sub>x</sub>, NO<sub>x</sub>, tropospheric O<sub>3</sub> and PM. This is because the lifetimes of these species are large enough (days to weeks) for them to be transported over large distances under favourable meteorological conditions. The long atmospheric lifetime of PM<sub>2.5</sub> means that, on an annual basis, long-range transport has a significant contribution (20%) towards UK PM<sub>2.5</sub> concentrations (Department for Environment Food and Rural Affairs, 2016) (Figure 10).

Secondary PM<sub>2.5</sub> has been shown to represent a relatively large fraction of total UK PM<sub>2.5</sub> (Figure 9) (Department for Environment Food and Rural Affairs, 2016). As a result, several studies have investigated the impact of reductions of precursor emissions on PM<sub>2.5</sub> concentrations to identify which precursors to target for the most effective reductions in PM<sub>2.5</sub> (Air Quality Expert Group, 2013; Harrison *et al.*, 2013; Megaritis *et al.*, 2013; Vieno *et al.*, 2016). All studies identified that reductions in precursors led to a much smaller reduction in total PM<sub>2.5</sub> (i.e. X% reduction in precursor → reduction in PM<sub>2.5</sub> < X%) due to the non-linear relationship between emissions and PM<sub>2.5</sub> concentrations. On a species specific basis studies suggest that the largest reduction in UK PM<sub>2.5</sub> concentrations could be achieved through reductions in ammonia (Air Quality Expert Group, 2013; Megaritis, *et al.*, 2013) or sulfate (Harrison *et al.*, 2013; Vieno *et al.*, 2016). However, there is less clarity between studies on the magnitude of resulting reduction in PM<sub>2.5</sub> from reductions in precursors, and whether the reduction in UK or continental European precursors are most important. Despite this, when public exposure is taken into account, reductions in primary PM<sub>2.5</sub> yield the largest reductions in population-weighted PM<sub>2.5</sub> (Air Quality Expert Group, 2013). In urban areas, where the largest proportion of the population live, primary PM<sub>2.5</sub> emissions dominate, while in rural areas reductions in ammonia lead to the greatest reductions in PM<sub>2.5</sub>.

UK concentrations of  $PM_{2.5}$  were not routinely monitored until 2008. Therefore, previous studies focussing on the drivers of high pollution episodes have analysed  $PM_{10}$  observations or specific pollution episode case-studies, using atmospheric chemistry transport models. Vieno *et al.* (2016) showed that a large spring pollution episode in 2014 was driven by ammonium nitrate, which was formed from agricultural emissions released outside of the UK and subsequently transported to the UK under favourable winds. Other studies have used back trajectories alongside  $PM_{10}$  observations to investigate possible source regions of  $PM_{10}$  episodes (King, and Dorling, 1997; Stedman, 1996). These studies found that on days that high  $PM_{10}$  concentrations were observed, the contribution of local emissions to the total concentration was small. The high  $PM_{10}$  days were dominated by easterly flow, suggesting that there was a large contribution from long-range transport to the overall  $PM_{10}$  concentrations observed, since the back trajectories emanated from mainland Europe. The study concluded that more work was required to confirm this, over a longer period with observations at rural sites. More recent studies have used  $PM_{2.5}$  observations, from 2009, to investigate processes affecting  $PM_{2.5}$  concentrations (Harrison, et al., 2012).  $PM_{2.5}$  concentrations were also found to be highest for south-easterly, easterly and north-easterly flows and lower for westerly flows. The increase in  $PM_{2.5}$  was attributed to the long-range transport of emissions from continental Europe under easterly and south-easterly flow. The results suggested that the long-range transport of pollutants to the UK is associated with specific meteorological conditions. However, due to the short observational record at the time, the sample size for individual wind directions was small. This meant relationships between wind direction and  $PM_{2.5}$  observations could not be established over a longer period of time to be statistically robust.

The influence of different synoptic conditions on total column  $NO_2$  and  $O_3$  across the UK was investigated using Lamb weather types, a classification system for synoptic meteorology (Pope *et al.*, 2015; Pope *et al.*, 2016). The study highlighted that pollutant concentrations are strongly

influenced by wind and circulation patterns. The highest O<sub>3</sub> concentrations occurred under summer anticyclonic conditions due to large scale subsidence limiting vertical mixing. South-easterly and north-easterly flow also increased mean UK O<sub>3</sub> concentrations by between 10 and 15 µg m<sup>-3</sup> (Pope *et al.*, 2016). NO<sub>2</sub> concentrations were found to significantly increase under winter-time anticyclonic conditions through pollutant accumulation. Concentrations were also enhanced under south-easterly flow due to long-range transport of pollutants from continental Europe (Pope, et al., 2015). The wintertime increase was attributed to the combined effect of increased emissions, more stable conditions and decreased photolysis, allowing accumulation over emission sources. Due to the relatively short UK PM<sub>2.5</sub> observational record and frequently cloudy conditions inhibiting satellite retrievals of aerosol optical depth (AOD) the same analysis is yet to be applied to UK PM<sub>2.5</sub> concentrations.

#### 1.2.2.2 Impact of Topography

The topography of regions can enhance or reduce pollution concentrations and is therefore an important factor controlling the ambient concentrations. The topography of some regions can be conducive to the development of temperature inversions, which can increase concentrations of pollutants at the surface, leading to high pollution events (Wallace, et al., 2010). A temperature inversion occurs when the potential temperature of air at the surface is lower than air above, leading to the cooler, denser surface air becoming trapped below less dense, warmer air aloft. These conditions aid the accumulation of pollutants by preventing vertical mixing and dispersion, trapping pollutants at the surface and therefore increasing their concentrations. There are three key types of inversions caused by topography, which subsequently impact pollutant concentrations at the surface:

- 1) **Radiation inversions** – usually occur on cold nights under clear skies. Radiation inversions are characterised by rapid heat loss at the Earth's surface, warming air above.

If this occurs in a valley or basin, cold air from the side of the valleys flows down slope, becoming trapped beneath the layer of warmer air that was heated by the surface.

- 2) **Advective inversions** – occur close to coastlines which are bordered by cold oceans or lakes. The differential heating between the air over the land and sea in the daytime causes a pressure gradient to form. As a result, a land-sea breeze is initiated where cold low-level oceanic/lake air moves landwards, underneath the warm continental air, setting up a return flow of continental air aloft.
- 3) **Subsidence inversions** – are associated with areas where high pressure dominates and a large layer of air descends. As the air descends it is heated by the increase in atmospheric pressure (adiabatic heating). This can also occur as air is compressed in flow over a hillside. The adiabatic heating can lead to the air aloft being warmer than at the surface, therefore forming a temperature inversion at the surface or within a valley.

## 1.3 UK PM<sub>2.5</sub> Concentrations

### 1.3.1 PM<sub>2.5</sub> Chemical Composition

The chemical composition of PM<sub>2.5</sub> can vary greatly, dependent upon emission source (Figure 2), chemical transformations and atmospheric conditions (Air Quality Expert Group, 2012). This means PM<sub>2.5</sub> concentrations measured in a specific location can be a mixture of many different chemical species from different sources. Some of the common species of PM<sub>2.5</sub> (and their emission sources) include:

- Elementary carbon (soot) (emitted by burning fossil fuel by traffic and biomass burning)
- Calcium salts (CaSO<sub>4</sub> • 2H<sub>2</sub>O) (from construction and demolition dust and wind-blown soil)

- Sea salt (NaCl) (from sea spray).
- Iron-rich dusts (emitted from combustion (traffic, shipping and industry), brake and tyre wear (traffic) and wind- and traffic-generated suspension of crustal material).
- Organic matter, including dioxins, polycyclic aromatic hydrocarbons and alkanes (emitted as a result of combustion in industry and engines and naturally from biomass burning).
- Secondary inorganic ions, such as nitrate, sulfate and ammonia (the primary precursors for which are emitted from agriculture, industry and transport).
- Secondary Organic Aerosol (SOA) (formed through the oxidization of VOC emissions from fuel combustion, industrial processes, vehicles and fires and BVOCs from vegetation).

The composition of UK PM<sub>2.5</sub> was characterised using observations from a background site in Birmingham between 2004 and 2006 (Figure 9) (Yin, and Harrison, 2008). Overall secondary species, including ammonium nitrate, sodium nitrate and ammonium sulfate, accounted for 45% of the total PM<sub>2.5</sub> mass (Figure 9 (a)). However, on high pollution days (PM<sub>10</sub> > 50 µg m<sup>-3</sup>) the contribution of secondary PM<sub>2.5</sub> increased to ~75%, with a doubling of the ammonium nitrate and sodium nitrate contribution (from 21% to 46%) (Figure 9 (b)). Although these findings are for one location, the increase in nitrate PM species during polluted days is in line with findings elsewhere in Europe (Vieno *et al.*, 2016). This also fits with the results of a modelling study which examined an extended pollution episode (Vieno *et al.*, 2016). This study indicated that nitrate, from a combination of local emissions and long-range transport dominated during the pollution episode (Vieno *et al.*, 2016).

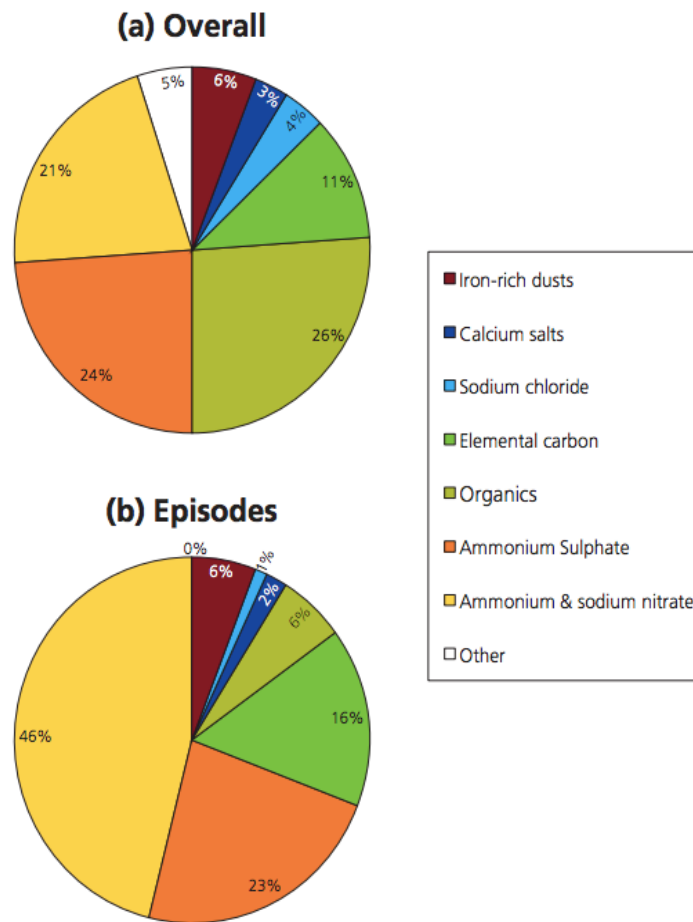


Figure 9. (a) Average composition of UK  $PM_{2.5}$  (2004-2006) and (b) on days where  $PM_{10} > 50 \mu g m^{-3}$ . From (Air Quality Expert Group, 2012), adapted from (Yin and Harrison, 2008).

### 1.3.2 $PM_{2.5}$ Sources

The relative contribution of UK emissions to total  $PM_{2.5}$  mass can vary between background conditions and high pollution events. On an annual basis a combination of local emissions (traffic and non-traffic) and long-range transport (regional and international emissions) have been shown to affect the concentration of  $PM_{2.5}$  at monitoring sites (Figure 10) (Department for Environment Food and Rural Affairs, 2016). The largest contributions to concentrations at background locations comes from regional UK emissions (45%) and then from international emissions (20%) and urban non-traffic emissions (21%). Regional and international emissions

can include primary emissions, such as those from anthropogenic sources (e.g. industry) or natural sources (e.g. dust or wildfires), and secondary species formed in the atmosphere from precursor emissions (e.g. ammonium nitrate from ammonia emissions) (Figure 9).

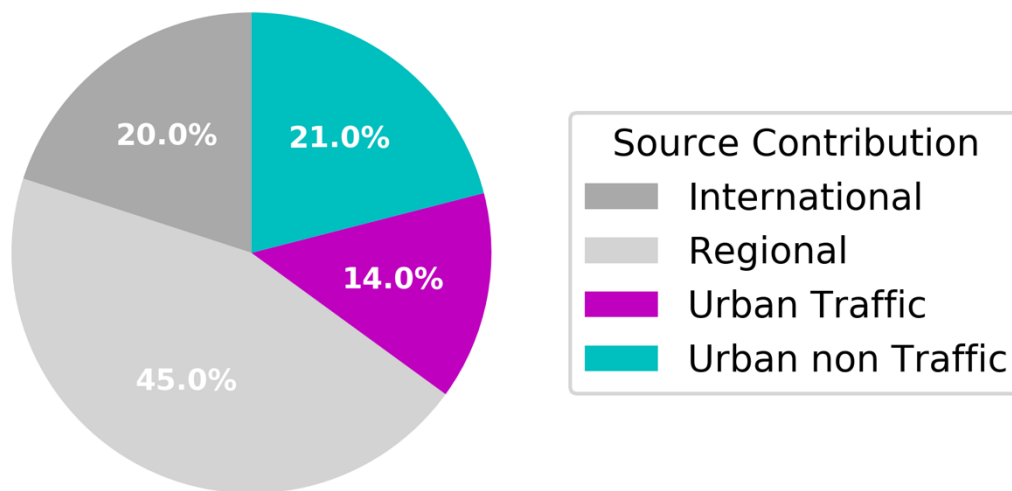


Figure 10. Percentage contributions (%) to total modelled annual mean ambient  $PM_{2.5}$  concentrations at UK urban background locations (Department for Environment Food and Rural Affairs, 2016).

However, the relative contribution of each source varies during high pollution episodes (Department for Environment Food & Rural Affairs, 2019), reflected by changes in composition (Figure 9 (a) and (b)). Increases in  $PM_{2.5}$  concentrations across the UK, which often occur under easterly winds, are thought to be linked to the long-range transport of  $PM_{2.5}$  and secondary  $PM_{2.5}$  precursor emissions (Harrison, et al., 2013). However, the relative contribution of UK and non-UK emissions on UK  $PM_{2.5}$  concentrations is yet to be quantified.

### 1.3.3 Seasonal Cycle in $PM_{2.5}$ Concentrations

There is clear seasonal variation in monthly  $PM_{2.5}$  concentrations across all regions of the UK (Figure 11), with the highest concentrations observed between January and April and the lowest

concentrations between June and September (Harrison, et al., 2012). The combination of an increase in local emissions of primary PM<sub>2.5</sub> and secondary PM precursors, alongside a more stable boundary layer during winter months is believed to lead to higher PM<sub>2.5</sub> concentrations. While in summer months, increased boundary layer height, a decrease in emissions and the evaporative loss of semi-volatile PM is believed to lead to lower PM<sub>2.5</sub> concentrations. However, the relative contributions of emission sources to PM<sub>2.5</sub> concentrations observed is yet to be quantified. Alongside this, the mechanisms leading to the large increase in PM<sub>2.5</sub> concentrations in April have not been studied.

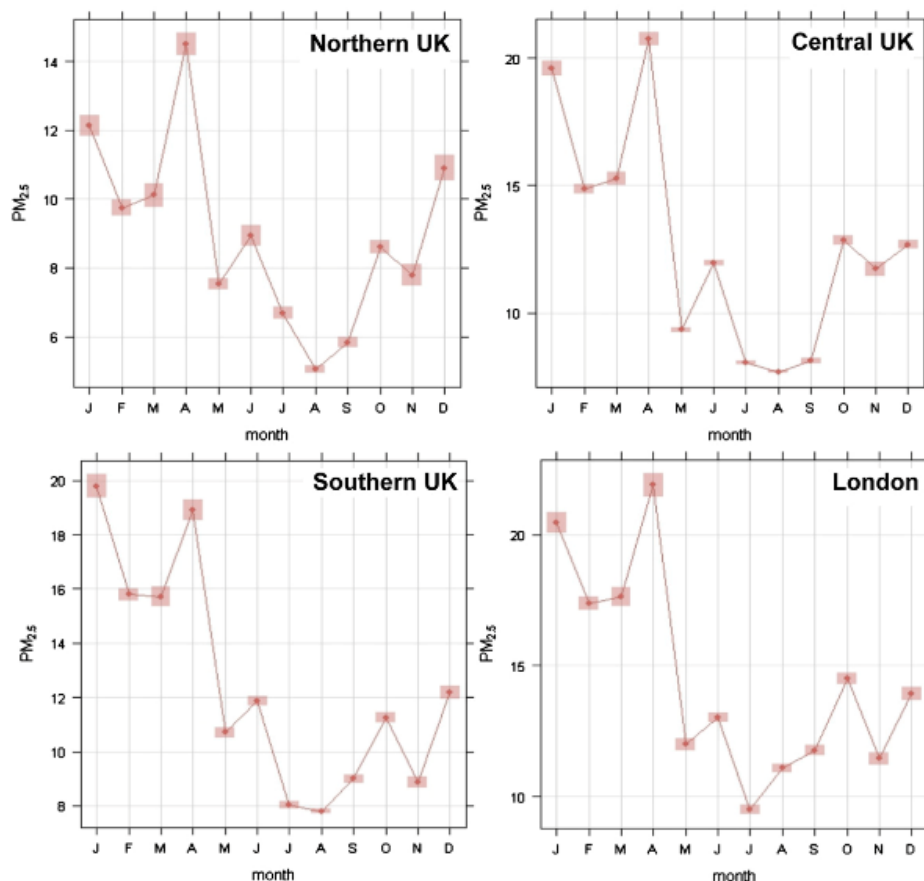


Figure 11. 2009 monthly variation in PM<sub>2.5</sub> concentrations ( $\mu\text{g m}^{-3}$ ) at urban background sites at sites in ‘Northern UK’ (n = 8), ‘Central UK’ (n = 17), ‘Southern UK’ (n = 8) and ‘London’ (n = 8). The 95% confidence interval is indicated by shading. (Harrison, et al., 2012).

### **1.3.4 Spatial Variations in Air Pollutant Concentrations**

Air pollutant concentrations also vary spatially, based on their emission sources, chemical reactions in the atmosphere and therefore lifetime, as pollutants disperse. Environmental inequality, especially with regards to air pollution, is well documented since socioeconomically disadvantaged areas are often located close to emissions sources, such as roads (Williams, et al., 2018). Socioeconomically disadvantaged communities may also have higher rates of morbidity and may therefore also be more susceptible to the negative health-effects of air pollution (Forastiere, et al., 2007; O'Neill, et al., 2003). This has been shown in urban areas where the negative health impacts of exposure to air pollutants are not as prevalent within less deprived populations (Forastiere, et al., 2007). It is estimated that in England 1.3-3.5 million years of life are lost as a result of health inequalities (Marmot, and Bell, 2012). Substantial differences in mean air pollutant concentrations were identified between the most and least deprived fifth of wards across the UK in 2011 (Williams, et al., 2018). The difference was highest for NO<sub>2</sub>, likely due to the short lifetime and steep concentration gradients in the pollutant from emissions sources (roads). In the UK, wards with higher proportions of Black, Asian and minority ethnicity (BAME) residents and deprivation were found to be closer to roads. The study found that the differences in NO<sub>2</sub> were larger between white and BAME populations than deprived and non-deprived populations (Williams, et al., 2018). Differences were also observed for PM<sub>2.5</sub> and O<sub>3</sub> between the most and least deprived fifth wards, though these were smaller (Williams, et al., 2018). This is likely to be due to the large secondary component and long lifetime of PM<sub>2.5</sub>, and due to O<sub>3</sub> being titrated in high NO<sub>x</sub> conditions (close to roads).

## **1.4 Pollution Monitoring and Legislation**

The concentration of an air pollutant can be measured in several ways. For emission sources, such as power generation, emissions are measured at source through point source measurement

within the stack (Environment Agency, 2019) or remote sensing (Liu, et al., 2016; Wang, et al., 2010). Emissions are reported to the United Nations Economic Commissions for Europe Convention on Long-Range Transboundary Air Pollutants (CLRTAP) and must fall within emissions ceilings guidelines (Department for Environment Food and Rural Affairs, 2011). Alongside this, the Gothenburg Protocol sets national emissions reductions targets to be achieved by 2020 (Department for Environment Food and Rural Affairs, 2011).

Once pollutants have been emitted they can be detected by ground-based observation sites (Lin, et al., 2010), satellites (Beirle, et al., 2011; Pope, et al., 2018) and aircraft (Martin, et al., 2006; Wang, et al., 2004) as the plume begins to disperse into the atmosphere. Ground observation sites are used by governments to monitor pollutant concentrations (Liang, 2013).

#### **1.4.1 Automatic Urban and Rural Network Observations**

In the UK, Automatic Urban and Rural Network (AURN) observation sites are used to ensure that concentrations are within the limits set by the European Union Air Quality Directive (European Parliament, 2008; Stevenson, et al., 2009), which are legally binding and must not be exceeded (European Environment Agency, 2017b). The concentration limits chosen for each pollutant are based on epidemiological and toxicological evidence for the adverse health impacts due to exposure (Liang, 2013). The concentrations at which adverse effects are seen in the human population vary with pollutant and exposure time, leading to different limits and averaging periods for different species (Table 2) (European Commission, 2017).

The 2005 World Health Organisation guideline limits are also shown (Table 2) (World Health Organization, 2005). These are global guidelines on thresholds for key air pollutants that pose health risks and limits are based on associations between exposure and increases in non-communicable diseases.

Table 2. EU Directive Limits (European Commission, 2017) and WHO Guidelines (World Health Organization, 2005) for air pollutants.

EU Air Quality Directive Limits				WHO Guidelines
Pollutant	Time Period	European Objective	Date to be achieved by	Concentration
<b>PM<sub>10</sub></b>	Annual mean	Limit - 40 $\mu\text{g m}^{-3}$	01/01/2005	20 $\mu\text{g m}^{-3}$
	24-hour mean	Limit - 50 $\mu\text{g m}^{-3}$ (<35 exceedances year <sup>-1</sup> )	01/01/2005	50 $\mu\text{g m}^{-3}$
<b>PM<sub>2.5</sub></b>	Annual mean	Limit - 25 $\mu\text{g m}^{-3}$	01/01/2015	10 $\mu\text{g m}^{-3}$
	24-hour mean	-		25 $\mu\text{g m}^{-3}$
<b>NO<sub>2</sub></b>	1-hour mean	Limit - 200 $\mu\text{g m}^{-3}$ (<18 exceedances year <sup>-1</sup> )	01/01/2010	200 $\mu\text{g m}^{-3}$
	Annual mean	Limit - 40 $\mu\text{g m}^{-3}$	01/01/2010	40 $\mu\text{g m}^{-3}$
<b>O<sub>3</sub></b>	8-hour mean	Target - 120 $\mu\text{g m}^{-3}$ (<25 exceedances year <sup>-1</sup> averaged over 3 years)	31/12/2010	100 $\mu\text{g m}^{-3}$
<b>CO</b>	Maximum daily 8-hour running mean	Limit - 10 $\mu\text{g m}^{-3}$	01/01/2005	-
<b>NO<sub>x</sub></b>	Daily mean	Limit - 30 $\mu\text{g m}^{-3}$	19/07/2021	-

The UK AURN includes ~170 sites, ranging from rural to kerbside sites and measures a large range of meteorological variables (e.g. wind speed, ambient temperature and relative humidity) as well as key air pollutants (including those in Table 2) (Stevenson, et al., 2009). The sites are generally situated in or close to areas of high population and provide high time-resolution (hourly) measurements of pollutants (Stevenson, et al., 2009).

PM<sub>2.5</sub> and NO<sub>2</sub> are the two pollutants of most concern in the UK and Europe currently. UK air-quality management areas have been declared (Committee on the Medical Effects of Air Pollutants, 2010; Royal College of Physicians, 2016; World Health Organization, 2013). For NO<sub>2</sub> an annual mean of 40 µg m<sup>-3</sup> and an hourly mean of 200 µg m<sup>-3</sup> (with no more than 18 exceedances per year) have been set as targets. While for PM<sub>2.5</sub> the annual mean target is 25 µg m<sup>-3</sup>. Alongside this, the European Commission (EC) Directive 2008 also required member states to determine the average exposure index (AEI) for PM<sub>2.5</sub> through measurements of PM<sub>2.5</sub> over a ten-year period. A national exposure reduction target (NERT) was then calculated for 2020, using the AEI. Measurements used to calculate the AEI were taken from background locations over a 3-year period between 2009-2011 and will be compared with measurements between 2018-2020 in order to assess compliance. The UK AEI was calculated to be 13.6 µg m<sup>-3</sup> using measurements from 47 of the UK AURN sites. The NERT for 2020 was therefore a reduction of 15%, equating to 2 µg m<sup>-3</sup> (i.e. an AEI of 11.6 µg m<sup>-3</sup>). However, since the monitoring network is sparse, representing the exposure of the whole population is challenging (Willocks, et al., 2012).

#### 1.4.2 Satellite Observations

Concentrations of air pollutants can also be measured by satellites; these measurements are more spatially complete than ground observations, which generally give sparse coverage. However, they lack the temporal detail of ground observations since they are often in sun-

synchronous polar-orbits, meaning they only pass over a region once a day. Satellites measure a range of air pollutants, including CO, NO<sub>2</sub> and O<sub>3</sub> (e.g. Tropospheric Monitoring Instrument (TROPOMI) (Veefkind, et al., 2012)). Satellites provide measurements of the total tropospheric column for NO<sub>2</sub> and CO, this is a measure of the total number of molecules (e.g. CO molecules) per unit area (e.g. cm<sup>-2</sup>) in the atmosphere (specifically between the surface of the Earth and the tropopause) (WMO OSCAR, 2020). Satellites use different spectral bands in order to measure the total column of different pollutants (e.g. ultraviolet-visible (UV), infrared (IR) and visible). Differential Optical Absorption Spectroscopy (DOAS), based on Lambert Beer's Law, is used to measure gaseous species. Since the intensity of light at the end of a light path is dependent upon the absorption by a particular air pollutant species, the total column of the air pollutant species can be derived based on the total absorption. O<sub>3</sub> is measured in the UV, visible, IR wavelengths (Gorshchev, et al., 2014). Satellite measurements focus on using the Hartley (200-300 nm) (Miles, et al., 2015), Huggins (310-340 nm) (Katayama, 1986; Miles, et al., 2015; Zhu, et al., 2005), Chappuis (450-650 nm) (Chappuis, 1880; Miles, et al., 2015) and infrared (4.7, 9.6 and 14.1 μm) (Boynard, et al., 2009; Miles, et al., 2015) bands, all of which are absorbed by O<sub>3</sub>, to measure the concentration of O<sub>3</sub> through the atmosphere. For aerosols, the extinction as a function of wavelength at specific points between the UV and IR, per km through the atmosphere, is used to measure concentrations (Remer, et al., 2013).

### 1.4.3 Aircraft Observations

Aircraft flights are also used to measure key air pollutants in field campaigns. They provide measurement at high temporal resolution (often a few seconds) through their flight path. However, they lack coverage over long time periods or large areas. The UK Facility for Airborne Atmospheric Measurements (FAAM) aircraft has been used for many field campaigns and measures a range of pollutants, including NO<sub>x</sub> (NO and NO<sub>2</sub>), PM, O<sub>3</sub>, and CO, among others (Harris, et al., 2017). The transect of measurements the aircraft can collect is

very useful in understanding the evolution of pollutants over space and time, from emission at source to a population's exposure, characterising emissions, meteorological and chemical processes.

#### 1.4.4 Model Predictions

Atmospheric-chemistry transport models, such as WRF-Chem (Grell, et al., 2005), can also be used to give more spatially complete predictions of many air pollutants, using ground and satellite observations to evaluate simulated concentrations. Concentrations can be simulated at a range of resolutions, from global models at ~100 km to regional models at ~5-30 km and to high resolution models at ~1 km (Seigneur, and Dennis, 2011). This allows concentrations to be predicted where observational networks are sparse or do not measure the species of interest. Models also allow for a range of scientific scenarios to be investigated (Jacob, 2006), for example emissions reductions or sectoral contributions to air pollutant concentrations. Therefore, they are a very useful tool in atmospheric science.

## 1.5 Health Impacts of air pollution

### 1.5.1 Attributing exposure to health impacts

Two main approaches are used to understand the effect of air pollutants on health:

- **Epidemiology** is used to determine if exposure to a pollutant is associated with disease outcomes; it is the study of how often diseases occur in an exposed population (Coggon, et al., 2009).
- **Toxicology** is able to identify the specific biologically plausible mechanism responsible for the associations found in epidemiology (United States Environmental Protection Agency (USEPA), 2009).

## Epidemiology

Epidemiological studies use comparisons between groups to discover whether exposure to a risk factor (e.g. air pollution) is associated with a particular outcome (e.g. death from heart disease). There are three main study designs used in epidemiology: cross sectional, cohort and case-control. For exposure to air pollution two study designs are primarily used, (1) cross sectional and (2) cohort:

### 1. cross-sectional

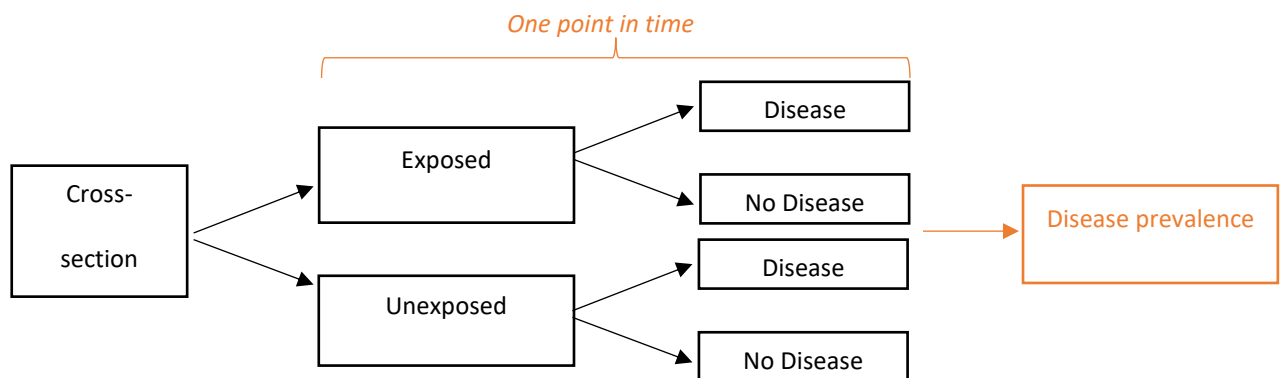


Figure 12. Cross-sectional study design and study outcome.

### 2. retrospective cohort studies.

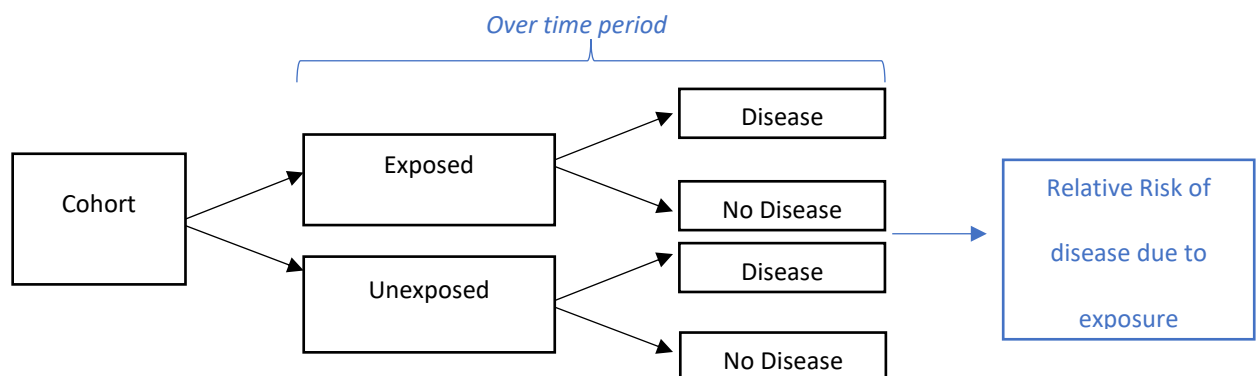


Figure 13. Cohort study design and outcome.

Cross-sectional studies allow a snapshot of a particular population at one point in time (Figure 12) (Song, and Chung, 2010). Usually, subjects are chosen because they are part of a target population at a certain time (e.g. smokers and non-smokers and in London). Data is collected

on participants regardless of exposure or disease status. This study design can determine disease prevalence within the population (e.g. how many smokers have lung cancer). However, a relative risk cannot be directly derived (i.e. how much smoking increases the relative risk of lung cancer) (Song, and Chung, 2010).

In contrast, cohort studies look at a population group over time retrospectively or prospectively (though for air pollution this is generally retrospectively) (Figure 13) (Song, and Chung, 2010). In this study design the population is categorised based on whether they were exposed to risk factors of interest, regardless of disease status. They are then followed over time to determine whether health outcomes develop. Since this study type follows participants over time, the relative risk can be directly derived (Song, and Chung, 2010).

Two key concerns in all epidemiology studies are confounding variables and effect-measure modification (Bovbjerg, 2020a, 2020b). Confounding variables distort the association observed, because both the exposure being measured and the outcome are affected by another factor (Bovbjerg, 2020a; Howards, 2018). Effect-measure modification occurs when the magnitude of a health outcome being measured varies dependent on a third variable (e.g. temperature) and can often vary based on circumstances (Bovbjerg, 2020b; Corraini, et al., 2017). Within epidemiology confounding variables and effect-measure modification are controlled for through statistical adjustments (Corraini, et al., 2017). For example, in the association of physical activity with heart disease, age is a confounding factor because old people tend to exercise less, but also have a higher risk of heart disease. Though confounders can be controlled for through statistical adjustments, identification and measurement of all confounding variables is required (Howards, 2018). Therefore, prior knowledge of both the likely sources and magnitudes of the confounders and effect-modifiers, as well as their distribution within the population, is needed.

## Toxicology

Alongside identifying associations, a plausible mechanism needs to be identified to infer causality of a relationship (Adami, et al., 2011). As a result, toxicology is used alongside epidemiological studies to identify causality through biologically plausible mechanisms, using tightly controlled conditions in a laboratory setting (Adami, et al., 2011; United States Environmental Protection Agency (USEPA), 2009).

Four key factors affect toxicity (Figure 14):

- 1) Dose – the amount of pollutant in the body, which is controlled by 3 variables:
  - a. *Intake*: how much pollutant someone is exposed to.
  - b. *Type/Route of exposure*: Inhalation, dermal, ingestion.
  - c. *Time period*: how long someone is exposed for.
- 2) Subject susceptibility – factors which could impact someone’s response to exposure e.g. underlying health conditions, age.
- 3) Substance – varying properties affecting absorption e.g. PM<sub>2.5</sub> composition.
- 4) Interactions – how different substances mix and affect response e.g. multi-pollutants.

The risk associated with a substance is then assessed against the four toxicity factors using a 3-step risk assessment:

- 1) **Exposure assessments** on mice/rats and humans. Within exposure assessments subjects are exposed to pollutants, and the effects are monitored in air and within the body (biomonitoring) using biomarkers of inflammation from urine and blood.
- 2) **Effects and consequence assessments** on mice and rats *in vivo* (live mice/rats) and *in vitro* (cells from mice/rats) methods. These assess the effects of exposure on organs.

- 3) **Risk characterization** integrates all of the toxicological information, including dose-response curves to estimate a risk associated with a substance.

The ethical concerns regarding randomised control trials of exposure to air pollutants means that causality of the associations identified between air pollutants and health impacts are determined by combining evidence from epidemiological and toxicological studies (Figure 14). There is overlap in many principles used to infer causality (Figure 14).

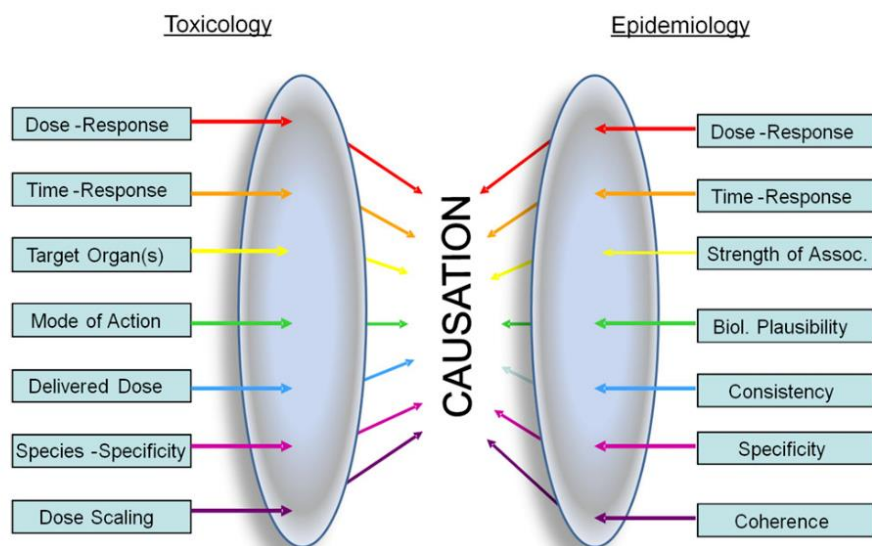


Figure 14. Evidence that is combined from toxicological and epidemiological studies to infer causal inference (Adami, et al., 2011).

The level of agreement between epidemiology studies over different time periods and locations, toxicological and controlled human exposure studies are combined to determine causality (Figure 14, Figure 15). Causality cannot be proven, only inferred with varying degrees of certainty (Adami, et al., 2011). For a 'likely' causal relationship, there must be strong epidemiological evidence for an association and toxicological evidence of a biologically plausible mechanism for the association (Figure 14, Figure 15) (Adami, et al., 2011).

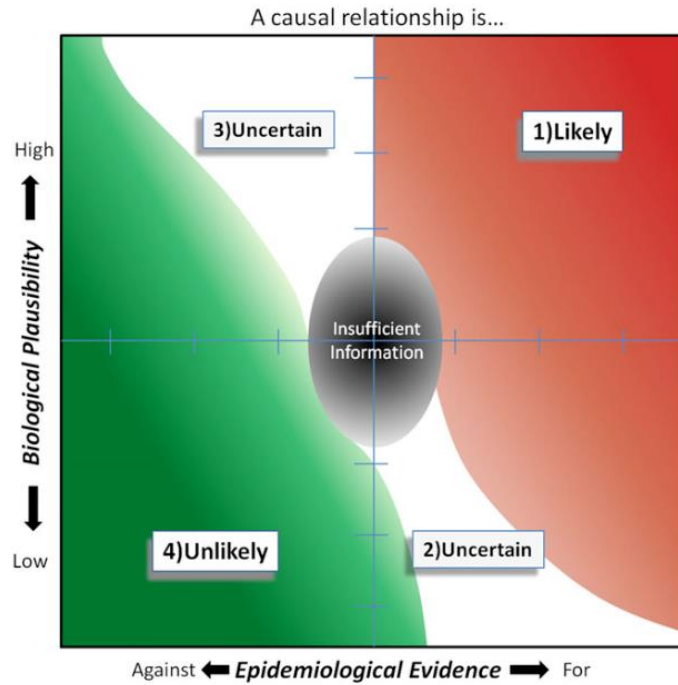


Figure 15. Schematic indicating how causal inference is inferred combining epidemiological and toxicological evidence (Adami, et al., 2011).

### 1.5.2 Mechanism for Health Impacts from PM<sub>2.5</sub>

The mechanism for the health impacts of PM exposure are complex and change with the length of exposure. Epidemiological studies suggest that the fine fraction of PM (PM<sub>2.5</sub>) plays a substantial role (Pope III, and Dockery, 2006). These particles are small enough to be inhaled deep into the lungs. Exposure and dose are also likely to be higher for PM<sub>2.5</sub> since atmospheric lifetime is long, meaning transport over long distances can occur and infiltration into indoor environments is much more likely due to the small diameter of PM<sub>2.5</sub> (Pope III, and Dockery, 2006).

Toxicological studies have identified a range of biologically plausible pathways, following inhalation, that may lead to the association between cardiovascular morbidity and mortality and long-term exposure to PM<sub>2.5</sub>, which have been identified in epidemiological studies (Pope III, and Dockery, 2006) (Figure 16). Exposure to PM<sub>2.5</sub> has been linked to inflammation and

oxidative stress within the lungs, changes in blood characteristics and changes to vein structure, altered heart function and changes within the brain (Figure 16) (Pope III, and Dockery, 2006). Though this is still an active area of research, it is now widely acknowledged that there is a causal, mechanistic link between exposure to PM<sub>2.5</sub> and cardiovascular morbidity and mortality (Pope III, and Dockery, 2006).

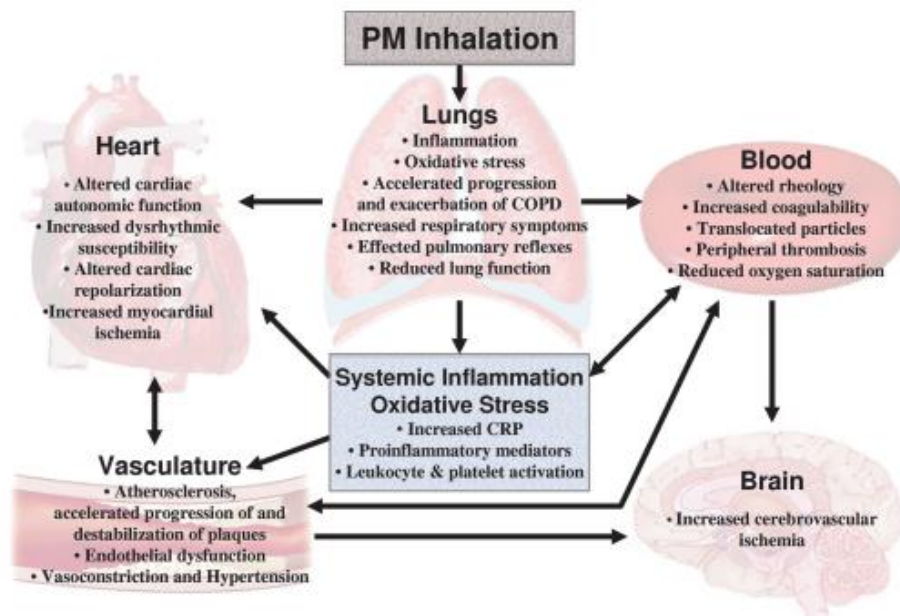


Figure 16. The hypothetical physiological processes that link PM exposure with cardiopulmonary morbidity and mortality (Pope III, and Dockery, 2006).

Although the composition of PM<sub>2.5</sub> can vary greatly, dependent upon emission source and chemical processes, the associations found between PM<sub>2.5</sub> and various disease endpoints has been fairly consistent (Pope III, and Dockery, 2006). However, there is currently a lack of understanding as to which characteristics of PM<sub>2.5</sub> are most responsible for toxicity. Alongside this, the role of specific pollutants, pollutant sources, co-pollutant mixtures and pollutant characteristics in the health outcomes observed is not well understood. The concept that characteristics of PM do not have any significance on its health effects contradicts basic

toxicological principles and has led to scepticism from some in the plausibility of the associations observed (Harrison, and Yin, 2000; Schwarze, et al., 2006). However, others studies have highlighted that the similarity in health outcomes of exposure, despite differences in PM components, may be due to the inflammatory reactions that are thought to be central to the development of cardiovascular and pulmonary diseases associated with PM exposure (Schwarze, et al., 2006).

Due to the lack of understanding regarding the specific components responsible for the health impacts of PM<sub>2.5</sub>, the concentration response functions currently used in health impact assessment studies assume that all PM<sub>2.5</sub> is equally toxic, independent of composition (Atkinson, et al., 2014; Liu, et al., 2019; World Health Organization, 2013).

### **1.5.3 Epidemiological Studies**

Prior to the 1990s it was largely believed that PM acted as a vector, which allowed SO<sub>2</sub> to be transferred deep into the lung. Thus, this SO<sub>2</sub> and PM mixture was believed to be the mechanism responsible for the negative health impacts associated with exposure (Harrison, and Yin, 2000). However, a number of studies later demonstrated that ambient concentrations of particulate matter previously thought to be safe, unless in the presence of high SO<sub>2</sub> concentrations, were associated with a negative effect on health (e.g. (Schwartz, et al., 1996)).

As a result, many studies have since investigated the association of exposure to particulate matter and mortality. The associations found by studies between PM and increased risk of cardiopulmonary morbidity and mortality over both long- and short-time scales have been relatively consistent (Nemery, et al., 2001; Pope III, 2007; Schrenk, et al., 1949). Exposure to PM<sub>2.5</sub> is the most consistent and robust predictor of mortality in studies of long-term air pollutant exposure (Kivimäki, et al., 2015; Yang, et al., 2013). Associations for long-term exposures have been found to be much larger than with exposures over short-time periods

(Pope III, 2007). Short-term studies focus on daily variations in ambient PM and the impacts of this on health, using time-series designs (Figure 12). Whereas long-term studies focus on the impacts of spatial changes in ambient PM between regions over years or decades on health, using cohort studies (Figure 13) (Pope III, 2007).

#### 1.5.3.1 Short-Term Exposure

Short-term exposure studies have developed in complexity, from simple methodologies that assumed a linear relationship between variables, to more complex methods that allowed flexible fitting for non-linear associations (e.g. season and temperature), through to case-crossover designs, multicity studies and meta-analyses most recently (Pope III, and Dockery, 2006). Case-crossover studies replace the need for statistical modelling to account for non-linear associations (e.g. seasonality) by choosing control periods which account for this. Case-crossover studies match exposures at the time of death (e.g. within a high pollution episode) to control periods when the death didn't occur, so that deceased individuals act as their own controls (Jaakkola, 2003). Excess risk is estimated using regression, where logistic regression is applied to the exposed and unexposed individuals (Jaakkola, 2003). A benefit of this study design is that it allows the impact of susceptibility to be observed (Pope III, and Dockery, 2006). However, results are sensitive to the selection of control periods and case-crossover studies also have a lower statistical power than the short-term time series analysis because only control periods are included (and so information is lost outside of these) (Pope III, and Dockery, 2006).

Multi-city studies reduce the risk of biases (e.g. city or publication) (Pope III, 2007) but are less common. A study of six US cities (Schwartz, et al., 1996) was one of the first multicity studies. The study found that daily mortality was significantly associated with PM<sub>10</sub>, PM<sub>2.5</sub> and sulfate exposure, and most strongly with PM<sub>2.5</sub>. Every 10- $\mu\text{g m}^{-3}$  increase in two-day mean

PM<sub>2.5</sub> was associated with a 1.5% increase in daily mortality. The study has been repeated several times (Klemm, et al., 2000; Laden, et al., 2000) and similar associations remain (1.2 % per 10 µg m<sup>-3</sup>).

Many short-term single-city PM mortality studies have been carried out since the 1990s, which means that it is possible to estimate the pooled effects by combining multiple published studies in a large quantitative review or meta-analyses (Pope III, and Dockery, 2006). There have been several multi-city and meta-analysis studies for short-term exposure of PM<sub>2.5</sub> in recent years (Atkinson, et al., 2014; Franklin, et al., 2007; Liu, et al., 2019; Mills, et al., 2015; Ostro, et al., 2006; World Health Organization, 2013; Zanobetti, and Schwartz, 2009). PM<sub>2.5</sub> associated mortality estimates ranged from 0.4 to 1.2 % per 10 µg m<sup>-3</sup> increase in concentrations. The meta-analysis of Atkinson *et al.* (2014) found that there was a large degree of variation in estimates worldwide (0.25% to 2.08%) and that associations for specific diseases varied.

Despite this, overall the results of short-term exposure mortality studies are very consistent, regardless of the method applied, indicating total mortality increases by ~1% (0.4 – 1.3%) per 10 µg m<sup>-3</sup> increase in PM concentrations (Atkinson, et al., 2014; Harrison, and Yin, 2000; Liu, et al., 2019; Pope III, 2007; World Health Organization, 2013). As with toxicological studies, this appears to be irrespective of location and therefore composition (Harrison, and Yin, 2000). However, since studies are observing small effects, the uncertainties in estimating these effects are relatively large (Harrison, and Yin, 2000).

### 1.5.3.2 Wildfire pollutant exposure and mortality

Emissions for biomass burning are the dominant air pollution source in many areas of the world, including Canada and Australia (Lelieveld, et al., 2015). Therefore, epidemiology of smoke exposure from wildfires is an area of increasing research (Johnston, et al., 2012). This is also owing to the increased statistical power gained from studying prolonged high exposure

fire events, regions with frequent wildfires and high populations or much more common outcomes (e.g. prescriptions for medicine) (Johnston, et al., 2012).

Studies have found consistent associations between wildfire smoke exposure and respiratory morbidity and asthma and chronic obstructive pulmonary disease (COPD) exacerbations (Alman, et al., 2016; Borchers Arriagada, et al., 2019; Cascio, 2018; Delfino, et al., 2009; Dennekamp, and Abramson, 2011; Liu, et al., 2015; Morgan, et al., 2010; Rappold, et al., 2011; Reid, et al., 2016; Shaposhnikov, et al., 2014). These have been documented through increased healthcare visits (including doctors, emergency departments and hospitalizations) (Borchers Arriagada, et al., 2019; Delfino, et al., 2009; Johnston, et al., 2014; Morgan, et al., 2010; Yao, et al., 2016). There is also increasing evidence to suggest that exposure to wildfire smoke is associated with all-cause mortality (Borchers Arriagada, et al., 2019; Faustini, et al., 2015; Johnston, et al., 2011).

However, in order to better understand the impact of wildfires on mortality and diseases (e.g. cardiovascular disease) more large studies with increased statistical power are needed. Alongside this, little information is currently available on whether health effects vary from different smoke pollutants or the age of smoke. However, recent toxicological evidence suggests the age of smoke may lead to changes in toxicity (Paraskevopoulou, et al., 2019). Due to there currently being very few epidemiological studies of wildfire health impacts, it is not possible to determine whether the shape of the concentration response function for PM represents the health impacts of wildfire smoke accurately (Cascio, 2018; Reid, et al., 2016). As a result, studies on the short-term health impacts of wildfires commonly use concentration response functions derived for un-specified anthropogenic PM (Borchers Arriagada, et al., 2020; Crippa, et al., 2016; Johnston, et al., 2012).

### 1.5.3.3 Long-Term Exposure

More recently, studies have used cohort populations to examine the effects of exposure on mortality over long-time periods. Some of the first cohort mortality studies focused on chronic exposure to PM<sub>2.5</sub> in the USA (the Harvard Six Cities Studies (HSCS) and the American Cancer Study (ACS)) (Dockery, et al., 1993, 1989; Pope, et al., 1995). The studies used a 14-16- year and 7- year follow-up of 8,000 and 500,000 adults in 6 cities and 151 areas, respectively. Information on pollutants was taken from the national air quality monitoring network in the ACS. Both studies controlled for confounders such as age, sex and smoking among others and both found cardiopulmonary mortality to be most strongly and significantly associated with exposure to PM<sub>2.5</sub> and sulfate. Long-term exposure to PM<sub>2.5</sub> is associated with a larger increase in mortality relative risk (~6 to 17% per 10 µg m<sup>-3</sup>) than short-term studies (~ 1 % per 10 µg m<sup>-3</sup>) (Pope III, 2007).

### 1.5.3.4 Concentration response function shape

The shape of the concentration response (CR) curve describes the increase in mortality with increasing air pollutant concentrations. In these relationships the population-weighted PM<sub>2.5</sub> concentration is used as a proxy for dose (Avery, et al., 2010). This is because PM<sub>2.5</sub> exposure is generally through inhalation, and the particles at this size are respirable, but also because there is currently a lack of data on personal exposures within populations. However, several recent studies have developed methods to account for population mobility in pollutant exposure estimates (de Nazelle, et al., 2009; Reis, et al., 2018; Shekarrizfard, et al., 2017).

The CR curve is affected by several variables:

- 1) the toxicity of a pollutant.
- 2) the susceptibility of the population.
- 3) the conditions that the pollutant interacts with (e.g. weather).

The shape of the PM-mortality concentration response functions and the no-effects threshold (theoretical minimum risk exposure level (TMREL)) is one of the large areas of continuing research. The TMREL is particularly important in setting and evaluating ambient air quality limits across the world and in public policy estimating the health costs of pollution (Pope III, and Dockery, 2006; Wong, et al., 2008).

Many studies have focused on trying to constrain the shape and no-effect threshold (TMREL), using methods that vary in complexity. Initially studies focused on single cities (Pope III, and Kalkstein, 1996; Schwartz, 1993; Schwartz, et al., 1996; Schwartz, and Marcus, 1990), finding that the function was linear or near-linear with no clear no-effects threshold (Schwartz, and Marcus, 1990). However, these single city studies could not be generalized for other areas and lacked statistical power to make strong statistical inferences regarding the shape of the function. As a result, studies moved onto calculating the shape of the concentration-response function across multiple cities using daily time-series studies (Daniels, et al., 2000; Samoli, et al., 2005; Schwartz, et al., 2001). These studies were based in North America and Europe and found the function shape to be near linear with no clear no-effect threshold. Therefore, for regions where concentrations are within those observed in these analyses, this suggests that reductions in ambient air quality are likely to improve health even at low levels. However, it should be noted that the shape of the concentration-response function remains uncertain at concentrations above those observed in these regions (i.e. developing countries) (Cohen, et al., 2004). This problem has become increasingly challenging as the ambient PM<sub>2.5</sub> concentrations in many developing countries, and during high pollution episodes, are much above the levels studied previously. As a result, integrated exposure-response (IER) functions were developed to help account for these high concentrations. IER functions combine risk estimates from studies of ambient air pollution, household air pollution, second-hand smoke and active smoking (GBD Collaborators 2015, 2017). This allows the shape of the IER to be determined

for much higher concentrations. However, this approach requires the assumption of equal exposure and toxicity between sources to be made. A recent study by Burnett *et al.* (2018) combined the results of 41 cohort studies, from 16 countries, examining PM<sub>2.5</sub> associated mortality to construct the Global Exposure Mortality Model (GEMM). The large number of cohort studies included allowed the study to consider population-weighted average PM<sub>2.5</sub> concentrations over a much larger range than any previous study (15 to 84 µg m<sup>-3</sup>). For the five specific causes of death that were examined in the Global Burden of Disease (GBD) (Lower Respiratory tract Infection, Stroke, Lung cancer, Ischemic Heart Disease and Chronic Obstructive Pulmonary Disease) the GEMM predicted a PM<sub>2.5</sub> disease burden that was 30% higher than the GBD estimate (GBD Collaborators 2015, 2017). This suggests that there may be additional causes of PM<sub>2.5</sub>-associated mortality that were not considered in the GBD (Burnett, et al., 2018). Additionally, it may suggest that creating an IER function using PM<sub>2.5</sub> sources such as cigarette smoking may underestimate the PM<sub>2.5</sub> disease burden, particularly at higher concentrations (Burnett, et al., 2018).

## **1.6 Burden of Disease from Air Pollutants**

### **1.6.1 Global and Regional Burden of Disease from PM<sub>2.5</sub>**

In the UK, long-term exposure to PM<sub>2.5</sub> and O<sub>3</sub> are the third and seventh leading environmental risk factors for mortality (Institute for Health Metrics and Evaluation, 2015). Long-term exposure to PM<sub>2.5</sub> is also the second leading environmental risk factor for Years Lived with Disability. Each year 29,000 deaths are brought forward across the UK due to long-term exposure to PM<sub>2.5</sub>.

Globally, exposure to ambient air pollution increases morbidity and mortality and is also a leading cause of disease burden (GBD Collaborators 2015, 2018). Ambient air pollution is the fourth highest-ranking risk factor for mortality globally, with 85% of the global population

living in areas where recommended air quality guidelines are exceeded (GBD Collaborators 2015, 2018). Long-term exposure to PM<sub>2.5</sub> alone is estimated to have caused 4.2 million deaths and 103.1 million lost years of healthy life in 2015 (GBD Collaborators 2015, 2016). This represents 7.6% of global mortality.

Thus, reducing population exposure to ambient PM<sub>2.5</sub> could yield large public health benefits. However, in order to achieve this, targeted reductions (e.g. sector specific/region specific) are necessary.

### **1.6.1.1 Long-Term (Chronic) Exposure**

#### **1.6.1.1.1 Global**

The most recent Global Burden of Disease (GBD) study estimated that long-term exposure to ambient PM<sub>2.5</sub> was responsible for 4.2 million deaths and 103.1 million lost years of healthy life in 2015 (GBD Collaborators 2015, 2018, 2017). This accounted for 7.6% of total global mortality in 2015. Mortality from PM<sub>2.5</sub> was calculated using disease-specific IERs developed by Cohen *et al.* (2017), for ischemic heart disease (IHD), cerebrovascular disease (ischemic stroke and haemorrhagic stroke (stroke)), lung cancer, chronic obstructive pulmonary disease (COPD) and lower respiratory infections (LRI). Age-specific functions were applied to IERs for IHD and stroke. The study found that PM<sub>2.5</sub> attributable mortality was dominated by cardiovascular disease.

Trends in PM<sub>2.5</sub> attributable mortality reflect population demographics and underlying mortality rates, as well as ambient PM<sub>2.5</sub> concentrations. Since there has been a decrease in both the underlying cardiovascular mortality rates and ambient PM<sub>2.5</sub> in World Bank high-income countries, such as the UK, this has led to a decrease in PM<sub>2.5</sub> attributable mortality (Figure 17) (GBD Collaborators 2015, 2017). Despite this, in England, where the majority of the UK population live, long-term exposure to ambient particulate matter led to ~12,500 (~23

per 100,000 population) deaths being brought forward in 2015 (Figure 17) (GBD Collaborators 2015, 2017; Institute for Health Metrics and Evaluation, 2015).

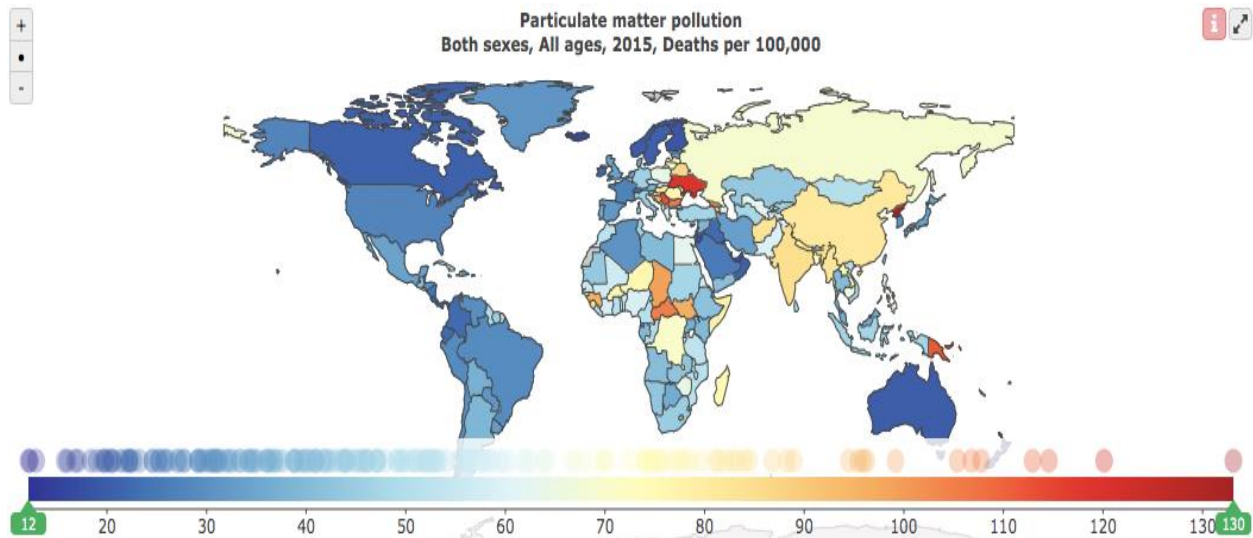


Figure 17. Total deaths (per 100,000 population) attributable to ambient particulate matter pollution in 2015 globally (GBD Collaborators 2015, 2017; Institute for Health Metrics and Evaluation, 2015).

In order to achieve targeted reductions in  $PM_{2.5}$  concentrations, and therefore the associated health impacts of exposure, the contribution of emission sectors to the total  $PM_{2.5}$  burden must be known. Atmospheric chemistry transport models can be used to simulate the impacts of removing/reducing emissions from individual source sectors (industry, land traffic, residential and commercial energy use, biomass burning, power generation, agriculture and power generation) on pollutant concentrations (Seigneur, and Dennis, 2011). This allows the change in annual mean  $PM_{2.5}$  concentrations and the sectoral contribution to ambient  $PM_{2.5}$  and  $PM_{2.5}$  attributable mortality due to population exposure to be investigated (Lelieveld, et al., 2015).

Regionally, source categories responsible for the largest contribution to PM<sub>2.5</sub> attributable mortality are shown in Figure 18.

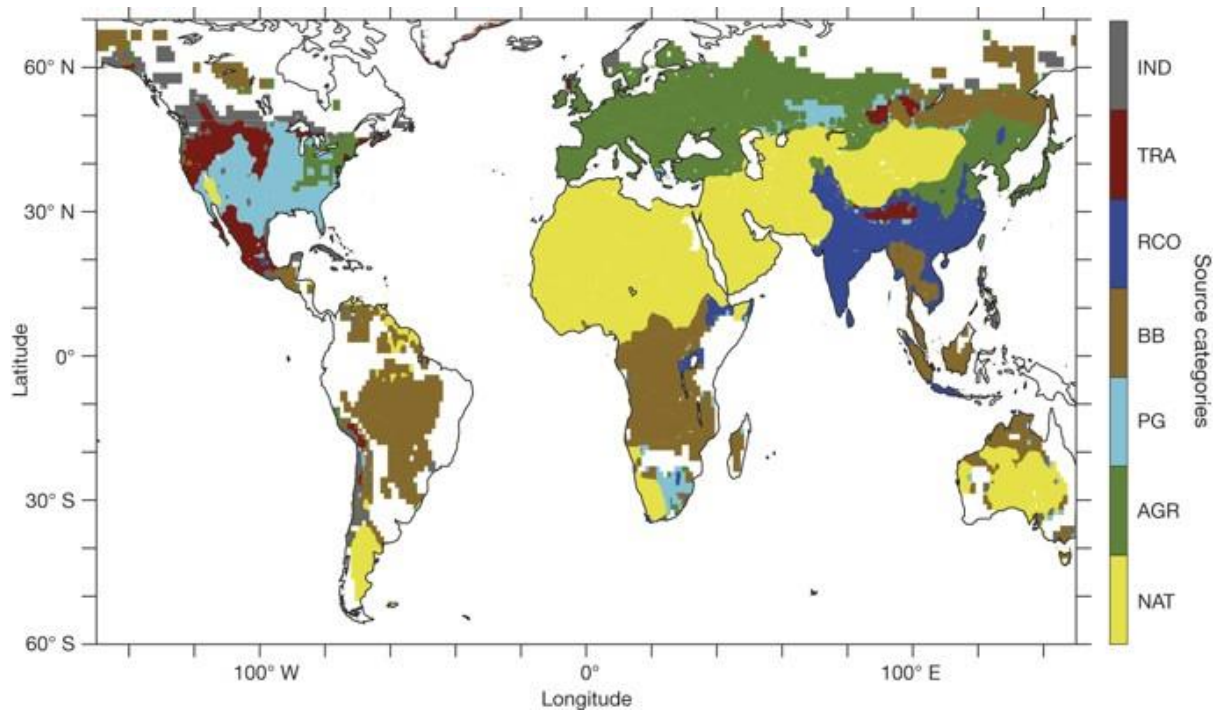


Figure 18. Source categories responsible for the largest impact on mortality linked to outdoor air pollution in 2010. Source categories that are colour coded are: IND, industry; TRA, land traffic; RCO, residential and commercial energy use (e.g. heating, cooking); BB, biomass burning; PG, power generation; AGR, agriculture; and NAT, natural. In the white areas, annual mean PM<sub>2.5</sub> is below the concentration–response threshold. (Lelieveld, et al., 2015).

Globally, residential and commercial energy use (RCO) dominates the PM<sub>2.5</sub> health impact, responsible for around a third of the total global PM<sub>2.5</sub> attributable mortality (~1 million deaths brought forward) (Lelieveld, et al., 2015). This is because a large proportion of the global population live in India and China where the RCO sector dominates the PM<sub>2.5</sub> contribution, annual mean ambient PM<sub>2.5</sub> concentrations are very high and underlying mortality rates from disease are also high (Figure 18). By land area, agricultural and natural emissions dominate

PM<sub>2.5</sub> concentrations (AGR and NAT). Agricultural emissions contribute to around a fifth of the total PM<sub>2.5</sub> attributable mortality, being the dominant source of PM<sub>2.5</sub> attributable mortality in Europe (one fifth of the total 285,000 deaths brought forward in 2010 in Europe). This is due to the release of ammonia from agricultural processes forming secondary PM<sub>2.5</sub> species (ammonium nitrate and ammonium sulphate). However, it should be noted that this study used a coarse global model (~100 km resolution). As a result, the model is likely to be unable to accurately represent local and regional scale processes, as well as the steep concentration gradients within urban areas.

In Europe ammonium nitrate contributes significantly to PM concentrations, with mean contributions of 6-16% to PM<sub>2.5</sub> and 6-20% to PM<sub>10</sub> (Putaud, et al., 2010). However, it should be highlighted that secondary formation is complex, dependent upon whether a region is nitrate or ammonia limited. In addition, the results of precursor reductions on total secondary PM<sub>2.5</sub> formation is non-linear (Petetin, et al., 2015). Therefore, global models, at coarse spatial resolutions, may not be able to capture these processes accurately. Observational sites across the European Monitoring and Evaluation Program network have indicated that secondary PM<sub>2.5</sub> formation is nitrate limited across continental Europe (Pay, et al., 2012). This indicates that continental Europe is ammonia rich and therefore there is enough ammonia to neutralise sulphate and nitrate, forming ammonia nitrate and ammonium sulphate (Petetin, et al., 2015). However, large areas close to coasts, such as Spain and England, have been found to be ammonia limited, meaning ammonium sulphate and ammonium nitrate formation are limited by the amount of ammonia available (Pay et al., 2012). This is due to high emissions of sulphur dioxide and nitrogen oxides from shipping and low emissions of ammonia over marine regions. The coarse model resolution (100 km) is also unlikely to capture the regional variation in regime seen in observational data. Particularly because the secondary fraction of PM<sub>2.5</sub> is difficult to quantify and predict from measurements due to the complexity of emitted precursors

and transformational processes (Department for Environment Food & Rural Affairs, 2015). A reduction in ammonia does not necessarily lead to a reduction in secondary PM<sub>2.5</sub> in either of these environments due to differences in the lifetime between the gas and aerosol phases of secondary PM<sub>2.5</sub>. For example, a reduction in sulphate emissions leads to an increase in secondary PM<sub>2.5</sub> concentrations due to an increase in ammonia availability for ammonium nitrate formation, and the increased lifetime of ammonium nitrate (Davidson, and Wu, 1990).

Biomass burning has a small global contribution to global mortality from PM<sub>2.5</sub> (~5% of the total 3,150,000 deaths brought forward in 2010 globally) (Lelieveld, et al., 2015). However, in regions of the world frequently affected by large wildfires (e.g. Canada, South America, South-east Asia and Australia) it is the main source of ambient PM<sub>2.5</sub>. However, since the health impacts of biomass burning emissions of PM<sub>2.5</sub> are uncertain, as well as the relative toxicity of specific components of PM<sub>2.5</sub>, this estimate is based on uniform PM<sub>2.5</sub> toxicity across species.

The global mortality burden from landscape fire smoke (LFS (PM<sub>2.5</sub>)) was estimated annually between 1997 and 2006, using GEOS-Chem (Johnston, et al., 2012). 339,000 deaths were attributed to LFS annually, of which 267,000 were in South-east Asia and sub-Saharan Africa. LFS associated mortality was lower in Australia but the burden was concentrated around the south-east coast of the country. 81% of the total global annual mortality due to LFS was a result of chronic exposure and 19% was due to sporadic exposure. The total mortality burden increased in El Niño years and decreased in La Niña years due to the associated change in rainfall that lead to changes in the number and intensity of fires (Johnston, et al., 2012).

#### **1.6.1.1.2 UK**

In the UK 29,000 deaths are brought forward due to long-term exposure to PM<sub>2.5</sub> annually (Committee on the Medical Effects of Air Pollutants, 2010) and the associated Years of Life

Lost (YLL) is 340,000. YLL is a measure of morbidity, calculated as a function of mortality and life-expectancy specific to an age group.

The number of deaths brought forward regionally due to long-term exposure to PM<sub>2.5</sub> has also been estimated (Gowers, et al., 2014). Since the total PM<sub>2.5</sub> attributable deaths are influenced by the total population, the population demographics and underlying mortality rate, comparison between different regions is difficult. Therefore, the attributable fraction (AF) was presented instead. The AF is the percentage of deaths that are attributable to long-term PM<sub>2.5</sub> exposure and is therefore independent of population characteristics and underlying mortality rates. Thus, it allows for easy comparison of different regions more easily. The AF and annual mean PM<sub>2.5</sub> concentrations indicated that England was worst affected by long-term exposure to PM<sub>2.5</sub> (5.6% and 9.9 µg m<sup>-3</sup>), compared with Wales (4.3% and 7.5 µg m<sup>-3</sup>), Scotland (3.9% and 6.8 µg m<sup>-3</sup>) and Northern Ireland (3.8% and 6.6 µg m<sup>-3</sup>) (Gowers, et al., 2014). In England, there were large regional variations in the AF and annual mean PM<sub>2.5</sub> concentrations (4.6% to 7.2% and 8.1 µg m<sup>-3</sup> to 12.7 µg m<sup>-3</sup>) (Gowers, et al., 2014). The London region was worst affected by long-term exposure to PM<sub>2.5</sub> (7.2%). In contrast, the South East had largest PM<sub>2.5</sub> attributable mortality (4,034 deaths brought forward) and years of life lost (YLL) (41,729 YLL). This reflects the much higher population and underlying mortality rate in the South East, since the annual mean PM<sub>2.5</sub> concentration and AF were lower in the South East (9.7 µg m<sup>-3</sup> and 5.5%) than London (12.7 µg m<sup>-3</sup> and 7.2%) (Gowers, et al., 2014).

Alongside this, a number of policy scenario experiments were also carried out in order to estimate the impact of reductions in ambient PM<sub>2.5</sub> on health (Committee on the Medical Effects of Air Pollutants, 2010). The effect on health was described as life-years gained, essentially a reduction in the YLL, and the corresponding increased life expectancy. Policies simulated included the removal of all anthropogenic PM<sub>2.5</sub> emissions, reducing annual average

PM<sub>2.5</sub> concentrations by 1 µg m<sup>-3</sup> and enforcing a maximum annual mean PM<sub>2.5</sub> concentration of 7 µg m<sup>-3</sup> (Table 3). All scenarios were for the UK.

Table 3. Change in life expectancy for 2008 UK population following implementation of different policy scenarios (Committee on the Medical Effects of Air Pollutants, 2010).

Policy	Population-weighted mean concentration removed	Increased life expectancy (days) for 2008 birth cohort	
		Men	Women
Annual mean PM <sub>2.5</sub> concentrations reduced by 1 µg m <sup>-3</sup>	1 µg m <sup>-3</sup>	21	21
All anthropogenic PM <sub>2.5</sub> removed	8.97 µg m <sup>-3</sup>	191	177
Maximum annual mean PM <sub>2.5</sub> concentration 7 µg m <sup>-3</sup>	3.50 µg m <sup>-3</sup>	74	69

Results from the scenarios tested indicated that there was a fairly linear response in life expectancy increase with population weighted mean PM<sub>2.5</sub> concentrations (Table 3). As would therefore be expected, the most effective scenario was to remove all anthropogenic PM<sub>2.5</sub>, which accounts for a population weighted mean concentration of 8.97 µg m<sup>-3</sup>. Removing all anthropogenic PM<sub>2.5</sub> led to an increase in life expectancy of between 177 and 191 days (~6 months) for the 2008 birth cohort throughout their lifetime (Table 3) (Committee on the Medical Effects of Air Pollutants, 2010). However, this is not plausible in a real-world scenario. Modest improvements were made in the 7 µg m<sup>-3</sup> maximum annual mean policy, accounting for the removal of a population-weighted mean concentration of 3.5 µg m<sup>-3</sup> (Table

3). This, more likely scenario, led to an increase in life expectancy of ~70-75 days (~2.5 months).

In order to achieve reductions in annual mean  $PM_{2.5}$  concentrations it is essential to first quantify the contribution of different emission sectors. Yim and Barrett (2012) investigated the contribution of combustion emissions sectors on annual mean  $PM_{2.5}$  across the UK and the subsequent impact on  $PM_{2.5}$ -attributable mortality (Figure 19). In the study combustion sectors were segregated into a) power generation, b) commercial, institutional, residential and agricultural sources, c) industry, d) road transport, e) other transport and f) all UK combustion sources.

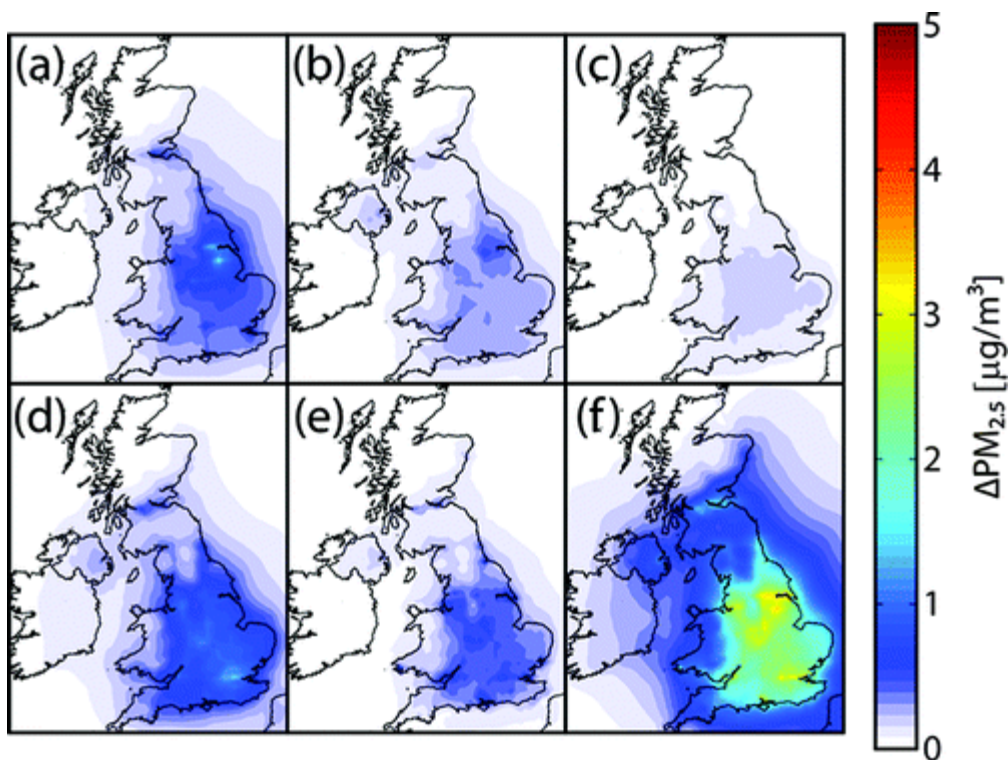


Figure 19. Annual average  $PM_{2.5}$  concentrations due to combustion emissions from (a) power generation; (b) commercial, institutional, residential, and agricultural sources; (c) industry; (d) road transport; (e) other transport; and (f) all UK combustion sources (Yim, and Barrett, 2012).

Road transport contributed the largest fraction of population weighted PM<sub>2.5</sub> (0.75 µg m<sup>-3</sup>), particularly in the south-east of England (Figure 19) (Yim, and Barrett, 2012). Other transport and power generation were the next largest contributors to population weighted PM<sub>2.5</sub> (0.51 and 0.42 µg m<sup>-3</sup>) (Figure 19) (Yim, and Barrett, 2012). The resulting annual health impact of exposure to combustion PM<sub>2.5</sub> indicated 9,000 deaths were brought forward in total, with the most substantial health burden from road transport, (3,300 deaths brought forward), other transport (1,800 deaths brought forward) and power generation (1,700 deaths brought forward) (Yim, and Barrett, 2012). Alongside this, the contribution of non-UK combustion emissions on PM<sub>2.5</sub>-attributable mortality was also estimated. Up to 2 µg m<sup>-3</sup> of the population-weighted PM<sub>2.5</sub> concentrations were from non-UK combustion emissions (Figure 19), this equated to 4,100 PM<sub>2.5</sub>-associated deaths (Yim, and Barrett, 2012). Thus, indicating non-UK combustion emissions have a considerable impact on UK PM<sub>2.5</sub>, and therefore health.

#### **1.6.1.2 Short Term Exposure**

Globally and regionally, short-lived high PM<sub>2.5</sub> concentration events can be caused by a variety of factors, including meteorology (e.g. inversions, long-range transport) and emissions (e.g. wildfires). Though short in duration these pollution events can have a substantial impact on population exposure to PM<sub>2.5</sub> and health.

##### **1.6.1.2.1 Global**

PM<sub>2.5</sub> emissions from wildfires in south-east Asia and Australia are so large that they are the dominant source of annual mean PM<sub>2.5</sub> concentrations in these regions (Lelieveld, et al., 2015). During the fire season populations in these regions can be exposed to concentrations far above the WHO guideline daily limit. Since these fires are generally episodic in nature, studies use short-term exposure response functions to estimate the acute health impact (Borchers Arriagada, et al., 2020; Crippa, et al., 2016).

Studies that have focused on the impacts of exposure to PM<sub>2.5</sub> from large wildfires, such as those in Asia and Australia, indicate the health impacts are considerable. The fires in Equatorial Asia in September and October 2015 led to an estimated 69 million people being exposed to unhealthy air quality, leading to 11,880 PM<sub>2.5</sub> associated deaths from short-term exposure (Crippa, et al., 2016). The first estimate of the impact of PM<sub>2.5</sub> exposure from fires during the 2019/2020 Australian wildfires indicates there were an estimated 417 PM<sub>2.5</sub>-associated deaths, 1124 cardiovascular and 2027 respiratory PM<sub>2.5</sub>-associated hospital admissions due to bushfire PM<sub>2.5</sub> between October 1<sup>st</sup> 2019 and February 10<sup>th</sup> 2020 (Borchers Arriagada, et al., 2020). However, this study may underestimate the impact on health due to reliance on estimating population exposure using ground-based observations from the Australian air quality monitoring network. The Australian monitoring network is sparse and sites are generally located in city centres, meaning it may be difficult to capture the steep concentration gradients between cities and suburban areas. The fire contribution to PM<sub>2.5</sub> concentrations was estimated by using the 95<sup>th</sup> percentile of historical PM<sub>2.5</sub> concentrations to identify ‘fire days’ and then subtracting the historical mean PM<sub>2.5</sub> concentration of all days. This may lead to an under or overestimation in the contribution of fires to PM<sub>2.5</sub> concentrations dependent upon whether this method accurately captures background concentrations.

#### **1.6.1.2.2 UK**

Due to the UK’s unique geographical location, close to continental Europe in the north Atlantic, concentrations of air pollutants are subject to many different meteorological processes (e.g. long-range transport, wash-out), which can influence concentrations on a range of time and spatial scales.

Synoptic meteorology plays a large role in controlling concentrations (Pope *et al.*, 2014; Pope *et al.*, 2016; Stirling *et al.*, 2020). Lamb weather types, a classification for synoptic

meteorology, have been used to investigate the influence of regional weather on NO<sub>2</sub> and O<sub>3</sub> concentrations throughout the year (Pope *et al.*, 2014; Pope *et al.*, 2016; Stirling *et al.*, 2020). Both NO<sub>2</sub> and O<sub>3</sub> were found to be strongly influenced by wind and circulation patterns. NO<sub>2</sub> concentrations were significantly increased under winter-time anticyclonic conditions, through pollutant accumulation, and were also enhanced under south-easterly flow due to long-range transport of pollutants from continental Europe (Pope, et al., 2014; Stirling, et al., 2020). The winter increase in NO<sub>2</sub> was attributed to the combined effect of increased emissions, more stable conditions and decreased photolysis allowing accumulation over emission sources (Pope, et al., 2014). The highest O<sub>3</sub> concentrations occurred under summer anticyclonic conditions due to large scale subsidence and limiting vertical mixing. The study also identified that south-easterly and north-easterly flow increased mean UK ozone concentrations by between 10 and 15 µg m<sup>-3</sup> (Pope *et al.*, 2016). The health burden of short-term exposure to O<sub>3</sub> was estimated to be 41 deaths per day under anticyclonic conditions and 42-53 deaths per day under easterly flows. The meteorological drivers of two episodes of high O<sub>3</sub> and PM<sub>2.5</sub> concentrations in 2006 were also found to be anticyclonic conditions with light easterly and south-easterly winds (Fenech, et al., 2019), broadly in agreement with Pope *et al.* (2016). The health impact from short-term exposure to O<sub>3</sub> was estimated to be 70 deaths brought forward, between 36% and 54% higher than if concentrations were at the seasonal-mean (Fenech, et al., 2019).

Other studies have focussed on the impacts of specific high pollution events on health (Stedman, 2004; Vieno *et al.*, 2016; Macintyre *et al.*, 2016). Population exposure to high PM<sub>2.5</sub> concentrations during a 10-day spring pollution episode in 2014 brought forward an estimated 600 deaths, 840 emergency respiratory and 730 emergency cardiovascular hospital admissions (Macintyre, et al., 2016). This equated to a doubling of hospital admissions compared with those under typical springtime conditions. The impact of high ozone and PM<sub>10</sub>

concentrations during the summer 2003 heatwave was also estimated (Stedman, 2004). The study found that 471 deaths were brought forward, attributable to exposure to PM<sub>10</sub> during the two-week pollution event, representing an increase of 207 deaths compared to the same period in 2002. This is in agreement with previous work that found a large proportion of the deaths brought forward resulted from elevation of pollutant concentrations rather than the direct impact of high temperatures (Rooney, et al., 1998). Previous work has therefore highlighted the substantial short-term, acute impact of air pollution episodes on public health.

## **1.7 Thesis Aims**

The work in this thesis aims to address several key gaps in current knowledge. This will be achieved through four key aims:

- Investigate the impact of synoptic weather on UK ambient PM<sub>2.5</sub> concentrations and quantify the relative contributions of local (UK) and regional (non-UK) emissions to PM<sub>2.5</sub>.
- Explore the air quality impacts of the 2018 Saddleworth Moor fire using observational data.
- Quantify the air quality and health impacts of the 2018 Saddleworth Moor fire using the WRF-Chem model.
- Quantify the air quality and health impacts of the 2019/2020 Australian mega fires using the WRF-Chem model.

## Chapter 2 - Methods

This thesis has two themes: the use of observational data and modelling. In Papers 1 and 2 observational datasets are used to understand factors affecting air quality at different spatial and temporal scales. While, Papers 3 and 4 use an atmospheric-chemistry transport model to quantify the impact of wildfires on PM<sub>2.5</sub> air quality and health. Papers 1, 2 and 3 are published and Paper 4 is in draft format. Table 4 and Table 5 give an overview of the datasets used in each of the papers. More detailed information on the datasets and methods is given in the following sections and within the papers themselves.

### Observational Papers

**Paper 1:** Ailish M. Graham, Kirsty J. Pringle, Stephen R. Arnold, Richard J. Pope, Massimo Vieno, Edward W. Butt, Luke A. Conibear, Ellen L. Stirling and James B. McQuaid. Impact of weather types on UK ambient particulate matter concentrations. *Atmospheric Environment: X*, **5**, p. 100061. DOI: <https://doi.org/10.1016/j.aeaoa.2019.100061>, 2019.

Paper 1 used ground-based observational data to investigate the influence of synoptic scale weather patterns (characterised by Lamb weather types) on ambient PM<sub>2.5</sub> across the UK (from AURN ground-based observational sites). The contributions of local and non-local primary PM<sub>2.5</sub> emissions to changes in ambient PM<sub>2.5</sub> concentrations under different weather patterns were investigated using the ROTRAJ back trajectory model and bottom-up anthropogenic emissions datasets.

**Paper 2:** Ailish M. Graham, Richard J. Pope, James B. McQuaid, Kirsty J. Pringle, Stephen R. Arnold, Antonio G. Bruno, David P. Moore, Jeremy J. Harrison, Martyn P. Chipperfield,

Richard Rigby, Alberto Sanchez-Marroquin, James Lee, Shona Wilde, Richard Siddans, Brian J. Kerridge, Lucy J. Ventress and Barry J. Latter. Impact of the June 2018 Saddleworth Moor wildfires on air quality in northern England. *Environmental Research Communications*, **2**(3), p.031001. DOI: <https://doi.org/10.1088/1748-9326/ab8496>, 2020.

Paper 2 used ground-based, satellite and aircraft observations to investigate the impact of the 2018 Saddleworth Moor fire on air pollutant concentrations across the north-west of England. The emission and evolution of key air pollutants, including CO, NO<sub>2</sub>, O<sub>3</sub> and PM<sub>2.5</sub>, were investigated using a combination of the time series and in-situ datasets that are listed above.

### **Modelling Papers**

**Paper 3:** Ailish M. Graham, Richard J. Pope, Kirsty P. Pringle, Stephen R. Arnold, Martyn P. Chipperfield, Luke A. Conibear, Edward W. Butt, Laura Kiely, Christoph Knote, James B. McQuaid. Impact on air quality and health due to the Saddleworth Moor Fire in Northern England. *Environmental Research Letters*. DOI: <https://doi.org/10.1088/2515-7620/ab7b92>, 2020.

**Paper 4:** Ailish M. Graham, Richard J. Pope, Kirsty P. Pringle, Stephen R. Arnold, Luke A. Conibear, Helen Burns, Richard Rigby, Nicolás Borchers-Arriagada, Edward W. Butt, Laura Kiely, Carly Reddington, Dominic V. Spracklen, Matt Woodhouse, Christoph Knote, James B. McQuaid. Impact of the 2019/2020 Australian megafires on Air Quality and Health. *Draft Format*

Papers 3 and 4 applied the same method to different regions of the world (UK and Australia). The WRF-Chem model was used to investigate the impacts of the 2018 Saddleworth Moor (Paper 3) and 2019/2020 Australian (Paper 4) wildfires on PM<sub>2.5</sub> concentrations. WRF-Chem was used to calculate the impacts of the fires on air quality by simulating PM<sub>2.5</sub> concentrations

with and without fire emissions. Observations of  $PM_{2.5}$  (from ground-based monitoring) were used to evaluate the model runs with fire emissions. Once the model performance was quantified the increase in  $PM_{2.5}$  concentrations due to the fires was calculated using the two simulations ( $PM_{2.5}$  Fires –  $PM_{2.5}$  No Fires). Using gridded population data (Australian Bureau of Statistics, 2019; NASA Socioeconomic Data and Applications Center (SEDAC) Center for International Earth Science Information Network (CIESIN), and Columbia, 2018) the population-weighted  $PM_{2.5}$  concentration was determined and used as a proxy for dose. A short-term concentration-response function (Atkinson, et al., 2014; World Health Organization, 2013) was applied to the population-weighted  $PM_{2.5}$  concentration, alongside underlying mortality rates (Australian Bureau of Statistics, 2020; Institute for Health Metrics and Evaluation, 2015) to quantify the health burden of population exposure to  $PM_{2.5}$  from the fires ( $PM_{2.5}$  Fires –  $PM_{2.5}$  No Fires).

Detailed information on the datasets used in the observational papers is provided in the supplementary material of Papers 1 and 2 – therefore only an overview is provided in Table 4. The focus of the following sections is to provide a more detailed model description and further information on the methods used in the modelling papers (Paper 3 and 4), as these are not described in detail in the papers themselves.

Table 4. Overview of datasets used in Papers 1 and 2. These papers focused on the use of observational datasets, using models to support understanding of relationships identified through the observational datasets.

Paper	Region	Air Pollutant Datasets			Emissions Datasets		Other Datasets	Model	
		Ground Observations	Satellite Observations	Aircraft Measurements	Anthropogenic Emissions	Fire Emissions	Synoptic Meteorology	Back Trajectories	Atmospheric Chemistry Transport Model
1	UK	AURN PM <sub>2.5</sub>			EDGAR-HTAP2, EMEP, NAEI PM <sub>2.5</sub>		Lamb Weather Types	Reading Offline Trajectory Model (ROTRAJ)	The European Monitoring and Evaluation Program Unified Model for the UK (EMEP4UK)
2	UK	AURN PM <sub>2.5</sub>	TROPOMI Tropospheric Column NO <sub>2</sub> , CO	FAAM NO <sub>2</sub> , CO, CO <sub>2</sub> , O <sub>3</sub> , PM <sub>2.5</sub>		FINN, MODIS Fire Radiative Power		The Hybrid Single Particle Lagrangian Integrated Trajectory Model (HYSPLIT)	

Table 5. Overview of datasets used in Papers 3 and 4. These papers focused on the application of air quality modelling to quantify the impacts of wildfires on health through population exposure to PM<sub>2.5</sub>.

Paper	Region	Air Pollutant Datasets	Emissions Datasets		Other Datasets			Model
		Ground Observations	Anthropogenic Emissions	Fire Emissions	Population Count	Mortality Rate	Concentration Response Function	Atmospheric Chemistry Transport Model
3	UK	AURN PM <sub>2.5</sub>	EDGAR-HTAP2	FINNv1.5	Gridded Population of the World v4 (GPWv4) (2015)	Global Burden of Disease (North-west England) (2015)	Atkinson <i>et al.</i> (2014): 1.04% (95% CI: 0.52 - 1.56%) per 10 µg m <sup>-3</sup>	Weather Research and Forecasting Model coupled with Chemistry (WRF-Chem) v3.7.1
4	Australia	PM <sub>2.5</sub> observations from government departments in Queensland, New South Wales, Australian Capital Territory and Victoria.	EDGAR-HTAP2	FINN near-real time	Australia Bureau of Statistics population count data (2018)	Australia Bureau of Statistics (state specific) (2018)	WHO (2013): 1.0123 (95% CI: 1.0045, 1.0201) per 10 µg m <sup>-3</sup>	Weather Research and Forecasting Model coupled with Chemistry (WRF-Chem) v3.7.1

## **2.1 WRF-Chem Model: Paper 3 and 4**

Concentrations of pollutants in the atmosphere are controlled by four key processes: emissions, chemistry, transport and removal (Jacob, 2006). These processes and interactions can be represented numerically in 3-D Atmospheric Chemical Transport Models (Dore, et al., 2015), such as the Weather Research and Forecasting Model with Chemistry (WRF-Chem) (Grell, et al., 2005). Models can therefore be used to simulate concentrations of pollutants across many scales, from global to local. Ground-based observations are often sparse, and are generally only representative of a small region surrounding their location. In contrast, satellite observations give a more complete picture spatially but often lack temporal detail due to their orbits (i.e. polar orbiters overpass only once per day). Modelled concentrations can be very useful in understanding the distribution of concentrations over larger areas than is available from ground-based monitoring and at higher temporal-resolution than is available from satellites. Despite this, ground-based and satellite observations are still useful in validating modelled pollutant concentrations both spatially and temporally. Provided the simulated concentrations agree well with observations, the impact of different scenarios can be simulated (e.g. changes in emissions). In papers 3 and 4  $PM_{2.5}$  concentrations were simulated for two scenarios: 1) with fire emissions 2) without fire emissions. This isolated the contribution of each wildfire event to  $PM_{2.5}$  concentrations and allowed the impact of pollutants emitted by wildfires on air quality and health to be quantified.

### **2.1.1 The WRF-Chem Model System**

The Weather Research and Forecasting Model with Chemistry (WRF-Chem) has become a popular tool for investigating regional air quality across the world in recent years. The model development was a collaborative effort, led by NOAA and ESRL scientists, to convert WRF

into a coupled model with chemistry that is free to use. WRF-Chem is a fully online-coupled model, in which the air quality and meteorology are fully integrated using the same coordinate system, transport and time-step (Grell, et al., 2005). This is achieved by including modules for both gas-phase and aerosol chemistry. Online chemistry allows complex interactions between emissions, chemistry, transport and removal to be captured (e.g. chemistry impacts on meteorology through interaction of aerosols on CCN), since these interactions occur on time-scales shorter than the model output (Grell, et al., 2005).

WRF is a fully compressible, non-hydrostatic model, which was designed for research and forecasting. There are two dynamical cores in the WRF model: The Advanced Research WRF (ARW) and Non-hydrostatic Mesoscale Model (NMM). Both cores are Eulerian mass dynamical that use terrain-following hydrostatic pressure vertical coordinates and include advection, Coriolis, diffusion, pressure gradients and time-stepping. The work presented in this thesis used the ARW core (within WRF-Chem version 3.7.1). The ARW solver is used to calculate chemistry and meteorology using the same coordinates, timestep and physics (Grell, et al., 2005; Skamarock, and Klemp, 2008).

The WRF and WRF-Chem modelling systems are constructed of two main components, which will be discussed in the following sections, with specific focus on the WRF-Chem model:

1. The WRF pre-processing system (WPS)
2. The WRF model (REAL and ARW model)

The WRF-Chem model differs from the WRF model due to the addition of chemistry, which needs additional gridded data for emissions of chemical species (see ‘External Data Source’ in Figure 20). This additional information is provided by the WPS (dust emissions) or read in (e.g. fire emissions, biogenic emissions) during initialisation (see ‘External Data Source’ in Figure 20). Alongside this, anthropogenic emissions are also read into the WRF ARW solver

(see ARW model in Figure 20) and an additional step is added in post processing (3) to calculate the concentrations of some air pollutant species (see ‘Post-Processing & Visualisation’ in Figure 20).

In this work a set of scripts (WRFotron) written by Christoph Knote were used to automate WRF-Chem simulations and scripts from Christoph Knote and Luke Conibear were used for post-processing. WRFotron scripts were used to submit the three key stages of simulations:

- pre-processing (pre.bash) (‘WPS’, ‘Real data’ and ‘wrfchembc’ Figure 20)
- the ARW model (main.bash) (‘ARW model’ Figure 20)
- post-processing (post.bash) using Python/NCL scripts (‘NCL’ Figure 20).

This work used the same model set-up as has been extensively used in air quality studies across many regions of the world previously (Conibear *et al.*, 2018a, 2018b; Conibear *et al.*, 2018; Kiely *et al.*, 2019, 2020; Reddington *et al.*, 2019; Conibear *et al.*, 2020; Silver *et al.*, 2020; Thorp *et al.*, 2020).

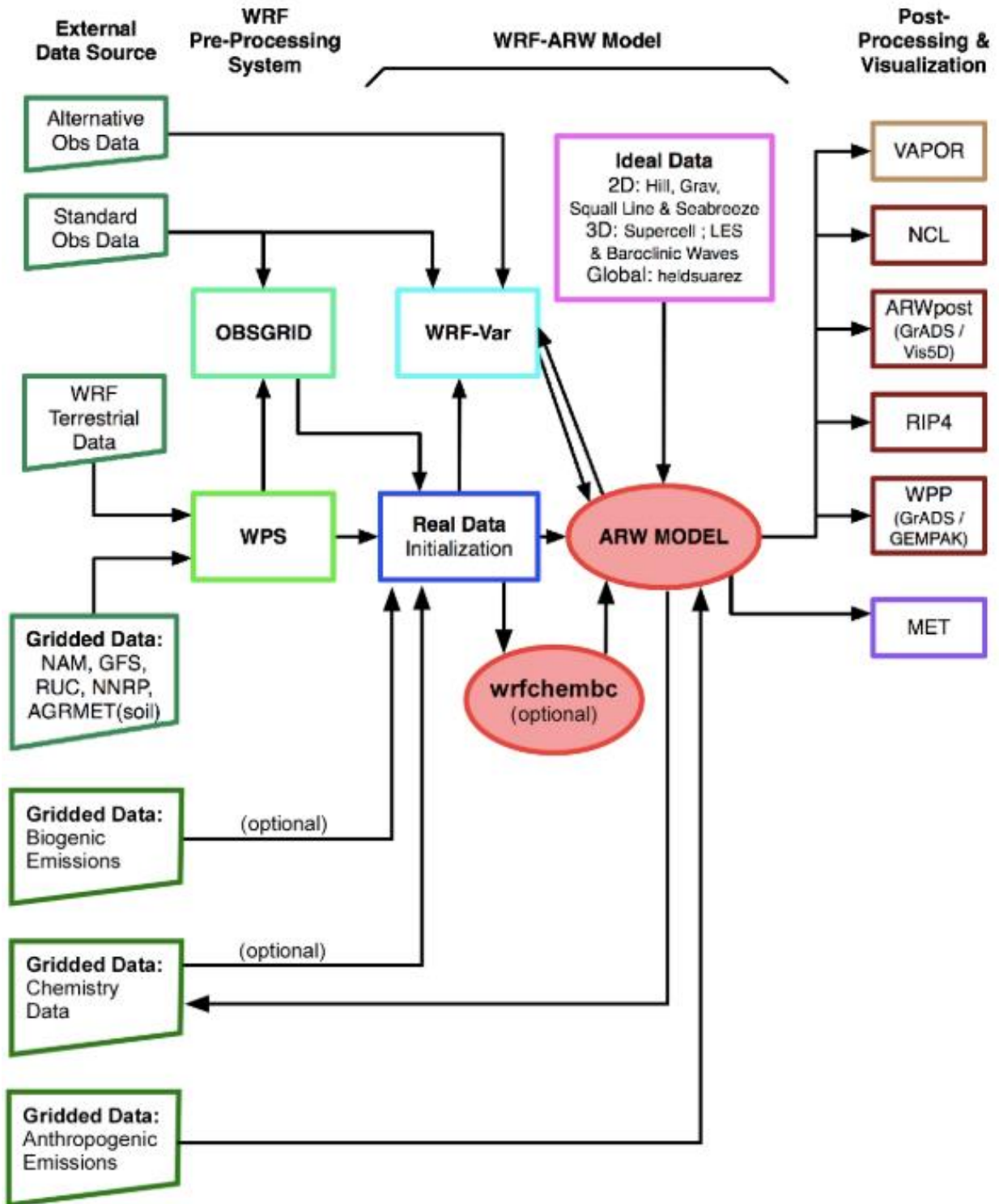


Figure 20. Flowchart of the WRF-Chem Modelling System (Peckham, et al., 2015).

### **2.1.2 Domain and Model Set-up**

An overview of the model set-up used for Papers 3 and 4 is provided in Table 6, further information on the settings used is given in the following sections and within the papers and their supplementary material.

Table 6. Model and Domain settings used for Paper 3 and 4.

<b>Model Configuration and Parametrizations</b>	<b>Paper 3</b>	<b>Paper 4</b>
<b>Model Simulation Time Period</b>	June 16 <sup>th</sup> – July 14 <sup>th</sup> 2018	September 1 <sup>st</sup> 2019 – January 31 <sup>st</sup> 2020
<b>Model Domain</b>	-4.9 – 0.7°E and 53.0 – 54.4°N	128.9 – 170.6°E and -9 – -48°N
<b>Horizontal Resolution</b>	17x39 grid boxes 10 km	130x150 grid boxes 30 km
<b>Vertical Resolution</b>	33 levels and 27 meteorological levels	33 levels and 38 meteorological levels
<b>Model Timestep</b>	60 seconds	180 seconds
<b>Meteorological Initial Boundary Conditions</b>	NCEP GFS and NCEP FNL 6-hourly analyses at 0.5°	ERA5 6-hourly analyses at 0.1° resolution
<b>Chemical Initial Boundary Conditions</b>	WACCM 6-hourly simulation data	WACCM 6-hourly simulation data
<b>Fire emissions</b>	FINNv1.5	FINN near-real time
<b>Fire emissions release</b>	100% at the surface called every 30 seconds	Evenly distributed through the boundary layer/plume-rise, both called every 30 seconds
<b>Anthropogenic emissions</b>	EDGAR-HTAP 2010	EDGAR-HTAP 2010
<b>Dust emissions</b>	GOCART with Air Force Weather Agency (AFWA) modifications	GOCART with Air Force Weather Agency (AFWA) modifications
<b>Land surface</b>	NOAH Land surface model	NOAH Land surface model
<b>Boundary Layer Scheme</b>	The Mellor-Yamada-Nakanishi-Niino Level 2.5(MYNN2) scheme called every 60 seconds	The Mellor-Yamada-Nakanishi-Niino Level 2.5(MYNN2) scheme called every 3 minutes
<b>Gas-phase Chemistry</b>	MOZART-4 with aqueous chemistry (202) called every 60 seconds	MOZART-4 with aqueous chemistry (202) called every 3 minutes
<b>Photolysis Scheme</b>	Madronich fTUV (phot_opt=3) called every 10 mins	New full fTUV (phot_opt=4) called every 30 mins
<b>Aerosol Scheme</b>	MOSAIC 4-bin with aqueous chemistry (202) (apart from in stratocumulus clouds) called every 60 seconds	MOSAIC 4-bin with aqueous chemistry (202) (apart from in stratocumulus clouds) called every 3 minutes
<b>Convection Parameterization</b>	Grell 3-D ensemble	Grell 3-D ensemble

<b>Microphysics</b>	Thompson scheme	Thompson scheme
<b>Radiation Scheme</b>	RRTM longwave called every 60 seconds and Shortwave radiation RRTM shortwave called every 60 seconds	RRTM longwave called every 3 minutes and Shortwave radiation RRTM shortwave called every 3 minutes
<b>Meteorological Nudging</b>	All vertical levels - potential temperature, horizontal and vertical winds and the water vapour mixing ratio using 3-hourly GFS reanalysis.	<p>1. All vertical levels - potential temperature, horizontal and vertical winds and the water vapour mixing ratio using 6-hourly ERA5 reanalysis.</p> <p>2. Within the boundary layer horizontal and vertical winds are nudged using 6-hourly ERA5 reanalysis. Above the boundary layer - potential temperature, horizontal and vertical winds and the water vapour mixing ratio using 6-hourly ERA5 reanalysis</p>

### 2.1.2.1 UK 2018 Saddleworth Moor Wildfire

Simulations for the Saddleworth Moor wildfire were performed between June 1<sup>st</sup> to July 14<sup>th</sup> 2018 at 10 km resolution for a domain covering northern England (Figure 21). The first two weeks of the simulation were discarded as model to spin-up. Therefore, the simulation analysed spanned June 16<sup>th</sup> to July 14<sup>th</sup> 2018. The domain size was 17x39 grid boxes with 33 pressure levels (from the surface to 10 hPa). The domain included the north-west England region, which ground-based and satellite observations indicated was most severely affected by pollutants from the fires. The spatial resolution was 10 km, therefore a model timestep of 60 seconds was used in order not to breach courant (C) stability (i.e. how much information (u) moves across a grid cell ( $\Delta x$ ) within a given model timestep ( $\Delta t$ ), since  $C = \frac{u \Delta t}{\Delta x}$ ). This allowed the model simulation time and cost to be reasonable, without the model becoming unstable.

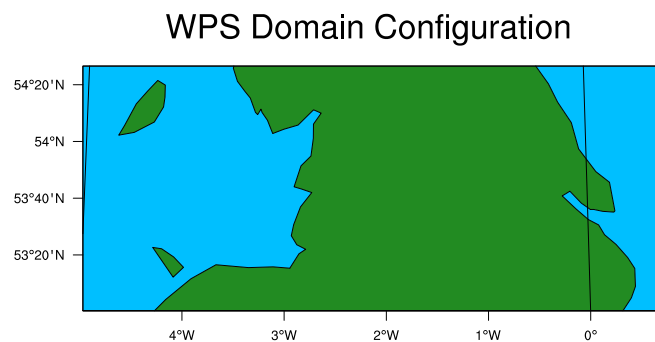


Figure 21. WRF-Chem domain for Saddleworth Moor Fires 2018 simulations

### 2.1.2.2 Australia

Simulations over Australia were performed for August 1<sup>st</sup> 2019 to January 31<sup>st</sup> 2020 at 30 km resolution for a domain covering eastern Australia and New Zealand (Figure 22). Model output was discarded between August 1<sup>st</sup> and August 31<sup>st</sup> to allow the model to spin-up in the first month. The domain size was 130x150 grid boxes with 33 pressure levels (from the surface to 10 hPa). For these simulations, only eastern Australia was included in the model domain for several reasons. Firstly, ~90% of the population live in this region, secondly this was the region the fires affected most severely, thirdly, satellite observations indicated that pollutants were transported within this region by prevailing winds, and finally, computing cost and time meant that including all of Australia and New Zealand would have been challenging. Since the resolution of this model simulation was coarser (30 km) a larger model timestep was used (3 minutes).

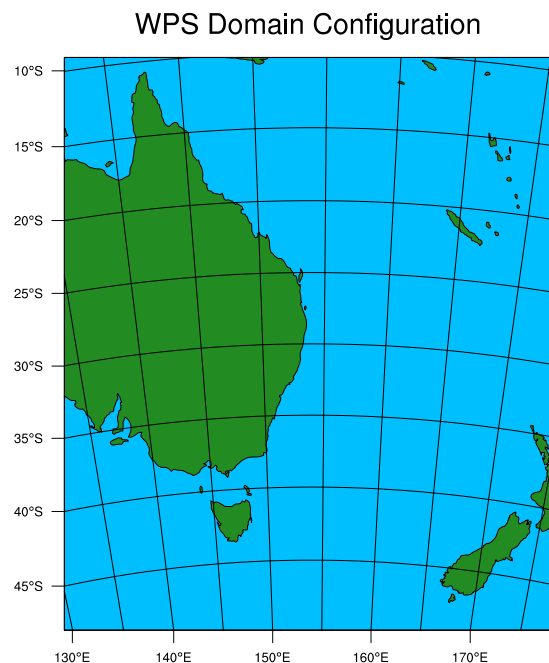


Figure 22. WRF-Chem domain for Australia wildfires 2019/2020 simulations

## **Data used for Initial Conditions**

### **2.1.2.3 Initial Boundary Meteorology**

#### **Meteorological Reanalysis**

##### **UK**

Meteorological conditions were initialised using NCEP GFS 6-hourly analyses at 0.5° resolution on 27 pressure levels (NCEP, 2007). In between the 6-hourly analyses, GFS 3-hourly forecasts were used for boundary conditions and nudging of meteorological variables (NOAA, 2020). Nudging was used in order to keep simulated meteorology in line with the meteorological analyses. The variables which were nudged in all of the vertical levels included, potential temperature, the horizontal and vertical winds and the water vapour mixing ratio. Meteorology was re-initialised every week using meteorological boundary conditions in order to minimise model drift.

##### **Australia**

Meteorological conditions were initialised using ERA5 6-hourly analyses at 0.1° resolution on 38 pressure levels (Hoffman et al., 2019; ECMWF, 2020). Nudging was performed in the same way as with GFS reanalysis but using 6-hourly ERA5 meteorological analysis. Two nudging options were tested, firstly, meteorological variables (potential temperature, horizontal and vertical winds and the water vapour mixing ratio) were nudged for all vertical levels. Secondly, only horizontal and vertical wind components were nudged within the boundary layer and above the boundary layer potential temperature, horizontal and vertical winds and the water vapour mixing ratio were nudged.

### **2.1.2.4 Initial Chemical Boundary Conditions**

Initial boundary chemistry was provided by the Whole Atmosphere Community Climate Model (WACCM) 6-hourly simulation data (Marsh, et al., 2013; UCAR, 2020a), since this is the only dataset available at near-real time. WACCM meteorology is driven by the NASA

GMAO GEOS-5 model. Anthropogenic emissions for 2014 from CEDS (used in CMIP6) and FINN-v1 fire emissions are used in WACCM. Model output is given on 88 vertical levels at  $0.9 \times 1.25^\circ$  (UCAR, 2020b). WACCM initial boundary conditions were used to initialise chemistry at the start of the simulation in both the UK and Australia model simulations.

#### 2.1.2.5 Anthropogenic Emissions

For both the UK and Australia model simulations, global anthropogenic emissions were taken from the Emission Database for Global Atmospheric Research with Task Force on Hemispheric Transport of Air Pollution version 2.2 (EDGAR-HTAP2) (Janssens-Maenhout, et al., 2015) at  $0.1^\circ$  resolution for 2010. Sector specific diurnal cycles were subsequently added to the emissions after they have been read in, using diurnal cycles from Olivier *et al.* (2003). EDGAR-HTAP2 is a global, gridded, air pollution emission inventory compiled of officially reported, national gridded inventories. Where national emissions datasets or specific sectors were not available EDGAR v4.3 grid maps are used. Emissions include  $\text{SO}_2$ ,  $\text{NO}_x$ , CO, NMVOC,  $\text{NH}_3$ ,  $\text{PM}_{10}$ ,  $\text{PM}_{2.5}$ , BC and OC. The resulting EDGAR-HTAP2 dataset provides emissions of these pollutants on a monthly and annual grid map and contains emission factors that are fuel-, technology-, process- and human activity- dependent, as well as considering end-of-pipe abatement. Emissions include all anthropogenic emissions except large-scale biomass burning (e.g. wildfires). Emissions are split into 7 sectors: aircraft, international shipping, power industry, industry, ground transport, residential and agriculture.

Within EDGAR-HTAP2, European emissions are from the TNO-MACC-II (EMEP-TNO) (Kuenen, et al., 2014) dataset at  $0.125^\circ \times 0.0625^\circ$  (converted to  $0.1^\circ \times 0.1^\circ$ ), spanning from  $30^\circ\text{W}$ - $60^\circ\text{E}$  and  $30^\circ$ - $72^\circ\text{N}$ . EDGAR-HTAP2 2010 data for Europe is based on EMEP-TNO 2009 data but uses the trend in EMEP-TNO data between 2006 and 2009 to estimate 2010 emissions. The EMEP-TNO dataset includes all activities, except international shipping and

international aviation (this was taken from EDGARv4.3), and all emissions, except OC and BC. OC and BC were derived using a ‘PM-split’ table, that provides recommendations on PM composition carbonaceous profiles for each sector and country (Visschedijk, et al., 2009) using PM<sub>2.5</sub> and PM<sub>10</sub>. From the annual totals, monthly profiles were calculated using monthly scaling factors for each country and sector.

Australian emissions in EDGAR-HTAP2 are taken from EDGAR v4.3. The dataset provides global emissions of anthropogenic and greenhouse gases between 1970 and 2010, including OC, BC and PM<sub>2.5</sub>. Emissions are provided at country level for individual sources. These are mapped onto the EDGAR-HTAP2 grid using proxy data such as population data, roads, railways and animal density, among others (more information in Janssens-Maenhout *et al.* (2013)). Once the data has been mapped, monthly profiles for each HTAP sector from EDGAR v4.3 are applied to create a monthly varying dataset – for Australia profiles for the southern hemisphere are used.

EDGAR-HTAP2 emissions are used in place of local emissions datasets (e.g. NAEI emissions for the UK) because during fire events the PM<sub>2.5</sub> signal is likely to be dominated by fire emissions of PM<sub>2.5</sub> (e.g. PM<sub>2.5</sub> fires – PM<sub>2.5</sub> no fires).

#### 2.1.2.6 Fire Emissions

Wildfire emissions were taken from the Fire Inventory from NCAR version 1.5 (FINNv1.5) (UK) and FINN version 1 near real time (FINNv1 NRT) (Australia), which were provided with chemical speciation profiles for MOZART-4. Both versions of FINN combine satellite observations, land cover, biomass consumption estimates and emissions factors to calculate daily fire emissions globally at 1 km resolution. FINN emissions are chosen over GFED due to their higher spatial resolution (1 km vs 5 km). FINN uses satellite observations from the MODIS Thermal Anomalies Product to provide detections of active fires. Burned area is

assumed to be 1 km<sup>2</sup> for each fire identified and scaled back based on the density of vegetation from the MODIS Vegetation Continuous Fields (VCF) (i.e. if 50% bare = 0.5 km<sup>2</sup> burned area). The type of vegetation burned during a detected fire is determined using the MODIS Collection 5 Land Cover Type (LCT). Each fire pixel is assigned to one of 16 possible land cover/land use classes and also the density of vegetation at 500 m resolution, scaled to 1 km. The 16 land cover types are then aggregated into 8 generic categories to which fuel loadings are applied (Wiedinmyer, et al., 2011). Fuel loadings are from Hoelzemann *et al.* (2004) and emissions factors are from Akago *et al.* (2011), Mcmeeking (2008) and Andrae and Merlet (2001). FINN includes all emissions from above ground vegetation but not from the combustion of peat (Kiely, et al., 2019). Fire types included are wildfires, prescribed and agricultural burning. However, trash burning or biofuel use are not included.

The key difference between FINN v1 NRT and FINN v1.5 is that FINN v1 NRT uses MODIS near real time fire counts rather than the reprocessed fire counts, which v1.5 uses. This is due to FINN v1 NRT being a near real time product. The near real time product (FINN v1 NRT) is used for paper 4 because FINNv1.5 emissions had not been released at the time of the model simulations. However, the differences between the two datasets over Australia for the year 2018 (and 2019 following the v1.5 release) were quantified to identify any differences in PM<sub>2.5</sub> emissions.

### **Release of Fire Emissions**

WRF-Chem is set-up to emit fire emissions using a plume-rise parameterisation by default (Freitas, et al., 2007). Plume-rise is a 1-D cloud-resolving model that parameterises how plumes transport hot gases and particles vertically. Plume-rise uses meteorological fields and land-use from the WRF-Chem simulation as input and then explicitly simulates each plume.

The height of each plume is then used as the injection height for flaming fire emissions within the model (Freitas, et al., 2007).

Several studies focussed on peat fires have found that, due to the lower burning temperatures, the plume-rise scheme potentially represents an incorrect vertical distribution of the emissions (Archer-Nicholls, et al., 2015; Crippa, et al., 2016). Given the relatively small size of the Saddleworth Moor fires (8 km<sup>2</sup>) and the low peak height of flames (4 m), the plume-rise parameterization is likely to overestimate the injection height of the emissions from the fires. Therefore, in these simulations 100% of emissions were released at the surface. The much larger Australia bushfires are likely to have had a substantially higher flame height and produced such intense heat that they created pyro-cumulonimbus clouds. Therefore, in these simulation two emissions release options were implemented in order to investigate which lead to the best comparison with observations:

- 1) distributing emissions evenly within the boundary layer, following the method of Kiely *et al.* (2020, 2019).
- 2) Plume-rise.

Kiely *et al.* (2020, 2019) used a similar WRF-Chem set-up to the Australia simulations and found that for simulations of Indonesian fires surface and boundary layer emission release options improved agreement between simulated surface PM<sub>2.5</sub> concentration and observations compared with the plume-rise module.

In both papers, the fire\_emiss pre-processor was used to re-grid FINN emissions to the domain spatial resolution and to map the FINN chemical speciation to the model aerosol scheme. The size distribution of aerosol was then calculated online. Fire\_emiss also applies separate diurnal cycles to emissions from wildfire, prescribed burning and agricultural burning, using WRAP

data (Western Regional Air Partnership, 2005). >90% of wildfire emissions are released between 10:00 and 19:00 local time.

#### 2.1.2.7 Dust Emissions

Three options to calculate dust emissions are available in WRF-Chem v3.7.1: 1) GOCART-WRF (dust\_opt=1) (LeGrand, et al., 2019), 2) GOCART AFWA (dust\_opt=3) (LeGrand, et al., 2019) and 3) GOCART UoC (dust\_opt=4) (Shao, 2001). In this work the GOCART with Air Force Weather Agency (AFWA) modifications (LeGrand, et al., 2019) scheme was used (dust\_opt=3), which calculates dust emissions online. The AFWA scheme is based on the parametrisation of Marticorena and Bergametti (1995) and builds upon the original GOCART dust emission scheme (Ginoux, et al., 2001), first incorporated into WRF-Chem as GOCART-WRF. GOCART was designed to use a topographically based source function to fixed geographic variability in substrate erodibility. This removed the need to obtain soil and surface characteristic data, which are difficult to acquire. In GOCART AFWA the erodible fraction of soil is fixed to a constant mix of sand, silt and clay. Dust emissions are calculated using wind speed, soil moisture and general soil characteristics, which are already available in WRF-Chem. Emissions are calculated separately for discrete soil grain size bins in a two-stage process, where wind shear triggers large particle saltation, leading to the emission of fine particles by saltation bombardment. The AFWA scheme is able to better represent dust emissions by saltation bombardment and particle disaggregation than the GOCART-WRF scheme by utilising an independent series of 9 bins for saltation (between 1.42  $\mu\text{m}$  and 250  $\mu\text{m}$ ) and 5 bins for emitted dust (0.2-2  $\mu\text{m}$  , 2-3.6  $\mu\text{m}$ , 3.6-6  $\mu\text{m}$ , 6-12  $\mu\text{m}$  and 12-20  $\mu\text{m}$ ) (LeGrand, et al., 2019). Dust mass fluxes calculated by the scheme are used to represent the dust mass flux that is injected into the surface atmospheric model level. Separate modules in the model, for atmospheric transport and removal, are then used to estimate dust concentrations in model levels above this.

#### **2.1.2.8 Land-use**

Land-use (vegetation) data is from MODIS at 30 arc-second resolution (~1km) using International Geosphere-Biosphere Programme (IGBP) classes. 18 land-use classes are used, with 7 tree/shrubland, 3 savanna/grassland, 2 cropland, wetland, ice and snow, urban, bare-ground and water categories. More information is available from UCAR (2020c).

#### **2.1.3 Model set-up**

##### **2.1.3.1 Land-surface Model**

The NOAH land-surface model (LSM) was used to represent land surface processes and provide lower boundary conditions (Ek, et al., 2003). The NOAH LSM simulates surface energy and water fluxes and the surface energy and water budgets due to near-surface atmospheric forcing. The associated changes in soil moisture and temperature and snowpack are important to the surface energy and water budgets on daily, seasonal and annual timescales. This allows the model to account for sub-grid fluxes and also has knock on effects on boundary layer and cumulus schemes. The three key inputs that the LSM needed as input were: land-use (vegetation) type, soil texture and slope. From this, the LSM provides WRF with: surface sensible heat flux, surface latent heat flux, upward long-wave radiation (or skin temperature and surface emissivity), upward (reflected) short-wave radiation (or surface albedo, including snow effect).

##### **2.1.3.2 Boundary Layer Scheme**

The planetary boundary-layer scheme (PBL) used was the Mellor-Yamada-Nakanishi-Niino Level 2.5 (MYNN2) scheme (Nakanishi, and Niino, 2006). The PBL is important in determining the concentration of pollutants. The most important variables within the PBL, which determine concentrations, are PBL height, wind speed and direction, temperature and relative humidity. These are characterised using parameterisations. Within the MYNN2

scheme a database of large eddy simulations was used to tune these variables, with the aim of overcoming typical biases seen in PBLs (e.g. a convective boundary layer which doesn't grow sufficiently and underestimated turbulent kinetic energy).

### 2.1.3.3 Gas-phase and Aerosol Chemistry Scheme

The Model for Ozone and Related Chemical Tracers, version 4 (MOZART-4) scheme was used for gas-phase chemistry (Emmons, et al., 2009), driven by model meteorology. The MOZART-4 scheme includes 85 gas-phase species, 12 bulk aerosol compounds, 39 photolysis (phot\_opt=3)/109 photolysis (phot\_opt=4) reactions relevant to tropospheric and stratospheric chemistry, and 157 gas-phase reactions (Emmons, et al., 2009). The scheme, which allows the online calculation of aerosol, updates MOZART-2 (Horowitz, et al., 2003), which was based on the Model of Atmospheric Transport and Chemistry (MATCH) (Rasch, et al., 1997). The scheme has also been extended to include detailed treatment of monoterpenes, aromatics, nitrous acid (HONO.- an important source of the hydroxyl radical), acetylene (C<sub>2</sub>H<sub>2</sub>) and an updated isoprene scheme (Knote *et al.*, 2014). This is coupled to the Model for Simulating Aerosol Interactions and Chemistry (MOSAIC) sectional aerosol scheme with the Kinetic Pre-Processor (KPP). Within MOSAIC, four sectional aerosol bin sizes are used: 0.039–0.156, 0.156–0.625, 0.625–2.5 and 2.5–10 μm. The MOSAIC scheme includes the interaction of aerosol with radiation through the direct effect of aerosol on radiation (scattering) and the effect of aerosols and clouds on photolysis (Emmons, et al., 2009). MOZART-4 also includes aerosol interactions with clouds via aerosol number determining cloud drop number and size, the first indirect aerosol effect, aqueous chemistry (in these simulations aqueous chemistry in stratocumulus clouds was not included) and wet removal through scavenging.

The physical processes within MOZART-4 are the same as within MOZART-2 (Horowitz, et al., 2003). Within the MOZART model convective mass fluxes are calculated, using the

shallow and mid-level convective transport formulation of Hack (1994) alongside the deep convection scheme of Zhang and McFarlane (1995). A parameterisation is used for vertical diffusion in the boundary layer (Holtslag, and Boville, 1993). Wet deposition is from Brasseur *et al.* (1998). A flux form semi-Lagrangian transport algorithm is used for advective transport (Lin, and Rood, 1996).

The updated gas-phase chemical mechanism in MOZART-4 uses a volatility basis set description of secondary organic aerosol (SOA) formation, based on Lane, Donahue and Pandis (2008a, 2008b) (Knote *et al.*, 2014). This allows the oxidation of several biogenic and anthropogenic precursor species to form new species with varying volatilities (Knote *et al.*, 2014). These then partition between the gas- and aerosol-phase, dependent upon total organic aerosol load and temperature. The effect of continuous oxidation on reducing the volatility is also included, as well as the removal of secondary inorganic VOCs. Primary organic aerosols (POAs) are considered non-volatile in the model. More detailed information on the updated scheme is available in Hodzic and Knote (2014) and Knote *et al.* (2014).

#### **2.1.3.3.1 Aerosols**

The MOZART-4 scheme includes the calculation of black carbon, sulfate, ammonium nitrate, primary and secondary organic aerosol (POA and SOA) and sea salt. Sulfate aerosols are formed from precursor emissions of SO<sub>2</sub> and DMS (Barth, et al., 2000). Black carbon (BC) and organic carbon (OC) emissions are split between hydrophobic (50%) and hydrophilic forms (80%) (Chin, et al., 2002). BC and OC are converted from hydrophobic to hydrophilic at a time constant of 1.6 days (Horowitz, 2006; Tie, et al., 2005). SOA is formed through the oxidation of monoterpenes and toluene (Chung, and Seinfeld, 2002). A parameterization of gas/aerosol partitioning (Metzger, et al., 2002) and ammonia emissions are combined to determine the distribution of ammonium nitrate. Based on the amount of sulphate present, the parametrisation

applies a set of approximations to the equilibrium constant calculation (Seinfeld, 1986). The uptake of dinitrogen pentoxide ( $\text{N}_2\text{O}_5$ ),  $\text{HO}_2$ ,  $\text{NO}_2$  and nitrate ( $\text{NO}_3$ ) onto aerosols is included. The surface area is calculated, using the assumption of a lognormal distribution, using a different geometric mean radius and standard deviation for each type of aerosol (Chin, et al., 2002). Sea salt aerosol is calculated online (Mahowald, et al., 2006) and is included using four size bins (0.1–0.5, 0.5–1.5, 1.5–5, and 5–10  $\mu\text{m}$ ). Monthly mean distributions of dust in the Community Atmosphere Model (CAM) are used to set the distribution of dust, in four size bins (0.05–0.5, 0.5–1.25, 1.25–2.5, and 2.5–5.0  $\mu\text{m}$ ). Ambient relative humidity is used to determine hygroscopic growth of aerosols, with different rates applied to individual types of aerosols (Chin, et al., 2002). While, washout is 20% of the  $\text{HNO}_3$  washout rate for all aerosol species, except hydrophobic OC and BC (Horowitz, 2006; Tie, et al., 2005).

#### **2.1.3.3.2 Photolysis**

The online f-TUV (fast Tropospheric Ultraviolet-Visible) scheme (Tie, et al., 2003) (39 reactions) and the new TUV scheme (UCAR, 2020d) (109 reactions) were used in the UK and Australia simulations, respectively. These settings are recommended for use with MOZART-4 (Hodzic, and Knote, 2014). The f-TUV scheme is a simplified, much faster and computationally cheaper version of the TUV model (Madronich, and Weller, 1990). The f-TUV scheme was updated to allow the impact of aerosols on clouds to also be included (Tie, et al., 2003). A lookup table, which is based on the Mie calculations in the NCAR Community Atmosphere Model (CAM3), is used in the treatment of aerosols in fixing photolysis frequencies and aerosol optical depth. The new TUV scheme uses the updated TUV model (TUV v5.3), which now includes aerosol and cloud feedback on photolysis rates, improving TUV model performance when compared with observations (UCAR, 2020e).

#### **2.1.3.3.3 Dry Deposition**

Dry deposition velocities were calculated online using the parameterisation of Wesley (2007), Walmsley and Wesley (1996) and Wesley and Hicks (2000). The parameterisation uses the distribution of vegetation, and the diffusion coefficient, reactivity and water-solubility of gases, to calculate surface resistance. The distribution of vegetation is taken from monthly land cover maps of plant functional type fraction and leaf area index (Bonan, et al., 2003). The flux of air pollutants (aerosols and gases) to the surface is calculated by multiplying the spatio-temporal deposition velocity by air pollutant concentrations in the model surface layer.

#### **2.1.3.3.4 Biogenic Emissions**

The Model of Emissions of Gases and Aerosols from Nature (MEGAN) (Guenther, et al., 2006) was used to calculate biogenic emissions of isoprene and monoterpenes online (at 1 km resolution). Therefore it should be used with the updated gas-phase chemical mechanism in MOZART-4 (Hodzic, and Knote, 2014). MEGAN online emissions are based on the emission factor of each compound, an emissions activity factor and a factor that accounts for canopy gain or loss. Other biogenic emissions are taken from the POET inventory, these vary at monthly temporal resolution but do not vary for different years. Lumped monoterpene emissions in MOZART-4 are the sum of alpha-pinene, beta-pinene, limonene, myrcene, ocimene, sabinene, and delta-3-carene in the MEGAN emission factor maps.

#### **2.1.3.4 Radiation Scheme**

The Rapid Radiative Transfer Model (RRTM) option was used for both short and long wave radiation (Iacono, et al., 2008). The RRTM includes several long-wave absorbing molecules: water vapour, carbon dioxide, ozone, methane, nitrous oxide, oxygen, nitrogen and the halocarbons, and short-wave absorbing molecules: water vapour, carbon dioxide, ozone, methane and oxygen. Extinction from aerosols, clouds and Rayleigh scattering are also included in the model.

#### **2.1.3.5 Microphysics Scheme**

The Thompson scheme was used for cloud microphysics (Thompson, et al., 2008). The scheme is a single-moment scheme, other than the double-moment ice. The mixing ratios of 5 liquid and ice species (cloud water, rain, cloud ice, snow and graupel), as well the number concentration of cloud ice, are explicitly simulated. The use of only one moment for all species (except ice) means that computing costs and run time for simulations are reduced.

#### **2.1.3.6 Convection Parameterisation Scheme**

The Grell 3-D scheme was used for convection parameterisation (Grell and Dévényi, 2002) as this is the only scheme integrated with cloud chemistry and tracer transport (Hodzic, and Knote, 2014). The parameterisation framework is based on an earlier convective parameterization, which used dynamic control, static control and feedback to split cumulus parameterisation (Grell, 1993). Dynamic control determines the modulation of convection by the environment, determining where convection will occur and how strong it will be. Feedback distributes the total integrated heating and drying in the vertical, therefore specifying the modification of the environment by convection. Finally, static control controls updraft and downdraft characteristics, including mechanisms such as entrainment, detrainment and microphysics. The Grell 3-D scheme expands this scheme to enable the inclusion of other commonly used assumptions. This gives a large spread in the solution calculated by the parameterisation. Ensemble and data assimilation are then used to identify the most likely solution.

#### **2.1.4 Model Uncertainties**

Model uncertainties can arise from a range of factors. Uncertainties from input datasets include the resolution of emissions datasets not capturing the strong concentration gradients of emissions due to averaging (Kushta, et al., 2018; Thompson, et al., 2014). Alongside this, model set-up can affect results. The trade-off between model resolution, computation time and expense means that simulations are often performed at resolutions that do not capture strong

concentration gradients in highly populated areas (Kushta, et al., 2018). This can lead to an underestimation of population exposure to pollutants and can therefore lead to an underestimation in the health impact calculated. Parameterisations of complex processes (e.g. boundary layer height diurnal cycle, convection), and the subsequent poor representation of them, can also lead to concentrations of air pollutants at the surface being in poor agreement with observations.

## **2.2 Health Impact Assessment**

### **2.2.1 Concentration-Response Function**

The concentration-response function (CRF) of Atkinson *et al* (2014) was used to estimate the impact of short-term exposure to PM<sub>2.5</sub> on mortality in Paper 3. The CRF was derived using a meta-analysis of 110 peer-reviewed time-series and case-crossover studies. The key strength of meta-analyses is that they strengthen evidence by combining findings of many studies.

Studies within the meta-analysis were found using keyword searches on the main medical journal databases and included studies published up to 2011. Once a relevant study was identified, it was only included if the study design, statistical methods and regression estimates fitted the criteria for the meta-analysis. This was achieved using 4 selection criteria:

- 1) estimates were for PM<sub>2.5</sub>
- 2) daily data for at least one year
- 3) confounding factors were controlled for
- 4) sufficient information was available for the calculation of a regression estimate and standard error for comparison in the meta-analysis.

Studies selected were also filtered for the time lag between population exposure to PM<sub>2.5</sub> and health effects presented, selecting the results from only one lag (the lag that the author focused on or was most statistically significant), if several were given. In order to reduce the over-representation of a single city within the meta-analysis, single-city studies were also filtered and only included if they were not within in any of the multi-city studies already selected.

Studies selected for the meta-analysis were grouped globally and also split into WHO regions (Africa, Eastern Mediterranean, Europe, Americas, South-East Asia and West Pacific), which were further split by the mortality rates for children and adults. For each of these regions, a meta-analysis was performed if 4 or more single city-estimates or a multi-city study estimate was available. Separate meta-analyses were performed for the single city-estimates and the multi-city estimates in each region. The single-city and multi-city effect estimates were then combined to calculate a global summary estimate. A random effects model was used to identify the proportion of variability in effect estimates that was due to unobserved differences (heterogeneity) across WHO regions. This indicated that there was a high level of heterogeneity in all-cause mortality effect estimates across regions ( $I^2 = 93\%$ ) from 0.25% to 2.08% per 10  $\mu\text{g m}^{-3}$  increment in PM<sub>2.5</sub>.

In order to ensure that the results of Paper 4 were directly comparable to previous work by Borchers Arriagada *et al.* (2020), the World Health Organisation (2013) CRF was used. The WHO CRF was derived using the Air Pollution Epidemiology Database (APED) meta-analysis, which included 12-single city time-series studies and 1 multi-city study, all of which were all-cause, all-age mortality studies. All studies included were based in Europe (WHO European region), with the multi-city study including 9 French cities. Studies included were carried out between 1991 and 2006. Single-city study estimates ranged between -0.66% and 2.57% per 10  $\mu\text{g m}^{-3}$ , while the multi-city study estimate was 1.59% per 10  $\mu\text{g m}^{-3}$ .

### 2.2.2 Premature Mortality Estimate

In order to calculate the health burden of short-term exposure from PM<sub>2.5</sub> three key factors were used. Firstly, the ‘safe limit’, known as the theoretical minimum risk exposure level (TMREL), below which there is no increase in mortality or morbidity. Secondly, the baseline mortality rate of the population exposed. Thirdly, a CRF, which relates population exposure above the ‘safe limit’ to an increase in mortality or morbidity.

Paper 3 and 4 used different CRFs (as discussed above). However, the CRFs were applied in the same way for both papers. For both papers, since there is little evidence to suggest a safe-limit of exposure to PM<sub>2.5</sub>, a TMREL ( $X_0$ ) of  $0.0 \mu\text{g m}^{-3}$  was assumed, in line with others (Borchers Arriagada, et al., 2020; Holgate, 1998; Macintyre, et al., 2016; Schmidt, et al., 2011). However, a sensitivity analysis was also carried out in paper 3 to investigate the impact of the assumed TMREL on the results, using a TMREL of 2.4 and  $5.9 \mu\text{g m}^{-3}$ . These values were chosen to match the lower and upper TMREL used in the Global Burden of Disease 2015 study (GBD Collaborators 2015, 2017). For Paper 3 the all-cause, all-age background mortality rate for north-west England was taken from the Global Burden of Disease (IHME, 2018). Whilst in paper 4 state specific all-cause, all-age background mortality rates were taken from the Australian Bureau of Statistics (Australian Bureau of Statistics, 2020).

In order to estimate the number of deaths brought forward due to exposure to PM<sub>2.5</sub> the CRF, TMREL and background mortality rate were combined together with population level exposure to PM<sub>2.5</sub> in three steps in Equation (11):

$$(a) \quad RR = \exp^{\beta(X-X_0)}$$

$$(b) \quad AF = \left(\frac{RR-1}{RR}\right) \quad (11)$$

$$(c) \quad E_m = \sum_{i=1}^N B_d \cdot pop_i \cdot AF_i$$

Firstly, the relative risk (RR) was calculated (Equation (11)(a)). This is the probability of mortality from a disease endpoint within an exposed population compared with the probability of mortality within an unexposed population ( $\beta$ ) (Equation (11)(a)).  $X$  is the concentration of  $PM_{2.5}$  the population is exposed to in a given grid box ( $i$ ) and  $X_0$  is the TMREL below which there is no risk from exposure. The beta values used were a 1.04% (95% CI: 0.52%, 1.56%) increase in mortality per  $10 \mu g m^{-3}$  increase in  $PM_{2.5}$  concentration in paper 3 (Atkinson, et al., 2014) and 1.0123% (95% CI: 1.0045%, 1.0201%) in paper 4 (World Health Organization, 2013). Most North American and Western European epidemiology studies clearly show a linear exposure-response relationship for short-term exposure to PM, without a threshold (Daniels et al. 2000; Pope and Dockery 2006; Samoli et al. 2005). Therefore, a linear exposure-response relationship was applied, like other studies (Crippa, et al., 2016; Macintyre, et al., 2016; Schmidt, et al., 2011).

Secondly, the relative risk was then used to calculate the attributable fraction (AF) (Equation (11)(b)). The AF is the fraction of the excess mortality attributable to exposure to  $PM_{2.5}$ . Finally, the AF was combined with population count, from each grid box, and the baseline mortality rate of the population to calculate the daily all-cause mortality burden of exposure to  $PM_{2.5}$ . Short-term health impacts are assumed to be equal across ages, therefore baseline all-cause, all-age mortality rates and population data for all ages were used in the calculations.

In both papers 3 and 4, the health impact assessment was carried out using the “subtraction” method, which is the one most commonly used in health impact studies (Crippa *et al.*, 2016; Macintyre *et al.*, 2016b; Conibear *et al.*, 2018a; Reddington *et al.*, 2019). The number of deaths brought forward due to exposure to PM<sub>2.5</sub> in the simulations with fire ( $E_{m \text{ FIRES}}$ ) and without fire ( $E_{m \text{ NO FIRES}}$ ) emissions were both calculated. The number of deaths brought forward due to PM<sub>2.5</sub> from fires alone ( $E_{m \text{ FIRES ONLY}}$ ) was then calculated as the difference between  $E_{m \text{ FIRES ON}}$  and  $E_{m \text{ FIRES OFF}}$  (Equation (12)).

$$E_{m \text{ FIRES ONLY}} = E_{m \text{ FIRES ON}} - E_{m \text{ FIRES OFF}} \quad (12)$$

### 2.2.3 Baseline Mortality Data

The 2015 baseline mortality rate data for north-west England was taken from the Institute for Health Metrics and Evaluation (IHME) (Institute for Health Metrics and Evaluation, 2018), originally from the Office of National Statistics (ONS) mortality statistics. The IHME is the overarching body responsible for the GBD studies and data stored by the IMHE is used in the Global Burden of Disease studies (GBD Collaborators 2015, 2016). Baseline mortality data for 2015 was used for this study since data for subsequent years is extrapolated.

State specific all-cause, all-age background mortality rates for 2018 were taken for Australia from the Australian Bureau of Statistics (Australian Bureau of Statistics, 2020) to match the method of Borchers Arriagada *et al.* (2020).

For both papers, the annual baseline mortality was equally divided by the number of days in the year as others have also done (Stedman, 2004; Macintyre *et al.*, 2016b; Pope *et al.*, 2016).

Uncertainties at the 95% confidence interval are provided in the IMHE baseline mortality data for north-west England and these were applied within the health impact assessment (11).

#### 2.2.4 Population Data

Population count data for north-west England was taken from the Gridded Population of the World dataset version 4 (GPWv4) at the Centre for International Earth Science Information Network () (v10.4) (CIESEN, 2018). GPWv4 is a minimally-modelled population dataset for the distribution of the human population on a continuous global raster (pixel) surface. In order to create a global dataset, population data was collected from the 2010 censuses (these were carried out between 2005 and 2014) at the highest possible resolution. Population estimates from the national statistics office or the United Nations were used for countries where census results were not available or yet released. In some countries, multiple levels of administrative data were available. In this case, the highest resolution data was always used for given regions in the country and was merged with lower level data for the rest of the country. Annualized growth rates were applied to the collected census data in order to account for discrepancies in when census data was available (since this was between 2005 and 2014). The annualized growth rate was then used to estimate the population count in the target years of 2000, 2005, 2010, 2015 and 2020 published in the GPWv4 dataset. The data was then proportionally allocated to pixels by uniform areal-weighting. The resulting population count estimates used in paper 3 were at 0.05° resolution for the year 2015.

Paper 4 used population count data for Australia from the Australian Bureau of Statistics (Australian Bureau of Statistics, 2019) to match the method of Borchers Arriagada *et al.* (2020). Population count data is from the 2016 census, with regional population growth applied each year. Population count data used were at 0.01° resolution for the year 2018.

## **Uncertainties**

Previous work has shown that the largest uncertainties in health impact assessments stem from the concentration-response function 95% CI ( $\pm 30\%$ ), rather than from model resolution (2.4%), vertical distribution of the PM<sub>2.5</sub> (0.6%) or resolution of the RR (0.8%) (Kushta, et al., 2018). Alongside this, uncertainty arises from the TMREL since it is not well established whether there is a safe level of exposure to PM<sub>2.5</sub> (Pope III, and Dockery, 2006; Schwarze, et al., 2006). Further work is required to reduce these uncertainties in the future.

# Impact of weather types on UK ambient particulate matter concentrations

**Ailish M. Graham<sup>1</sup>, Kirsty J. Pringle<sup>1</sup>, Stephen R. Arnold<sup>1</sup>,  
Richard J. Pope<sup>1,2</sup>, Massimo Vieno<sup>3</sup>, Edward W. Butt<sup>1</sup>, Luke  
Conibear<sup>1</sup>, Ellen L. Stirling<sup>1</sup> and James B. McQuaid<sup>1</sup>**

<sup>1</sup> School of Earth and Environment, University of Leeds, Leeds, LS2 9JT, UK

<sup>2</sup> National Centre for Earth Observation, University of Leeds, Leeds, LS2 9JT, UK

<sup>3</sup> Natural Environment Research Council, Centre for Ecology and Hydrology, Penicuik, EH26 0QB, UK

Correspondence to: Ailish M. Graham (ee15amg@leeds.ac.uk)

## 3.1 Abstract

Each year more than 29,000 premature deaths in the UK are linked to long term-exposure to ambient particulate matter (PM) with a diameter less than 2.5  $\mu\text{m}$  ( $\text{PM}_{2.5}$ ). Many studies have focused on the long-term impacts of exposure to PM, but short-term increases in pollution can also exacerbate health effects, leading to deaths brought forward within exposed populations. This study investigates the impact of different atmospheric circulation patterns on UK  $\text{PM}_{2.5}$  concentrations and the relative contribution of local and transboundary pollutants to variations in  $\text{PM}_{2.5}$  concentrations. Daily mean  $\text{PM}_{2.5}$  observations from 42 UK background sites indicate that easterly, south-easterly and southerly wind directions and anticyclonic circulation patterns enhance background concentrations of  $\text{PM}_{2.5}$  at all UK sites by up to 12  $\mu\text{g m}^{-3}$ . Results from back trajectory analysis and the European Monitoring and Evaluation Programme for UK model (EMEP4UK) show this is due to the transboundary transport of pollutants from continental Europe. While back trajectories indicate under easterly, south-easterly and

southerly flow 25-50% of the total accumulated primary PM<sub>2.5</sub> emissions originate outside of the UK, with a very polluted footprint (0.25-0.35 µg m<sup>-2</sup>). Anticyclonic conditions, which occur frequently (21%), also lead to increases in PM<sub>2.5</sub> concentrations (UK multi-annual mean 14.7 µg m<sup>-3</sup>). EMEP4UK results indicate this is likely due the build-up of local emissions due to slack winds. Under westerly and north-westerly flow 15-30% of the total accumulated primary PM<sub>2.5</sub> emissions originate outside of the UK, and are much less polluted (0.1 µg m<sup>-2</sup>) with model results indicating transport of clean maritime air masses from the Atlantic. Results indicate that both wind-direction and stability under anticyclonic conditions are important in controlling ambient PM<sub>2.5</sub> concentrations across the UK. There is also a strong dependence of high PM<sub>2.5</sub> Daily Air Quality Index (DAQI) values on easterly, south-easterly and southerly wind-directions, with >70% of occurrences of observed 48-71+ µg m<sup>-3</sup> concentrations occurring under these wind directions. While north-westerly and cyclonic conditions reduce PM<sub>2.5</sub> concentrations at all sites by up to 8 µg m<sup>-3</sup>. PM<sub>2.5</sub> DAQI values are also lowest under these conditions, with >80% of 0-11 µg m<sup>-3</sup> concentrations and >50% of 12 to 23 µg m<sup>-3</sup> concentrations observed during westerly, north-westerly and northerly wind directions. Indicating that these conditions are likely to be associated with a reduction in the potential health effects from exposure to ambient levels of PM<sub>2.5</sub>.

### **3.2 Introduction**

Air pollution is the fourth highest-ranking risk factor for mortality globally, with 85% of the global population living in areas where the WHO recommended air quality guidelines (10 µg m<sup>-3</sup> for particulate matter with a diameter less than 2.5 µm (PM<sub>2.5</sub>)) are exceeded (GBD Collaborators 2015, 2018). Exposure to air pollutants, including PM<sub>2.5</sub>, on both short and long-time scales has been shown to be strongly associated with mortality and morbidity (GBD Collaborators 2015, 2018). Exposure to PM<sub>2.5</sub> is associated with increases in diseases such as cardiovascular disease, ischemic heart disease, stroke, lower respiratory tract infections and

chronic obstructive pulmonary disorder (Atkinson, et al., 2014; GBD Collaborators 2015, 2017). In the UK, it is estimated that more than 29,000 premature deaths each year are linked to long term-exposure to ambient PM<sub>2.5</sub> (Committee on the Medical Effects of Air Pollutants, 2010). Short-lived high pollution episodes can lead to acute health impacts from exposure to PM<sub>2.5</sub> over shorter time periods, leading to deaths being brought forward among an exposed population (Stedman, 2004). PM<sub>2.5</sub> is composed of both solid and liquid droplets suspended in the atmosphere, which are small enough to be inhaled deep into the lungs (Raaschou-Nielsen, et al., 2013). Emissions of primary PM<sub>2.5</sub> and secondary PM<sub>2.5</sub> precursors come from a wide range of sources including combustion for power generation, heating and from vehicles, as well as dust and sea spray. There is little evidence to suggest which chemical constituents of the PM present an increased health risk and whether there is a safe limit of exposure for health effects (Committee on the Medical Effects of Air Pollutants, 2009).

Previous research on UK air pollution has focussed on the health impacts or mechanisms of short-term high pollution event case-studies (Stedman, 2004; Vieno *et al.*, 2016; Macintyre *et al.*, 2016b). Macintyre *et al.* (2016) found exposure to high PM<sub>2.5</sub> concentrations (maximum hourly concentration - 83 µg m<sup>-3</sup> at urban background sites) during a 10-day spring pollution episode in 2014 brought forward 600 deaths, 840 emergency respiratory and 730 emergency cardiovascular hospital admissions. This equated to a doubling of hospital admissions compared with those under typical springtime conditions. Stedman (2004) quantified the impact of high ozone and particulate matter with a diameter less than 10 µm (PM<sub>10</sub>) concentrations during the summer 2003 heatwave using a dose-response function. They found that 471 deaths were brought forward, attributable to exposure to PM<sub>10</sub> during the two-week pollution event, representing an increase of 207 deaths compared to the same period in 2002. This agrees with previous work that found a large proportion of the deaths brought forward

resulted from elevation of pollutant concentrations rather than the direct impact of high temperatures (Rooney, et al., 1998).

Since UK concentrations of PM<sub>2.5</sub> were not routinely monitored until 2008, when the New Air Quality Directive was introduced by the European Union, previous studies focussing on the drivers of high pollution episodes have analysed PM<sub>10</sub> observations. These studies used back trajectories to link observations of high PM<sub>10</sub> concentrations with possible source regions (King, and Dorling, 1997; Stedman, 1996). King and Dorling (1997) found that on days where PM<sub>10</sub> concentrations exceeded 50 µg m<sup>-3</sup> in 12 UK cities and at two rural sites, local emissions represented a small fraction of the total concentration and each episode was dominated by easterly flow. They suggested that, since the back trajectories emanated from mainland Europe, long-range transport has a large contribution in the overall PM<sub>10</sub> concentrations observed. They concluded that more work was required to confirm this, over a longer period with observations at rural sites.

Harrison *et al.* (2012) used 37 urban-background observational sites from the UK Automated Urban and Rural Network (AURN) to examine PM<sub>2.5</sub> concentrations for the year 2009 in order to better understand processes affecting concentrations across the UK. The study used meteorological data from 8 sites to determine the wind direction and wind speed at the AURN sites. They found that PM<sub>2.5</sub> concentrations were below the annual mean when winds were from westerly flows, while for south-easterly, easterly and north-easterly flows they were above the annual mean. This was attributed to emissions from continental Europe under easterly and south-easterly flow. The work of Harrison *et al.* (2012) suggest that the long-range transport of pollutants to the UK is associated with specific meteorological conditions. However, due to the short observational record at the time, the research used only one year of PM<sub>2.5</sub> observations, the sample size for individual wind directions was small. This meant

relationships between wind direction and PM<sub>2.5</sub> observations could not be established over a longer period of time to be statistically robust.

This study builds upon the work of Harrison *et al.* (2012) with observations that have increased coverage both spatially (42 sites compared to 37) and temporally (2010-2016). Additionally, we use Lamb Weather Types (LWTs) rather than local meteorological observations to investigate the relationship between synoptic meteorology and the transport of pollutants. LWTs reflect the synoptic-scale conditions, rather than local meteorology, and so are more closely related to the transport of pollutants.

In recent years Lamb weather types (LWT) (Lamb, 1972) and circulation weather types (CWT) have become an increasingly popular method of investigating the impact of regional atmospheric circulation patterns on pollutant concentrations (Demuzere *et al.*, 2009; Tang *et al.*, 2009; Tang, Rayner and Haeger-eugensson, 2011; Pope *et al.*, 2014; Russo *et al.*, 2014; Grundstrom *et al.*, 2015; Pope *et al.*, 2016; Grundström *et al.*, 2017). These can be used to classify synoptic scale atmospheric circulation patterns over regions such as the UK using wind direction, speed and circulation strength. The application of LWTs alongside observations of pollutant concentrations (PM<sub>10</sub>, NO<sub>2</sub>, O<sub>3</sub> and birch pollen) allows the association of different wind directions with the long-range transport of pollutants and the build-up or dispersion of pollutants for large areas. This allows relationships to be derived between specific weather types and higher pollutant concentrations over longer time periods. Previous work by Demuzere *et al.* (2009) in the Netherlands found that PM<sub>10</sub> concentrations increased when air was transported from the east and south during summer when there were dry conditions and high temperatures. Liu *et al.* (2017) also found that PM<sub>2.5</sub> concentrations in the United States were closely controlled by temperature, finding tropical weather types were associated with

significantly higher PM<sub>2.5</sub> concentrations and polar weather types with low PM<sub>2.5</sub> concentrations.

The UK, given its close proximity to Europe, is often subject to pollution episodes propagating from the continent. Pope *et al.* (2016, 2014) used LWTs to investigate the influence of meteorology on NO<sub>2</sub> and O<sub>3</sub> concentrations in the UK. The research found that both pollutants are strongly influenced by wind and circulation patterns. The highest O<sub>3</sub> concentrations occurred under summer anticyclonic conditions due to large scale subsidence limiting vertical mixing. The study also identified that south-easterly and north-easterly flow increased mean UK O<sub>3</sub> concentrations by between 10 to 15 µg m<sup>-3</sup> (Pope *et al.*, 2016). NO<sub>2</sub> concentrations were found to significantly increase under winter-time anticyclonic conditions through pollutant accumulation and were enhanced under south-easterly flow due to long-range transport of pollutants from continental Europe (Pope, et al., 2014). They attributed the winter increase to be a result of the combined effect of increased emissions, more stable conditions and decreased photolysis allowing accumulation over emission sources.

Here, we present the first study to use long-term (2010-2016) observations of PM<sub>2.5</sub>, subsampled under LWTs, back trajectories and an atmospheric chemistry transport model, to investigate how climatological weather regimes influence UK surface particulate matter air quality.

### **3.3 Data and Methods**

An overview of the methods used in this study can be found in Figure 23 for reference.

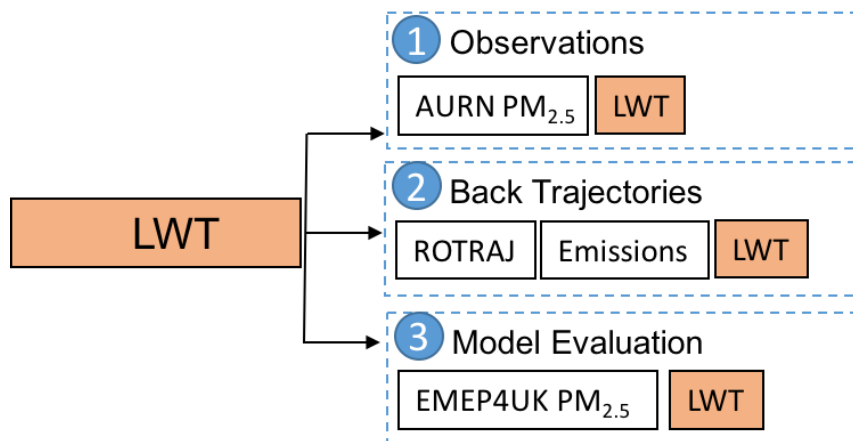


Figure 23. An overview of the datasets and method used in this study. Lamb weather types (LWT) are combined with observations of PM<sub>2.5</sub> concentrations from the Automated Urban and Rural Network (AURN), back trajectories from the Reading Offline Trajectory Model (ROTRAJ) and a gridded emission dataset. We also compare our results to a chemistry transport model (EMEP4UK).

### 3.3.1 Observations

#### 3.3.1.1 Lamb Weather Types

Lamb Weather Types (LWTs) are a synoptic classification of daily weather patterns across the UK (Lamb, 1972). LWTs are a useful tool for UK air pollution studies. They indicate the large-scale atmospheric flow and air mass origins, linking each air mass to specific dispersion conditions and mesoscale meteorology that control the regional transport of air pollution (Dayan, and Levy, 2004). In this work we use LWTs calculated automatically (using the algorithm from Jenkinson and Collinson (1977)) from NCEP reanalysis between 1948 and present (Jones, et al., 2013). NCEP reanalysis are available at 2.5° at 00, 06, 12 and 18Z each day (Kalnay, et al., 1996). The 12Z reanalysis is used to calculate the LWT each day. We have confidence in the reliability of LWT classification from NCEP reanalysis since Jones *et al.* (2013) found LWT calculated from NCEP reanalysis correlated well (0.65-0.79) with the subjective LWTs of Lamb (1972). Each LWT is calculated using the daily mean of three

variables from NCEP reanalysis, which characterise the circulation at the surface over the UK at 1200Z. Variables used are (i) the mean flow direction, (ii) the strength of mean flow and (iii) the mean strength of the circulation pattern (vorticity) (Jones, et al., 2013). Based on this analysis, conditions on a given day are classified as one of 28 LWTs. The 28 different LWTs comprise of three circulation types: Anticyclonic (0), Cyclonic (20) and Unclassified (-1), and eight wind types: N, NE, E, SE, S, SW, W, NW. We use a similar grouping method to O'Hare and Wilby (1995) and Pope *et al.* (2014), grouping the LWTs into eight wind types (Table 7). We however, use 0, 20 and -1 to classify the synoptic types, like Otero *et al.* (2018). This allows the independent examination of circulation and wind direction on pollutant concentrations.

Table 7. 27 LWT classifications (Jenkinson, and Collison, 1977), the 11 LWTs used in this study are indicated in **bold** (NE, E, SE, S, SW, W, NW, N, Anticyclonic, Neutral & Cyclonic). There are 8 wind types (NE, E, SE, S, SW, W, NW & N, shown in the left columns, and 2 circulation types (anticyclonic, cyclonic), in the top row, and unclassified days, where wind speed and shear were too low to allow classification. Following our grouping of LWT into 11 types, LWT index 3 (ASE) would fall under the anticyclonic and south-easterly classifications (see outer column and row of Table 7). There is also one other LWT (-9: non-existent day) not used in this study.

<b>This Study</b>	<b>Anticyclonic</b>	<b>Neutral</b>	<b>Cyclonic</b>
		-1 UC	
-	0 A	-	20 C
<b>NE</b>	1 ANE	11 NE	21 CNE
<b>E</b>	2 AE	12 E	22 CE
<b>SE</b>	3 ASE	13 SE	23 CSE
<b>S</b>	4 AS	14 S	24 CS
<b>SW</b>	5 ASW	15 SW	25 CSW
<b>W</b>	6 AW	16 W	26 CW
<b>NW</b>	7 ANW	17 NW	27 CNW
<b>N</b>	8 AN	18 N	28 CN

### 3.3.1.2 Automated Urban and Rural Network

We use observed PM<sub>2.5</sub> concentrations taken from the Automated Urban and Rural Network (AURN). AURN is the largest automated air quality monitoring network in the UK with 145 sites measuring species including PM<sub>2.5</sub>, NO<sub>2</sub>, SO<sub>2</sub> and O<sub>3</sub>. AURN sites are classified as urban traffic/kerbside, urban or suburban background, and rural background. For this study background sites are used (urban background, suburban background and rural background). Background sites are chosen as they are considered to be more representative of the surrounding region than kerbside sites. This is because their locations are chosen so as to be influenced by the integrated contribution of all sources upwind rather than by a single source or street (Department for Environment Food and Rural Affairs, 2018a). Data from 42 sites is used; 39 of which are urban background (UB), 2 rural background (RB) and 1 background suburban (BS) (Supplementary Material: Table 10). We use daily mean PM<sub>2.5</sub> concentrations (calculated from hourly measurements) from the 42 background sites for the period of 1<sup>st</sup> January 2010 – 31<sup>st</sup> December 2016. Quality assurance checks are performed by Department for Environment Food and Rural Affairs before data release (DEFRA, 2009). Thus, we only perform basic data quality control on the daily data on two different time scales: annual and monthly. For annual statistics, sites are only used if fewer than 10% of days (per year) are missing. Monthly data for seasonal statistics is only used if fewer than 10% of days (per month) have missing data.

## 3.4 Back Trajectories and Integrated Emissions

Reddington *et al.* (2014) showed that the use of back trajectories and emissions can be a powerful tool in understanding the influence of emissions on local air quality due to long-range transport in air masses arriving in Singapore. Following a similar method, we quantify the importance of the relationship between LWT and AURN PM<sub>2.5</sub> concentrations.

### 3.4.1 Emissions

Emissions from the National Atmospheric Emission Inventory (NAEI), European Monitoring and Evaluation Programme (EMEP) and Emission Database for Global Atmospheric Research with Task Force on Hemispheric Transport of Air Pollution (EDGAR-HTAP) are combined to create a gridded emission dataset (Figure 24). More details in Supplementary Material: Emissions section.

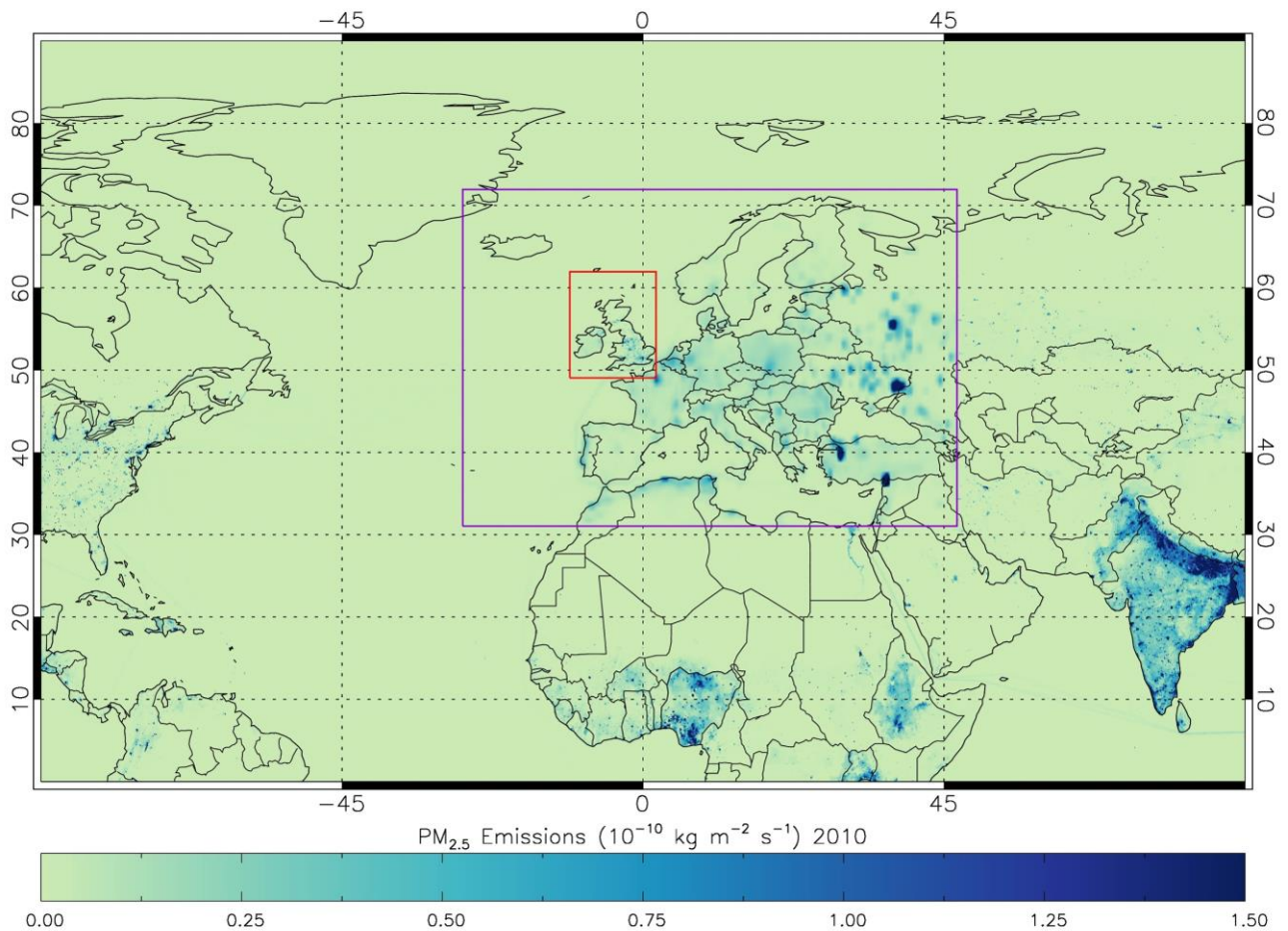


Figure 24. Gridded emissions of primary PM<sub>2.5</sub> for 2010 are shown as an example (annual varying emissions were used between 2010 and 2014). For the outer domain (Purple Box), gridded annual EMEP emissions at 0.5° resolution from the Centre for Emission Inventories and Projections (CEIP, [www.ceip.at](http://www.ceip.at)) are used. While for the inner domain (Red Box) gridded annual National Atmospheric Emissions Inventories (NAEI) emissions at 0.01° resolution are aggregated to 0.05° resolution. Emissions outside of Europe are provided by the Emission Database for Global Atmospheric Research with Task Force on Hemispheric Transport of Air Pollution (EDGAR-HTAP) version 2.2 emissions for 2010 at 0.1° resolution (Janssens-Maenhout, et al., 2015). More information in Supplementary Material: Emissions section.

### 3.4.2 Reading Offline Trajectory Model (ROTRAJ)

We combine back trajectories and bottom-up emission estimates in order to investigate the influence of long-range transport of pollutants on ambient pollutant concentrations under different LWTs in the UK. We use primary PM<sub>2.5</sub> emissions integrated over air mass back-trajectories to determine the relative influence of direct PM<sub>2.5</sub> emissions on air masses (i.e. ROTRAJ back trajectories) arriving at different times and locations over the UK. Back-trajectories are calculated using the ROTRAJ offline Lagrangian transport model (Methven, 2003). The model uses ERA-Interim reanalysis from the European Centre for Medium Range Weather Forecasting (ECMWF) to provide velocity fields for the simulations at 1.0125° horizontal resolution. After a trajectory parcel is released the location of each trajectory parcel is calculated every 6 hours by vertical cubic Lagrange interpolation and horizontal bilinear interpolation. This method accounts for large scale advection since the winds are resolved but does not resolve small scale sub-grid turbulent transport.

In this study, ROTRAJ back trajectories were initialised from just above the surface (0.99 sigma level; a terrain following coordinate system where 1 is the surface) at 12:00 UTC to match the LWT dataset between 2010 and 2014 at all background AURN sites (42 sites), extending back 4 days in 6-hourly time steps. PM<sub>2.5</sub> emissions were accumulated along each trajectory over 4 days at 15-minute time intervals (interpolated linearly from 6-hourly position output). PM<sub>2.5</sub> emissions were only accumulated when the trajectory path was at pressures

greater than 850 hPa (as an approximation of being within the boundary layer). At each location, we accumulate the entire emission within an emission grid box over which the trajectory passes. The surface area of each grid box that the trajectory points passed over is also accumulated over time. To approximate for dilution and chemical loss of PM<sub>2.5</sub> along the trajectory path, e-folding lifetimes were applied to the total PM<sub>2.5</sub> accumulated emission in the air parcel. A range of lifetimes of 1, 3, 7 and 14 days were applied to investigate the sensitivity of the final PM<sub>2.5</sub> accumulation, on arrival to the respective AURN sites, to loss processes (Supplementary Material: Sensitivity of Integrated Back Trajectories to assumed e-folding lifetime). The along-trajectory emission accumulation can be represented by Equation (13):

$$E_i = [E_{i-1} + \phi_i \cdot \Delta t \cdot \alpha_i] e^{-\Delta t / \tau} \quad (13)$$

$$i=1, N (=384) \text{ and } E_0=0.0$$

where  $E_N$  is total accumulated PM<sub>2.5</sub> mass (kg),  $N$  is the number of time steps within the trajectory (384),  $E_i$  is accumulated PM<sub>2.5</sub> (kg) at any given point  $i$  along the trajectory,  $\phi_i$  is the emissions flux of PM<sub>2.5</sub> (kg m<sup>-2</sup> s<sup>-1</sup>) at point  $i$ ,  $\Delta t$  is the 15-minute time step,  $\alpha_i$  is the surface area of the grid box (m<sup>2</sup>) at point  $i$  and  $\tau$  is the assumed e-folding PM<sub>2.5</sub> lifetime(s).

To remove the dependence on emission grid resolution (since we assumed the air mass has the same width as the emission grid box), the total accumulated PM<sub>2.5</sub> mass ( $E$ ) was divided by accumulated surface area ( $S$ ) and then scaled by 10<sup>9</sup>. This results in  $E$  having units of μg m<sup>-2</sup>.  $S$  is given by Equation (14):

$$S = \sum_{i=1}^N \alpha_i \quad (14)$$

$E_{UK}$  is also determined using the same approach, but only implemented when the trajectories enter the UK region defined by a longitudinal-latitude box (8°W-2°E, 50-60°N). To derive  $E_{UK}$  in units of  $\mu\text{g m}^{-2}$  the accumulated  $\text{PM}_{2.5}$  mass from the UK is divided by the accumulated surface area (S) over the full trajectory path. The ratio between  $E_{UK}/E$  represents the fractional contribution of UK sources towards the total accumulated  $\text{PM}_{2.5}$  emissions.

Finally, the daily (12:00 UTC) total accumulated emission and  $E_{UK}/E$  ratios from all sites are binned by the LWTs. This methodology provides a powerful tool to identify which flow directions, as classified by the LWTs, are the most polluted and the proportion of pollutant emissions from long range transport (e.g. continental Europe) versus local sources.

### 3.4.3 European Modelling and Evaluation Programme for the UK (EMEP4UK) $\text{PM}_{2.5}$ Data

Since the UK observational network is very sparse and so only gives limited spatial coverage we sample the European Modelling and Evaluation Programme for the UK (EMEP4UK) (v4.17) model (Centre for Ecology and Hydrology, 2018) under different LWTs to look further into the spatial distribution of  $\text{PM}_{2.5}$  concentrations. The model covers the UK at 0.05° resolution using a nested approach from the coarser European wide EMEP model (Simpson, et al., 2012). Further details of the model set-up can be found in the Supplementary Material: EMEP4UK Evaluation section.

We tested the model's skill in reproducing variability in UK  $\text{PM}_{2.5}$  concentrations both temporally and spatially. The model captures the variability in  $\text{PM}_{2.5}$  concentrations and their relationship with LWT well and shows strong correlation with observations and anomalies at

each site ( $r = 0.887$  and  $0.905$  respectively) with only a small negative bias ( $1 \mu\text{g m}^{-3}$ ) (Supplementary Material: EMEP4UK Evaluation section). Therefore, we can have good confidence in the model's ability to represent ambient  $\text{PM}_{2.5}$  concentrations.

### 3.5 Results

#### 3.6 AURN $\text{PM}_{2.5}$ Observations 2010-2016

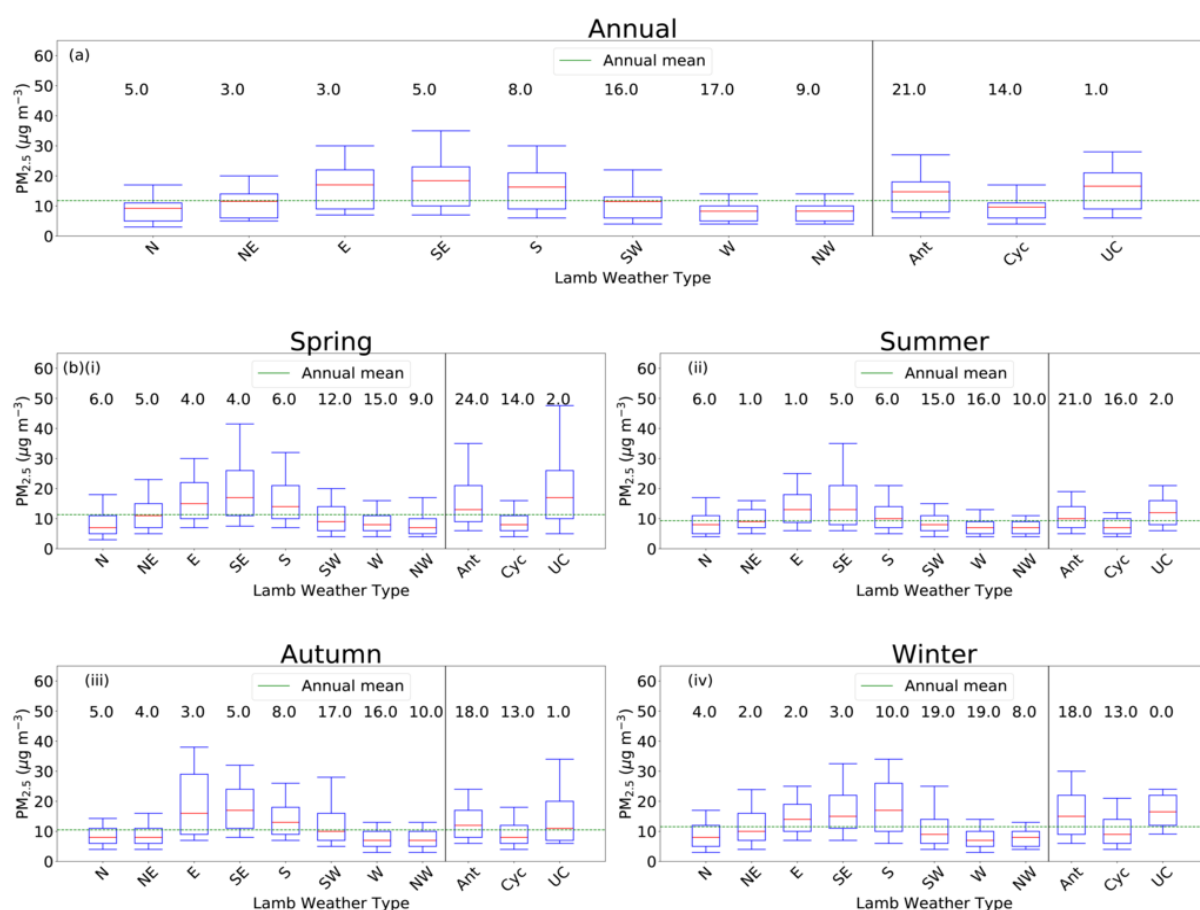


Figure 25. (a) Annual observations and (b) seasonal: (i) spring (ii) summer (iii) autumn (iv) winter observations of  $\text{PM}_{2.5}$  concentrations from 42 UK AURN sites between 2010-2016 under different Lamb Weather Types (LWTs) ( $\mu\text{g m}^{-3}$ ). Mean concentrations are shown in red, with the 10<sup>th</sup>, 25<sup>th</sup>, 75<sup>th</sup> and 90<sup>th</sup> percentiles in blue. The mean of all LWTs, is shown by the green dashed line. The frequency of each LWT (in %) for the 2010-2016 period, annually and seasonally is also indicated.

We find a strong dependency of observed PM<sub>2.5</sub> abundance on wind flow and circulation pattern, as characterised by the LWTs, with enhanced PM<sub>2.5</sub> concentrations under easterly, south-easterly and southerly flow and anticyclonic and unclassified weather types. Figure 25 (a) shows the daily mean AURN concentrations of PM<sub>2.5</sub> binned into the 11 different LWT regimes for the years 2010 to 2016. The multi-annual mean for all sites and all LWTs is 11 µg m<sup>-3</sup>. We find that the average PM<sub>2.5</sub> concentrations binned according to LWT regimes follow a coherent pattern; mean concentrations of PM<sub>2.5</sub> in easterly, southerly and south-easterly flow directions are elevated above the annual mean (15 to 20 µg m<sup>-3</sup>). Easterly, southerly and south-easterly flow regimes also have 90<sup>th</sup> percentile concentrations of 28 to 35 µg m<sup>-3</sup> (10 to 20 µg m<sup>-3</sup> higher than other flow directions). 10<sup>th</sup> percentile concentrations under these regimes are also elevated (2.5 to 4.5 µg m<sup>-3</sup> higher than other regimes). These flow types occur on 3, 5 and 8% days of the year. Northerly, north-easterly, south-westerly, westerly and north-westerly flows all give mean PM<sub>2.5</sub> concentrations below the multi-annual mean. The lowest concentrations in the 75<sup>th</sup> and 90<sup>th</sup> percentiles also occur under westerly, north-westerly and northerly flow types (<10.0, <11.0 & <20.0 µg m<sup>-3</sup> respectively). Westerly, north-westerly and south-westerly weather types occur on a larger proportion of days each year (17, 9 and 16% of days). Mean PM<sub>2.5</sub> concentrations are also affected by the circulation type; elevated concentrations are found under anticyclonic and unclassified conditions (mean concentrations of 14.7 and 16.6 µg m<sup>-3</sup>), exceeding the annual mean concentration. Although anticyclonic conditions are associated with lower mean PM<sub>2.5</sub> concentrations than easterly, south-easterly and southerly flow, they occur much more frequently (21% of days). Therefore, they have a more important contribution to the annual mean concentration and thus, the population's long-term exposure to PM<sub>2.5</sub>. In contrast, PM<sub>2.5</sub> below the annual mean concentrations are found under cyclonic flows (9.6 µg m<sup>-3</sup>), occurring on 14% of days.

The distribution of observed concentrations with LWT and proportion of occurrences of LWT for spring (MAM), summer (JJA) and winter (DJF) follows a similar pattern as that seen annually (Figure 25 (b) (i, ii, iv)), although there is some seasonal variability. In autumn (SON) (Figure 25 (b) (iii)) the highest PM<sub>2.5</sub> concentrations are found under easterly, south-easterly and unclassified flows, occurring 2-8% of the time. Whereas in winter the highest concentrations are found in southerly, south-easterly and anticyclonic flows, with a small increase in the number of occurrences of southerly types (10%). 90<sup>th</sup> percentile concentrations are highest in spring under the unclassified type and are the highest observed of any season (47.6 µg m<sup>-3</sup>), although they only occur 2% of the time.

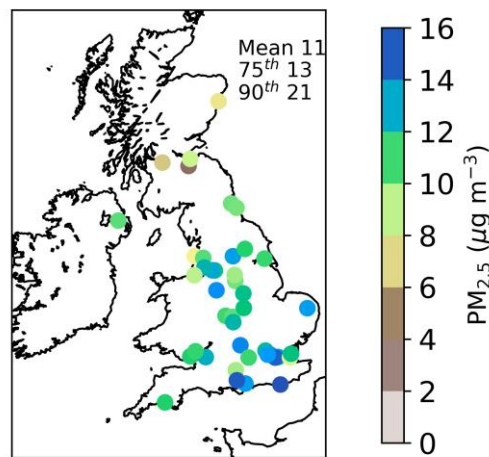


Figure 26. Multi-annual mean PM<sub>2.5</sub> concentrations from 42 UK AURN monitoring sites (2010-2016 average in µg m<sup>-3</sup>) averaged over all LWT regimes. The mean, 75<sup>th</sup> and 90<sup>th</sup> percentile PM<sub>2.5</sub> concentration calculated from all sites is shown on the top right of each panel.

Figure 26 shows the geographical distribution of annual mean PM<sub>2.5</sub> concentrations under all LWTs. Concentrations are highest in the south of England (12 to 16 µg m<sup>-3</sup>) and decrease northward, with the lowest concentrations observed in Scotland and Northern Ireland (0 to 4

$\mu\text{g m}^{-3}$ ). 33 of the 42 sites in England have multi-annual mean concentrations above  $10 \mu\text{g m}^{-3}$ , the WHO recommended limit, and 20 are above the multi-annual mean of all sites ( $11 \mu\text{g m}^{-3}$ ).

To examine the geographic distribution of the effect of LWT on  $\text{PM}_{2.5}$  concentrations (Figure 27 (a-f)), we calculate the  $\text{PM}_{2.5}$  anomaly under each LWT for individual sites with respect to the multi-annual mean concentration at that site (Figure 26). We also test for statistical significance at each AURN site under each LWT using a one million sample Monte Carlo simulation, in which we randomly sample  $\text{PM}_{2.5}$  concentrations for all LWT between 2010 and 2016 to build up a distribution of concentrations containing one million random samples. We then take the mean  $\text{PM}_{2.5}$  concentration for a given LWT and site (e.g. SE site 1), if this lies above the 95<sup>th</sup> or below the 5<sup>th</sup> percentile of the one million-sample distribution we can conclude that the concentration observed did not occur by chance and is significantly different statistically. The process is repeated for each LWT, creating a new distribution each time. Statistically significant anomalies ( $p < 0.05$ ) are subsequently circled in black (Figure 27 (a-f)). In line with the previous analysis,  $\text{PM}_{2.5}$  concentrations are enhanced by between 28-35% under easterly, south-easterly and southerly flow (Figure 27 (a), (b) and (c)). Some sites experience LWT flow direction anomalies of up to  $12 \mu\text{g m}^{-3}$  (Wigan Centre), and 40 of the 42 sites exhibit a positive anomaly under south-easterly and southerly flow with a mean anomaly of  $6.1 \mu\text{g m}^{-3}$  and  $4.4 \mu\text{g m}^{-3}$  respectively under these flows.  $\text{PM}_{2.5}$  concentrations are affected by LWT across the whole of the UK with the northernmost extent reaching to Scotland and Northern Ireland. Northerly, westerly and north-westerly are the three flow directions associated with the largest  $\text{PM}_{2.5}$  reductions ( $-5 \mu\text{g m}^{-3}$ , equivalent to a 30-44% reduction) (Figure 27 (e), (f) and (g)). The negative anomalies under these flow regimes are present at the same number of sites (40 of 42) but the anomaly is smaller in magnitude than the positive anomaly from the easterly, south-easterly and southerly flows with mean negative anomalies of  $-2$  to  $-3 \mu\text{g m}^{-3}$ .

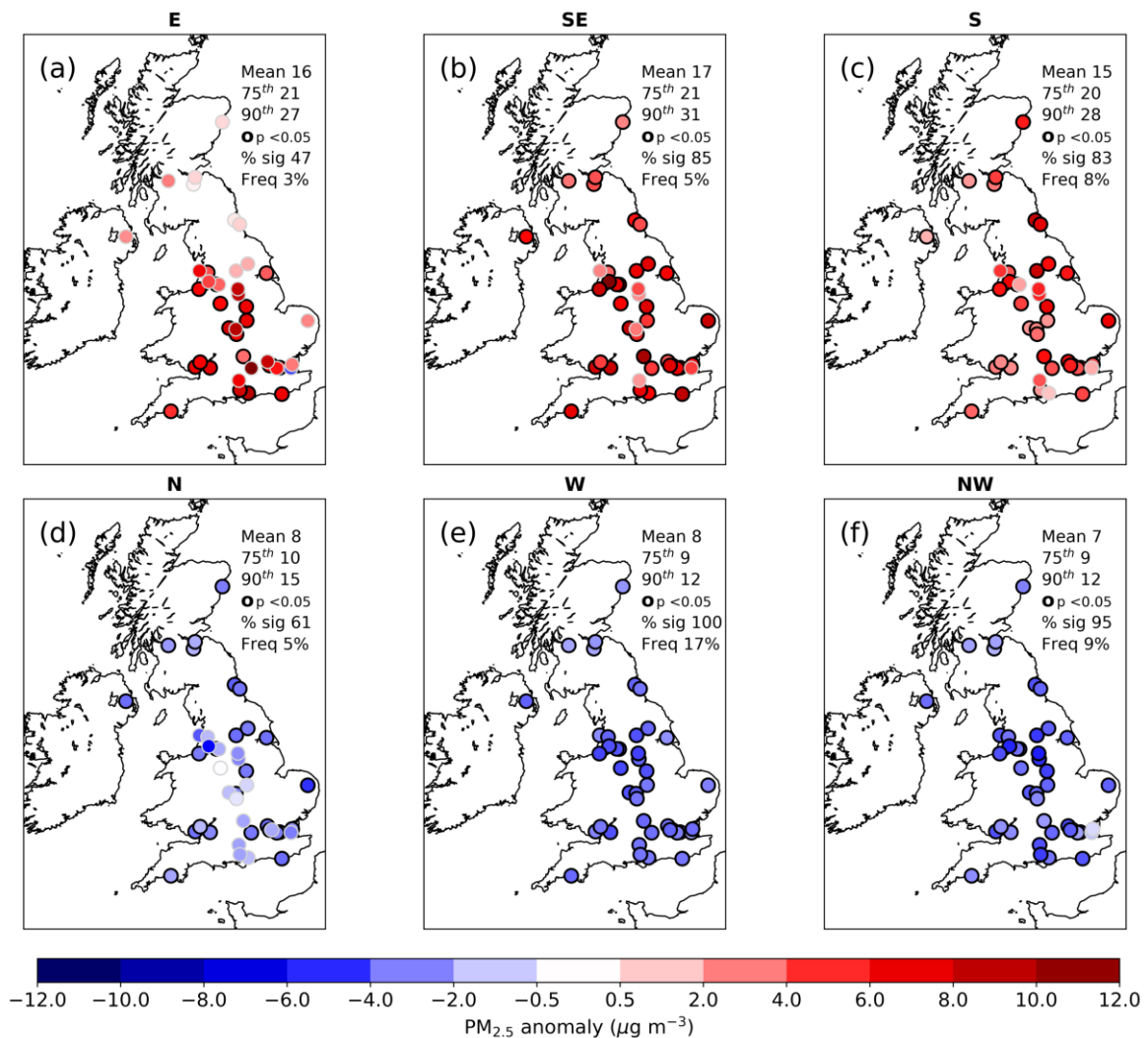


Figure 27. The multi-annual mean PM<sub>2.5</sub> anomaly relative to annual mean concentration averaged over all LWT regimes (relative to multi-annual mean concentration averaged over all LWT regimes (2010-2016) (in  $\mu\text{g m}^{-3}$ ), shown in Figure 26) under different flows directions is shown in panels (a) to (f). For clarity, we show the three flow directions with the largest positive anomaly ((a) easterly, (b) south-easterly and (c) southerly) and the three flow directions with the largest negative anomaly ((d) northerly, (e) westerly and (f) north-westerly). The mean, 75<sup>th</sup> and 90<sup>th</sup> percentile PM<sub>2.5</sub> concentrations calculated from all sites are shown on the top right of each panel. Sites where the anomaly is statistically significant ( $p < 0.05$ ) are indicated by black contouring and the percentage of sites where anomalies are statistically significant is also indicated in the top right panel (% sig). The frequency of each LWT (in %) for the 2010-2016 period is also indicated.

The effect of circulation pattern on PM<sub>2.5</sub> concentrations is generally weaker than that of flow direction. This suggests that long-range transport of PM<sub>2.5</sub> rather than the build-up of local pollutant emissions is more important in controlling PM<sub>2.5</sub> concentrations. Despite this, the

presence of anticyclonic and cyclonic conditions has an influence on PM<sub>2.5</sub> across the UK, with a maximum multi-annual anomaly of 4.6 and -4.4 μg m<sup>-3</sup> respectively (Figure 28 (a) and (b)). This represents a 20% increase and 24% decrease, respectively. Both of these flow types also occur more frequently (21% and 14%), meaning they are more important in contributing to the annual mean concentration and thus, the population's long-term exposure to PM<sub>2.5</sub>.

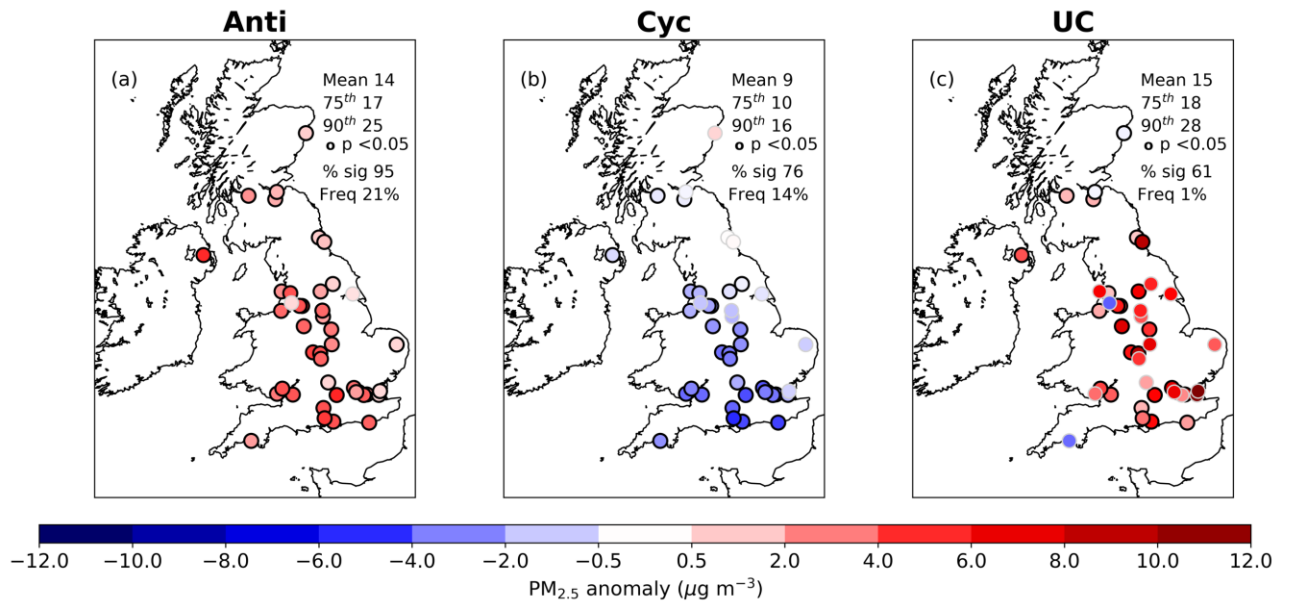


Figure 28. AURN annual mean PM<sub>2.5</sub> anomalies (relative to multi-annual mean concentration averaged over all LWT regimes (2010-2016 (in μg m<sup>-3</sup>), shown in Figure 26). Concentrations and anomalies sampled under (a) anticyclonic (b) cyclonic and (c) unclassified weather types are shown. The mean, 75<sup>th</sup> and 90<sup>th</sup> percentile PM<sub>2.5</sub> concentration calculated from all sites is shown on the top right of each panel. Sites where the anomaly is statistically significant (p < 0.05) are indicated by black contouring and the percentage of sites where anomalies are statistically significant is also indicated in the top right panel (% sig). The frequency of each LWT (in %) for the 2010-2016 period is also indicated.

### 3.6.1 Back Trajectories and Integrated Emissions

Variability in the back-trajectory integrated emissions sampled at the UK AURN sites further supports the relationships between in-situ observed  $PM_{2.5}$  and wind direction discussed above. Figure 29 shows the median accumulated primary  $PM_{2.5}$  emissions along ROTRAJ back trajectories arriving between 2010 and 2014, binned by the LWT flow directions. Here a representative 7-day e-folding lifetime (Seinfeld and Pandis, 2006) is used to approximate for physical/chemical loss processes from the air parcel. In the supplementary material (Supplementary Material: Sensitivity of Integrated Back Trajectories to assumed e-folding lifetime section) we explore the sensitivity of the accumulated  $PM_{2.5}$  emissions to different e-folding lifetimes. This showed that for shorter e-folding lifetimes (1 and 3 days) integrated emissions are dominated by UK emissions and there is little change between the total summed emission with different LWT. While, at larger e-folding lifetimes (7 and 14 days) the total integrated emission UK contribution and the total summed emission varies more between LWT. Since this method cannot account for secondary  $PM_{2.5}$ , the total accumulated  $PM_{2.5}$  emissions should be interpreted as a proxy of how polluted each air mass is, and the fractional contribution of emissions inside and outside of the UK to the total loading (akin to using CO as a tracer), rather than an estimate of  $PM_{2.5}$  in the atmosphere.

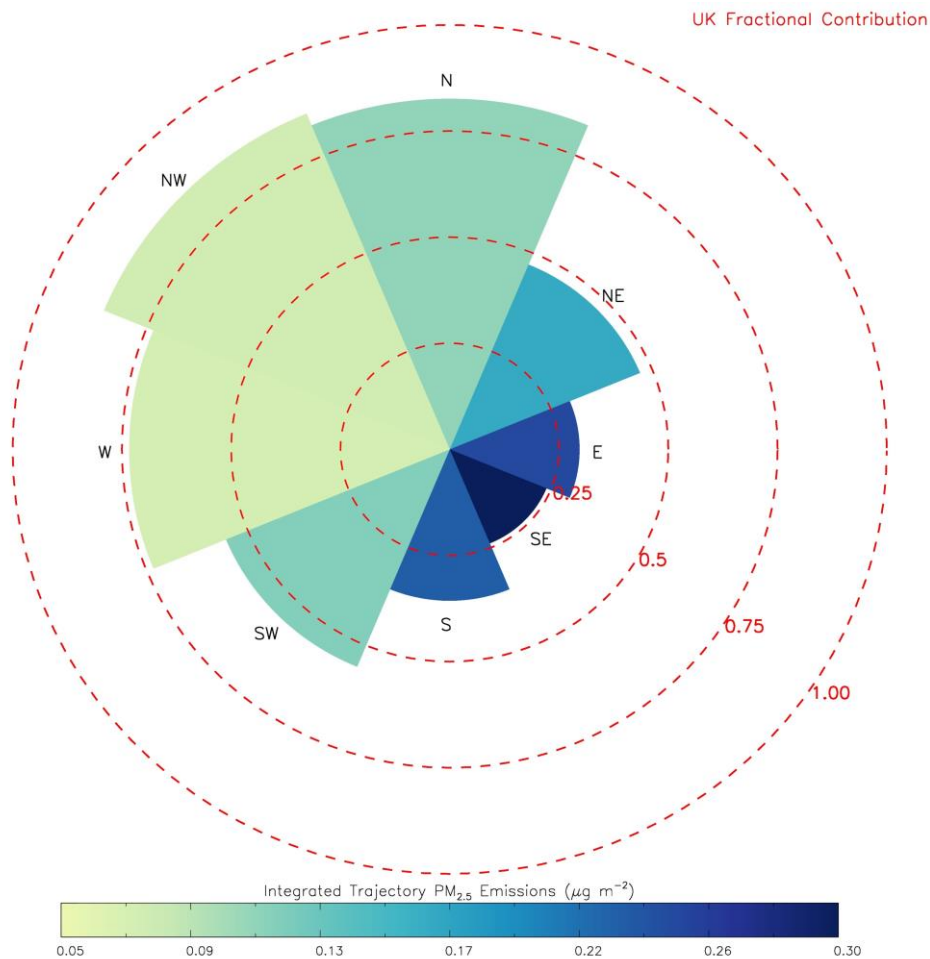


Figure 29. Median UK (background AURN sites) integrated PM<sub>2.5</sub> emissions (µg m<sup>-2</sup>) accumulated over the daily (12 UTC, 2010-2014) ROTRAJ back trajectories (4 days – 15-minute time steps), with a 7-day e-folding lifetime, binned by LWT flow directions. Red circles represent the UK fractional contribution to trajectory accumulated PM<sub>2.5</sub> emissions.

Overall, the results support the LWT-AURN PM<sub>2.5</sub> relationships with peak median accumulated emissions (*E*) from the south-easterly, southerly and easterly directions (0.25 to 0.3 µg m<sup>-2</sup> accumulated primary PM<sub>2.5</sub> emission). This supports the idea that continental European primary emissions are contributing to poor UK air quality when UK-bound air masses pass over polluted source regions (e.g. the Benelux region and west Germany). The fractional contribution from UK emissions under these flow directions is between 25-50%, indicating that under these flows more than 50% of emissions contributing to UK primary

particulate pollution originates in continental Europe. The north-westerly and westerly flow directions correspond to the cleanest air masses ( $< 0.1 \mu\text{g m}^{-2}$  accumulated primary  $\text{PM}_{2.5}$  emission), again in agreement with the LWT-AURN  $\text{PM}_{2.5}$ , as the back trajectories primarily originate from over the North Atlantic. Here, the UK fractional contribution is much larger ( $\sim 70\text{-}85\%$ ) as the majority of the accumulated  $\text{PM}_{2.5}$  emission ( $E$ ) is from within the UK domain (i.e.  $E_{UK}$  is relatively large). Exterior emissions sources will include Ireland and potentially sources where back trajectories tails originate in Europe, over source regions, but loop around to the UK west coast.

### 3.6.2 EMEP4UK modelled $\text{PM}_{2.5}$ and LWT

Since AURN observations give sparse coverage of the UK, we use EMEP4UK surface  $\text{PM}_{2.5}$  fields to further investigate the processes affecting ambient  $\text{PM}_{2.5}$  concentrations under different LWT classifications. In the supplementary material, we show that the model has skill in reproducing  $\text{PM}_{2.5}$  concentrations ( $r=0.887$ ) and anomalies ( $r=0.905$ ) under different LWTs when compared with AURN observations. Therefore, we have confidence in EMEP4UK's representation of ambient  $\text{PM}_{2.5}$  concentrations when sub-sampled under the LWTs.

EMEP4UK reproduces the back trajectory and AURN-LWT analysis with the largest positive  $\text{PM}_{2.5}$  anomalies observed under easterly, south-easterly and southerly weather types due to the long-range transport of  $\text{PM}_{2.5}$  from continental Europe (positive anomalies of  $6\text{-}12 \mu\text{g m}^{-3}$ ). The addition of the model 10-m winds, also sub-sampled under the LWTs, adds valuable information of the flow characteristics. Here, the flow clearly originates from the continent (typically around  $5 \text{ m s}^{-1}$ ) and is closely aligned with the spatial anomaly features (Figure 30).

The largest negative anomalies ( $-10$  to  $-4 \mu\text{g m}^{-3}$ ) are associated with the transport of clean air masses from the Atlantic, as indicated by the back-trajectory analysis. Northerly, north-westerly and westerly flow all have wind speeds between  $5$  and  $10 \text{ m s}^{-1}$  transporting  $\text{PM}_{2.5}$

offshore away from source regions. However, under north-easterly and south-westerly flow directions, a strong  $PM_{2.5}$  anomaly gradient can be observed across the UK. Negative anomalies ( $-6$  to  $-2 \mu\text{g m}^{-3}$ ) over the northern (south-western) UK represent the more gradual replacement of polluted air masses under north-easterly (south-westerly) flow. Transport of the polluted air mass yields positive anomalies ( $2$ - $6 \mu\text{g m}^{-3}$ ) over the southern (north-eastern) UK region. Here, the model adds important spatial details which are less reliably captured in the observations.

Circulation influences are also further investigated using the model, where anticyclonic conditions show reduced onshore transport of pollutants due to relatively weak easterly winds (under  $5 \text{ m s}^{-1}$ ) from continental Europe. This leads to conditions favourable for the build-up of  $PM_{2.5}$  ( $2$ - $6 \mu\text{g m}^{-3}$ ) predominantly from local emissions/formation. While under cyclonic conditions,  $PM_{2.5}$  is transported offshore, into the North Sea, by strong westerly winds ( $10 \text{ m s}^{-1}$ ) from the Atlantic leading to decreased concentrations over the UK mainland ( $-6$  to  $-2 \mu\text{g m}^{-3}$ ). Unclassified weather types are characterised by slack winds ( $0$ - $2 \text{ m s}^{-1}$ ) over the UK leading to the build-up of local emissions due to stagnant air masses ( $4$ - $10 \mu\text{g m}^{-3}$ ). This all further supports the importance of how flow characteristics (i.e. long-range transport and stagnation) influence UK  $PM_{2.5}$  concentrations.

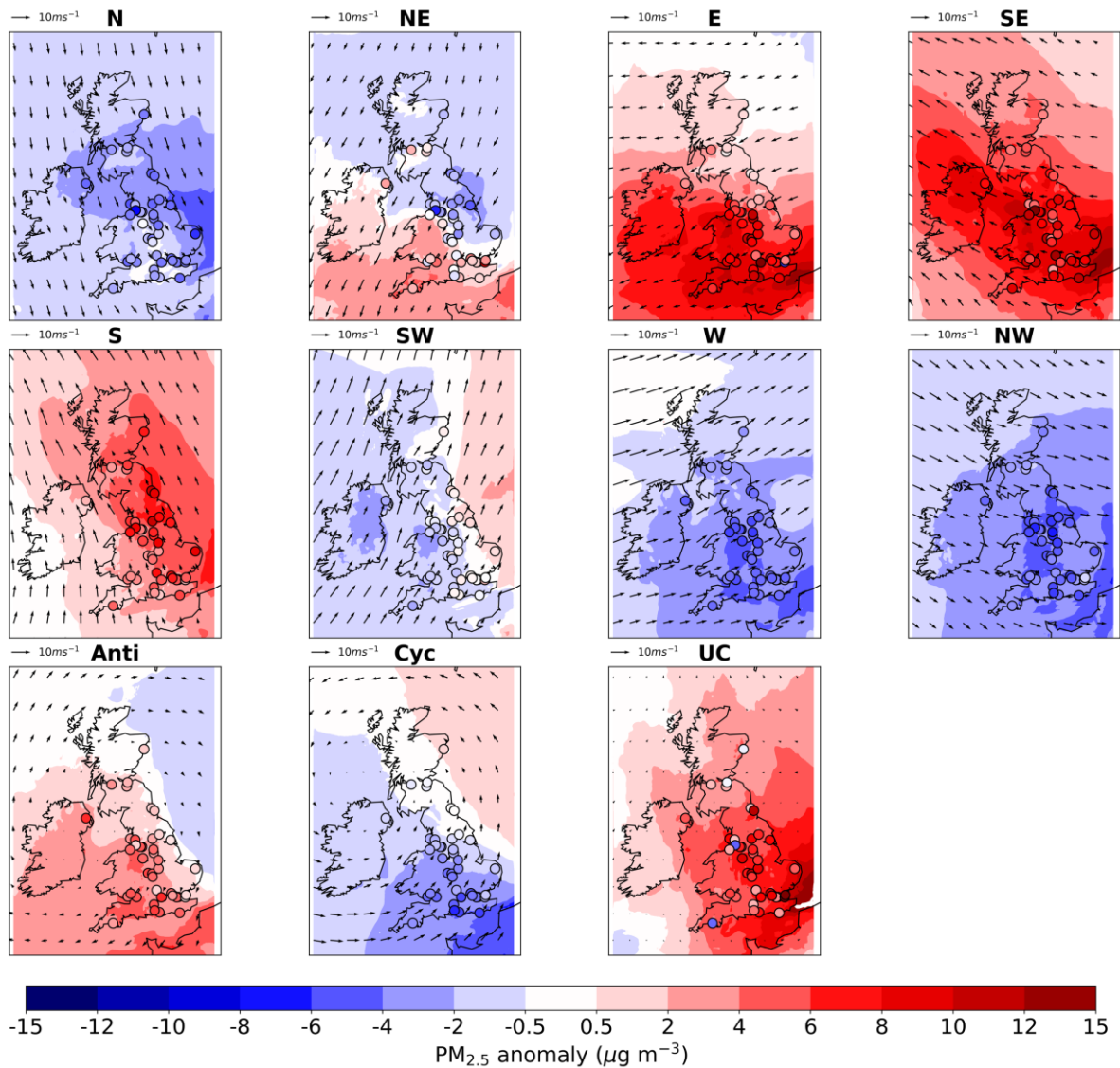


Figure 30. The multi-annual mean  $PM_{2.5}$  anomaly relative to annual mean concentration averaged over all LWT regimes (relative to multi-annual mean concentration averaged over all LWT regimes (2010-2016) (in  $\mu g m^{-3}$ )) under different flow directions from the EMEP4UK model. 10m winds, also from the EMEP4UK model (nudged to 3-hourly GFS analysis), are over plotted. All LWT wind directions and synoptic types are shown.

### 3.6.3 Contribution of LWTs to the Daily Air Quality Index (DAQI)

To put the results of AURN PM<sub>2.5</sub> Observations 2010-2016 in a public health context, we bin the daily mean PM<sub>2.5</sub> concentrations under the different LWTs according to the 10 UK Daily Air Quality Index (DAQI) PM<sub>2.5</sub> concentration bands. The UK Daily Air Quality Index (DAQI) is a public health air quality warning system used by the UK Department for Environment, Food and Rural Affairs (DEFRA) to communicate current and future pollutant levels in the UK to the general public (COMEAP, 2011). Five key pollutants have been identified to monitor by the Committee on the Medical Effects of Air Pollutants (PM<sub>10</sub>, O<sub>3</sub>, NO<sub>x</sub>, SO<sub>2</sub> and PM<sub>2.5</sub>). In order to gain an overall DAQI each of these pollutants are given an individual score between 1 (low) and 10 (very polluted). The overall DAQI is then assigned based on the highest individual DAQI value for each of the 5 pollutants at a given time. For example, if O<sub>3</sub> scored a DAQI value of 9, and all other species scored a value of 2, the overall DAQI would be 9. As we only investigate PM<sub>2.5</sub>, we can only comment on the effect of LWT on PM<sub>2.5</sub> within the DAQI (PM DAQI). However, since the DAQI score is assigned the highest individual species score from each of the 5 pollutants, air masses with high or very high PM<sub>2.5</sub> scores are likely to have the same overall DAQI score.

We find that 71% of days classed as “very polluted” (PM DAQI of 10) occur with south easterly, southerly and south westerly flows, whereas only 12% of days with the cleanest air (PM DAQI of 1) occur with these air masses (Figure 31). North westerly, northerly and westerly air flows dominate the cleanest air days (59% of days with PM DAQI of 1 occur with these flows) and there are no occurrences of the highest PM DAQI values (9 and 10) on days with north westerly, northerly or westerly air flows (Figure 31). For PM DAQI values of 4 and above, at-risk individuals (e.g. those with asthma or heart conditions) are advised to reduce strenuous activity if they experience symptoms. These results suggest a strong dependence of periods of increased risk for such individuals on meteorological conditions.

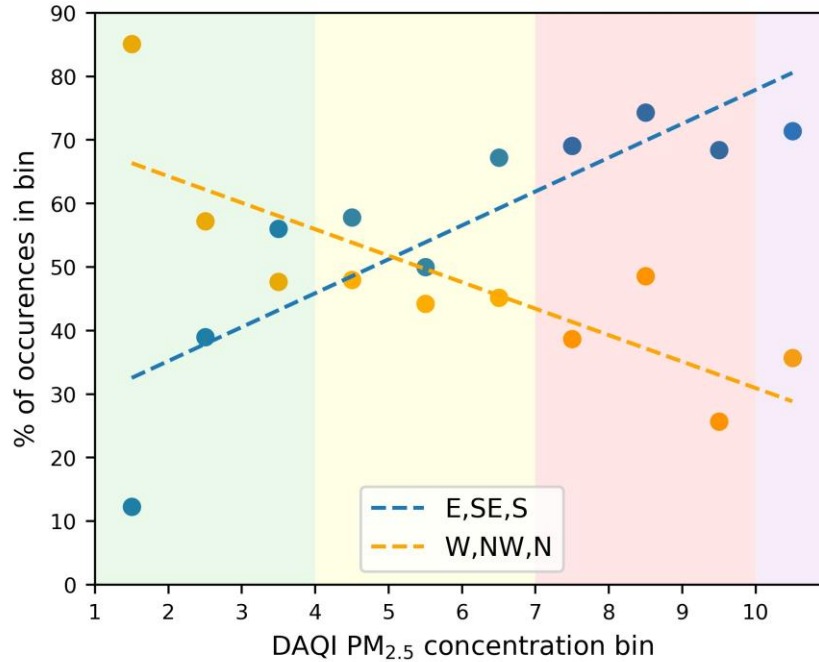


Figure 31. Percentage occurrence (defined as the percentage of occurrences of easterly, south-easterly and southerly (and westerly north-westerly and northerly) LWTs in each bin) of easterly, south-easterly and southerly weather types and westerly, north-westerly and northerly in each DAQI PM<sub>2.5</sub> concentration bin. Bins 1-10 indicate PM<sub>2.5</sub> concentrations of 0-11, 12-23, 24-35, 36-41, 42-47, 48-53, 54-58, 59-64, 65-70, >71 (all in  $\mu\text{g m}^{-3}$ ).

## Discussion and Conclusions

This study investigated the role that synoptic weather plays in controlling variability of ambient PM<sub>2.5</sub> concentrations in the UK.

Observations of PM<sub>2.5</sub> concentrations under different LWTs indicate that both annually and seasonally, anticyclonic circulation and easterly, south-easterly and southerly flow increase the mean PM<sub>2.5</sub> concentrations observed. Results from the EMEP4UK model suggest transboundary transport is likely responsible for the increases in PM<sub>2.5</sub> observed under the wind types (easterly, south-easterly and southerly flow) and the build-up of local emissions under

stagnant air masses under anticyclonic and unclassified types. Results also indicate that although PM<sub>2.5</sub> concentrations are higher under easterly, south-easterly and southerly flow than under anticyclonic conditions, anticyclonic conditions occur on a much larger fraction of days and so have a larger impact on the annual PM<sub>2.5</sub> concentration and the population's exposure to increased PM<sub>2.5</sub> concentrations. These findings are in agreement with previous work which has examined different species and short-lived pollution episodes as case studies (Vieno *et al.*, 2010, 2014; Pope *et al.*, 2014; Vieno *et al.*, 2016; Pope *et al.*, 2016). Pope *et al.* (2014) also found that under anticyclonic conditions NO<sub>2</sub> concentrations were significantly increased through pollutant accumulation and that south-easterly flow enhanced NO<sub>2</sub> concentrations. They attributed this to long-range transport from continental Europe. A similar relationship was found for ozone in summer months, with enhanced concentrations under north-easterly and south-easterly flow and anticyclonic conditions leading to increased ozone concentrations due to large scale subsidence and little vertical mixing (Pope *et al.*, 2016). Demuzere *et al.* (2009) found PM<sub>10</sub> concentrations were highest in the Netherlands under easterly, south-easterly and southerly wind directions, attributing the increase in PM<sub>10</sub> concentrations to air masses passing over large source regions.

The results of the back-trajectory analysis indicate that the transport of pollutants from large source regions outside of the UK is an important contributor to the total accumulated emission under easterly, south-easterly and southerly flow. Since secondary PM<sub>2.5</sub> typically represents 3 - 8 µg m<sup>-3</sup> (20-50%) of the total PM<sub>2.5</sub> concentration at background sites in Europe (Querol, *et al.*, 2004) a method accounting for secondary PM<sub>2.5</sub> (nitrate, sulphate and ammonium) would need to be applied to quantify the contribution of non-UK emissions to total PM<sub>2.5</sub> in the UK. Nevertheless, our results suggest a substantial non-UK burden on UK pollution under continental air masses.

This study further reinforces that synoptic weather in the UK plays an important role in controlling PM<sub>2.5</sub>. It is important, therefore, that air quality models are able to accurately simulate synoptic meteorology in order to reliably forecast PM<sub>2.5</sub> concentrations in forecasts. Given the large impact on health that short-term exposure to PM<sub>2.5</sub> has been shown to have in previous studies (e.g. Macintyre *et al.* (2016)), the ability of air quality forecast models to accurately predict PM<sub>2.5</sub> concentrations is key in preparing for and mitigating the associated health impacts of exposure.

The results of the back-trajectory analysis indicate that quantifying the contribution of UK and non-UK pollution sources is extremely important in evaluating the impact of local emission controls on UK pollutant concentrations. This is particularly relevant given that we have shown variations in background PM<sub>2.5</sub> concentrations are highly variable under different weather patterns.

### **3.7 Acknowledgements**

We acknowledge the use of AURN PM<sub>2.5</sub> data from the Department for Environment, Food and Rural Affairs (<https://uk-air.defra.gov.uk/data>), as well as the Lamb Weather Type Dataset from the Climate and Research Unit (<https://crudata.uea.ac.uk/cru/data/lwt>).

This work was supported by NCEO and the Natural Environment Research Council award number NE/R016429/1 as part of the UK-SCaPE programme delivering National Capability.

### 3.8 References

- 1) Atkinson, R.W., Kang, S., Anderson, H.R., Mills, I.C., Walton, H.A., 2014. Epidemiological time series studies of PM<sub>2.5</sub> and daily mortality and hospital admissions: A systematic review and meta-analysis. *Thorax* 69, 660–665. <https://doi.org/10.1136/thoraxjnl-2013-204492>
- 2) Centre for Ecology and Hydrology, 2018. The European Monitoring and Evaluation Programme for the UK (EMEP4UK) [WWW Document]. URL <http://www.emep4uk.ceh.ac.uk/> (accessed 12.1.18).
- 3) Cohen, A.J., Brauer, M., Burnett, R., Anderson, H.R., Frostad, J., Estep, K., Balakrishnan, K., Brunekreef, B., Dandona, L., Dandona, R., Feigin, V., Freedman, G., Hubbell, B., Jobling, A., Kan, H., Knibbs, L., Liu, Y., Martin, R., Morawska, L., Pope III, C.A., Shin, H., Straif, K., Shaddick, G., Thomas, M., van Dingenen, R., van Donkelaar, A., Vos, T., Murray, C.J.L., Forouzanfar, M.H., 2017. Estimates and 25-year trends of the global burden of disease attributable to ambient air pollution: an analysis of data from the Global Burden of Diseases Study 2015. *Lancet* 389, 1907–1918. [https://doi.org/10.1016/S0140-6736\(17\)30505-6](https://doi.org/10.1016/S0140-6736(17)30505-6)
- 4) Committee on the Medical Effects of Air Pollutants, 2010. The Mortality Effects of Long-Term Exposure to Particulate Air Pollution in the United Kingdom. [https://doi.org/ISBN 978-0-85951-685-3](https://doi.org/ISBN%20978-0-85951-685-3)
- 5) Committee on the Medical Effects of Air Pollutants, 2009. Long-term Exposure to Air Pollution: Effect on Mortality.
- 6) Dayan, U., Levy, I., 2004. The Influence of Meteorological Conditions and Atmospheric Circulation Types on PM<sub>10</sub> and Visibility in Tel Aviv. *J. Appl. Meteorol.* 44, 606–619.
- 7) Demuzere, M., Trigo, R.M., Vila-Guerau de Arellano, J., van Lipzig, N.P.M., 2009. The impact of weather and atmospheric circulation on O<sub>3</sub> and PM<sub>10</sub> levels at a rural mid-latitude site. *Atmos. Chem. Phys.* 9, 2695–2714. <https://doi.org/10.5194/acp-9-2695-2009>

- 8) Department for Environment Food and Rural Affairs, 2018. Pollutant information.
- 9) Department for Environment Food and Rural Affairs, 2011. Emissions of Air Quality Pollutants.
- 10) Grundström, M., Dahl, Å., Ou, T., Chen, D., Pleijel, H., 2017. The relationship between birch pollen, air pollution and weather types and their effect on antihistamine purchase in two Swedish cities. *Aerobiologia (Bologna)*. 33, 457–471. <https://doi.org/10.1007/s10453-017-9478-2>
- 11) Grundstrom, M., Tang, L., Hallquist, M., Nguyen, H., Chen, D., Pleijel, H., 2015. Influence of atmospheric circulation patterns on urban air quality during the winter. *Atmos. Pollut. Res.* 6, 278–285. <https://doi.org/10.5094/APR.2015.032>
- 12) Harrison, R.M., Laxen, D., Moorcroft, S., Laxen, K., 2012. Processes affecting concentrations of fine particulate matter (PM<sub>2.5</sub>) in the UK atmosphere. *Atmos. Environ.* 46, 115–124. <https://doi.org/10.1016/j.atmosenv.2011.10.028>
- 13) Janssens-Maenhout, G., Crippa, M., Guizzardi, D., Dentener, F., Muntean, M., Pouliot, G., Keating, T., Zhang, Q., Kurokawa, J., Wankmüller, R., Denier Van Der Gon, H., Kuenen, J.J.P., Klimont, Z., Frost, G., Darras, S., Koffi, B., Li, M., 2015. HTAP-v2.2: A mosaic of regional and global emission grid maps for 2008 and 2010 to study hemispheric transport of air pollution. *Atmos. Chem. Phys.* 15, 11411–11432. <https://doi.org/10.5194/acp-15-11411-2015>
- 14) Jenkinson, A., Collison, F., 1977. An Initial Climatology of Gales over the North Sea, Synoptic Branch Memorandum.
- 15) Jones, P.D., Harpham, C., Briffa, K.R., 2013. Lamb weather types derived from reanalysis products. *Int. J. Climatol.* 33, 1129–1139. <https://doi.org/10.1002/joc.3498>

- 16) Kalnay, E., Collins, W., Deaven, D., Gandin, L., Iredell, M., Jenne, R., Joseph, D., 1996. The NCEP NCAR 40-year reanalysis project. *Bull. Am. Meteorol. Soc.* 77, 437–472.
- 17) King, A., Dorling, S., 1997. New directions special issue on the origins of PM<sub>10</sub> particulate matter: particulate matter PM<sub>10</sub> - the significance of ambient levels. *Atmos. Environ.* 31, 2379–2381. [https://doi.org/10.1016/S1352-2310\(97\)00001-0](https://doi.org/10.1016/S1352-2310(97)00001-0)
- 18) Lamb, H., 1972. British Isles weather types and a register of daily sequence of circulation patterns. *Geophys. Mem.* 116, 1861–1971.
- 19) Liu, Y., Zhao, N., Vanos, J.K., Cao, G., 2017. Effects of synoptic weather on ground-level PM<sub>2.5</sub> concentrations in the United States. *Atmos. Environ.* 148, 297–305. <https://doi.org/10.1016/j.atmosenv.2016.10.052>
- 20) Macintyre, H.L., Heaviside, C., Neal, L.S., Agnew, P., Thornes, J., Vardoulakis, S., 2016. Mortality and emergency hospitalizations associated with atmospheric particulate matter episodes across the UK in spring 2014. *Environ. Int.* 97, 108–116. <https://doi.org/10.1016/j.envint.2016.07.018>
- 21) Methven, J., 2003. Estimating photochemically produced ozone throughout a domain using flight data and a Lagrangian model. *J. Geophys. Res.* 108, 4271. <https://doi.org/10.1029/2002JD002955>
- 22) O’Hare, G., Wilby, R., 1995. A Review of Ozone Pollution in the United Kingdom and Ireland with an Analysis Using Lamb Weather Types. *Geogr. J.* 161, 1–20.
- 23) Otero, N., Sillmann, J., Butler, T., 2018. Assessment of an extended version of the Jenkinson–Collinson classification on CMIP5 models over Europe. *Clim. Dyn.* 50, 1559–1579. <https://doi.org/10.1007/s00382-017-3705-y>
- 24) Pope, R.J., Butt, E.W., Chipperfield, M.P., Doherty, R.M., Fenech, S., Schmidt, A., Arnold, S.R., Savage, N.H., 2016. The impact of synoptic weather on UK surface ozone and

implications for premature mortality. *Environ. Res. Lett.* 11, 124004.

<https://doi.org/10.1088/1748-9326/11/12/124004>

- 25) Pope, R.J., Savage, N.H., Chipperfield, M.P., Arnold, S.R., Osborn, T.J., 2014. The influence of synoptic weather regimes on UK air quality: Analysis of satellite column NO<sub>2</sub>. *Atmos. Sci. Lett.* 15, 211–217. <https://doi.org/10.1002/asl2.492>
- 26) Querol, X., Alastuey, A., Ruiz, C.R., Artiñano, B., Hansson, H.C., Harrison, R.M., Buringh, E., Ten Brink, H.M., Lutz, M., Bruckmann, P., Straehl, P., Schneider, J., 2004. Speciation and origin of PM<sub>10</sub> and PM<sub>2.5</sub> in selected European cities. *Atmos. Environ.* 38, 6547–6555. <https://doi.org/10.1016/j.atmosenv.2004.08.037>
- 27) Raaschou-Nielsen, O., Andersen, Z.J., Beelen, R., Samoli, E., Stafoggia, M., Weinmayr, G., Hoffmann, B., Fischer, P., Nieuwenhuijsen, M.J., Brunekreef, B., Xun, W.W., Katsouyanni, K., Dimakopoulou, K., Sommar, J., Forsberg, B., Modig, L., Oudin, A., Oftedal, B., Schwarze, P.E., Nafstad, P., De Faire, U., Pedersen, N.L., Östenson, C.G., Fratiglioni, L., Penell, J., Korek, M., Pershagen, G., Eriksen, K.T., Sørensen, M., Tjønneland, A., Ellermann, T., Eeftens, M., Peeters, P.H., Meliefste, K., Wang, M., Bueno-de-Mesquita, B., Key, T.J., de Hoogh, K., Concin, H., Nagel, G., Vilier, A., Grioni, S., Krogh, V., Tsai, M.Y., Ricceri, F., Sacerdote, C., Galassi, C., Migliore, E., Ranzi, A., Cesaroni, G., Badaloni, C., Forastiere, F., Tamayo, I., Amiano, P., Dorronsoro, M., Trichopoulou, A., Bamia, C., Vineis, P., Hoek, G., 2013. Air pollution and lung cancer incidence in 17 European cohorts: Prospective analyses from the European Study of Cohorts for Air Pollution Effects (ESCAPE). *Lancet Oncol.* 14, 813–822. [https://doi.org/10.1016/S1470-2045\(13\)70279-1](https://doi.org/10.1016/S1470-2045(13)70279-1)
- 28) Reddington, C.L., Yoshioka, M., Balasubramanian, R., Ridley, D., Toh, Y.Y., Arnold, S.R., Spracklen, D. V., 2014. Contribution of vegetation and peat fires to particulate air pollution in Southeast Asia. *Environ. Res. Lett.* 9, 094006. <https://doi.org/10.1088/1748-9326/9/9/094006>

- 29) Rooney, C., McMichael, A.J., Kovats, R.S., Coleman, M.P., 1998. Excess mortality in England and Wales, and in Greater London, during the 1995 heatwave. *J. Epidemiol. Community Health* 52, 482–486. <https://doi.org/10.1136/jech.52.8.482>
- 30) Russo, A., Trigo, R.M., Martins, H., Mendes, M.T., 2014. NO<sub>2</sub>, PM<sub>10</sub> and O<sub>3</sub> urban concentrations and its association with circulation weather types in Portugal. *Atmos. Environ.* 89, 768–785. <https://doi.org/10.1016/j.atmosenv.2014.02.010>
- 31) Simpson, D., Benedictow, A., Berge, H., Bergström, R., Emberson, L.D., Fagerli, H., Flechard, C.R., Hayman, G.D., Gauss, M., Jonson, J.E., Jenkin, M.E., Nyúri, A., Richter, C., Semeena, V.S., Tsyro, S., Tuovinen, J.P., Valdebenito, A., Wind, P., 2012. The EMEP MSC-W chemical transport model Technical description. *Atmos. Chem. Phys.* 12, 7825–7865. <https://doi.org/10.5194/acp-12-7825-2012>
- 32) Stanaway, J.D., Afshin, A., Gakidou, E., Lim, S.S., Abate, D., Abate, K.H., Abbafati, C., Abbasi, N., Abbastabar, H., Abd-Allah, F., Abdela, J., Abdelalim, A., Abdollahpour, I., Abdulkader, R.S., Abebe, M., Abebe, Z., Abera, S.F., Abil, O.Z., Abraha, H.N., Abrham, A.R., Abu-Raddad, L.J., Abu-Rmeileh, N.M.E., Accrombessi, M.M.K., Acharya, D., Acharya, P., Adamu, A.A., Adane, A.A., Adebayo, O.M., Adedoyin, R.A., Adekanmbi, V., Ademi, Z., Adetokunboh, O.O., Adib, M.G., Admasie, A., Adsuar, J.C., Afanvi, K.A., Afarideh, M., Agarwal, G., Aggarwal, A., Aghayan, S.A., Agrawal, A., Agrawal, S., Ahmadi, A., Ahmadi, M., Ahmadieh, H., Ahmed, M.B., Aichour, A.N., Aichour, I., Aichour, M.T.E., Akbari, M.E., Akinyemiju, T., Akseer, N., Al-Aly, Z., Al-Eyadhy, A., Al-Mekhlafi, H.M., et al., 2018. Global, regional, and national comparative risk assessment of 84 behavioural, environmental and occupational, and metabolic risks or clusters of risks for 195 countries and territories, 1990-2017: A systematic analysis for the Global Burden of Disease Stu. *Lancet* 392, 1923–1994. [https://doi.org/10.1016/S0140-6736\(18\)32225-6](https://doi.org/10.1016/S0140-6736(18)32225-6)

- 33) Stedman, J.R., 2004. The predicted number of air pollution related deaths in the UK during the August 2003 heatwave. *Atmos. Environ.* 38, 1087–1090.  
<https://doi.org/10.1016/j.atmosenv.2003.11.011>
- 34) Stedman, J.R., 1996. A UK-wide episode of elevated particulate matter (PM) concentrations in March 1996. *Science*. 80. [https://doi.org/https://doi.org/10.1016/S1352-2310\(97\)88638-4](https://doi.org/https://doi.org/10.1016/S1352-2310(97)88638-4)
- 35) Tang, L., Chen, D., Karlsson, P.E., Gu, Y., Ou, T., 2009. Synoptic circulation and its influence on spring and summer surface ozone concentrations in southern Sweden. *Boreal Environ. Res.* 14, 889–902.
- 36) Tang, L., Rayner, D., Haeger-Eugensson, M., 2011. Have Meteorological Conditions Reduced NO<sub>2</sub> Concentrations from Local Emission Sources in Gothenburg? *Water, Air, Soil Pollut.* 221, 275–286. <https://doi.org/10.1007/s11270-011-0789-6>
- 37) Vieno, M., Dore, A.J., Stevenson, D.S., Doherty, R., Heal, M.R., Reis, S., Hallsworth, S., Tarrason, L., Wind, P., Fowler, D., Simpson, D., Sutton, M.A., 2010. Modelling surface ozone during the 2003 heat-wave in the UK. *Atmos. Chem. Phys.* 10, 7963–7978.  
<https://doi.org/10.5194/acp-10-7963-2010>
- 38) Vieno, M., Heal, M.R., Hallsworth, S., Famulari, D., Doherty, R.M., Dore, A.J., Tang, Y.S., Braban, C.F., Leaver, D., Sutton, M.A., Reis, S., 2014. The role of long-range transport and domestic emissions in determining atmospheric secondary inorganic particle concentrations across the UK. *Atmos. Chem. Phys.* 14, 8435–8447. <https://doi.org/10.5194/acp-14-8435-2014>
- 39) Vieno, M., Heal, M.R., Twigg, M.M., MacKenzie, I.A., Braban, C.F., Lingard, J.J.N., Ritchie, S., Beck, R.C., Möring, A., Ots, R., Di Marco, C.F., Nemitz, E., Sutton, M.A., Reis, S., 2016. Corrigendum: The UK particulate matter air pollution episode of March–April 2014: more than Saharan dust (2016 *Environ. Res. Lett.* 11 044004). *Environ. Res. Lett.* 11, 059501.  
<https://doi.org/10.1088/1748-9326/11/5/059501>

# Impact of the June 2018 Saddleworth Moor wildfires on air quality in northern England

**Graham AM<sup>1</sup>, Pope RJ<sup>1,2</sup>, McQuaid JB<sup>1</sup>, Pringle KP<sup>1</sup>, Arnold SR<sup>1</sup>, Bruno AG<sup>3,4</sup>, Moore DP<sup>3,4</sup>, Harrison JJ<sup>3,4</sup>, Chipperfield MP<sup>1,2</sup>, Rigby R<sup>1,5</sup>, Sanchez-Marroquin, A<sup>1</sup>, Lee J<sup>6,7</sup>, Wilde, S<sup>6</sup>, Siddans, R<sup>8,9</sup>, Kerridge, BJ<sup>8,9</sup>, Ventress, LJ<sup>8,9</sup>, Latter, BG<sup>8,9</sup>**

<sup>1</sup> School of Earth and Environment, University of Leeds, Leeds, United Kingdom

<sup>2</sup> National Centre for Earth Observation, University of Leeds, Leeds, United Kingdom

<sup>3</sup> Department of Physics and Astronomy, University of Leicester, Leicester, UK

<sup>4</sup> National Centre for Earth Observation, University of Leicester, Leicester, UK

<sup>5</sup> Centre for Environmental Modelling and Computation, University of Leeds, Leeds, UK

<sup>6</sup> Department of Chemistry, University of York, York, UK

<sup>7</sup> National Centre for Atmospheric Science, University of York, York

<sup>8</sup> Remote Sensing Group, STFC Rutherford Appleton Laboratory, Chilton, United Kingdom

<sup>9</sup> National Centre for Earth Observation, STFC Rutherford Appleton Laboratory, Chilton, United Kingdom

## **4.1 Abstract**

The June 2018 Saddleworth Moor fires were some of the largest UK wildfires on record and lasted for approximately three weeks. They emitted large quantities of smoke, trace gases and aerosols which were transported downwind over the highly populated regions of Manchester and Liverpool. Surface observations of PM<sub>2.5</sub> indicate that concentrations were 4-5.5 times higher than the recent seasonal average. State-of-the-art satellite measurements of total column

carbon monoxide (TCCO) from the TROPOMI instrument on the Sentinel 5 – Precursor (S5P) platform, coupled with measurements from a flight of the UK BAe-146-301 research aircraft, are used to quantify the substantial enhancement in emitted trace gases. The aircraft measured in-plume enhancements with near-fire CO and PM<sub>2.5</sub> concentrations >1500 ppbv and >125 µg m<sup>-3</sup> (compared to ~100 ppbv and ~5 µg m<sup>-3</sup> background concentrations). Downwind in-plume ozone (O<sub>3</sub>) values were larger than the near-fire location, indicating O<sub>3</sub> production with distance from source. The near-fire O<sub>3</sub>:CO ratio was ( $\Delta O_3/\Delta CO$ ) 0.001 ppbv/ppbv, increasing downwind to 0.060-0.105 ppbv/ppbv, suggestive of O<sub>3</sub> production enhancement downwind of the fires. Emission rates of CO and CO<sub>2</sub> ranged between 1.07 (0.07-4.69) kg s<sup>-1</sup> and 13.7 (1.73-50.1) kg s<sup>-1</sup>, respectively, similar to values expected from a medium sized power station.

## 4.2 Introduction

Vegetation fires contribute a large source of trace gases and aerosols into the Earth's atmosphere (Cheng, et al., 1998; HelasGand Pienaar, 1996; Lobert, and Warnatz, 1993; Peterson, et al., 2018; Reddington, et al., 2014; Wooster, et al., 2018), which have substantial implications for climate (Cruz Núñez, et al., 2014; Hamilton, et al., 2018; Liu, et al., 2014; Rowlinson, et al., 2019; Sommers, et al., 2014) and air quality (AQ) (Bravo, et al., 2002; Konovalov, et al., 2011; Moore, 2019; Phuleria, et al., 2005; Reddington, et al., 2015). Unlike many fire-prone regions, vegetation fires in the United Kingdom (UK) are relatively small and rare (Davies, et al., 2016; Van Der Werf, et al., 2017; Yallop, et al., 2006). However, on the June 24th 2018, large-scale wildfires broke out for approximately three weeks over Saddleworth Moor and Winter Hill, in north west England (BBC, 2018), requiring over 100 firefighters to tackle the blaze (Day, and Green, 2018). At their peak, the Saddleworth Moor fires covered approximately 8 km<sup>2</sup> of moorland (Greater Manchester Combined Authority,

2019), representing the largest wildfires close to an urban population in the UK on record (Figure 38) (NASA Socioeconomic Data and Applications Center (SEDAC) Center for International Earth Science Information Network (CIESIN), and Columbia, 2018). Therefore, this provided the first opportunity to measure the mixing of fire emissions with anthropogenic emissions in the UK. The fires forced the evacuation of several dozen properties and closure of many schools (Pidd, and Rawlinson, 2018). The fires primarily burned heather-dominated moorland with an underlying area of dry peat (Bain, et al., 2011; Greater Manchester Combined Authority, 2019; Xu, et al., 2018). Flames ranged between to 2-4 m in height, depending on the overlying vegetation type and wind conditions (Greater Manchester Combined Authority, 2019). Fires also propagated vertically and laterally through the peat layer, which would be expected to lead to large emissions of greenhouse gases and air pollutants (Wooster, et al., 2018). As peat is a substantially oxygenated fuel source, it can burn underground for long periods (e.g. weeks to months (Hu, et al., 2018; Roulston, et al., 2018)) making peat fires extremely difficult to control. Emissions from peat are poorly understood but it is thought that during the flaming stage, fires emit large amounts of soot and nitrogen oxides ( $\text{NO}_x$ ), while in the smouldering stage they emit much more carbon monoxide (CO), methane ( $\text{CH}_4$ ), volatile organic compounds (VOCs) and particulate matter (PM) (Turetsky, et al., 2015).

Throughout the period of June 22<sup>nd</sup> to 29<sup>th</sup>, meteorological conditions were favourable for the development and spread of the Saddleworth Moor and Winter Hill fires. Between June 22<sup>nd</sup> and 29<sup>th</sup> 2018, the UK experienced strong anticyclonic conditions from enhancement of the Azores high pressure system in the North Atlantic. Mean sea level pressure (MSLP) and geopotential height at 850 hPa (850GPH), from ERA-Interim and ERA5 reanalysis, indicate the stable high-pressure system (MLSP >1020 hPa and 850GPH 1560-1600 m over northern

England) resulted in low 10 m wind speeds (<5 m/s) and high surface temperatures (~27 °C on June 26<sup>th</sup>) (ERA-Interim, ECMWF), which dried out vegetation and reduced the likelihood of precipitation (see Supplementary Material: Meteorological Conditions and Figure 57 - Figure 59). In the future, conditions such as this are likely to become more common within the UK (Guerreiro, et al., 2018). Projections suggest that, as a result, UK wildfires are likely to become more frequent and intense (Albertson, et al., 2010) yielding more hazardous AQ situations in nearby populated areas.

Visible images between the June 25<sup>th</sup> to 30<sup>th</sup>, from the Moderate Resolution Imaging Spectroradiometer (MODIS) instruments, on-board NASA's Aura and Terra satellites, clearly show fire initiation followed by a westward propagation of the fire smoke plume (see Supplementary Material: Figure 60). Following the substantial visible impact (i.e. smoke and burned area) of the Saddleworth Moor and Winter Hill fires and the related high-level media coverage, we use state-of-the-art satellite observations from the newly launched (October 2017) TROPOMI instrument on-board ESA's Sentinel-5 Precursor (S5P), which provides, for the first time, high resolution observations of trace gases to quantify the impact of the pollutants from fires from space. We combine these observations with ground and specialised aircraft campaign observations to investigate the influence these fires had on atmospheric composition and AQ across north-western England. The Data & Methods section describes the observations used, the Results section presents our results and the Discussion and Conclusions section summarises the implications of our findings.

## 4.3 Data & Methods

### 4.3.1 Automated Urban and Rural Network Observations

Surface observations of particulate matter (PM<sub>2.5</sub> – atmospheric aerosol with a diameter less than 2.5 microns) are taken from Manchester Piccadilly, Salford Eccles and Wigan Centre Automated Urban and Rural Network (AURN) sites. AURN is the largest automated air quality monitoring network in the UK with 145 sites. These sites use the FDMS (Filter Dynamics Measurement System) analyser, which is based on the TEOM (Tapered Element Oscillating Microbalance) (Department for Environment Food & Rural Affairs, 2008). Air is drawn in through inlets for PM<sub>2.5</sub> and PM<sub>10</sub> where it is dried and weighed on a filter held at 30°C. This system measures non-volatile and volatile fractions by cycling through cold and warm chambers to evaporate volatile species before re-weighing the sample. Further information on data quality checks and uncertainties can be found in Stevenson *et al.* (2009). We use daily mean PM<sub>2.5</sub> concentrations (calculated from hourly measurements, where > 75% of hourly measurements each day are available) for June 16<sup>th</sup> to July 12<sup>th</sup> 2013-2018 to assess the impact of the fires on downwind populated areas (e.g. Manchester Piccadilly, Salford Eccles and Wigan) (see Figure 33) and to compare with longer term averages for the particular time of year.

### 4.3.2 Satellite Observations

Satellite measurements of total column carbon monoxide (TCCO) and tropospheric column nitrogen dioxide (TCNO<sub>2</sub>) are obtained from the TROPOMI instrument on-board ESA's Sentinel-5 Precursor (S5P) satellite (Veefkind, et al., 2012). S5P was launched in October 2017 into a sun-synchronous polar orbit with a local overpass time of 13:30 (Veefkind, et al., 2012). The instrument has a nadir-viewing spectral range of 270-500 nm (ultraviolet-visible, UV-Vis),

675-775 nm (near-infrared, NIR) and 2305-2385 nm (short wave-infrared, SWIR). TROPOMI represents the next generation of satellite instruments for observing global and regional AQ (Pope, et al., 2019) with an unparalleled nadir horizontal spatial resolution of  $3.5 \text{ km} \times 7.0 \text{ km}$  for UV-NIR bands and  $7.0 \text{ km} \times 7.0 \text{ km}$  for SWIR bands. For comparison, its predecessor, the Ozone Monitoring Instrument (OMI), had a horizontal spatial resolution of  $24 \text{ km} \times 13 \text{ km}$  (Boersma, et al., 2011). We also use fire radiative power (FRP) data from the MODIS instruments on-board NASA's Aqua and Terra satellites, launched in 1999 and 2002, respectively. Both instruments are nadir viewing (spectral range, 0.41-15  $\mu\text{m}$ ) with sun-synchronous local overpass times of 10:30 and 13:30, respectively (Remer, et al., 2005). The approach of Pope *et al.* (2018) is used to map TROPOMI TCCO data onto a  $0.03^\circ \times 0.03^\circ$  grid over the UK, while the FRP data (Level 3 product) is on a  $0.1^\circ \times 0.1^\circ$  grid.

Garane *et al.* (2019) find a typical global bias of 0-1.5% between TROPOMI TCCO and surface validation sites. For the Saddleworth Moor fires, we see precision errors of approximately 3.3-4.3%. Further information on the instrumentation and uncertainties can be found in Lambert *et al.* (2019).

### 4.3.3 FAAM Aircraft Data

The UK's BAe-146-301 Large Atmospheric Research Aircraft flew on June 29<sup>th</sup> 2018 to target the Saddleworth Moor fires (flight number C110). The aircraft is operated by the Facility for Airborne Atmospheric Measurements (FAAM, Ryder et al., 2015) and detailed information on the aircraft instrumentation and their uncertainties is given by Harris *et al.* (2017). For this flight, in-situ measurements of carbon monoxide (CO), ozone (O<sub>3</sub>) nitrogen dioxide (NO<sub>2</sub>) and particulate matter with a diameter less than 2.5  $\mu\text{m}$  (PM<sub>2.5</sub>) amongst other species, were obtained.

PM<sub>2.5</sub> data is calculated from data collected by optical particle counters mounted under the wing that measure aerosol size distributions. The instrument used was the passive cavity aerosol spectrometer probe 100-X (PCASP). The PCASP measures particles in the 0.1 - 3 μm diameter size range. Further information on the method the instruments used to calculate aerosol diameter and the calibration method used is described in Rosenberg *et al.* (2012). We find uncertainty within the integrated volume in the PM<sub>2.5</sub> range dataset to be ~30-35% at the 1-sigma confidence interval. Further information on sources of these uncertainties can be found in the Supplementary Material: Instrumentation section.

Measurements of NO were made using a custom built chemiluminescence instrument (Air Quality Design Inc), with NO<sub>2</sub> measured on a second channel by photolytic conversion to NO at 395 nm using a blue light converter (BLC), followed by detection by chemiluminescence (Lee, et al., 2009). Estimated accuracies are 4% for NO and 5% for NO<sub>2</sub>, with associated precision of 31 and 45 pptv, respectively (for 1Hz data). Further information is in the Supplementary Material: Instrumentation section.

Ozone was measured by an ultraviolet (UV) absorption photometer (Thermo Fisher, model 49C) with an uncertainty of 2% and a precision of 1 ppb for 4-s measurements (Harris, et al., 2017).

CO was measured by a vacuum UV fluorescence analyzer (Aero Laser GmbH, model AL5002; (Gerbig, et al., 1999)). The instrument was calibrated in flight every ~45 min using a synthetic-air working standard (Air Liquide, ~500 ppb). The 1-Hz CO measurements have a 2% uncertainty and 3-ppb precision (Harris, et al., 2017).

The aircraft left Cranfield, Bedfordshire at approximately 10:00 UTC, then undertook targeted fire plume measurements over Saddleworth Moor (near-field) at 10:30-11:30 UTC (Supplementary Material: Figure 60 and Figure 35 (a)) before taking downwind measurements over the Irish Sea (12:00-13:00 UTC). The aircraft returned to Cranfield around 15:00 UTC.

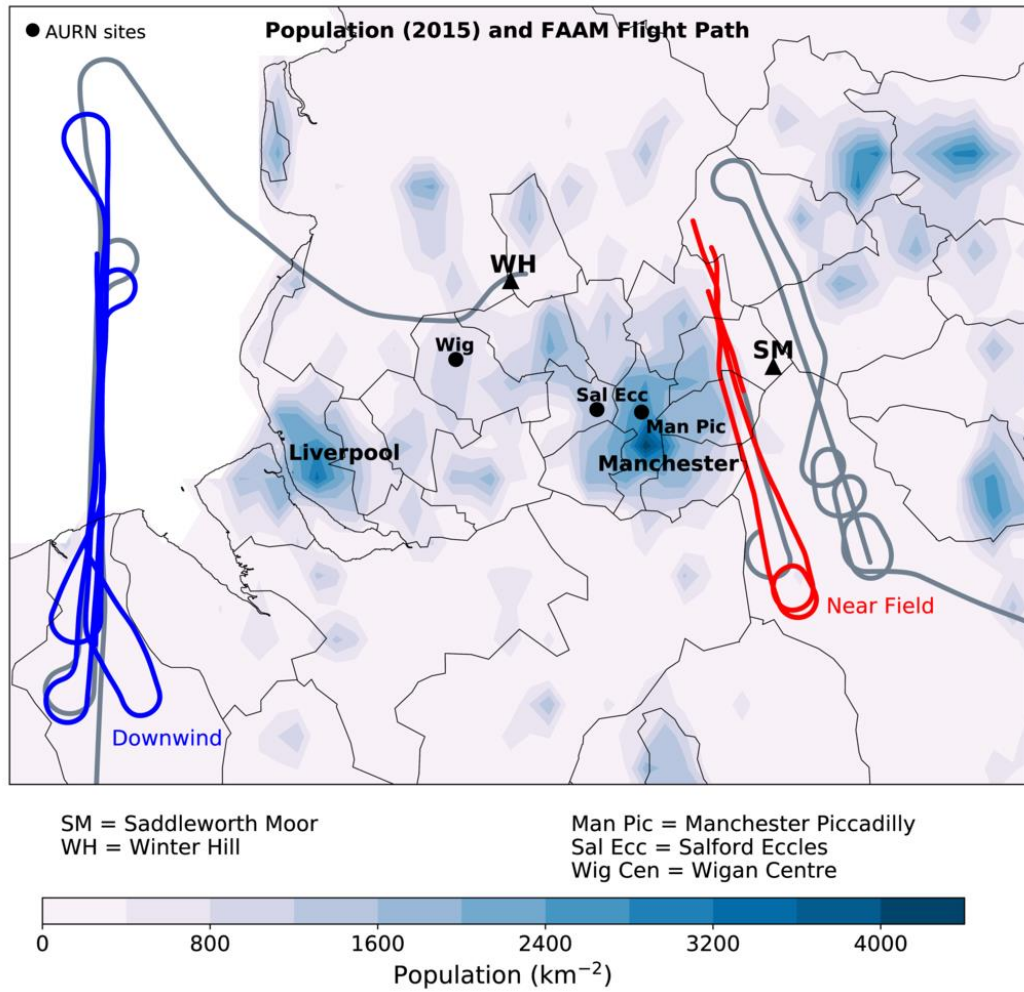


Figure 32. CEISIN population count (2015). Black triangles indicate the locations of Saddleworth Moor (SM) and Winter Hill (WH), the cities of Manchester (Man) and Liverpool are also marked. Black circles indicate AURN observation sites used in Figure 33. The flight path of the FAAM aircraft on 29<sup>th</sup> June 2018 is also shown in grey, with near-field and downwind sections (Figure 35-Figure 37) of the flight highlighted in red and blue.

## 4.4 Results

### 4.4.1 MODIS visible images

MODIS visible images (Supplementary Material: Figure 54) clearly show the ignition and time-evolution of the Saddleworth Moor and Winter Hill fires. Fire ignition occurs on June 25<sup>th</sup> 2018 on Saddleworth Moor. The smoke plume initially moves northwards (26<sup>th</sup> June) before shifting westwards, propagating over Manchester and Liverpool (27<sup>th</sup>-30<sup>th</sup> June). The size of the smoke plume peaks on 27<sup>th</sup> June. The Winter Hill fire then begins on June 30<sup>th</sup> and propagates westwards towards the Lancashire coast.

### 4.4.2 Automated Urban and Rural Network Observations

Observations of surface PM<sub>2.5</sub> at the Manchester Piccadilly, Salford Eccles and Wigan Centre AURN sites show enhanced concentrations during the fire period (grey shading in Figure 33). At all sites, PM<sub>2.5</sub> concentrations peak above 40  $\mu\text{g m}^{-3}$  (black dashed line), which is substantially larger than concentrations before and after the fire event (note Manchester Piccadilly is the only site where July 2018 data was available). These concentrations are well above the World Health Organisation (WHO) 24-hour guideline limit of 25  $\mu\text{g m}^{-3}$ , highlighting the potential population exposure risks even over this short time period.

We also use volatile and non-volatile PM<sub>2.5</sub> observations to investigate the relative influence of the primary and secondary components of PM<sub>2.5</sub> from the fire. Non-volatile PM<sub>2.5</sub> comprises of unreactive solid particles (e.g. elemental carbon, primary organic aerosol) (Chowdhury, et al., 2007; Tian, et al., 2009) whereas volatile PM<sub>2.5</sub> comprises of gaseous reactive precursors (e.g. sulfate, nitrate and VOCs) which can switch between the gas and solid phase through condensation. Considerable uncertainties exist in the apportionment of fire-emitted PM<sub>2.5</sub> due to the complex range of factors controlling emissions, which include fuel type, fuel moisture

content and organic aerosol mass concentration. Here, the AURN measurements indicate that during the Saddleworth Moor fires non-volatile  $PM_{2.5}$  was strongly correlated with total  $PM_{2.5}$  during the fire period. In 2018, the non-volatile fraction of total  $PM_{2.5}$  is between 3 and 18% higher than between 2013 and 2017, contributing to up to 93% of total  $PM_{2.5}$  (see Supplementary Material: Table 11). Compared with previous years (June 2013-2017 observational spread), the non-volatile  $PM_{2.5}$  concentrations are 4-5.5 times higher than average.

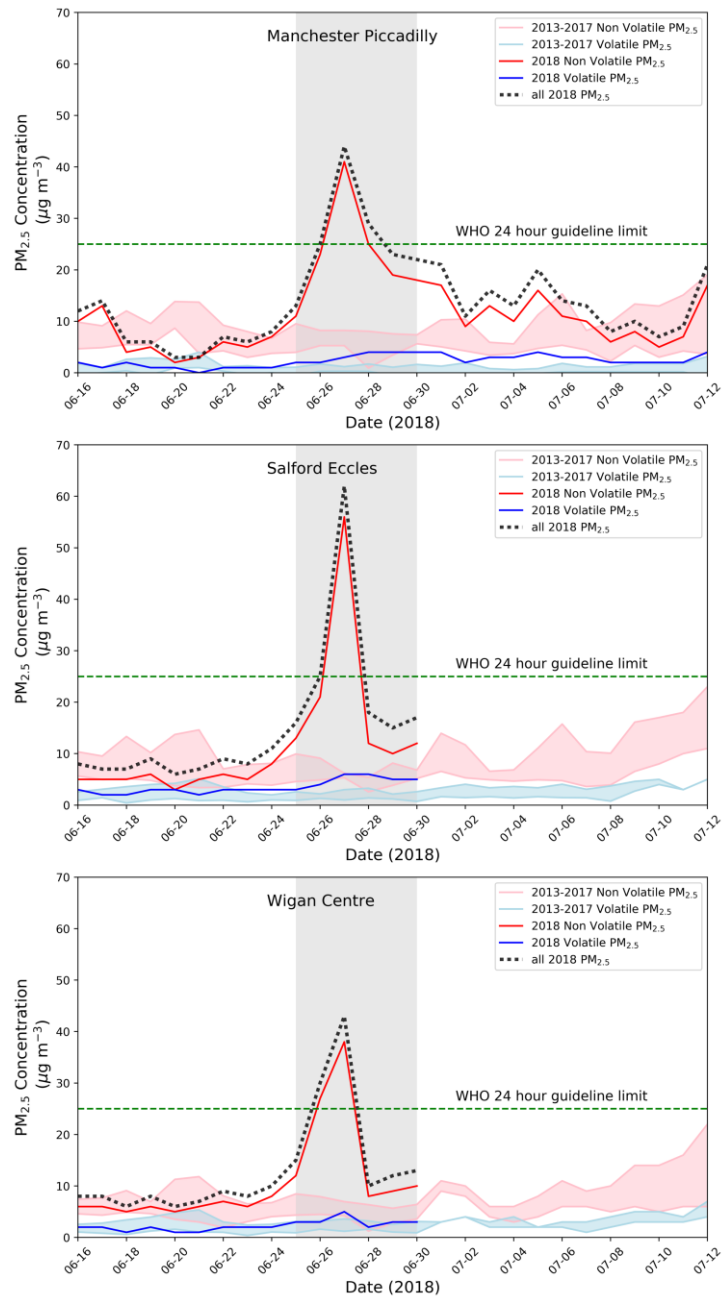


Figure 33. AURN observations of volatile and non-volatile PM<sub>2.5</sub> for 16<sup>th</sup> June – 14<sup>th</sup> July 2018. Non-volatile PM<sub>2.5</sub> is indicated by the red solid line (2018) and pink shading (2013-2017 standard deviation). Volatile PM<sub>2.5</sub> is indicated by the blue solid line (2018) and light blue shading (2013-2017 standard deviation). The total PM<sub>2.5</sub> concentration for 2018 is also indicated by the black dashed line and the fire period in grey. The WHO 24-hour guideline limit is also in green for reference.

### 4.4.3 TROPOMI Observations

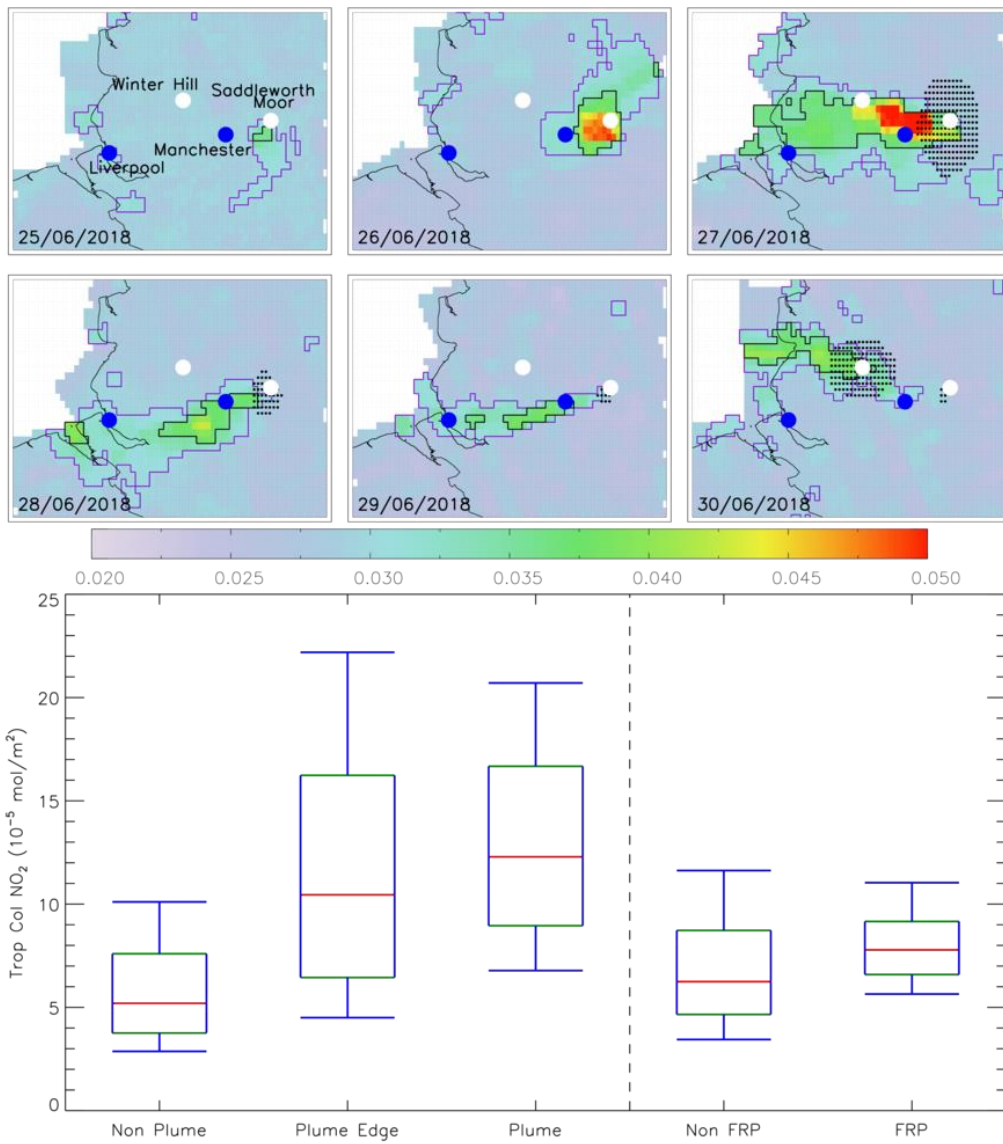


Figure 34. TROPOMI total carbon monoxide (TCCO, moles  $\text{m}^{-2}$ ) measurements of the Saddleworth Moor wildfire (25<sup>th</sup> – 30<sup>th</sup> June 2018). Black and purple polygon-outlined regions represent the fire plume ( $>0.03$  moles  $\text{m}^{-2}$ ) and edge of plume (0.025-0.03 moles  $\text{m}^{-2}$ ). Black dots show pixels where MODIS fire radiative power (FRP) is  $> 50$   $\text{mW m}^{-2}$ . White dots show the location of the Saddleworth Moor and Winter Hill fires. Blue dots show the location of Manchester and Liverpool. The box and whisker schematics represent TROPOMI tropospheric column nitrogen dioxide (TCNO<sub>2</sub>, 10-5 moles  $\text{m}^{-2}$ ) sub-sampled “in-plume”, “edge of plume” and “out of plume” TCCO thresholds. TCNO<sub>2</sub> is also sub-sampled under fire pixels (FRP  $> 50$   $\text{mW m}^{-2}$ ) and non-fire pixels (FRP  $< 50$   $\text{mW m}^{-2}$ ). Red, green and blue represent the median, 25<sup>th</sup> and 75<sup>th</sup> percentiles and 10<sup>th</sup> and 90<sup>th</sup> percentiles, respectively.

The time evolution (25<sup>th</sup>-30<sup>th</sup> June) of the Saddleworth Moor and Winter Hill fires can also clearly be seen in the TROPOMI TCCO data where the fire plume propagates westwards (top six panels of Figure 34) over Manchester and Liverpool (blue circles). Over Saddleworth Moor, TCCO peaks at over 0.04-0.05 moles  $\text{m}^{-2}$  (26<sup>th</sup> and 27<sup>th</sup> June) with background concentrations of 0.02-0.025 moles  $\text{m}^{-2}$ . Between June 27<sup>th</sup>–29<sup>th</sup> the plume has dispersed westwards with “in-plume” concentrations remaining above 0.030 moles  $\text{m}^{-2}$ . By the 30<sup>th</sup> June, the Saddleworth Moor plume has diminished but the Winter Hill fires have fully developed with a north-westerly plume direction (TCCO  $>0.04$  moles  $\text{m}^{-2}$ ). The time-evolution of the TCCO plume correlates strongly with the MODIS visible images (see Supplementary Material: Figure 54) supporting the robustness of the novel TROPOMI composition data. This is also seen in TCCO data from the Infrared Atmospheric Sounding Interferometer (IASI) satellite (see Supplementary Material: Comparison of TROPOMI with IASI (Infrared Atmospheric Sounding Interferometer) and Supplementary Material: Figure 64), further supporting TROPOMI. As TCCO enhancements flow out over Manchester and Liverpool, both densely populated, there will likely be substantial increases in other prominent air pollutants (e.g. NO<sub>2</sub>, PM<sub>2.5</sub> and O<sub>3</sub>) as shown in Figure 33.

Inspection of the TROPOMI TCNO<sub>2</sub> data (see Supplementary Material: Satellite Observations of Tropospheric Column Nitrogen Dioxide section and Supplementary Material: Figure 57) highlights concentration enhancements over both Manchester and Liverpool during the Saddleworth Moor fire time period. However, the prevailing anticyclonic meteorological conditions have been shown in other studies (e.g. Pope *et al.* (2015, 2014)) to significantly increase NO<sub>2</sub> concentrations over urban regions due to accumulation of anthropogenic emissions. Therefore, to isolate potential fire-sourced NO<sub>2</sub> signal, a quantitative classification of “fire-influenced” pixels was used to sub-sample the TCNO<sub>2</sub> data. Firstly, satellite pixels with FRP > 50 mW m<sup>-2</sup> were classed as “fire” (black circles in Figure 34), while those with FRP < 50 mW m<sup>-2</sup> were classed as “non-fire”. Secondly, the TCCO was used to identify the observations as “in-plume” (TCCO > 0.03 moles m<sup>-2</sup>, black polygon-outlining - Figure 34), “edge of plume” (0.025 moles m<sup>-2</sup> < TCCO < 0.030 moles m<sup>-2</sup>, purple polygon-outlining) and “out of plume” (0.020 moles m<sup>-2</sup> < TCCO < 0.025 moles m<sup>-2</sup>). The “out of plume” lower limit was set to 0.020 moles m<sup>-2</sup> to ensure that near-plume satellite pixels are used and not background pixels across the domain. Several different thresholds were tested and this combination yielded the most realistic spatial plume distributions when compared to MODIS visible images.

When sub-sampled under “fire” pixels (bottom panel, Figure 34) the median TCNO<sub>2</sub> concentration is approximately 8.0 x10<sup>-5</sup> moles m<sup>-2</sup>, which is significantly larger than the “non-fire” pixel TCNO<sub>2</sub> median (6.0-7.0 x10<sup>-5</sup> moles m<sup>-2</sup>) (95% confidence level (CL) based on student t-test, using the mean). The “fire” TCNO<sub>2</sub> 10<sup>th</sup>, 25<sup>th</sup> and 75<sup>th</sup> percentile concentrations are also larger than the non-fire-TCNO<sub>2</sub> equivalent. However, the “non-fire” TCNO<sub>2</sub> 90<sup>th</sup> percentile value is marginally larger. The TCNO<sub>2</sub> data sub-sampled under the TCCO plume

definitions show a similar pattern. “Out of plume” median TCNO<sub>2</sub> is the lowest (5-6 x10<sup>-5</sup> moles m<sup>-2</sup>) of all classifications (also true for the 10<sup>th</sup>, 25<sup>th</sup>, 75<sup>th</sup> and 90<sup>th</sup> percentiles). Though downwind of the fire location, the “edge of plume” and “in plume” classifications have the largest median TCNO<sub>2</sub> values of 10.0-11.0 x10<sup>-5</sup> moles m<sup>-2</sup> and 12.0-13.0 x10<sup>-5</sup> moles m<sup>-2</sup>, respectively. These two classifications both overlap regions of enhanced anthropogenic NO<sub>2</sub> sources (i.e. Manchester and Liverpool), so their median and percentile concentrations are larger (see Supplementary Material: Satellite Observations of Tropospheric Column Nitrogen Dioxide section and Supplementary Material: Figure 57). By using the TCCO data as a tracer for the fire plume, we detect a NO<sub>2</sub> fire response on top of the anthropogenic NO<sub>2</sub> signal. This is supported by aircraft results in the FAAM Aircraft Observations section, though we note that there is a substantial level of noise in the TROPOMI NO<sub>2</sub> data (unlike for CO). Here, the median and percentile concentrations are all larger “in plume” than “edge of plume” where the medians are significantly different at the 95% CL (student t-test, using the mean). This indicates that the increased spatial resolution of TROPOMI (when compared to previous satellites such as OMI) is able to both, detect the impacts of fires on air pollutants and to quantify them, something not possible with the sparse coverage of the AURN sites. We can therefore conclude that the Saddleworth Moor and Winter Hill fires, observed by TROPOMI, significantly enhanced observed NO<sub>2</sub> and CO concentrations.

#### 4.4.4 FAAM Aircraft Observations

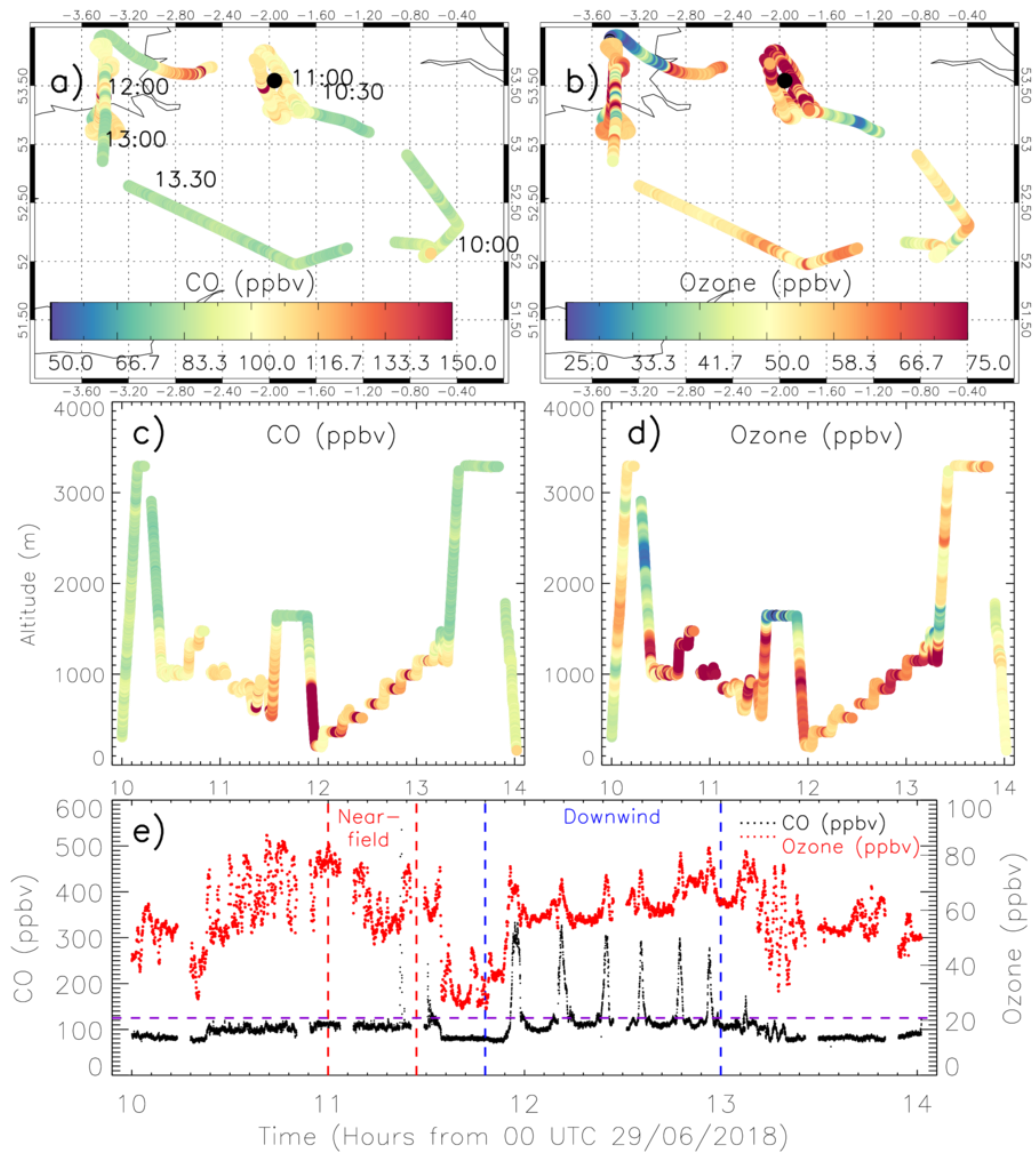


Figure 35. Facility of Airborne Atmospheric Measurements (FAAM) observations of carbon monoxide (CO, ppbv) and ozone (O<sub>3</sub>, ppbv) from the Saddleworth Moor wildfires on 29th June 2018. (a) CO concentration along flight path (b) O<sub>3</sub> concentration along flight path (c) time-altitude CO profile, (d) time-altitude O<sub>3</sub> profile, (e) CO (black) and O<sub>3</sub> (red) time-series. Time stamps for the flight are included in (a) for reference to in (c) and (d). The sections bounded by the red and blue dashed lines in panels (a), (b), (e) and (f) represent the near-field (NF) and downwind (DW) time phases of the flight. The horizontal purple dashed line in (e) indicates the “in-plume” (> 125 ppbv) versus “out of plume” (< 125 ppbv) threshold.

#### 4.4.4.1 Pollutant Concentrations “in-plume” and “out-of-plume” Near-Field and Downwind

To verify the satellite results and investigate other air pollutants, we use FAAM aircraft observations of CO, O<sub>3</sub> and NO<sub>2</sub>, from June 29<sup>th</sup> 2018. Between approximately 11:00-11:30 UTC the aircraft was sampling the near-field fire plume southwest-west of Saddleworth Moor (black circle – Figure 35 (a) and (b)) at 500-1000 m above ground level (AGL). Measurements within the plume show enhanced CO concentrations peaking at over 1500 ppbv, while background CO ranged between 80-100 ppbv (Figure 35 (c) and (e)). This correlates well with measurements of PM<sub>2.5</sub> aerosol concentration, which also indicate enhanced PM<sub>2.5</sub> in the plume (15 - >120 µg m<sup>-3</sup>) and much lower background values (~5 µg m<sup>-3</sup>) (Supplementary Material: Figure 61). Here, we define this segment of the flight as “near-field” (NF) (Figure 35 (e)). While there was a large step-change in CO and PM<sub>2.5</sub> measurements, there were no clear changes in the measured O<sub>3</sub> concentrations. Before the NF flight segment, O<sub>3</sub> concentrations ranged between 45-85 ppbv, when the aircraft was north-northeast-east of Saddleworth Moor (i.e. ~10:30-11:00 UTC, Figure 35 (a), (d) and (e)). The NF O<sub>3</sub> concentrations are slightly lower, ranging between 45-80 ppbv.

In the “downwind” (DW) flight segment (approximately 12:00-13:00 UTC– Figure 35 (e)), the aircraft made plume measurements over the Irish Sea. Here, the aircraft flew between 250-1000 m making multiple passes in and out of the plume. This can be clearly seen in Figure 35 (c) and (d) where there are sudden step-changes in CO (100-115 ppbv to > 150 ppbv) and O<sub>3</sub> (50-60 to > 80 ppbv) concentrations with change in altitude. Figure 35 (e) and Supplementary Material: Figure 60 and Figure 61 indicate this even more clearly, with CO, O<sub>3</sub>, NO<sub>2</sub> and PM<sub>2.5</sub> concentrations varying between 100-300 ppbv, 45-80 ppbv, ~1-8 ppbv and ~5-130 µg m<sup>-3</sup>, respectively, as the aircraft samples the composition in and out of the plume. To isolate in and out of plume concentrations, a CO threshold of 125 ppbv was used to define plume from background concentrations (purple dashed line – Figure 35 (e)).

Figure 36 shows CO, O<sub>3</sub> and NO<sub>2</sub> concentrations sub-sampled “in-plume” and “out of plume” (based on the CO 125 ppbv threshold) for the NF and DW flight segments. In the NF, the median CO concentrations are substantially larger “in-plume” than “out of plume” at approximately 725 (220-860, 25<sup>th</sup>-75<sup>th</sup> percentiles) ppbv and 107 (104-111) ppbv, respectively. In the DW flight segment, median CO concentrations are substantially lower “in-plume” at approximately 190 (90-260) ppbv, while “out of plume” concentrations are slightly larger (111, 102-115 ppbv) than the NF “out of plume”. Again, the same pattern is seen in the results for PM<sub>2.5</sub> (Supplementary Material: Figure 62). NF “in-plume” concentrations are also much larger for PM<sub>2.5</sub> (55.9 µg m<sup>-3</sup>, 14.1-71.8 µg m<sup>-3</sup>) than the “out-of-plume” median (7.5 µg m<sup>-3</sup>, 5.8-10.0 µg m<sup>-3</sup>). PM<sub>2.5</sub> is also substantially lower DW “in-plume” (18.43 µg m<sup>-3</sup>) than NF “in-plume” (55.9 µg m<sup>-3</sup>) and DW “in-plume” (18.43, 11.1 and 28.2 µg m<sup>-3</sup>) is also higher than DW “out-of-plume” (7.15, 4.47 and 9.61 µg m<sup>-3</sup>).

NF O<sub>3</sub> is larger “out of plume” (68, 47-76 ppbv) than “in-plume” (60, 58-61 ppbv). This is consistent with other studies, which show that fire plumes decrease local O<sub>3</sub> concentrations, primarily through titration with freshly emitted NO (Verma et al., 2009). The opposite occurs for NO<sub>2</sub> where concentrations are larger “in-plume” (2.05, 1.9-2.2 ppbv) than “out of plume” (0.9, 0.1-2.1 ppbv). However, the “out of plume” NO<sub>2</sub> range (10<sup>th</sup>-90<sup>th</sup> percentiles) is much larger with concentrations peaking above 5 ppbv as the NF NO<sub>2</sub> “in-plume” sample size is small with less spread (n=27). In the DW, O<sub>3</sub> concentrations show enhancements “in-plume” when compared with the NF. DW “in-plume” concentrations are 66 (61-70) ppbv, this is substantially larger than the DW “out of plume” concentrations (O<sub>3</sub> is 59 (57-63) ppbv). This enhancement compared with the surrounding air mass is suggestive of production of O<sub>3</sub> “in-plume” with distance away from the Saddleworth Moor. However, this O<sub>3</sub> enhancement may also be influenced by downwind NO<sub>x</sub> sources (i.e. Liverpool and Manchester). The DW NO<sub>2</sub> concentrations are larger “in-plume” (3.2 (2.1-4.1) ppbv) than “out of plume” (1.2 (0.8-1.8) ppbv), while also larger than the NF “in-plume” concentrations of 2.05 (1.9-2.2) ppbv. This enhancement of NO<sub>2</sub> concentrations “in-plume” corroborates the satellite TCNO<sub>2</sub> results in Figure 34, but also the larger DW NO<sub>2</sub> levels. To determine if these pollutant samples were significantly different from each other, the student t-test was used to compare the mean NF “in-plume” with NF “out of plume”, NF “in-plume” with DW “in-plume” and DW “in-plume” with DW “out of plume” for each pollutant separately. Overall, we found that all combinations were significantly different for each pollutant at the 95% CL. Thus, concentrations of NO<sub>2</sub>, O<sub>3</sub>, PM<sub>2.5</sub> and CO within the plume are statistically significantly enhanced compared to outside of the plume in NF and DW locations. Alongside this, concentrations are statistically significantly enhanced within the plume NF compared to within the plume DW.

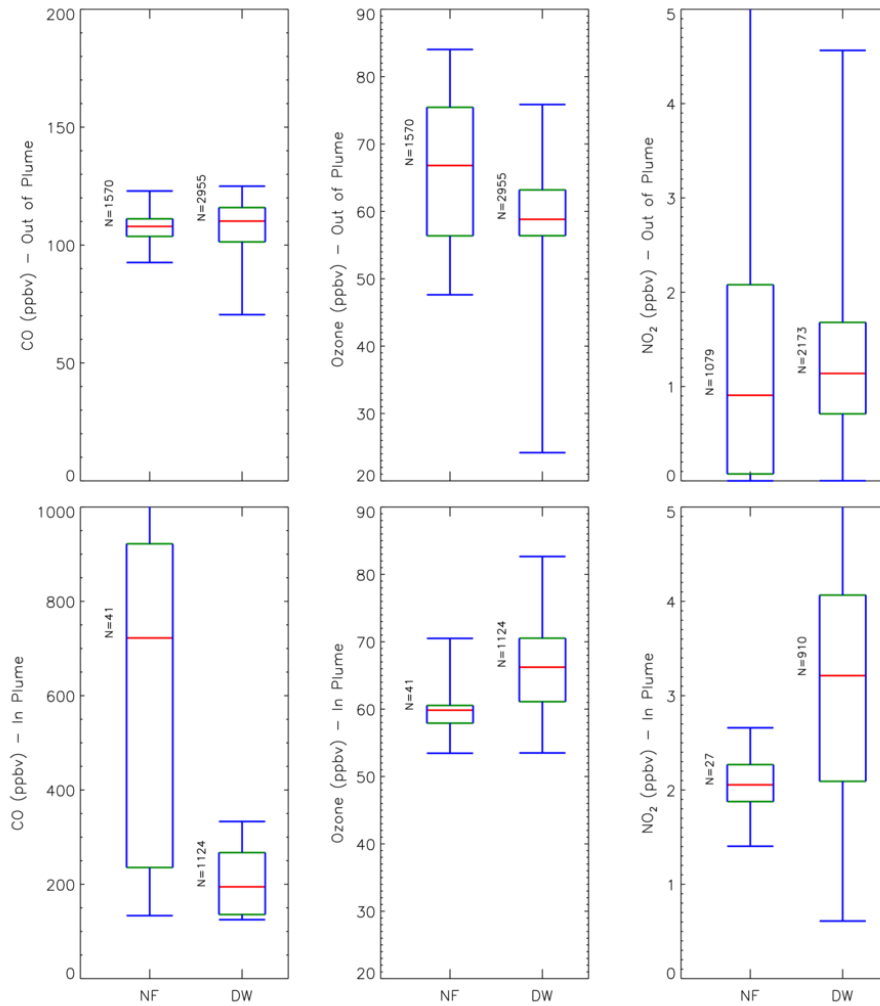


Figure 36. Box and whisker schematic of CO (left, ppbv), O<sub>3</sub> (centre, ppbv) and NO<sub>2</sub> (right, ppbv) “in-” and “out of plume” (CO > 125 ppbv). Red, green and blue represent the median, 25th and 75th percentiles and minimum and maximum concentrations, respectively. NF and DW represent the near-field and downwind phases of the plume.

#### 4.4.4.2 “In Plume” Ozone Production Near-Field and Downwind

To quantify the enhancement of “in-plume” O<sub>3</sub> with distance from source, we have used a similar approach to Arnold *et al.* (2015) and Jaffe and Wigder (2012). The linear fit between CO and O<sub>3</sub> concentrations was determined for the NF (red symbols) and DW (blue symbols)

flight segments (Figure 37), where measurements with CO concentrations < 125 ppbv were excluded (black circles). NF CO ranges between 125 to > 500 ppbv (i.e. CO data > 500 ppbv is used for the statistics, but not plotted to clearly display the DW relationship), whereas O<sub>3</sub> remains between 53-60 ppbv (note two points peak at ~70 ppbv). The O<sub>3</sub> enhancement, as a function of CO concentration, for the NF is  $\Delta O_3/\Delta CO = 0.001$  ppbv/ppbv indicating no clear O<sub>3</sub> enhancement with increasing CO. In the DW flight segment there are three distinct positive CO:O<sub>3</sub> slopes at approximately 0.25-0.5 km (crosses), 0.6-0.85 km (diamonds) and above 0.9 km (circles) altitudes. Here, the O<sub>3</sub> enhancements are  $\Delta O_3/\Delta CO = 0.060$ , 0.067 and 0.105 ppbv/ppbv, respectively, all of which are significant at the 95% CL (i.e. the trends lie outside of the variation observed in the data (outside of  $\pm 2$  standard deviations)). This indicates a significant enhancement of “in-plume” O<sub>3</sub> production increasing with altitude. One likely reason for the larger  $\Delta O_3/\Delta CO$  rate with altitude is that there is more photochemical production of ozone at top of the plume (i.e. incoming solar radiation reaches this part of the plume first and is attenuated further into the plume) (Jaffe and Wigder, 2012). However, we do not have the detailed chemical measurements necessary to test this hypothesis. Though NO<sub>2</sub> is enhanced DW from urban sources, the  $\Delta O_3/\Delta CO$  variation with altitude is predominantly from the Saddleworth Moor fires. As shown in Figure 35 and Supplementary Material: Figure 60, there is a strong correlation with enhancements in all pollutants as the aircraft flies in and out of the plume (also see Aircraft Instrumentation and Cross-section section). The  $\Delta NO_2/\Delta CO$  ratio (not shown here) has the opposite pattern to  $\Delta O_3/\Delta CO$  ratio and decreases with height. This potentially suggests that the anthropogenic signal is reducing with altitude or that NO<sub>2</sub> is being processed more quickly with more active photochemistry. However, to accurately diagnose the influence of anthropogenic and fire NO<sub>x</sub> sources on O<sub>3</sub> production, a high-resolution regional modelling frame work is required, which is beyond the scope of this study.

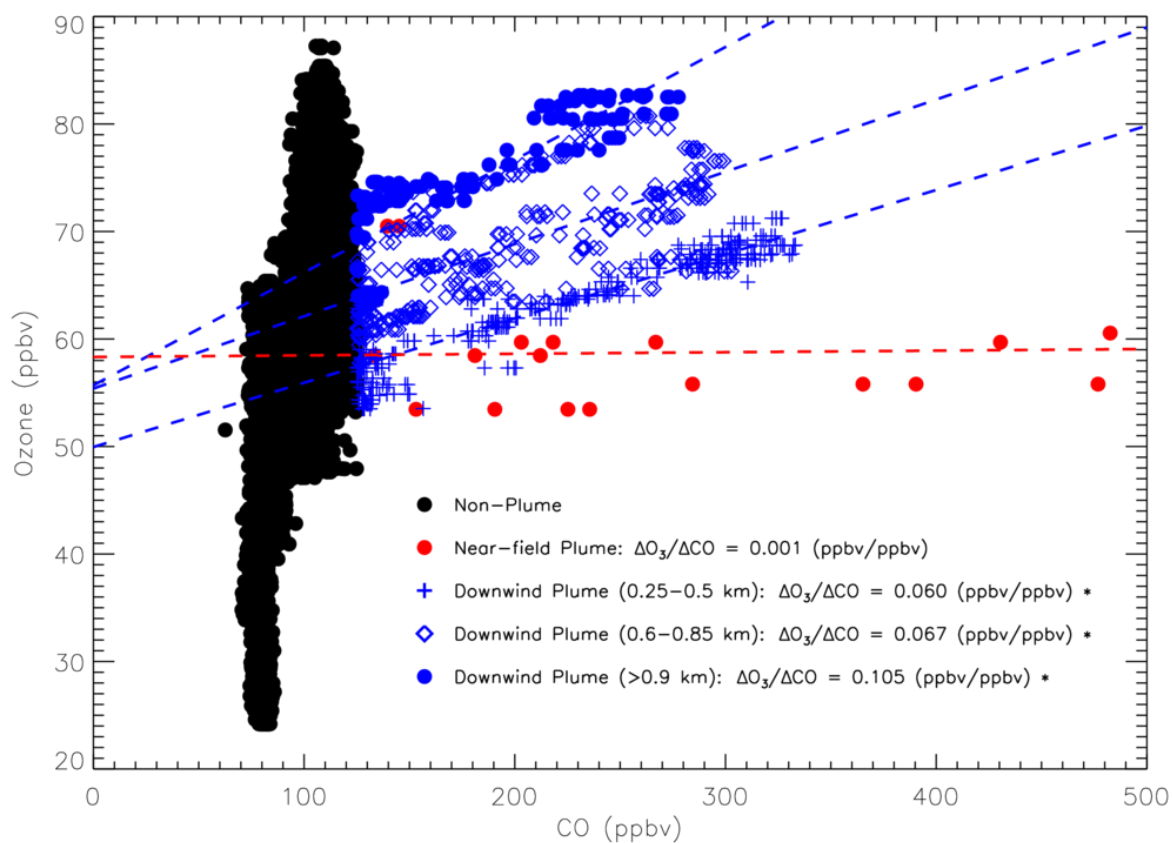


Figure 37. CO (ppbv) and O<sub>3</sub> (ppbv) relationship for different Saddleworth Moor fire plume phases (29th June 2018). Black circles represent all data defined as “out of plume” (<125 ppbv CO), red circles are “in plume” near field and blue symbols are “in plume” downwind. Blue crosses, diamonds and circles represent measurements between 0.25–0.5 km, 0.6–0.85 km and above 0.9 km. Dashed lines represent the CO–O<sub>3</sub> regression for different fire plume altitudes where all downwind relationships are significant at the 95% confidence level (\*).

#### 4.4.4.3 Back Trajectories

Backward trajectories from the NOAA Hybrid Single-Particle Lagrangian Integrated Trajectory model (HYSPLIT) (Stein, et al., 2015) released from the aircraft sampling regions near-field and downwind can assist estimating the age of air mass which the smoke plume was in when pollutants were sampled. Trajectories were released from the most northerly and

southerly points of the near-field (2.2°W, 53.75°N at 1100 UTC and 1.9°W, 53.25°N at 1200 UTC) and downwind (3.4°W, 53.75°N at 1200 UTC and 3.4°W, 52.75°N at 1300 UTC) sections of the flight from a range of altitudes during these profiles (500, 750 & 1000 m and 250, 500 and 1000 m, respectively) (Figure 56). The results of the back-trajectory analysis indicate the air mass which near-field samples were taken from was likely 30 mins – 1 hour in age, showing little variation in age with changes in sample height (500, 750 and 1000 m). The air mass of the downwind samples was likely 2-7 hours in age, with the age of the air mass decreasing with increasing altitude (250, 500 and 1000 m) in the northernmost (southernmost) sample location from 4-6, 3-4 and 2-3 hours (6-7, 4-5 and 3-4 hours).

### **Deriving CO emissions from the fires**

To determine CO emissions from the Saddleworth Moor fires, we consider the cross section made by the aircraft through the plume on June 29<sup>th</sup> (see Supplementary Material: Figure 63). Here, the plume has an approximate width and thickness of 4482 m and 52 m, respectively. The fire emissions were calculated by:

$$E_{CO} = \overline{\Delta CO} \bar{w} h d \quad (15)$$

where  $E_{CO}$  ( $\text{kg s}^{-1}$ ) represents the emissions of CO,  $\overline{\Delta CO}$  ( $\text{kg m}^{-3}$ ) is the mean fire enhancement between the “in-plume” and “out of plume” CO concentrations,  $\bar{w}$  ( $\text{m s}^{-1}$ ) is the mean wind speed at the flight altitude (assumed to be in the direction of plume flow and perpendicular to the aircraft flight path),  $h$  (m) is the plume thickness and  $d$  (m) is the plume width. The limitations of this approach are the assumptions that  $\bar{w}$  is representative of the full plume wind speed, that the plume cross-section is regular, and the estimate values of  $h$  and  $d$  (the aircraft might not have included the entire plume in the transect). Here,  $\bar{w} = 7.31 \text{ m s}^{-1}$  and  $\overline{\Delta CO} =$

$6.4 \times 10^{-7} \text{ kg m}^{-3}$ , so  $E_{CO} = 1.07 \text{ kg s}^{-1}$ . To estimate the uncertain range of this emission rate, we perturb the values of  $h$  and  $d$  by 50% (these variables represent the largest source of uncertainty) and use lower and upper limits of  $\bar{w}$  and  $\overline{\Delta CO} \pm 1.0$  standard deviation. This provides a range of  $E_{CO} = 1.07 (0.07-4.69) \text{ kg s}^{-1}$ , which is in reasonable agreement with remote sensing estimates from the Global Fire Assimilation System (GFAS,  $0.54 \text{ kg s}^{-1}$ ) and the Fire Inventory from NCAR (FINN,  $2.15 \text{ kg s}^{-1}$ ). When this is repeated for  $\text{CO}_2$ , also measured during the aircraft campaign,  $E_{\text{CO}_2} = 13.7 (1.73-50.1) \text{ kg s}^{-1}$  while GFAS and FINN have emission rates of  $7.84 \text{ kg s}^{-1}$  and  $33.1 \text{ kg s}^{-1}$ , respectively.

## 4.5 Discussion and Conclusions

Historically, the UK is prone to relatively small vegetation fires (e.g. in comparison to tropical and other boreal fire, van der Werf *et al.* (2017)) often used in moorland burning for the purposes of agricultural grazing (Davies, et al., 2016; Yallop, et al., 2006). However, in recent years, the UK has experienced several substantially larger fires which have gained much media interest and resulted in the evacuation of surrounding populated areas. In this study, we have successfully used ground-based observations, state-of-the-art satellite and aircraft measurements to quantify the impact of the Saddleworth Moor and Winter Hill fires on regional atmospheric composition and air quality.

Using ground-based observations, the impact of pollutants from the fire can be quantified at the surface. Pollutants from the fire were transported westwards during the peak of the fires (27<sup>th</sup>, 29<sup>th</sup> and 30<sup>th</sup> June) over large populations (e.g. Manchester). Consequently, the fire had a significant impact on  $\text{PM}_{2.5}$  concentrations in Manchester and in regions further afield (including Wigan – 50 km away). Surface  $\text{PM}_{2.5}$  during the fires was 4-5.5 higher than average and dominated by the non-volatile  $\text{PM}_{2.5}$  fraction. Since concentrations were up to 2 times the

WHO recommended guideline limit ( $25 \mu\text{g m}^{-3}$ ) there are likely to have been considerable negative health impacts for individuals exposed, particularly those with underlying health conditions.

The unprecedented spatial resolution of the new S5P TROPOMI satellite instrument now allows us to detect trace gases from such fires. The time-evolution of total column carbon monoxide (TCCO) measurements during June 25<sup>th</sup>-30<sup>th</sup> shows the westward propagation of the Saddleworth Moor fire plume out towards the Irish Sea over the highly populated cities of Manchester and Liverpool. By using quantitative classification of the fire plume (i.e. TCCO concentration and fire radiative power, FRP), we have isolated a significant enhancement in tropospheric column  $\text{NO}_2$  (TCNO<sub>2</sub>), a key air pollutant, on top of the enhanced anthropogenic signal from prevailing anticyclonic meteorological conditions (i.e. accumulation of pollutants over source regions). Measurements from the FAAM aircraft flight on June 29<sup>th</sup> support this, with clear enhancement of boundary layer (<1 km) CO concentrations within the plume. Near Saddleworth Moor, in-plume CO and PM<sub>2.5</sub> measurements peak at over 1500 ppbv and  $127.5 \mu\text{g m}^{-3}$ , while downwind of the plume over the Irish Sea they are somewhat lower at 200-400 ppbv and  $96.1 \mu\text{g m}^{-3}$ . The opposite occurs for ozone (O<sub>3</sub>) where the downwind plume shows a significant increase, highlighting its downwind production. Based on CO:O<sub>3</sub> correlations within the plume, the O<sub>3</sub> production increases significantly from  $\Delta\text{O}_3/\Delta\text{CO} = 0.001$  ppbv/ppbv near-field to  $\Delta\text{O}_3/\Delta\text{CO} = 0.060$ - $0.105$  ppbv/ppbv (depending on the altitude between 250-1000 m) downwind. Our estimates lie within the range of values found in previous studies of similar fires (boreal region mean: 0.018-0.15) (Jaffe, and Wigder, 2012). Though urban sources of NO<sub>x</sub> (i.e. Manchester and Liverpool) may also be contributing to the DW O<sub>3</sub> enhancements as has been found in previous studies of wildfires near highly populated urban areas (McKeen et

al., 2002; Morris et al., 2006). Emission rates from Saddleworth Moor, during the smouldering stage of the fire's life cycle, are estimated to be 1.07 (0.07-4.69) kg s<sup>-1</sup> and 13.7 (1.73-50.1) kg s<sup>-1</sup> for CO and CO<sub>2</sub>, respectively. This CO<sub>2</sub> emission rate is similar to those of the Grangemouth (near Edinburgh) or Enfield (north of London) power stations (~16.0 kg s<sup>-1</sup>; (NAEI, 2018)).

We have shown that the Saddleworth Moor and Winter Hill fires produced large quantities of some key air pollutants, including O<sub>3</sub>, PM<sub>2.5</sub> and CO, which were transported over Manchester and Liverpool yielding a substantial degradation in AQ. In the future, with accelerating climate change leading to enhanced temperatures and drought conditions within the UK (Guerreiro, et al., 2018), wildfires are likely to become more frequent and intense (Albertson, et al., 2010) yielding more hazardous AQ situations in nearby populated areas. Therefore, work is required to accurately determine the surface enhancement in air pollutant concentrations from such fires. As the surface monitoring network (Automated Urban and Rural Network, (Department for Environment Food and Rural Affairs, 2018b)) is sparse, satellite observations and modelling can play an important role. Future work is also needed to assess the corresponding health impacts of exposure to air pollutants from wildfires.

## **4.6 Acknowledgements**

This work was supported by the UK Natural Environment Research Council (NERC) by providing funding for the National Centre for Earth Observation (NCEO) through grant number NE/R016518/1. The contribution of Alberto Sanchez-Marroquin has been supported by the European Research Council (MarineIce (grant no. 648661)).

Surface pressure reanalysis charts from the UK Met Office were accessed from University of Leeds archive. Surface PM<sub>2.5</sub> concentration observations were taken from the AURN network

via <https://uk-air.defra.gov.uk/>. The TROPOMI total column CO and tropospheric column NO<sub>2</sub> data were obtained from ESA's Copernicus Open Access Hub (<https://scihub.copernicus.eu/>) and the Tropospheric Emissions Monitoring Internet Service (TEMIS, <http://www.temis.nl/airpollution/no2.html>), respectively. MODIS fire radiative power (FRP) data was provided by the ECMWF Global Fire Assimilation System (<https://apps.ecmwf.int/datasets/data/cams-gfas/>). ECMWF ERA-Interim meteorological reanalysis data came from <https://apps.ecmwf.int/datasets/data/interim-full-daily/levtype=sfc/>. The Saddleworth Moor aircraft data were taken using the Facility for Airborne Atmospheric Measurements (FAAM) BAe-146-301 Large Atmospheric Research Aircraft and are available from the Centre for Environmental Data Analysis (CEDA) at <https://old.faam.ac.uk/index.php/data>. The authors also gratefully acknowledge the NOAA Air Resources Laboratory (ARL) for the provision of the HYSPLIT transport and dispersion model and/or READY website (<https://www.ready.noaa.gov>) used in this publication.

## 4.7 References

- 1) Albertson, K., Ayles, J., Cavan, G., McMorrow, J., 2010. Climate change and the future occurrence of moorland wildfires in the Peak District of the UK. *Clim. Res.* 45, 105–118. <https://doi.org/10.3354/cr00926>
- 2) Arnold, S.R., Emmons, L.K., Monks, S.A., Law, K.S., Ridley, D.A., Turquety, S., Tilmes, S., Thomas, J.L., Bouarar, I., Flemming, J., Huijnen, V., Mao, J., Duncan, B.N., Steenrod, S., Yoshida, Y., Langner, J., Long, Y., 2015. Biomass burning influence on high-latitude tropospheric ozone and reactive nitrogen in summer 2008: A multi-model analysis based on POLMIP simulations. *Atmos. Chem. Phys.* 15, 6047–6068. <https://doi.org/10.5194/acp-15-6047-2015>
- 3) Bain, C., Bonn, A., Stoneman, R., Chapman, S., Coupar, A., Evans, M., Gearey, B., Howat, M., Joosten, H., Keenleyside, C., Labadz, J., Lindsay, R., Littlewood, N., Lunt, P., Miller, C., Moxey, A., Orr, H., Reed, M., Smith, P., Swales, V., Thompson, D., Thompson, P., Van de Noort, R., Wilson, J., Worrall, F., 2011. IUCN UK Commission of Inquiry on Peatlands.
- 4) BBC, 2018. Saddleworth Moorfire is out after more than three weeks.
- 5) Boersma, K.F., Eskes, H.J., Dirksen, R.J., Van Der A, R.J., Veefkind, J.P., Stammes, P., Huijnen, V., Kleipool, Q.L., Sneep, M., Claas, J., Leitão, J., Richter, A., Zhou, Y., Brunner, D., 2011. An improved tropospheric NO<sub>2</sub> column retrieval algorithm for the Ozone Monitoring Instrument. *Atmos. Meas. Tech.* 4, 1905–1928. <https://doi.org/10.5194/amt-4-1905-2011>
- 6) Bravo, A.H., Sosa, E.R., Sánchez, A.P., Jaimes, P.M., Saavedra, R.M.I., 2002. Impact of wildfires on the air quality of Mexico City, 1992-1999. *Environ. Pollut.* 117, 243–253. [https://doi.org/10.1016/S0269-7491\(01\)00277-9](https://doi.org/10.1016/S0269-7491(01)00277-9)

- 7) Cheng, L., McDonald, K.M., Angle, R.P., Sandhu, H.S., 1998. Forest fire enhanced photochemical air pollution. A case study. *Atmos. Environ.* 32, 673–681.  
[https://doi.org/10.1016/S1352-2310\(97\)00319-1](https://doi.org/10.1016/S1352-2310(97)00319-1)
- 8) Chowdhury, Z., Zheng, M., Schauer, J.J., Sheesley, R.J., Salmon, L.G., Cass, G.R., Russell, A.G., 2007. Speciation of ambient fine organic carbon particles and source apportionment of PM<sub>2.5</sub> in Indian cities. *J. Geophys. Res. Atmos.* 112. <https://doi.org/10.1029/2007JD008386>
- 9) Cruz Núñez, X., Ruiz, L.V., García, C.G., 2014. Black carbon and organic carbon emissions from wildfires in Mexico. *Atmosfera*, 27, 165–172. [https://doi.org/10.1016/S0187-6236\(14\)71107-5](https://doi.org/10.1016/S0187-6236(14)71107-5)
- 10) Davies, G.M., Kettridge, N., Stoof, C.R., Gray, A., Ascoli, D., Fernandes, P.M., Marrs, R., Allen, K.A., Doerr, S.H., Clay, G.D., McMorrow, J., Vandvik, V., 2016. The role of fire in UK peatland and moorland management: The need for informed, unbiased debate. *Philos. Trans. R. Soc. B Biol. Sci.* 371. <https://doi.org/10.1098/rstb.2015.0342>
- 11) Day, R., Green, C., 2018. The devastating toll of this summer's moorland wildfires has been revealed - as firefighters tackle another blaze - Manchester Evening News. Manchester Evening News.
- 12) Department for Environment Food & Rural Affairs, 2008. Site Operational Procedures for TEOM FDMS Analysers. Wiley.
- 13) Department for Environment Food and Rural Affairs, 2018. Automatic Urban and Rural Network (AURN) [WWW Document]. URL <https://uk-air.defra.gov.uk/networks/network-info?view=aurn> (accessed 12.10.20).
- 14) Garane, K., Koukouli, M.-E., Verhoelst, T., Fioletov, V., Lerot, C., Heue, K.-P., Bais, A., Balis, D., Bazureau, A., Dehn, A., Goutail, F., Granville, J., Griffin, D., Hubert, D., Keppens,

- A., Lambert, J.-C., Loyola, D., McLinden, C., Pazmino, A., Pommereau, J.-P., Redondas, A., Romahn, F., Valks, P., Van Roozendaal, M., Xu, J., Zehner, C., Zerefos, C., Zimmer, W., 2019. TROPOMI/S5p total ozone column data: global ground-based validation & consistency with other satellite missions. *Atmos. Meas. Tech. Discuss.* 1–38. <https://doi.org/10.5194/amt-2019-147>
- 15) Gerbig, C., Schmitgen, S., Kley, D., Volz-thomas, A., Dewey, K., 1999. An improved fast-response vacuum-UV resonance fluorescence CO instrument. *J. Geophys. Res.* 104, 1699–1704.
- 16) Greater Manchester Combined Authority, 2019. Response to Freedom of Information Request 1920-057.
- 17) Guerreiro, S.B., Dawson, R.J., Kilsby, C., Lewis, E., Ford, A., 2018. Future heat-waves, droughts and floods in 571 European cities. *Environ. Res. Lett.* 13. <https://doi.org/10.1088/1748-9326/aaaad3>
- 18) Hamilton, D.S., Hantson, S., Scott, C.E., Kaplan, J.O., Pringle, K.J., Nieradzik, L.P., Rap, A., Folberth, G.A., Spracklen, D. V., Carslaw, K.S., 2018. Reassessment of pre-industrial fire emissions strongly affects anthropogenic aerosol forcing. *Nat. Commun.* 9. <https://doi.org/10.1038/s41467-018-05592-9>
- 19) Harris, N.R.P., Carpenter, L.J., Lee, J.D., Vaughan, G., Filus, M.T., Jones, R.L., Ouyang, B., Pyle, J.A., Robinson, A.D., Andrews, S.J., Lewis, A.C., Minaeian, J., Vaughan, A., Dorsey, J.R., Gallagher, M.W., Le Breton, M., Newton, R., Percival, C.J., Ricketts, H.M.A., Bauguitte, S.J.B., Nott, G.J., Wellpott, A., Ashfold, M.J., Flemming, J., Butler, R., Palmer, P.I., Kaye, P.H., Stopford, C., Chemel, C., Boesch, H., Humpage, N., Vick, A., MacKenzie, A.R., Hyde, R., Angelov, P., Meneguz, E., Manning, A.J., 2017. Coordinated airborne studies

in the tropics (CAST). *Bull. Am. Meteorol. Soc.* 98, 145–162. <https://doi.org/10.1175/BAMS-D-14-00290.1>

- 20) HelasGand Pienaar, J., 1996. The influence of vegetation fires on the chemical composition of the atmosphere. *S. Afr. J. Sci.* 92, 132–136.
- 21) Hu, Y., Fernandez-Anez, N., Smith, T.E.L., Rein, G., 2018. Review of emissions from smouldering peat fires and their contribution to regional haze episodes. *Int. J. Wildl. Fire* 27, 293–312. <https://doi.org/10.1071/WF17084>
- 22) Jaffe, D.A., Wigder, N.L., 2012. Ozone production from wildfires: A critical review. *Atmos. Environ.* 51, 1–10. <https://doi.org/10.1016/j.atmosenv.2011.11.063>
- 23) Jones, P.D., Harpham, C., Briffa, K.R., 2013. Lamb weather types derived from reanalysis products. *Int. J. Climatol.* 33, 1129–1139. <https://doi.org/10.1002/joc.3498>
- 24) Kanamitsu, M., 1989. Description of the NMC Global Data Assimilation and Forecast System. *Weather Forecast.* 4, 335–342. [https://doi.org/10.1175/1520-0434\(1989\)004<0335:DOTNGD>2.0.CO;2](https://doi.org/10.1175/1520-0434(1989)004<0335:DOTNGD>2.0.CO;2)
- 25) Konovalov, I.B., Beekmann, M., Kuznetsova, I.N., Yurova, A., Zvyagintsev, A.M., 2011. Atmospheric impacts of the 2010 Russian wildfires: Integrating modelling and measurements of an extreme air pollution episode in the Moscow region. *Atmos. Chem. Phys.* 11, 10031–10056. <https://doi.org/10.5194/acp-11-10031-2011>
- 26) Lambert, J.-C., Keppens, A., Hubert, D., Langerock, B., Eichmann, K.-U., Kleipool, Q., Sneep, M., Verhoelst, T., Wagner, T., Weber, M., Ahn, C., Argyrouli, A., Balis, D., Chan, K.L., Compernelle, S., Smedt, I. De, Eskes, H., Fjæraa, A.M., Garane, K., Gleason, J.F., Goutail, F., Granville, J., Hedelt, P., Heue, K.-P., Jaross, G., Koukouli, M., Landgraf, J., Lutz, R., Niemejer, S., Pazmiño, A., Pinaridi, G., Pommereau, J.-P., Richter, A., Rozemeijer, N.,

- Sha, M.K., Zweers, D.S., Theys, N., Tilstra, G., Torres, O., Valks, P., Vigouroux, C., P. Wang, 2019. Sentinel-5 Precursor Mission Performance Centre Quarterly Validation Report of the Copernicus Sentinel-5 Precursor Operational Data Products # 03 : July 2018 – May 2019. S5P MPC Routine Oper. Consol. Valid. Rep. Ser. 2, 1–125.
- 27) Lee, J.D., Moller, S.J., Read, K.A., Lewis, A.C., Mendes, L., Carpenter, L.J., 2009. Year-round measurements of nitrogen oxides and ozone in the tropical North Atlantic marine boundary layer. *J. Geophys. Res. Atmos.* 114, 1–14. <https://doi.org/10.1029/2009JD011878>
- 28) Liu, Y., Goodrick, S., Heilman, W., 2014. Wildland fire emissions, carbon, and climate: Wildfire-climate interactions. *For. Ecol. Manage.* 317, 80–96. <https://doi.org/10.1016/j.foreco.2013.02.020>
- 29) Lobert, J., Warnatz, J., 1993. Emissions from the combustion process in vegetation. *Fire Environ.* 13, 15–37.
- 30) Long, C.M., Nascarella, M.A., Valberg, P.A., 2013. Carbon black vs. black carbon and other airborne materials containing elemental carbon: Physical and chemical distinctions. *Environ. Pollut.* 181, 271–286. <https://doi.org/10.1016/j.envpol.2013.06.009>
- 31) Moore, D.P., 2019. The October 2017 red sun phenomenon over the UK. *Weather* 74, 348–353. <https://doi.org/10.1002/wea.3440>
- 32) NAEI, 2018. Download emission maps [WWW Document]. URL [https://naei.beis.gov.uk/data/map-uk-das?pollutant\\_id=2&emiss\\_maps\\_submit=naei-20190625105934](https://naei.beis.gov.uk/data/map-uk-das?pollutant_id=2&emiss_maps_submit=naei-20190625105934) (accessed 12.10.20).
- 33) NASA Socioeconomic Data and Applications Center (SEDAC) Center for International Earth Science Information Network (CIESIN), Columbia, U. of, 2018. Gridded Population of the

World, Version 4 (GPWv4): Population Count, Revision 11.

<https://doi.org/https://doi.org/10.7927/H4JW8BX5>

- 34) Peterson, D.A., Campbell, J.R., Hyer, E.J., Fromm, M.D., Kablick, G.P., Cossuth, J.H., DeLand, M.T., 2018. Wildfire-driven thunderstorms cause a volcano-like stratospheric injection of smoke. *Clim. Atmos. Sci.* 1, 1–8. <https://doi.org/10.1038/s41612-018-0039-3>
- 35) Phuleria, H.C., Fine, P.M., Zhu, Y., Sioutas, C., 2005. Air quality impacts of the October 2003 Southern California wildfires. *J. Geophys. Res. Atmos.* 110, 1–11. <https://doi.org/10.1029/2004JD004626>
- 36) Pidd, H., Rawlinson, K., 2018. Saddleworth Moor fire declared major incident as residents evacuated. *The Guardian*.
- 37) Pope, R.J., Arnold, S.R., Chipperfield, M.P., Latter, B.G., Siddans, R., Kerridge, B.J., 2018. Widespread changes in UK air quality observed from space. *Atmos. Sci. Lett.* 19, 1–8. <https://doi.org/10.1002/asl.817>
- 38) Pope, R.J., Graham, A.M., Chipperfield, M.P., Veeffkind, J.P., 2019. High resolution satellite observations give new view of UK air quality. *Weather* 2, 2–6. <https://doi.org/10.1002/wea.3441>
- 39) Pope, R.J., Savage, N.H., Chipperfield, M.P., Arnold, S.R., Osborn, T.J., 2014. The influence of synoptic weather regimes on UK air quality: Analysis of satellite column NO<sub>2</sub>. *Atmos. Sci. Lett.* 15, 211–217. <https://doi.org/10.1002/asl2.492>
- 40) Pope, R.J., Savage, N.H., Chipperfield, M.P., Ordóñez, C., Neal, L.S., 2015. The influence of synoptic weather regimes on UK air quality: Regional model studies of tropospheric column NO<sub>2</sub>. *Atmos. Chem. Phys. Discuss.* 15, 18577–18607. <https://doi.org/10.5194/acpd-15-18577-2015>

- 41) Reddington, C.L., Butt, E.W., Ridley, D.A., Artaxo, P., Morgan, W.T., Coe, H., Spracklen, D. V., 2015. Air quality and human health improvements from reductions in deforestation-related fire in Brazil. *Nat. Geosci.* 8, 768–771. <https://doi.org/10.1038/ngeo2535>
- 42) Reddington, C.L., Yoshioka, M., Balasubramanian, R., Ridley, D., Toh, Y.Y., Arnold, S.R., Spracklen, D. V., 2014. Contribution of vegetation and peat fires to particulate air pollution in Southeast Asia. *Environ. Res. Lett.* 9, 094006. <https://doi.org/10.1088/1748-9326/9/9/094006>
- 43) Remer, L.A., Kaufman, Y.J., Tanré, D., Mattoo, S., Chu, D.A., Martins, J. V., Li, R.R., Ichoku, C., Levy, R.C., Kleidman, R.G., Eck, T.F., Vermote, E., Holben, B.N., 2005. The MODIS aerosol algorithm, products, and validation. *J. Atmos. Sci.* 62, 947–973. <https://doi.org/10.1175/JAS3385.1>
- 44) Rosenberg, P.D., Dean, A.R., Williams, P.I., Dorsey, J.R., Minikin, A., Pickering, M.A., Petzold, A., 2012. Particle sizing calibration with refractive index correction for light scattering optical particle counters and impacts upon PCASP and CDP data collected during the Fennec campaign. *Atmos. Meas. Tech.* 5, 1147–1163. <https://doi.org/10.5194/amt-5-1147-2012>
- 45) Roulston, C., Paton-Walsh, C., Smith, T.E.L., Guérette, A., Evers, S., Yule, C.M., Rein, G., Van der Werf, G.R., 2018. Fine Particle Emissions from Tropical Peat Fires Decrease Rapidly With Time Since Ignition. *J. Geophys. Res. Atmos.* 123, 5607–5617. <https://doi.org/10.1029/2017JD027827>
- 46) Rowlinson, M.J., Rap, A., Arnold, S.R., Pope, R.J., Chipperfield, M.P., McNorton, J., Forster, P., Gordon, H., Pringle, K.J., Feng, W., Kerridge, B.J., Latter, B.L., Siddans, R., 2019. Impact of El Niño Southern Oscillation on the interannual variability of methane and tropospheric ozone. *Atmos. Chem. Phys. Discuss.* 2, 1–20. <https://doi.org/10.5194/acp-2019-222>

- 47) Sanchez-Marroquin, A., Hedges, D.H.P., Hiscock, M., Parker, S.T., Rosenberg, P.D., Trembath, J., Walshaw, R., Burke, I., McQuaid, J., Murray, B., 2019. Characterisation of the filter inlet system on the BAE-146 research aircraft and its use for size resolved aerosol composition measurements. *Atmos. Meas. Tech.* 12, 5741–5763.  
<https://doi.org/10.5194/amt-12-5741-2019>
- 48) Siddans, R., Gerber, D., Miles, G., 2015. Optimal Estimation Method retrievals with IASI, AMSU and MHS measurements.
- 49) Sommers, W.T., Loehman, R.A., Hardy, C.C., 2014. Wildland fire emissions, carbon, and climate: Science overview and knowledge needs. *For. Ecol. Manage.* 317, 1–8.  
<https://doi.org/10.1016/j.foreco.2013.12.014>
- 50) Stein, A.F., Draxler, R.R., Rolph, G.D., Stunder, B.J.B., Cohen, M.D., Ngan, F., 2015. Noaa's hysplit atmospheric transport and dispersion modeling system. *Bull. Am. Meteorol. Soc.* 96, 2059–2077. <https://doi.org/10.1175/BAMS-D-14-00110.1>
- 51) Stevenson, K., Yardley, R., Stacey-Aea, B., Maggs, R., Veritas, B., 2009. QA/QC Procedures for the UK Automatic Urban and Rural Air Quality Monitoring Network (AURN). Executive summary.
- 52) Tian, D., Hu, Y., Wang, Y., Boylan, J., Zheng, M., Armistead, R., 2009. Assessment of biomass burning emissions and their impacts on urban and regional PM<sub>2.5</sub>: A Georgia case study. *Environ. Sci. Technol.* 43, 299–305. <https://doi.org/10.1021/es801827s>
- 53) Turetsky, M.R., Benscoter, B., Page, S., Rein, G., Van Der Werf, G.R., Watts, A., 2015. Global vulnerability of peatlands to fire and carbon loss. *Nat. Geosci.* 8, 11–14.  
<https://doi.org/10.1038/ngeo2325>

- 54) Van Der Werf, G.R., Randerson, J.T., Giglio, L., Van Leeuwen, T.T., Chen, Y., Rogers, B.M., Mu, M., Van Marle, M.J.E., Morton, D.C., Collatz, G.J., Yokelson, R.J., Kasibhatla, P.S., 2017. Global fire emissions estimates during 1997-2016. *Earth Syst. Sci. Data* 9, 697–720. <https://doi.org/10.5194/essd-9-697-2017>
- 55) Veefkind, J.P., Aben, I., McMullan, K., Förster, H., de Vries, J., Otter, G., Claas, J., Eskes, H.J., de Haan, J.F., Kleipool, Q., van Weele, M., Hasekamp, O., Hoogeveen, R., Landgraf, J., Snel, R., Tol, P., Ingmann, P., Voors, R., Kruizinga, B., Vink, R., Visser, H., Levelt, P.F., 2012. TROPOMI on the ESA Sentinel-5 Precursor: A GMES mission for global observations of the atmospheric composition for climate, air quality and ozone layer applications. *Remote Sens. Environ.* 120, 70–83. <https://doi.org/10.1016/j.rse.2011.09.027>
- 56) Wagner, R., Jähn, M., Schepanski, K., 2018. Wildfires as a source of airborne mineral dust - Revisiting a conceptual model using large-eddy simulation (LES). *Atmos. Chem. Phys.* 18, 11863–11884. <https://doi.org/10.5194/acp-18-11863-2018>
- 57) Wooster, M.J., Gaveau, D.L.A., Salim, M.A., Zhang, T., Xu, W., Green, D.C., Huijnen, V., Murdiyarso, D., Gunawan, D., Borchard, N., Schirrmann, M., Main, B., Sepriando, A., 2018. New tropical peatland gas and particulate emissions factors indicate 2015 Indonesian fires released far more particulate matter (but less methane) than current inventories imply. *Remote Sens.* 10, 1–31. <https://doi.org/10.3390/rs10040495>
- 58) Xu, J., Morris, P.J., Liu, J., Holden, J., 2018. PEATMAP: Refining estimates of global peatland distribution based on a meta-analysis. *Catena* 160, 134–140. <https://doi.org/10.1016/j.catena.2017.09.010>

59) Yallop, A.R., Thacker, J.I., Thomas, G., Stephens, M., Clutterbuck, B., Brewer, T., Sannier, C.A.D., 2006. The extent and intensity of management burning in the English uplands. *J. Appl. Ecol.* 43, 1138–1148. <https://doi.org/10.1111/j.1365-2664.2006.01222.x>

# Impact on Air Quality and Health due to the Saddleworth Moor Fire in Northern England

Graham A.M<sup>1</sup>, Pope R.J<sup>1,2</sup>, Pringle K.P<sup>1</sup>, Arnold S.<sup>1</sup>,  
Chipperfield, M.P<sup>1,2</sup>, Conibear, L.A<sup>1</sup>, Butt, E.W<sup>1</sup>, Kiely L.<sup>1</sup>,  
Knote, C.<sup>3</sup>, and McQuaid, J.B<sup>1</sup>

<sup>1</sup> Institute for Climate and Atmospheric Science, School of Earth and Environment, University of Leeds, Leeds, LS2 9JT

<sup>2</sup> National Centre for Earth Observation, University of Leeds, Leeds, LS2 9JT

<sup>3</sup> Meteorological Institute, LMU Munich, Munich, Germany

E-mail: ee15amg@leeds.ac.uk

## 5.1 Abstract

On June 24th 2018 one of the largest UK wildfires in recent history broke out on Saddleworth Moor, close to Manchester, in north-west England. Since wildfires close to large populations in the UK have been relatively small and rare in the past, there is little knowledge about the impacts. This has prevented the development of effective strategies to reduce them. This paper uses a high-resolution coupled atmospheric-chemistry model to assess the impact of the fires on particulate matter with a diameter less than 2.5  $\mu\text{m}$  ( $\text{PM}_{2.5}$ ) across the region and the impact on health from short-term exposure. We find that the fires substantially degraded air quality.  $\text{PM}_{2.5}$  concentrations increased by more than 300% in Oldham and Manchester and up to 50% in areas up to 80 km away, such as Liverpool and Wigan. This led to one quarter of the population (2.9 million

people) in the simulation domain (-4.9-0.7°E and 53.0-54.4°N) being exposed to moderate PM<sub>2.5</sub> concentrations on at least one day, according to the Daily Air Quality Index (36-53 µg m<sup>-3</sup>), between June 23<sup>rd</sup> and 30<sup>th</sup> 2018. This equates to 4.5 million people being exposed to PM<sub>2.5</sub> above the WHO 24-hour guideline of 25 µg m<sup>-3</sup> on at least one day. Using a concentration-response function we calculate the short-term health impact, which indicates that in total over the 7-day period 28 (95% CI: 14.1-42.1) deaths were brought forward, with a mean daily excess mortality of 3.5 deaths per day (95% CI: 1.8-5.3). The excess mortalities from PM<sub>2.5</sub> due to the fires represented up to 60% of the total excess mortality (5.7 of 9.5 excess deaths), representing an increase of 3.8 excess mortalities (165% increase) compared to if there were no fires. We find the impact of mortality due to PM<sub>2.5</sub> from the fires on the economy was also substantial (£21.1m).

## 5.2 Introduction

The Saddleworth Moor fire in June 2018 was the largest UK wildfire in recent decades, with over double the burnt area of the most recent large wildfire in 2011, in Swinley, Berkshire (Royal Berkshire Fire and Rescue Service, 2011). It led to the evacuation of many residents from their homes, and caused elevated atmospheric pollutant concentrations across the Greater Manchester urban region. The fires began on June 24<sup>th</sup> 2018 and burned for three weeks over Saddleworth Moor (1.96°W, 53.54°N) and Winter Hill (2.52°W, 53.63°N) (Figure 38). The fires, which are thought to have been deliberately started, peaked in size on 27<sup>th</sup> June, covering 8 km<sup>2</sup> with flames reaching 4 m in height (Greater Manchester Combined Authority, 2019). The fires burned on moorland that was dominated by heather with an underlying layer of peat (Greater Manchester Combined Authority, 2019) (Supplementary Material: Figure 65). Peat is exceptionally vulnerable to ignition during periods of drought and once alight it is extremely

difficult to control and extinguish because it is a well oxygenated fuel source (Rappold, et al., 2011). As a result, peat fires can smoulder underground for long periods, re-emerging away from the original source (Rappold, et al., 2011). Fuel consumption is relatively large in peat fires, emissions per unit area are much higher than for other fuel types (Geron, and Hays, 2013). Consequently, peat fires emit large dense ground level plumes, meaning that local populations may be more susceptible to smoke exposure than for other wildfire types (Tinling, et al., 2016). Alongside this, although other studies have suggested that flaming smoke may be more toxic than smouldering smoke on a mass basis (Kim, et al., 2019, 2018), peat burning produces more smoke and so it has been suggested that the toxicity of smoke from peat fires is different to other wildfires (Reisen, et al., 2015; Tinling, et al., 2016), however there is currently limited research on this topic.

June 2018 was anomalously warm and dry across the UK. Average daily maximum temperatures were between 18 - 22 °C (2.5 °C warmer than the 1981-2010 average) (UK Met Office, 2018) and less than 75 mm rainfall fell during the month (50% of the 1981-2010 average rainfall). There were fewer than 4 days with > 10mm rainfall (UK Met Office, 2018). These conditions led to the peat on the moor becoming particularly susceptible to ignition.

Wildfires emit large amounts of pollutants and have substantial impacts globally on the radiative balance (Hodzic, et al., 2007; Rappold, et al., 2011), cloud microphysical properties (Jiang, et al., 2016; Lu, and Sokolik, 2013), air quality (Crippa, et al., 2016; Jaffe, and Wigder, 2012; Reddington, et al., 2014) and therefore health (Johnston, et al., 2012; Jones, et al., 2015; Liu, et al., 2015; Rappold, et al., 2011). Wildfires are an increasing environmental and health concern that are projected to occur more frequently, become more intense and spread much more quickly in the future (Barros, et al., 2014). It is projected that by 2080 the combination

of higher temperatures, decreased summer rainfall and drier soils could lead to a 30-50% increase in UK wildfire risk (HM Government, 2012). Peat bogs, which account for over 22,000 km<sup>2</sup> of UK land cover (Xu, et al., 2018), are particularly vulnerable to wildfire.

As a result of the predicted increase in wildfires, population exposure to pollutants from fires is also expected to increase. Substantial evidence supports the association of short-term exposure to PM<sub>2.5</sub> from fires and respiratory and cardiac morbidity and mortality from both epidemiological (Delfino, et al., 2009; Johnston, et al., 2011; Reid, et al., 2016; Zanobetti, and Schwartz, 2009) and toxicology studies (Naeher, et al., 2007). However, there is a large amount of conflicting research on the toxicity of different species and so equal toxicity between PM components is still commonly assumed but is an active area of research (Atkinson, et al., 2014). The health burden of fires in the tropics and United States, Australia and Canada is well documented in the literature (Crippa, et al., 2016; Finlay, et al., 2012; Johnston, et al., 2011; Landis, et al., 2018; Liu, et al., 2015; Reid, et al., 2016; Reisen, et al., 2015) and is significant. The large wildfires during 2015 in Equatorial Asia led to 69 million people being exposed to unhealthy levels of PM<sub>2.5</sub> and are estimated to have caused 11,880 excess mortalities due to short-term exposure (Crippa, et al., 2016).

Alongside the significant health impacts of wildfires, there is also a large associated socioeconomic cost (Fann, et al., 2018; Kochi, et al., 2012). The concept of Value of Statistical Life, how much society is willing to pay to preserve a life or extend it, is used by studies to estimate the economic value of short-term excess deaths and hospital admissions during wildfires. Using this method it is estimated that in the US between 2008 and 2012 the economic cost of short-term exposure to wildfire air pollutants was \$63bn (95% CI \$6bn-\$170bn), while

for long-term wildfire air pollutant exposure the cost was \$450bn (95% CI \$42bn-\$1200bn) (Fann, et al., 2018).

Since wildfires close to highly populated areas are relatively rare in the UK, little research into the health and economic impacts of UK wildfires has been carried out. However, as fires are predicted to increase with the warming climate and land-use change it is becoming increasingly important to examine wildfires in a UK context. Previous studies elsewhere in the world have found that public health tools and educational programmes to reduce exposure yield significant health benefits from reduced mortality and exacerbations of underlying illnesses (Rappold, et al., 2014). Many countries also have both 'Fire Danger Ratings' and 'Fire Warning Systems'. These are used to inform the public of the daily fire risk, based on weather forecasts and fuel loading, and provide updates on current active fires. Other countries also often have severe penalties for arson, with high conviction rates every year, and high rewards for information on suspected arsonists (up to \$50 K (Department of Fire and Emergency Services, 2018)). However, at present, a lack of knowledge about the impacts of wildfires in the UK prohibits the development of effective strategies to reduce their impacts.

In this paper we use the Saddleworth Moor Fires in June 2018 as a case study to calculate the potential health and economic impacts of exposure to PM<sub>2.5</sub> from wildfire on the UK population using a high-resolution air quality model. The results of this study aim to quantify the population's exposure to PM<sub>2.5</sub> from the fires and the subsequent health impact. This will help to inform legislation makers, based on the impacts of the Saddleworth Moor Fires, whether there is a need to introduce preventative measures and emergency planning for fires to reduce the population's exposure to harmful pollutants.

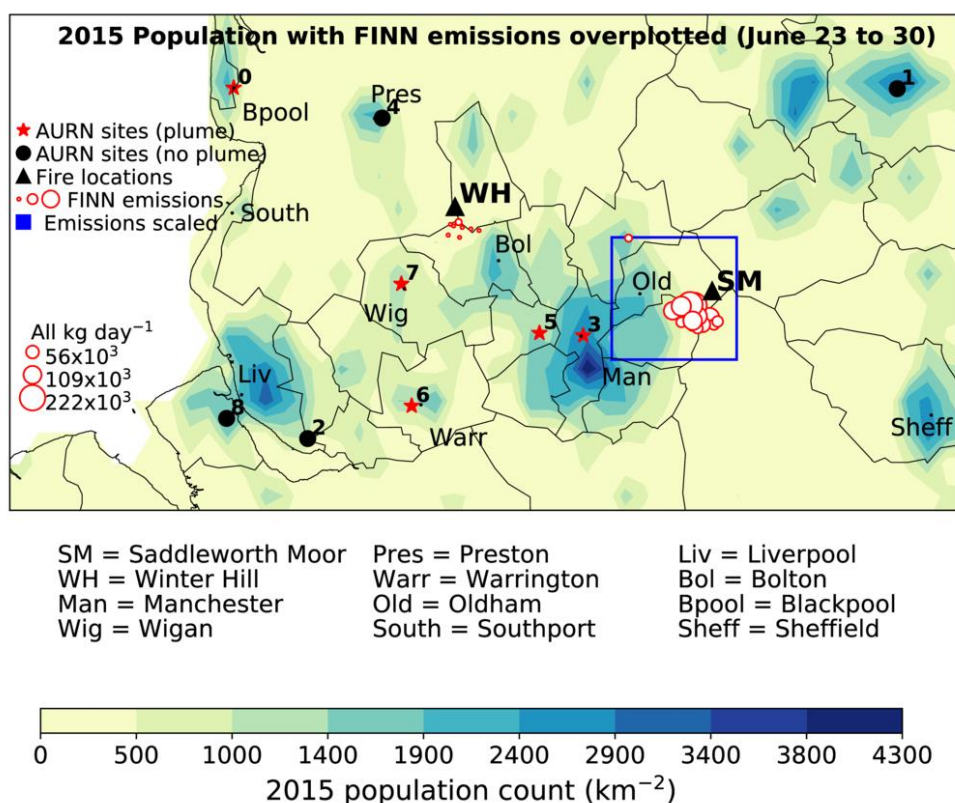


Figure 38. Population count (km<sup>-2</sup>) (2015) in model domain with Automated Urban and Rural Network (AURN) sites used in model evaluation overplotted (Supplementary Material: Table 12). Sites where elevated PM<sub>2.5</sub> was observed are indicated by red stars and those where concentrations remained below 50 µg m<sup>-3</sup> by black circles. The locations of Saddleworth Moor and Winter Hill are indicated by black triangles. Fire emissions, from FINNv1.5 (time-varying scaling), between June 23<sup>rd</sup> and June 30<sup>th</sup> are indicated by red circles – each circle represents a fire hotspot from MODIS, while the size of the circles is relative to the mass of PM<sub>2.5</sub> emitted in kg day<sup>-1</sup> (scale on left). The area over which scaling was applied to the FINN fire emissions is also shown by the blue box. More details on AURN sites can be found in Supplementary Material: Table 12.

## 5.3 Method

### 5.3.1 WRF-Chem

This study uses WRF-Chem v3.7.1 (Grell, et al., 2005), a fully coupled atmospheric chemistry model at 10 km resolution, to simulate hourly PM<sub>2.5</sub> concentrations during the Saddleworth Moor fires 2018. The study domain covers northern England (-4.9-0.7°E and 53.0-54.4°N) and

a population of 14 million people. Our simulations are performed using the same model version and set-up as Conibear *et al.* (2018a), Reddington *et al.* (2019) and Kiely *et al.* (2019). For a more detailed model description refer to Conibear *et al.* (2018a).

Meteorological initial boundary conditions (IBC) were provided by the National Centers for Environmental Prediction (NCEP) Global Forecasting System (GFS) reanalysis (meteorology) at 6-hour time steps and 0.5° resolution. Chemical IBC are from the Whole Atmosphere Community Climate Model (WACCM) (Marsh, et al., 2013) (UCAR, 2020a). An updated MOZART-4 (Emmons, et al., 2009) scheme is used to calculate gas-phase chemical reactions. Aerosol dynamics and processes were represented by the Model for Simulating Aerosol Interactions and Chemistry (MOSAIC), which included aqueous chemistry and extended treatment of organic aerosol (Hodzic, and Knote, 2014). Four bins were used represent aerosol size: 0.039-0.156 µm, 0.156-0.625 µm, 0.625-2.5 µm and 2.5-10 µm. WRF was nudged on all 33-vertical terrain following levels every 3 hours in order to keep mesoscale meteorology in line with the reanalysis meteorology from GFS (National Centre for Atmospheric Research, 2007). Variables nudged included horizontal and vertical wind, potential temperature and water vapour mixing ratio.

Monthly anthropogenic emissions were from the Emission Database for Global Atmospheric Research with Task Force on Hemispheric Transport of Air Pollution version 2.2 (EDGAR-HTAP2) (Janssens-Maenhout, et al., 2015) at 0.1° resolution for 2010 (see Supplementary Material: Anthropogenic Emissions for more information). Biogenic emissions were calculated online by the Model of Emissions of Gases and Aerosols from Nature (MEGAN) (Guenther, et al., 2006). Dust emissions are also calculated online using the GOCART with Air Force Weather Agency (AFWA) modifications (LeGrand, et al., 2019).

We calculate the contribution of the fires between June 16<sup>th</sup> and July 14<sup>th</sup> 2018 on PM<sub>2.5</sub> surface concentrations by comparing simulations with and without fire emissions included.

### 5.3.2 Wildfire emissions

Wildfire emissions are taken from the Fire Inventory from NCAR version 1.5 (FINNv1.5). The FINNv1.5 emissions dataset combines satellite observations, land cover, biomass consumption estimates and emissions factors to calculate fire emissions globally at 1 km resolution every day. Satellite observations from the MODIS Thermal Anomalies Product provide detections of active fires with a nominal horizontal resolution of  $\sim 1 \text{ km}^2$ . Burned area is assumed to be  $1 \text{ km}^2$  for each fire identified and scaled back based on the density of vegetation from the MODIS Vegetation Continuous Fields (VCF) (i.e. if 50% bare =  $0.5 \text{ km}^2$  burned area). The type of vegetation burned during a detected fire is determined using the MODIS Collection 5 Land Cover Type (LCT). This assigns each fire pixel to one of 16 possible land cover/land use classes and also the density of vegetation at 500 m resolution, scaled to 1 km. The 16 land cover types are then aggregated into 8 generic categories to which fuel loadings are applied (Wiedinmyer, et al., 2011). Fuel loadings are from Hoelzemann *et al.* (2004) and emissions factors are from Akagi *et al.* (2011), McMeeking (2008) and Andrae and Merlet (2001). FINNv1.5 includes all emissions from above ground vegetation but not from the combustion of peat (Kiely, et al., 2019).

We compare the FINN burned area (1 km resolution) with MODIS burned area (500 m resolution) in order to evaluate whether the resolution of the MODIS hotspot data used within FINN to estimate emissions is able to represent the fire size correctly, and thus emissions. We find the burned areas to be very similar for FINN ( $9.77 \text{ km}^2$ ) and MODIS ( $8.43 \text{ km}^2$ ) and the datasets to be in agreement spatially. The burned area in FINN is likely to be slightly higher

than MODIS because of the lower resolution of the dataset. Since the Saddleworth Moor fires occurred on an area that is dominated by peat bog, with overlying vegetation including heather, grass and juniper (Greater Manchester Combined Authority, 2019; Xu, et al., 2018) (Supplementary Material: Figure 65), we are confident the need for scaling emissions is due to the missing peat emissions rather than an error relating to fire size.

We therefore scale all FINN emissions over the Saddleworth Moor region (Figure 38 and Supplementary Material: Figure 65) to account for the underestimation of emissions in the dataset due to the missing peat emissions. Scaling is performed equally across all FINN emission species, and is altered daily to match the daily mean observations of  $PM_{2.5}$  at AURN sites (see Supplementary Material: Table 12 for AURN sites). We scale emissions by a factor 5 on June 26<sup>th</sup> and a factor 10 on 27<sup>th</sup>, 28<sup>th</sup> and 29<sup>th</sup>. On all other days, we use the original unscaled FINN emissions. More details on the evaluation of FINN scaling can be found in the Supplementary Material (Supplementary Material: Wildfire Emissions Scaling and Model Evaluation and Supplementary Material: Figure 66 and Figure 67).

### 5.3.3 Model Evaluation

Hourly observations of  $PM_{2.5}$  from the Automated Rural and Urban Network (AURN) in the UK are used to evaluate the model's performance at hourly and daily temporal resolution. We evaluate the model against all AURN sites in the north-west and Yorkshire and Humber regions of England, which are mostly urban sites (see Supplementary Material: Table 12 and Figure 38 for more details). Daily means are calculated from hourly data for days where >90% of data is available at a given site.

### 5.3.4 Health Impact Assessment

The health impact from short-term exposure to elevated pollutants from the Saddleworth Moor fires can be calculated using an exposure response function:

$$E_m = \sum_{i=1}^N B_d \cdot pop_i \cdot AF_i \quad (16)$$

where:

$$AF = \left( \frac{RR - 1}{RR} \right) \quad (17)$$

and:

$$RR = \exp^{\beta(X-X_0)} \quad (18)$$

$E_m$  represents the excess mortality caused by exposure to  $PM_{2.5}$  over the safe limit of exposure ( $X-X_0$ ) each day.  $N$  is the number of days within the simulation and  $i$  is the day in simulation,  $B_d$  is the baseline death rate,  $pop$  is the population exposed and  $AF$  is the attributable fraction of mortality due to exposure to  $PM_{2.5}$ . The  $AF$  is calculated using the concept of relative risk ( $RR$ ), this is the probability of mortality from a disease endpoint within an exposed population to the probability of mortality within an unexposed population ( $\beta$ ). The concentration a population is exposed to is given by  $X$  and the safe-limit of exposure is  $X_0$ . Since there is little evidence to suggest a safe-limit of exposure to  $PM_{2.5}$  we assume  $X_0$  to be zero (Holgate, 1998; Macintyre, et al., 2016; Schmidt, et al., 2011). We use beta values from Atkinson *et al.* (2014) for  $PM_{2.5}$  (1.04% (95% CI: 0.52%,1.56%) per  $10 \mu g m^{-3}$  increase). Since short-term health

impacts are assumed to be equal across ages, we use baseline mortality rates for all ages and population for all ages in the calculations (Atkinson, et al., 2014).

The health impact assessment is carried out using the “subtraction” method, which is the method most commonly used in short-term health impact studies (Crippa, et al., 2016; Macintyre, et al., 2016). This method calculates the excess mortality from fires ( $E_{m \text{ FIRES ONLY}}$ ) to be the difference between the excess mortality from  $\text{PM}_{2.5}$  in the simulation with fires on ( $E_{m \text{ FIRES ON}}$ ) and excess mortality from  $\text{PM}_{2.5}$  when there are no fires in the simulation ( $E_{m \text{ FIRES OFF}}$ ) (Equation (19)).

$$E_{m \text{ FIRES ONLY}} = E_{m \text{ FIRES ON}} - E_{m \text{ FIRES OFF}} \quad (19)$$

We use population count data from the Gridded Population of the World, Version 4.11 (NASA Socioeconomic Data and Applications Center (SEDAC) Center for International Earth Science Information Network (CIESIN), and Columbia, 2018) for 2015 at 5 km resolution. The dataset is created by the Centre for International Earth Science Information Network (CIESIN) and was accessed from the National Aeronautics and Space Administration (NASA) Socioeconomic Data and Applications Centre (SEDAC). The dataset uses estimates of human population based on the national census and population registers. Input data from 2005-2014 are extrapolated to produce estimates of population for 5-year increments. A map of this population data in the north-west of England is available for reference (Figure 38). Baseline mortality rate data for north-west England is taken from the Global Burden of Disease for 2015 (Institute for Health Metrics and Evaluation, 2018).

### 5.3.5 Economic Cost of Fires

The economic cost of mortality caused by exposure to PM<sub>2.5</sub> from the fires is calculated using the ‘Value of Prevented Fatality’ (VPF) from the UK Department for Transport. The VPF was initially used to evaluate transport projects which entail expected reductions in fatalities (Guria, et al., 2005). However, in recent years, many other government sectors, such as the UK Environment Agency and Health Protection Agency, have begun to utilise the concept (Deloitte UK, 2009). Several other studies have used this method to quantify the benefits of air quality improvements from reduced mortality (Krupnick, et al., 1996; US Environmental Protection Agency, 1997). There is a large range in estimates for VPF so we use values from the Department for Transport since these are based on UK costs of mortality and lie within the range of other estimates (see Supplementary Material: Table 15 and Supplementary Material: Economic Cost of the fires for more details). The estimates are broken down into human costs, medical costs, lost output and other costs. Values are given in GBP for 2008, which we scale to 2018 values in line with inflation (Bank of England, 2019). The human cost component reflects the pain and suffering felt by the victim and relatives and the reduction in life quality during the period of injury. Thus, the human cost is derived from the ‘Willingness to Pay’ of the population to reduce this risk. Medical costs represent all treatment costs and lost output represents working days lost and therefore, the total expected lost earnings before tax, as well as national insurance payments. Other costs represent emergency services and benefits.

## 5.4 Results

### 5.4.1 AURN Observations

AURN observations (Figure 39) indicate PM<sub>2.5</sub> concentrations at 5 locations in the north-west exceeded 100 µg m<sup>-3</sup> between June 16<sup>th</sup> and July 14<sup>th</sup> 2018. As expected, concentrations were

highest at sites near to Saddleworth Moor, reaching 140 and 225  $\mu\text{g m}^{-3}$  on June 27<sup>th</sup> and 28<sup>th</sup> at Manchester Piccadilly and Salford Eccles respectively (Figure 39). They also reached  $>175 \mu\text{g m}^{-3}$  at Wigan Centre, 50 km from the fires. Other sites in the network were relatively unaffected by the fires, with little variation in concentrations during the fires (Figure 39).

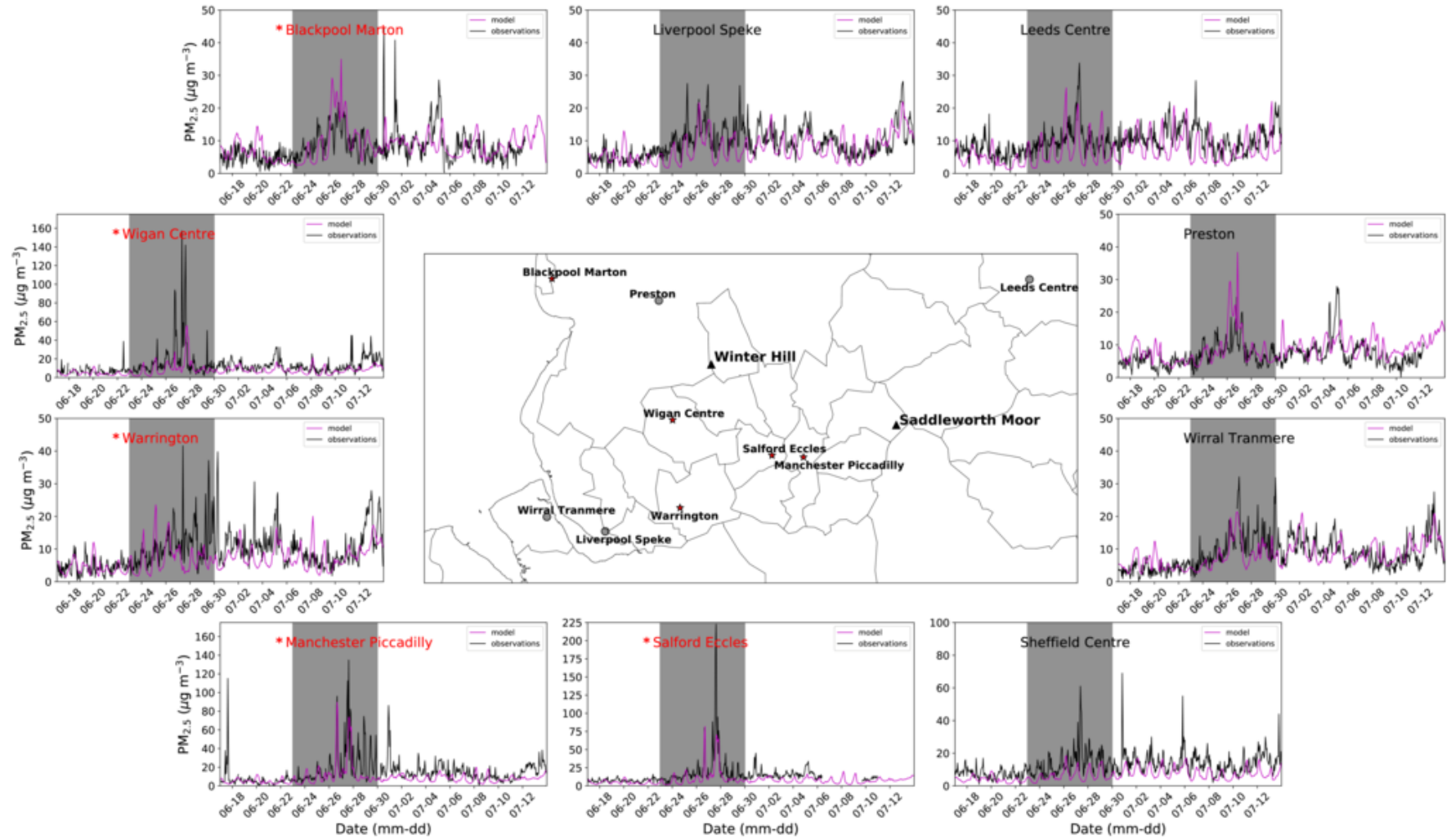


Figure 39. Hourly observed and simulated surface PM<sub>2.5</sub> between June 16<sup>th</sup> 2018 and July 14<sup>th</sup> 2018. Modelled values are from the time-varying scaling simulation (see Wildfire emissions and Model Evaluation sections and Table 8), in magenta, and observations from AURN sites are in black. Locations where PM<sub>2.5</sub> observations are elevated are shown by red stars and time series site names in red. The period when the Saddleworth Moor and Winter Hill fires occurred is indicated in grey shading.

#### 5.4.2 Model Evaluation

The model is evaluated using Pearson correlation coefficient ( $r$ ), mean bias (MB), normalised mean bias (NMB), root mean square error (RMSE), mean absolute error (MAE) and normalised mean absolute error (NMAE). Firstly, when assessing model performance at the daily resolution, without scaling FINN fire emissions (no scaling), the model performs relatively poorly (Table 8 and Supplementary Material: Figure 66). The Pearson correlation score is similar to the simulation without fire emissions (no fires) (0.69 and 0.62 respectively). RMSE ( $5.06 \mu\text{g m}^{-3}$ ), NMB (-0.22) and NMAE (0.33) are also similar to with no fire emissions ( $5.30 \mu\text{g m}^{-3}$ , -0.24 and 0.34 respectively). Referring to the time series from each AURN site it becomes clear the poor performance of the model is dominated by sites where fire emissions are not being captured well (see Supplementary Material: Figure 66 and Figure 67). When a factor 10 scaling ( $10\times$  scaling) is applied to FINN emissions over Saddleworth Moor the correlation is improved (0.74) and NMB is substantially improved (0.10) (Table 8). The RMSE ( $4.31 \mu\text{g m}^{-3}$ ) and NMAE (0.31) also improve. However, the model still over predicts PM<sub>2.5</sub> in the early stages of the fire (see Supplementary Material: Figure 66). The over prediction may be due to a changing fuel source through the fire lifetime, from the surface vegetation (heather and grass) initially, which FINN accounts for, to underlying peat once the surface vegetation has been consumed (Greater Manchester Combined Authority, 2019). Peat has much higher emissions per unit burnt ( $9.1 \text{ g kg}^{-1}$  burned (but estimates range from 6-30  $\text{g kg}^{-1}$ ) compared with 6.3–15.3  $\text{g kg}^{-1}$  for other vegetation types burned (GFEDv4) (Giglio, et al., 2013)).

Alongside this, FINNv1.5 does not account for whether burning is smouldering or flaming, which can change emissions significantly, particularly in peat fires where emissions are highest during smouldering due to colder combustion temperatures (Stockwell, et al., 2016). To try to account for the change in fuel type we perform a simulation where we adjust the scaling of the fire emissions each day (see Wildfire emissions and Model Evaluation section for more details on scaling). Using a daily time-variant scaling (Time-varying scaling) we improve RMSE ( $4.27 \mu\text{g m}^{-3}$ ) and Pearson correlation (0.77) and find the simulation has a similar NMAE (0.31) when compared with factor 10 scaling (10× scaling: RMSE =  $4.31 \mu\text{g m}^{-3}$ ,  $r = 0.74$  and NMAE = 0.31) (see Table 8). Time-varying scaling also performs best at hourly time resolution with improved correlation (0.42), RMSE ( $7.11 \mu\text{g m}^{-3}$ ) and NMAE to 0.47 (compared with factor 10 scaling and no scaling simulations ( $r = 0.37$  and  $0.351$ , RMSE =  $7.78$  and  $7.557 \mu\text{g m}^{-3}$ )) and the removal of the over prediction at the start of the fires (see Supplementary Material: Figure 66). We therefore use the time-variant scaling of FINN emissions as our best-estimate (more details in Supplementary Material: Wildfire Emissions Scaling and Model Evaluation).

Table 8. Model evaluation statistics for WRF-Chem simulations with different FINNv1.5 options for daily mean PM<sub>2.5</sub>. Statistics shown are the mean value of Pearson correlation coefficient (r), mean bias (MB), normalised mean bias (NMB), root mean squared error (RMSE), mean absolute error (MAE) and normalised mean absolute error (NMAE) at each AURN site for the entire simulation (June 16<sup>th</sup> 2018 to July 14<sup>th</sup> 2018). Simulations shown are for FINNv1.5 with no alterations (no scaling), FINN v1.5 with factor 10 scaling over Saddleworth Moor (10x scaling), FINN v1.5 with changing scaling to account for the different stages of the fire (time-varying scaling) and simulations with (no fire emissions). See Model Evaluation and Supplementary Material: Figure 65 for more details on time-varying scaling.

Daily Evaluation Statistic	Time-varying Scaling	10x Scaling	No Scaling	No Fire Emissions
<b>Pearson Correlation (r)</b>	0.77	0.74	0.69	0.62
<b>Mean Bias (MB)</b>	-1.59	-0.95	-1.84	-1.98
<b>Normalised Mean Bias (NMB)</b>	-0.19	-0.10	-0.22	-0.24
<b>Root Mean Square Error (RMSE)</b>	4.27	4.31	5.06	5.30
<b>Mean Absolute Error (MAE)</b>	2.30	2.22	2.48	2.59
<b>Normalised Mean Absolute Error (NMAE)</b>	0.31	0.31	0.33	0.34

### 5.4.3 Impact on Air Quality

Using WRF-Chem simulations we calculate the percentage increase in  $PM_{2.5}$  at the surface due to fires as  $\left(\frac{PM_{2.5\text{ Fires}} - PM_{2.5\text{ No Fires}}}{PM_{2.5\text{ No Fires}}} \times 100\right)$ , where  $PM_{2.5}$  from the simulation with fire emissions is labelled as  $PM_{2.5\text{ Fires}}$  and  $PM_{2.5}$  from the simulation without fire emissions is labelled as  $PM_{2.5\text{ No Fires}}$ . Between June 23<sup>rd</sup> and June 30<sup>th</sup> 2018 model simulations indicate the mean increase in  $PM_{2.5}$  due to fires (Figure 40 (c)) is largest in the area surrounding Oldham (> 300% increase). However, there is also a 150-200% increase in  $PM_{2.5}$  in Manchester, Bolton and Wigan. Areas as far away as Liverpool, Preston and Warrington are also affected with 10-50% increases in  $PM_{2.5}$  observed. Daily mean percentage increase in  $PM_{2.5}$  from fires indicates that the largest increase in  $PM_{2.5}$  observed is due to the Saddleworth Moor fires (Supplementary Material: Figure 70) on the 26<sup>th</sup> and 27<sup>th</sup> June. Results indicate  $PM_{2.5}$  increases of > 600% in Manchester, Bolton and Wigan and >1000% in Oldham are due to the fires (Supplementary Material: Figure 70). Large areas of the north-west also experience > 350% increase in  $PM_{2.5}$ , including Wigan, 50 km from the fires, and a 100% increase is observed as far west as the Irish Sea. Simulations indicate the Winter Hill fires on June 29<sup>th</sup> and 30<sup>th</sup> were also associated with  $PM_{2.5}$  increases of 100 to >600% in Bolton, Wigan and Southport (40 km away) (Supplementary Material: Figure 70). The Winter Hill fire was substantially smaller and occurred further north where the population density is lower. In summary, WRF-Chem simulations of wildfire impacts on atmospheric composition indicate an extensive area in which particulate matter concentrations are enhanced, far above normal regional and UK levels.

### 5.4.4 Daily Air Quality Index and WHO guideline

To put these results into the context of air quality guidelines, we use the Daily Air Quality Index (DAQI) values and the World Health Organisation (WHO) 24-hour guideline for  $PM_{2.5}$  combined with population count to estimate the population exposure (Figure 40 (a) and (b)). A limitation of this method is that it assumes the population living in the affected area is exposed

to PM<sub>2.5</sub> from the fires, however this may vary based on whether the environment they are in provides any passive or active filtration (e.g. indoor air filtration) and does not account for how much time is spent outdoors. The DAQI is used to advise the UK population on recommended behaviour changes during air pollution events. For example, the advice for PM<sub>2.5</sub> within the very high DAQI band is for everyone to reduce outdoor activity, and for those with asthma to be aware for the potential need for increased medication (see Supplementary Material: Table 13 for more details on DAQI bands). Between June 23<sup>rd</sup> and June 30<sup>th</sup> 0.8 million people were exposed to the highest DAQI band (very high: >71 µg m<sup>-3</sup>) in areas close to the Saddleworth Moor fire (Figure 40 (a)). This exposure was dominated by PM<sub>2.5</sub> on June 27<sup>th</sup> (0.5 million exposed) but 0.2 million people were also exposed to very high levels of PM<sub>2.5</sub> on June 26<sup>th</sup> (see Supplementary Material: Figure 68) (note totals may not add up due to rounding). 0.8 million people were exposed to concentrations above 54 µg m<sup>-3</sup> (high DAQI: 54-70 µg m<sup>-3</sup>) and 1.3 million people to 36-54 µg m<sup>-3</sup> (moderate DAQI) (Figure 40 (a)). The degradation in air quality was dominated by the Saddleworth Moor fires since exposure to the Winter Hill fire accounted for only 5% of the total moderate DAQI exposure (0.06 million to moderate DAQI levels on June 30<sup>th</sup>) (see Supplementary Material: Figure 68). This is likely in part because the area surrounding Winter Hill is more sparsely populated. Nonetheless, these results indicate almost a quarter of the population within our simulation domain (22% of the total 14 million people in the model domain) were exposed to concentrations of > 36 µg m<sup>-3</sup> on at least one day between June 23<sup>rd</sup> and 30<sup>th</sup> due to the Saddleworth Moor and Winter Hill fires. When we compare these results with the PM<sub>2.5</sub> No Fires simulation (Supplementary Material: Figure 71), in which no day exceeds the low DAQI, it is clear that the fires are responsible for the degradation in air quality during this time period.

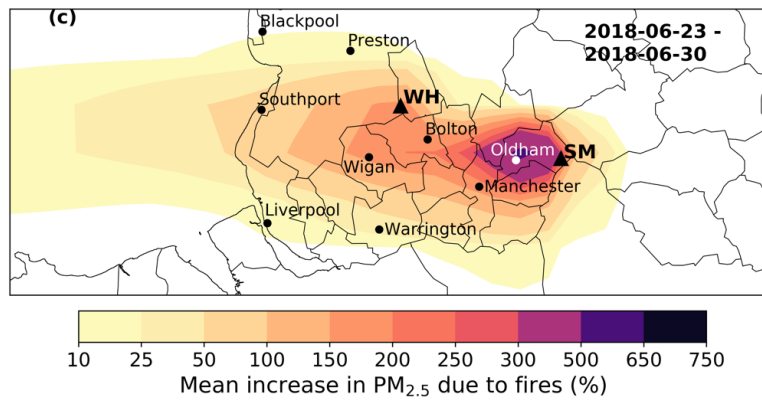
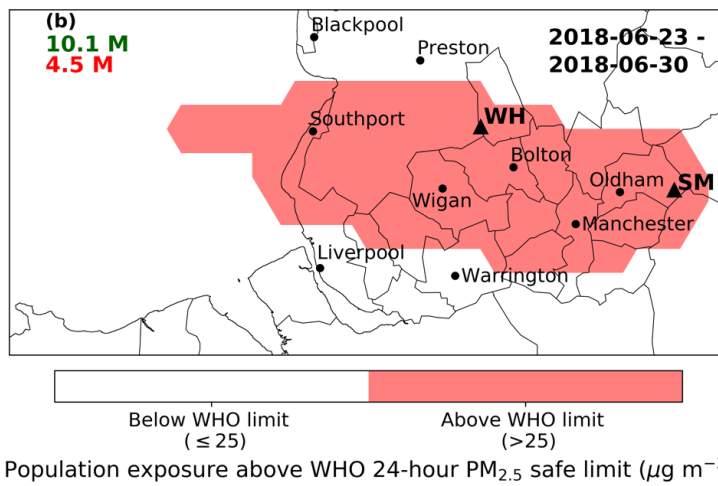
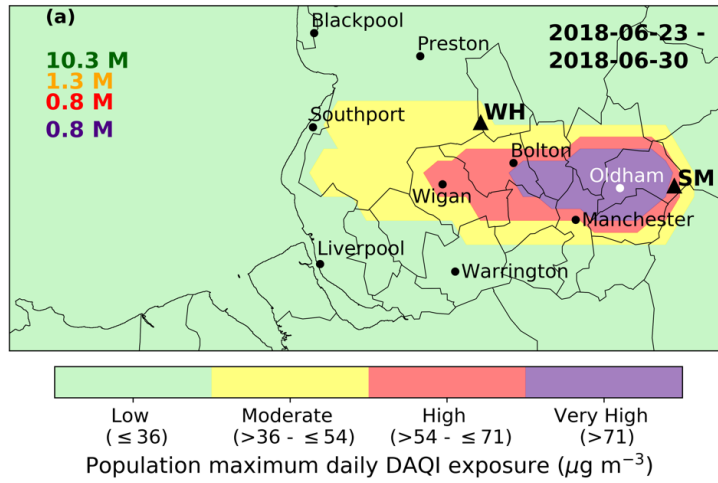


Figure 40. (a) Areas of low ( $\leq 36 \mu\text{g m}^{-3}$ ), moderate ( $36 - \leq 53 \mu\text{g m}^{-3}$ ), high ( $54 - \leq 70 \mu\text{g m}^{-3}$ ) and very high ( $>71 \mu\text{g m}^{-3}$ )  $\text{PM}_{2.5}$  as defined by the Daily Air Quality Index (DAQI). Coloured numbers correspond to total number of people exposed to each DAQI level on at least one day between June 23<sup>rd</sup> and June 30<sup>th</sup> 2018. See Supplementary Material: Table 13 for more information on the DAQI. (b) Areas where  $\text{PM}_{2.5}$  is above the WHO 24-hour limit of  $25 \mu\text{g m}^{-3}$  and total population exposed to  $\text{PM}_{2.5}$  below (green) and above (red) this threshold on at least one day between June 23<sup>rd</sup> – June 30<sup>th</sup>. (c) Mean increase (%) in  $\text{PM}_{2.5}$  due to fires between June 23<sup>rd</sup> and June 30<sup>th</sup> 2018. Calculated as,  $\left(\frac{\text{PM}_{2.5 \text{ Fires}} - \text{PM}_{2.5 \text{ No Fires}}}{\text{PM}_{2.5 \text{ No Fires}}} \times 100\right)$ , where 10 represents a 10% increase in  $\text{PM}_{2.5}$ . Locations of large urban areas and Saddleworth Moor (SM) and Winter Hill (WH) are also indicated for reference.

We also frame our results in the context of the WHO 24-hour guideline of  $25 \mu\text{g m}^{-3}$  (Figure 40 (b)). Results show that 4.5 million people were exposed to  $\text{PM}_{2.5}$  above this guideline for at least one 24-hour period between June 23<sup>rd</sup> and 30<sup>th</sup>. The impact was widespread, affecting Oldham, Manchester, Wigan and areas of high population on the coast north of Liverpool (for further detail see Supplementary Material: Figure 69).

In addition, we examine the fraction of the total annual DAQI high (48-71) and very high (71+) hourly exceedances which the fires represent at each of the AURN sites used in this study. We find that hourly DAQI exceedances during the fire period (June 23<sup>rd</sup> – June 30<sup>th</sup>) represent a large fraction of the total annual high (48-71) and very high (71+) DAQI hourly exceedances at many sites (Supplementary Material: Table 16 (a)). At Manchester Piccadilly, Salford Eccles and Wirral Tranmere 31%, 77% and 58% of total annual hourly DAQI very high exceedances occurred within the week of the fires (see Supplementary Material: Table 16 (b) for more details). Thus, not only did the fires have a large impact on air quality between June 23<sup>rd</sup> and 30<sup>th</sup> but they also represented a large fraction of the annual hourly DAQI exceedances.

### 5.4.5 Health Impact Assessment

Finally, we calculate the short-term mortality burden due to exposure to PM<sub>2.5</sub> from the fires and the economic cost, using the subtraction method detailed in the Health Impact Assessment Section. We use the concentration response function of Atkinson *et al.* (2014) with zero assumed safe-limit of exposure (0 µg m<sup>-3</sup>) since there is little evidence in the current literature to suggest that there is a safe level. In total over the 7-day period of the fires there were 28 (95% CI: 14.1-42.1) deaths brought forward with a mean daily excess mortality of 3.53 deaths per day (95% CI: 1.77-5.26) (Figure 41 (a)). This comprises a large fraction of the total 81 deaths brought forward over the four-week simulation (16<sup>th</sup> June – 14<sup>th</sup> July). When the fraction of daily mortality from fires is calculated (i.e.  $\frac{E_m \text{ Fires} - E_m \text{ No Fires}}{E_m \text{ Fires}} \times 100$ ) the impact of the fires is even more apparent (Figure 41 (a)). On June 23<sup>rd</sup> and 24<sup>th</sup>, the fraction of total excess mortality caused by fires is very low (0.08-0.9%) but substantially increases during the fires (25<sup>th</sup> and 26<sup>th</sup> – 11-39%), peaking at ~60% on June 27<sup>th</sup> and 33% on June 30<sup>th</sup>. Thus, the increase in excess mortality observed during June 23<sup>rd</sup> – 30<sup>th</sup> 2018 was dominated by the Saddleworth Moor and Winter Hill fires

In order to make our results comparable to other research in the literature we also calculate the percentage increase in excess mortality (E<sub>m</sub>) due to short-term exposure to PM<sub>2.5</sub> from the fires only ( $\frac{E_m \text{ Fires} - E_m \text{ No Fires}}{E_m \text{ No Fires}} \times 100$ ). This gives a result that is independent of the population size, since the population in the domain is relatively small (14 million) in comparison to other studies. The results indicate that up to 3.8 of 6.4 excess mortalities were due to exposure to PM<sub>2.5</sub> from the fires, representing a 165% (95% CI: 84-246%) increase in E<sub>m</sub> across the region due to exposure to PM<sub>2.5</sub> from the fires (Figure 41 (b)). While, the Winter Hill fire was associated with 1.9 of 2.8 total excess mortalities, a 96% (95% CI: 48-131%) increase in E<sub>m</sub>. In total over the 7-day period of the fires there were 7 (95% CI: 4-11) deaths brought forward

with a mean daily excess mortality of 0.9 deaths per day (95% CI: 0.5-1.4) (Figure 41 (a)). This comprises a large fraction of the total 20 deaths brought forward over the four-week period simulated (June 16<sup>th</sup> –July 14<sup>th</sup> 2018).

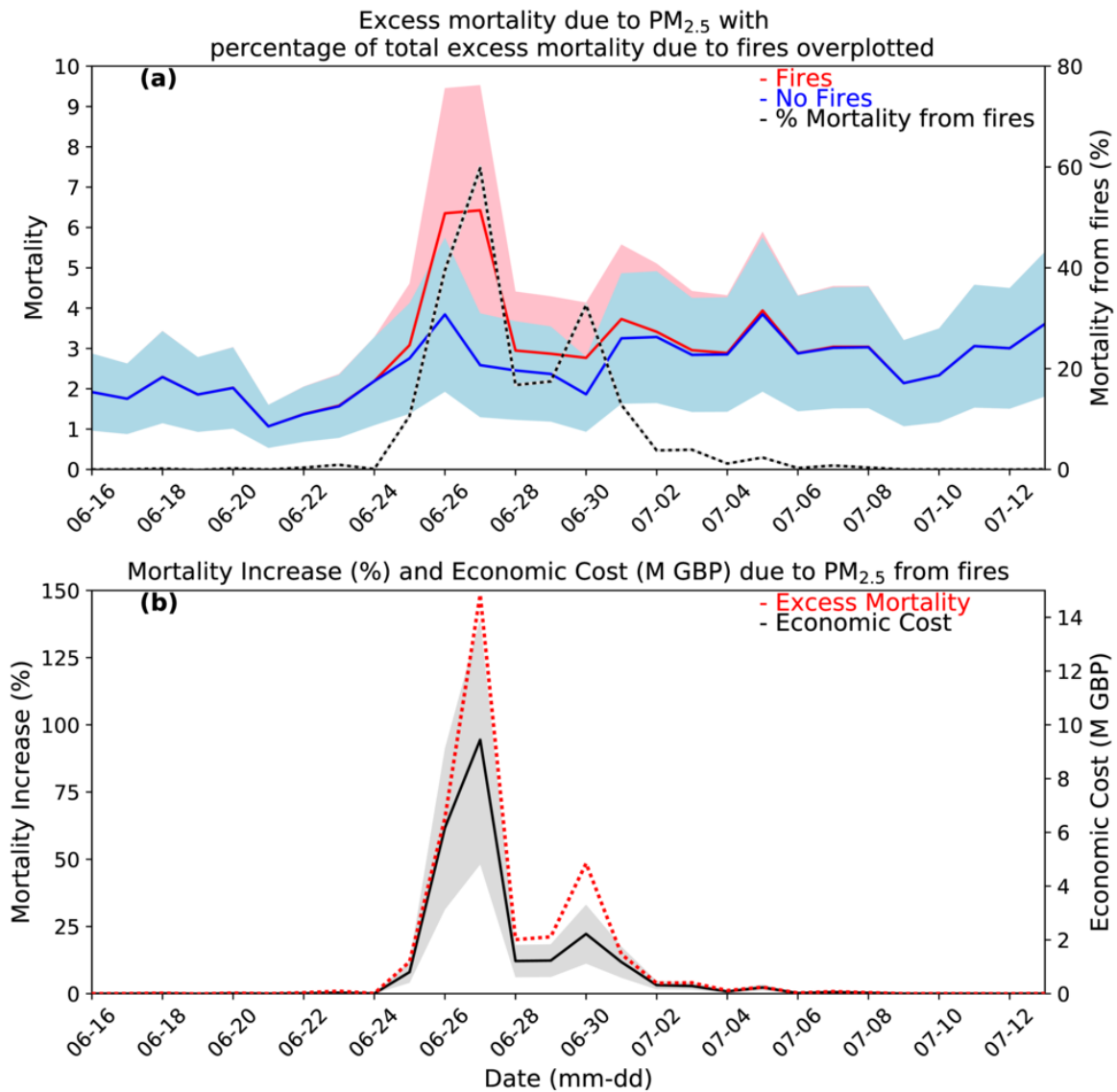


Figure 41. (a) Total Excess Mortality ( $E_m$ ) across the entire simulation domain from PM<sub>2.5</sub> in the fires and no fires simulations. The fraction of mortality due to fires across the model domain between June 16<sup>th</sup> – July 14<sup>th</sup> 2018 is also shown, calculated as  $\left(\frac{E_{m \text{ FIRES}} - E_{m \text{ NO FIRES}}}{E_{m \text{ FIRES}}}\right) \times 100$ . 95% confidence intervals, based on uncertainty in the concentration-response function, are indicated by red and blue shading. (b) Percentage increase in excess mortality ( $E_m$ ) due to fires  $\left(\frac{E_{m \text{ FIRES}} - E_{m \text{ NO FIRES}}}{E_{m \text{ NO FIRES}}}\right) \times 100$ , with the economic cost of mortality from fires (in millions of pounds (M GBP)) also shown.

Table 9. (a) The economic cost of fatality during the Saddleworth Moor Fires, calculated using the value of protected fatality (VPF) from the Department for Transport (DfT). The cost is calculated using the lower, mid and upper excess mortality from short-term exposure to PM<sub>2.5</sub> between June 23<sup>rd</sup> and 30<sup>th</sup> 2018 and the VPF for 2018 (£1.9M - see Supplementary Material Table 15 (a) for more details). (b) The cost breakdown is also shown (see Supplementary Material: Table 15 (b) for further details), based on the central excess-mortality estimates.

a)	Lower	Mid	Upper
<b>Excess Mortality Estimate (June 23<sup>rd</sup> -30<sup>th</sup>)</b>	4.4	<b>8.6</b>	12.7
<b>Economic Cost of Fatality (using 2018 DfT VPF)</b>	£ 10.7 M	<b>£ 21.1 M</b>	£ 31.3 M
<b>b) Cost breakdown based on mid excess-mortality values</b>		<b>2018 £</b>	
<b>Total VPF</b>	<b>21.1 M</b>		
Human Cost	13.9 M		
Medical	0.07 M		
Lost Output	7.0 M		
Other costs	0.15 M		

### 5.4.6 Economic Impact

The economic cost of mortality caused by exposure to PM<sub>2.5</sub> from the fires is calculated using the 'Value of Prevented Fatality' (VPF) from the Department for Transport (see Economic Cost of Fires section, Supplementary Material: Table 15 and Supplementary Material: Economic Cost of the fires section for more details). Our results indicate the fires were associated with a £21.1m economic cost between 23<sup>rd</sup>-30<sup>th</sup> June (95% CI: £10.7m – 31.2m based on calculated excess mortality uncertainty (95% CI)) (see Table 9 (a) for more details). The estimates are broken down into human costs, medical costs, lost output and other costs (Table 9 (b)) (see Economic Cost of Fires section for more details). This indicates the economic cost of the fires is dominated by the human cost (£13.9m) and lost output (£7.0m). The estimated economic cost of the fires suggests there are large economic gains to be made through the introduction of policies and education programmes to reduce the population's exposure to harmful air pollutants from fires.

## 5.5 Discussion and Conclusions

In order to contextualise our work, we compare our results to previous studies on wildfires and UK air quality. Work by Kollanus *et al.* (2017) calculated the mortality across Europe from vegetation fires during 2005 and 2008, aggregated by country. They found that in the UK the total attributable deaths in 2005 and 2008 from vegetation fires were 52 (95% CI: 40 & 65) and 42 (95% CI: 32 & 52), respectively. Equivalent to a total of 0.08 (95% CI: 0.06 & 0.11) and 0.07 (95% CI: 0.05 & 0.08) deaths per 100,000 population. Although our results are not directly comparable to those of Kollanus *et al.* (2017), due to their estimate being for long-term exposure, it is still interesting to note that the Saddleworth Moor and Winter Hill fires alone led to 0.008 deaths per day per 100,000 population.

Our results lie within the range of estimates from studies on the short-term health impacts of fires elsewhere in the world. Hänninen *et al.* (2009) found that long-range transport of PM from wildfires in eastern Europe led to an additional population-weighted exposure of  $15.7 \mu\text{g m}^{-3}$  for 2 weeks in August 2002. The study estimated the excess mortality burden to be 17 deaths in a population of 3.4 million during the 2-week period. This equated to 0.0353 deaths per day per 100,000 population – substantially higher than the estimates in this study (0.008). This may be as a result of Hänninen *et al.* (2009) overestimating exposure in non-urban areas of Finland, since they used 8 monitoring sites to characterise exposure over a  $100,000 \text{ km}^2$  area with 3.4 million inhabitants. Our estimates are closer to those of Fann *et al.* (2018) who calculated the health and economic impact of wildfires across the US between 2008-2012. The study used the same method as this study but using the CMAQ air quality model run with and without fire emissions. They found that on average 0.00171 excess mortalities per 100,000 population each day were caused by  $\text{PM}_{2.5}$  exposure from wildfires. A limitation of our work and previous work is that the exposure response function used treats all  $\text{PM}_{2.5}$  as equally toxic and the effects of concentration to be linear. This is because of a lack of studies in the literature investigating toxicity of  $\text{PM}_{2.5}$  and composition. Despite this, recent toxicology and epidemiological studies suggest that particulate matter from peat fires causes lung inflammation and cardiac responses and has a significant effect on respiratory and cardiac health (Kim, et al., 2014; Rappold, et al., 2012).

Finally, although they are not directly comparable, it is important to put the calculated health impact of the fires into context of the long-term impact of exposure to ambient pollution in this region. The long-term impact of ambient  $\text{PM}_{2.5}$  on the population in the north-west and Yorkshire regions is ~4,400 deaths per year, based on 2010  $\text{PM}_{2.5}$  concentrations (Gowers, et al., 2014). This long-term chronic effect of ambient  $\text{PM}_{2.5}$  is somewhat larger than the

calculated impact of the fires, however the impact of the fire episode represents an important acute increase in mortality over the short-term.

To conclude, this study is the first to quantify the impact of the 2018 UK wildfires on human health. We have shown that the fires had a substantial impact on air quality in the north-west of England, with observations of PM<sub>2.5</sub> concentrations reaching up to 225 µg m<sup>-3</sup> at some locations. This equated to up to a > 1000% increase in PM<sub>2.5</sub> and led to 22% of the population (2.9 million) in the simulation domain being exposed to PM<sub>2.5</sub> concentrations of 36 µg m<sup>-3</sup> or above on at least one day during the fires (June 23<sup>rd</sup> -30<sup>th</sup>). 4.5 million people (or 32% of the population) were exposed to PM<sub>2.5</sub> above the WHO 24-hour guideline of 25 µg m<sup>-3</sup> on at least one day. When we calculated the excess mortality from fires we found that there were 81 (28) excess deaths over the month (fire week) simulation due to PM<sub>2.5</sub> exposure, with 8.6 (8.6) excess deaths attributable to PM<sub>2.5</sub> from fires. Daily excess mortality indicated that during the fires (June 23<sup>rd</sup> - 30<sup>th</sup> 2018), up to 60% of mortality (3.8 of 6.4 excess mortalities) was attributable to PM<sub>2.5</sub> from fires. This represented up to a 165% increase in excess mortality compared to without fires. In addition to this, the fires also had a substantial economic impact (£21.1m). Previous studies have found public health tools and educational programs to reduce exposure yield significant health and economic benefits from reduced mortality and exacerbations of underlying illnesses. Since wildfires are likely to become more common due to climate change our work demonstrates the importance of the introduction of both public health tools and educational programs to reduce the impacts of such events.

## 5.6 Acknowledgements

Observations of PM<sub>2.5</sub> were accessed from the Department of Environment, Food and Rural Affairs (DEFRA) online from: <https://uk-air.defra.gov.uk/data/>. Gridded population data was accessed from: Center for International Earth Science Information Network (CIESIN)

<http://dx.doi.org/10.7927/H4639MPP>. All-cause mortality data was taken from the Global Burden of Disease for 2015: <http://vizhub.healthdata.org/gbd-compare>.

This work was supported by the UK Natural Environment Research Council (NERC) by providing funding for the National Centre for Earth Observation (NCEO), grant number NE/R016518/1.

## **5.7 Data Availability**

The data that support the findings of this study are available upon request from the authors.

## 5.8 References

- 1) Akagi, S.K., Yokelson, R.J., Wiedinmyer, C., Alvarado, M.J., Reid, J.S., Karl, T., Crouse, J.D., Wennberg, P.O., 2011. Emission factors for open and domestic biomass burning for use in atmospheric models. *Atmos. Chem. Phys.* 11, 4039–4072. <https://doi.org/10.5194/acp-11-4039-2011>
- 2) Andreae, M.O., Melret, P., Merlet, P., Metlet, P., 2001. Emission of trace gases and aerosols from biomass burning. *Global Biogeochem. Cycles* 15, 955–966. <https://doi.org/10.1029/2000GB001382>
- 3) Archer-Nicholls, S., Lowe, D., Darbyshire, E., Morgan, W.T., Bela, M.M., Pereira, G., Trembath, J., Kaiser, J.W., Longo, K.M., Freitas, S.R., Coe, H., McFiggans, G., 2015. Characterising Brazilian biomass burning emissions using WRF-Chem with MOSAIC sectional aerosol. *Geosci. Model Dev.* 8, 549–577. <https://doi.org/10.5194/gmd-8-549-2015>
- 4) Atkinson, R.W., Kang, S., Anderson, H.R., Mills, I.C., Walton, H.A., 2014. Epidemiological time series studies of PM<sub>2.5</sub> and daily mortality and hospital admissions: A systematic review and meta-analysis. *Thorax* 69, 660–665. <https://doi.org/10.1136/thoraxjnl-2013-204492>
- 5) Bank of England, 2019. Bank of England 2019 Inflation Calculator [WWW Document]. URL <https://www.bankofengland.co.uk/monetary-policy/inflation/inflation-calculator?number.Sections%5B0%5D.Fields%5B0%5D.Value=4900000&start-year=671.8&end-year=1110.8>
- 6) Barros, V., Field, C., Dokken, D., Mach, K., Bilir, T., MChatterjee, K., Ebi, K., Estrada, Y., Genova, R., Girma, B., Kissel, E., Levy, A., Maccracken, S., Mastandrea, P., White, L., 2014. IPCC 2014 Climate Change 2014: Impacts, Adaptation, and Vulnerability. Part B: Regional Aspects. Contribution of Working Group II to the Fifth Assessment Report of the Intergovernmental Panel on Climate Change.

- 7) Carthy, T., Chilton, S., Covey, J., Hopkins, L., Jones-Lee, M., Loomes, G., Pidgeon, N., Spencer, A., 1998. On the Contingent Valuation of Safety and the Safety of Contingent Valuation: Part 2 - The CV/SG “Chained” Approach. *J. Risk Uncertain.* 17, 187–214.  
<https://doi.org/10.1023/a:1007782800868>
- 8) Cohen, A.J., Brauer, M., Burnett, R., Anderson, H.R., Frostad, J., Estep, K., Balakrishnan, K., Brunekreef, B., Dandona, L., Dandona, R., Feigin, V., Freedman, G., Hubbell, B., Jobling, A., Kan, H., Knibbs, L., Liu, Y., Martin, R., Morawska, L., Pope III, C.A., Shin, H., Straif, K., Shaddick, G., Thomas, M., van Dingenen, R., van Donkelaar, A., Vos, T., Murray, C.J.L., Forouzanfar, M.H., 2017. Estimates and 25-year trends of the global burden of disease attributable to ambient air pollution: an analysis of data from the Global Burden of Diseases Study 2015. *Lancet* 389, 1907–1918. [https://doi.org/10.1016/S0140-6736\(17\)30505-6](https://doi.org/10.1016/S0140-6736(17)30505-6)
- 9) Conibear, L., Butt, E., Knote, C., Arnold, S., Spracklen, D., 2018. Residential energy use emissions dominate health impacts from exposure to ambient particulate matter in India. *Nat. Commun.* 9, 1–9. <https://doi.org/10.1038/s41467-018-02986-7>
- 10) Crippa, P., Castruccio, S., Archer-Nicholls, S., Lebron, G., Kuwata, M., Thota, A., Sumin, S., Butt, E., Wiedinmyer, C., Spracklen, D., 2016. Population exposure to hazardous air quality due to the 2015 fires in Equatorial Asia. *Sci. Rep.* 6, 1–9. <https://doi.org/10.1038/srep37074>
- 11) Delfino, R.J., Brummel, S., Wu, J., Stern, H., Ostro, B., Lipsett, M., Winer, A., Street, D.H., Zhang, L., Tjoa, T., Gillen, D.L., Ostro, B., Zhang, L., Street, D.H., Lipsett, M., Brummel, S., Delfino, R.J., Gillen, D.L., Stern, H., 2009. The relationship of respiratory and cardiovascular hospital admissions to the southern California wildfires of 2003. *Occup. Environ. Med.* 66, 189–197. <https://doi.org/10.1136/oem.2008.041376>
- 12) Deloitte UK, 2009. Highways Agency Value of Life Estimates for the Purposes of Project.

- 13) Department of Fire and Emergency Services, 2018. Prepare for a Bushfire - Department of Fire and Emergency Services [WWW Document]. URL <https://www.dfes.wa.gov.au/bushfire/prepare/> (accessed 12.11.20).
- 14) Emmons, L.K., Walters, S., Hess, P.G., Lamarque, J.-F., Pfister, G.G., Fillmore, D., Granier, C., Guenther, A., Kinnison, D., Laepple, T., Orlando, J., Tie, X., Tyndall, G., Wiedinmyer, C., Baughcum, S.L., Kloster, S., 2009. Description and evaluation of the Model for Ozone and Related chemical Tracers, version 4 (MOZART-4). *Geosci. Model Dev. Discuss.* 2, 1157–1213. <https://doi.org/10.5194/gmdd-2-1157-2009>
- 15) Fann, N., Alman, B., Broome, R.A., Morgan, G.G., Johnston, F.H., Pouliot, G., Rappold, A.G., 2018. The health impacts and economic value of wildland fire episodes in the U.S.: 2008–2012. *Sci. Total Environ.* 610–611, 802–809. <https://doi.org/10.1016/j.scitotenv.2017.08.024>
- 16) Finlay, S.E., Moffat, A., Gazzard, R., Baker, D., Murray, V., 2012. Health impacts of wildfires. *PLoS Curr.* 1–23. <https://doi.org/10.1371/4f959951cce2c>
- 17) Freitas, S.R., Longo, K.M., Chatfield, R., Latham, D., Silva Dias, M.A.F., Andreae, M.O., Prins, E., Santos, J.C., Gielow, R., Carvalho, J.A., 2007. Including the sub-grid scale plume rise of vegetation fires in low resolution atmospheric transport models. *Atmos. Chem. Phys.* 7, 3385–3398. <https://doi.org/10.5194/acp-7-3385-2007>
- 18) Geron, C., Hays, M., 2013. Air emissions from organic soil burning on the coastal plain of North Carolina. *Atmos. Environ.* 64, 192–199. <https://doi.org/10.1016/j.atmosenv.2012.09.065>
- 19) Giglio, L., Randerson, J.T., Van Der Werf, G.R., 2013. Analysis of daily, monthly, and annual burned area using the fourth-generation global fire emissions database (GFED4). *J. Geophys. Res. Biogeosciences* 118, 317–328. <https://doi.org/10.1002/jgrg.20042>

- 20) Gowers, A.M., Miller, B.G., Stedman, J.R., 2014. Estimating Local Mortality Burdens associated with Particulate Air Pollution About Public Health England.
- 21) Greater Manchester Combined Authority, 2019. Response to Freedom of Information Request 1920-057.
- 22) Grell, G.A., Peckham, S.E., Schmitz, R., McKeen, S.A., Frost, G., Skamarock, W.C., Eder, B., 2005. Fully coupled “online” chemistry within the WRF model. *Atmos. Environ.* 39, 6957–6975. <https://doi.org/10.1016/j.atmosenv.2005.04.027>
- 23) Guenther, A., Karl, T., Harley, P., Wiedinmyer, C., Palmer, P.I., Geron, C., 2006. Estimates of global terrestrial isoprene emissions using MEGAN (Model of Emissions of Gases and Aerosols from Nature). *Atmos. Chem. Phys.* 6, 3181–3210. <https://doi.org/10.5194/acp-6-3181-2006>
- 24) Guria, J., Leung, J., Jones-Lee, M., Loomes, G., 2005. The willingness to accept value of statistical life relative to the willingness to pay value: Evidence and policy implications. *Environ. Resour. Econ.* 32, 113–127. <https://doi.org/10.1007/s10640-005-6030-6>
- 25) Hänninen, O.O., Salonen, R.O., Koistinen, K., Lanki, T., Barregard, L., Jantunen, M., 2009. Population exposure to fine particles and estimated excess mortality in Finland from an East European wildfire episode. *J. Expo. Sci. Environ. Epidemiol.* 19, 414–422. <https://doi.org/10.1038/jes.2008.31>
- 26) HM Government, 2012. UK Climate Change Risk Assessment.
- 27) Hodzic, A., Knote, C., 2014. MOZART gas-phase chemistry with MOSAIC aerosols 7.
- 28) Hodzic, A., Madronich, S., Bonn, B., Massie, S., Menut, L., Wiedinmyer, C., 2007. Wildfire particulate matter in Europe during summer 2003: Meso-scale modeling of smoke emissions, transport and radiative effects. *Atmos. Chem. Phys.* 7, 4043–4064. <https://doi.org/10.5194/acp-7-4043-2007>

- 29) Hoelzemann, J.J., Schultz, M.G., Brasseur, G.P., Granier, C., Simon, M., 2004. Global Wildland Fire Emission Model (GWEM): Evaluating the use of global area burnt satellite data. *J. Geophys. Res.* 109, 14–18. <https://doi.org/10.1029/2003JD003666>
- 30) Holgate, S., 1998. Quantification of the Effects of Air Pollution on Health in the United Kingdom. The Stationary Office, London.
- 31) Institute for Health Metrics and Evaluation, 2018. GBD Compare Data Visualization [WWW Document]. URL <https://vizhub.healthdata.org/gbd-compare/> (accessed 3.6.18).
- 32) Jaffe, D.A., Wigder, N.L., 2012. Ozone production from wildfires: A critical review. *Atmos. Environ.* 51, 1–10. <https://doi.org/10.1016/j.atmosenv.2011.11.063>
- 33) Janssens-Maenhout, G., Crippa, M., Guizzardi, D., Dentener, F., Muntean, M., Pouliot, G., Keating, T., Zhang, Q., Kurokawa, J., Wankmüller, R., Denier Van Der Gon, H., Kuenen, J.J.P., Klimont, Z., Frost, G., Darras, S., Koffi, B., Li, M., 2015. HTAP-v2.2: A mosaic of regional and global emission grid maps for 2008 and 2010 to study hemispheric transport of air pollution. *Atmos. Chem. Phys.* 15, 11411–11432. <https://doi.org/10.5194/acp-15-11411-2015>
- 34) Jiang, Y., Lu, Z., Liu, X., Qian, Y., Zhang, K., Wang, Y., Yang, X.Q., 2016. Impacts of global open-fire aerosols on direct radiative, cloud and surface-albedo effects simulated with CAM5. *Atmos. Chem. Phys.* 16, 14805–14824. <https://doi.org/10.5194/acp-16-14805-2016>
- 35) Johnston, F., Hanigan, I., Henderson, S., Morgan, G., Bowman, D., 2011. Extreme air pollution events from bushfires and dust storms and their association with mortality in Sydney, Australia 1994-2007. *Environ. Res.* 111, 811–816. <https://doi.org/10.1016/j.envres.2011.05.007>
- 36) Johnston, F.H., Henderson, S.B., Chen, Y., Marlier, M., DeFries, R.S., Kinney, P., Bowman, D.M.J.S., Randerson, J.T., Marlier, M., DeFries, R.S., Kinney, P., Bowman, D.M.J.S., Brauer,

- M., 2012. Estimated global mortality attributable to smoke from landscape fires. *Environ. Health Perspect.* 120, 695–701. <https://doi.org/10.1289/ehp.1104422>
- 37) Jones, R.R., Hogrefe, C., Fitzgerald, E.F., Hwang, S., Garcia, V.C., Lin, S., Jones, R.R., Hogrefe, C., Fitzgerald, E.F., Hwang, S., Özkaynak, H., Garcia, V.C., Lin, S., Jones, R.R., Hogrefe, C., Fitzgerald, E.F., Hwang, S., Özkaynak, H., Garcia, V.C., Lin, S., 2015. Respiratory hospitalizations in association with fine PM and its components in New York State. *J. Air Waste Manage. Assoc.* 65, 559–569. <https://doi.org/10.1080/10962247.2014.1001500>
- 38) Kiely, L., Spracklen, D. V., Wiedinmyer, C., Conibear, L., Reddington, C.L., Archer-Nicholls, S., Lowe, D., Arnold, S.R., Knote, C., Firoz Khan, M., Talib Latif, M., Kuwata, M., Hapsari Budisulistiorini, S., Syaufina, L., 2019. New estimate of particulate emissions from Indonesian peat fires in 2015. *Atmos. Chem. Phys.* 19, 11105–11121. <https://doi.org/10.5194/acp-19-11105-2019>
- 39) Kim, Y., Tong, H., Daniels, M., Boykin, E., Krantz, Q., McGee, J., Hays, M., Kovalcik, K., Dye, J.A., Gilmour, M., 2014. Cardiopulmonary toxicity of peat wildfire particulate matter and the predictive utility of precision cut lung slices. *Part. Fibre Toxicol.* 11, 29. <https://doi.org/10.1186/1743-8977-11-29>
- 40) Kim, Y.H., King, C., Krantz, T., Hargrove, M.M., George, I.J., McGee, J., Copeland, L., Hays, M.D., Landis, M.S., Higuchi, M., Gavett, S.H., Gilmour, M.I., 2019. The role of fuel type and combustion phase on the toxicity of biomass smoke following inhalation exposure in mice. *Arch. Toxicol.* 93, 1501–1513. <https://doi.org/10.1007/s00204-019-02450-5>
- 41) Kim, Y.H., Warren, S.H., Krantz, Q.T., King, C., Jaskot, R., Preston, W.T., George, B.J., Hays, M.D., Landis, M.S., Higuchi, M., Demarini, D.M., Gilmour, M.I., 2018. Mutagenicity and lung toxicity of smoldering vs. flaming emissions from various biomass fuels:

Implications for health effects from wildland fires. *Environ. Health Perspect.* 126, 1–14.  
<https://doi.org/10.1289/EHP2200>

42) Kochi, I., Champ, P.A., Loomis, J.B., Donovan, G.H., 2012. Valuing mortality impacts of smoke exposure from major southern California wildfires. *J. For. Econ.* 18, 61–75.  
<https://doi.org/10.1016/j.jfe.2011.10.002>

43) Kollanus, V., Prank, M., Gens, A., Soares, J., Vira, J., Kukkonen, J., Sofiev, M., Salonen, R.O., Lanki, T., 2017. Mortality due to Vegetation Fire–Originated PM<sub>2.5</sub> Exposure in Europe—Assessment for the Years 2005 and 2008. *Environ. Health Perspect.* 125, 30–37.  
<https://doi.org/10.1289/EHP194>

44) Krupnick, A., Harrison, K., Nickell, E., Toman, M., 1996. The value of health benefits from ambient air quality improvements in Central and Eastern Europe: An exercise in benefits transfer. *Environ. Resour. Econ.* 7, 307–332. <https://doi.org/10.1007/bf00369622>

45) Landis, M.S., Edgerton, E.S., White, E.M., Wentworth, G.R., Sullivan, A.P., Dillner, A.M., 2018. The impact of the 2016 Fort McMurray Horse River Wildfire on ambient air pollution levels in the Athabasca Oil Sands Region, Alberta, Canada. *Sci. Total Environ.* 618, 1665–1676. <https://doi.org/10.1016/j.scitotenv.2017.10.008>

46) LeGrand, S.L., Polashenski, C., Letcher, T.W., Creighton, G.A., Peckham, S.E., Cetola, J.D., 2019. The AFWA dust emission scheme for the GOCART aerosol model in WRF-Chem v3.8.1. *Geosci. Model Dev.* 12, 131–166. <https://doi.org/10.5194/gmd-12-131-2019>

47) Liu, J.C., Pereira, G., Uhl, S.A., Bravo, M.A., Bell, M.L., 2015. A systematic review of the physical health impacts from non-occupational exposure to wildfire smoke. *Environ. Res.* 136, 120–132. <https://doi.org/10.1016/j.envres.2014.10.015>

- 48) Lu, Z., Sokolik, I.N., 2013. The effect of smoke emission amount on changes in cloud properties and precipitation: A case study of Canadian boreal wildfires of 2007. *J. Geophys. Res. Atmos.* 118, 11,777-11,793. <https://doi.org/10.1002/2013JD019860>
- 49) Macintyre, H.L., Heaviside, C., Neal, L.S., Agnew, P., Thornes, J., Vardoulakis, S., 2016. Mortality and emergency hospitalizations associated with atmospheric particulate matter episodes across the UK in spring 2014. *Environ. Int.* 97, 108–116. <https://doi.org/10.1016/j.envint.2016.07.018>
- 50) Marsh, D.R., Mills, M.J., Kinnison, D.E., Lamarque, J.F., Calvo, N., Polvani, L.M., 2013. Climate change from 1850 to 2005 simulated in CESM1(WACCM). *J. Clim.* 26, 7372–7391. <https://doi.org/10.1175/JCLI-D-12-00558.1>
- 51) Mcmeeking, G.R., 2008. The Optical, Chemical, and Physical Properties of Aerosols and Gases Emitted by the Laboratory Combustion of Wildland Fires 321.
- 52) Naeher, L.P., Brauer, M., Lipsett, M., Zelikoff, J.T., Simpson, C.D., Koenig, J.Q., Smith, K.R., 2007. Woodsmoke health effects: A review. *Inhal. Toxicol.* 19, 67–106. <https://doi.org/10.1080/08958370600985875>
- 53) NASA Socioeconomic Data and Applications Center (SEDAC) Center for International Earth Science Information Network (CIESIN), Columbia, U. of, 2018. Gridded Population of the World, Version 4 (GPWv4): Population Count, Revision 11. <https://doi.org/https://doi.org/10.7927/H4JW8BX5>
- 54) National Centre for Atmospheric Research, 2007. NCEP Global Forecast System (GFS) Analyses and Forecasts [WWW Document]. URL <https://rda.ucar.edu/datasets/ds084.6/> (accessed 12.11.20).

- 55) Rappold, A.G., Cascio, W.E., Kilaru, V.J., Stone, S.L., Neas, L.M., Devlin, R.B., Diaz-sanchez, D., 2012. Cardio-respiratory outcomes associated with exposure to wildfire smoke are modified by measures of community health 1–9.
- 56) Rappold, A.G., Fann, N.L., Crooks, J., Huang, J., Cascio, W.E., Devlin, R.B., Diaz-Sanchez, D., 2014. Forecast-based interventions can reduce the health and economic burden of wildfires. *Environ. Sci. Technol.* 48, 10571–10579. <https://doi.org/10.1021/es5012725>
- 57) Rappold, A.G., Stone, S.L., Cascio, W.E., Neas, L.M., Kilaru, V.J., Carraway, M.S., Szykman, J.J., Ising, A., Cleve, W.E., Meredith, J.T., Vaughan-Batten, H., Deyneka, L., Devlin, R.B., 2011. Peat Bog Wildfire Smoke Exposure in Rural North Carolina Is Associated with Cardiopulmonary Emergency Department Visits Assessed through Syndromic Surveillance. *Environ. Health Perspect.* 119, 1415–1420. <https://doi.org/10.1289/ehp.1003206>
- 58) Reddington, C., Conibear, L., Knote, C., Silver, B., Li, Y., Chan, C., Arnold, S., Spracklen, D., 2019. Exploring the impacts of anthropogenic emission sectors on PM<sub>2.5</sub> and human health in South and East Asia. *Atmos. Chem. Phys.* 19, 11887–11910. <https://doi.org/10.5194/acp-19-11887-2019>
- 59) Reddington, C.L., Yoshioka, M., Balasubramanian, R., Ridley, D., Toh, Y.Y., Arnold, S.R., Spracklen, D. V., 2014. Contribution of vegetation and peat fires to particulate air pollution in Southeast Asia. *Environ. Res. Lett.* 9, 094006. <https://doi.org/10.1088/1748-9326/9/9/094006>
- 60) Reid, C.E., Brauer, M., Johnston, F.H., Jerrett, M., Balmes, J.R., Elliott, C.T., E., R.C., Michael, B., H., J.F., Michael, J., R., B.J., T., E.C., 2016. Critical review of health impacts of wildfire smoke exposure. *Environ. Health Perspect.* 124, 1334–1343. <https://doi.org/10.1289/ehp.1409277>
- 61) Reisen, F., Duran, S.M., Flannigan, M., Elliott, C., Rideout, K., 2015. Wildfire smoke and public health risk. *Int. J. Wildl. Fire* 24, 1029. <https://doi.org/10.1071/WF15034>

- 62) Royal Berkshire Fire and Rescue Service, 2011. Press Release: Freedom of Information.
- 63) Schmidt, A., Ostro, B., Carslaw, K.S., Wilson, M., Thordarson, T., Mann, G.W., Simmons, A.J., 2011. Excess mortality in Europe following a future Laki-style Icelandic eruption. *Proc. Natl. Acad. Sci.* 108, 15710–15715. <https://doi.org/10.1073/pnas.1108569108>
- 64) Stockwell, C.E., Jayarathne, T., Cochrane, M.A., Ryan, K.C., Putra, E.I., Saharjo, B.H., Nurhayati, A.D., Albar, I., Blake, D.R., Simpson, I.J., Stone, E.A., Yokelson, R.J., 2016. Field measurements of trace gases and aerosols emitted by peat fires in Central Kalimantan, Indonesia, during the 2015 El Niño. *Atmos. Chem. Phys.* 16, 11711–11732. <https://doi.org/10.5194/acp-16-11711-2016>
- 65) Tinling, M.A., West, J.J., Cascio, W.E., Kilaru, V., Rappold, A.G., 2016. Repeating cardiopulmonary health effects in rural North Carolina population during a second large peat wildfire. *Environ. Heal. A Glob. Access Sci. Source* 15, 1–12. <https://doi.org/10.1186/s12940-016-0093-4>
- 66) UCAR, 2020. WRF-Chem MOZART-4 DOWNLOAD [WWW Document]. URL <https://www.aom.ucar.edu/wrf-chem/mozart.shtml> (accessed 9.16.20).
- 67) UK Met Office, 2018. UK actual and anomaly maps [WWW Document]. URL <https://www.metoffice.gov.uk/research/climate/maps-and-data/uk-actual-and-anomaly-maps> (accessed 12.11.20).
- 68) US Environmental Protection Agency, 1997. The Benefits and Costs of the Clean Air Act 1970 to 1990 (Appendix G) 45, 327–331.
- 69) Wiedinmyer, C., Akagi, S.K., Yokelson, R.J., Emmons, L.K., Al-Saadi, J.A., Orlando, J.J., Soja, A.J., 2011. The Fire INventory from NCAR (FINN): a high-resolution global model to estimate the emissions from open burning. *Geosci. Model Dev.* 4, 625–641. <https://doi.org/10.5194/gmd-4-625-2011>

70) Xu, J., Morris, P.J., Liu, J., Holden, J., 2018. PEATMAP: Refining estimates of global peatland distribution based on a meta-analysis. *Catena* 160, 134–140.

<https://doi.org/10.1016/j.catena.2017.09.010>

71) Zanobetti, A., Schwartz, J., 2009. The effect of fine and coarse particulate air pollution on mortality: A national analysis. *Environ. Health Perspect.* 117, 898–903.

<https://doi.org/10.1289/ehp.0800108>

# Impact of the 2019/2020 Australian megafires on Air Quality and Health

**Ailish M. Graham<sup>1</sup>, Richard J. Pope<sup>1,2</sup>, Kirsty P. Pringle<sup>1,3</sup>,  
Stephen R. Arnold<sup>1</sup>, Luke A. Conibear<sup>1</sup>, Helen Burns<sup>1</sup>, Richard  
Rigby<sup>1</sup>, Nicolás Borchers-Arriagada<sup>4</sup>, Edward W. Butt, <sup>1</sup>  
Laura Kiely<sup>1</sup>, Carly Reddington<sup>1</sup>, Dominic V. Spracklen<sup>1</sup>, Matt  
Woodhouse<sup>5</sup>, Christoph Knote<sup>6</sup>, James B. McQuaid<sup>1</sup>**

1 School of Earth and Environment, University of Leeds, Leeds, LS2 9JT, UK

2 National Centre for Earth Observation, University of Leeds, Leeds, LS2 9JT, UK

3 Edinburgh Parallel Computing Centre, Bayes Centre, Edinburgh, EH8 9BT, UK

4 Menzies Institute for Medical Research, University of Tasmania, Hobart, TAS 7000

Australia

5 The Commonwealth Scientific and Industrial Research Organisation, Australia

6 Meteorological Institute, LMU Munich, Munich, Germany

Correspondence to: Ailish M. Graham ([ee15amg@leeds.ac.uk](mailto:ee15amg@leeds.ac.uk))

## 6.1 Abstract

The Australian 2019/2020 bushfires were unprecedented in both their extent and intensity, causing a catastrophic loss of habitat and human and animal life across eastern-Australia. Between October 2019 and February 2020 hundreds of fires burned, peaking in size in December and January and releasing the equivalent of half of Australia's annual carbon emissions. We use a high-resolution

atmospheric-chemistry transport model to assess the impact of the bushfires on particulate matter with a diameter less than 2.5  $\mu\text{m}$  ( $\text{PM}_{2.5}$ ) concentrations across south-east Australia. The health burden from short-term population exposure to  $\text{PM}_{2.5}$  is also quantified. We find that between September 1<sup>st</sup> 2019 and January 31<sup>st</sup> 2020 large proportions of the population in eastern-Australia were exposed to dangerous ('Poor', 'Very Poor' and 'Hazardous') air quality index levels. The impact of the bushfires on AQ was concentrated in the cities of Sydney, Newcastle-Maitland and Canberra-Queanbeyan during November, December and, also in Melbourne, in January. The health impact of exposure to  $\text{PM}_{2.5}$  from bushfires across eastern-Australia, regionally and at city level is also estimated using a short-term exposure response function. Our estimate indicates that between October 1<sup>st</sup> and January 31<sup>st</sup> 180 (95% CI: 74-294) deaths were brought forward due to the fires. The number of deaths brought forward from exposure to bushfire  $\text{PM}_{2.5}$  was largest in New South Wales (109 (95% CI: 41-176)), Queensland (24 (95% CI: 15-41)) and Victoria (35 (95% CI: 13-56)). At a city level the health impacts of  $\text{PM}_{2.5}$  exposure due to the bushfires were concentrated in Sydney (65 (95% CI: 24-105)), Melbourne (23 (95% CI: 9-38)) and Canberra-Queanbeyan (9 (95% CI: 4-14)), where large populations were exposed to high  $\text{PM}_{2.5}$  concentrations due to the bushfires.

## **6.2 Introduction**

The Australian 2019/2020 bushfires were unprecedented in both their extent and intensity (Brew, et al., 2020), causing a catastrophic loss of habitat and human and animal life. Between October 2019 and February 2020 hundreds of fires burned in the south-east of the country, peaking in size in December and January. By burned area the bushfires were the largest in south-east Australia since European occupation (Wintle, et al., 2020), burning more than 10 million hectares of vegetation. The burned area for the 2019/2020 fires was larger than the Ash Wednesday and Black Saturday (1983 and 2009) fires combined (Brew, et al., 2020). The immediate impacts of the bushfires included the destruction of almost 6,000 buildings and the

deaths of 34 people and more than three billion terrestrial vertebrates. However, the impacts of the bushfires on biodiversity are not likely to be fully understood for many years (Wintle, et al., 2020). More than 100 of the significantly impacted species have lost at least 50% of their habitat and almost 50 of these species have lost >80% of their habitat. Therefore the impacts of extinction debts are yet to be realised (Wintle, et al., 2020).

The severity of the 2019/2020 bushfire season was promoted by a decrease in rainfall and increase in temperatures due to a combination of meteorological and climatic conditions (Australian Bureau of Meteorology, 2019a). Australia had experienced two very dry years prior to 2019 (2017, 2018), with 2019 being the warmest and driest on record (van Oldenborgh, et al., 2020). This was combined with a strong positive Indian Ocean Dipole (IOD) phase from July 2019 onwards (Australian Bureau of Meteorology, 2020) and a negative Southern Annular Mode (SAM) event (Australian Bureau of Meteorology, 2019b), both of which reduce rainfall across south-eastern Australia.

The vegetation cover in east Australia is dominated by native tree and grass species (native forests and woodlands, native shrublands and heathlands, native grasslands and minimally modified pasture), annual crops and highly modified pastures (Australia State of the Environment, 2016). The forests are temperate broadleaf and are principally eucalypts, one of the most fire prone species in the world. Fires in eucalypt forests spread largely through leaf litter layer, the dryness of this layer effectively controls the occurrence of fires (Boer, et al., 2020). In 2019, the moisture content of leaf litter reached record low levels and the total area of leaf litter exceeded critical flammability levels; being the highest in the past 30 years (van Oldenborgh, et al., 2020). Typically, <2% of eucalypt forests burn in the most extreme fire seasons (Boer, et al., 2020). However, during the 2019/2020 bushfires 21% of the biome burned, well above the burned percentages seen anywhere else in the world.

Emissions from the bushfires also had a large impact at a global scale, releasing >300 tonnes of CO<sub>2</sub> between August and January, equivalent to half of Australia's annual carbon emissions (Lee, 2019). In addition, plumes from the fires (carbon monoxide) circumvented the Southern hemisphere (Pope, et al., *in press.*).

Substantial epidemiological and toxicological evidence supports the association between wildfire PM<sub>2.5</sub> exposure and respiratory and cardiac morbidity (Delfino, et al., 2009; Johnston, et al., 2011; Naeher, et al., 2007; Reid, et al., 2016; Zanobetti, and Schwartz, 2009). There is also increasing evidence to suggest that exposure to wildfire smoke is associated with all-cause mortality (Faustini, et al., 2015; Johnston, et al., 2011). However, research to identify the toxicity of different PM<sub>2.5</sub> species is ongoing and so equal toxicity is commonly assumed in health impact assessments. The health burden of wildfires is concentrated in the tropics, Australia, Canada and the USA and is substantial (Black, et al., 2017; Crippa, et al., 2016; Johnston, et al., 2012; Liu, et al., 2015; Reid, et al., 2016). In these countries the PM<sub>2.5</sub> associated health burden from long-term exposure is dominated by exposure to wildfires (Lelieveld, et al., 2015). Therefore, reducing population exposure to pollutants from wildfires is likely to yield an immediate, large health benefit in these regions (Johnston, et al., 2012).

Alongside the immediate impacts of wildfires on health, from exposure to air pollutants, many studies have highlighted the psychological impacts of these disasters (Norris *et al.*, 2002; Norris *et al.*, 2002; Bryant *et al.*, 2014). An increase in the number of adults experiencing distress (42% compared to 23%) was reported in adults affected by the Ash Wednesday bushfires, compared to those who were unaffected (McFarlane, 1988; McFarlane, et al., 1997). Alongside this, children (12%) also suffered from severe emotional distress in the months following bushfires (McDermott, and Palmer, 1999).

Climate change is projected to increase the frequency, intensity and spread of wildfires globally (Sutton, et al., 2011) and in Australia (Lucas, et al., 2007). Fire weather conditions in Australia are predicted to worsen, with forest fire danger index (FFDI) projected to increase in all climate change scenarios (0-10% by 2020 and 0-30% by 2050) (Lucas, et al., 2007). Alongside this, the number of days where fire danger is ‘very-high’ or ‘extreme’ was projected to increase by between 5-65% by the end of 2020, with an increase in the length of the fire season (Lucas, et al., 2007). The largest changes in FFDI were predicted to be seen in New South Wales due to the Mediterranean climate of the region. Mild, wet winters encourage the growth of fuel, and hot, dry summers lead to an increase in the FFDI (Lucas, et al., 2007). The increase in bushfire frequency and intensity is likely to increase population exposure to pollutants from bushfires, and therefore the health burden of bushfire events.

The first study to investigate the impact of the 2019/2020 bushfires on mortality from exposure to PM<sub>2.5</sub> used PM<sub>2.5</sub> concentrations observed at ground-based air quality monitoring sites across eastern Australia to estimate daily mean PM<sub>2.5</sub> exposure (Borchers Arriagada et al., 2020). Inverse distance weighting was used to interpolate PM<sub>2.5</sub> monitoring data spatially to statistical area level 2 (SA2s) centroids within 100 km of each monitoring site. SA2s generally include a population of ~10,000 (3,000 – 25,000) and are designed to be representative of individual communities that interact together socio-economically. The entire SA2 population was then assumed to be exposed to a the interpolated PM<sub>2.5</sub> concentration. Bushfire smoke affected days were defined, at each monitoring site, as days where the daily mean PM<sub>2.5</sub> concentration exceeded the 95<sup>th</sup> percentile of historical daily mean PM<sub>2.5</sub> concentrations. The contribution of bushfire smoke to the total PM<sub>2.5</sub> mass (bushfire smoke PM<sub>2.5</sub>) was estimated using the difference between the observed PM<sub>2.5</sub> concentration and the long-term historical monthly-mean PM<sub>2.5</sub> concentration at each monitoring site. Using the bushfire smoke PM<sub>2.5</sub> the health impacts of bushfire PM<sub>2.5</sub> exposure were estimated, applying the WHO (2013) short-term

exposure-response function for all-cause, all-age mortality. The estimated health impact on mortality was substantial, with 417 (153 – 680) deaths brought forward across eastern-Australia due to bushfire smoke between October 1<sup>st</sup> 2019 and February 10<sup>th</sup> 2020. The health impact on mortality was highest in New South Wales and Victoria (219 (95% CI: 81 – 357) and 120 (95% CI: 44 – 195)).

Another study by Ryan *et al.* (2021) used a random forest model, trained using ground-based observations, to predict air pollutant concentrations, including PM<sub>2.5</sub>, without bushfires. These were compared with ground-based observations during the period of the bushfires to estimate the bushfire contribution to PM<sub>2.5</sub> concentrations each day. Population-weighted bushfire PM<sub>2.5</sub> exposure and short-term health impact in Victoria and New South Wales was then estimated in the same way as Borchers Arriagada *et al.* (2020). The estimated health impact lay within the lower limit of Borchers Arriagada *et al.* (2020) in Victoria and New South Wales at 92 (95% CI: 57 – 126) and 152 (95% CI: 95 – 209), compared with 120 (95% CI: 44 – 195) and 219 (95% CI: 81 – 357). The difference was attributed to the different approaches to quantifying the bushfire fraction of PM<sub>2.5</sub>, as well as the study by Ryan *et al.* (2021) only including populations within the large cities (~80% of the state) rather than the entire state population.

This research will build upon the work of Borchers Arriagada *et al.* (2020) and Ryan *et al.* (2021) by using an atmospheric chemistry transport model (ACTM) to simulate PM<sub>2.5</sub> concentrations between September 1<sup>st</sup> 2019 and January 31<sup>st</sup> 2020 at 30 km resolution. This will provide a more accurate daily estimation of the bushfire smoke contribution to total PM<sub>2.5</sub> mass due to explicitly simulating PM<sub>2.5</sub> concentrations for the same meteorological conditions without fires. Alongside this, regionally, population exposure is likely to be better captured,

given the sparse monitoring network and strong concentration gradients likely to have been observed.

## 6.3 Method

### 6.3.1 Model Description

PM<sub>2.5</sub> concentrations between September 1<sup>st</sup> 2019 to January 31<sup>st</sup> 2020 were simulated using WRF-Chem (version 3.7.1), a fully coupled atmospheric chemistry model. The model set-up and version used in this study is the same as (Conibear *et al.*, 2018a,2018b; Conibear *et al.*, 2018; Kiely *et al.*, 2019,2020; Reddington *et al.*, 2019; Silver *et al.*, 2020). A detailed model description can be found in Conibear *et al.* (2018a). The model domain covered eastern-Australia (128.9 to 170.6°E and -9 to -48°N) at 30 km horizontal resolution (130x150 grid boxes), with 33 vertical levels (to 10 hPa) and included 89% (22.1 m) of the Australian population. The contribution of bushfires to surface PM<sub>2.5</sub> concentrations between September 1<sup>st</sup> and January 31<sup>st</sup> was calculated by simulating two scenarios, with and without fire emissions. This allowed the contribution of the fires to air quality and health be quantified (PM<sub>2.5</sub> Fires - PM<sub>2.5</sub> NO Fires = PM<sub>2.5</sub> Fires Only).

Meteorological conditions were initialised using ERA5 6-hourly analyses at 0.1° resolution on 38 pressure levels (Hoffmann, et al., 2018). Nudging was used in order to keep simulated meteorology in line with the meteorological analyses. Several nudging sensitivity experiments were carried out to investigate the sensitivity of simulated PM<sub>2.5</sub> concentrations to the nudging option used (Supplementary Material: Figure 75). Nudging of potential temperature, the horizontal and vertical winds and the water vapour mixing ratio in all vertical levels improved simulated PM<sub>2.5</sub> concentrations by reducing the Root Mean Square Error (RMSE), Normalised Mean Absolute Error (NMAE) and Normalised Mean Bias (NMB) ( $r = 0.42$ , RMSE = 24.1, NMB = -0.49, NMAE = 0.74 compared with  $r = 0.39$ , RMSE = 22.9  $\mu\text{g m}^{-3}$ , NMB = -0.17,

NMAE = 0.72) (Supplementary Material: Table 17). Therefore, the results of the simulations where all meteorological variables in all vertical levels were nudged are presented here.

Initial boundary chemistry was provided by the Whole Atmosphere Community Climate Model (WACCM) 6-hourly simulation data (Marsh, et al., 2013; UCAR, 2020a). WACCM meteorology is driven by the NASA GMAO GEOS-5 model. Anthropogenic emissions for 2014 from CEDS (used in CMIP6) and FINN-v1 fire emissions are used in WACCM. Model output is given on 88 vertical levels at  $0.9 \times 1.25^\circ$  (UCAR, 2020b).

Global anthropogenic emissions were taken from the Emission Database for Global Atmospheric Research with Task Force on Hemispheric Transport of Air Pollution version 2.2 (EDGAR-HTAP2) (Janssens-Maenhout, et al., 2015) at  $0.1^\circ$  resolution for 2010. Sector specific diurnal cycles were subsequently added to the emissions, using diurnal cycles from Olivier *et al.* (2003). EDGAR-HTAP2 is a global, gridded, air pollution emission inventory compiled of officially reported, national gridded inventories. Where national emissions datasets or specific sectors are not available EDGAR v4.3 grid maps are used. Emissions include  $\text{SO}_2$ ,  $\text{NO}_x$ , CO, NMVOC,  $\text{NH}_3$ ,  $\text{PM}_{10}$ ,  $\text{PM}_{2.5}$ , BC and OC. Emissions include all anthropogenic emissions except large-scale biomass burning (e.g. wildfires).

### 6.3.2 Wildfire emissions

Wildfire emissions were taken from the Fire Inventory from FINN v1 near real time (FINNv1 NRT), since FINNv1.5 was not available at the time model simulations were run. FINN combines satellite observations, land cover, biomass consumption estimates and emissions factors to calculate daily fire emissions globally at 1 km resolution. FINN emissions are chosen over GFED due to their higher spatial resolution (1 km vs 5 km) and availability at near-real time. FINN uses satellite observations from the MODIS Thermal Anomalies Product to provide detections of active fires. Burned area is assumed to be  $1 \text{ km}^2$  for each fire identified and scaled

back based on the density of vegetation from the MODIS Continuous Fields (VCF) (i.e. if 50% bare = 0.5 km<sup>2</sup> burned area). The type of vegetation burned during a detected fire is determined using the MODIS Collection 5 Land Cover Type (LCT). This assigns each fire pixel to one of 16 possible land cover/land use classes and also the density of vegetation at 500 m resolution, scaled to 1 km. The 16 land cover types are then aggregated into 8 generic categories to which fuel loadings are applied (Wiedinmyer, et al., 2011). Fuel loadings are from Hoelzemann *et al.* (2004) and emissions factors are from Akagi *et al.* (2011), Mcmeeking (2008) and Andrae and Merlet (2001). Fire types included are wildfires, prescribed and agricultural burning. However, trash burning or biofuel use are not included.

The key difference between FINN v1 NRT and FINN v1.5 is that FINN v1 NRT uses MODIS near real time fire counts rather than the reprocessed fire counts, which FINN v1.5 uses. The differences between the two datasets over Australia for the year 2018 (and 2019 following the v1.5 release) are quantified (Supplementary Material: Figure 72) to identify any differences in emissions. Generally, emissions for 2019 indicate that emissions per fire hotspot were much higher than previous years (2010-2018). This is likely due to the high levels of dry fuel availability during 2019 (van Oldenborgh, et al., 2020). Emissions in FINN v1.5 and NRT are in good agreement for 2018, while for 2019 FINN NRT PM<sub>2.5</sub> (~1 Tg) are slightly higher than FINNv1.5 (~0.9 Tg). However, there is a much larger range of disagreement in the estimates of 2019 annual fire emissions between the five key fire emissions datasets (~1 to >7.5 Tg) (Supplementary Material: Figure 73).

#### 6.3.2.1 Release of Fire Emissions

The high temperatures associated with combustion mean that wildfires can often inject emissions above the surface. Therefore, in WRF-Chem, a plume-rise parameterisation is set-up to release fire emissions at the appropriate height by default (Freitas, et al., 2007). Plume-

rise uses meteorological fields and land-use from the WRF-Chem simulation as input and then explicitly simulates each plume. The height of each plume is then used as the injection height for flaming fire emissions within the model (Freitas, et al., 2007). Despite this, several studies have found that the plume-rise scheme potentially represents an incorrect vertical distribution of the emissions (Archer-Nicholls, et al., 2015; Crippa, et al., 2016). Kiely *et al.* (2020, 2019) found that releasing emissions evenly through the boundary layer improved agreement between simulated surface PM<sub>2.5</sub> concentration and observations for Indonesian fires. Therefore, we test two options: 1) releasing emissions evenly through the boundary layer and 2) plume-rise. The results of this sensitivity study indicate that simulated PM<sub>2.5</sub> concentrations are relatively insensitive to the emission option was used (Supplementary Material: Figure 75) but that releasing emissions evenly through the BL performs better. Therefore, we present the results of releasing emissions evenly through the boundary layer in this paper.

### 6.3.3 Observations

#### 6.3.3.1 Ground-based monitoring sites

Hourly PM<sub>2.5</sub> observations from ground-based monitoring are used to assess model performance in simulating PM<sub>2.5</sub> concentrations. Data from the New South Wales, Queensland, Australian Capital Territory Government and the Victoria EPA monitoring networks were combined, providing data across 80 observational sites. A map of sites used is available in the Supplementary Material (Supplementary Material: Figure 74). Daily means were calculated from hourly data if >18 hours of data was available each day, otherwise a missing data flag was applied. Model performance was evaluated using Pearson correlation (*r*), Normalised Mean Bias (NMB), Root Mean Square Error (RMSE) and Normalised Mean Absolute Error (NMAE) (Supplementary Material: Table 17). Multiple observations were available in many of the large cities (Newcastle, Sydney, Canberra, Melbourne), allowing the model performance to be evaluated in locations where populations are likely to have been exposed to high concentrations of PM<sub>2.5</sub>.

#### 6.3.4 Health Impact Assessment

The health impact from short-term exposure to elevated PM<sub>2.5</sub> from the Australian fires can be calculated using a concentration-response function (CRF). The CRF of the World Health Organisation (2013) was used to estimate the impact of short-term exposure to PM<sub>2.5</sub> on mortality.

$$E_m = \sum_{i=1}^N B_d \cdot pop_i \cdot AF_i \quad (20)$$

$$AF = \left( \frac{RR - 1}{RR} \right) \quad (21)$$

$$RR = \exp^{\beta(X-X_0)} \quad (22)$$

$$\beta = \frac{\ln(RR)}{\Delta C} \quad (23)$$

Here,  $E_m$  represents the excess mortality caused by exposure to  $PM_{2.5}$  over the safe limit of exposure ( $X-X_0$ ) each day.  $N$  is the number of days within the simulation and  $i$  is the day in simulation,  $B_d$  is the baseline death rate,  $pop_i$  is the population exposed each day and  $AF_i$  is the attributable fraction of mortality each day due to exposure to  $PM_{2.5}$ . The AF is calculated using the concept of relative risk (RR), which is the probability of mortality from a disease endpoint within an exposed population compared to within an unexposed population ( $\beta$ ). The concentration a population is exposed to is given by  $X$  and the safe-limit of exposure is  $X_0$ . Since there is little evidence to suggest a safe-limit of exposure to  $PM_{2.5}$  we assume  $X_0$  to be zero (Holgate, 1998; Macintyre, et al., 2016; Schmidt, et al., 2011). We use relative risk values from the World Health Organisation (2013) of 1.0123 (95% CI: 1.0045, 1.0201) per  $10 \mu g m^{-3}$ , which we use to estimate beta ( $\beta$ ) using Equation (23). Since short-term health impacts are assumed to be equal across ages, we use all-cause, all-age baseline mortality rates in the calculations.

### 6.3.5 Population and Baseline Mortality Data

Population count data for 2018 is from the Australia Bureau of Statistics (Australian Bureau of Statistics, 2019) at 1 km resolution. This indicates our model domain includes 89% of the Australian population. Baseline all-cause, all-age 2018 mortality rate data for each state in our

model domain is taken from the Australia Bureau of Statistics (Australian Bureau of Statistics, 2020) (Supplementary Material: Table 22).

## 6.4 Results

### 6.4.1 Fire Emissions

FINN emissions clearly indicate that the  $PM_{2.5}$  emissions between late-October 2019 and mid-January 2020 were unprecedented, lying far above the 95<sup>th</sup> percentile of emissions observed in the previous 8 years (Figure 42 and Supplementary Material: Table 17). The Australian bushfires in 2019-2020 began in the northern region of east-Australia (close to Brisbane and Newcastle) and shifted south through the season (Figure 42). As the fires moved southwards,  $PM_{2.5}$  emissions also increased, with the highest  $PM_{2.5}$  emissions occurring in south-eastern Australia in late December- early January.

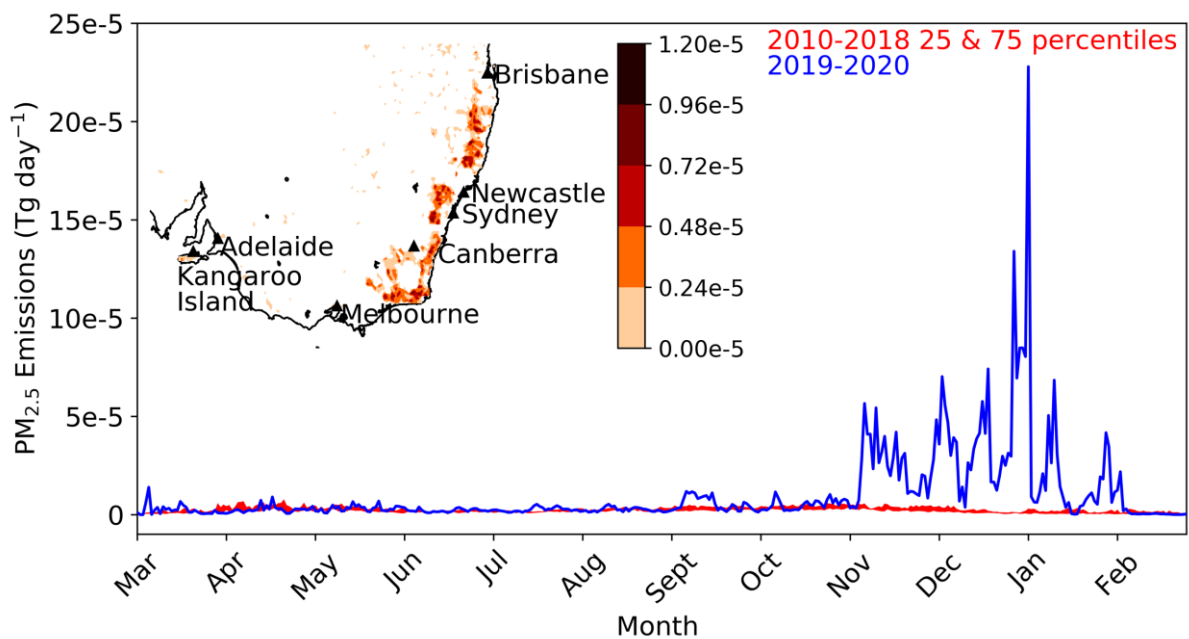


Figure 42.  $PM_{2.5}$  fire emissions (Tg day<sup>-1</sup>) across Australia between March 2019 and March 2020 from the FINN near-real time fire emission dataset. The timeseries shows the 2010-2018 25<sup>th</sup> and 75<sup>th</sup> percentiles of daily  $PM_{2.5}$  emissions each day (red) and the mean 2019-2020 daily  $PM_{2.5}$  emissions (blue). Inset map: Map of  $PM_{2.5}$  fire emissions (Tg day<sup>-1</sup>) across eastern Australia between March 2019 and March 2020.

The impact of the fires on PM<sub>2.5</sub> air quality (AQ) is clear from ground-based observations across south-east Australia (Figure 43). Observations indicate that between October 2019 and February 2020 daily mean PM<sub>2.5</sub> concentrations averaged across all sites reached 70 µg m<sup>-3</sup> on several days. Whereas, in the no fires simulation concentrations remain below 20 µg m<sup>-3</sup>. Therefore, indicating that a large fraction of the total PM<sub>2.5</sub> mass observed is due to fires. The impact of the fires on populations can be more clearly seen when PM<sub>2.5</sub> concentrations individual cities are examined (Figure 43). Newcastle-Maitland and Sydney exhibit the same pattern of PM<sub>2.5</sub> variability, following the pattern seen regionally across eastern-Australia closely. High PM<sub>2.5</sub> concentrations are first observed in late October and affect the cities sporadically until mid-January, reaching ~75 µg m<sup>-3</sup>. In contrast, the impacts of the fires on PM<sub>2.5</sub> AQ in Canberra are not seen until November and December. However, concentrations are much higher in Canberra, reaching >100 µg m<sup>-3</sup> in November and >300 µg m<sup>-3</sup> in December. PM<sub>2.5</sub> AQ in Melbourne is affected latest, with PM<sub>2.5</sub> concentrations reaching 50 to >150 µg m<sup>-3</sup> in December and January.

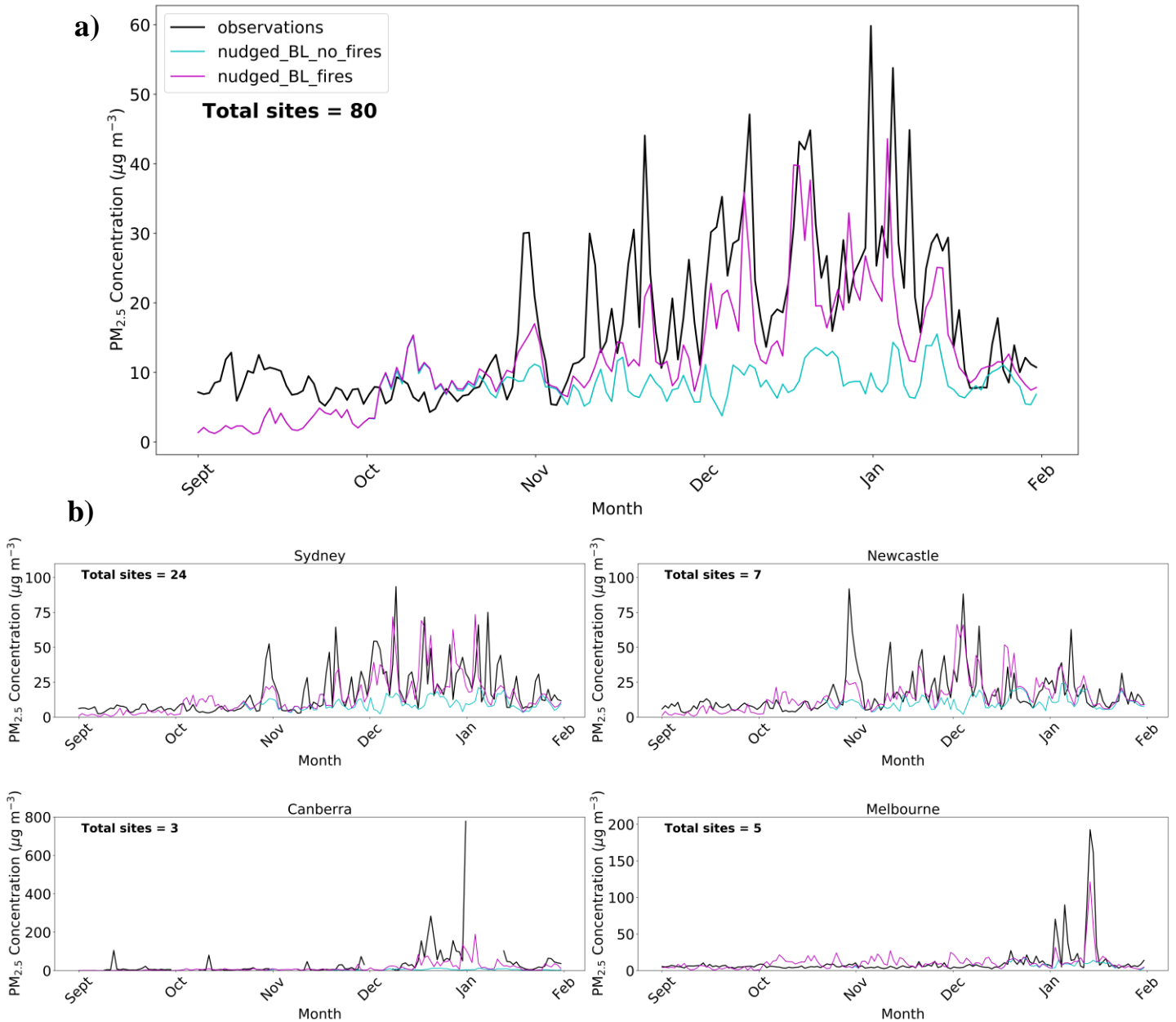


Figure 43. (a) Observed (black) and simulated (magenta and cyan) daily mean PM<sub>2.5</sub> concentrations. Simulations shown are no fires (cyan) and fires (magenta). The mean PM<sub>2.5</sub> concentration from all 64 observational sites across eastern-Australia is shown for the model and observations. (b) The same as above but for individual cities. The observed (black) and simulated (magenta and cyan) mean PM<sub>2.5</sub> concentrations are shown for each city. The total number of sites in each city is also shown on the left of each panel.

### 6.4.2 Model Evaluation

Evaluation of the WRF-Chem model indicates that the model generally underestimates PM<sub>2.5</sub> in early September (by ~70%) but then tends to overestimate PM<sub>2.5</sub> (by ~30%) in early October (before the fires) across all sites (Figure 43). This is also generally true at city scale (Figure 43). During the fire period (late-October – November) there is a substantial enhancement in PM<sub>2.5</sub> in both the observations and WRF-Chem nudged\_BL\_fires simulation. The nudged\_BL\_fires simulation captures the variability in PM<sub>2.5</sub> observations reasonably well ( $r=0.39$ ), particularly compared to the nudged\_BL\_no\_fires simulation ( $r=0.14$ ). The nudged\_BL\_fires simulation also captures the concentrations observed in the peaks and ambient conditions well (RMSE = 22.9  $\mu\text{g m}^{-3}$ , NMB = -0.17), compared to the nudged\_BL\_no\_fires simulation (RMSE = 25.3  $\mu\text{g m}^{-3}$ , NMB = -0.45) and the nudged\_BL\_1.5 simulation (RMSE = 24.3  $\mu\text{g m}^{-3}$ , NMB = -0.03). The model performs well in all of the cities which have several observational sites (Sydney, Newcastle-Maitland and Melbourne), capturing the variability and magnitude of the peaks in PM<sub>2.5</sub> well. The model struggles more to capture the magnitude of the PM<sub>2.5</sub> peaks observed in Canberra-Queanbeyan but this is likely due to the lack of observations (3 sites), meaning the model struggles to represent a small number of point measurements. Whereas the cities where PM<sub>2.5</sub> concentrations are represented better by the model had many more observations (5 - 24 sites). The improvement in model performance in cities where there are multiple observations gives confidence in the ability of the model to represent the population exposure to PM<sub>2.5</sub> from the fires.

### 6.4.3 Monthly mean PM<sub>2.5</sub> concentration (Supplementary Material)

Monthly mean PM<sub>2.5</sub> concentrations are calculated for the model and observations between October and February (Supplementary Material: Figure 77). This indicates monthly mean concentrations are low across east-Australia (0-30  $\mu\text{g m}^{-3}$ ) in October but increase through November in Newcastle-Maitland and Sydney (10-75  $\mu\text{g m}^{-3}$ ), both in New South Wales

(NSW) (Supplementary Material: Figure 77). As the fires shift southwards, concentrations increase in the NSW region and to the south, around Canberra-Queanbeyan, Australia Capital Territory (ACT), and Melbourne, South Australia, ( $10-100 \mu\text{g m}^{-3}$ ) in December. Using the nudged\_BL\_fires and nudged\_BL\_no\_fires simulations the percentage of  $\text{PM}_{2.5}$  due to fires ( $\frac{\text{PM}_{2.5 \text{ fires}} - \text{PM}_{2.5 \text{ no fires}}}{\text{PM}_{2.5 \text{ fires}}} \times 100$ ) and the increase in  $\text{PM}_{2.5}$  due to fires ( $\frac{\text{PM}_{2.5 \text{ nudged\_BL\_fires}} - \text{PM}_{2.5 \text{ nudged\_BL\_no\_fires}}}{\text{PM}_{2.5 \text{ nudged\_BL\_no\_fires}}} \times 100$ ) can be estimated. This indicates that increases in December monthly mean  $\text{PM}_{2.5}$  concentrations around Sydney, Newcastle-Maitland and Canberra-Queanbeyan of 250-1500% are observed due to the fires (Supplementary Material: Figure 78). The highest concentrations are seen in January in the region between Melbourne and Canberra-Queanbeyan ( $>150 \mu\text{g m}^{-3}$ ). This represents an increase in  $\text{PM}_{2.5}$  due to fires of  $>3500\%$ . From Supplementary Material: Figure 78 it is clear that the fires had a considerable impact on the monthly mean  $\text{PM}_{2.5}$  concentrations observed. Although monthly mean concentrations are relatively low in October and November (monthly mean  $\leq 25 \mu\text{g m}^{-3}$ ), a large fraction of  $\text{PM}_{2.5}$  is from fires. In the region to the south of Brisbane, 20-30% of the total  $\text{PM}_{2.5}$  is from fires in October. While, in the area around Newcastle and Sydney 20-100% of  $\text{PM}_{2.5}$  is from fires. In December and January, the impact of the fires on  $\text{PM}_{2.5}$  air quality is widespread, when  $>70\%$  of  $\text{PM}_{2.5}$  is from fires over a large region including Melbourne, Canberra-Queanbeyan, Sydney, Newcastle-Maitland and Brisbane.

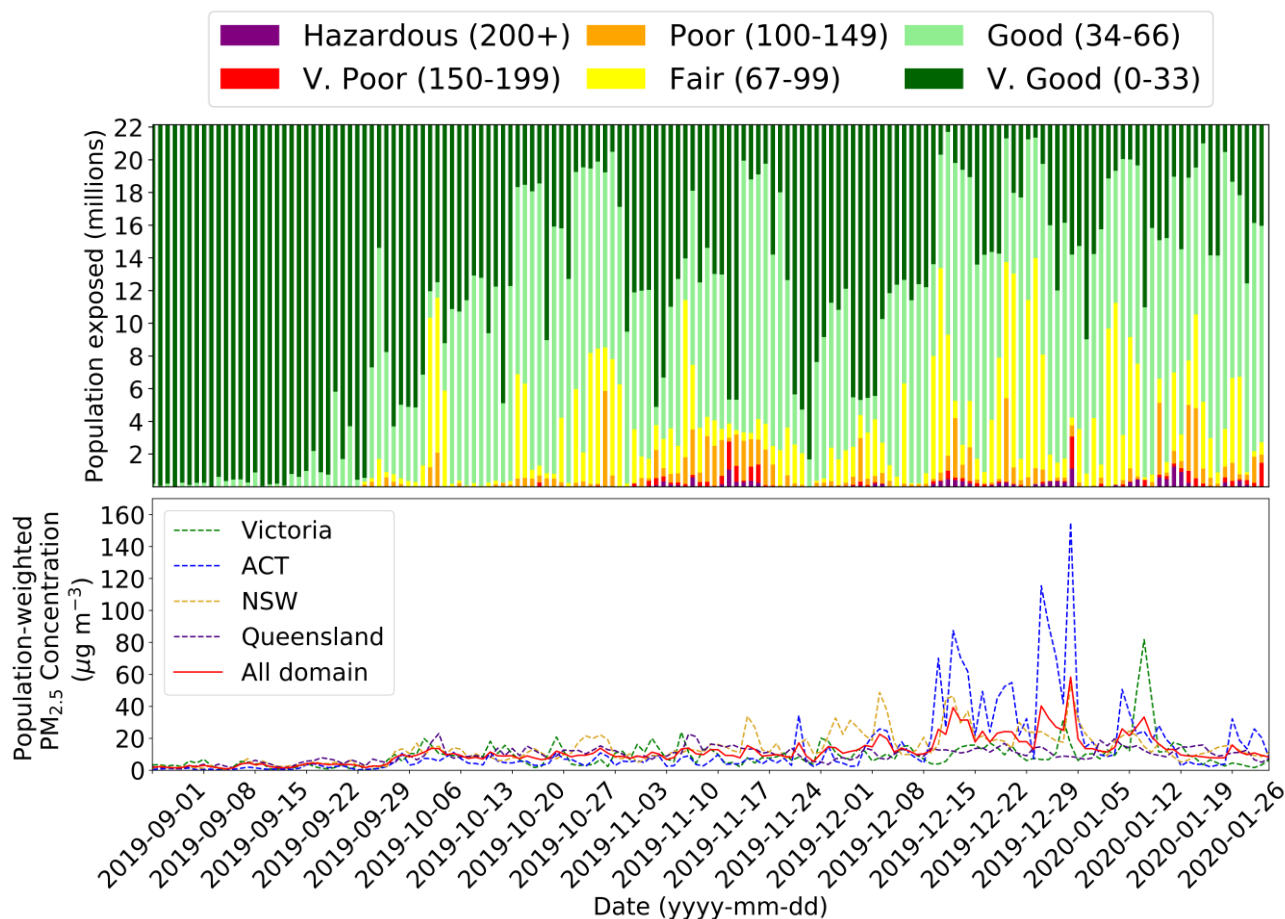


Figure 44. Daily population exposure (in millions) to Australian Air Quality Index Values across eastern-Australia (nudged\_BL\_fires simulation) between September 1<sup>st</sup> and January 31<sup>st</sup>. More information on how the AQI is calculated in Supplementary Material: Table 25. Daily population-weighted bushfire PM<sub>2.5</sub> exposure across all states in model domain (red) and regionally for Victoria (green), Australian Capital Territory blue (yellow) and Queensland (purple) (nudged\_BL\_fires-nudged\_BL\_no\_fires simulation) between September 1<sup>st</sup> and January 31<sup>st</sup>.

#### 6.4.4 Air Quality Impacts

Combining simulated PM<sub>2.5</sub> concentrations with population data (at 1 km) allows the impact of the fires on population exposure to poor AQ to be estimated across eastern-Australia (Figure 44, Supplementary Material: Figure 80) and in individual cities (Figure 45). Across eastern-Australia exposure to Air Quality Index (AQI) values in September and October dominated by ‘V.Good’ and ‘Good’ values (Figure 44 and Supplementary Material: Table 18). During

September ~21.4 million people were exposed to ‘V. Good’ and ‘Good’ AQI concentrations (Supplementary Material: Table 18), while ~6,000 people were exposed to concentrations poorer than ‘Good’ AQI. In October, there was an increase in population exposure to poor PM<sub>2.5</sub> AQ (‘Fair’, ‘Poor’, ‘V.Poor’ and ‘Hazardous’ PM<sub>2.5</sub> AQI values) (Figure 44). Throughout October an average of 2.1 m, 298,000, 12,100 and 93 people were exposed to ‘Fair’, ‘Poor’, ‘V.Poor’ and ‘Hazardous’ PM<sub>2.5</sub> AQI values. This increased throughout October and November as a large proportion of the population are exposed to ‘Fair’, ‘Poor’ or ‘V.Poor’ PM<sub>2.5</sub> AQI from November onwards (Figure 44). Between November 1<sup>st</sup> and January 1<sup>st</sup> the average population exposed to ‘Poor’, ‘V.Poor’ and ‘Hazardous’ PM<sub>2.5</sub> AQI values was ~1.5 m in November, 935,000 in December and ~1.3 m in January.

By comparing population AQI exposure with fires to if there were no fires (Supplementary Material: Table 18 and Table 19) exposure to high DAQI value can be attributed to the fires rather than as a result of other effects (e.g. long-range transport of PM<sub>2.5</sub>). This indicates that in the no fires simulation between September and the end of January ~163,000 people in total would have been exposed to AQI values of ‘V. Poor’ and 130,000 people were exposed to ‘Hazardous’ AQI values if there were no fires.

Population-weighted bushfire PM<sub>2.5</sub> concentrations for the states most severely affected by the fires (Figure 44 and Supplementary Material: Table 21) indicate that the population in ACT was exposed to the highest PM<sub>2.5</sub> due to the fires. Here, population-weighted concentrations reaching 155.1 µg m<sup>-3</sup> on January 4<sup>th</sup> and exceeding 100 µg m<sup>-3</sup> on several days. This is far above the maximum population-weighted PM<sub>2.5</sub> concentrations in any of the other states (Queensland (22.9 µg m<sup>-3</sup>) NSW (53.4 µg m<sup>-3</sup>) Victoria (81.8 µg m<sup>-3</sup>)) and far above the maximum between September 1<sup>st</sup> and January 31<sup>st</sup> across all states of 58.3 µg m<sup>-3</sup>. The mean population-weighted PM<sub>2.5</sub> concentration between September 1<sup>st</sup> and January 31<sup>st</sup> across all

states was  $11.6 \mu\text{g m}^{-3}$ , with the highest mean population-weighted  $\text{PM}_{2.5}$  concentrations in ACT ( $14.1 \mu\text{g m}^{-3}$ ) and NSW ( $13.4 \mu\text{g m}^{-3}$ ). Comparing these results with Borchers Arriagada *et al.* (2020), population-weighted bushfire  $\text{PM}_{2.5}$  concentrations are considerably lower in this study (Supplementary Material: Table 21). This is evident from the difference in the mean and maximum population-weighted  $\text{PM}_{2.5}$  concentrations across all states (mean:  $11.6 \mu\text{g m}^{-3}$  vs  $23.7 \mu\text{g m}^{-3}$  and maximum:  $58.3 \mu\text{g m}^{-3}$  vs  $98.5 \mu\text{g m}^{-3}$ ). The disparity is dominated by the large differences between estimates for ACT and Victoria (Supplementary Material: Table 21), where observations were relatively sparse.

When individual cities are considered (Figure 45) the effect of the southward shift of fires between October and January on population exposure to 'Fair', 'Poor', 'V. Poor' and 'Hazardous'  $\text{PM}_{2.5}$  AQI can be clearly seen. In October, there is widespread exposure to 'Fair' and 'Poor'  $\text{PM}_{2.5}$  AQ. The effects of population exposure are largest in Brisbane, Newcastle-Maitland, Sydney and Melbourne with 343,000, 897,000, 780,000, and ~2.2 m people exposed to 'Fair' and 'Poor'  $\text{PM}_{2.5}$  AQ (Figure 45 and Supplementary Material: Table 20). The impacts of fires on  $\text{PM}_{2.5}$  AQ becomes most evident from November. During November population exposure to 'Poor', 'V. Poor' and 'Hazardous'  $\text{PM}_{2.5}$  AQ is evident in Sydney (112,000, 86,000 and 10,000) and Newcastle-Maitland (235,000, 170,000, and 2,500). Alongside this, in Canberra-Queanbeyan 15,000, 1,100 and 174 people are exposed to 'Poor', 'V. Poor' and 'Hazardous'  $\text{PM}_{2.5}$  AQ. The pattern of increasing population exposure to poor  $\text{PM}_{2.5}$  AQ continues in December, as the fires intensify, with a clear southward shift (Figure 45). Populations in Sydney, Newcastle-Maitland and Canberra-Queanbeyan continue to be exposed to 'Poor' and worse AQ. This leads to 3.6 m, 1.7 m and 237,000 people being exposed to 'Poor' or worse AQ in Sydney, Newcastle-Maitland and Canberra-Queanbeyan, respectively in December (Supplementary Material: Table 20). During this time in Brisbane, Melbourne and

Adelaide ~5,000, 1.1 m and 53,000 people are exposed to 'Poor' or worse AQ. Finally, in January, the southward shift in fires continues, with a clear decrease in exposure to 'Poor' or worse AQI in Brisbane, Sydney and Newcastle-Maitland but increases in exposure to poor AQ in Canberra-Queanbeyan, Melbourne and Adelaide. This leads to 286,000, 979,000 and ~48,000 people being exposed to 'Poor', 'V. Poor' and 'Hazardous' PM<sub>2.5</sub> AQI values in Canberra-Queanbeyan, Melbourne and Adelaide (Supplementary Material: Table 20). Despite reductions in the total population exposed to hazardous AQI values in Newcastle-Maitland and Sydney, widespread population exposure to 'Poor', 'V. Poor' and 'Hazardous' PM<sub>2.5</sub> AQI values continues during January. In total 515,000 and ~820,000 people are exposed to 'Poor', 'V. Poor' and 'Hazardous' PM<sub>2.5</sub> AQ in Newcastle-Maitland and Sydney (Supplementary Material: Table 20).

Population-weighted bushfire PM<sub>2.5</sub> (nudged\_BL\_fires- nudged\_BL\_no\_fires) for individual cities can be used to identify the cities most severely affected by the fires (Figure 45, Supplementary Material: Table 21). In line with the state population-weighted PM<sub>2.5</sub> concentrations, Canberra-Queanbeyan (ACT) is affected most severely by PM<sub>2.5</sub> from the fires. Population-weighted PM<sub>2.5</sub> concentrations in Canberra-Queanbeyan reach 156.2 µg m<sup>-3</sup> and average 14.2 µg m<sup>-3</sup> between September 1<sup>st</sup> and January 31<sup>st</sup>. The maximum population-weighted PM<sub>2.5</sub> concentrations in Sydney (58.4 µg m<sup>-3</sup>) and Newcastle-Maitland (48.7 µg m<sup>-3</sup>) is much below Canberra-Queanbeyan. However, as a result of the prolonged exposure to poor AQ in Sydney and Newcastle-Maitland, the mean population-weighted PM<sub>2.5</sub> concentrations in both cities (13.8 µg m<sup>-3</sup> and 14.3 µg m<sup>-3</sup>) are similar to Canberra-Queanbeyan.

This clearly indicates widespread population exposure to dangerous PM<sub>2.5</sub> AQI levels throughout November, December and January. This is likely to have a large impact on public health due to short-term exposure to high PM<sub>2.5</sub> concentrations.

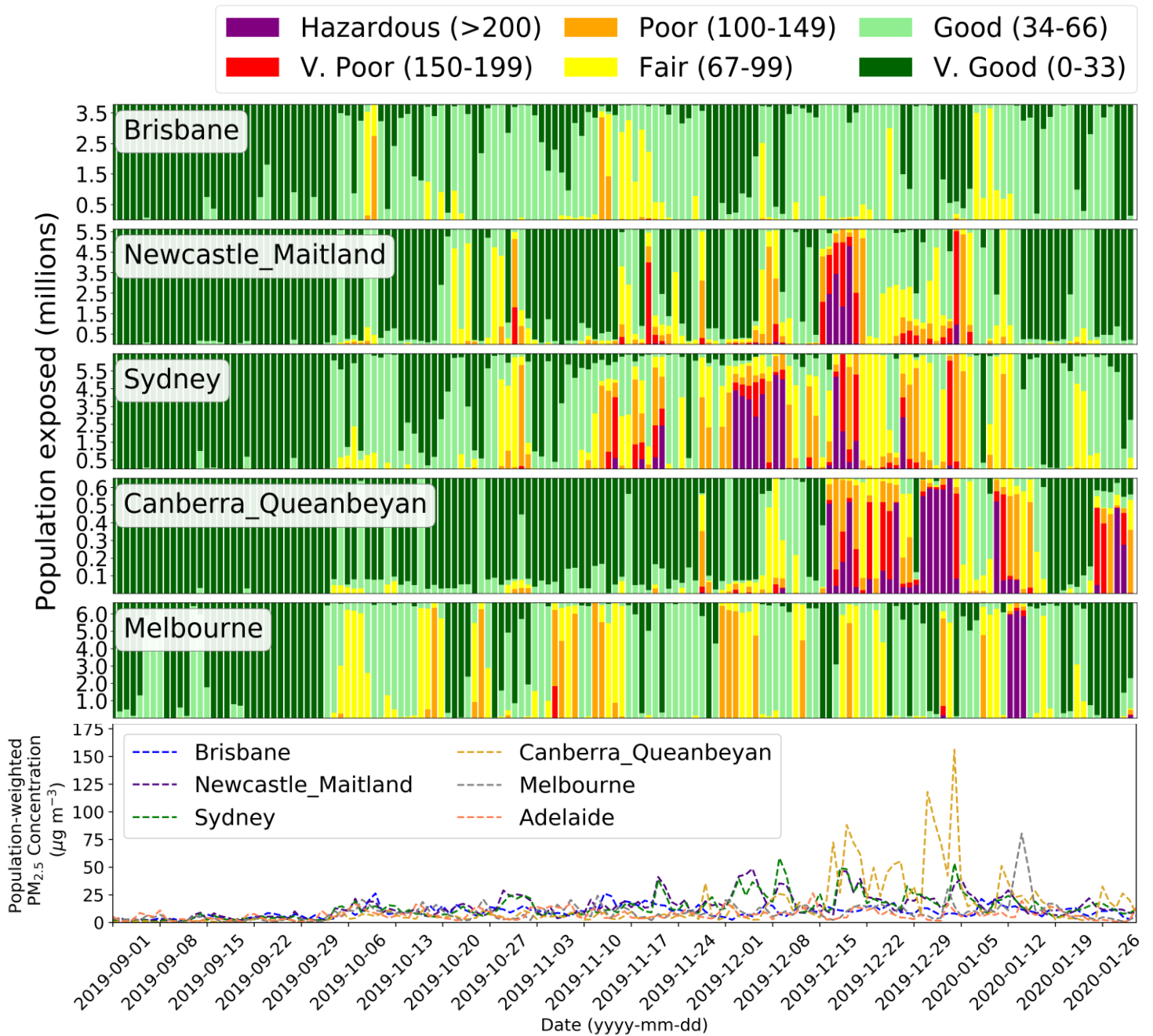


Figure 45. Daily population exposure (in millions) to Australian Air Quality Index Values in individual cities (Brisbane (Queensland), Sydney (NSW), Newcastle-Maitland (NSW), Canberra-Queanbeyan (ACT) and Melbourne (Victoria)) between September 1<sup>st</sup> and January 31<sup>st</sup>. More information on how the AQI is calculated in Supplementary Material: Table 25. Daily population-weighted bushfire PM<sub>2.5</sub> concentration in the cities of Brisbane (blue), Newcastle-Maitland (purple), Sydney (green), Canberra-Queanbeyan (yellow), Melbourne (grey) and Adelaide (orange) (nudged\_BL\_fires- nudged\_BL\_no\_fires simulation) between September 1<sup>st</sup> and January 31<sup>st</sup>.

#### 6.4.5 Health Impacts

Using the World Health Organisation (2013) concentration response function the number of deaths brought forward by the fires between October 1<sup>st</sup> and January 31<sup>st</sup> can be estimated as the difference between the number of deaths brought forward in the nudged\_BL\_fires and nudged\_BL\_no\_fires simulations (Figure 46). This indicates the impact of short-term exposure to bushfire PM<sub>2.5</sub> has a substantial impact on health from mid-October to mid-January (Figure 46). In total 180 (95% CI: 74-294) deaths were brought forward as a result of PM<sub>2.5</sub> exposure from the bushfires (Supplementary Material: Health Impacts and Table 23) and 624 (95% CI: 229-1008) from exposure to all PM<sub>2.5</sub>.

The health impact of exposure to PM<sub>2.5</sub> was largest in New South Wales (NSW), Queensland and Victoria (Figure 46). We estimate that exposure to PM<sub>2.5</sub> between October 1<sup>st</sup> 2019 and January 31<sup>st</sup> 2020 led to 287 (95% CI: 107-463), 112 (95% CI: 41-181), and 155 (95% CI: 57-250) deaths being brought forward in New South Wales (NSW), Queensland and Victoria, respectively. Of these deaths, 109 (95% CI: 41-176), 24 (95% CI: 15-41) and 35 (95% CI: 13-56) deaths brought forward were due to exposure to PM<sub>2.5</sub> from the bushfires (Supplementary Material: Table 24). Comparing these estimates with the results of Borchers Arriagada *et al.* (2020) and Ryan *et al.* (2021) (Figure 46) the estimates in this study are within the range of both studies in New South Wales (109 deaths brought forward (95% CI: 41 – 176) compared with Borchers Arriagada *et al.* (2020): 219 (95% CI: 81 – 357) and Ryan *et al.* (2021): 152.1 (95% CI: 95 – 209) and lie below the lower end of estimates in Victoria (35 deaths brought forward (95% CI: 13 – 56) compared with Borchers Arriagada *et al.* (2020): 120 (95% CI: 44 – 195) and Ryan *et al.* (2021): 92 (95% CI: 57 – 126)). The differences found between these studies are despite of all three using the same population and baseline mortality datasets and concentration-response function. The disparity in results between the studies is likely due to a number of factors. Firstly, our study uses modelled PM<sub>2.5</sub> concentrations, rather than

observations. Since the model generally underestimates PM<sub>2.5</sub> concentrations, the overall health impact estimated is likely to be underestimated due to a reduction in the population-weighted PM<sub>2.5</sub>. Additionally, the bushfire fraction of the total PM<sub>2.5</sub> mass could be overestimated in the Borchers Arriagada *et al.* (2020) study due the use of monthly mean historical PM<sub>2.5</sub> concentrations to account for the no fire fraction of PM<sub>2.5</sub>. The estimate of Ryan *et al.* (2021), which used a random forest model to account for the non-bushfire PM<sub>2.5</sub> fraction, is also lower than Borchers Arriagada *et al.* (2020), further supporting this. Additionally, the disparity between results could be, in part, due to the methods used to calculate population-exposure in the studies. The inverse weighting method used to estimate PM<sub>2.5</sub> concentrations in the Borchers Arriagada *et al.* (2020) and Ryan *et al.* (2021) studies may struggle to account for meteorological or orographic effects on PM<sub>2.5</sub> concentration gradients. However this is also a limitation in this study given the relatively coarse model resolution (30 km) which may also struggle to resolve the strong concentration gradients around cities and the fires.

When individual cities are considered in the health impact assessment it becomes clear that the health impact is concentrated in cities with high populations, where PM<sub>2.5</sub> concentrations due to fires were high (Figure 46). Of the large cities we investigated, the health impact of exposure to PM<sub>2.5</sub> from fires was largest in Sydney (65 (95% CI: 24-105)), Melbourne (23 (95% CI: 9-38)) and Canberra-Queanbeyan (9 (95% CI: 4-14)) (Figure 46, Supplementary Material: Table 24).

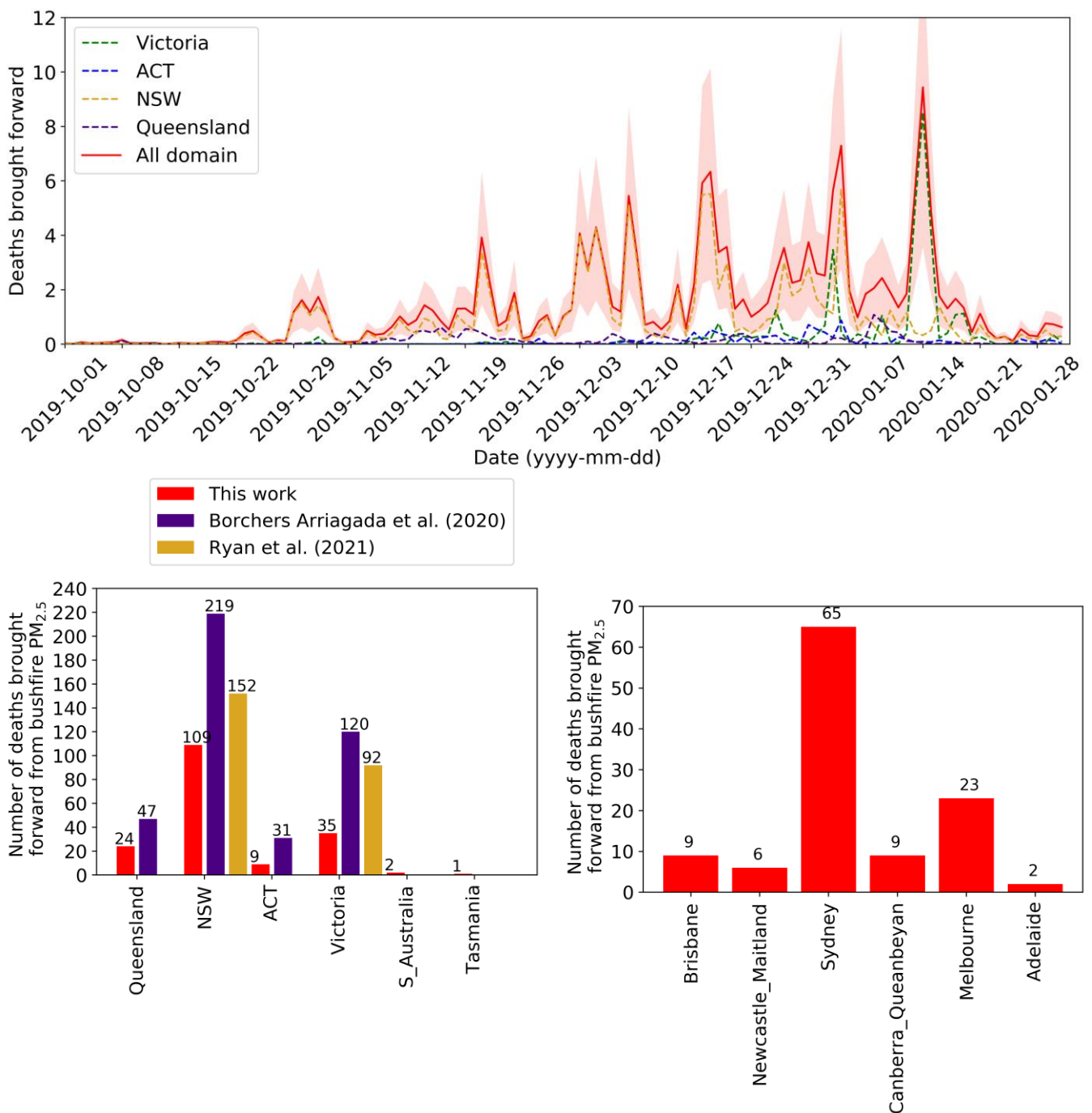


Figure 46. Estimated increase in the number of deaths brought forward across model domain (red) and the states of Victoria (green), Australia Capital Territory [ACT] (blue), New South Wales [NSW] (yellow) and Queensland (purple) due to PM<sub>2.5</sub> from bushfires (fires only) between October 1<sup>st</sup> and January 31<sup>st</sup>. Shading indicates the 95% confidence intervals of the estimate. The number of deaths brought forward due to bushfire PM<sub>2.5</sub> (fires only) (red) between October 1<sup>st</sup> and January 31<sup>st</sup> is also broken down by city and region and the total number of deaths shown above the bars. The estimated number of deaths brought forward in each state due to bushfire PM<sub>2.5</sub> (fires only) (red) in this study are compared to the Borchers Arriagada *et al.* (2020) estimate (indigo) and Ryan *et al.* (2021) for the same period.

## 6.5 Conclusions

We use the WRF-Chem regional air quality model to estimate the impact of the 2019/2020 Australian bushfires across eastern Australia, building upon the work of Borchers Arriagada *et al.* (2020). FINN fire emissions indicate PM<sub>2.5</sub> emissions from the 2019/2020 bushfires were unprecedented. Around 1 Tg of PM<sub>2.5</sub> was emitted during 2019 and ~0.3 Tg between January and February 2020. This is likely due to the high levels of dry fuel availability across the region during 2019 (van Oldenborgh, et al., 2020).

Two model simulations were performed 1) with FINN fire emissions (nudged\_BL\_fires) and 2) without FINN fire emissions (nudged\_BL\_no\_fires), which allowed the impact of the bushfires on PM<sub>2.5</sub> air quality (AQ) and health to be quantified. Simulated PM<sub>2.5</sub> concentrations from the nudged\_BL\_fires simulation reproduced observed daily mean concentrations relatively well but with a low bias ( $r = 0.39$ ,  $RMSE = 22.9 \mu\text{g m}^{-3}$ ,  $NMB = -0.17$ ,  $NMAE = 0.72$ ). Despite this, modelled PM<sub>2.5</sub> concentrations captured the variability and magnitude of peaks seen in the observations across eastern-Australia and for specific cities.

We find that between September 1<sup>st</sup> 2019 and January 31<sup>st</sup> 2020 large proportions of the population were exposed to dangerous ('Poor', 'V.Poor' and 'Hazardous') air quality levels. Almost 350,000 people were exposed to hazardous AQI levels in December and January, compared with 130,000 across December and January people in the nudged\_BL\_no\_fires simulations. The impact of the bushfires on AQ was concentrated in the cities of Sydney, Newcastle-Maitland and Canberra-Queanbeyan during November, December and, also in Melbourne, in January. While, generally Brisbane and Adelaide were less severely affected by the fires, with only 14 people exposed to Hazardous AQ.

We estimate the health impacts of exposure to PM<sub>2.5</sub> from fires across eastern-Australia, regionally and at city level using a short-term exposure response function (World Health

Organization, 2013). Our estimate indicates that between October 1<sup>st</sup> and January 31<sup>st</sup> 180 (95% CI: 74-294) deaths were brought forward due to the fires, 624 (95% CI: 229-1008) due to all PM<sub>2.5</sub> and 444 (95% CI: 155, 714) if there were no fires. The health impacts were largest in New South Wales, Queensland and Victoria with 109 (95% CI: 41, 176), 24 (95% CI: 15, 41) and 35 (95% CI: 13-56) deaths brought forward due to fires in these regions (287 (95% CI:107-463), 112 (95% CI: 41-181) and 155 (95% CI: 57-250) all PM<sub>2.5</sub>), respectively. Our results lie within the range of estimated bushfire PM<sub>2.5</sub> health impacts from both Borchers Arriagada *et al.* (2020) and Ryan *et al.* (2021) for New South Wales but below the lower limit for other states, such as Victoria. This is most likely due to differences in how PM<sub>2.5</sub> attributable to fires was estimated in each study and also differences in the estimated population-weighted bushfire PM<sub>2.5</sub> concentrations. This study builds upon previous work by using an atmospheric chemistry transport model to isolate the impacts of the fires on air quality and also to investigate the impacts regionally, away from observational sites. At a city-level, the health impacts of PM<sub>2.5</sub> exposure due to fires were concentrated in the cities with large populations and high PM<sub>2.5</sub> concentrations due to fires (Sydney (65 (95% CI: 24-105)), Melbourne (23 (95% CI: 9-38)) and Canberra-Queanbeyan (9 (95% CI: 4-14))).

This work confirms that there was a substantial AQ and health impact across eastern-Australia from the 2019/2020 bushfires. Our study only considered one health outcome, therefore the full health impact of exposure to PM<sub>2.5</sub> is likely to be higher and requires further studies addressing the impacts on hospital admissions, ambulance call outs and primary health care visits. Alongside this, the impact of other pollutants on health (e.g. O<sub>3</sub>) could also be quantified. In the future, further work is required to characterise the health impacts of exposure to pollutants for wildfires. This would allow for more comprehensive estimates of the health impacts associated with population exposure. Finally, with more dry years like 2019/2020 projected to occur in the future due to climate change the impact of wildfires such as 2019/2020

are likely to be seen again. Therefore, fire risk management policies should be developed further to consider the impact of climate change on wildfire frequency and intensity across the country.

## 6.6 References

- 1) Akagi, S.K., Yokelson, R.J., Wiedinmyer, C., Alvarado, M.J., Reid, J.S., Karl, T., Crouse, J.D., Wennberg, P.O., 2011. Emission factors for open and domestic biomass burning for use in atmospheric models. *Atmos. Chem. Phys.* 11, 4039–4072. <https://doi.org/10.5194/acp-11-4039-2011>
- 2) Andreae, M.O., Metlet, P., 2001. Emission of trace gases and aerosols from biomass burning, *Global Biogeochemical Cycles*. <https://doi.org/10.1029/2000GB001382>
- 3) Archer-Nicholls, S., Lowe, D., Darbyshire, E., Morgan, W.T., Bela, M.M., Pereira, G., Trembath, J., Kaiser, J.W., Longo, K.M., Freitas, S.R., Coe, H., McFiggans, G., 2015. Characterising Brazilian biomass burning emissions using WRF-Chem with MOSAIC sectional aerosol. *Geosci. Model Dev.* 8, 549–577. <https://doi.org/10.5194/gmd-8-549-2015>
- 4) Australia State of the Environment, 2016. Vegetation.
- 5) Australian Bureau of Meteorology, 2020. Australian Climate Influences: IOD [WWW Document]. URL <http://www.bom.gov.au/climate/about/?bookmark=iod>
- 6) Australian Bureau of Meteorology, 2019a. Tracking Australia’s climate through 2019 [WWW Document]. URL <http://www.bom.gov.au/climate/updates/articles/a036.shtml>
- 7) Australian Bureau of Meteorology, 2019b. Southern Annular Mode [WWW Document]. URL <http://www.bom.gov.au/climate/about/?bookmark=sam>
- 8) Australian Bureau of Statistics, 2020. Deaths, Year of occurrence, Age at death, Age-specific death rates, Sex, States, Territories and Australia [WWW Document]. URL

[http://stat.data.abs.gov.au/Index.aspx?DataSetCode=DEATHS\\_AGESPECIFIC\\_OCCURENCEYEAR](http://stat.data.abs.gov.au/Index.aspx?DataSetCode=DEATHS_AGESPECIFIC_OCCURENCEYEAR) (accessed 1.7.21).

- 9) Australian Bureau of Statistics, 2019. Regional Population Growth, Australia, 2017-18 [WWW Document]. URL <https://www.abs.gov.au/AUSSTATS/abs@.nsf/DetailsPage/3218.02017-18?OpenDocument> (accessed 1.7.21).
- 10) Black, C., Tesfaigzi, Y., Bassein, J.A., Miller, L.A., 2017. Wildfire smoke exposure and human health: Significant gaps in research for a growing public health issue. *Environ. Toxicol. Pharmacol.* 55, 186–195. <https://doi.org/10.1016/j.etap.2017.08.022>
- 11) Boer, M., Resco de Dios, V., Bradstock, R., 2020. Unprecedented burn area of Australian mega forest fires. *Nat. Clim. Chang.* 10, 170. <https://doi.org/10.1038/s41558-020-0710-7>
- 12) Borchers Arriagada, N., Palmer, A.J., Bowman, D.M.J.S., Morgan, G.G., Jalaludin, B.B., Johnston, F.H., 2020. Unprecedented smoke-related health burden associated with the 2019–20 bushfires in eastern Australia. *Med. J. Aust.* 2019–2020. <https://doi.org/10.5694/mja2.50545>
- 13) Brew, N., Richards, L., Smith, L., 2020. 2019–20 Australian bushfires—frequently asked questions: a quick guide.
- 14) Bryant, R.A., Waters, E., Gibbs, L., Gallagher, H.C., Pattison, P., Lusher, D., Macdougall, C., Harms, L., Block, K., Snowdon, E., Sinnott, V., Ireton, G., Richardson, J., Forbes, D., 2014. Psychological outcomes following the Victorian Black Saturday bushfires. *Aust. N. Z. J. Psychiatry* 48, 634–643. <https://doi.org/10.1177/0004867414534476>
- 15) Cohen, A.J., Brauer, M., Burnett, R., Anderson, H.R., Frostad, J., Estep, K., Balakrishnan, K., Brunekreef, B., Dandona, L., Dandona, R., Feigin, V., Freedman, G., Hubbell, B., Jobling, A.,

- Kan, H., Knibbs, L., Liu, Y., Martin, R., Morawska, L., Pope III, C.A., Shin, H., Straif, K., Shaddick, G., Thomas, M., van Dingenen, R., van Donkelaar, A., Vos, T., Murray, C.J.L., Forouzanfar, M.H., 2017. Estimates and 25-year trends of the global burden of disease attributable to ambient air pollution: an analysis of data from the Global Burden of Diseases Study 2015. *Lancet* 389, 1907–1918. [https://doi.org/10.1016/S0140-6736\(17\)30505-6](https://doi.org/10.1016/S0140-6736(17)30505-6)
- 16) Conibear, L., Butt, E., Knote, C., Arnold, S., Spracklen, D., 2018a. Residential energy use emissions dominate health impacts from exposure to ambient particulate matter in India. *Nat. Commun.* 9, 1–9. <https://doi.org/10.1038/s41467-018-02986-7>
- 17) Conibear, L., Butt, E., Knote, C., Arnold, S., Spracklen, D., 2018b. Stringent Emission Control Policies Can Provide Large Improvements in Air Quality and Public Health in India. *GeoHealth* 2, 196–211. <https://doi.org/10.1029/2018gh000139>
- 18) Conibear, L., Butt, E., Knote, C., Spracklen, D., Arnold, S., 2018c. Current and Future Disease Burden From Ambient Ozone Exposure in India. *GeoHealth* 2, 334–355. <https://doi.org/10.1029/2018gh000168>
- 19) Crippa, P., Castruccio, S., Archer-Nicholls, S., Lebron, G., Kuwata, M., Thota, A., Sumin, S., Butt, E., Wiedinmyer, C., Spracklen, D., 2016. Population exposure to hazardous air quality due to the 2015 fires in Equatorial Asia. *Sci. Rep.* 6, 1–9. <https://doi.org/10.1038/srep37074>
- 20) Delfino, R.J., Brummel, S., Wu, J., Stern, H., Ostro, B., Lipsett, M., Winer, A., Street, D.H., Zhang, L., Tjoa, T., Gillen, D.L., 2009. The relationship of respiratory and cardiovascular hospital admissions to the southern California wildfires of 2003. *Occup. Environ. Med.* 66, 189–197. <https://doi.org/10.1136/oem.2008.041376>
- 21) Faustini, A., Alessandrini, E.R., Pey, J., Perez, N., Samoli, E., Querol, X., Cadum, E., Perrino, C., Ostro, B., Ranzi, A., Sunyer, J., Stafoggia, M., Forastiere, F., Angelini, P., Berti, G.,

- Bisanti, L., Catrambone, M., Chiusolo, M., Davoli, M., De' donato, F., Demaria, M., Gandini, M., Grosa, M., Ferrari, S., Pandolfi, P., Pelosini, R., Pietrodangelo, A., Pizzi, L., Poluzzi, V., Priod, G., Randi, G., Rowinski, M., Scarinzi, C., Stivanello, E., Zauli-Sajani, S., Dimakopoulou, K., Eleftheriadis, K., Katsouyanni, K., Kelessis, A., Maggos, T., Michalopoulos, N., Pateraki, S., Petrakakis, M., Rodopoulou, S., Sypsa, V., Agis, D., Artiñano, B., Barrera-Gómez, J., Basagaña, X., De La Rosa, J., Diaz, J., Fernandez, R., Jacquemin, B., Karanasiou, A., Linares, C., Sanchez, A.M., Tobias, A., Bidondo, M., Declercq, C., Le Tertre, A., Lozano, P., Medina, S., Pascal, L., Pascal, M., 2015. Short-term effects of particulate matter on mortality during forest fires in Southern Europe: Results of the MED-PARTICLES project. *Occup. Environ. Med.* 72, 323–329. <https://doi.org/10.1136/oemed-2014-102459>
- 22) Freitas, S.R., Longo, K.M., Chatfield, R., Latham, D., Silva Dias, M.A.F., Andreae, M.O., Prins, E., Santos, J.C., Gielow, R., Carvalho, J.A., 2007. Including the sub-grid scale plume rise of vegetation fires in low resolution atmospheric transport models. *Atmos. Chem. Phys.* 7, 3385–3398. <https://doi.org/10.5194/acp-7-3385-2007>
- 23) Hoelzemann, J.J., Schultz, M.G., Brasseur, G.P., Granier, C., Simon, M., 2004. Global Wildland Fire Emission Model (GWEM): Evaluating the use of global area burnt satellite data. *J. Geophys. Res* 109, 14–18. <https://doi.org/10.1029/2003JD003666>
- 24) Hoffmann, L., Günther, G., Li, D., Stein, O., Wu, X., Griessbach, S., Heng, Y., Konopka, P., Müller, R., Vogel, B., Wright, J.S., 2018. From ERA-Interim to ERA5: considerable impact of ECMWF's next-generation reanalysis on Lagrangian transport simulations. *Atmos. Chem. Phys. Discuss.* 1–38. <https://doi.org/10.5194/acp-2018-1199>
- 25) Holgate, S., 1998. Quantification of the Effects of Air Pollution on Health in the United Kingdom. The Stationary Office, London.

- 26) Janssens-Maenhout, G., Crippa, M., Guizzardi, D., Dentener, F., Muntean, M., Pouliot, G., Keating, T., Zhang, Q., Kurokawa, J., Wankmüller, R., Denier Van Der Gon, H., Kuenen, J.J.P., Klimont, Z., Frost, G., Darras, S., Koffi, B., Li, M., 2015. HTAP-v2.2: A mosaic of regional and global emission grid maps for 2008 and 2010 to study hemispheric transport of air pollution. *Atmos. Chem. Phys.* 15, 11411–11432. <https://doi.org/10.5194/acp-15-11411-2015>
- 27) Johnston, F., Hanigan, I., Henderson, S., Morgan, G., Bowman, D., 2011. Extreme air pollution events from bushfires and dust storms and their association with mortality in Sydney, Australia 1994-2007. *Environ. Res.* 111, 811–816. <https://doi.org/10.1016/j.envres.2011.05.007>
- 28) Johnston, F.H., Henderson, S.B., Chen, Y., Marlier, M., DeFries, R.S., Kinney, P., Bowman, D.M.J.S., Randerson, J.T., Marlier, M., DeFries, R.S., Kinney, P., Bowman, D.M.J.S., Brauer, M., 2012. Estimated global mortality attributable to smoke from landscape fires. *Environ. Health Perspect.* 120, 695–701. <https://doi.org/10.1289/ehp.1104422>
- 29) Kiely, L., Spracklen, D. V., Wiedinmyer, C., Conibear, L., Reddington, C.L., Archer-Nicholls, S., Lowe, D., Arnold, S.R., Knote, C., Firoz Khan, M., Talib Latif, M., Kuwata, M., Hapsari Budisulistiorini, S., Syaufina, L., 2019. New estimate of particulate emissions from Indonesian peat fires in 2015. *Atmos. Chem. Phys.* 19, 11105–11121. <https://doi.org/10.5194/acp-19-11105-2019>
- 30) Kiely, L., Spracklen, D. V., Wiedinmyer, C., Conibear, L.A., Reddington, C.L., Arnold, S.R., Knote, C., Khan, M.F., Latif, M.T., Syaufina, L., Adrianto, H.A., 2020. Air quality and health impacts of vegetation and peat fires in Equatorial Asia during 2004 – 2015. *Environ. Res. Lett.* <https://doi.org/10.1088/1748-9326/ab9a6c>

- 31) Lee, H., 2019. Bushfires Release Over Half Australia's Annual Carbon Emissions. Bloom. Green.
- 32) Lelieveld, J., Evans, J.S., Fnais, M., Giannadaki, D., Pozzer, A., 2015. The contribution of outdoor air pollution sources to premature mortality on a global scale. *Nature* 525, 367–371. <https://doi.org/10.1038/nature15371>
- 33) Liu, J.C., Pereira, G., Uhl, S.A., Bravo, M.A., Bell, M.L., 2015. A systematic review of the physical health impacts from non-occupational exposure to wildfire smoke. *Environ. Res.* 136, 120–132. <https://doi.org/10.1016/j.envres.2014.10.015>
- 34) Lucas, C., Hennessy, K., Mills, G., Bathols, J., 2007. Bushfire Weather in Southeast Australia : Recent Trends and Projected Climate Change Impacts. Consult. Rep. Prep. Clim. Inst. Aust. 84.
- 35) Macintyre, H.L., Heaviside, C., Neal, L.S., Agnew, P., Thornes, J., Vardoulakis, S., 2016. Mortality and emergency hospitalizations associated with atmospheric particulate matter episodes across the UK in spring 2014. *Environ. Int.* 97, 108–116. <https://doi.org/10.1016/j.envint.2016.07.018>
- 36) Marsh, D.R., Mills, M.J., Kinnison, D.E., Lamarque, J.F., Calvo, N., Polvani, L.M., 2013. Climate change from 1850 to 2005 simulated in CESM1(WACCM). *J. Clim.* 26, 7372–7391. <https://doi.org/10.1175/JCLI-D-12-00558.1>
- 37) McDermott, B.M.C., Palmer, L.J., 1999. Post-disaster service provision following proactive identification of children with emotional distress and depression. *Aust. N. Z. J. Psychiatry* 33, 855–863. <https://doi.org/10.1046/j.1440-1614.1999.00611.x>

- 38) McFarlane, A.C., 1988. The phenomenology of posttraumatic stress disorders following a natural disaster. *J. Nerv. Ment. Dis.* 176, 22–29. <https://doi.org/10.1097/00005053-198801000-00003>
- 39) McFarlane, A.C., Clayer, J.R., Bookless, C.L., 1997. Psychiatric morbidity following a natural disaster: An Australian bushfire. *Soc. Psychiatry Psychiatr. Epidemiol.* 32, 261–268. <https://doi.org/10.1007/BF00789038>
- 40) Mcmeeking, G.R., 2008. The Optical, Chemical, and Physical Properties of Aerosols and Gases Emitted by the Laboratory Combustion of Wildland Fires 321.
- 41) Naeher, L.P., Brauer, M., Lipsett, M., Zelikoff, J.T., Simpson, C.D., Koenig, J.Q., Smith, K.R., 2007. Woodsmoke health effects: A review. *Inhal. Toxicol.* 19, 67–106. <https://doi.org/10.1080/08958370600985875>
- 42) Norris, Fran H., Friedman, M.J., Watson, P.J., 2002. 60,000 Disaster victims speak: Part II. Summary and implications of the disaster mental health research. *Psychiatry* 65, 240–260. <https://doi.org/10.1521/psyc.65.3.240.20169>
- 43) Norris, Fran H, Friedman, M.J., Watson, P.J., Byrne, C.M., 2002. 60 , 000 disaster victims speak : Part I . an empirical review of the empirical ... *Heal. (San Fr.* 2747.
- 44) Olivier, J., Peters, J., Granier, C., Pétron, G., Müller, J., Wallens, S., 2003. Present and future surface emissions of atmospheric compounds.
- 45) Pope, R., Kerridge, B., Siddans, R., Latter, B., Ventress, L., Chipperfield, M., Arnold, S., Pimlott, M., Graham, A., Rigby, R., n.d. Large enhancements in southern hemisphere satellite-observed carbon monoxide due to 2019/2020 Australian wildfires. “unpublished.”

- 46) Reddington, C., Conibear, L., Knote, C., Silver, B., Li, Y., Chan, C., Arnold, S., Spracklen, D., 2019. Exploring the impacts of anthropogenic emission sectors on PM<sub>2.5</sub> and human health in South and East Asia. *Atmos. Chem. Phys.* 19, 11887–11910.  
<https://doi.org/10.5194/acp-19-11887-2019>
- 47) Reid, C., Brauer, M., Johnston, F., Jerrett, M., Balmes, J., Elliott, C., 2016. Critical review of health impacts of wildfire smoke exposure. *Environ. Health Perspect.* 124, 1334–1343.  
<https://doi.org/10.1289/ehp.1409277>
- 48) Schmidt, A., Ostro, B., Carslaw, K.S., Wilson, M., Thordarson, T., Mann, G.W., Simmons, A.J., 2011. Excess mortality in Europe following a future Laki-style Icelandic eruption. *Proc. Natl. Acad. Sci.* 108, 15710–15715. <https://doi.org/10.1073/pnas.1108569108>
- 49) Silver, B., Conibear, L., Reddington, C., Knote, C., Arnold, S., Spracklen, D., 2020. Pollutant emission reductions deliver decreased PM<sub>2.5</sub>-caused mortality across China during 2015–2017. *Atmos. Chem. Phys.* 2017, 1–18. <https://doi.org/10.5194/acp-2019-1141>
- 50) Sutton, M.A., van Grinsven, H., Billen, G., Bleeker, A., Bouwman, A.F., Bull, K., Erisman, J.W., Grennfelt, P., Grizzetti, B., Howard, C.M., Oenema, O., Spranger, T., Winiwarter, W., 2011. Summary for policy makers. *Eur. Nitrogen Assess.* xxiv–xxxiv.  
<https://doi.org/10.1017/cbo9780511976988.002>
- 51) UCAR, 2020a. WRF-Chem MOZART-4 DOWNLOAD [WWW Document]. URL  
<https://www.acom.ucar.edu/wrf-chem/mozart.shtml> (accessed 9.16.20).
- 52) UCAR, 2020b. WACCM Download [WWW Document]. URL  
<https://www.acom.ucar.edu/waccm/download.shtml> (accessed 9.16.20).
- 53) van Oldenborgh, G.J., Krikken, F., Lewis, S., Leach, N., Lehner, F., Saunders, K., van Weele, M., Haustein, K., Li, S., Wallom, D., Sparrow, S., Arrighi, J., Singh, R., van Aalst, M., Philip,

- S., Vautard, R., Otto, F., 2020. Attribution of the Australian bushfire risk to anthropogenic climate change. *Nat. Hazards Earth Syst. Sci.* 1–46. <https://doi.org/10.5194/nhess-2020-69>
- 54) Wiedinmyer, C., Akagi, S.K., Yokelson, R.J., Emmons, L.K., Al-Saadi, J.A., Orlando, J.J., Soja, A.J., 2011. The Fire INventory from NCAR (FINN): a high resolution global model to estimate the emissions from open burning. *Geosci. Model Dev.* 4, 625–641. <https://doi.org/10.5194/gmd-4-625-2011>
- 55) Wintle, B.A., Legge, S., Woinarski, J.C.Z., 2020. After the Megafires: What Next for Australian Wildlife? *Trends Ecol. Evol.* xx, 1–5. <https://doi.org/10.1016/j.tree.2020.06.009>
- 56) World Health Organization, 2013. Health risks of air pollution in Europe – HRAPIE project. 0-60pp.
- 57) Zanobetti, A., Schwartz, J., 2009. The effect of fine and coarse particulate air pollution on mortality: A national analysis. *Environ. Health Perspect.* 117, 898–903. <https://doi.org/10.1289/ehp.0800108>

## Chapter 7 - Summary

The work in this thesis was divided into four papers which aimed to investigate some of the key factors affecting air pollutant concentrations over different time-scales. Two main focusses were chosen, the impact of variability in synoptic weather on UK PM<sub>2.5</sub> concentrations (Paper 1) and the impact of case-study wildfire events on PM<sub>2.5</sub> air quality and human health in the UK (Papers 2 and 3) and Australia (Paper 4). In Papers 1 and 2 observational datasets were used to understand factors affecting air quality at different spatial and temporal scales. While, Papers 3 and 4 used an atmospheric-chemistry transport model to quantify the impact of wildfires on PM<sub>2.5</sub> air quality and health.

Paper 1 focussed on the influence of synoptic weather on the local and long-range transport of emissions on PM<sub>2.5</sub> concentrations in the UK. The key aims of this work were:

- To investigate the influence of synoptic weather on UK ambient PM<sub>2.5</sub> concentrations using Lamb weather types (LWTs).
- To identify the mechanisms responsible for variations in UK ambient PM<sub>2.5</sub> concentrations under different LWTs.
- To quantify the contribution of UK and non-UK emissions to local summed emissions.

Paper 2 used observational data to investigate the spatio-temporal evolution of pollutants within the 2018 Saddleworth Moor wildfire plume. The key aims were:

- To investigate the temporal and spatial evolution of the plume using satellite observations of tropospheric column carbon monoxide (TCCO) and nitrogen dioxide (TCNO<sub>2</sub>).

- To explore population exposure to fire pollutants at the surface using ground-based observations.
- To explore how key air pollutants in the plume evolve between emission (near-field) and downwind over the Irish Sea (downwind) using aircraft data.
- To quantify emissions of CO and CO<sub>2</sub> from the fire using aircraft data.

Papers 3 and 4 used the WRF-Chem model to quantify the impacts of the 2018 Saddleworth Moor wildfire and 2019/2020 Australian megafires on PM<sub>2.5</sub> air quality and health. The key aims of both studies were:

- To simulate PM<sub>2.5</sub> concentrations and quantify the contribution of the wildfires to simulated PM<sub>2.5</sub> concentrations using WRF-Chem simulations with and without fire emissions.
- To investigate the impact of the wildfires on population exposure to poor PM<sub>2.5</sub> air quality, using the country-specific air quality index (AQI) bands and the WHO 24-hour guideline limit for PM<sub>2.5</sub>.
- To quantify the health impact of exposure to PM<sub>2.5</sub> from the fires due to short-term exposure.

The motivation and key results from this work will be discussed below.

## **7.1 Paper 1: Impact of weather types on UK ambient particulate matter concentrations**

Previous work, primarily based on satellite data, investigated the impact of synoptic scale meteorology on nitrogen dioxide (NO<sub>2</sub>) and ozone (O<sub>3</sub>) concentrations across the UK using the

Lamb weather types (LWTs) (Pope, et al., 2016, 2015). Increases in concentrations of both NO<sub>2</sub> and O<sub>3</sub> were found to be strongly associated with synoptic conditions that lead to boundary layer pollutant accumulation (e.g. anticyclonic) or with long-range transport of pollutants from continental Europe (e.g. easterly flows). Due to the relatively short time period that routine ground-based monitoring of PM<sub>2.5</sub> had been carried out for (since the late 2000s), there was previously not enough data to carry out the same analysis using ground-based observations of PM<sub>2.5</sub>. This work used ground-based observations of PM<sub>2.5</sub> from 42 background sites, spanning 2010 to 2016, sampled under LWTs. The relationships found between particulate matter with a diameter less than 2.5 micrometres (PM<sub>2.5</sub>) observations and LWTs were investigated further using EMEP4UK modelled PM<sub>2.5</sub> concentrations and a back-trajectory methodology (Stirling, et al., 2020).

The key findings of the work were:

- i) Both annually and seasonally anticyclonic circulation and easterly (easterly, south-easterly) and southerly flow were associated with increases in mean ambient UK PM<sub>2.5</sub> concentrations.
- ii) The EMEP4UK model indicated the increase in PM<sub>2.5</sub> concentrations observed was likely due to trans-boundary transport of PM<sub>2.5</sub> under the easterly, south-easterly and southerly flow. While, under anticyclonic and un-classified conditions, the accumulation of local emissions under stagnant air masses led to increases in PM<sub>2.5</sub> concentrations.
- iii) Anticyclonic conditions had the largest impact on the population's exposure to increased PM<sub>2.5</sub> concentrations due to their increased frequency compared to the wind flows.

- iv) The back-trajectory model indicated that the long-range transport of pollutants from outside of the UK was an important contributor (25–50%) to total accumulated emissions under the wind flows. However, this only accounted for primary PM<sub>2.5</sub>, and 20-50% of total PM<sub>2.5</sub> has been found to be secondary at European background sites (Querol, et al., 2004). Therefore, a method that accounts for the secondary fraction of PM<sub>2.5</sub> would be necessary to quantify the contribution of non-UK emissions to total UK PM<sub>2.5</sub>. Despite this, these results indicated there was a substantial contribution from non-UK emissions to UK PM<sub>2.5</sub> under continental air masses.
- v) Synoptic weather plays an important role in controlling PM<sub>2.5</sub> concentrations, therefore, it is vital that air quality models can accurately simulate synoptic meteorology in order to reliably forecast PM<sub>2.5</sub> concentrations. This is also key in preparing for and mitigating the associated health impacts of short-term exposure to increased PM<sub>2.5</sub> concentrations.
- vi) The back-trajectory analysis indicated that quantifying the contribution of UK and non-UK pollution sources is important in evaluating the impact of local emission controls on UK pollutant concentrations. This is particularly relevant given that variations in background PM<sub>2.5</sub> concentrations are highly variable under different weather patterns.

## **7.2 Paper 2: Impact of the June 2018 Saddleworth Moor wildfires on air quality in northern England**

In the past wildfires in the UK have generally been small. However, in recent years the UK has begun to experience an increase in the number of larger fires ( $> 5 \text{ km}^2$ ). These fires have the potential to:

- i) expose urban populations, close to moorlands, to high concentrations of air pollutants.
- ii) lead to chemical interactions between fire emitted air pollutants and those from anthropogenic sources (e.g. urban emissions).

Analysis of observations was used to quantify the impact of the fires on atmospheric composition. A wide range of observations were used to investigate how pollutant concentrations evolved spatio-temporally due to the Saddleworth Moor and Winter Hill fires. Ground-based observations of  $\text{PM}_{2.5}$  in large urban centres (Manchester and Wigan) downwind of the fires were used to investigate the impact of the fires on surface concentrations and  $\text{PM}_{2.5}$  type. Satellite observations of  $\text{CO}$  and  $\text{NO}_2$  from TROPOMI were combined with fire-radiative power to investigate the temporal evolution of the plumes from the fires. Finally, observations of  $\text{CO}$ ,  $\text{NO}_2$ ,  $\text{O}_3$  and  $\text{PM}_{2.5}$  from the FAAM aircraft flight on 29<sup>th</sup> June were used to explore the in-plume composition evolution of key air pollutants between near-field and down-wind samples.

The key findings of this work were:

### **Ground-based Observations**

- i) Increased PM<sub>2.5</sub> concentrations were observed in Manchester and areas further afield (e.g. Wigan) during the peak of the fires (27<sup>th</sup>, 29<sup>th</sup> and 30<sup>th</sup> June). Surface concentrations were 4-5.5 times higher than the average of previous years (2013-2017).
- ii) Concentrations were up to 2 times the WHO guideline 24-hour limit (25 µg m<sup>-3</sup>). There are likely to have been considerable negative health impacts for individuals exposed, particularly for those with underlying health conditions.
- iii) PM<sub>2.5</sub> mass was dominated by the non-volatile PM<sub>2.5</sub> fraction and the largest increase in concentrations from the 2013-2017 mean was observed in this fraction.

### **Satellite Observations**

- i) Total column CO (TCCO) observations between June 25<sup>th</sup> and June 30<sup>th</sup> exhibited a clear westward propagation of the plume from the Saddleworth Moor fire to the Irish Sea, over the cities of Manchester and Liverpool.
- ii) Fire-radiative power and TCCO concentrations were used alongside visible images to define threshold concentrations for the boundary of the plume. Values chosen for TCCO plume boundaries were therefore based on a best-match to both TCCO concentrations and visible images.
- iii) TCCO was used as a tracer of fire and allowed the isolation of enhancements in total column NO<sub>2</sub> (TCNO<sub>2</sub>) due to the fires. This indicated that the TCNO<sub>2</sub> concentrations observed were composed of:
  - iv) fire emissions

- v) anthropogenic emissions, from the accumulation of NO<sub>2</sub> over source regions (e.g. Manchester) (due to stagnant meteorology conditions during the fire period).

### **Aircraft Observations**

- i) Measurements from the FAAM aircraft flight on June 29<sup>th</sup> allowed the composition of the plume near-source (close to Saddleworth Moor) and downwind (over the Irish Sea) to be investigated.
- ii) Measurements indicated clear enhancement in CO concentrations within the plume, throughout the boundary layer (0-1 km). In-plume CO concentrations peaked at >1500 ppbv, while downwind concentrations peaked at 200-400 ppbv.
- iii) In-plume PM<sub>2.5</sub> concentrations peaked at 127.5 µg m<sup>-3</sup> and downwind concentrations peaked at 96.1 µg m<sup>-3</sup>.
- iv) The relative enhancement of O<sub>3</sub> compared to CO (the  $\Delta O_3/\Delta CO$  ratio) was used to evaluate photochemical O<sub>3</sub> formation in-plume near-field and downwind of the fires, using CO as a plume tracer. The  $\Delta O_3/\Delta CO$  ratio indicated O<sub>3</sub> concentrations significantly increased downwind ( $\Delta O_3/\Delta CO = 0.001$  ppbv/ppbv) compared to near-field ( $\Delta O_3/\Delta CO = 0.060-0.105$  ppbv/ppbv, 250m-1000m). This suggested downwind production of O<sub>3</sub> and titration of O<sub>3</sub> near-source by freshly emitted NO.
- v) The interaction of pollutants within the plume, with anthropogenic NO<sub>2</sub>, as the plume passed over Manchester and other urban areas may have contributed to the downwind O<sub>3</sub> enhancements, through photochemical production of O<sub>3</sub>. The  $\Delta NO_2/\Delta CO$  ratio supported this, exhibiting the opposite pattern to the  $\Delta O_3/\Delta CO$  ratio, and decreasing

with increasing height. This suggested that either the anthropogenic signal was reducing with altitude or that  $\text{NO}_2$  was being processed more quickly with more active photochemistry closer to the surface. However, data was not available to investigate this further.

vi) Downwind  $\text{O}_3$  increases (higher  $\Delta\text{O}_3/\Delta\text{CO}$  ratios) were also larger with increasing altitude. One possible reason for this is an increase in photochemical production of  $\text{O}_3$  at the top of the plume. Incoming solar radiation would reach the top of the plume first and then be attenuated further into the plume, leading to decreasing  $\text{O}_3$  production with decreasing altitude.

vii)  $\text{CO}$  and  $\text{CO}_2$  emission rates of the fires, on the 29<sup>th</sup> June (when the fire was smoldering), were 1.07 (0.07-4.69)  $\text{kg s}^{-1}$  and 13.7 (1.73-50.1)  $\text{kg s}^{-1}$ . The  $\text{CO}_2$  emission rate was similar to that of a moderately sized power station such as Grangemouth or Enfield (Edinburgh and London) ( $\sim 16.0 \text{ kg s}^{-1}$ ).

### **7.3 Paper 3: Impact on air quality and health due to the Saddleworth Moor fire in northern England**

Observational data used in Paper 2 (Paper 2: Impact of the June 2018 Saddleworth Moor wildfires on air quality in northern England) indicated the potential for wide-spread negative health impacts due to poor air quality. Therefore, in paper 3 a regional air quality model (WRF-Chem) was used to simulate  $\text{PM}_{2.5}$  concentrations due to the Saddleworth Moor fire in 2018 (June 23<sup>rd</sup> – June 30<sup>th</sup>). The model simulation was carried out at 10 km resolution between June 16<sup>th</sup> and July 14<sup>th</sup>. Two simulations were performed; one with wildfire emissions, and one without wildfire emissions. This approach allowed the impacts of the fires on  $\text{PM}_{2.5}$

concentrations to be isolated from other processes (e.g. meteorology) and allowed the impact of PM<sub>2.5</sub> from the fires on air quality and health to be quantified.

The key findings of the work were:

- i) Simulated daily mean surface PM<sub>2.5</sub> concentrations from the WRF-Chem model captured the peaks in PM<sub>2.5</sub> concentrations observed at ground-based monitoring sites ( $r=0.69$ ), but underestimated the absolute concentrations (NMB = -0.22, RMSE = 5.06  $\mu\text{g m}^{-3}$ ). This was likely because the fires burned peat moorland and the fire emissions (FINN) used in the model did not include emissions for peat. Since these fires would have burned through the surface vegetation (i.e. heather, grass and juniper), FINN does provide some estimation of emission, though with a low bias. Therefore, a time-varying scaling was applied to the original emissions to account for the missing peat source. This yielded a more robust comparison between the model and ground-based observations with  $r=0.77$ , NMB=-0.19 and RMSE = 4.27  $\mu\text{g m}^{-3}$ .
- ii) The wildfires had a substantial impact on PM<sub>2.5</sub> concentrations across the north-west of England with hourly concentrations reaching 225  $\mu\text{g m}^{-3}$  in some locations.
  - a. million people were exposed to PM<sub>2.5</sub> concentrations  $\geq 36 \mu\text{g m}^{-3}$  (moderate DAQI and above) on at least one day between June 23<sup>rd</sup> and 30<sup>th</sup>.
- iii) 4.5 million people were exposed to PM<sub>2.5</sub> concentrations above the WHO 24-hour guideline limit of 25  $\mu\text{g m}^{-3}$  on at least one day in the same period.
- iv) The health impact of exposure to PM<sub>2.5</sub> was estimated using the concentration-response function of Atkinson *et al.* (2014) alongside the population-weighted PM<sub>2.5</sub> concentrations and the baseline mortality rate for north-west England (both for 2015). This indicated the fires brought forward 6.4 deaths (95% CI: 4–11) during the week of

June 23<sup>rd</sup>-30<sup>th</sup> due to exposure to PM<sub>2.5</sub>. During this period the up to 60% (3.6 of 6.4) of the total deaths brought forward due to PM<sub>2.5</sub> exposure were attributable to PM<sub>2.5</sub> from the fires, representing an increase of up to 165% compared to without fires.

- v) The economic impact of the fires was also estimated using the number of deaths brought forward and the value of prevented fatality (VPF) from the Department for Transport. This indicated that the cost of the fires was £21.1 m (95% CI: 10.7 – 31.1 m).

Papers 2 and 3 indicate the impacts of wildfires in the UK have the potential to have measurable effects on air quality and health. The health impacts are likely to be underestimated in paper 3 since the modelled PM<sub>2.5</sub> concentrations exhibit a negative bias and only the health impacts of exposure to PM<sub>2.5</sub> were considered. Additionally, wildfires are likely to become more common due to climate change. This work demonstrates the importance of the introduction of public health tools and educational programmes to reduce the impacts of such events. The impacts of changes in land-management on the likelihood of fire occurrence could also be studied further in order to identify whether this could reduce fire risk on moorlands under a warmer, drier summer climate.

## **7.4 Paper 4: Impact of the 2019/2020 mega-fires on air quality and health in Australia**

Following the same method as Paper 3, a regional air quality model (WRF-Chem) was used to simulate PM<sub>2.5</sub> concentrations due to the Australia bushfires in 2019 and 2020. Simulations were carried out at 30 km resolution between September 1<sup>st</sup> and January 31<sup>st</sup>. Two simulations were performed; one with wildfire emissions, and one without wildfire emissions, in the same way as in paper 3.

- i) FINN fire emissions indicated PM<sub>2.5</sub> emissions from the 2019/2020 bushfires were unprecedented compared with emissions between 2010-2018. Around 1 Tg of PM<sub>2.5</sub> was emitted during 2019 and ~0.3 Tg between January and February 2020. The high emissions were likely attributable to the high levels of dry fuel availability across the region during 2019.
- ii) Simulated PM<sub>2.5</sub> concentrations from the nudged\_BL\_fires simulation reproduced observed daily mean concentrations from 80 ground-based observation sites well but with a low bias ( $r = 0.39$ ,  $RMSE = 22.9 \mu\text{g m}^{-3}$ ,  $NMB = -0.17$ ,  $NMAE = 0.72$ ). Model simulations captured the variability and magnitude of peaks seen in PM<sub>2.5</sub> observations across eastern-Australia and for specific cities.
- iii) Between September 1<sup>st</sup> 2019 and January 31<sup>st</sup> 2020 large proportions of the population were exposed to dangerous ('Poor', 'V.Poor' and 'Hazardous') air quality levels. Almost 350,000 people were exposed to hazardous AQI levels in December and January, compared with 130,000 across December and January people in the nudged\_BL\_no\_fires simulations. The impact of the bushfires on AQ was concentrated in the cities of Sydney, Newcastle-Maitland and Canberra-Queanbeyan during

November, December and, also in Melbourne, in January. While, generally Brisbane and Adelaide were minorly affected by the fires, with only 14 people exposed to Hazardous AQ.

- iv) A short-term exposure response function (World Health Organization, 2013) was used to estimate the health impacts of exposure to PM<sub>2.5</sub> from fires across eastern-Australia, regionally and at city level. An estimated 180 (95% CI: 74-294) deaths were brought forward due to the fires between October 1<sup>st</sup> and January 31<sup>st</sup>, 624 (95% CI: 229-1008) from all PM<sub>2.5</sub> and 444 (95% CI: 155-714) if there were no fires.
- v) The health impacts were largest in New South Wales, Queensland and Victoria with 109 (95% CI: 41-176), 24 (95% CI: 15-41) and 35 (95% CI: 13-56) deaths brought forward due to fires in these regions (287 (95% CI:107-463), 112 (95% CI: 41-181) and 155 (95% CI: 57-250) all PM<sub>2.5</sub>), respectively. These results estimated a lower regional health impact from PM<sub>2.5</sub> from the bushfires than Borchers Arriagada *et al.* (2020) and Ryan *et al.* (2021). This is most likely due to differences in how PM<sub>2.5</sub> attributable to fires was estimated in each study and also differences in the estimated bushfire population-weighted PM<sub>2.5</sub> concentrations. This study builds upon previous work by using an atmospheric chemistry transport model to investigate the impacts of the fires on air quality.
- vi) At a city-level, the health impacts of PM<sub>2.5</sub> exposure due to fires were concentrated in the cities with large populations and high PM<sub>2.5</sub> concentrations due to fires (Sydney (65 (95% CI: 24-105)), Melbourne (23 (95% CI: 9-38)) and Canberra (9 (95% CI: 4-15))).
- vii) This work confirms that there was a substantial AQ and health impact across eastern-Australia from the 2019/2020 bushfires. However, this study only considered one pollutant, therefore the full health impact of exposure to PM<sub>2.5</sub> is likely to be higher and

require further studies addressing the impacts on hospital admissions, ambulance call outs and primary health care visits. Alongside this, the impact of other pollutants on health (e.g. O<sub>3</sub>) could also be quantified.

viii) In the future, further work is required to characterise the health impacts of exposure to pollutants for wildfires. This would allow for more comprehensive estimates of the health impacts associated with population exposure. Finally, with more dry years like 2019/2020 projected to occur in the future due to climate change the impact of wildfires such as 2019/2020 are likely to be seen again. Therefore, fire risk management policies should be developed further to consider the impact of climate change on wildfire frequency and intensity across the country.

## **Critical Discussion and Implications for Future Work**

### **7.5 Uncertainties**

#### **7.5.1 Back-trajectory method**

In paper 1 a back-trajectory method was used to investigate the influence of UK and non-UK primary PM<sub>2.5</sub> emissions on summed emissions arriving at observational sites across the UK. In order to represent atmospheric loss processes an e-folding lifetime was applied to the summed emissions along the back-trajectory path. The sensitivity of results to the assumed lifetime was also tested. The representation of loss processes could be developed further to account for changes in deposition velocity with changes in wind speed using meteorological reanalysis to adjust the e-folding lifetime at each timestep. Alongside this, the boundary layer height was assumed to be 850 hPa and emissions were only summed if the pressure of trajectory points was higher than this. However, boundary layer height varies on temporal (diurnally, seasonally) and spatial (marine and continental) scales. Therefore, in future meteorological reanalysis could be used to determine boundary layer height for each trajectory point.

#### **7.5.2 Satellite Data**

In paper 2 TCCO and TCNO<sub>2</sub> data from the TROPOMI satellite were used to investigate the impact of the Saddleworth Moor wildfires. This analysis would not have been possible with its predecessor (OMI) due to the much spatial lower resolution of OMI. However, the polar orbit of both satellites means it is only possible to measure the concentration of air pollutants once each day. This means that a large amount of valuable information on the spatio-temporal evolution of fire plumes is lost. Alongside this cloud cover is often an issue, meaning often multiple days or weeks of measurements need to be averaged together. The new geostationary satellites (Geostationary Operational Environmental Satellite (GOES) (Zhang, et al., 2020) and

Tropospheric Emissions: Monitoring of Pollution (TEMPO) (Zoogman, et al., 2017)) will provide observations of fires (FRP), aerosols (AOD) and trace-gases (including O<sub>3</sub> and NO<sub>2</sub>) at even higher spatial resolution than TROPOMI (2 km and 2.1 km) and temporal resolution (5-minutes and hourly) in the future.

### 7.5.3 Modelling

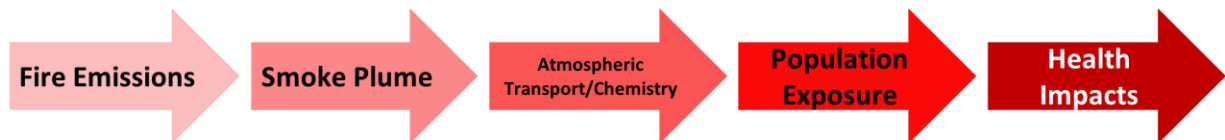


Figure 47. Sources of uncertainties within modelling health impacts from wildfire pollutants.

Uncertainties within this work arise from several factors, from uncertainties within the input data used (e.g. emissions, concentration-response function) to model parameterisations of processes (e.g. plume height, atmospheric chemistry processes) and finally, to gaps in our current understanding that mean assumptions have to be made.

Gaps in our current knowledge and uncertainties that were not covered in detail in the supplementary material of the papers will be discussed below. The uncertainties in the estimated health impacts from wildfires can be split into 5 main factors (Figure 47). These can be grouped into emissions (fire emissions), modelling (smoke plume, atmospheric chemistry/transport) and health impact assessments (population exposure, health impacts).

#### 7.5.3.1 Emissions

##### 7.5.3.1.1 Fire Emissions

There are large differences between different global fire emissions datasets, which arise from uncertainties detecting fires based on satellite product used and uncertainties within the

emissions factors applied (though many are known with an uncertainty of ~30% (Andreae, et al., 2001)) (Liu, et al., 2020). These differences can lead to large spatial and temporal variability in emissions datasets and can therefore impact on simulated concentrations of air pollutants. Unfortunately, due to time and computational cost limits, it is rare that multiple simulations with different emissions datasets can be carried out in modelling studies. Liu *et al.* (2020) identified 5 key sources of bias in the major global fire emission datasets (GFEDv4s, FINNv1.5, GFASv1.2 Quick Fire Emissions Dataset (QFEDv2.5r1) and Fire Energetics and Emissions Research (FEERv1.0-G1.2)), which lead to uncertainties. Biases stem from the satellite product used to derive fire emissions (active fires/burned area), difficulties detecting fires through cloud/haze, burned area fragmentation, complex topography leading to shadowing, and difficulties with small fire detection. As a result of these biases, in some regions emissions estimates can vary by an order of magnitude, dependent upon the remote sensing technique used (Andreae, et al., 2001). Difficulty detecting small fires could be improved through the use of new high spatial and temporal resolution satellite datasets, such as the Geostationary Operational Environmental Satellite (GOES) (Zhang, et al., 2020). GOES will provide observations of fires (FRP) and aerosols (AOD) at high spatial (2 km) and temporal resolution (5-minutes) (Zhang, et al., 2020). This will provide new temporal information about wildfire life-cycles and emissions. The increased temporal resolution will also help in constraining model simulations through assimilation of FRP data on fires throughout the day, rather than by a single overpass. Therefore, aiding the constraint of uncertainties in fire emissions and plume characteristics. Alongside issues with detection, there are discrepancies in speciation and emissions factors between the five main fire emissions datasets. These arise from the inherent difficulties estimating fire emissions. The largest differences in emissions factors are between  $PM_{2.5}$  and  $CH_4$ , where the coefficient of variation

is 20.3 and 26.7% (Liu, et al., 2020). This is, in part, due to the absence of peat emissions in FINN, QFED and FFER, since the emission factors for peat emissions of CH<sub>4</sub> (and CO) are much higher than other land use types (Wiedinmyer, et al., 2011). Peat emissions were the dominant source of emissions for the 2018 UK moorland fires, likely leading to underestimation in FINN emissions. However, over the past few years there has been continued work to incorporate peat emissions in to FINN where fire emissions from peat are high. Peat emissions have now been added into FINN (FINNpeat) for Indonesia (Kiely, et al., 2019). In the future, this work could be extended for global peat fire emissions.

#### **7.5.3.1.2 Anthropogenic Emissions**

Uncertainties arise when combining regional anthropogenic emission inventories to create global anthropogenic emissions inventories (EDGAR HTAP v2.2). Uncertainties stem from considerable discrepancies between the assumptions made (activity, technology, end-of-pipe) and emissions factors applied during the construction of each of the regional inventories. This leads to inconsistencies at the borders of regions (Janssens-Maenhout, et al., 2015). Uncertainties in emissions are generally smaller for industrialised countries (e.g. UK and Australia) but vary for species and sector. The largest uncertainties are within NH<sub>3</sub>, PM<sub>10</sub>, PM<sub>2.5</sub> and BC/OC in the shipping (PM, BC/OC), transport (NH<sub>3</sub>, PM<sub>10</sub>, PM<sub>2.5</sub> and BC/OC), residential (NH<sub>3</sub>, PM<sub>10</sub>, PM<sub>2.5</sub> and BC/OC) and agriculture (NH<sub>3</sub>, PM<sub>10</sub>, PM<sub>2.5</sub> and BC/OC) sectors ( $\leq 100\%$  uncertainty). Anthropogenic emissions from 2010, which were used in papers 3 and 4 are likely to be higher than the years simulated (2018 and 2019/2020). However, since both papers focus on the fire contribution to PM<sub>2.5</sub>, rather than that of the background anthropogenic emissions, this is unlikely to have any effect on the calculated health impact due to fires. Uncertainties in anthropogenic emissions datasets could be reduced through the use of

new high spatial resolution satellite measurements to derive emission rates of different species (e.g. (Beirle, et al., 2011)) and improved activity and diurnal cycle information, particularly in developing countries.

#### 7.5.3.2 Modelling

Initial and boundary conditions can have a large impact on simulated air pollutant concentrations. Previous studies have found simulated PM<sub>2.5</sub> concentrations are strongly influenced by meteorological initial and boundary conditions (Ritter, et al., 2013). Additionally, climatological dust-fields are often currently used within initially boundary chemical conditions, which has led to overestimations in some regions (Georgiou, et al., 2018). Updates to future model runs could include higher resolution chemical and meteorological boundary conditions and CAM-Chem (Community Atmosphere Model with Chemistry) dust, which uses simulated wind speed and surface conditions (e.g. Crippa *et al.* (2016)). Alongside this, chemical assimilation could be implemented to improve agreement between simulated pollutant concentrations and observations (Li, et al., 2013; Ukhov, et al., 2020; Werner, et al., 2019).

#### 7.5.3.3 Health Impact Assessment

##### **7.5.3.3.1 Health Impacts**

Emissions from wildfires are complex, varying based upon the fire type, landscape, fuel consumption and meteorology (Cascio, 2018). Alongside this, the chemical composition of smoke plumes change with aging, as secondary pollutants are formed (e.g. O<sub>3</sub>) and if plumes interact with anthropogenic emissions (Jaffe, and Wigder, 2012). Wildfire smoke is likely to become a more important source of air pollutants to populations in future years. This is due to the combined effect of reductions in anthropogenic air pollution, due to increased regulatory

efforts, and the increasing risk of wildfires due to climate change (Black, et al., 2017). This has led to increased research into the impacts of wildfires on health. Recent work has identified an association between exposure to PM<sub>2.5</sub> from wildfires and respiratory morbidity, with increasing evidence suggesting an association with all-cause mortality (Reid, et al., 2016). Despite this, further research is required to clearly identify the link with cause-specific mortality and to identify whether using un-specified PM adequately characterises the health effects of exposure to wildfire smoke (Reid, et al., 2016). The effect of co-pollutant mixtures, which are found in wildfire smoke, on health also require further research in order to provide more comprehensive health impact assessments for wildfire events. An improved understanding of these relationships would allow for more targeted policies regarding fires and would help to identify and mitigate the health impacts of exposure for the most at-risk groups.

Another key gap in current knowledge stems from a lack of understanding of which components (e.g. species of PM<sub>2.5</sub>), sources (e.g. industry/transport) and characteristics of air pollution are responsible for the health impacts observed (Pope III, and Dockery, 2006). Currently, evidence suggests that, for PM, particle size plays the main role in the health impacts observed. This is due to particle size controlling whether it is of respirable size, able to penetrate into indoor environments and controlling its atmospheric lifetime (Pope III, and Dockery, 2006). Similar associations between exposure and mortality are observed across developed and less developed regions, despite differences in PM<sub>2.5</sub> composition (Harrison, and Yin, 2000), further supporting this. However, other factors which may affect PM<sub>2.5</sub> toxicity (e.g. reactivity and solubility) still require further research.

As a result, in most current work focussing on the health impacts of sporadic events, short-term concentration response function (CRF) derived from ambient PM<sub>2.5</sub> exposure (Atkinson, et al.,

2014; World Health Organization, 2013) are applied for all-age, all-cause mortality. This assumes all species of PM<sub>2.5</sub> are equally toxic, which may not be true. Alongside this, there is a large degree of uncertainty in the exposure-response, which stems from uncertainties in population response to air pollution exposure. The effect of the uncertainty in the CRF has been shown to dominate the uncertainty in health impact assessments (Kushta, et al., 2018). There is continued work to understand the health impacts of short-term exposure to PM<sub>2.5</sub>, in the future this may allow disease-specific mortality and morbidity exposure-response functions to be derived, similar to those for long-term exposure (Burnett, et al., 2018; GBD Collaborators 2015, 2017).

#### **7.5.3.3.2 Population Exposure**

In addition to this, the assumption that population weighted concentration is a proxy for exposure, which is commonly applied in health impact assessments (Crippa *et al.*, 2016; Macintyre *et al.*, 2016b; Conibear *et al.*, 2018a) introduces the potential for inaccuracy. Generally, population data (from residential censuses) is combined with modelled concentrations of pollutants, without adjusting for variation in personal exposure (e.g. time spent in the home compared to at work, time spent outside, filtration in buildings). Several studies have developed methods to account for population mobility (e.g. workday vs home, active vs home and travel-time), finding this changed population exposure to NO<sub>2</sub>, O<sub>3</sub> and PM<sub>2.5</sub> in large conurbations (de Nazelle, et al., 2009; Reis, et al., 2018; Shekarrizfard, et al., 2017). In addition, computing packages have been developed that use synthetic data to mimic the relationships found in confidential population datasets (Nowok, et al., 2016). This avoids the need for access to sensitive personal data. In the future, with the addition of data on personal exposures in populations, better representation of exposure could improve results (Kanjo, et al., 2018). Since modelled pollutant concentrations are used to represent exposure, model

resolution also plays an important role in capturing accurate population exposure to pollutants. At a resolution of 10 or 30 km, gradients in concentrations at local levels (e.g. street canyons) are not captured and this therefore introduces error in exposure estimations. Increased model resolution could improve the representation of concentration gradients and diurnal cycles in concentrations.

## 7.6 Implications for Future Work

Wildfires close to populated areas have generally been rare in many regions of the world in the past, including the UK. However, they are projected to become more common in the future, both globally and in Europe (Krawchuk, et al., 2009; Liu, et al., 2010; Syphard, et al., 2018). The impact of increased wildfire frequency on health due to short-term acute exposure has not yet been quantified. However, this could prove useful to policy makers in quantifying the cost-benefits of the introduction of policy and land management techniques to reduce fire risk (Cascio, 2018).

Coordinated emission estimates of CO, using FRP and burned area remote-sensing, alongside inversion modelling, may help to constrain emission estimates (Andreae, 2019). For PM specifically, emission estimates could be improved through increased understanding of the impact of fuel moisture and fire type on emission factors (Andreae, 2019). Studies in the future could also focus on how emissions vary regionally and seasonally, in order to better capture spatial and temporal variability in fire emissions (Andreae, 2019). This is important in modelling the impacts of wildfire pollutants on populations exposed.

New high-resolution satellite data, such as the GOES (Zhang, et al., 2020) and TEMPO (Zoogman, et al., 2017), will provide observations of fires (FRP), aerosols (AOD) and trace-gases (including O<sub>3</sub> and NO<sub>2</sub>) at high spatial (2 km and 2.1 km) and temporal resolution (5-minutes and hourly) in the future (Zhang, et al., 2020; Zoogman, et al., 2017). This will provide new temporal information about emissions from wildfires and their day-time evolution, as well as plume height (from TEMPO). The increased temporal resolution of these instruments will

also help to better predict the precursor emissions for secondary species, such as SOA and O<sub>3</sub>, and therefore the downwind formation of these pollutants. Furthermore, the improved spatial and temporal resolution of GOES and TEMPO will help in constraining model simulations both through validation and data assimilation. Therefore, aiding the constraint of uncertainties in emissions, fire and plume characteristics and chemical interactions as plumes age.

Health impact assessments, which calculate the number of deaths brought forward due to exposure to PM<sub>2.5</sub>, have large uncertainties, which stem from the exposure-response relationships used within them and assumptions made about exposure. A particular weakness of the exposure-response functions used in this thesis (Atkinson, et al., 2014; World Health Organization, 2013) is that short-term exposure-response functions generally do not include studies looking mortality risk at high PM<sub>2.5</sub> concentrations (e.g. those observed in pollution from fires). Therefore, the shape of the exposure response is assumed to be linear (Harrison, and Yin, 2000; Pope III, and Dockery, 2006). In future work, a similar approach could be adopted to Burnett *et al.* (2018), where the shape of the exposure-response is constrained using studies that derive associations for mortality at higher PM<sub>2.5</sub> concentrations, but for short-term exposure in this case. This method also has the added benefit of avoiding the need to integrate exposure-responses from several sources (e.g. ambient air pollution with passive and active smoking) meaning assumptions about equal toxicity can be avoided.

Many gaps remain in our understanding of the health impacts of exposure to PM from wildfires (Reid, et al., 2016). Currently, associations between wildfire smoke/PM and all-cause mortality, respiratory morbidity, hospitalisations and accident and emergency visits are best understood (Cascio, 2018; Reid, et al., 2016). Research focused on ambient PM has found much stronger associations between chronic PM exposure and mortality (Pope III, and

Dockery, 2006), though work is yet to identify whether PM composition is important. As yet no study has quantified the health impact of chronic PM exposure, such as that seen in southeast Asia (Black, et al., 2017; Reid, et al., 2016). Finally, since the composition of wildfire PM can vary greatly, it is not known whether the current concentrations used for public health warnings (based on evidence of health impacts from anthropogenic emissions) adequately characterise the health effects of wildfire PM. However, recent work by Borchers Arriagada *et al.* (2019) derived wildfire smoke PM<sub>2.5</sub>-specific summary effect estimate for asthma-related outcomes. The study found the relative risk was higher for wildfire PM<sub>2.5</sub> than for a typical ambient PM<sub>2.5</sub> mixture. These results suggest that health impact assessments using relative risk estimates from ambient PM<sub>2.5</sub> may underestimate the health impacts of wildfire smoke PM<sub>2.5</sub>. Future work could focus on other disease endpoints, such as cardiovascular morbidity and mortality and a range of PM<sub>2.5</sub> sources. These could then be used in future health impact assessments for wildfire pollutant impacts.

Alongside this, few studies have quantified the health impacts of exposure to ozone (O<sub>3</sub>) from wildfires (Black, et al., 2017). This is likely due to very few epidemiology studies having addressed the impact of wildfire pollutants other than PM (e.g. O<sub>3</sub>) on morbidity or mortality (Black, et al., 2017). A study by Reid *et al.* (2019) that examined a case-study US wildfire in 2008 found that there was no association between O<sub>3</sub> and emergency respiratory admissions during wildfires, when PM<sub>2.5</sub> was adjusted for. The study also highlighted that the health impacts of wildfire O<sub>3</sub> are understudied and further research was needed for different fire types and regions. Given that the interaction between wildfire smoke and anthropogenic pollutants can produce secondary pollutants, such as O<sub>3</sub>, downwind, an increase in the number of studies

addressing the health impacts of exposure to wildfire ozone would help to quantify the full impact of pollutants from wildfires on health.

The impact of interactions between pollutants on exposure-response is also yet to be uncovered, since epidemiology studies generally report the associations between a single pollutant and health. However, it is not clear whether the calculation of health impacts for pollutants individually is realistic, given that the population is exposed to multiple pollutants simultaneously. Further work is needed to better understand the effect of multi-pollutant mixtures on health.

A better representation of population exposure would also enhance our ability to quantify the health impacts of population pollutant exposure. This could be achieved by improving the representativeness of dose, through increasing information on population mobility and/or using population level exposure data, collected from personal monitors (for pollutants and heart-rate/respiratory rate/oxygen consumption) (Kanjo, et al., 2018). Better representativeness of dose could be combined with increased model resolution, as computational power advances and models become quicker and therefore cheaper to run. Increased model resolution would allow the strong air pollutant concentrations seen in urban areas to be better represented (Kushta, et al., 2018). However, the largest uncertainties in health impact assessments stem from the estimates of population response to air pollutant concentrations, which are derived from epidemiology studies ( $\pm 30\%$  (Kushta, et al., 2018)). Therefore, constraining uncertainties in health responses, through better understanding of factors such as composition and source (e.g. wildfires, anthropogenic, natural) are a key factor in improving the quantification of health impacts.

## Chapter 8 - Conclusions

Within the UK, air quality is the largest environmental health risk (Department for Environment Food & Rural Affairs, 2019). Health is adversely affected through both exposure to short-term high pollution events and long-term lower-level pollution (Department for Environment Food & Rural Affairs, 2019). This results in more than 29,000 premature deaths each year being linked to long term-exposure to ambient PM<sub>2.5</sub> (Committee on the Medical Effects of Air Pollutants, 2010). Despite this, previously the impact of synoptic meteorology on ambient PM<sub>2.5</sub> concentrations had not been quantified. Alongside this, wildfires close to large populations had been relatively rare in the UK in the past so little work had looked at their impacts. As ambient pollutant concentrations continue to decrease, through decreased anthropogenic emissions, improved emission abatement and tighter legislation, short-term high pollution events (including wildfires) are likely to have an increased impact on overall population exposure and health. Alongside this, wildfires are projected to become more common in the future due to climate change and as a result are likely to represent a larger fraction of the population's annual exposure to air pollution in the future.

The aims of this thesis were to quantify the impact of different sources and processes on short-term changes in ambient PM<sub>2.5</sub> across the UK. Synoptic meteorology has a considerable influence on ambient PM<sub>2.5</sub> across the UK. Easterly, south-easterly and southerly winds were shown to transport pollutants from continental Europe, increasing ambient concentrations observed. In contrast, anticyclonic conditions led to the build-up of local emissions under slack winds.

Wildfires, such as the Saddleworth Moor and Winter Hill fires in 2018, have the potential to substantially influence regional pollutant concentrations. Concentrations of pollutants close to

the fires were high but, in areas downwind (> 80 km away), concentrations were also enhanced above background concentrations, exposing populations to high concentrations far from the fires. Secondary pollutants, such as ozone, were formed in the downwind smoke plume. More research is required to investigate the interaction between pollutants from fires and anthropogenic emissions when plumes pass over large urban areas, as this may happen more commonly in the future with the increased likelihood of wildfires in the future due to climate change. The WRF-Chem model was used to quantify the air quality and health impacts of PM<sub>2.5</sub> from the fires. A large proportion of the population in the region around Saddleworth Moor and Winter Hill were exposed to PM<sub>2.5</sub> concentrations above the WHO guideline limit and the moderate DAQI limit. The fires led to increases in the number of deaths brought forward due to exposure to PM<sub>2.5</sub> (165%) compared to if there were no fires and as a result had a large economic impact (£21.1m).

The 2019/2020 Australian bushfires were unprecedented in their burned area size (10 million hectares) and PM<sub>2.5</sub> emissions (1.3 Tg), burning from October 2019 through to February 2020. Again, the WRF-Chem model was used to quantify the air quality and health impacts of PM<sub>2.5</sub> from the fires. Between September 1<sup>st</sup> 2019 and January 31<sup>st</sup> 2020 large proportions of the population were exposed to dangerous ('Poor', 'V.Poor' and 'Hazardous') air quality levels. The impact of the bushfires on AQ was concentrated in the cities of Sydney, Newcastle-Maitland and Canberra-Queanbeyan during November, December and, also in Melbourne, in January. While, generally Brisbane and Adelaide were much less severely affected by the fires, with few people exposed to Hazardous AQ. Exposure to PM<sub>2.5</sub> from the fires led to an estimated 180 (95% CI: 74-294) deaths being brought forward between October 1<sup>st</sup> and January 31<sup>st</sup>. The health impacts were largest in New South Wales, Queensland and Victoria. In line with this, at

a city-level the health impacts of PM<sub>2.5</sub> exposure due to fires were concentrated in cities within Queensland and Victoria that have large populations that were exposed to high PM<sub>2.5</sub> concentrations due to fires, including Sydney, Melbourne and also Canberra.

This thesis highlighted that there are a range of factors affecting the population's exposure to PM<sub>2.5</sub> on short time scales. The build-up of local emissions and long-range transport of pollutants to the UK under continental air masses were shown to play an important role in controlling ambient UK PM<sub>2.5</sub> concentrations. Thus, highlighting the need for continued cooperation in reducing emissions across Europe in order to improve air quality. The impact of short-term emerging threats, such as wildfires, was quantified, indicating that short-lived high pollution events have the potential to have a substantial impact on air quality and health. With a warming climate and increased wildfire frequency projected in the future, the results of this work highlight that more research is required to quantify the cost-benefits of public health interventions or changes in land-management practices that may reduce the risk of wildfires.

## 8.1 References

- 1) Adami, H.O., Berry, S.C.L., Breckenridge, C.B., Smith, L.L., Swenberg, J.A., Trichopoulos, D., Weiss, N.S., Pastoor, T.P., 2011. Toxicology and epidemiology: Improving the science with a framework for combining toxicological and epidemiological evidence to establish causal inference. *Toxicol. Sci.* 122, 223–234. <https://doi.org/10.1093/toxsci/kfr113>
- 2) Air Quality Expert Group, 2013. Mitigation of United Kingdom PM<sub>2.5</sub> Concentrations Mitigation of.
- 3) Air Quality Expert Group, 2012. Fine Particulate Matter (PM<sub>2.5</sub>) in the United Kingdom.
- 4) Air Quality Expert Group, 2005. Particulate Matter in the UK: Summary. <https://doi.org/10.1201/9780203743676-3>
- 5) Akagi, S.K., Yokelson, R.J., Wiedinmyer, C., Alvarado, M.J., Reid, J.S., Karl, T., Crouse, J.D., Wennberg, P.O., 2011. Emission factors for open and domestic biomass burning for use in atmospheric models. *Atmos. Chem. Phys.* 11, 4039–4072. <https://doi.org/10.5194/acp-11-4039-2011>
- 6) Albertson, K., Ayles, J., Cavan, G., McMorrow, J., 2010. Climate change and the future occurrence of moorland wildfires in the Peak District of the UK. *Clim. Res.* 45, 105–118. <https://doi.org/10.3354/cr00926>
- 7) Alman, B.L., Pfister, G., Hao, H., Stowell, J., Hu, X., Liu, Y., Strickland, M.J., 2016. The association of wildfire smoke with respiratory and cardiovascular emergency department visits in Colorado in 2012: A case crossover study. *Environ. Heal. A Glob. Access Sci. Source* 15, 1–9. <https://doi.org/10.1186/s12940-016-0146-8>
- 8) Andreae, M.O., 2019. Emission of trace gases and aerosols from biomass burning - An updated assessment. *Atmos. Chem. Phys.* 19, 8523–8546. <https://doi.org/10.5194/acp-19-8523-2019>
- 9) Andreae, M.O., Melret, P., Merlet, P., Metlet, P., 2001. Emission of trace gases and aerosols from biomass burning. *Global Biogeochem. Cycles* 15, 955–966. <https://doi.org/10.1029/2000GB001382>

- 10) Archer-Nicholls, S., Lowe, D., Darbyshire, E., Morgan, W.T., Bela, M.M., Pereira, G., Trembath, J., Kaiser, J.W., Longo, K.M., Freitas, S.R., Coe, H., McFiggans, G., 2015. Characterising Brazilian biomass burning emissions using WRF-Chem with MOSAIC sectional aerosol. *Geosci. Model Dev.* 8, 549–577. <https://doi.org/10.5194/gmd-8-549-2015>
- 11) Archibald, A.T., Levine, J.G., Abraham, N.L., Cooke, M.C., Edwards, P.M., Heard, D.E., Jenkin, M.E., Karunaharan, A., Pike, R.C., Monks, P.S., Shallcross, D.E., Telford, P.J., Whalley, L.K., Pyle, J.A., 2011. Impacts of HO<sub>x</sub> regeneration and recycling in the oxidation of isoprene: Consequences for the composition of past, present and future atmospheres. *Geophys. Res. Lett.* 38, 1–6. <https://doi.org/10.1029/2010GL046520>
- 12) Arnold, S.R., Emmons, L.K., Monks, S.A., Law, K.S., Ridley, D.A., Turquety, S., Tilmes, S., Thomas, J.L., Bouarar, I., Flemming, J., Huijnen, V., Mao, J., Duncan, B.N., Steenrod, S., Yoshida, Y., Langner, J., Long, Y., 2015. Biomass burning influence on high-latitude tropospheric ozone and reactive nitrogen in summer 2008: A multi-model analysis based on POLMIP simulations. *Atmos. Chem. Phys.* 15, 6047–6068. <https://doi.org/10.5194/acp-15-6047-2015>
- 13) Atkinson, R.W., Butland, B.K., Dimitroulopoulou, C., Heal, M.R., Stedman, J.R., Carslaw, N., Jarvis, D., Heaviside, C., Vardoulakis, S., Walton, H., Anderson, H.R., 2016. Long-term exposure to ambient ozone and mortality: A quantitative systematic review and meta-analysis of evidence from cohort studies. *BMJ Open* 6, 1–10. <https://doi.org/10.1136/bmjopen-2015-009493>
- 14) Atkinson, R.W., Kang, S., Anderson, H.R., Mills, I.C., Walton, H.A., 2014. Epidemiological time series studies of PM<sub>2.5</sub> and daily mortality and hospital admissions: A systematic review and meta-analysis. *Thorax* 69, 660–665. <https://doi.org/10.1136/thoraxjnl-2013-204492>
- 15) Australia State of the Environment, 2016. Vegetation.
- 16) Australian Bureau of Meteorology, 2020. Australian Climate Influences: IOD [WWW Document]. URL <http://www.bom.gov.au/climate/about/?bookmark=iod>

- 17) Australian Bureau of Meteorology, 2019a. Tracking Australia's climate through 2019 [WWW Document]. URL <http://www.bom.gov.au/climate/updates/articles/a036.shtml>
- 18) Australian Bureau of Meteorology, 2019b. Southern Annular Mode [WWW Document]. URL <http://www.bom.gov.au/climate/about/?bookmark=sam>
- 19) Australian Bureau of Statistics, 2020. Deaths, Year of occurrence, Age at death, Age-specific death rates, Sex, States, Territories and Australia [WWW Document]. URL [http://stat.data.abs.gov.au/Index.aspx?DataSetCode=DEATHS\\_AGESPECIFIC\\_OCCURENCEYEAR](http://stat.data.abs.gov.au/Index.aspx?DataSetCode=DEATHS_AGESPECIFIC_OCCURENCEYEAR) (accessed 1.7.21).
- 20) Australian Bureau of Statistics, 2019. Regional Population Growth, Australia, 2017-18 [WWW Document]. URL <https://www.abs.gov.au/AUSSTATS/abs@.nsf/DetailsPage/3218.02017-18?OpenDocument> (accessed 1.7.21).
- 21) Avery, C.L., Mills, K.T., Williams, R., McGraw, K.A., Poole, C., Smith, R.L., Whitsel, E.A., 2010. Proxies for Personal Exposures. *Epidemiology* 21, 215–223. <https://doi.org/10.1097/EDE.0b013e3181cb41f7>. Estimating
- 22) Bain, C., Bonn, A., Stoneman, R., Chapman, S., Coupar, A., Evans, M., Gearey, B., Howat, M., Joosten, H., Keenleyside, C., Labadz, J., Lindsay, R., Littlewood, N., Lunt, P., Miller, C., Moxey, A., Orr, H., Reed, M., Smith, P., Swales, V., Thompson, D., Thompson, P., Van de Noort, R., Wilson, J., Worrall, F., 2011. IUCN UK Commission of Inquiry on Peatlands.
- 23) Bank of England, 2019. Bank of England 2019 Inflation Calculator [WWW Document]. URL <https://www.bankofengland.co.uk/monetary-policy/inflation/inflation-calculator?number.Sections%5B0%5D.Fields%5B0%5D.Value=4900000&start-year=671.8&end-year=1110.8>
- 24) Barros, V., Field, C., Dokken, D., Mach, K., Bilir, T., MChatterjee, K., Ebi, K., Estrada, Y., Genova, R., Girma, B., Kissel, E., Levy, A., MacCracken, S., Mastandrea, P., White, L., 2014. IPCC 2014 Climate Change 2014: Impacts, Adaptation, and Vulnerability. Part B: Regional Aspects. Contribution of Working Group II to the Fifth Assessment Report of the

Intergovernmental Panel on Climate Change.

- 25) Barth, M.C., Rasch, P.J., Kiehl, J.T., Benkovitz, C.M., Schwartz, S.E., 2000. Sulfur chemistry in the National Center for Atmospheric Research Community Climate Model: Description, evaluation, features, and sensitivity to aqueous chemistry. *J. Geophys. Res. Atmos.* 105, 1387–1415. <https://doi.org/10.1029/1999JD900773>
- 26) BBC, 2018. Saddleworth Moorfire is out after more than three weeks.
- 27) Beirle, S., Boersma, K.F., Platt, U., Lawrence, M.G., Wagner, T., 2011. Megacity emissions and lifetimes of nitrogen oxides probed from space. *Science*, 333, 1737–1739. <https://doi.org/10.1126/science.1207824>
- 28) Black, C., Tesfaigzi, Y., Bassein, J.A., Miller, L.A., 2017. Wildfire smoke exposure and human health: Significant gaps in research for a growing public health issue. *Environ. Toxicol. Pharmacol.* 55, 186–195. <https://doi.org/10.1016/j.etap.2017.08.022>
- 29) Boer, M., Resco de Dios, V., Bradstock, R., 2020. Unprecedented burn area of Australian mega forest fires. *Nat. Clim. Chang.* 10, 170. <https://doi.org/10.1038/s41558-020-0710-7>
- 30) Boersma, K.F., Eskes, H.J., Dirksen, R.J., Van Der A, R.J., Veefkind, J.P., Stammes, P., Huijnen, V., Kleipool, Q.L., Sneep, M., Claas, J., Leitão, J., Richter, A., Zhou, Y., Brunner, D., 2011. An improved tropospheric NO<sub>2</sub> column retrieval algorithm for the Ozone Monitoring Instrument. *Atmos. Meas. Tech.* 4, 1905–1928. <https://doi.org/10.5194/amt-4-1905-2011>
- 31) Bonan, G.B., Levis, S., Sitch, S., Vertenstein, M., Oleson, K.W., 2003. A dynamic global vegetation model for use with climate models: Concepts and description of simulated vegetation dynamics. *Glob. Chang. Biol.* 9, 1543–1566. <https://doi.org/10.1046/j.1365-2486.2003.00681.x>
- 32) Borchers Arriagada, N., Horsley, J.A., Palmer, A.J., Morgan, G.G., Tham, R., Johnston, F.H., 2019. Association between fire smoke fine particulate matter and asthma-related outcomes: Systematic review and meta-analysis. *Environ. Res.* 179, 108777. <https://doi.org/10.1016/j.envres.2019.108777>

- 33) Borchers Arriagada, N., Palmer, A.J., Bowman, D.M.J.S., Morgan, G.G., Jalaludin, B.B., Johnston, F.H., 2020. Unprecedented smoke-related health burden associated with the 2019–20 bushfires in eastern Australia. *Med. J. Aust.* 2019–2020. <https://doi.org/10.5694/mja2.50545>
- 34) Bovbjerg, M., 2020a. Confounding, in: *Foundations of Epidemiology*. Oregon State University.
- 35) Bovbjerg, M., 2020b. Effect Modification, in: *Foundations of Epidemiology*. Oregon State University.
- 36) Boynard, A., Clerbaux, C., Coheur, P.F., Hurtmans, D., Turquety, S., George, M., Hadji-Lazaro, J., Keim, C., Meyer-Arnek, J., 2009. Measurements of total and tropospheric ozone from IASI: Comparison with correlative satellite, ground-based and ozonesonde observations. *Atmos. Chem. Phys.* 9, 6255–6271. <https://doi.org/10.5194/acp-9-6255-2009>
- 37) Brasseur, G.P., Hauglustaine, D.A., Walters, S., Rasch, P.J., Mfiller, J., Granter, C., Tie, X.X., 1998. MOZART, a global chemical transport model for ozone. Model description (called MOZART) developed in the framework of the NCAR Community Climate Model (CCM) and aimed at studying the distribution and budget of tropospheric and boundary layer transp. *J. Geophys. Res.* 103.
- 38) Bravo, A.H., Sosa, E.R., Sánchez, A.P., Jaimes, P.M., Saavedra, R.M.I., 2002. Impact of wildfires on the air quality of Mexico City, 1992-1999. *Environ. Pollut.* 117, 243–253. [https://doi.org/10.1016/S0269-7491\(01\)00277-9](https://doi.org/10.1016/S0269-7491(01)00277-9)
- 39) Brew, N., Richards, L., Smith, L., 2020. 2019–20 Australian bushfires—frequently asked questions: a quick guide.
- 40) Bryant, R.A., Waters, E., Gibbs, L., Gallagher, H.C., Pattison, P., Lusher, D., Macdougall, C., Harms, L., Block, K., Snowdon, E., Sinnott, V., Ireton, G., Richardson, J., Forbes, D., 2014. Psychological outcomes following the Victorian Black Saturday bushfires. *Aust. N. Z. J. Psychiatry* 48, 634–643. <https://doi.org/10.1177/0004867414534476>
- 41) Burnett, R., Chen, H., Szyszkowicz, M., Fann, N., Hubbell, B., Pope, C.A., Apte, J.S., Brauer,

- M., Cohen, A., Weichenthal, S., Coggins, J., Di, Q., Brunekreef, B., Frostad, J., Lim, S.S., Kan, H., Walker, K.D., Thurston, G.D., Hayes, R.B., Lim, C.C., Turner, M.C., Jerrett, M., Krewski, D., Gapstur, S.M., Diver, W.R., Ostro, B., Goldberg, D., Crouse, D.L., Martin, R. V., Peters, P., Pinault, L., Tjepkema, M., Van Donkelaar, A., Villeneuve, P.J., Miller, A.B., Yin, P., Zhou, M., Wang, L., Janssen, N.A.H., Marra, M., Atkinson, R.W., Tsang, H., Thach, T.Q., Cannon, J.B., Allen, R.T., Hart, J.E., Laden, F., Cesaroni, G., Forastiere, F., Weinmayr, G., Jaensch, A., Nagel, G., Concin, H., Spadaro, J. V., 2018. Global estimates of mortality associated with longterm exposure to outdoor fine particulate matter. *Proc. Natl. Acad. Sci. U. S. A.* 115, 9592–9597. <https://doi.org/10.1073/pnas.1803222115>
- 42) Carlton, A.G., Wiedinmyer, C., Kroll, J.H., 2009. A review of Secondary organic aerosol (SOA) formation from isoprene. *Atmos. Chem. Phys.* 9, 4987–5005. <https://doi.org/10.5194/acp-9-4987-2009>
- 43) Carthy, T., Chilton, S., Covey, J., Hopkins, L., Jones-Lee, M., Loomes, G., Pidgeon, N., Spencer, A., 1998. On the Contingent Valuation of Safety and the Safety of Contingent Valuation: Part 2 - The CV/SG “Chained” Approach. *J. Risk Uncertain.* 17, 187–214. <https://doi.org/10.1023/a:1007782800868>
- 44) Cascio, W.E., 2018. Wildland fire smoke and human health. *Sci. Total Environ.* 624, 586–595. <https://doi.org/10.1016/j.scitotenv.2017.12.086>
- 45) CENR, 2000. Atmospheric Ammonia: Sources and Fate A Review of Ongoing Federal Research and. October.
- 46) Centre for Ecology and Hydrology, 2018. The European Monitoring and Evaluation Programme for the UK (EMEP4UK) [WWW Document]. URL <http://www.emep4uk.ceh.ac.uk/> (accessed 12.1.18).
- 47) Centre for Ecology and Hydrology, 2016. Air Pollution Information System: Ozone [WWW Document]. URL [http://www.apis.ac.uk/overview/pollutants/overview\\_o3.htm](http://www.apis.ac.uk/overview/pollutants/overview_o3.htm)
- 48) Chappuis, J., 1880. Sur le spectre d’absorption de l’ozone. *C. R. Acad. Sci. Paris.* 91, 985.

- 49) Cheng, L., McDonald, K.M., Angle, R.P., Sandhu, H.S., 1998. Forest fire enhanced photochemical air pollution. A case study. *Atmos. Environ.* 32, 673–681. [https://doi.org/10.1016/S1352-2310\(97\)00319-1](https://doi.org/10.1016/S1352-2310(97)00319-1)
- 50) Cheremisinoff, N., 2002. Handbook of Air Pollution Prevention and Control, Handbook of Air Pollution Prevention and Control. <https://doi.org/10.1016/b978-0-7506-7499-7.x5000-7>
- 51) Chin, M., Ginoux, P., Kinne, S., Torres, O., Holben, B.N., Duncan, B.N., Martin, R. V., Logan, J.A., Higurashi, A., Nakajima, T., 2002. Tropospheric aerosol optical thickness from the GOCART model and comparisons with satellite and sun photometer measurements. *J. Atmos. Sci.* 59, 461–483. [https://doi.org/10.1175/1520-0469\(2002\)059<0461:taotft>2.0.co;2](https://doi.org/10.1175/1520-0469(2002)059<0461:taotft>2.0.co;2)
- 52) Chowdhury, Z., Zheng, M., Schauer, J.J., Sheesley, R.J., Salmon, L.G., Cass, G.R., Russell, A.G., 2007. Speciation of ambient fine organic carbon particles and source apportionment of PM<sub>2.5</sub> in Indian cities. *J. Geophys. Res. Atmos.* 112. <https://doi.org/10.1029/2007JD008386>
- 53) Chung, S.H., Seinfeld, J.H., 2002. Global distribution and climate forcing of carbonaceous aerosols. *J. Geophys. Res.* 107, 4407. <https://doi.org/10.1029/2001JD001397>
- 54) Clean Fuels Development Coalition, 2019. What’s in our gasoline is killing us Mobile Source Air Toxics (MSATs) and the Threat to Public Health.
- 55) Coggon, D., Barker, D., Rose, G., 2009. *Epidemiology for the Uninitiated*, 5th ed, Wiley. BMJ Books.
- 56) Cohen, A.J., Anderson, H.R., Ostro, B., Pandey, K.D., Krzyzanowski, M., Kunzli, N., Gutschmidt, K., Pope III, C.A., Romieu, I., Samet, J.M., Smith, K.R., 2004. Comparative Quantification of Health Risks Global and Regional Burden of Disease Attributable to Selected Major Risk Factors, in: Ezzati, M., Lopez, A.D., Rodgers, A., Murray, C.J. (Eds.), *World Health Organization*. Geneva, Switzerland, pp. 1353–1433.
- 57) Committee on the Medical Effects of Air Pollutants, 2010. *The Mortality Effects of Long-Term Exposure to Particulate Air Pollution in the United Kingdom*. <https://doi.org/ISBN 978-0-85951-685-3>

- 58) Committee on the Medical Effects of Air Pollutants, 2009. Long-term Exposure to Air Pollution: Effect on Mortality.
- 59) Conibear, L., Butt, E., Knote, C., Arnold, S., Spracklen, D., 2018a. Residential energy use emissions dominate health impacts from exposure to ambient particulate matter in India. *Nat. Commun.* 9, 1–9. <https://doi.org/10.1038/s41467-018-02986-7>
- 60) Conibear, L., Butt, E., Knote, C., Arnold, S., Spracklen, D., 2018b. Stringent Emission Control Policies Can Provide Large Improvements in Air Quality and Public Health in India. *GeoHealth* 2, 196–211. <https://doi.org/10.1029/2018gh000139>
- 61) Conibear, L., Butt, E., Knote, C., Spracklen, D., Arnold, S., 2018c. Current and Future Disease Burden From Ambient Ozone Exposure in India. *GeoHealth* 2, 334–355. <https://doi.org/10.1029/2018gh000168>
- 62) Conibear, L.A., Butt, E.W., Knote, C., Lam, N.L., Arnold, S., Tibrewal, K., Venkataraman, C., Spracklen, D. V, Bond, T.C., 2020. A complete transition to clean household energy can save one-quarter of the healthy life lost to particulate matter pollution exposure in India. *Environ. Res. Lett.* <https://doi.org/10.1088/1748-9326/ab8e8a>
- 63) Corraini, P., Olsen, M., Pedersen, L., Dekkers, O.M., Vandenbroucke, J.P., 2017. Effect modification, interaction and mediation: An overview of theoretical insights for clinical investigators. *Clin. Epidemiol.* 9, 331–338. <https://doi.org/10.2147/CLEP.S129728>
- 64) Crippa, P., Castruccio, S., Archer-Nicholls, S., Lebron, G., Kuwata, M., Thota, A., Sumin, S., Butt, E., Wiedinmyer, C., Spracklen, D., 2016. Population exposure to hazardous air quality due to the 2015 fires in Equatorial Asia. *Sci. Rep.* 6, 1–9. <https://doi.org/10.1038/srep37074>
- 65) Crutzen, P., Lawrence, M., Pöschl, U., 1999. On the background photochemistry of tropospheric ozone. *Tellus B Chem. Phys. Meteorol.* 51, 123–146. <https://doi.org/10.1034/j.1600-0870.1999.t01-1-00010.x>
- 66) Cruz Núñez, X., Ruiz, L.V., García, C.G., 2014. Black carbon and organic carbon emissions from wildfires in Mexico. *Atmosfera* 27, 165–172. <https://doi.org/10.1016/S0187->

- 67) Daniels, M., Dominici, F., Samet, J.M., Zeger, S.L., 2000. Estimating Particulate Matter-Mortality Dose-Response Curves and Threshold Levels: An Analysis of Daily Time-Series for the 20 Largest US Cities. *Am. J. Epidemiol.* 152, 397–406.
- 68) Davidson, C.I., Wu, Y.-L., 1990. *Dry Deposition of Particles and Vapors*. Springer, New York, NY, pp. 103–216. [https://doi.org/10.1007/978-1-4612-4454-7\\_5](https://doi.org/10.1007/978-1-4612-4454-7_5)
- 69) Davies, G.M., Kettridge, N., Stoof, C.R., Gray, A., Ascoli, D., Fernandes, P.M., Marrs, R., Allen, K.A., Doerr, S.H., Clay, G.D., McMorrow, J., Vandvik, V., 2016. The role of fire in UK peatland and moorland management: The need for informed, unbiased debate. *Philos. Trans. R. Soc. B Biol. Sci.* 371. <https://doi.org/10.1098/rstb.2015.0342>
- 70) Day, R., Green, C., 2018. The devastating toll of this summer’s moorland wildfires has been revealed - as firefighters tackle ANOTHER blaze - Manchester Evening News. Manchester Evening News.
- 71) Dayan, U., Levy, I., 2004. The Influence of Meteorological Conditions and Atmospheric Circulation Types on PM<sub>10</sub> and Visibility in Tel Aviv. *J. Appl. Meteorol.* 44, 606–619.
- 72) de Nazelle, A., Rodríguez, D.A., Crawford-Brown, D., 2009. The built environment and health: Impacts of pedestrian-friendly designs on air pollution exposure. *Sci. Total Environ.* 407, 2525–2535. <https://doi.org/10.1016/j.scitotenv.2009.01.006>
- 73) Delfino, R.J., Brummel, S., Wu, J., Stern, H., Ostro, B., Lipsett, M., Winer, A., Street, D.H., Zhang, L., Tjoa, T., Gillen, D.L., Ostro, B., Zhang, L., Street, D.H., Lipsett, M., Brummel, S., Delfino, R.J., Gillen, D.L., Stern, H., 2009. The relationship of respiratory and cardiovascular hospital admissions to the southern California wildfires of 2003. *Occup. Environ. Med.* 66, 189–197. <https://doi.org/10.1136/oem.2008.041376>
- 74) Deloitte UK, 2009. *Highways Agency Value of Life Estimates for the Purposes of Project*.
- 75) Demuzere, M., Trigo, R.M., Vila-Guerau de Arellano, J., van Lipzig, N.P.M., 2009. The impact of weather and atmospheric circulation on O<sub>3</sub> and PM<sub>10</sub> levels at a rural mid-latitude site.

Atmos. Chem. Phys. 9, 2695–2714. <https://doi.org/10.5194/acp-9-2695-2009>

- 76) Denman, K.L., Brasseur, G., Chidthaisong, A., Ciais, P., Cox, P.M., Dickinson, R.E., Hauglustaine, D., Heinze, C., Holland, E., Jacob, D., Lohmann, U., Ramachandran, S., Dias, P.L. da S., Wofsy, S.C., Zhang, X., 2007. Couplings Between Changes in the Climate System and Biogeochemistry, *Climate Change 2007: The Physical Science Basis. Contribution of Working Group I to the Fourth Report of the Intergovernmental Panel on Climate Change.* Cambridge, United Kingdom and New York, NY, USA.
- 77) Dennekamp, M., Abramson, M.J., 2011. The effects of bushfire smoke on respiratory health. *Respirology* 16, 198–209. <https://doi.org/10.1111/j.1440-1843.2010.01868.x>
- 78) Department for Environment Food & Rural Affairs, 2019. Clean air strategy.
- 79) Department for Environment Food & Rural Affairs, 2015. A review of the state-of-the-science relating to secondary particulate matter of relevance to the composition of the UK atmosphere.
- 80) Department for Environment Food & Rural Affairs, 2008. Site Operational Procedures For TEOM FDMS Analysers. Wiley.
- 81) Department for Environment Food and Rural Affairs, 2018a. Pollutant information.
- 82) Department for Environment Food and Rural Affairs, 2018b. Automatic Urban and Rural Network (AURN) [WWW Document]. URL <https://uk-air.defra.gov.uk/networks/network-info?view=aur> (accessed 12.10.20).
- 83) Department for Environment Food and Rural Affairs, 2017. Improving air quality in the UK: tackling nitrogen dioxide in our towns and cities Draft UK Air Quality Plan for tackling nitrogen dioxide.
- 84) Department for Environment Food and Rural Affairs, 2016. Sources and Effects of PM<sub>2.5</sub> [WWW Document]. Air Pollut. UK. <https://doi.org/10.1111/j.1528-1167.2012.03717.x>
- 85) Department for Environment Food and Rural Affairs, 2011. Emissions of Air Quality Pollutants.
- 86) Department for Environment Food and Rural Affairs, 2007. The Air Quality Strategy for

England , Scotland , Wales and Northern Ireland: Volume 1.

- 87) Department for Environment Food and Rural Affairs, Department for Transport, 2017. UK plan for tackling roadside nitrogen dioxide concentrations: An overview 1–11.
- 88) Department of Environmental Affairs and Tourism, 2018. Air Pollution Dispersion and Topographical Effects, in: National Air Quality Management Programme Phase Transition Project. pp. 1–113.
- 89) Department of Fire and Emergency Services, 2018. Prepare For a Bushfire - Department of Fire and Emergency Services [WWW Document]. URL <https://www.dfes.wa.gov.au/bushfire/prepare/> (accessed 12.11.20).
- 90) Deutscher Wetterdienst, 2017. Wetter und Klima - Deutscher Wetterdienst - Überblick [WWW Document]. URL [https://www.dwd.de/EN/research/observing\\_atmosphere/composition\\_atmosphere/aerosol/content\\_nav/particle\\_size\\_distribution\\_node.html](https://www.dwd.de/EN/research/observing_atmosphere/composition_atmosphere/aerosol/content_nav/particle_size_distribution_node.html) (accessed 6.29.20).
- 91) Dockery, D.W., Pope III, C.A., Xu, X., Spengler, J.D., Ware, J.H., Fay, M.E., Ferris, B.G., Speizer, F.E., 1993. An Association between Air Pollution and Mortality in Six U.S. Cities. *N. Engl. J. Med.* 329, 1753–1759. <https://doi.org/10.1056/NEJM199312093292401>
- 92) Dockery, D.W., Speizer, F.E., Stram, D.O., Ware, J.H., Spengler, J.D., Ferris, B.G., 1989. Effects of Inhalable Particles on Respiratory Health of Children. *Am. Rev. Respir. Dis.* 139, 587–594. <https://doi.org/10.1164/ajrccm/139.3.587>
- 93) Dore, A.J., Carslaw, D.C., Braban, C., Cain, M., Chemel, C., Conolly, C., Derwent, R.G., Griffiths, S.J., Hall, J., Hayman, G., Lawrence, S., Metcalfe, S.E., Redington, A., Simpson, D., Sutton, M.A., Sutton, P., Tang, Y.S., Vieno, M., Werner, M., Whyatt, J.D., 2015. Evaluation of the performance of different atmospheric chemical transport models and inter-comparison of nitrogen and sulphur deposition estimates for the UK. *Atmos. Environ.* 119, 131–143. <https://doi.org/10.1016/j.atmosenv.2015.08.008>
- 94) Ek, M.B., Mitchell, K.E., Lin, Y., Rogers, E., Grunmann, P., Koren, V., Gayno, G., Tarpley,

- J.D., 2003. Implementation of Noah land surface model advances in the National Centers for Environmental Prediction operational mesoscale Eta model. *J. Geophys. Res. Atmos.* 108, 1–16. <https://doi.org/10.1029/2002jd003296>
- 95) Emberson, L.D., Pleijel, H., Ainsworth, E.A., van den Berg, M., Ren, W., Osborne, S., Mills, G., Pandey, D., Dentener, F., Büker, P., Ewert, F., Koeble, R., Van Dingenen, R., 2018. Ozone effects on crops and consideration in crop models. *Eur. J. Agron.* 100, 19–34. <https://doi.org/10.1016/j.eja.2018.06.002>
- 96) Emmons, L.K., Walters, S., Hess, P.G., Lamarque, J.-F., Pfister, G.G., Fillmore, D., Granier, C., Guenther, A., Kinnison, D., Laepple, T., Orlando, J., Tie, X., Tyndall, G., Wiedinmyer, C., Baughcum, S.L., Kloster, S., 2009. Description and evaluation of the Model for Ozone and Related chemical Tracers, version 4 (MOZART-4). *Geosci. Model Dev. Discuss.* 2, 1157–1213. <https://doi.org/10.5194/gmdd-2-1157-2009>
- 97) Environment Agency, 2019. Guidance: Monitoring stack emissions: technical guidance for selecting a monitoring approach [WWW Document]. URL <https://www.gov.uk/guidance/monitoring-stack-emissions-technical-guidance-for-selecting-a-monitoring-approach#the-different-approaches-to-monitoring-stack-emissions>
- 98) European Commission, 2017. Standards - Air Quality - Environment - European Commission. Europa. <https://doi.org/10.1016/j.vetimm.2013.04.003>
- 99) European Environment Agency, 2017a. Air quality in Europe — 2017 report, EEA Technical Report. <https://doi.org/10.2800/22775>
- 100) European Environment Agency, 2017b. Air quality standards — European Environment Agency [WWW Document]. *Eur. Environ. Agency.* URL <https://www.eea.europa.eu/themes/air/air-quality-concentrations/air-quality-standards> (accessed 6.29.20).
- 101) European Environment Agency, 2016. Tropospheric ozone: background information [WWW Document]. URL <https://www.eea.europa.eu/publications/TOP08-98/page004.html>

- 102) European Environment Agency, 2013. Air quality in Europe—2013 Report: EEA report no 9/2013, European Union.
- 103) European Parliament, C. of the E.U., 2008. DIRECTIVE 2008/50/EC OF THE EUROPEAN PARLIAMENT AND OF THE COUNCIL.
- 104) Fann, N., Alman, B., Broome, R.A., Morgan, G.G., Johnston, F.H., Pouliot, G., Rappold, A.G., 2018. The health impacts and economic value of wildland fire episodes in the U.S.: 2008–2012. *Sci. Total Environ.* 610–611, 802–809. <https://doi.org/10.1016/j.scitotenv.2017.08.024>
- 105) Faustini, A., Alessandrini, E.R., Pey, J., Perez, N., Samoli, E., Querol, X., Cadum, E., Perrino, C., Ostro, B., Ranzi, A., Sunyer, J., Stafoggia, M., Forastiere, F., Angelini, P., Berti, G., Bisanti, L., Catrambone, M., Chiusolo, M., Davoli, M., De'donato, F., Demaria, M., Gandini, M., Grosa, M., Ferrari, S., Pandolfi, P., Pelosini, R., Pietrodangelo, A., Pizzi, L., Poluzzi, V., Priod, G., Randi, G., Rowinski, M., Scarinzi, C., Stivanello, E., Zauli-Sajani, S., Dimakopoulou, K., Eleftheriadis, K., Katsouyanni, K., Kelessis, A., Maggos, T., Michalopoulos, N., Pateraki, S., Petrakakis, M., Rodopoulou, S., Sypsa, V., Agis, D., Artiñano, B., Barrera-Gómez, J., Basagaña, X., De La Rosa, J., Diaz, J., Fernandez, R., Jacquemin, B., Karanasiou, A., Linares, C., Sanchez, A.M., Tobias, A., Bidondo, M., Declercq, C., Le Tertre, A., Lozano, P., Medina, S., Pascal, L., Pascal, M., 2015. Short-term effects of particulate matter on mortality during forest fires in Southern Europe: Results of the MED-PARTICLES project. *Occup. Environ. Med.* 72, 323–329. <https://doi.org/10.1136/oemed-2014-102459>
- 106) Fenech, S., Doherty, R.M., Heaviside, C., Macintyre, H.L., O'Connor, F.M., Vardoulakis, S., Neal, L., Agnew, P., 2019. Meteorological drivers and mortality associated with O<sub>3</sub> and PM<sub>2.5</sub> air pollution episodes in the UK in 2006. *Atmos. Environ.* 213, 699–710. <https://doi.org/10.1016/j.atmosenv.2019.06.030>
- 107) Finlay, S.E., Moffat, A., Gazzard, R., Baker, D., Murray, V., 2012. Health impacts of wildfires. *PLoS Curr.* 1–23. <https://doi.org/10.1371/4f959951cce2c>

- 108) Forastiere, F., Stafoggia, M., Tasco, C., Picciotto, S., Agabiti, N., Cesaroni, G., Perucci, C.A., 2007. Socioeconomic status, particulate air pollution, and daily mortality: Differential exposure or differential susceptibility. *Am. J. Ind. Med.* 50, 208–216. <https://doi.org/10.1002/ajim.20368>
- 109) Franklin, M., Zeka, A., Schwartz, J., 2007. Association between PM<sub>2.5</sub> and all-cause and specific-cause mortality in 27 US communities. *J. Expo. Sci. Environ. Epidemiol.* 17, 279–287. <https://doi.org/10.1038/sj.jes.7500530>
- 110) Freitas, S.R., Longo, K.M., Chatfield, R., Latham, D., Silva Dias, M.A.F., Andreae, M.O., Prins, E., Santos, J.C., Gielow, R., Carvalho, J.A., 2007. Including the sub-grid scale plume rise of vegetation fires in low resolution atmospheric transport models. *Atmos. Chem. Phys.* 7, 3385–3398. <https://doi.org/10.5194/acp-7-3385-2007>
- 111) Garane, K., Koukouli, M.-E., Verhoelst, T., Fioletov, V., Lerot, C., Heue, K.-P., Bais, A., Balis, D., Bazureau, A., Dehn, A., Goutail, F., Granville, J., Griffin, D., Hubert, D., Keppens, A., Lambert, J.-C., Loyola, D., McLinden, C., Pazmino, A., Pommereau, J.-P., Redondas, A., Romahn, F., Valks, P., Van Roozendaal, M., Xu, J., Zehner, C., Zerefos, C., Zimmer, W., 2019. TROPOMI/S5P total ozone column data: global ground-based validation & consistency with other satellite missions. *Atmos. Meas. Tech. Discuss.* 1–38. <https://doi.org/10.5194/amt-2019-147>
- 112) GBD Collaborators 2015, 2018. Global, regional, and national comparative risk assessment of 84 behavioural, environmental and occupational, and metabolic risks or clusters of risks for 195 countries and territories, 1990-2017: A systematic analysis for the Global Burden of Disease Stu. *Lancet* 392, 1923–1994. [https://doi.org/10.1016/S0140-6736\(18\)32225-6](https://doi.org/10.1016/S0140-6736(18)32225-6)
- 113) GBD Collaborators 2015, 2017. Estimates and 25-year trends of the global burden of disease attributable to ambient air pollution: an analysis of data from the Global Burden of Diseases Study 2015. *Lancet* 389, 1907–1918. [https://doi.org/10.1016/S0140-6736\(17\)30505-](https://doi.org/10.1016/S0140-6736(17)30505-)

- 114) GBD Collaborators 2015, 2016. Global, regional, and national comparative risk assessment of 79 behavioural, environmental and occupational, and metabolic risks or clusters of risks, 1990–2015: a systematic analysis for the Global Burden of Disease Study 2015. *Lancet* 388, 1659–1724. [https://doi.org/10.1016/S0140-6736\(16\)31679-8](https://doi.org/10.1016/S0140-6736(16)31679-8)
- 115) Georgiou, G.K., Christoudias, T., Proestos, Y., Kushta, J., Hadjinicolaou, P., Lelieveld, J., 2018. Air quality modelling in the summer over the eastern Mediterranean using WRF-Chem: Chemistry and aerosol mechanism intercomparison. *Atmos. Chem. Phys.* 18, 1555–1571. <https://doi.org/10.5194/acp-18-1555-2018>
- 116) Gerbig, C., Schmitgen, S., Kley, D., Volz-thomas, A., Dewey, K., 1999. An improved fast-response vacuum-UV resonance fluorescence CO instrument. *J. Geophys. Res.* 104, 1699–1704.
- 117) Geron, C., Hays, M., 2013. Air emissions from organic soil burning on the coastal plain of North Carolina. *Atmos. Environ.* 64, 192–199. <https://doi.org/10.1016/j.atmosenv.2012.09.065>
- 118) Giglio, L., Randerson, J.T., Van Der Werf, G.R., 2013. Analysis of daily, monthly, and annual burned area using the fourth-generation global fire emissions database (GFED4). *J. Geophys. Res. Biogeosciences* 118, 317–328. <https://doi.org/10.1002/jgrg.20042>
- 119) Ginoux, P., Chin, M., Tegen, I., Goddard, T., In, G., 2001. Sources and distributions of dust aerosols simulated with the GOCART model. *J. Geophys. Res.* 106, 20255–20273.
- 120) Gorshelev, V., Serdyuchenko, A., Weber, M., Chehade, W., Burrows, J.P., 2014. High spectral resolution ozone absorption cross-sections - Part 1: Measurements, data analysis and comparison with previous measurements around 293 K. *Atmos. Meas. Tech.* 7, 609–624. <https://doi.org/10.5194/amt-7-609-2014>
- 121) Gowers, A.M., Miller, B.G., Stedman, J.R., 2014. Estimating Local Mortality Burdens associated with Particulate Air Pollution About Public Health England.

- 122) Greater Manchester Combined Authority, 2019. Response to Freedom of Information Request 1920-057.
- 123) Grell, G.A., 1993. Prognostic Evaluation of Assumptions Used by Cumulus Parameterisations. *Mon. Weather Rev.* 764–787.
- 124) Grell, G.A., Peckham, S.E., Schmitz, R., McKeen, S.A., Frost, G., Skamarock, W.C., Eder, B., 2005. Fully coupled “online” chemistry within the WRF model. *Atmos. Environ.* 39, 6957–6975. <https://doi.org/10.1016/j.atmosenv.2005.04.027>
- 125) Grundström, M., Dahl, Å., Ou, T., Chen, D., Pleijel, H., 2017. The relationship between birch pollen, air pollution and weather types and their effect on antihistamine purchase in two Swedish cities. *Aerobiologia (Bologna)*. 33, 457–471. <https://doi.org/10.1007/s10453-017-9478-2>
- 126) Grundstrom, M., Tang, L., Hallquist, M., Nguyen, H., Chen, D., Pleijel, H., 2015. Influence of atmospheric circulation patterns on urban air quality during the winter. *Atmos. Pollut. Res.* 6, 278–285. <https://doi.org/10.5094/APR.2015.032>
- 127) Guenther, A., Karl, T., Harley, P., Wiedinmyer, C., Palmer, P.I., Geron, C., 2006. Estimates of global terrestrial isoprene emissions using MEGAN (Model of Emissions of Gases and Aerosols from Nature). *Atmos. Chem. Phys.* 6, 3181–3210. <https://doi.org/10.5194/acp-6-3181-2006>
- 128) Guerreiro, S.B., Dawson, R.J., Kilsby, C., Lewis, E., Ford, A., 2018. Future heat-waves, droughts and floods in 571 European cities. *Environ. Res. Lett.* 13. <https://doi.org/10.1088/1748-9326/aaaad3>
- 129) Guria, J., Leung, J., Jones-Lee, M., Loomes, G., 2005. The willingness to accept value of statistical life relative to the willingness to pay value: Evidence and policy implications. *Environ. Resour. Econ.* 32, 113–127. <https://doi.org/10.1007/s10640-005-6030-6>
- 130) Hack, J.J., 1994. Parameterization of moist convection in the National Center for Atmospheric Research community climate model (CCM2). *J. Geophys. Res.* 99, 5551–5568.

<https://doi.org/10.1029/93JD03478>

- 131) Hamilton, D.S., Hantson, S., Scott, C.E., Kaplan, J.O., Pringle, K.J., Nieradzik, L.P., Rap, A., Folberth, G.A., Spracklen, D. V., Carslaw, K.S., 2018. Reassessment of pre-industrial fire emissions strongly affects anthropogenic aerosol forcing. *Nat. Commun.* 9. <https://doi.org/10.1038/s41467-018-05592-9>
- 132) Hänninen, O.O., Salonen, R.O., Koistinen, K., Lanki, T., Barregard, L., Jantunen, M., 2009. Population exposure to fine particles and estimated excess mortality in Finland from an East European wildfire episode. *J. Expo. Sci. Environ. Epidemiol.* 19, 414–422. <https://doi.org/10.1038/jes.2008.31>
- 133) Harris, N.R.P., Carpenter, L.J., Lee, J.D., Vaughan, G., Filus, M.T., Jones, R.L., Ouyang, B., Pyle, J.A., Robinson, A.D., Andrews, S.J., Lewis, A.C., Minaeian, J., Vaughan, A., Dorsey, J.R., Gallagher, M.W., Le Breton, M., Newton, R., Percival, C.J., Ricketts, H.M.A., Bauguitte, S.J.B., Nott, G.J., Wellpott, A., Ashfold, M.J., Flemming, J., Butler, R., Palmer, P.I., Kaye, P.H., Stopford, C., Chemel, C., Boesch, H., Humpage, N., Vick, A., MacKenzie, A.R., Hyde, R., Angelov, P., Meneguz, E., Manning, A.J., 2017. Coordinated airborne studies in the tropics (CAST). *Bull. Am. Meteorol. Soc.* 98, 145–162. <https://doi.org/10.1175/BAMS-D-14-00290.1>
- 134) Harrison, R.M., 2014. *Pollution: Causes, Effects and Control* - Google Books, 5th ed. Royal Society of Chemistry, London.
- 135) Harrison, R.M., Jones, A.M., Beddows, D.C.S., Derwent, R.G., 2013. The effect of varying primary emissions on the concentrations of inorganic aerosols predicted by the enhanced UK Photochemical Trajectory Model. *Atmos. Environ.* 69, 211–218. <https://doi.org/10.1016/j.atmosenv.2012.12.016>
- 136) Harrison, R.M., Laxen, D., Moorcroft, S., Laxen, K., 2012. Processes affecting concentrations of fine particulate matter (PM<sub>2.5</sub>) in the UK atmosphere. *Atmos. Environ.* 46, 115–124. <https://doi.org/10.1016/j.atmosenv.2011.10.028>

- 137) Harrison, R.M., Smith, D.J.T., Kibble, A.J., 2004. What is responsible for the carcinogenicity of PM<sub>2.5</sub>? *Occup. Environ. Med.* 61, 799–805. <https://doi.org/10.1136/oem.2003.010504>
- 138) Harrison, R.M., Yin, J., 2000. Particulate matter in the atmosphere: Which particle properties are important for its effects on health? *Sci. Total Environ.* 249, 85–101. [https://doi.org/10.1016/S0048-9697\(99\)00513-6](https://doi.org/10.1016/S0048-9697(99)00513-6)
- 139) HelasGand Pienaar, J., 1996. The influence of vegetation fires on the chemical composition of the atmosphere. *S. Afr. J. Sci.* 92, 132–136.
- 140) HM Government, 2012. UK Climate Change Risk Assessment.
- 141) Hodzic, A., Knote, C., 2014. MOZART gas-phase chemistry with MOSAIC aerosols 7.
- 142) Hodzic, A., Madronich, S., Bonn, B., Massie, S., Menut, L., Wiedinmyer, C., 2007. Wildfire particulate matter in Europe during summer 2003: Meso-scale modeling of smoke emissions, transport and radiative effects. *Atmos. Chem. Phys.* 7, 4043–4064. <https://doi.org/10.5194/acp-7-4043-2007>
- 143) Hoelzemann, J.J., Schultz, M.G., Brasseur, G.P., Granier, C., Simon, M., 2004. Global Wildland Fire Emission Model (GWEM): Evaluating the use of global area burnt satellite data. *J. Geophys. Res* 109, 14–18. <https://doi.org/10.1029/2003JD003666>
- 144) Hoffmann, L., Günther, G., Li, D., Stein, O., Wu, X., Griessbach, S., Heng, Y., Konopka, P., Müller, R., Vogel, B., Wright, J.S., 2018. From ERA-Interim to ERA5: considerable impact of ECMWF's next-generation reanalysis on Lagrangian transport simulations. *Atmos. Chem. Phys. Discuss.* 1–38. <https://doi.org/10.5194/acp-2018-1199>
- 145) Holgate, S., 1998. Quantification of the Effects of Air Pollution on Health in the United Kingdom. The Stationary Office, London.
- 146) Holtslag, B., Boville, A., 1993. Local Versus Nonlocal Boundary-Layer Diffusion in a Global Climate Model. *J. Clim.* 6, 1825–1842. <https://doi.org/https://doi.org/10.1175/1520->

0442(1993)006<1825:LVNBLD>2.0.CO;2

- 147) Horowitz, L.W., 2006. Past, present and future concentrations of tropospheric ozone and aerosols: Methodology, ozone evaluation, and sensitivity to aerosol wet removal. *J. Geophys. Res. Atmos.* 111, 22211. <https://doi.org/10.1029/2005JD006937>
- 148) Horowitz, L.W., Walters, S., Mauzerall, D.L., Emmons, L.K., Rasch, P.J., Granier, C., Tie, X., Lamarque, J.F., Schultz, M.G., Tyndall, G.S., Orlando, J.J., Brasseur, G.P., 2003. A global simulation of tropospheric ozone and related tracers: Description and evaluation of MOZART, version 2. *J. Geophys. Res. Atmos.* 108. <https://doi.org/10.1029/2002jd002853>
- 149) Howards, P.P., 2018. An overview of confounding. Part 1: the concept and how to address it. *Acta Obstet. Gynecol. Scand.* 97, 394–399. <https://doi.org/10.1111/aogs.13295>
- 150) Hu, X.M., 2015. Boundary Layer (Atmospheric) and Air Pollution: Air Pollution Meteorology. *Encycl. Atmos. Sci. Second Ed.* 1, 227–236. <https://doi.org/10.1016/B978-0-12-382225-3.00499-0>
- 151) Hu, Y., Fernandez-Anez, N., Smith, T.E.L., Rein, G., 2018. Review of emissions from smouldering peat fires and their contribution to regional haze episodes. *Int. J. Wildl. Fire* 27, 293–312. <https://doi.org/10.1071/WF17084>
- 152) Iacono, M.J., Delamere, J.S., Mlawer, E.J., Shephard, M.W., Clough, S.A., Collins, W.D., 2008. Radiative forcing by long-lived greenhouse gases: Calculations with the AER radiative transfer models. *J. Geophys. Res.* 113, 13103. <https://doi.org/10.1029/2008JD009944>
- 153) Institute for Health Metrics and Evaluation, 2018. GBD Compare Data Visualization [WWW Document]. URL <https://vizhub.healthdata.org/gbd-compare/> (accessed 3.6.18).
- 154) Institute for Health Metrics and Evaluation, 2015. GBD Compare: IHME Viz Hub [WWW Document]. *Glob. Burd. Dis.* <https://doi.org/http://ihmeuw.org/3pgz>
- 155) Jaakkola, J., 2003. Case-crossover design in air pollution epidemiology. *Eur. Respir. Journal, Suppl.* 21. <https://doi.org/10.1183/09031936.03.00402703>
- 156) Jacob, D., 2006. Chapter 1: Chemical Trace Models - An Introduction. *Atmos. Model.*

- Transp. Chem. 1–9.
- 157) Jacob, D.J., 2000. Introduction to atmospheric chemistry. *Choice Rev. Online* 37, 37-6318-37–6318. <https://doi.org/10.5860/choice.37-6318>
- 158) Jaffe, D.A., Wigder, N.L., 2012. Ozone production from wildfires: A critical review. *Atmos. Environ.* 51, 1–10. <https://doi.org/10.1016/j.atmosenv.2011.11.063>
- 159) Janssens-Maenhout, G., Crippa, M., Guizzardi, D., Dentener, F., Muntean, M., Pouliot, G., Keating, T., Zhang, Q., Kurokawa, J., Wankmüller, R., Denier Van Der Gon, H., Kuenen, J.J.P., Klimont, Z., Frost, G., Darras, S., Koffi, B., Li, M., 2015. HTAP-v2.2: A mosaic of regional and global emission grid maps for 2008 and 2010 to study hemispheric transport of air pollution. *Atmos. Chem. Phys.* 15, 11411–11432. <https://doi.org/10.5194/acp-15-11411-2015>
- 160) Janssens-Maenhout, G., Pagliari, V., Guizzardi, D., Muntean, M., 2013. Global emission inventories in the Emission Database for Global Atmospheric Research (EDGAR)–Manual (I). <https://doi.org/10.2788/81454>
- 161) Jenkinson, A., Collison, F., 1977. An Initial Climatology of Gales over the North Sea, Synoptic Branch Memorandum.
- 162) Jerrett, M., Burnett, R.T., Pope III, C.A., Ito, K., Thurston, G., Krewski, D., Shi, Y., Calle, E., Thun, M., 2009. Long-Term Ozone Exposure and Mortality. *N. Engl. J. Med.* 360, 1085–1095. <https://doi.org/10.1056/nejmoa0803894>
- 163) Jiang, Y., Lu, Z., Liu, X., Qian, Y., Zhang, K., Wang, Y., Yang, X.Q., 2016. Impacts of global open-fire aerosols on direct radiative, cloud and surface-albedo effects simulated with CAM5. *Atmos. Chem. Phys.* 16, 14805–14824. <https://doi.org/10.5194/acp-16-14805-2016>
- 164) Johnston, F., Hanigan, I., Henderson, S., Morgan, G., Bowman, D., 2011. Extreme air pollution events from bushfires and dust storms and their association with mortality in Sydney, Australia 1994-2007. *Environ. Res.* 111, 811–816. <https://doi.org/10.1016/j.envres.2011.05.007>
- 165) Johnston, F.H., Henderson, S.B., Chen, Y., Marlier, M., DeFries, R.S., Kinney, P.,

- Bowman, D.M.J.S., Randerson, J.T., Marlier, M., DeFries, R.S., Kinney, P., Bowman, D.M.J.S., Brauer, M., 2012. Estimated global mortality attributable to smoke from landscape fires. *Environ. Health Perspect.* 120, 695–701. <https://doi.org/10.1289/ehp.1104422>
- 166) Johnston, F.H., Purdie, S., Jalaludin, B., Martin, K.L., Henderson, S.B., Morgan, G.G., 2014. Air pollution events from forest fires and emergency department attendances in Sydney, Australia 1996-2007: A case-crossover analysis. *Environ. Heal. A Glob. Access Sci. Source* 13, 1–9. <https://doi.org/10.1186/1476-069X-13-105>
- 167) Jones, P.D., Harpham, C., Briffa, K.R., 2013. Lamb weather types derived from reanalysis products. *Int. J. Climatol.* 33, 1129–1139. <https://doi.org/10.1002/joc.3498>
- 168) Jones, R.R., Hogrefe, C., Fitzgerald, E.F., Hwang, S., Garcia, V.C., Lin, S., Jones, R.R., Hogrefe, C., Fitzgerald, E.F., Hwang, S., Özkaynak, H., Garcia, V.C., Lin, S., Jones, R.R., Hogrefe, C., Fitzgerald, E.F., Hwang, S., Özkaynak, H., Garcia, V.C., Lin, S., 2015. Respiratory hospitalizations in association with fine PM and its components in New York State. *J. Air Waste Manage. Assoc.* 65, 559–569. <https://doi.org/10.1080/10962247.2014.1001500>
- 169) Kalnay, E., Collins, W., Deaven, D., Gandin, L., Iredell, M., Jenne, R., Joseph, D., 1996. The NCEP\_NCAR 40-year reanalysis project. *Bull. Am. Meteorol. Soc.* 77, 437–472.
- 170) Kanamitsu, M., 1989. Description of the NMC Global Data Assimilation and Forecast System. *Weather Forecast.* 4, 335–342. [https://doi.org/10.1175/1520-0434\(1989\)004<0335:DOTNGD>2.0.CO;2](https://doi.org/10.1175/1520-0434(1989)004<0335:DOTNGD>2.0.CO;2)
- 171) Kanjo, E., Younis, E.M.G., Sherkat, N., 2018. Towards unravelling the relationship between on-body, environmental and emotion data using sensor information fusion approach. *Inf. Fusion* 40, 18–31. <https://doi.org/10.1016/j.inffus.2017.05.005>
- 172) Katayama, D.H., 1986. The UV Huggins bands of ozone. *J. Chem. Phys.* 85, 6809–6810. <https://doi.org/10.1063/1.451416>
- 173) Kiely, L., Spracklen, D. V., Wiedinmyer, C., Conibear, L., Reddington, C.L., Archer-

- Nicholls, S., Lowe, D., Arnold, S.R., Knote, C., Firoz Khan, M., Talib Latif, M., Kuwata, M., Hapsari Budisulistiorini, S., Syaufina, L., 2019. New estimate of particulate emissions from Indonesian peat fires in 2015. *Atmos. Chem. Phys.* 19, 11105–11121. <https://doi.org/10.5194/acp-19-11105-2019>
- 174) Kiely, L., Spracklen, D. V, Wiedinmyer, C., Conibear, L.A., Reddington, C.L., Arnold, S.R., Knote, C., Khan, M.F., Latif, M.T., Syaufina, L., Adrianto, H.A., 2020. Air quality and health impacts of vegetation and peat fires in Equatorial Asia during 2004 – 2015. *Environ. Res. Lett.* <https://doi.org/10.1088/1748-9326/ab9a6c>
- 175) Kim, Y., Tong, H., Daniels, M., Boykin, E., Krantz, Q., McGee, J., Hays, M., Kovalcik, K., Dye, J.A., Gilmour, M., 2014. Cardiopulmonary toxicity of peat wildfire particulate matter and the predictive utility of precision cut lung slices. *Part. Fibre Toxicol.* 11, 29. <https://doi.org/10.1186/1743-8977-11-29>
- 176) Kim, Y.H., King, C., Krantz, T., Hargrove, M.M., George, I.J., McGee, J., Copeland, L., Hays, M.D., Landis, M.S., Higuchi, M., Gavett, S.H., Gilmour, M.I., 2019. The role of fuel type and combustion phase on the toxicity of biomass smoke following inhalation exposure in mice. *Arch. Toxicol.* 93, 1501–1513. <https://doi.org/10.1007/s00204-019-02450-5>
- 177) Kim, Y.H., Warren, S.H., Krantz, Q.T., King, C., Jaskot, R., Preston, W.T., George, B.J., Hays, M.D., Landis, M.S., Higuchi, M., Demarini, D.M., Gilmour, M.I., 2018. Mutagenicity and lung toxicity of smoldering vs. flaming emissions from various biomass fuels: Implications for health effects from wildland fires. *Environ. Health Perspect.* 126, 1–14. <https://doi.org/10.1289/EHP2200>
- 178) King, A., Dorling, S., 1997. New directions special issue on the origins of PM<sub>10</sub> particulate matter: particulate matter PM<sub>10</sub> - the significance of ambient levels. *Atmos. Environ.* 31, 2379–2381. [https://doi.org/https://doi.org/10.1016/S1352-2310\(97\)00001-0](https://doi.org/https://doi.org/10.1016/S1352-2310(97)00001-0)
- 179) Kivimäki, M., Vineis, P., Brunner, E.J., 2015. How can we reduce the global burden of disease? *Lancet* 386, 2235–2237. [https://doi.org/10.1016/S0140-6736\(15\)00129-4](https://doi.org/10.1016/S0140-6736(15)00129-4)

- 180) Klemm, R.J., Mason, R.M., Heilig, C.M., Neas, L.M., Dockery, D.W., 2000. Is daily mortality associated specifically with fine particles? data reconstruction and replication of analyses. *J. Air Waste Manag. Assoc.* 50, 1215–1222. <https://doi.org/10.1080/10473289.2000.10464149>
- 181) Knote, C., Hodzic, A., Jimenez, J.L., 2014. The effect of dry and wet deposition of condensable vapors on secondary organic aerosols concentrations over the continental US, *Atmospheric Chemistry and Physics Discussions*. <https://doi.org/10.5194/acpd-14-13731-2014>
- 182) Knote, C., Hodzic, A., Jimenez, J.L., Volkamer, R., Orlando, J.J., Baidar, S., Brioude, J., Fast, J., Gentner, D.R., Goldstein, A.H., Hayes, P.L., Knighton, W.B., Oetjen, H., Setyan, A., Stark, H., Thalman, R., Tyndall, G., Washenfelder, R., Waxman, E., Zhang, Q., 2014. SOA formation from glyoxal in a 3-D model Atmospheric Chemistry and Physics Simulation of semi-explicit mechanisms of SOA formation from glyoxal in a 3-D model SOA formation from glyoxal in a 3-D model. *Atmos. Chem. Phys. Discuss* 13, 26699–26759. <https://doi.org/10.5194/acpd-13-26699-2013>
- 183) Kochi, I., Champ, P.A., Loomis, J.B., Donovan, G.H., 2012. Valuing mortality impacts of smoke exposure from major southern California wildfires. *J. For. Econ.* 18, 61–75. <https://doi.org/10.1016/j.jfe.2011.10.002>
- 184) Kollanus, V., Prank, M., Gens, A., Soares, J., Vira, J., Kukkonen, J., Sofiev, M., Salonen, R.O., Lanki, T., 2017. Mortality due to Vegetation Fire–Originated PM<sub>2.5</sub> Exposure in Europe—Assessment for the Years 2005 and 2008. *Environ. Health Perspect.* 125, 30–37. <https://doi.org/10.1289/EHP194>
- 185) Konovalov, I.B., Beekmann, M., Kuznetsova, I.N., Yurova, A., Zvyagintsev, A.M., 2011. Atmospheric impacts of the 2010 Russian wildfires: Integrating modelling and measurements of an extreme air pollution episode in the Moscow region. *Atmos. Chem. Phys.* 11, 10031–10056. <https://doi.org/10.5194/acp-11-10031-2011>
- 186) Krawchuk, M.A., Moritz, M.A., Parisien, M.A., Van Dorn, J., Hayhoe, K., 2009.

- Global pyrogeography: The current and future distribution of wildfire. *PLoS One* 4.  
<https://doi.org/10.1371/journal.pone.0005102>
- 187) Kroll, J.H., Seinfeld, J.H., 2008. Chemistry of secondary organic aerosol: Formation and evolution of low-volatility organics in the atmosphere. *Atmos. Environ.* 42, 3593–3624.  
<https://doi.org/10.1016/j.atmosenv.2008.01.003>
- 188) Krupnick, A., Harrison, K., Nickell, E., Toman, M., 1996. The value of health benefits from ambient air quality improvements in Central and Eastern Europe: An exercise in benefits transfer. *Environ. Resour. Econ.* 7, 307–332. <https://doi.org/10.1007/bf00369622>
- 189) Kuenen, J.J.P., Visschedijk, A.J.H., Jozwicka, M., Denier Van Der Gon, H.A.C., 2014. TNO-MACC-II emission inventory; A multi-year (2003-2009) consistent high-resolution European emission inventory for air quality modelling. *Atmos. Chem. Phys.* 14, 10963–10976.  
<https://doi.org/10.5194/acp-14-10963-2014>
- 190) Kushta, J., Pozzer, A., Lelieveld, J., 2018. Uncertainties in estimates of mortality attributable to ambient PM<sub>2.5</sub> in Europe. *Environ. Res. Lett.* 13. <https://doi.org/10.1088/1748-9326/aabf29>
- 191) Laden, F., Neas, L.M., Dockery, D.W., Schwartz, J., 2000. Association of Fine Particulate Matter from Different Sources with Daily Mortality in Six U.S. *Environ. Health Perspect.* 108, 941–947.
- 192) Lamb, H., 1972. British Isles weather types and a register of daily sequence of circulation patterns. *Geophys. Mem.* 116, 1861–1971.
- 193) Lambert, J.-C., Keppens, A., Hubert, D., Langerock, B., Eichmann, K.-U., Kleipool, Q., Sneep, M., Verhoelst, T., Wagner, T., Weber, M., Ahn, C., Argyrouli, A., Balis, D., Chan, K.L., Compennolle, S., Smedt, I. De, Eskes, H., Fjærraa, A.M., Garane, K., Gleason, J.F., Goutail, F., Granville, J., Hedelt, P., Heue, K.-P., Jaross, G., Koukouli, M., Landgraf, J., Lutz, R., Niemejer, S., Pazmiño, A., Pinaridi, G., Pommereau, J.-P., Richter, A., Rozemeijer, N., Sha, M.K., Zweers, D.S., Theys, N., Tilstra, G., Torres, O., Valks, P., Vigouroux, C., P. Wang, 2019.

Sentinel-5 Precursor Mission Performance Centre Quarterly Validation Report of the Copernicus Sentinel-5 Precursor Operational Data Products # 03 : July 2018 – May 2019. S5P MPC Routine Oper. Consol. Valid. Rep. Ser. 2, 1–125.

- 194) Landis, M.S., Edgerton, E.S., White, E.M., Wentworth, G.R., Sullivan, A.P., Dillner, A.M., 2018. The impact of the 2016 Fort McMurray Horse River Wildfire on ambient air pollution levels in the Athabasca Oil Sands Region, Alberta, Canada. *Sci. Total Environ.* 618, 1665–1676. <https://doi.org/10.1016/j.scitotenv.2017.10.008>
- 195) Lane, T.E., Donahue, N.M., Pandis, S.N., 2008a. Simulating secondary organic aerosol formation using the volatility basis-set approach in a chemical transport model. *Atmos. Environ.* 42, 7439–7451. <https://doi.org/10.1016/j.atmosenv.2008.06.026>
- 196) Lane, T.E., Donahue, N.M., Pandis, S.N., 2008b. Effect of NO<sub>x</sub> on secondary organic aerosol concentrations. *Environ. Sci. Technol.* 42, 6022–6027. <https://doi.org/10.1021/es703225a>
- 197) Lee, H., 2019. Bushfires Release Over Half Australia’s Annual Carbon Emissions. Bloom. Green.
- 198) Lee, J.D., Moller, S.J., Read, K.A., Lewis, A.C., Mendes, L., Carpenter, L.J., 2009. Year-round measurements of nitrogen oxides and ozone in the tropical North Atlantic marine boundary layer. *J. Geophys. Res. Atmos.* 114, 1–14. <https://doi.org/10.1029/2009JD011878>
- 199) LeGrand, S.L., Polashenski, C., Letcher, T.W., Creighton, G.A., Peckham, S.E., Cetola, J.D., 2019. The AFWA dust emission scheme for the GOCART aerosol model in WRF-Chem v3.8.1. *Geosci. Model Dev.* 12, 131–166. <https://doi.org/10.5194/gmd-12-131-2019>
- 200) Lelieveld, J., Evans, J.S., Fnais, M., Giannadaki, D., Pozzer, A., 2015. The contribution of outdoor air pollution sources to premature mortality on a global scale. *Nature* 525, 367–371. <https://doi.org/10.1038/nature15371>
- 201) Li, Z., Zang, Z., Li, Q.B., Chao, Y., Chen, D., Ye, Z., Liu, Y., Liou, K.N., 2013. A three-dimensional variational data assimilation system for multiple aerosol species with WRF-

- Chem and an application to PM<sub>2.5</sub> prediction. *Atmos. Chem. Phys.* 13, 4265–4278.  
<https://doi.org/10.5194/acp-13-4265-2013>
- 202) Liang, J., 2013. Particulate matter, in: *Chemical Modeling for Air Resources*. Elsevier, pp. 189–219. <https://doi.org/10.1016/B978-0-12-408135-2.00009-4>
- 203) Lin, J., Nielsen, C.P., Zhao, Y., Lei, Y., Liu, Y., McElroy, M.B., 2010. Recent changes in particulate air pollution over china observed from space and the ground: Effectiveness of emission control. *Environ. Sci. Technol.* 44, 7771–7776. <https://doi.org/10.1021/es101094t>
- 204) Lin, S.J., Rood, R.B., 1996. Multidimensional flux-form semi-lagrangian transport schemes. *Mon. Weather Rev.* 124, 2046–2070. <https://doi.org/10.6052/j.issn.1000-4750.2015.05.0420>
- 205) Liu, C., Chen, R., Sera, F., Vicedo-Cabrera, A.M., Guo, Y., Tong, S., Coelho, M.S.Z.S., Saldiva, P.H.N., Lavigne, E., Matus, P., Valdes Ortega, N., Osorio Garcia, S., Pascal, M., Stafoggia, M., Scortichini, M., Hashizume, M., Honda, Y., Hurtado-Díaz, M., Cruz, J., Nunes, B., Teixeira, J.P., Kim, H., Tobias, A., Íñiguez, C., Forsberg, B., Åström, C., Ragettli, M.S., Guo, Y.-L., Chen, B.-Y., Bell, M.L., Wright, C.Y., Scovronick, N., Garland, R.M., Milojevic, A., Kyselý, J., Urban, A., Orru, H., Indermitte, E., Jaakkola, J.J.K., Rytí, N.R.I., Katsouyanni, K., Analitis, A., Zanobetti, A., Schwartz, J., Chen, J., Wu, T., Cohen, A., Gasparri, A., Kan, H., 2019. Ambient Particulate Air Pollution and Daily Mortality in 652 Cities. *N. Engl. J. Med.* 381, 705–715. <https://doi.org/10.1056/nejmoa1817364>
- 206) Liu, F., Beirle, S., Zhang, Q., Dörner, S., He, K., Wagner, T., 2016. NO<sub>x</sub> lifetimes and emissions of cities and power plants in polluted background estimated by satellite observations. *Atmos. Chem. Phys.* 16, 5283–5298. <https://doi.org/10.5194/acp-16-5283-2016>
- 207) Liu, J.C., Pereira, G., Uhl, S.A., Bravo, M.A., Bell, M.L., 2015. A systematic review of the physical health impacts from non-occupational exposure to wildfire smoke. *Environ. Res.* 136, 120–132. <https://doi.org/10.1016/j.envres.2014.10.015>
- 208) Liu, T., Mickley, L.J., Marlier, M.E., DeFries, R.S., Khan, M.F., Latif, M.T.,

- Karambelas, A., 2020. Diagnosing spatial biases and uncertainties in global fire emissions inventories: Indonesia as regional case study. *Remote Sens. Environ.* 237, 111557. <https://doi.org/10.1016/j.rse.2019.111557>
- 209) Liu, Y., Goodrick, S., Heilman, W., 2014. Wildland fire emissions, carbon, and climate: Wildfire-climate interactions. *For. Ecol. Manage.* 317, 80–96. <https://doi.org/10.1016/j.foreco.2013.02.020>
- 210) Liu, Y., Stanturf, J., Goodrick, S., 2010. Trends in global wildfire potential in a changing climate. *For. Ecol. Manage.* 259, 685–697. <https://doi.org/10.1016/j.foreco.2009.09.002>
- 211) Liu, Y., Zhao, N., Vanos, J.K., Cao, G., 2017. Effects of synoptic weather on ground-level PM<sub>2.5</sub> concentrations in the United States. *Atmos. Environ.* 148, 297–305. <https://doi.org/10.1016/j.atmosenv.2016.10.052>
- 212) Lobert, J., Warnatz, J., 1993. Emissions from the combustion process in vegetation. *Fire Environ.* 13, 15–37.
- 213) Long, C.M., Nascarella, M.A., Valberg, P.A., 2013. Carbon black vs. black carbon and other airborne materials containing elemental carbon: Physical and chemical distinctions. *Environ. Pollut.* 181, 271–286. <https://doi.org/10.1016/j.envpol.2013.06.009>
- 214) Lu, Z., Sokolik, I.N., 2013. The effect of smoke emission amount on changes in cloud properties and precipitation: A case study of Canadian boreal wildfires of 2007. *J. Geophys. Res. Atmos.* 118, 11,777–11,793. <https://doi.org/10.1002/2013JD019860>
- 215) Lucas, C., Hennessy, K., Mills, G., Bathols, J., 2007. Bushfire Weather in Southeast Australia : Recent Trends and Projected Climate Change Impacts. Consult. Rep. Prep. Clim. Inst. Aust. 84.
- 216) Macintyre, H.L., Heaviside, C., Neal, L.S., Agnew, P., Thornes, J., Vardoulakis, S., 2016. Mortality and emergency hospitalizations associated with atmospheric particulate matter episodes across the UK in spring 2014. *Environ. Int.* 97, 108–116.

<https://doi.org/10.1016/j.envint.2016.07.018>

- 217) Madronich, S., Weller, G., 1990. Numerical integration errors in calculated tropospheric photodissociation rate coefficients. *J. Atmos. Chem.* 10, 289–300. <https://doi.org/10.1007/BF00053864>
- 218) Mahowald, N.M., Lamarque, J.F., Tie, X.X., Wolff, E., 2006. Sea-salt aerosol response to climate change: Last Glacial Maximum, preindustrial, and doubled carbon dioxide climates. *J. Geophys. Res. Atmos.* 111, 1–11. <https://doi.org/10.1029/2005JD006459>
- 219) Marmot, M., Bell, R., 2012. Fair society, healthy lives (Full report). *Public Health* 126, S4–S10. <https://doi.org/10.1016/j.puhe.2012.05.014>
- 220) Marsh, D.R., Mills, M.J., Kinnison, D.E., Lamarque, J.F., Calvo, N., Polvani, L.M., 2013. Climate change from 1850 to 2005 simulated in CESM1(WACCM). *J. Clim.* 26, 7372–7391. <https://doi.org/10.1175/JCLI-D-12-00558.1>
- 221) Marticorena, B., Bergametti, G., 1995. Modeling the atmospheric dust cycle: Design of a soil-derived dust emission scheme. *J. Geophys. Res.* 100, 16415–16430. <https://doi.org/10.1029/95jd00690>
- 222) Martin, R. V., Sioris, C.E., Chance, K., Ryerson, T.B., Bertram, T.H., Wooldridge, P.J., Cohen, R.C., Neuman, J.A., Swanson, A., Flocke, F.M., 2006. Evaluation of space-based constraints on global nitrogen oxide emissions with regional aircraft measurements over and downwind of eastern North America. *J. Geophys. Res. Atmos.* 111, 1–15. <https://doi.org/10.1029/2005JD006680>
- 223) McDermott, B.M.C., Palmer, L.J., 1999. Post-disaster service provision following proactive identification of children with emotional distress and depression. *Aust. N. Z. J. Psychiatry* 33, 855–863. <https://doi.org/10.1046/j.1440-1614.1999.00611.x>
- 224) McFarlane, A.C., 1988. The phenomenology of posttraumatic stress disorders following a natural disaster. *J. Nerv. Ment. Dis.* 176, 22–29. <https://doi.org/10.1097/00005053-198801000-00003>

- 225) McFarlane, A.C., Clayer, J.R., Bookless, C.L., 1997. Psychiatric morbidity following a natural disaster: An Australian bushfire. *Soc. Psychiatry Psychiatr. Epidemiol.* 32, 261–268. <https://doi.org/10.1007/BF00789038>
- 226) Mcmeeking, G.R., 2008. The Optical, Chemical, and Physical Properties of Aerosols and Gases Emitted by the Laboratory Combustion of Wildland Fires 321.
- 227) Megaritis, A.G., Fountoukis, C., Charalampidis, P.E., Pilinis, C., Pandis, S.N., 2013. Response of fine particulate matter concentrations to changes of emissions and temperature in Europe. *Atmos. Chem. Phys.* 13, 3423–3443. <https://doi.org/10.5194/acp-13-3423-2013>
- 228) Methven, J., 2003. Estimating photochemically produced ozone throughout a domain using flight data and a Lagrangian model. *J. Geophys. Res.* 108, 4271. <https://doi.org/10.1029/2002JD002955>
- 229) Metzger, S., Dentener, F., Pandis, S., Lelieveld, J., 2002. Gas/aerosol partitioning: A computationally efficient model. <https://doi.org/10.1029/2001JD001102>
- 230) Miles, G.M., Siddans, R., Kerridge, B.J., Latter, B.G., Richards, N.A.D., 2015. Tropospheric ozone and ozone profiles retrieved from GOME-2 and their validation. *Atmos. Meas. Tech.* 8, 385–398. <https://doi.org/10.5194/amt-8-385-2015>
- 231) Mills, I.C., Atkinson, R.W., Kang, S., Walton, H., Anderson, H.R., 2015. Quantitative systematic review of the associations between short-term exposure to nitrogen dioxide and mortality and hospital admissions. *BMJ Open* 5, 1–8. <https://doi.org/10.1136/bmjopen-2014-006946>
- 232) Monks, P.S., Archibald, A.T., Colette, A., Cooper, O., Coyle, M., Derwent, R., Fowler, D., Granier, C., Law, K.S., Mills, G.E., Stevenson, D.S., Tarasova, O., Thouret, V., Von Schneidmesser, E., Sommariva, R., Wild, O., Williams, M.L., 2015. Tropospheric ozone and its precursors from the urban to the global scale from air quality to short-lived climate forcer. *Atmos. Chem. Phys.* 15, 8889–8973. <https://doi.org/10.5194/acp-15-8889-2015>
- 233) Moore, D.P., 2019. The October 2017 red sun phenomenon over the UK. *Weather* 74,

- 348–353. <https://doi.org/10.1002/wea.3440>
- 234) Morgan, G., Sheppard, V., Khalaj, B., Ayyar, A., Lincoln, D., Jalaludin, B., Beard, J., Corbett, S., Lumley, T., 2010. Effects of bushfire smoke on daily mortality and hospital admissions in Sydney, Australia. *Epidemiology* 21, 47–55. <https://doi.org/10.1097/EDE.0b013e3181c15d5a>
- 235) Naeher, L.P., Brauer, M., Lipsett, M., Zelikoff, J.T., Simpson, C.D., Koenig, J.Q., Smith, K.R., 2007. Woodsmoke health effects: A review. *Inhal. Toxicol.* 19, 67–106. <https://doi.org/10.1080/08958370600985875>
- 236) NAEI, 2018. Download emission maps [WWW Document]. URL [https://naei.beis.gov.uk/data/map-uk-das?pollutant\\_id=2&emiss\\_maps\\_submit=naei-20190625105934](https://naei.beis.gov.uk/data/map-uk-das?pollutant_id=2&emiss_maps_submit=naei-20190625105934) (accessed 12.10.20).
- 237) Nakanishi, M., Niino, H., 2006. An improved Mellor-Yamada Level-3 model: Its numerical stability and application to a regional prediction of advection fog. *Boundary-Layer Meteorol.* 119, 397–407. <https://doi.org/10.1007/s10546-005-9030-8>
- 238) NASA Socioeconomic Data and Applications Center (SEDAC) Center for International Earth Science Information Network (CIESIN), Columbia, U. of, 2018. Gridded Population of the World, Version 4 (GPWv4): Population Count, Revision 11. <https://doi.org/https://doi.org/10.7927/H4JW8BX5>
- 239) National Atmosphere Emissions Inventory, 2017a. Pollutant information - NAEI, UK [WWW Document]. URL [https://naei.beis.gov.uk/overview/pollutants?pollutant\\_id=8](https://naei.beis.gov.uk/overview/pollutants?pollutant_id=8) (accessed 6.30.20).
- 240) National Atmosphere Emissions Inventory, 2017b. Pollutant Information: Non-Methane VOC [WWW Document]. URL [https://naei.beis.gov.uk/overview/pollutants?pollutant\\_id=9](https://naei.beis.gov.uk/overview/pollutants?pollutant_id=9)
- 241) National Atmospheric Emission Inventory, 2016. Air Pollutants [WWW Document]. URL <https://naei.beis.gov.uk/overview/ap-overview>

- 242) National Centre for Atmospheric Research, 2007. NCEP Global Forecast System (GFS) Analyses and Forecasts [WWW Document]. URL <https://rda.ucar.edu/datasets/ds084.6/> (accessed 12.11.20).
- 243) Nemery, B., Hoet, P.H.M., Nemmar, A., 2001. The Meuse Valley fog of 1930: An air pollution disaster. *Lancet*. [https://doi.org/10.1016/S0140-6736\(00\)04135-0](https://doi.org/10.1016/S0140-6736(00)04135-0)
- 244) Norris, Fran H., Friedman, M.J., Watson, P.J., 2002. 60,000 Disaster victims speak: Part II. Summary and implications of the disaster mental health research. *Psychiatry* 65, 240–260. <https://doi.org/10.1521/psyc.65.3.240.20169>
- 245) Norris, Fran H, Friedman, M.J., Watson, P.J., Byrne, C.M., 2002. 60,000 disaster victims speak : Part I . an empirical review of the empirical ... *Heal.* (San Fr. 2747.
- 246) Nowok, B., Raab, G.M., Dibben, C., 2016. Synthpop: Bespoke creation of synthetic data in R. *J. Stat. Softw.* 74. <https://doi.org/10.18637/jss.v074.i11>
- 247) Nugent, A., DeCou, D., Russell, S., Alison Nugent, David DeCou, Shintaro Russell, 2019. *Atmo 200: Atmospheric Processes and Phenomenon*. Press Books, University of Hawai'i, Mānoa.
- 248) O'Hare, G., Wilby, R., 1995. A Review of Ozone Pollution in the United Kingdom and Ireland with an Analysis Using Lamb Weather Types. *Geogr. J.* 161, 1–20.
- 249) O'Neill, M.S., Jerrett, M., Kawachi, I., Levy, J.I., Cohen, A.J., Gouveia, N., Wilkinson, P., Fletcher, T., Cifuentes, L., Schwartz, J., Bateson, T.F., Cann, C., Dockery, D., Gold, D., Laden, F., London, S., Loomis, D., Speizer, F., Van den Eeden, S., Zanobetti, A., 2003. Health, wealth, and air pollution: Advancing theory and methods. *Environ. Health Perspect.* 111, 1861–1870. <https://doi.org/10.1289/ehp.6334>
- 250) Olivier, J., Peters, J., Granier, C., Pétron, G., Müller, J., Wallens, S., 2003. Present and future surface emissions of atmospheric compounds.
- 251) Ostro, B., Broadwin, R., Green, S., Feng, W.Y., Lipsett, M., 2006. Fine particulate air pollution and mortality in nine California counties: Results from CALFINE. *Environ. Health*

- Perspect. 114, 29–33. <https://doi.org/10.1289/ehp.8335>
- 252) Otero, N., Sillmann, J., Butler, T., 2018. Assessment of an extended version of the Jenkinson–Collison classification on CMIP5 models over Europe. *Clim. Dyn.* 50, 1559–1579. <https://doi.org/10.1007/s00382-017-3705-y>
- 253) Paraskevopoulou, D., Bougiatioti, A., Stavroulas, I., Fang, T., Lianou, M., Liakakou, E., Gerasopoulos, E., Weber, R., Nenes, A., Mihalopoulos, N., 2019. Yearlong variability of oxidative potential of particulate matter in an urban Mediterranean environment. *Atmos. Environ.* 206, 183–196. <https://doi.org/10.1016/j.atmosenv.2019.02.027>
- 254) Pay, M.T., Jiménez-Guerrero, P., Baldasano, J.M., 2012. Assessing sensitivity regimes of secondary inorganic aerosol formation in Europe with the CALIOPE-EU modeling system. *Atmos. Environ.* 51, 146–164. <https://doi.org/10.1016/j.atmosenv.2012.01.027>
- 255) Peckham, S., Grell, G., McKeen, S., Ahmadov, R., Marrapu, P., 2015. WRF-Chem version 3.7 user’s guide. *User’s Guid.* 1, 73. <https://doi.org/10.1017/CBO9781107415324.004>
- 256) Peterson, D.A., Campbell, J.R., Hyer, E.J., Fromm, M.D., Kablick, G.P., Cossuth, J.H., DeLand, M.T., 2018. Wildfire-driven thunderstorms cause a volcano-like stratospheric injection of smoke. *Clim. Atmos. Sci.* 1, 1–8. <https://doi.org/10.1038/s41612-018-0039-3>
- 257) Petetin, H., Sciare, J., Bressi, M., Rosso, A., Sanchez, O., Sarda-Estève, R., Petit, J.E., Beekmann, M., 2015. Assessing the ammonium nitrate formation regime in the Paris megacity and its representation in the CHIMERE model. *Atmos. Chem. Phys. Discuss.* 15, 23731–23794. <https://doi.org/10.5194/acpd-15-23731-2015>
- 258) Phuleria, H.C., Fine, P.M., Zhu, Y., Sioutas, C., 2005. Air quality impacts of the October 2003 Southern California wildfires. *J. Geophys. Res. Atmos.* 110, 1–11. <https://doi.org/10.1029/2004JD004626>
- 259) Pidd, H., Rawlinson, K., 2018. Saddleworth Moor fire declared major incident as residents evacuated. *The Guardian*.
- 260) Pope, C.A., Thun, M.J., Namboodiri, M.M., Dockery, D.W., Evans, J.S., Speizer, F.E.,

- Heath, C.W., 1995. Particulate Air Pollution as a Predictor of Mortality in a Prospective Study of U.S. Adults. *Am. J. Respir. Crit. Care Med.* 151, 669–674.  
[https://doi.org/10.1164/ajrccm/151.3\\_Pt\\_1.669](https://doi.org/10.1164/ajrccm/151.3_Pt_1.669)
- 261) Pope III, C.A., 2007. Mortality effects of longer term exposures to fine particulate air pollution: Review of recent epidemiological evidence. *Inhal. Toxicol.* 19, 33–38.  
<https://doi.org/10.1080/08958370701492961>
- 262) Pope III, C.A., Dockery, D.W., 2006. Health effects of fine particulate air pollution: Lines that connect. *J. Air Waste Manag. Assoc.* 56, 709–742.  
<https://doi.org/10.1080/10473289.2006.10464485>
- 263) Pope III, C.A., Kalkstein, L.S., 1996. Synoptic weather modeling and estimates of the exposure-response relationship between daily mortality and particulate air pollution. *Environ. Health Perspect.* 104, 414–420. <https://doi.org/10.2307/3432686>
- 264) Pope, R., Kerridge, B., Siddans, R., Latter, B., Ventress, L., Chipperfield, M., Arnold, S., Pimlott, M., Graham, A., Rigby, R., n.d. Large enhancements in southern hemisphere satellite-observed carbon monoxide due to 2019/2020 Australian wildfires. “unpublished.”
- 265) Pope, R.J., Arnold, S.R., Chipperfield, M.P., Latter, B.G., Siddans, R., Kerridge, B.J., 2018. Widespread changes in UK air quality observed from space. *Atmos. Sci. Lett.* 19, 1–8.  
<https://doi.org/10.1002/asl.817>
- 266) Pope, R.J., Butt, E.W., Chipperfield, M.P., Doherty, R.M., Fenech, S., Schmidt, A., Arnold, S.R., Savage, N.H., 2016. The impact of synoptic weather on UK surface ozone and implications for premature mortality. *Environ. Res. Lett.* 11, 124004.  
<https://doi.org/10.1088/1748-9326/11/12/124004>
- 267) Pope, R.J., Graham, A.M., Chipperfield, M.P., Veefkind, J.P., 2019. High resolution satellite observations give new view of UK air quality. *Weather* 2, 2–6.  
<https://doi.org/10.1002/wea.3441>
- 268) Pope, R.J., Savage, N.H., Chipperfield, M.P., Arnold, S.R., Osborn, T.J., 2014. The

- influence of synoptic weather regimes on UK air quality: Analysis of satellite column NO<sub>2</sub>. *Atmos. Sci. Lett.* 15, 211–217. <https://doi.org/10.1002/asl2.492>
- 269) Pope, R.J., Savage, N.H., Chipperfield, M.P., Ordóñez, C., Neal, L.S., 2015. The influence of synoptic weather regimes on UK air quality: Regional model studies of tropospheric column NO<sub>2</sub>. *Atmos. Chem. Phys. Discuss.* 15, 18577–18607. <https://doi.org/10.5194/acpd-15-18577-2015>
- 270) Public Health England, 2018. Health matters: air pollution.
- 271) Putaud, J.P., Van Dingenen, R., Alastuey, A., Bauer, H., Birmili, W., Cyrys, J., Flentje, H., Fuzzi, S., Gehrig, R., Hansson, H.C., Harrison, R.M., Herrmann, H., Hitzenberger, R., Hüglin, C., Jones, A.M., Kasper-Giebl, A., Kiss, G., Koussa, A., Kuhlbusch, T.A.J., Löschau, G., Maenhaut, W., Molnar, A., Moreno, T., Pekkanen, J., Perrino, C., Pitz, M., Puxbaum, H., Querol, X., Rodriguez, S., Salma, I., Schwarz, J., Smolik, J., Schneider, J., Spindler, G., ten Brink, H., Tursic, J., Viana, M., Wiedensohler, A., Raes, F., 2010. A European aerosol phenomenology: Physical and chemical characteristics of particulate matter from 60 rural, urban, and kerbside sites across Europe. *Atmos. Environ.* 44, 1308–1320. <https://doi.org/10.1016/j.atmosenv.2009.12.011>
- 272) Querol, X., Alastuey, A., Ruiz, C.R., Artiñano, B., Hansson, H.C., Harrison, R.M., Buringh, E., Ten Brink, H.M., Lutz, M., Bruckmann, P., Straehl, P., Schneider, J., 2004. Speciation and origin of PM<sub>10</sub> and PM<sub>2.5</sub> in selected European cities. *Atmos. Environ.* 38, 6547–6555. <https://doi.org/10.1016/j.atmosenv.2004.08.037>
- 273) Raaschou-Nielsen, O., Andersen, Z.J., Beelen, R., Samoli, E., Stafoggia, M., Weinmayr, G., Hoffmann, B., Fischer, P., Nieuwenhuijsen, M.J., Brunekreef, B., Xun, W.W., Katsouyanni, K., Dimakopoulou, K., Sommar, J., Forsberg, B., Modig, L., Oudin, A., Oftedal, B., Schwarze, P.E., Nafstad, P., De Faire, U., Pedersen, N.L., Östenson, C.G., Fratiglioni, L., Penell, J., Korek, M., Pershagen, G., Eriksen, K.T., Sørensen, M., Tjønneland, A., Ellermann, T., Eeftens, M., Peeters, P.H., Meliefste, K., Wang, M., Bueno-de-Mesquita, B., Key, T.J., de

- Hoogh, K., Concin, H., Nagel, G., Vilier, A., Grioni, S., Krogh, V., Tsai, M.Y., Ricceri, F., Sacerdote, C., Galassi, C., Migliore, E., Ranzi, A., Cesaroni, G., Badaloni, C., Forastiere, F., Tamayo, I., Amiano, P., Dorronsoro, M., Trichopoulou, A., Bamia, C., Vineis, P., Hoek, G., 2013. Air pollution and lung cancer incidence in 17 European cohorts: Prospective analyses from the European Study of Cohorts for Air Pollution Effects (ESCAPE). *Lancet Oncol.* 14, 813–822. [https://doi.org/10.1016/S1470-2045\(13\)70279-1](https://doi.org/10.1016/S1470-2045(13)70279-1)
- 274) Rappold, A.G., Cascio, W.E., Kilaru, V.J., Stone, S.L., Neas, L.M., Devlin, R.B., Diaz-sanchez, D., 2012. Cardio-respiratory outcomes associated with exposure to wildfire smoke are modified by measures of community health 1–9.
- 275) Rappold, A.G., Fann, N.L., Crooks, J., Huang, J., Cascio, W.E., Devlin, R.B., Diaz-Sanchez, D., 2014. Forecast-based interventions can reduce the health and economic burden of wildfires. *Environ. Sci. Technol.* 48, 10571–10579. <https://doi.org/10.1021/es5012725>
- 276) Rappold, A.G., Stone, S.L., Cascio, W.E., Neas, L.M., Kilaru, V.J., Carraway, M.S., Szykman, J.J., Ising, A., Cleve, W.E., Meredith, J.T., Vaughan-Batten, H., Deyneka, L., Devlin, R.B., 2011. Peat Bog Wildfire Smoke Exposure in Rural North Carolina Is Associated with Cardiopulmonary Emergency Department Visits Assessed through Syndromic Surveillance. *Environ. Health Perspect.* 119, 1415–1420. <https://doi.org/10.1289/ehp.1003206>
- 277) Rasch, P.J., Mahowald, N.M., Eaton, B.E., 1997. Representations of transport, convection, and the hydrologic cycle in chemical transport models: Implications for the modeling of short-lived and soluble species. *J. Geophys. Res. Atmos.* 102, 28127–28138. <https://doi.org/10.1029/97jd02087>
- 278) Reddington, C., Conibear, L., Knute, C., Silver, B., Li, Y., Chan, C., Arnold, S., Spracklen, D., 2019. Exploring the impacts of anthropogenic emission sectors on PM<sub>2.5</sub> and human health in South and East Asia. *Atmos. Chem. Phys.* 19, 11887–11910. <https://doi.org/10.5194/acp-19-11887-2019>
- 279) Reddington, C.L., Butt, E.W., Ridley, D.A., Artaxo, P., Morgan, W.T., Coe, H.,

- Spracklen, D. V., 2015. Air quality and human health improvements from reductions in deforestation-related fire in Brazil. *Nat. Geosci.* 8, 768–771. <https://doi.org/10.1038/ngeo2535>
- 280) Reddington, C.L., Yoshioka, M., Balasubramanian, R., Ridley, D., Toh, Y.Y., Arnold, S.R., Spracklen, D. V., 2014. Contribution of vegetation and peat fires to particulate air pollution in Southeast Asia. *Environ. Res. Lett.* 9, 094006. <https://doi.org/10.1088/1748-9326/9/9/094006>
- 281) Reid, C.E., Brauer, M., Johnston, F.H., Jerrett, M., Balmes, J.R., Elliott, C.T., E., R.C., Michael, B., H., J.F., Michael, J., R., B.J., T., E.C., 2016. Critical review of health impacts of wildfire smoke exposure. *Environ. Health Perspect.* 124, 1334–1343. <https://doi.org/10.1289/ehp.1409277>
- 282) Reid, C.E., Considine, E.M., Watson, G.L., Telesca, D., Pfister, G.G., Jerrett, M., 2019. Associations between respiratory health and ozone and fine particulate matter during a wildfire event. *Environ. Int.* 129, 291–298. <https://doi.org/10.1016/j.envint.2019.04.033>
- 283) Reis, S., Liška, T., Vieno, M., Carnell, E.J., Beck, R., Clemens, T., Dragosits, U., Tomlinson, S.J., Leaver, D., Heal, M.R., 2018. The influence of residential and workday population mobility on exposure to air pollution in the UK. *Environ. Int.* 121, 803–813. <https://doi.org/10.1016/j.envint.2018.10.005>
- 284) Reisen, F., Duran, S.M., Flannigan, M., Elliott, C., Rideout, K., 2015. Wildfire smoke and public health risk. *Int. J. Wildl. Fire* 24, 1029. <https://doi.org/10.1071/WF15034>
- 285) Remer, L.A., Kaufman, Y.J., Tanré, D., Mattoo, S., Chu, D.A., Martins, J. V., Li, R.R., Ichoku, C., Levy, R.C., Kleidman, R.G., Eck, T.F., Vermote, E., Holben, B.N., 2005. The MODIS aerosol algorithm, products, and validation. *J. Atmos. Sci.* 62, 947–973. <https://doi.org/10.1175/JAS3385.1>
- 286) Remer, L.A., Mattoo, S., Levy, R.C., Munchak, L.A., 2013. MODIS 3 km aerosol product: Algorithm and global perspective. *Atmos. Meas. Tech.* 6, 1829–1844. <https://doi.org/10.5194/amt-6-1829-2013>

- 287) Ritter, M., Müller, M.D., Jorba, O., Parlow, E., Liu, L.J.S., 2013. Impact of chemical and meteorological boundary and initial conditions on air quality modeling: WRF-Chem sensitivity evaluation for a European domain. *Meteorol. Atmos. Phys.* 119, 59–70. <https://doi.org/10.1007/s00703-012-0222-8>
- 288) Rooney, C., McMichael, A.J., Kovats, R.S., Coleman, M.P., 1998. Excess mortality in England and Wales, and in Greater London, during the 1995 heatwave. *J. Epidemiol. Community Health* 52, 482–486. <https://doi.org/10.1136/jech.52.8.482>
- 289) Rosenberg, P.D., Dean, A.R., Williams, P.I., Dorsey, J.R., Minikin, A., Pickering, M.A., Petzold, A., 2012. Particle sizing calibration with refractive index correction for light scattering optical particle counters and impacts upon PCASP and CDP data collected during the Fennec campaign. *Atmos. Meas. Tech.* 5, 1147–1163. <https://doi.org/10.5194/amt-5-1147-2012>
- 290) Rossi, M.J., 2003. Heterogeneous Reactions on Salts. *Chem. Rev.* 103, 4823–4882. <https://doi.org/10.1021/cr020507n>
- 291) Roulston, C., Paton-Walsh, C., Smith, T.E.L., Guérette, A., Evers, S., Yule, C.M., Rein, G., Van der Werf, G.R., 2018. Fine Particle Emissions From Tropical Peat Fires Decrease Rapidly With Time Since Ignition. *J. Geophys. Res. Atmos.* 123, 5607–5617. <https://doi.org/10.1029/2017JD027827>
- 292) Rowlinson, M.J., Rap, A., Arnold, S.R., Pope, R.J., Chipperfield, M.P., McNorton, J., Forster, P., Gordon, H., Pringle, K.J., Feng, W., Kerridge, B.J., Latter, B.L., Siddans, R., 2019. Impact of El Niño Southern Oscillation on the interannual variability of methane and tropospheric ozone. *Atmos. Chem. Phys. Discuss.* 2, 1–20. <https://doi.org/10.5194/acp-2019-222>
- 293) Royal Berkshire Fire and Rescue Service, 2011. Press Release: Freedom of Information.
- 294) Royal College of Physicians, 2016. Report of a working party February 2016.

- 295) Russo, A., Trigo, R.M., Martins, H., Mendes, M.T., 2014. NO<sub>2</sub>, PM<sub>10</sub> and O<sub>3</sub> urban concentrations and its association with circulation weather types in Portugal. *Atmos. Environ.* 89, 768–785. <https://doi.org/10.1016/j.atmosenv.2014.02.010>
- 296) Samoli, E., Analitis, A., Touloumi, G., Schwartz, J., Anderson, H.R., Sunyer, J., Bisanti, L., Zmirou, D., Vonk, J.M., Pekkanen, J., Goodman, P., Paldy, A., Schindler, C., Katsouyanni, K., 2005. Estimating the exposure-response relationships between particulate matter and mortality within the APHEA multicity project. *Environ. Health Perspect.* 113, 88–95. <https://doi.org/10.1289/ehp.7387>
- 297) Sanchez-Marroquin, A., Hedges, D.H.P., Hiscock, M., Parker, S.T., Rosenberg, P.D., Trembath, J., Walshaw, R., Burke, I., McQuaid, J., Murray, B., 2019. Characterisation of the filter inlet system on the BAE-146 research aircraft and its use for size resolved aerosol composition measurements. *Atmos. Meas. Tech.* 12, 5741–5763. <https://doi.org/10.5194/amt-12-5741-2019>
- 298) Schmidt, A., Ostro, B., Carslaw, K.S., Wilson, M., Thordarson, T., Mann, G.W., Simmons, A.J., 2011. Excess mortality in Europe following a future Laki-style Icelandic eruption. *Proc. Natl. Acad. Sci.* 108, 15710–15715. <https://doi.org/10.1073/pnas.1108569108>
- 299) Schrenk, H.H., Heimann, H., Clayton, G.D., Gafafer, W.M., Wexler, H., 1949. Air Pollution in Donora, Pa.- Epidemiology of the Unusual Smog Episode of October 1948, in: Public Health Service. Washington, DC. <https://doi.org/10.1017/CBO9781107415324.004>
- 300) Schwartz, J., 1993. Air Pollution and Daily Mortality in Birmingham, Alabama. *Am. J. Epidemiol.* 137, 1136–1147. <https://doi.org/10.1093/oxfordjournals.aje.a116617>
- 301) Schwartz, J., Ballester, F., Saez, M., Pérez-Hoyos, S., Bellido, J., Cambra, K., Arribas, F., Cañada, A., Pérez-Boillos, M.J., Sunyer, J., 2001. The concentration-response relation between air pollution and daily deaths. *Environ. Health Perspect.* 109, 1001–1006. <https://doi.org/10.1289/ehp.011091001>
- 302) Schwartz, J., Dockery, D.W., Neas, L.M., 1996. Is Daily Mortality Associated

- Specifically with Fine Particles? *J. Air Waste Manag. Assoc.* 46, 927–939.  
<https://doi.org/10.1080/10473289.1996.10467528>
- 303) Schwartz, J., Marcus, A., 1990. Mortality and air pollution J London: A time series analysis. *Am. J. Epidemiol.* 131, 185–194. <https://doi.org/10.1093/oxfordjournals.aje.a115473>
- 304) Schwarze, P.E., Øvrevik, J., Låg, M., Refsnes, M., Nafstad, P., Hetland, R.B., Dybing, E., 2006. Particulate matter properties and health effects: Consistency of epidemiological and toxicological studies. *Hum. Exp. Toxicol.* 25, 559–579.  
<https://doi.org/10.1177/096032706072520>
- 305) Scott, C.E., Rap, A., Spracklen, D. V., Forster, P.M., Carslaw, K.S., Mann, G.W., Pringle, K.J., Kivekäs, N., Kulmala, M., Lihavainen, H., Tunved, P., 2014. The direct and indirect radiative effects of biogenic secondary organic aerosol. *Atmos. Chem. Phys.* 14, 447–470. <https://doi.org/10.5194/acp-14-447-2014>
- 306) Seigneur, C., Dennis, R., 2011. Atmospheric Modeling. Tech. Challenges Multipollutant Air Qual. Manag. 299–337. [https://doi.org/10.1007/978-94-007-0304-9\\_9](https://doi.org/10.1007/978-94-007-0304-9_9)
- 307) Seinfeld, J., 1986. *Atmospheric Chemistry and Physics of Air Pollution* - John H. Seinfeld, Professor Department of Chemistry John H Seinfeld - Google Books. Wiley, University of Michigan.
- 308) Seinfeld, J., Pandis, S., Steinfeld, J.I., 2016. *Atmospheric Chemistry and Physics: From Air Pollution to Climate Change*, 5th ed, Environment: Science and Policy for Sustainable Development. Wiley. <https://doi.org/10.1080/00139157.1999.10544295>
- 309) Shao, Y., 2001. A model for mineral dust emission. *J. Geophys. Res.* 106, 20239–20254.
- 310) Shaposhnikov, D., Revich, B., Bellander, T., Bedada, G.B., Bottai, M., Kharkova, T., Kvasha, E., Lezina, E., Lind, T., Semutnikova, E., Pershagen, G., 2014. Mortality related to air pollution with the Moscow heat wave and wildfire of 2010. *Epidemiology* 25, 359–364.  
<https://doi.org/10.1097/EDE.0000000000000090>

- 311) Sharma, M., Kishore, S., Tripathi, S.N., Behera, S.N., 2007. Role of atmospheric ammonia in the formation of inorganic secondary particulate matter: A study at Kanpur, India. *J. Atmos. Chem.* 58, 1–17. <https://doi.org/10.1007/s10874-007-9074-x>
- 312) Shekarrizfard, M., Faghieh-Imani, A., Tétreault, L.F., Yasmin, S., Reynaud, F., Morency, P., Plante, C., Drouin, L., Smargiassi, A., Eluru, N., Hatzopoulou, M., 2017. Regional assessment of exposure to traffic-related air pollution: Impacts of individual mobility and transit investment scenarios. *Sustain. Cities Soc.* 29, 68–76. <https://doi.org/10.1016/j.scs.2016.12.002>
- 313) Siddans, R., Gerber, D., Miles, G., 2015. Optimal Estimation Method retrievals with IASI, AMSU and MHS measurements.
- 314) Silver, B., Conibear, L., Reddington, C., Knote, C., Arnold, S., Spracklen, D., 2020. Pollutant emission reductions deliver decreased PM<sub>2.5</sub>-caused mortality across China during 2015–2017. *Atmos. Chem. Phys.* 2017, 1–18. <https://doi.org/10.5194/acp-2019-1141>
- 315) Simpson, D., Benedictow, A., Berge, H., Bergström, R., Emberson, L.D., Fagerli, H., Flechard, C.R., Hayman, G.D., Gauss, M., Jonson, J.E., Jenkin, M.E., Nyúri, A., Richter, C., Semeena, V.S., Tsyro, S., Tuovinen, J.P., Valdebenito, A., Wind, P., 2012. The EMEP MSC-W chemical transport model Technical description. *Atmos. Chem. Phys.* 12, 7825–7865. <https://doi.org/10.5194/acp-12-7825-2012>
- 316) Skamarock, W.C., Klemp, J.B., 2008. A time-split nonhydrostatic atmospheric model for weather research and forecasting applications. *J. Comput. Phys.* 227, 3465–3485. <https://doi.org/10.1016/j.jcp.2007.01.037>
- 317) Sommers, W.T., Loehman, R.A., Hardy, C.C., 2014. Wildland fire emissions, carbon, and climate: Science overview and knowledge needs. *For. Ecol. Manage.* 317, 1–8. <https://doi.org/10.1016/j.foreco.2013.12.014>
- 318) Song, J., Chung, K., 2010. Observational Studies: Cohort and Case-Control Studies. *Plast. Reconstr. Surg.* 126, 2234–2242. <https://doi.org/10.1007/s00415-017-8487-y>
- 319) Stedman, J.R., 2004. The predicted number of air pollution related deaths in the UK

- during the August 2003 heatwave. *Atmos. Environ.* 38, 1087–1090.  
<https://doi.org/10.1016/j.atmosenv.2003.11.011>
- 320) Stedman, J.R., 1996. A U.K.-wide episode of elevated particle (PM) concentration in March 1996. *Science*, 80. [https://doi.org/https://doi.org/10.1016/S1352-2310\(97\)88638-4](https://doi.org/10.1016/S1352-2310(97)88638-4)
- 321) Stein, A.F., Draxler, R.R., Rolph, G.D., Stunder, B.J.B., Cohen, M.D., Ngan, F., 2015. NOAA's hybrid atmospheric transport and dispersion modeling system. *Bull. Am. Meteorol. Soc.* 96, 2059–2077. <https://doi.org/10.1175/BAMS-D-14-00110.1>
- 322) Stevenson, K., Yardley, R., Stacey-Aea, B., Maggs, R., Veritas, B., 2009. QA/QC Procedures for the UK Automatic Urban and Rural Air Quality Monitoring Network (AURN): Executive summary.
- 323) Stirling, E.L., Pope, R.J., Graham, A.M., Chipperfield, M.P., Arnold, S.R., 2020. Quantifying the transboundary contribution of nitrogen oxides to UK air quality. *Atmos. Sci. Lett.* 21, 1–11. <https://doi.org/10.1002/asl.955>
- 324) Stockwell, C.E., Jayarathne, T., Cochrane, M.A., Ryan, K.C., Putra, E.I., Saharjo, B.H., Nurhayati, A.D., Albar, I., Blake, D.R., Simpson, I.J., Stone, E.A., Yokelson, R.J., 2016. Field measurements of trace gases and aerosols emitted by peat fires in Central Kalimantan, Indonesia, during the 2015 El Niño. *Atmos. Chem. Phys.* 16, 11711–11732. <https://doi.org/10.5194/acp-16-11711-2016>
- 325) Sutton, M.A., van Grinsven, H., Billen, G., Bleeker, A., Bouwman, A.F., Bull, K., Erisman, J.W., Grennfelt, P., Grizzetti, B., Howard, C.M., Oenema, O., Spranger, T., Winiwarter, W., 2011. Summary for policy makers. *Eur. Nitrogen Assess.* <https://doi.org/10.1017/cbo9780511976988.002>
- 326) Syphard, A.D., Sheehan, T., Rustigian-Romsos, H., Ferschweiler, K., 2018. Mapping future fire probability under climate change: Does vegetation matter? *PLoS One* 13, 1–23. <https://doi.org/10.1371/journal.pone.0201680>
- 327) Tadic, I., Crowley, J.N., Dienhart, D., Eger, P., Harder, H., Hottmann, B., Martinez,

- M., Parchatka, U., Pari, J.D., Pozzer, A., Rohloff, R., Schuladen, J., Shenolikar, J., Tauer, S., Lelieveld, J., Fischer, H., 2020. Net ozone production and its relationship to nitrogen oxides and volatile organic compounds in the marine boundary layer around the Arabian Peninsula. *Atmos. Chem. Phys.* 20, 6769–6787. <https://doi.org/10.5194/acp-20-6769-2020>
- 328) Tang, L., Chen, D., Karlsson, P.E., Gu, Y., Ou, T., 2009. Synoptic circulation and its influence on spring and summer surface ozone concentrations in southern Sweden. *Boreal Environ. Res.* 14, 889–902.
- 329) Tang, L., Rayner, D., Haeger-Eugensson, M., 2011. Have Meteorological Conditions Reduced NO<sub>2</sub> Concentrations from Local Emission Sources in Gothenburg? *Water, Air, Soil Pollut.* 221, 275–286. <https://doi.org/10.1007/s11270-011-0789-6>
- 330) Thompson, G., Field, P.R., Rasmussen, R.M., Hall, W.D., 2008. Explicit forecasts of winter precipitation using an improved bulk microphysics scheme. Part II: Implementation of a new snow parameterization. *Mon. Weather Rev.* 136, 5095–5115. <https://doi.org/10.1175/2008MWR2387.1>
- 331) Thompson, T.M., Saari, R.K., Selin, N.E., 2014. Air quality resolution for health impact assessment: Influence of regional characteristics. *Atmos. Chem. Phys.* 14, 969–978. <https://doi.org/10.5194/acp-14-969-2014>
- 332) Thorp, T., Arnold, S.R., Pope, R.J., Spracklen, D. V, Conibear, L., Knote, C., 2020. Late-Spring and Summertime Tropospheric Ozone and NO<sub>2</sub> in Western Siberia and the Russian Arctic: Regional Model Evaluation and Sensitivities. *Atmos. Chem. Phys. Discuss.* <https://doi.org/10.5194/acp-2020-426>
- 333) Tian, D., Hu, Y., Wang, Y., Boylan, J., Zheng, M., Armistead, R., 2009. Assessment of biomass burning emissions and their impacts on urban and regional PM<sub>2.5</sub>: A Georgia case study. *Environ. Sci. Technol.* 43, 299–305. <https://doi.org/10.1021/es801827s>
- 334) Tie, X., Madronich, S., Walters, S., Edwards, D.P., Ginoux, P., Mahowald, N., Zhang,

- R.Y., Lou, C., Brasseur, G., 2005. Assessment of the global impact of aerosols on tropospheric oxidants. *J. Geophys. Res. D Atmos.* 110, 1–32. <https://doi.org/10.1029/2004JD005359>
- 335) Tie, X., Madronich, S., Walters, S., Zhang, R., Racsh, P., Collins, W., 2003. Effect of clouds on photolysis and oxidants in the troposphere. *J. Geophys. Res.* 108, 4642. <https://doi.org/10.1029/2003JD003659>
- 336) Tinling, M.A., West, J.J., Cascio, W.E., Kilaru, V., Rappold, A.G., 2016. Repeating cardiopulmonary health effects in rural North Carolina population during a second large peat wildfire. *Environ. Heal. A Glob. Access Sci. Source* 15, 1–12. <https://doi.org/10.1186/s12940-016-0093-4>
- 337) Turetsky, M.R., Benscoter, B., Page, S., Rein, G., Van Der Werf, G.R., Watts, A., 2015. Global vulnerability of peatlands to fire and carbon loss. *Nat. Geosci.* 8, 11–14. <https://doi.org/10.1038/ngeo2325>
- 338) Twigg, M., Ilyinskaya, E., Beccaceci, S., Green, D., Jones, M., Langford, B., Leeson, S., Lingard, J., Pereira, G., Carter, H., Poskitt, J., Richter, A., Ritchie, S., Simmons, I., Smith, R., Sim Tang, Y., Van Dijk, N., Vincent, K., Nemitz, E., Vieno, M., Braban, C., 2016. Impacts of the 2014-2015 Holuhraun eruption on the UK atmosphere. *Atmos. Chem. Phys.* 16, 11415–11431. <https://doi.org/10.5194/acp-16-11415-2016>
- 339) UCAR, 2020a. WRF-Chem MOZART-4 Download [WWW Document]. URL <https://www.acom.ucar.edu/wrf-chem/mozart.shtml> (accessed 9.16.20).
- 340) UCAR, 2020b. WACCM Download [WWW Document]. URL <https://www.acom.ucar.edu/wacm/download.shtml> (accessed 9.16.20).
- 341) UCAR, 2020c. Static Data Downloads [WWW Document]. URL [http://www2.mmm.ucar.edu/wrf/users/download/get\\_sources\\_wps\\_geog.html](http://www2.mmm.ucar.edu/wrf/users/download/get_sources_wps_geog.html) (accessed 9.16.20).
- 342) UCAR, 2020d. Release of Tropospheric Ultraviolet-Visible (TUV) Model Version 5.3 [WWW Document]. URL <https://nar.ucar.edu/2016/acom/31-release-tropospheric-ultraviolet->

- visible-tuv-model-version-53 (accessed 11.6.20).
- 343) UCAR, 2020e. WRF-Chem Model Development [WWW Document]. URL <https://nar.ucar.edu/2016/acom/32-wrf-chem-model-development> (accessed 11.6.20).
- 344) UK Met Office, 2018. UK actual and anomaly maps [WWW Document]. URL <https://www.metoffice.gov.uk/research/climate/maps-and-data/uk-actual-and-anomaly-maps> (accessed 12.11.20).
- 345) Ukhov, A., Mostamandi, S., Da Silva, A., Flemming, J., Alshehri, Y., Shevchenko, I., Stenchikov, G., 2020. Assessment of natural and anthropogenic aerosol air pollution in the Middle East using MERRA-2, CAMS data assimilation products, and high-resolution WRF-Chem model simulations. *Atmos. Chem. Phys.* 20, 9281–9310. <https://doi.org/10.5194/acp-20-9281-2020>
- 346) United Nations Economic Commission for Europe, 1979. The Convention and its achievements - Air Pollution - Environmental Policy.
- 347) United States Environmental Protection Agency (USEPA), 2009. Integrated Science Assessment for Particulate Matter.
- 348) US Environmental Protection Agency, 2020. Ozone Effects on Plants.
- 349) US Environmental Protection Agency, 1997. The Benefits and Costs of the Clean Air Act 1970 to 1990 (Appendix G) 45, 327–331.
- 350) Vallero, D.A., 2014. Fundamentals of Air Pollution, Fundamentals of Air Pollution. <https://doi.org/10.1016/B978-0-12-373615-4.X5000-6>
- 351) Van Der Werf, G.R., Randerson, J.T., Giglio, L., Van Leeuwen, T.T., Chen, Y., Rogers, B.M., Mu, M., Van Marle, M.J.E., Morton, D.C., Collatz, G.J., Yokelson, R.J., Kasibhatla, P.S., 2017. Global fire emissions estimates during 1997-2016. *Earth Syst. Sci. Data* 9, 697–720. <https://doi.org/10.5194/essd-9-697-2017>
- 352) van Oldenborgh, G.J., Krikken, F., Lewis, S., Leach, N., Lehner, F., Saunders, K., van Weele, M., Haustein, K., Li, S., Wallom, D., Sparrow, S., Arrighi, J., Singh, R., van Aalst, M.,

- Philip, S., Vautard, R., Otto, F., 2020. Attribution of the Australian bushfire risk to anthropogenic climate change. *Nat. Hazards Earth Syst. Sci.* 1–46. <https://doi.org/10.5194/nhess-2020-69>
- 353) Veefkind, J.P., Aben, I., McMullan, K., Förster, H., de Vries, J., Otter, G., Claas, J., Eskes, H.J., de Haan, J.F., Kleipool, Q., van Weele, M., Hasekamp, O., Hoogeveen, R., Landgraf, J., Snel, R., Tol, P., Ingmann, P., Voors, R., Kruizinga, B., Vink, R., Visser, H., Levelt, P.F., 2012. TROPOMI on the ESA Sentinel-5 Precursor: A GMES mission for global observations of the atmospheric composition for climate, air quality and ozone layer applications. *Remote Sens. Environ.* 120, 70–83. <https://doi.org/10.1016/j.rse.2011.09.027>
- 354) Vieno, M., Dore, A.J., Stevenson, D.S., Doherty, R., Heal, M.R., Reis, S., Hallsworth, S., Tarrason, L., Wind, P., Fowler, D., Simpson, D., Sutton, M.A., 2010. Modelling surface ozone during the 2003 heat-wave in the UK. *Atmos. Chem. Phys.* 10, 7963–7978. <https://doi.org/10.5194/acp-10-7963-2010>
- 355) Vieno, M., Heal, M., Twigg, M., MacKenzie, I., Braban, C., Lingard, J., Ritchie, S., Beck, R., Möring, A., Ots, R., Di Marco, C., Nemitz, E., Sutton, M., Reis, S., 2016. The UK particulate matter air pollution episode of March–April 2014: More than Saharan dust. *Environ. Res. Lett.* 11, 044004. <https://doi.org/10.1088/1748-9326/11/4/044004>
- 356) Vieno, M., Heal, M.R., Hallsworth, S., Famulari, D., Doherty, R.M., Dore, A.J., Tang, Y.S., Braban, C.F., Leaver, D., Sutton, M.A., Reis, S., 2014. The role of long-range transport and domestic emissions in determining atmospheric secondary inorganic particle concentrations across the UK. *Atmos. Chem. Phys.* 14, 8435–8447. <https://doi.org/10.5194/acp-14-8435-2014>
- 357) Vieno, M., Heal, M.R., Twigg, M.M., MacKenzie, I.A., Braban, C.F., Lingard, J.J.N., Ritchie, S., Beck, R.C., Möring, A., Ots, R., Di Marco, C.F., Nemitz, E., Sutton, M.A., Reis, S., 2016a. Corrigendum: The UK particulate matter air pollution episode of March–April 2014: more than Saharan dust (2016 *Environ. Res. Lett.* 11 044004). *Environ. Res. Lett.* 11, 059501.

<https://doi.org/10.1088/1748-9326/11/5/059501>

- 358) Vieno, M., Heal, M.R., Williams, M.L., Carnell, E.J., Nemitz, E., Stedman, J.R., Reis, S., 2016b. The sensitivities of emissions reductions for the mitigation of UK PM<sub>2.5</sub>. *Atmos. Chem. Phys.* 16, 265–276. <https://doi.org/10.5194/acp-16-265-2016>
- 359) Visschedijk, A., Denier van der Gon, H., Droege, R., 2009. A European high resolution and size-differentiated emission inventory for elemental and organic carbon for the year 2005. Utrecht, the Netherlands.
- 360) Wagner, R., Jähn, M., Schepanski, K., 2018. Wildfires as a source of airborne mineral dust - Revisiting a conceptual model using large-eddy simulation (LES). *Atmos. Chem. Phys.* 18, 11863–11884. <https://doi.org/10.5194/acp-18-11863-2018>
- 361) Wallace, J., Corr, D., Kanaroglou, P., 2010. Topographic and spatial impacts of temperature inversions on air quality using mobile air pollution surveys. *Sci. Total Environ.* 408, 5086–5096. <https://doi.org/10.1016/j.scitotenv.2010.06.020>
- 362) Walmsley, J.L., Wesely, M.L., 1996. Modification of coded parametrizations of surface resistances to gaseous dry deposition. *Atmos. Environ.* 30, 1181–1188. [https://doi.org/10.1016/1352-2310\(95\)00403-3](https://doi.org/10.1016/1352-2310(95)00403-3)
- 363) Wang, S., Streets, D.G., Zhang, Q., He, K., Chen, D., Kang, S., Lu, Z., Wang, Y., 2010. Satellite detection and model verification of NO<sub>x</sub> emissions from power plants in Northern China. *Environ. Res. Lett.* 5. <https://doi.org/10.1088/1748-9326/5/4/044007>
- 364) Wang, Y.X., McElroy, M.B., Wang, T., Palmer, P.I., 2004. Asian emissions of CO and NO<sub>x</sub>: Constraints from aircraft and Chinese station data. *J. Geophys. Res. D Atmos.* 109, 1–26. <https://doi.org/10.1029/2004JD005250>
- 365) Werner, M., Kryza, M., Pagowski, M., Guzikowski, J., 2019. Assimilation of PM<sub>2.5</sub> ground base observations to two chemical schemes in WRF-Chem – The results for the winter and summer period. *Atmos. Environ.* 200, 178–189. <https://doi.org/10.1016/j.atmosenv.2018.12.016>

- 366) Wesely, M.L., 2007. Parameterization of surface resistances to gaseous dry deposition in regional-scale numerical models. *Atmos. Environ.* 41, 52–63. <https://doi.org/10.1016/j.atmosenv.2007.10.058>
- 367) Wesely, M.L., Hicks, B.B., 2000. A review of the current status of knowledge on dry deposition. *Atmos. Environ.* 34, 2261–2282. [https://doi.org/10.1016/S1352-2310\(99\)00467-7](https://doi.org/10.1016/S1352-2310(99)00467-7)
- 368) Western Regional Air Partnership, 2005. 2002 Fire Emission Inventory for the WRAP Region – Phase II, Prepared for the Western Governors Association/Western Regional Air Partnership.
- 369) Wiedinmyer, C., Akagi, S.K., Yokelson, R.J., Emmons, L.K., Al-Saadi, J.A., Orlando, J.J., Soja, A.J., 2011. The Fire INventory from NCAR (FINN): a high resolution global model to estimate the emissions from open burning. *Geosci. Model Dev.* 4, 625–641. <https://doi.org/10.5194/gmd-4-625-2011>
- 370) Willeke, K., Whitby, K.T., 1975. Atmospheric aerosols: size distribution interpretation. *J. Air Pollut. Control Assoc.* 25, 529–534. <https://doi.org/10.1080/00022470.1975.10470110>
- 371) Williams, M.L., Beevers, S., Kitwiroon, N., Dajnak, D., Walton, H., Lott, M.C., Pye, S., Fehst, D., Toledano, M.B., Holland, M., 2018. Public health air pollution impacts of pathway options to meet the 2050 UK Climate Change Act target: a modelling study. *Public Heal. Res.* 6, 1–124. <https://doi.org/10.3310/phr06070>
- 372) Willocks, L.J., Bhaskar, A., Ramsay, C.N., Lee, D., Brewster, D.H., Fischbacher, C.M., Chalmers, J., Morris, G., Scott, E.M., 2012. Cardiovascular disease and air pollution in Scotland: No association or insufficient data and study design? *BMC Public Health* 12. <https://doi.org/10.1186/1471-2458-12-227>
- 373) Wintle, B.A., Legge, S., Woinarski, J.C.Z., 2020. After the Megafires: What Next for Australian Wildlife? *Trends Ecol. Evol.*, 1–5. <https://doi.org/10.1016/j.tree.2020.06.009>
- 374) WMO OSCAR, 2020. Details for Instrument ALADIN [WWW Document]. URL <https://www.wmo-sat.info/oscar/variables/view/342> (accessed 6.30.20).

- 375) Wong, Chit Ming, Vichit-Vadakan, N., Kan, Haidong, Qian, Zhengmin, Vajanapoom, N., Ostro, B., Wong, C. M., Thach, T.Q., Chau, P.Y.K., Chan, K.P., Chung, R.Y., Qu, C.Q., Yang, L., Thomas, G.N., Lam, T.H., Hadley, A.J., Peiris, J.S.M., Wong, T.W., Kan, H., Chen, B., Zhao, N., Zhang, Y., Kan, H., London, S.J., Song, G., Jiang, L., Chen, G., Qian, Z., Lin, H.M., Bentley, C.M., Lin, H.M., He, Q., Kong, L., Yang, N., Zhou, D., Xu, S., Liu, W., 2008. Public Health and Air Pollution in Asia (PAPA): A multicity study of short-term effects of air pollution on mortality. *Environ. Health Perspect.* 116, 1195–1202. <https://doi.org/10.1289/ehp.11257>
- 376) Wood, E.C., Herndon, S.C., Onasch, T.B., Kroll, J.H., Canagaratna, M.R., Kolb, C.E., Worsnop, D.R., Neuman, J.A., Seila, R., Zavala, M., Knighton, W.B., 2009. A case study of ozone production, nitrogen oxides, and the radical budget in Mexico City. *Atmos. Chem. Phys.* 9, 2499–2517. <https://doi.org/10.5194/acp-9-2499-2009>
- 377) Wooster, M.J., Gaveau, D.L.A., Salim, M.A., Zhang, T., Xu, W., Green, D.C., Huijnen, V., Murdiyarso, D., Gunawan, D., Borchard, N., Schirrmann, M., Main, B., Sepriando, A., 2018. New tropical peatland gas and particulate emissions factors indicate 2015 Indonesian fires released far more particulate matter (but Less Methane) than current inventories imply. *Remote Sens.* 10, 1–31. <https://doi.org/10.3390/rs10040495>
- 378) World Health Organization, 2013. Health risks of air pollution in Europe – HRAPIE project. World Health Organ.
- 379) World Health Organization, 2005. Air quality guidelines—global update 2005.
- 380) Xu, J., Morris, P.J., Liu, J., Holden, J., 2018. PEATMAP: Refining estimates of global peatland distribution based on a meta-analysis. *Catena* 160, 134–140. <https://doi.org/10.1016/j.catena.2017.09.010>
- 381) Yallop, A.R., Thacker, J.I., Thomas, G., Stephens, M., Clutterbuck, B., Brewer, T., Sannier, C.A.D., 2006. The extent and intensity of management burning in the English uplands. *J. Appl. Ecol.* 43, 1138–1148. <https://doi.org/10.1111/j.1365-2664.2006.01222.x>

- 382) Yang, G., Wang, Y., Zeng, Y., Gao, G.F., Liang, X., Zhou, M., Wan, X., Yu, S., Jiang, Y., Naghavi, M., Vos, T., Wang, H., Lopez, A.D., Murray, C.J.L., 2013. Rapid health transition in China, 1990-2010: Findings from the Global Burden of disease study 2010. *Lancet* 381, 1987–2015. [https://doi.org/10.1016/S0140-6736\(13\)61097-1](https://doi.org/10.1016/S0140-6736(13)61097-1)
- 383) Yao, J., Eyamie, J., Henderson, S.B., 2016. Evaluation of a spatially resolved forest fire smoke model for population-based epidemiologic exposure assessment. *J. Expo. Sci. Environ. Epidemiol.* 26, 233–240. <https://doi.org/10.1038/jes.2014.67>
- 384) Yim, S.H.L., Barrett, S.R.H., 2012. Public health impacts of combustion emissions in the United Kingdom. *Environ. Sci. Technol.* 46, 4291–4296. <https://doi.org/10.1021/es2040416>
- 385) Yin, J., Harrison, R.M., 2008. Pragmatic mass closure study for PM<sub>1.0</sub>, PM<sub>2.5</sub> and PM<sub>10</sub> at roadside, urban background and rural sites. *Atmos. Environ.* 42, 980–988. <https://doi.org/10.1016/j.atmosenv.2007.10.005>
- 386) Zanobetti, A., Schwartz, J., 2009. The effect of fine and coarse particulate air pollution on mortality: A national analysis. *Environ. Health Perspect.* 117, 898–903. <https://doi.org/10.1289/ehp.0800108>
- 387) Zhang, G.J., McFarlane, N.A., 1995. Sensitivity of climate simulations to the parameterization of cumulus convection in the canadian climate centre general circulation model. *Atmos. - Ocean* 33, 407–446. <https://doi.org/10.1080/07055900.1995.9649539>
- 388) Zhang, H., Kondragunta, S., Laszlo, I., Zhou, M., 2020. Improving GOES Advanced Baseline Imager (ABI) aerosol optical depth (AOD) retrievals using an empirical bias correction algorithm. *Atmos. Meas. Tech.* 13, 5955–5975. <https://doi.org/10.5194/amt-13-5955-2020>
- 389) Zhu, H., Qu, Z.W., Grebenshchikov, S.Y., Schinke, R., Malicet, J., Brion, J., Daumont, D., 2005. The Huggins band of ozone: Assignment of hot bands. *J. Chem. Phys.* 122. <https://doi.org/10.1063/1.1825380>

390) Zoogman, P., Liu, X., Suleiman, R.M., Pennington, W.F., Flittner, D.E., Al-Saadi, J.A., Hilton, B.B., Nicks, D.K., Newchurch, M.J., Carr, J.L., Janz, S.J., Andraschko, M.R., Arola, A., Baker, B.D., Canova, B.P., Chan Miller, C., Cohen, R.C., Davis, J.E., Dussault, M.E., Edwards, D.P., Fishman, J., Ghulam, A., González Abad, G., Grutter, M., Herman, J.R., Houck, J., Jacob, D.J., Joiner, J., Kerridge, B.J., Kim, J., Krotkov, N.A., Lamsal, L., Li, C., Lindfors, A., Martin, R. V., McElroy, C.T., McLinden, C., Natraj, V., Neil, D.O., Nowlan, C.R., O'Sullivan, E.J., Palmer, P.I., Pierce, R.B., Pippin, M.R., Saiz-Lopez, A., Spurr, R.J.D., Szykman, J.J., Torres, O., Veefkind, J.P., Veihelmann, B., Wang, H., Wang, J., Chance, K., 2017. Tropospheric emissions: Monitoring of pollution (TEMPO). *J. Quant. Spectrosc. Radiat. Transf.* 186, 17–39. <https://doi.org/10.1016/j.jqsrt.2016.05.008>

# Supplementary Material: Impact of weather types on UK ambient particulate matter concentrations

**Ailish M. Graham<sup>1</sup>, Kirsty J. Pringle<sup>1</sup>, Stephen R. Arnold<sup>1</sup>,  
Richard J. Pope<sup>1,2</sup>, Massimo Vieno<sup>3</sup>, Edward W. Butt<sup>1</sup>, Luke  
Conibear<sup>1</sup>, Ellen L. Stirling<sup>1</sup> and James B. McQuaid<sup>1</sup>**

<sup>1</sup> School of Earth and Environment, University of Leeds, Leeds, LS2 9JT, UK

<sup>2</sup> National Centre for Earth Observation, University of Leeds, Leeds, LS2 9JT, UK

<sup>3</sup> Natural Environment Research Council, Centre for Ecology and Hydrology, Penicuik, EH26 0QB, UK

*Correspondence to:* Ailish M. Graham ([ee15amg@leeds.ac.uk](mailto:ee15amg@leeds.ac.uk))

## 9.1 Site Information

AURN sites are classified as urban traffic/kerbside, urban or suburban background, and rural background. For this study background sites are used (urban background, suburban background and rural background). Background sites are chosen as they are considered to be more representative of the surrounding region than urban sites. This is because their locations are chosen so as to be influenced by the integrated contribution of all sources upwind rather than by a single source or street (Department for Environment Food and Rural Affairs, 2011). Data from 42 sites is used; 39 of which are urban background (UB), 2 rural background (RB) and 1 background suburban (BS) (Table 10).

Table 10. Automated Urban and Rural Network sites used for PM<sub>2.5</sub> analysis. AURN sites and classifications (UB = Urban Background, RB = Rural Background, BS = Background Suburban).

Site Name	Type	Site Name	Type
Aberdeen (1)	UB	London N. Kensington (23)	UB
Auchencorth Moss (2)	RB	London Teddington Bushy Park (24)	UB
Belfast Centre (3)	UB	Manchester Piccadilly (25)	UB
Birmingham Acocks Green (4)	UB	Newcastle Centre (26)	UB
Blackpool Marton (5)	UB	Newport (27)	UB
Bristol St Paul's (6)	UB	Norwich Lakenfields (28)	UB
Cardiff Centre (7)	UB	Nottingham Centre (29)	UB
Chesterfield Loudsley Green (8)	UB	Oxford St Ebbes (30)	UB
Chilbolton Observatory (9)	RB	Plymouth Centre (31)	UB
Coventry Allesley (10)	UB	Portsmouth (32)	UB
Derry Rosemount (11)	UB	Preston (33)	UB

Eastbourne (12)	UB	Reading New Town (34)	UB
Edinburgh St Leonards (13)	UB	Rochester Stoke (35)	UB
Glasgow Townhead (14)	UB	Salford Eccles (36)	UB
Hull Freetown (15)	UB	Sheffield Devonshire Green (37)	UB
Leamington Spa (16)	UB	Southampton Centre (38)	UB
Leeds Centre (17)	UB	Southend-on-Sea (39)	UB
Leicester University (18)	UB	Stoke-on-Trent Centre (40)	UB
London Bexley (19)	BS	Sunderland Silksworth (41)	UB
London Bloomsbury (20)	UB	Wigan Centre (42)	UB

## 9.2 Emissions

The emissions used for the back trajectories are the same as those used in the EMEP4UK model, which uses two emissions datasets and a nested domain to cover the UK within the coarser European domain. Annually varying emissions for the 2010 – 2014 period were used as this matches the time period the back trajectories were available for. Emissions of primary PM<sub>2.5</sub> for 2010 are shown in Figure 24 for reference. For the outer domain (Figure 24: Purple Box), gridded annual EMEP emissions at 0.5° resolution from the Centre for Emission Inventories and Projections (CEIP, [www.ceip.at](http://www.ceip.at)) are used. While for the inner domain (Figure 24: Red Box) gridded annual National Atmospheric Emissions Inventories (NAEI) emissions

at 0.01° resolution are aggregated to 5 km resolution. Within the UK domain where emissions are not available at 0.05° resolution or less, EMEP 0.5° resolution emissions are interpolated to the required resolution of 0.05°. Emissions outside of Europe are provided by the Emission Database for Global Atmospheric Research with Task Force on Hemispheric Transport of Air Pollution (EDGAR-HTAP) version 2.2 emissions for 2010 at 0.1° resolution (Janssens-Maenhout, et al., 2015). The EDGAR-HTAP emission dataset uses emissions databases from the US Environmental Protection Agency (US EPA) including Canada, the model inter-comparison study for Asia Phase II (MICS –Asia) and EMEP-TNO emissions for Europe (which are replaced with emissions from the EMEP4UK model). EMEP4UK PM<sub>2.5</sub> emissions are interpolated onto the EDGAR-HTAP emissions grid to replace EDGAR-HTAP PM<sub>2.5</sub> emissions for the European domain.

PM emissions for all datasets also include elemental carbon (EC), organic matter (OM) and other compounds. Emissions of each species are provided for 10 anthropogenic source-sectors (SNAP sectors) (Simpson, et al., 2012).

### 9.3 Sensitivity of Integrated Back Trajectories to assumed e-folding lifetime

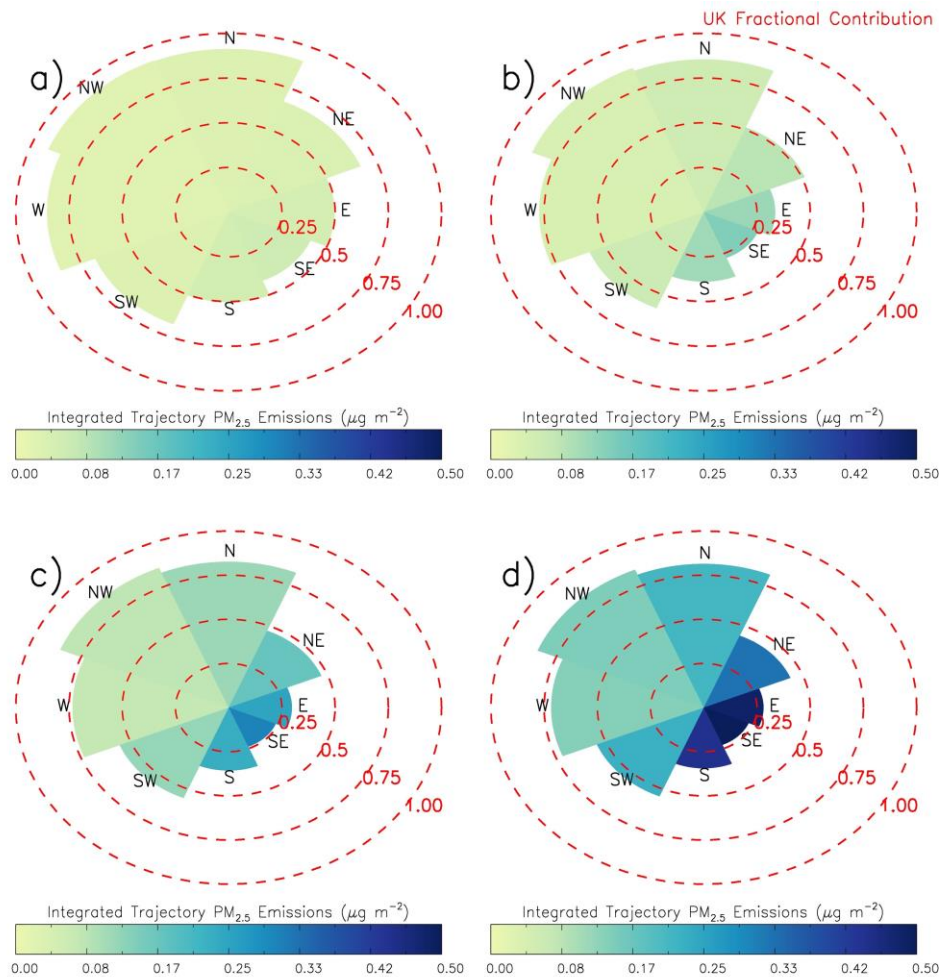


Figure 48. Median UK (background AURN sites) total accumulated  $\text{PM}_{2.5}$  emissions ( $\mu\text{g m}^{-2}$ ) accumulated over the daily (12 UTC, 2010-2014) ROTRAJ back trajectories (4 days – 15-minute time steps), with a (a) 1-day (b) 3-day (c) 7-day and (d) 14-day e-folding lifetime, binned by LWT flow directions. Red circles represent the UK fractional contribution to trajectory accumulated  $\text{PM}_{2.5}$  emissions.

Integrated  $\text{PM}_{2.5}$  emissions (Figure 48) indicate that the total integrated emission of the parcel accumulated along the trajectory path is sensitive to the e-folding lifetime chosen however the fractional contribution is less sensitive. With a change in the e-folding lifetime the fractional

contribution changes by less than 15% for all LWTs, however the total emission changes by an order of magnitude, from  $< 0.05 \mu\text{g m}^{-2}$  (1 hour) to  $< 0.5 \mu\text{g m}^{-2}$  (14 days) (Figure 48 (a) and (d)).

At a 1-hour life time total accumulated emissions are dominated by UK emissions for NW and N flows (10% from outside of the UK). This increases to around 30% under NE, W and SW flows and almost 70% under E, SE and S flow. The total emissions accumulated over the back trajectory show very little variation over this e-folding lifetime with NE, N and NW flows indicating the same emission total as E, SE and S flow. This suggests that the e-folding lifetime of  $\text{PM}_{2.5}$  emissions is very important in predicting the total accumulated emission over the back-trajectory path. At lifetimes of 3 and 7 hours large changes are observed in the total accumulated emission but not the fractional contribution. Between a lifetime of 3 and 7 hours (Figure 48 (b) and (c)) there is negligible change in the fractional contribution of UK emissions to the total accumulated emission. However, the total accumulated emission of  $\text{PM}_{2.5}$  observed under different flow directions changes substantially. This is seen most clearly under E, SE and S flow, doubling from  $\sim 0.2$  to  $\sim 0.4 \mu\text{g m}^{-2}$  (SE), but is also seen in the cleaner wind directions (N, NW, W from  $0.05$  to  $> 0.15 \mu\text{g m}^{-2}$ ). The same is seen when the lifetime is increased from 7 to 14 hours (Figure 48 (c) and (d)), with negligible changes in fractional contribution but substantial changes in total accumulated emissions. Although the total accumulated emission under all flow directions increases with the increased e-folding lifetime, the contrast in total accumulated emissions between N, NW and W flow regimes and E, SE and S flow regimes increases significantly. This follows the same pattern as that seen in the AURN  $\text{PM}_{2.5}$  concentration observations, indicative that under E, SE and S flow a large proportion of the

primary PM<sub>2.5</sub> emission total originates outside of the UK. This indicates long-range transport due to changing meteorology plays an important role in UK pollutant concentrations.

#### **9.4 EMEP4UK Evaluation**

Here we evaluate EMEP4UK against observations to test the model skill to simulating surface PM<sub>2.5</sub>. When daily modelled PM<sub>2.5</sub> concentrations at each site are compared with observations under each LWT, the model captures the distribution of concentrations well (Figure 49). The model also has skill in predicting mean PM<sub>2.5</sub> concentrations, with a negative bias  $\leq 1 \mu\text{g m}^{-3}$  under most LWTs and an annual mean negative bias of  $\sim 1 \mu\text{g m}^{-3}$  across all LWTs (Figure 49). Positive biases are also evident, of similar magnitude under most LWTs and under easterly and south-easterly flows biases of up to  $15 \mu\text{g m}^{-3}$  are apparent at some sites (Figure 50). Despite this, the model shows good overall agreement with observations, with a Pearson correlation coefficient of 0.887 (Figure 50). PM<sub>2.5</sub> anomalies are also well captured by the model (Figure 50), with the same pattern as was seen in the observations and a Pearson correlation coefficient of 0.905.

In conclusion, overall the model captures the variability in PM<sub>2.5</sub> concentrations with LWT well and shows good correlation with observations at each site ( $r = 0.887$ ) with only a small negative bias. Therefore, we can have good confidence in the model's ability to predict regional PM<sub>2.5</sub> changes with different LWTs.

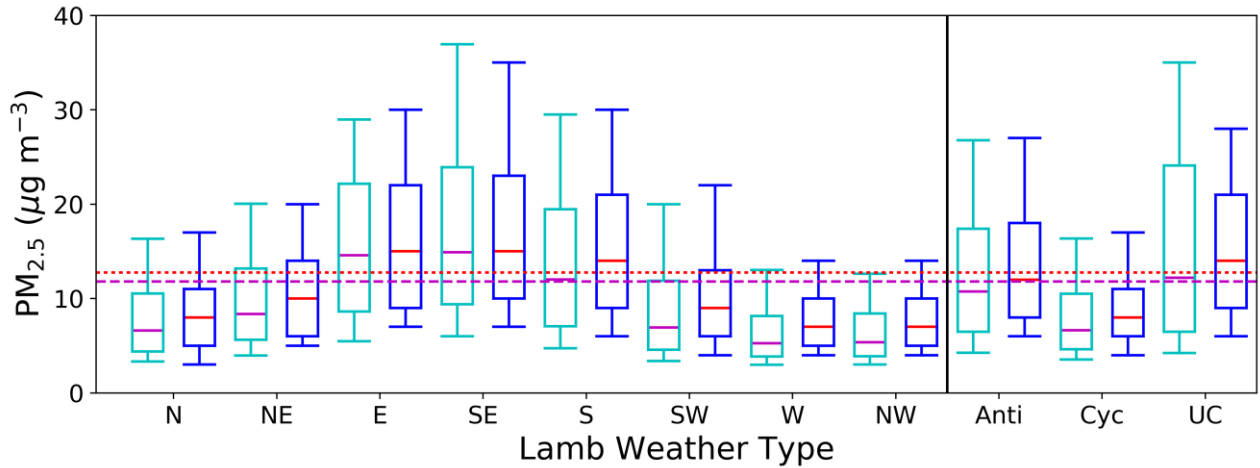


Figure 49. 2010-2016 daily modelled (cyan and magenta) and observed (blue and red) PM<sub>2.5</sub> concentrations, binned by LWT. Mean (red/magenta), 10th, 25th, 75th and 90th percentiles are shown. The mean modelled (magenta) and observed (red) PM<sub>2.5</sub> concentration for all LWTs is shown by the dashed line.

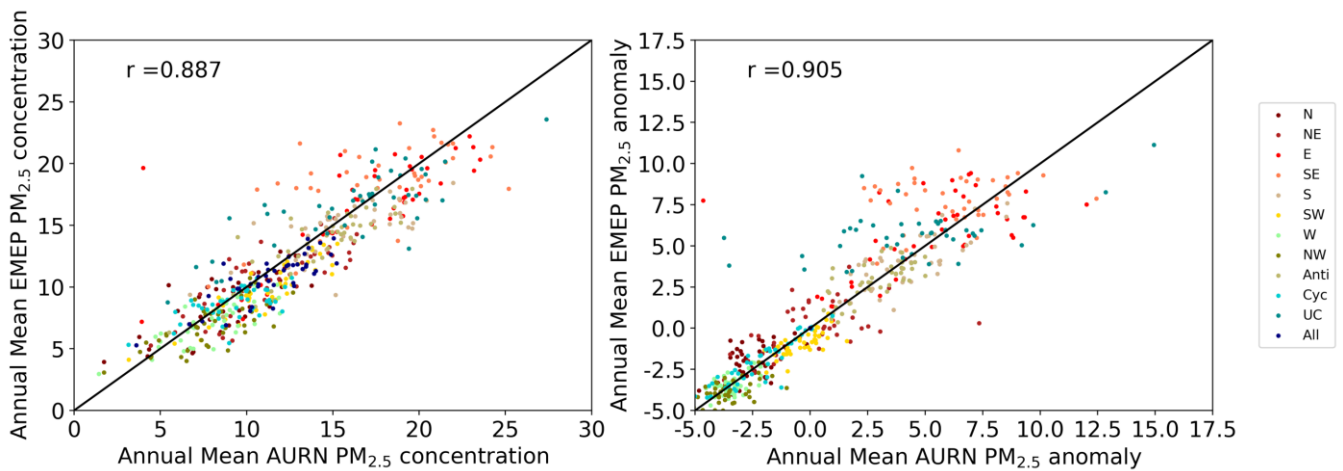


Figure 50. Annual mean concentration and anomaly between 2010-2016 for daily modelled (EMEP4UK) and observed PM<sub>2.5</sub> concentrations at AURN observation sites, binned by LWT. The Pearson correlation ( $r$ ) is shown at the top of each panel.

## 9.5 References

- 1) Department for Environment Food and Rural Affairs (2011) Emissions of Air Quality Pollutants.
- 2) Janssens-Maenhout, G., Crippa, M., Guizzardi, D., Dentener, F., Muntean, M., Pouliot, G., Keating, T., Zhang, Q., Kurokawa, J., Wankmüller, R., Denier Van Der Gon, H., Kuenen, J.J.P., Klimont, Z., Frost, G., Darras, S., Koffi, B., Li, M., 2015. HTAP-v2.2: A mosaic of regional and global emission grid maps for 2008 and 2010 to study hemispheric transport of air pollution. *Atmos. Chem. Phys.* 15, 11411–11432. <https://doi.org/10.5194/acp-15-11411-2015>.
- 3) Simpson, D., Benedictow, A., Berge, H., Bergström, R., Emberson, L.D., Fagerli, H., Flechard, C.R., Hayman, G.D., Gauss, M., Jonson, J.E., Jenkin, M.E., Nyúri, A., Richter, C., Semeena, V.S., Tsyro, S., Tuovinen, J.P., Valdebenito, A., Wind, P., 2012. The EMEP MSC-W chemical transport model: Technical description. *Atmos. Chem. Phys.* 12, 7825–7865. <https://doi.org/10.5194/acp-12-7825-2012>.

# Supplementary Material: Impact of the June 2018 Saddleworth Moor wildfires on air quality in northern England

Graham AM<sup>1</sup>, Pope RJ<sup>1,2</sup>, McQuaid JB<sup>1</sup>, Pringle KP<sup>1</sup>, Arnold SR<sup>1</sup>, Bruno AG<sup>3,4</sup>, Moore DP<sup>3,4</sup>, Harrison JJ<sup>3,4</sup>, Chipperfield MP<sup>1,2</sup>, Rigby R<sup>1,5</sup>, Sanchez-Marroquin, A<sup>1</sup>, Lee J<sup>6,7</sup>, Wilde, S<sup>6</sup>, Siddans, R<sup>8,9</sup>, Kerridge, BJ<sup>8,9</sup>, Ventress, LJ<sup>8,9</sup>, Latter, BG<sup>8,9</sup>

<sup>1</sup> School of Earth and Environment, University of Leeds, Leeds, United Kingdom

<sup>2</sup> National Centre for Earth Observation, University of Leeds, Leeds, United Kingdom

<sup>3</sup> Department of Physics and Astronomy, University of Leicester, Leicester, UK

<sup>4</sup> National Centre for Earth Observation, University of Leicester, Leicester, UK

<sup>5</sup> Centre for Environmental Modelling and Computation, University of Leeds, Leeds, UK

<sup>6</sup> Department of Chemistry, University of York, York, UK

<sup>7</sup> National Centre for Atmospheric Science, University of York, York

<sup>8</sup> Remote Sensing Group, STFC Rutherford Appleton Laboratory, Chilton, United Kingdom

<sup>9</sup> National Centre for Earth Observation, STFC Rutherford Appleton Laboratory, Chilton, United Kingdom

## 10.1 Meteorological Conditions

Meteorological reanalysis data (i.e. ERA-Interim and UK Met Office surface charts) were obtained from the European Centre for Medium-Range Weather Forecasts (ECMWF) on a  $0.5^\circ \times 0.5^\circ$  horizontal grid and the UK Met Office data archive. ERA-interim meteorological

variables include mean sea level pressure (MSLP), ERA5 geopotential, 2-m temperature and 10 m u & v wind components.. The ERA-Interim data were downloaded from <https://apps.ecmwf.int/datasets/data/interim-full-daily/levtype=sfc/>.

Figure 51 shows the time evolution of 1200 Z mean sea level pressure and geopotential height at 850 hPa (850GPH) from the 19<sup>th</sup>-30<sup>th</sup> June 2018. Over northern England pressure minima occur on June 19<sup>th</sup> and 20<sup>th</sup> (1010-1020 hPa), with 850GPH between 1400-1560 m and indicating a westerly flow. From the 21<sup>st</sup> June high pressure begins to build from the west (>1030 hPa) (850GPH 1580 m), peaking at >1030 hPa over much of the UK over Saddleworth Moor on June 22<sup>nd</sup> and 850GPH of 1560-1620 m, and persisting (>1020 hPa and 1540-1620 m) until the 30<sup>th</sup> June (1010-1020 hPa and 850GPH 1520-1540 m). These high pressure conditions are associated with enhancements in synoptic pressure in the North Atlantic yielding strong anticyclonic conditions over the UK. This is confirmed by the Lamb Weather Types (LWTs, (Jones, et al., 2013)) which represent the daily classification of UK circulation patterns. Based on data from the University of East Anglia, ([https://crudata.uea.ac.uk/cru/data/lwt/static\\_files/ERA5\\_1979\\_2018\\_12hrs\\_UK.dat](https://crudata.uea.ac.uk/cru/data/lwt/static_files/ERA5_1979_2018_12hrs_UK.dat)), June 22<sup>nd</sup>-29<sup>th</sup> experienced strong anticyclonic conditions (LWT = 0).

This enhancement in pressure across the UK yielded substantial increases in temperature and reduced wind speeds. Temperatures increased from June 22<sup>nd</sup>, peaking at 22-27 °C (~295-300°K) over Saddleworth Moor on the 26<sup>th</sup> June (Figure 52). This coincided with the full development of the Saddleworth Moor fire. The high temperatures helped to dry out the surface vegetation (and underlying peat) which led to the rapid spreading of the fire once ignition had occurred. From June 24<sup>th</sup> – 30<sup>th</sup>, temperatures never dropped below 22°C (~290°K) at Saddleworth Moor. Between June 24<sup>th</sup>-26<sup>th</sup>, when peak temperatures occurred, the 10 m wind

speeds never rose above  $3 \text{ m s}^{-1}$  (Figure 53), likely to have aided the fire development. On the other days of the observation period, the wind speeds over the land (sea) ranged between 3 and  $9 \text{ m s}^{-1}$  (5 to  $> 10 \text{ m s}^{-1}$ ).

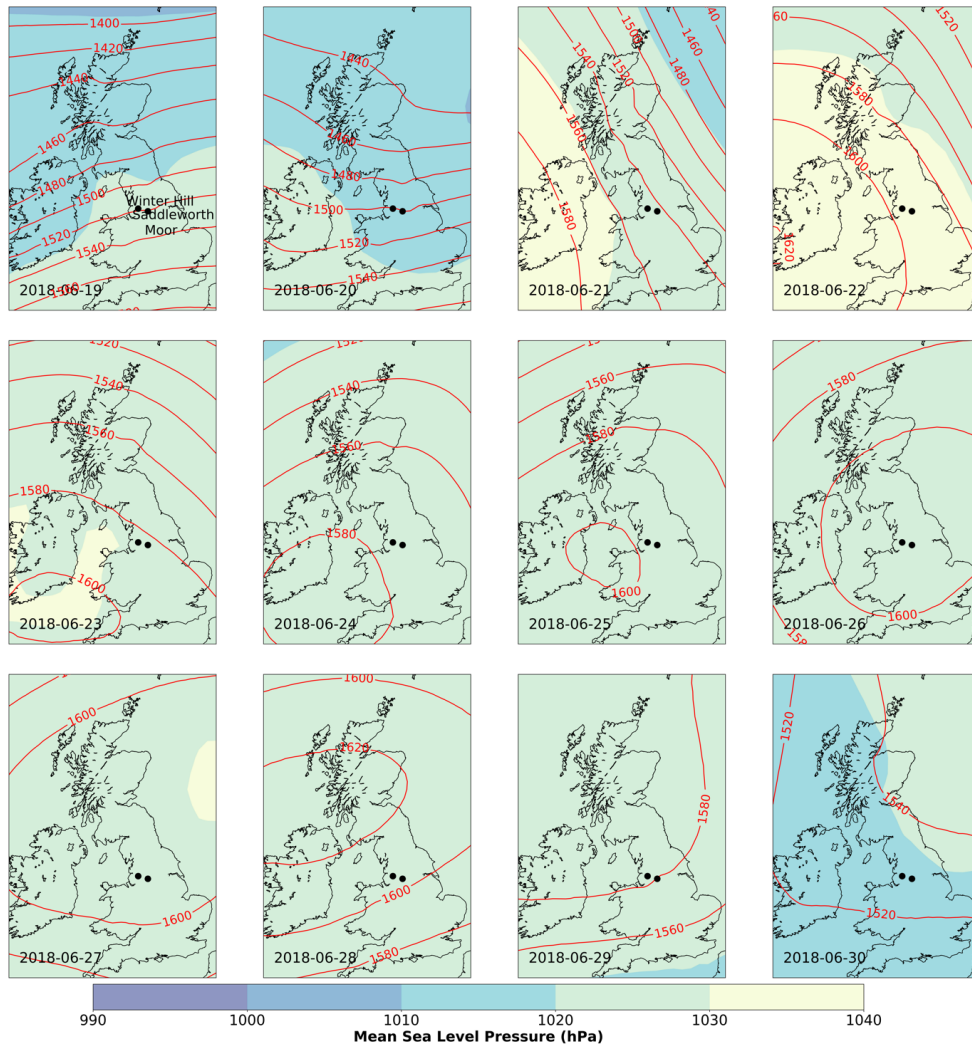


Figure 51. ERA-Interim 1200Z mean sea level pressure (hPa  $0.5^\circ \times 0.5^\circ$  grid)) with ERA5 geopotential height (m) at 850 hPa overplotted in red for June 19<sup>th</sup>-30<sup>th</sup> 2018 over Northern England. The black dots represent the location of Saddleworth Moor and Winter Hill.

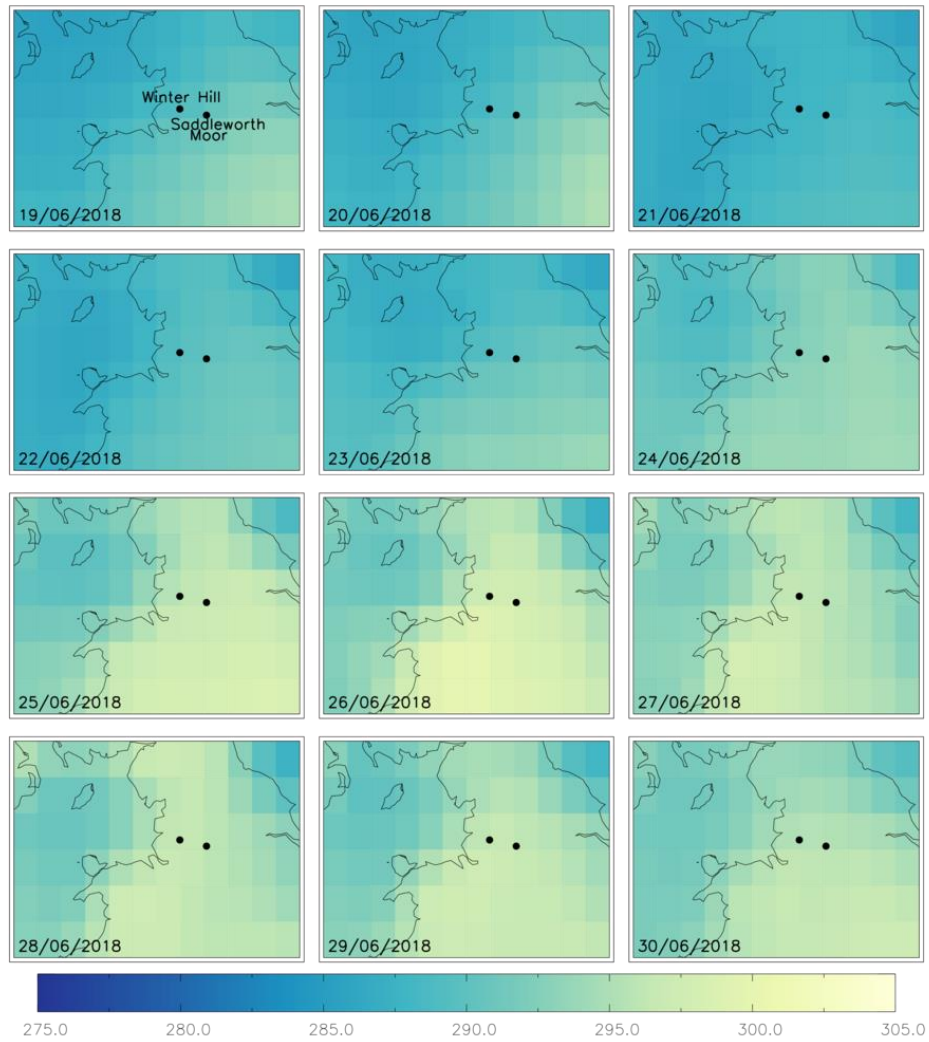


Figure 52. ECMWF ERA-Interim 2-m temperature (K,  $0.5^\circ \times 0.5^\circ$  grid) for June 19<sup>th</sup>-30<sup>th</sup> 2018 over Northern England. The black dots represent the location of Saddleworth Moor and Winter Hill.

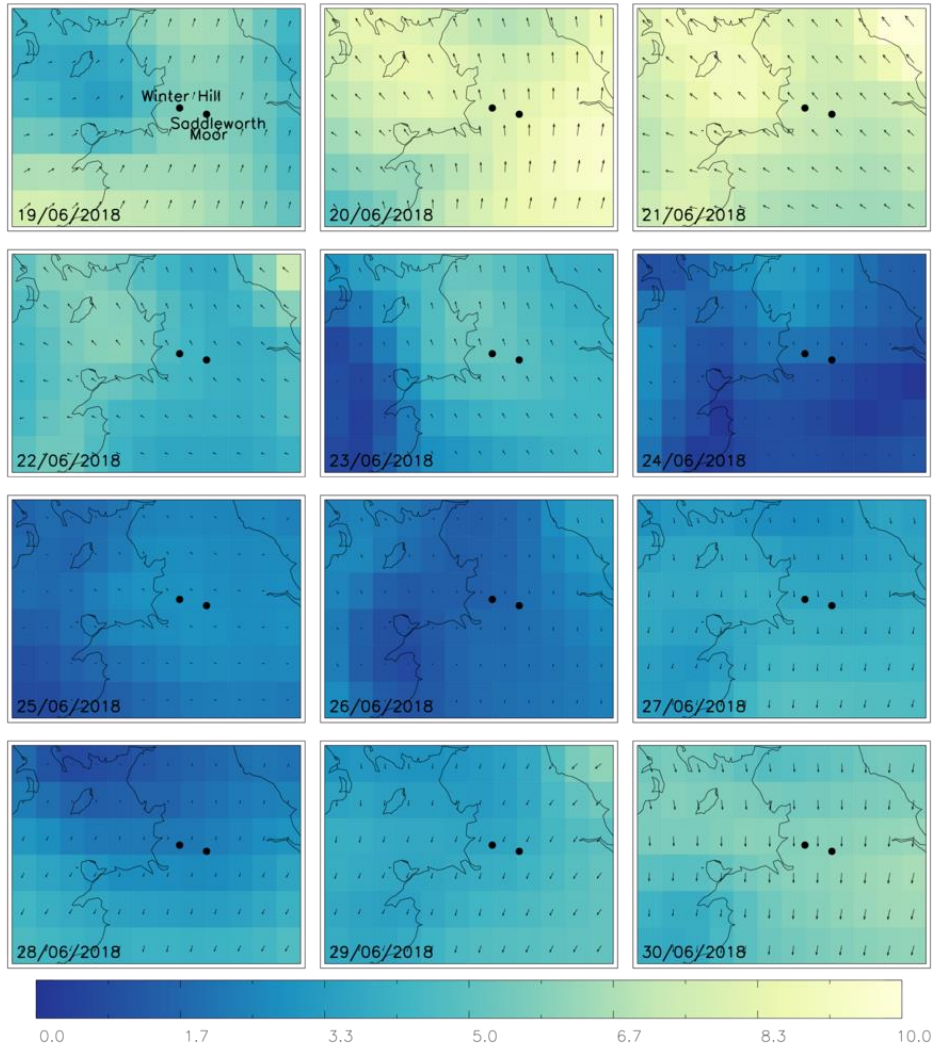


Figure 53. ECMWF ERA-Interim 10-m wind speed ( $\text{m s}^{-1}$ ,  $0.5^\circ \times 0.5^\circ$  grid) for June 19<sup>th</sup>-30<sup>th</sup> 2018 over Northern England. The black dots represent the location of Saddleworth Moor and Winter Hill.

## **10.2 Satellite Visible Images of Saddleworth Moor Fire Development**

The Moderate Resolution Imaging Spectroradiometer (MODIS) visible images of the Saddleworth Moor (Figure 54) show the time-evolution of the fire smoke plume from space. The first detection of the fire plume can be seen on the 25<sup>th</sup> June and remains in-situ until the 26<sup>th</sup> June. On the 27<sup>th</sup> June, there is a westwards propagation of the plume out towards Manchester and Liverpool. On June 28<sup>th</sup> and 29<sup>th</sup>, the plume has become more dispersed but is still visible and shifted slightly southwards. On the 30<sup>th</sup> June, the Saddleworth Moor plume is no longer detectable in the visible image, but now the Winter Hill fire plume is clearly flowing out towards the Irish Sea with a north-west trajectory. On later days, the MODIS instruments on both satellite platforms (local overpass times of 13.30 and 10.30) are obstructed by cloud when retrieving the visible images.



Figure 54. MODIS visible images, from NASA's Aura and Terra satellites, of the Saddleworth Moor and Winter Hill fires between June 25<sup>th</sup>-30<sup>th</sup>. The locations of Saddleworth Moor and Winter Hill are indicated in white, while the locations of Manchester and Liverpool are shown in cyan.

### 10.3 MODIS Fire Radiative Power

Figure 55 represents the fire radiative power (FRP,  $\text{mW m}^{-2}$ ) observed by the MODIS instruments over the northern England between June 19<sup>th</sup> and 30<sup>th</sup>. The data was downloaded from the Global Fire Assimilation System (GFAS, <https://apps.ecmwf.int/datasets/data/cams-gfas/>). Between June 19<sup>th</sup> to 26<sup>th</sup> MODIS detected no fires in north-western England. On June 25<sup>th</sup> and 26<sup>th</sup>, when MODIS visible images capture the Saddleworth Moor fire (Figure 55), the strength of the fire was insufficient for detection of thermal anomalies. On June 27<sup>th</sup>, MODIS FRP detects the fire over Saddleworth Moor peaking at over  $100 \text{ mW m}^{-2}$ . On June 28<sup>th</sup> and 29<sup>th</sup>, as seen in the visible images, the fire intensity has decreased to under  $100 \text{ mW m}^{-2}$  and covers a smaller area. On June 29<sup>th</sup>, the Winter Hill fires are detected at approximately  $30 \text{ mW m}^{-2}$  and on the 30<sup>th</sup> June this has increased to over  $100 \text{ mW m}^{-2}$ , while Saddleworth Moor retains the same thermal intensity over both days.

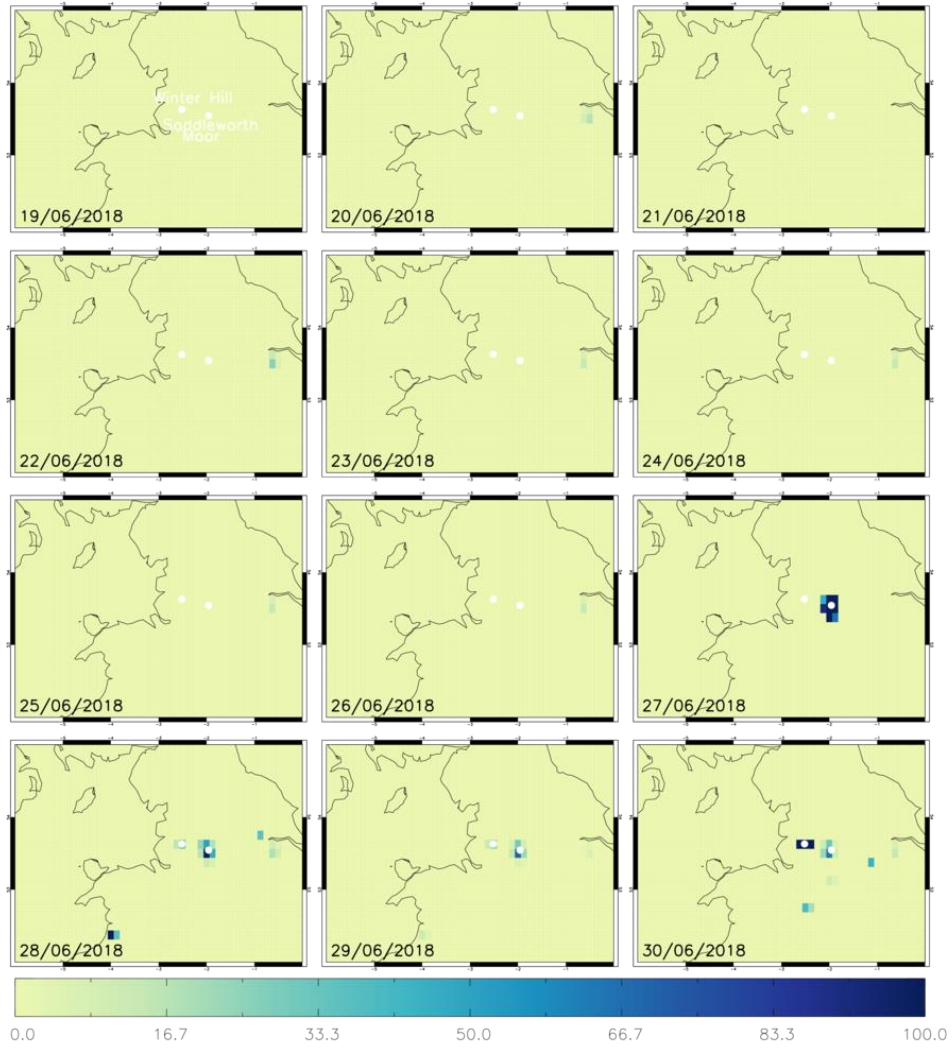


Figure 55. MODIS fire radiative power (FRP,  $\text{mW m}^{-2}$ ,  $0.1^\circ \times 0.1^\circ$  grid) for June 19<sup>th</sup>-30<sup>th</sup> 2018 over Northern England. The white dots represent the location of Saddlworth Moor and Winter Hill.

## 10.4 HYSPLIT Trajectories

Meteorological data for the HYSPLIT model is taken from The Global Data Assimilation System (GDAS), used by the National Centre for Environmental Prediction (NCEP) Global Forecast System (GFS) model to place observations into a gridded model space for the purpose of starting, or initializing, weather forecasts with observed data (<https://www.ncdc.noaa.gov/data-access/model-data/model-datasets/global-data-assimilation-system-gdas>). Meteorological data is at  $0.5^\circ$  spatial resolution and 3-hourly temporal resolution. Meteorological data is interpolated on the 18 model levels, which extend from ~995 hPa to 20 hPa (Kanamitsu, 1989)

The HYSPLIT model results shown are from single release points at aircraft sampling points in the near-field and downwind regions. Trajectories were released from the most northerly and southerly points of the near-field ( $2.2^\circ\text{W}$ ,  $53.75^\circ\text{N}$  and  $1.9^\circ\text{W}$ ,  $53.25^\circ\text{N}$ ) and downwind ( $3.4^\circ\text{W}$ ,  $53.75^\circ\text{N}$  and  $3.4^\circ\text{W}$ ,  $52.75^\circ\text{N}$ ) sections of the flight from a range of altitudes during these profiles (500, 750 & 1000 m and 250, 500 and 1000 m, respectively). The age of the air mass the sample was taken within can be estimated using the time at which these back-trajectories pass over Saddleworth Moor. See Stein *et al.* (2015) for more information on the HYSPLIT model (Figure 56).

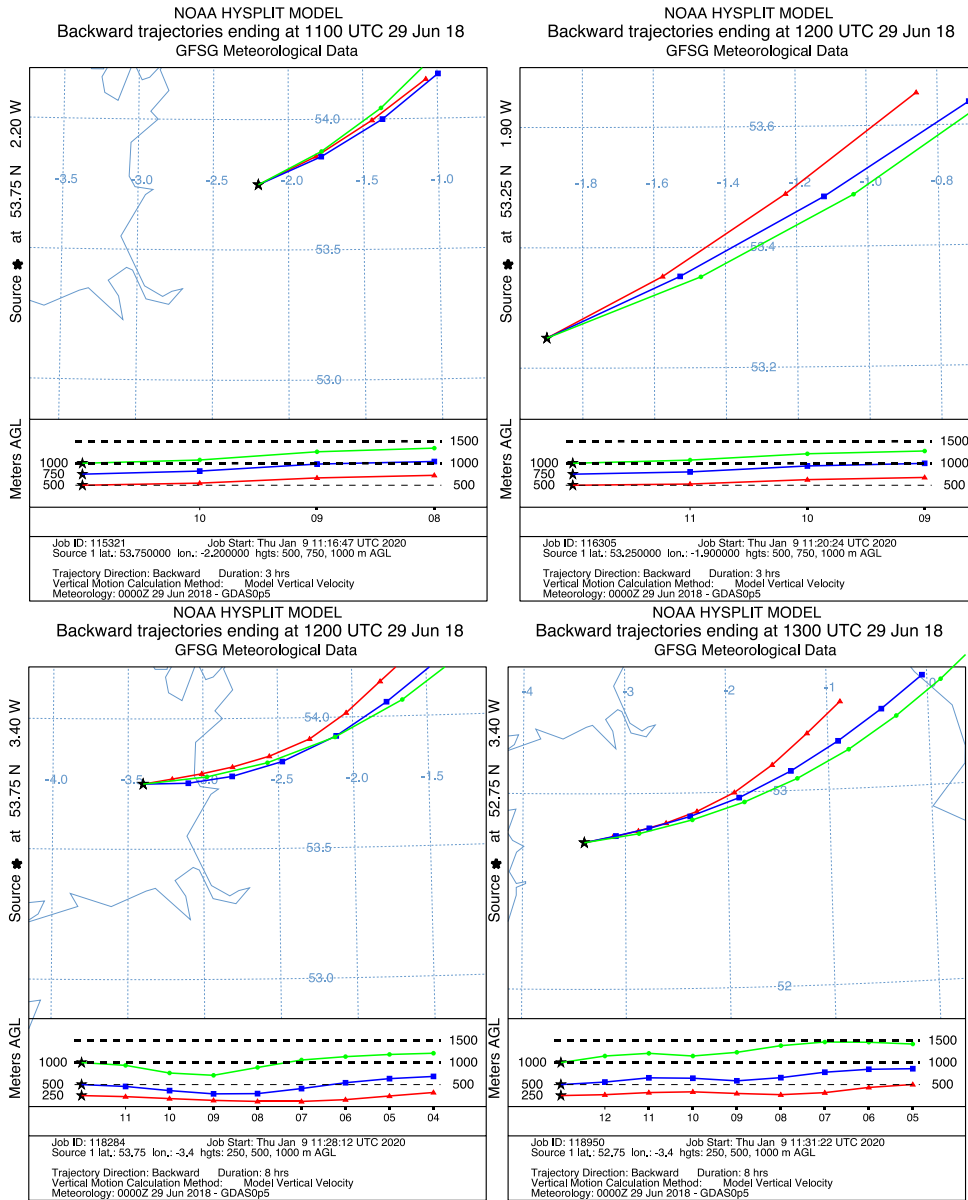


Figure 56. Back trajectories from HYSPLIT for the aircraft flight on June 29<sup>th</sup> 2018. Trajectories are released from various locations at 250-1000m heights based on the aircraft altitude and track during the near-field and downwind sections of the flight. The path of each trajectory is indicated on the map, while the altitude above ground level is indicated on the bottom plot.

## 10.5 Satellite Observations of Tropospheric Column Nitrogen Dioxide

TROPOMI measurements of tropospheric column nitrogen dioxide (TCNO<sub>2</sub>, 10<sup>-5</sup> moles m<sup>-2</sup>) increase in magnitude coinciding with the Saddleworth Moor fire occurrence (Figure 57). This is most noticeable on June 27<sup>th</sup> to 29<sup>th</sup> as TCNO<sub>2</sub> peaks at over 20 x10<sup>-5</sup> moles m<sup>-2</sup> with a substantial spatial extent coinciding with the fire plume (Figure 57). This is reinforced by the total column carbon monoxide (TCCO) plume location (black polygon-outlined region, TCCO > 0.03 moles m<sup>-2</sup>) as seen in the main manuscript. However, while the CO sources over Manchester and Liverpool are barely detectable by TROPOMI (see Figure 34 and Figure 57), the Saddleworth Moor and Winter Hill fires show strong enhancements relative to the background concentrations (see Satellite Observations of Tropospheric Column Nitrogen Dioxide section and Figure 60 for more details). The enhancement of TCNO<sub>2</sub> on June 27<sup>th</sup>-29<sup>th</sup> is linked to fire nitrogen oxide (NO<sub>x</sub>) emissions and increases from other NO<sub>2</sub> sources. As shown by Pope *et al.* (2015, 2014), anticyclonic conditions lead to the accumulation of NO<sub>2</sub>, yielding larger concentrations than the seasonal average. When comparing TROPOMI TCNO<sub>2</sub> over Manchester and other cities (e.g. London) for these few days against the June-July 2018 average, there are substantial enhancements over the source regions (not shown here) across the UK. Unfortunately, given the relatively short TROPOMI data record, it is difficult to find other meteorological situations similar to that of the Saddleworth Moor fires to investigate whether the 27<sup>th</sup>-29<sup>th</sup> June 2018 NO<sub>2</sub> enhancement was more extreme than at other times. Therefore, the TCCO plume is used to sub-sample the TCNO<sub>2</sub> data “in-plume”, “edge of plume” and “out of plume” with TCCO thresholds of >0.03 moles m<sup>-2</sup>, 0.025-0.03 moles m<sup>-2</sup> and 0.02-0.025 moles m<sup>-2</sup>, respectively. A minimum threshold for “out of plume” was set at

0.020 moles  $\text{m}^{-2}$  so  $\text{NO}_2$  was sampled close to but not within the plume, and to ensure large swaths of background  $\text{NO}_2$  within the domain were not used in this classification.

When  $\text{TCNO}_2$  is sub-sampled under the fire pixels ( $\text{FRP} > 50 \text{ mW m}^{-2}$ ), the median concentration is approximately  $8.0 \times 10^{-5}$  moles  $\text{m}^{-2}$ , which is significantly larger than the median  $\text{TCNO}_2$  concentration ( $6.0\text{-}7.0 \times 10^{-5}$  moles  $\text{m}^{-2}$ ) in non-fire pixels (same locations as fire pixels but on days were  $\text{FRP} < 50 \text{ mW m}^{-2}$ ) at the 95% confidence level (based on the student t-test). The fire- $\text{TCNO}_2$  10<sup>th</sup>, 25<sup>th</sup> and 75<sup>th</sup> percentile concentrations are also larger than the non-fire- $\text{TCNO}_2$  equivalent. However, the non-fire- $\text{TCNO}_2$  90<sup>th</sup> percentile value is marginally larger. The  $\text{TCNO}_2$  data sub-sampled under the TCCO plume definitions show a similar pattern. “Out of plume” median  $\text{TCNO}_2$  is the lowest ( $5\text{-}6 \times 10^{-5}$  moles  $\text{m}^{-2}$ ) of all classifications (true for the 10<sup>th</sup>, 25<sup>th</sup>, 75<sup>th</sup> and 90<sup>th</sup> percentiles as well). Though downwind of the fire location, the “edge of plume” and “in plume” classifications have the largest median  $\text{TCNO}_2$  values of  $10.0\text{-}11.0 \times 10^{-5}$  moles  $\text{m}^{-2}$  and  $12.0\text{-}13.0 \times 10^{-5}$  moles  $\text{m}^{-2}$ , respectively. These two classifications both overlap with regions of enhanced anthropogenic  $\text{NO}_2$  sources (i.e. Manchester and Liverpool), so their median and percentile concentrations are larger. In the six time panels of Figure 57, the “edge of plume” and “in plume” classifications both experience larger  $\text{TCNO}_2$  concentrations depending on the day. Therefore, by using the TCCO data as a tracer for the fire plume, we can detect an  $\text{NO}_2$  fire response on top of the anthropogenic  $\text{NO}_2$  signal. Here, the median and percentile concentrations are all larger “in plume” than “edge of plume”, compared with out of plume, where the medians are significantly different at the 95% confidence level (student t-test). So, our results suggest that, while not as clear as the TROPOMI TCCO signal, the Saddleworth Moor and Winter Hill fires significantly enhanced observed  $\text{NO}_2$  concentrations.

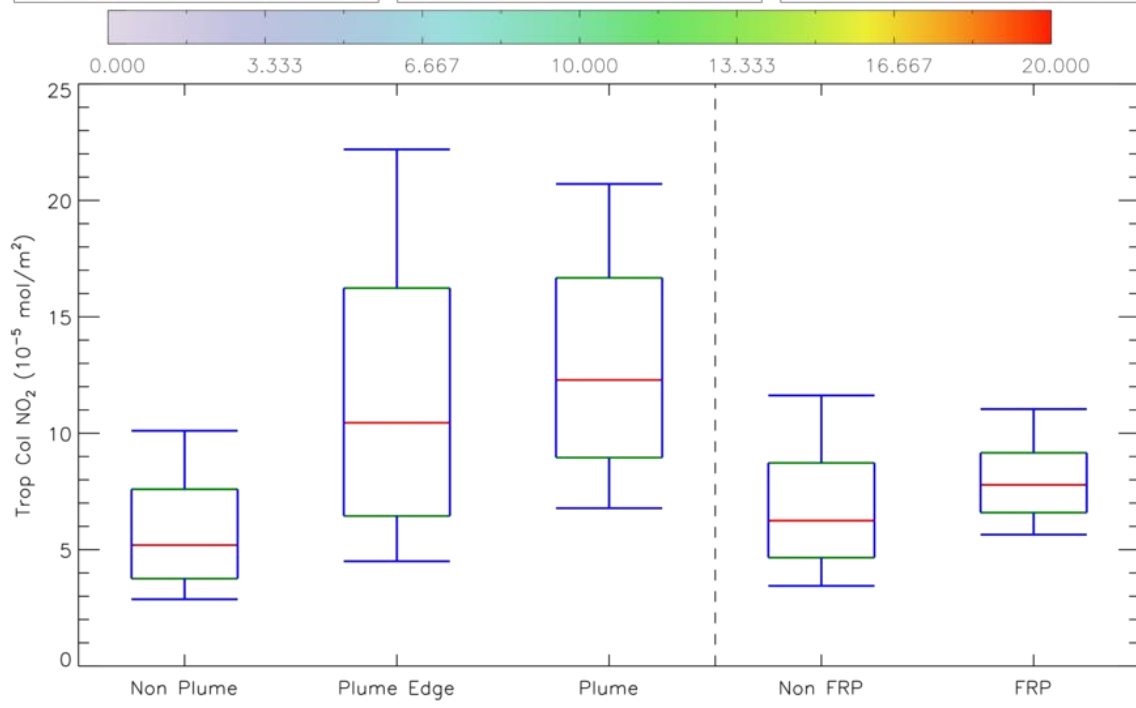
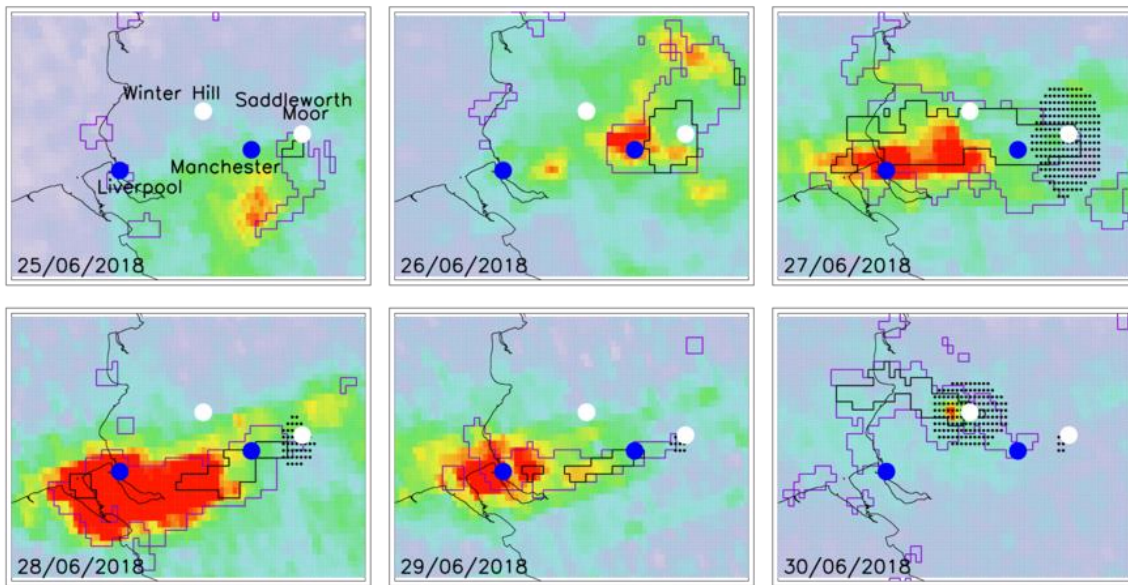


Figure 57. TROPOMI tropospheric column nitrogen dioxide (TCNO<sub>2</sub>, 10<sup>-5</sup> moles m<sup>-2</sup>) measurements of the Saddleworth Moor wildfire (June 25<sup>th</sup> – 30<sup>th</sup> 2019). Black and purple polygon-outlined regions represent the TROPOMI total column carbon monoxide (TCCO) fire plume (>0.03 moles m<sup>-2</sup>) and edge of plume (0.025-0.03 moles m<sup>-2</sup>). Black dots show pixels where MODIS fire radiative power (FRP) is > 50 mW m<sup>-2</sup>. White dots show the location of the Saddleworth Moor and Winter Hill fires. Blue dots show the location of Manchester and Liverpool. The box and whisker schematics represent TCNO<sub>2</sub> sub-sampled under the plume, edge of plume and out of the plume TCCO thresholds. TCNO<sub>2</sub> is also sub-sampled under fire pixels (FRP > 50 mW m<sup>-2</sup>) and non-fire pixels (FRP < 50 mW m<sup>-2</sup>). Red, green and blue represent the median, 25<sup>th</sup> & 75<sup>th</sup> percentiles and 10<sup>th</sup> & 90<sup>th</sup> percentiles, respectively.

## 10.6 TROPOMI Total Column Carbon Monoxide Averaging Kernels

The total column averaging kernels (AKs) reflect the altitude sensitivity of the CO total column retrieval. The AKs for three different locations (Saddleworth Moor, Manchester and Liverpool) during the Saddleworth Moor fire days are shown in the six panels of Figure 58. The AKs indicate a significant reduction of the retrieval sensitivity near the surface on the 27<sup>th</sup> June at Saddleworth Moor (Figure 58 (c)) and in Manchester and Liverpool on June 28<sup>th</sup> (Figure 58 (d)). TROPOMI detects reflected sunlight in the SWIR and, in principle, a TROPOMI measurement of CO is sensitive from the surface upwards. However, there can be reduced sensitivity in TROPOMI measurements near the surface due to smoke and aerosols.

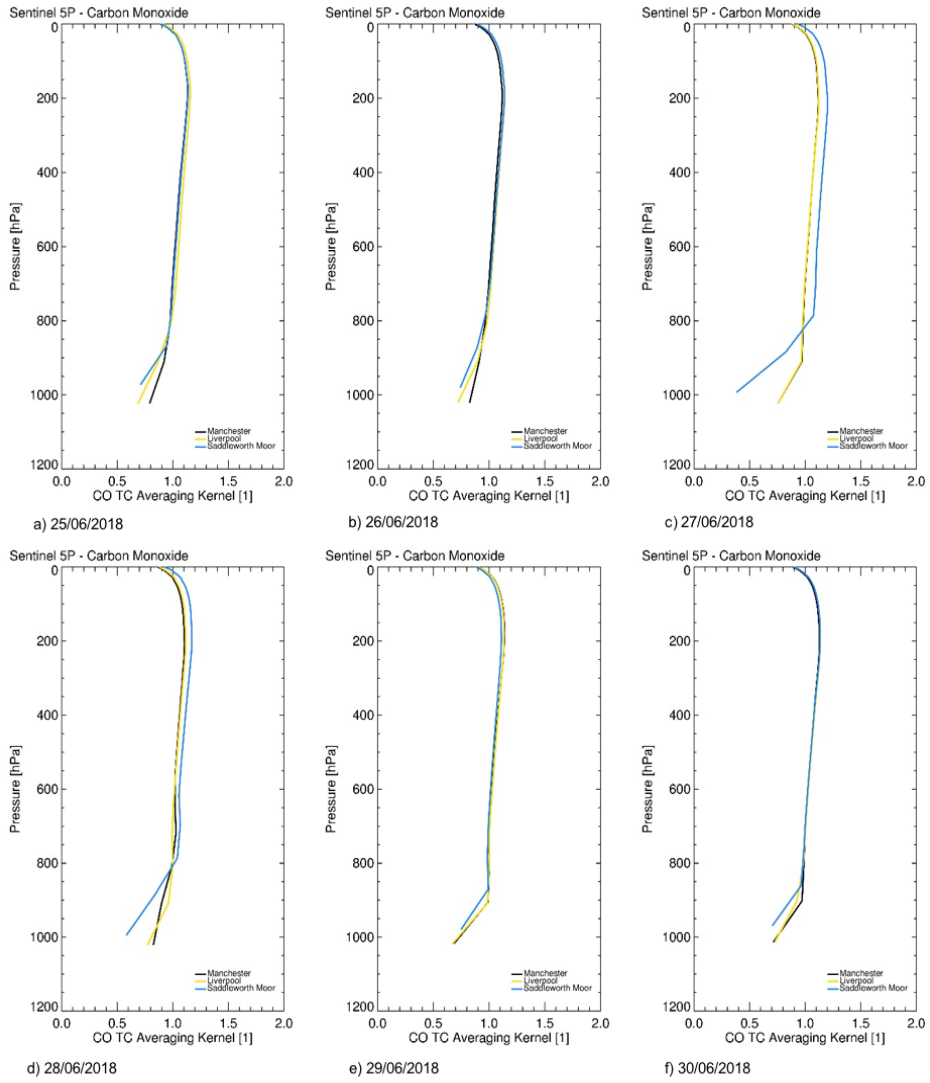


Figure 58. Total column averaging kernels reflecting the altitude sensitivity of the CO total column TROPOMI retrieval during the Saddleworth Moor fire days (June 25<sup>th</sup>-30<sup>th</sup> 2018) for three specific location, Manchester, Liverpool and Saddleworth Moor.

On June 25<sup>th</sup> and 26<sup>th</sup>, the AKs over the urban regions lose some sensitivity near the surface, independent of the fire signal. The Saddleworth Moor AKs have already lost sensitivity near the surface below approximately 800 hPa due to the influence of smoke particles within the plume. On June 27<sup>th</sup>, the Saddleworth Moor AK has greater sensitivity (just over 1.0) than the urban regions above 800 hPa. As winds transport the smoke plume over Manchester and Liverpool (June 29<sup>th</sup> and 30<sup>th</sup>), the AK loses sensitivity at approximately 900 hPa and reduces to approximately 0.7.

Typically, the signal from surface urban CO is smeared out over the satellite pixel (with some loss of sensitivity if there are aerosols) and it can be difficult to distinguish from the background due to instrumental noise. The SWIR CO overtone band is relatively weak, so detecting small CO enhancements above the background can be difficult. The fires are likely to emit more CO than the urban regions, so sources such as Manchester and Liverpool are more difficult to detect, but with clear enhancements from the fires.

## 10.7 Aircraft Instrumentation and Cross-section

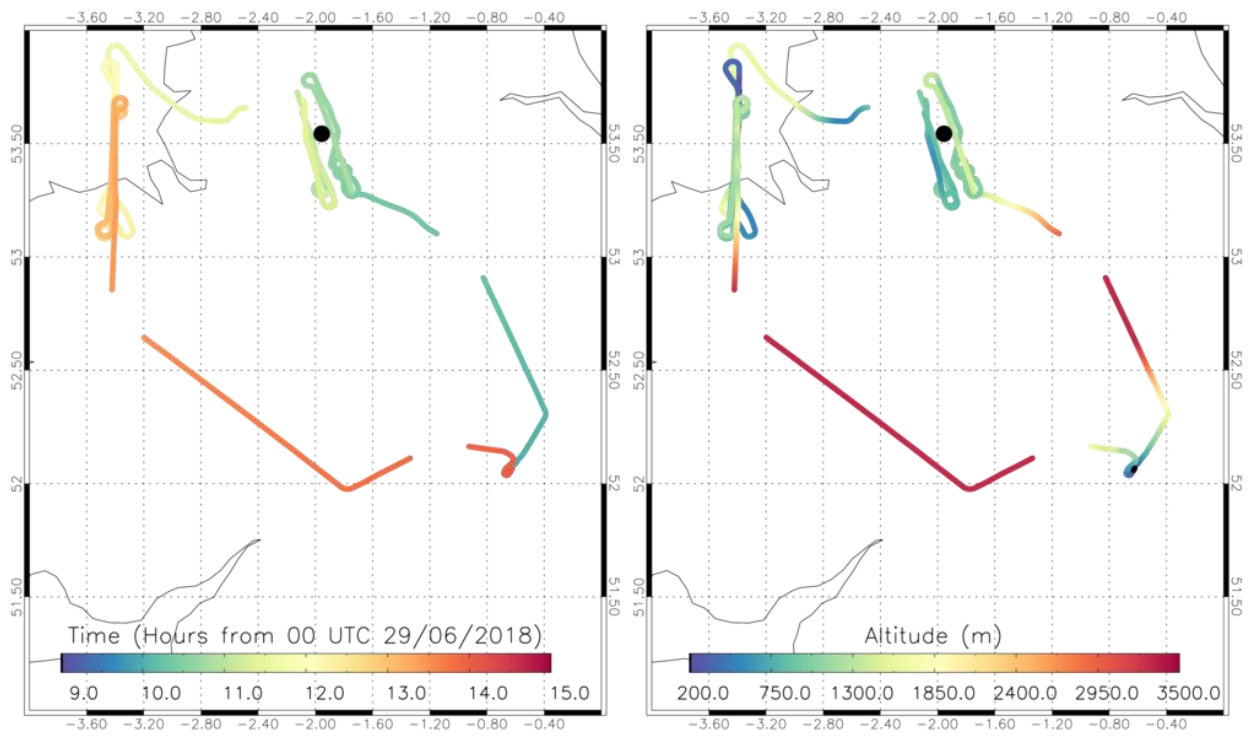


Figure 59. Facility of Airborne Atmospheric Measurements (FAAM) aircraft path (hours since 00 UTC) and altitude(m above ground level (AGL)) from the Saddleworth Moor wildfires on June 29<sup>th</sup> 2018.

### 10.7.1 Instrumentation

PM<sub>2.5</sub> mass was calculated using data from the passive cavity aerosol spectrometer probe 100-X (PCASP) instrument. Uncertainty in the PCASP dataset comes from poisson counting (i.e. the number of particles in each of the size bins) and the bin width (originating in the optical property corrections that are applied) (Sanchez-Marroquin, et al., 2019). We find this to be ~30-35% at the 1-sigma confidence interval for the integrated volume in the PM<sub>2.5</sub> range. Further uncertainty in the PM<sub>2.5</sub> concentration data (which we calculate from the raw dataset) comes from our assumption of density of the particles, which we apply to the dataset to calculate the mass of PM<sub>2.5</sub>. We take this value to be 1.4 kg m<sup>-3</sup> (black carbon), which is in the range of values (1.2 -1.8 kg m<sup>-3</sup>) given by Long *et al.* (2013). We believe this is a conservative estimation since the flight sample will likely also include dust particles, which have a higher density (Wagner, et al., 2018). We carried out a sensitivity analysis to the density value used and found that changing the density value by ±10% lead to a linear change in the PM<sub>2.5</sub> mass calculated (i.e. ±10%). We also use a refractive index of 1.56+0i, which we believe to be a good choice given that the aerosol sampled are very likely heterogeneous (Sanchez-Marroquin, et al., 2019). Finally, since the data is based on particles in the 0.1 - 3µm diameter size range, we are likely to slightly underestimate the total PM<sub>2.5</sub> mass. Though this this is likely to be small since the ultrafine section (< 0.1 µm) contains very little mass.

Measurements of NO were made using a custom built chemiluminescence instrument (Air Quality Design Inc), with NO<sub>2</sub> measured on a second channel by photolytic conversion to NO at 395 nm using a blue light converter (BLC), followed by detection by chemiluminescence (Lee, et al., 2009). In flight calibrations were carried out by adding a small flow of NO calibration gas (5 ppm NO in nitrogen, BOC) to the sample inlet, such that the calibration was

in the same humidity regime as the ambient measurements. The NO<sub>2</sub> conversion efficiency was measured by titration of the NO in the calibration to NO<sub>2</sub> using O<sub>3</sub>. Calibrations were carried out at the beginning and end of each flight whilst the aircraft was above the boundary layer and hence flying in very low and stable NO<sub>x</sub> conditions. The calibration factors were interpolated throughout the flight to account for any sensitivity drifts in the instrument. Estimated accuracies are 4% for NO 5% for NO<sub>2</sub>, with associated precision of 31 and 45 pptv respectively (for 1Hz data).

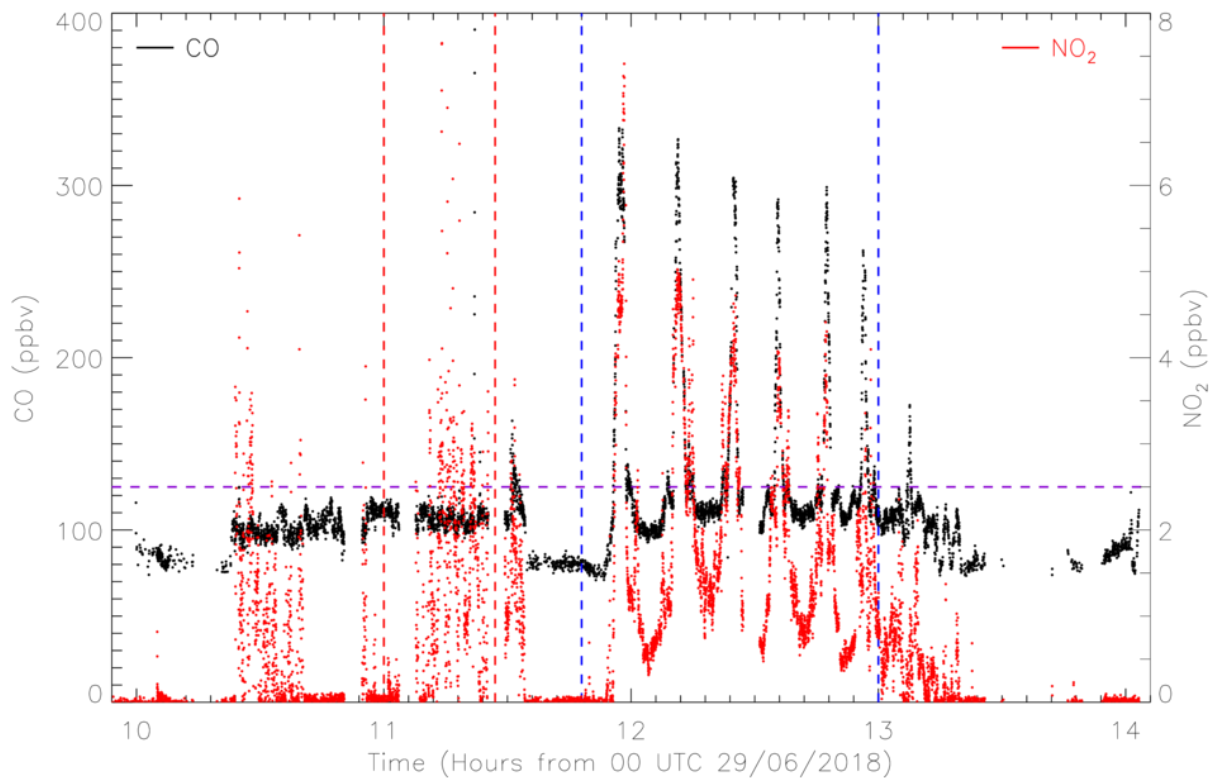


Figure 60. Facility of Airborne Atmospheric Measurements (FAAM) aircraft measurements of nitrogen dioxide ( $\text{NO}_2$ , ppbv) (red) and carbon monoxide (CO, ppbv) (black) from the Saddleworth Moor wildfires on June 29th 2018. The sections bounded by the red and blue dashed lines represent the near-field (NF) and downwind (DW) time phases of the flight. The horizontal purple dashed line indicates the “in-plume” ( $> 125$  ppbv) versus “out of plume” ( $< 125$  ppbv) threshold.

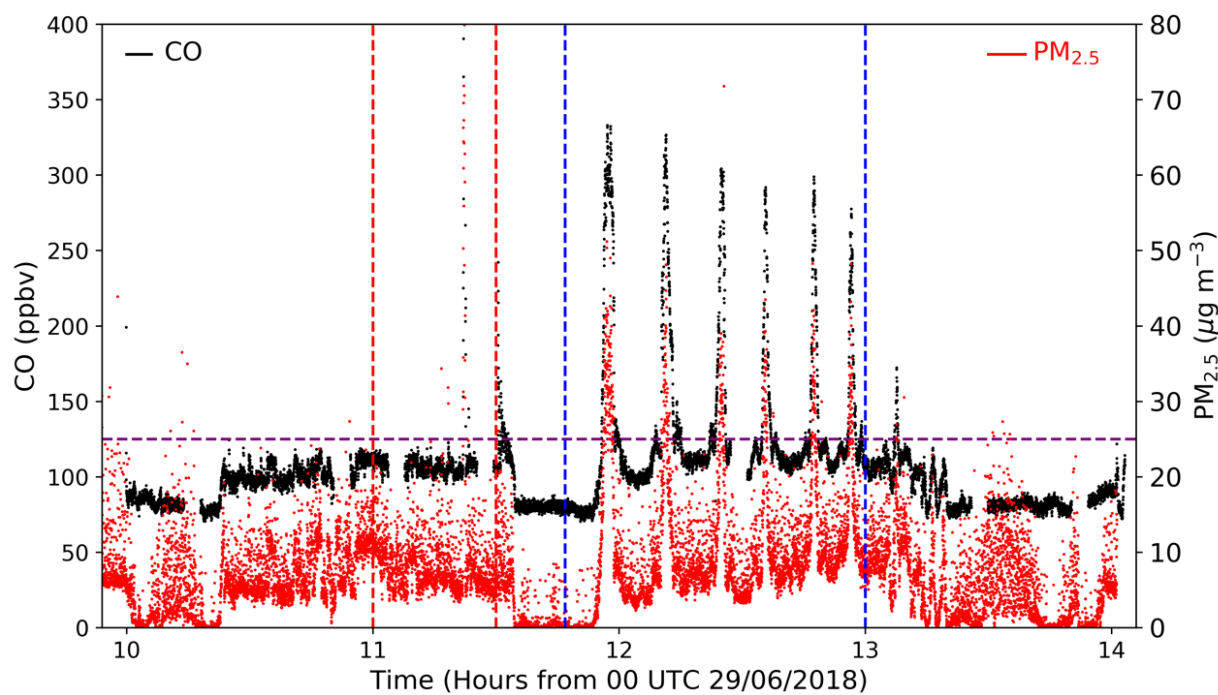


Figure 61. Facility of Airborne Atmospheric Measurements (FAAM) time-series observations of carbon monoxide (CO, ppbv) (black) and PM<sub>2.5</sub> concentration ( $\mu\text{g m}^{-3}$ ) (red) from the Saddleworth Moor wildfires on June 29<sup>th</sup> 2018. The sections bounded by the red and blue dashed lines represent the near-field (NF) and downwind (DW) time phases of the flight. The horizontal purple dashed line indicates the “in-plume” ( $> 125$  ppbv) versus “out of plume” ( $< 125$  ppbv) threshold.

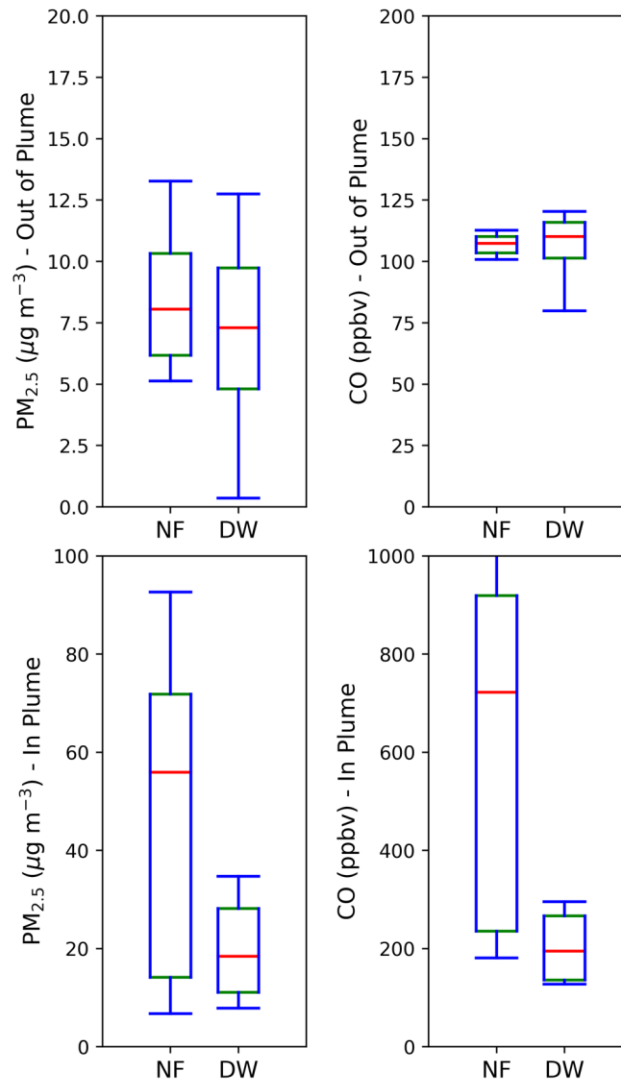


Figure 62. Box and whisker schematic of PM<sub>2.5</sub> aerosol concentration ( $\mu\text{g m}^{-3}$ ) and CO (right, ppbv “in-” and “out of plume” (CO > 125 ppbv). Red, green and blue represent the median, 25<sup>th</sup> and 75<sup>th</sup> percentiles and minimum and maximum concentrations, respectively. NF and DW represent the near-field and downwind phases of the plume.

### 10.7.2 Cross section

Figure 63 represents the “in-plume” flight transect (CO concentration > 125 ppbv) used for the emissions calculation in Equation (15) of the main manuscript. Here, the plume width is 4482 m and plume thickness is 52 m, and we assign a 50% uncertainty to these values which are assumed to be fixed. We tried different CO concentration thresholds, but 125 ppbv gave the best results. For example, if 100 ppbv were used then background values from other transects would be included and the plume transect would not be continuous. If larger values were used, the sample size within the transect would rapidly reduce. It is also possible that the aircraft might not have flown through the centre of the plume, so the values here might be underestimated. Finally, we assume the cross-section of this part of the transect is regular (i.e. approximately rectangular), providing further uncertainty in our methodology. However, the emission rates for CO and carbon dioxide (CO<sub>2</sub>) compare reasonably with remote sensing estimates, thus providing some confidence in our results.

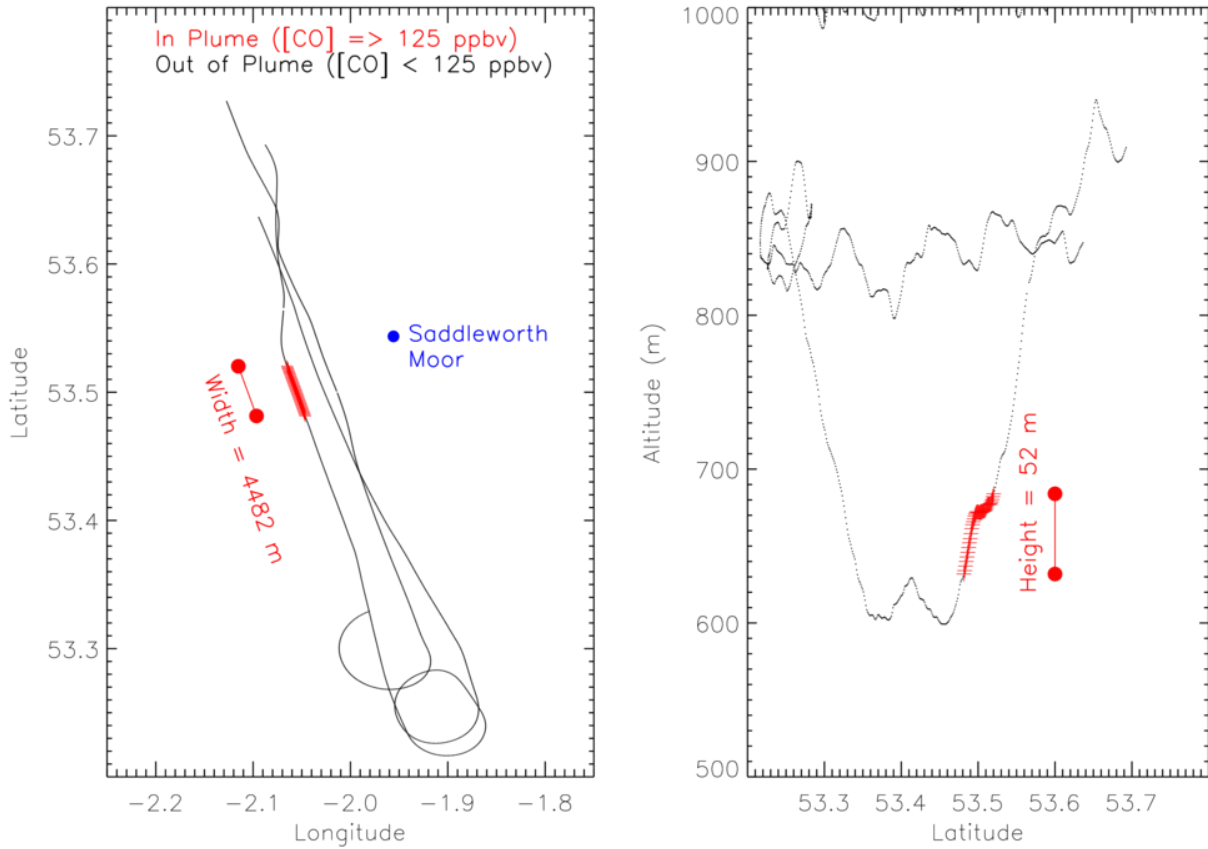


Figure 63. Aircraft transect representing the fire plume the near-field (NF) flight segment. Red crosses represent where the aircraft was sampling “in-plume” air defined as CO concentrations > 125 ppbv. The plume width is approximately 4482 m and the plume thickness is approximately 52 m, representing an approximate rectangular cross-section.

## 10.8 Comparison of TROPOMI with IASI (Infrared Atmospheric Sounding Interferometer)

Evaluation of total column carbon monoxide (TCCO) from the TROPOMI satellite is not possible using the aircraft data due to a lack of vertical information in the aircraft dataset, which prevents the derivation of a total column. We therefore use the Infrared Atmospheric Sounding Interferometer (IASI), onboard ESA's MetOP-A to evaluate TCCO from TROPOMI. The IASI TCCO data is provided by the Rutherford Appleton Laboratory (RAL), which uses their Infrared & Microwave Sounding (IMS) scheme (Siddans, et al., 2015). Typical precision uncertainty in the data used is approximately 12%. More information is provided by Siddans, Gerber and Miles (2015).

TCCO data from IASI clearly detects fire-enhanced TCCO, despite much less dense sampling from this satellite (Figure 64). However, daily background column values show large variability so we calculate a daily fire anomaly using the average background TCCO between 1-0°W and 55-56°N. Consistent with TROPOMI TCCO (Figure 34), on June 26<sup>th</sup>, a large enhancement in TCCO can be observed over the fire region of enhancement between  $0.3 \times 10^{18}$  molecules  $\text{cm}^{-2}$  and  $0.4 \times 10^{18}$  molecules  $\text{cm}^{-2}$  (Figure 64). On June 27<sup>th</sup>, free tropospheric winds transport CO towards the urban regions of Manchester and Liverpool ( $> 0.4 \times 10^{18}$  molecules  $\text{cm}^{-2}$ ). This is less well captured on June 28<sup>th</sup> and 29<sup>th</sup>, but TCCO enhancements are still co-located with that of TROPOMI. On June 30<sup>th</sup>, the Saddleworth Moor fires are no longer detected, but the Winter Hill fires show slight CO enhancements ( $0.25\text{-}0.3 \times 10^{18}$  molecules  $\text{cm}^{-2}$ ) consistent with TROPOMI TCCO.

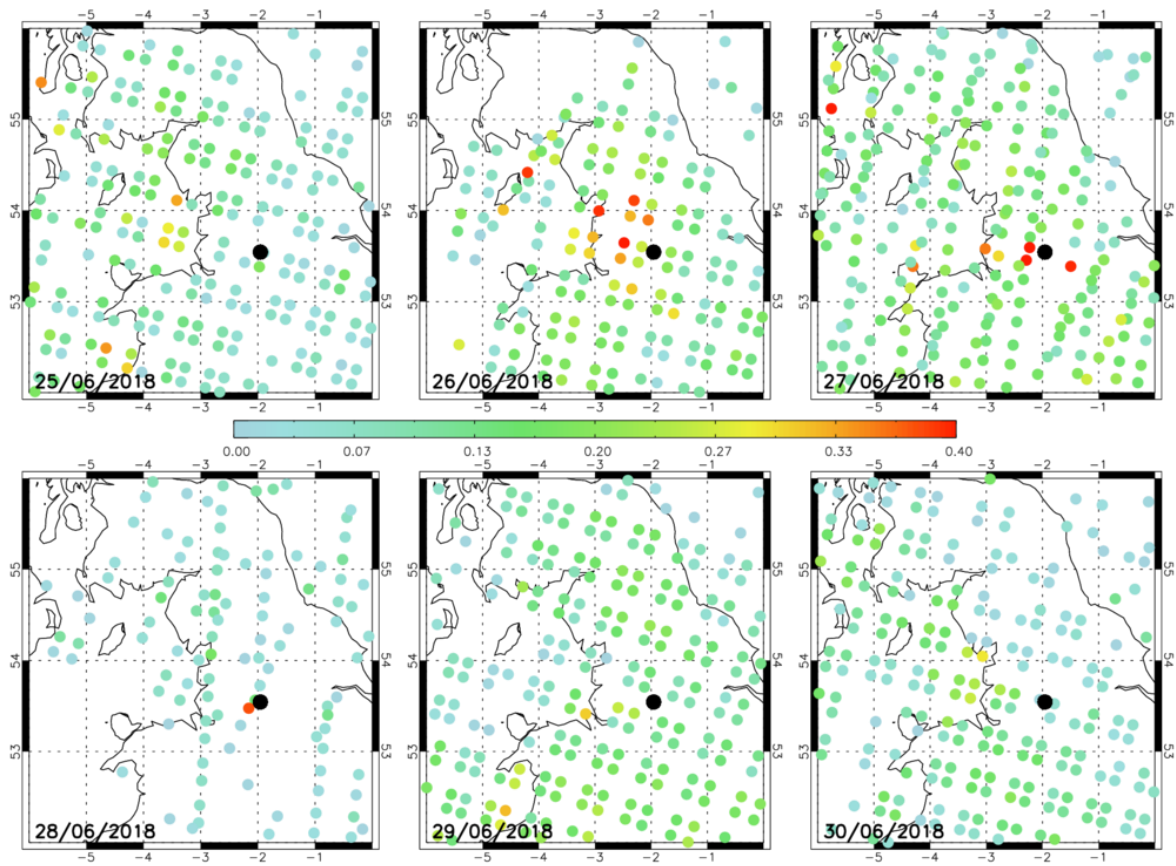


Figure 64. IASI total column carbon monoxide (TCCO, 1018 molecules cm<sup>-2</sup>) for June 25<sup>th</sup> - 30<sup>th</sup> 2018. Daily background concentrations have been subtracted based on the 1-0°W, 55-56°N average sub-region column value. The black circle representations the location of the Saddleworth Moor fires.

## 10.9 AURN PM<sub>2.5</sub> observations

Table 11. Mean daily non-volatile fraction of PM<sub>2.5</sub> for 2013-2017 and 2018 at Manchester Piccadilly, Salford Eccles and Wigan Centre AURN sites.

Date	Manchester Piccadilly		Salford Eccles		Wigan Centre	
	Non-volatile fraction 2013-2017	Non-volatile fraction 2018	Non-volatile fraction 2013-2017	Non-volatile fraction 2018	Non-volatile fraction 2013-2017	Non-volatile fraction 2018
<b>25/06/18</b>	0.96	0.84	0.81	0.81	0.76	0.80
<b>26/06/18</b>	0.87	0.92	0.80	0.84	0.72	0.90
<b>27/06/18</b>	0.90	0.93	0.74	0.90	0.70	0.88
<b>28/06/18</b>	0.82	0.86	0.63	0.66	0.61	0.80
<b>29/06/18</b>	0.96	0.83	0.76	0.80	0.70	0.75

## 10.10 References

- 1) Jones, P. D., Harpham, C. and Briffa, K. R. 2013. Lamb weather types derived from reanalysis products. *International Journal of Climatology* 33(5), 1129–1139. doi: 10.1002/joc.3498.
- 2) Kanamitsu, M. 1989. Description of the NMC Global Data Assimilation and Forecast System. *Weather and Forecasting* 4(3), 335–342. doi: 10.1175/1520-0434(1989)004<0335:DOTNGD>2.0.CO;2.
- 3) Lee, J.D., Moller, S.J., Read, K.A., Lewis, A.C., Mendes, L., Carpenter, L.J., 2009. Year-round measurements of nitrogen oxides and ozone in the tropical North Atlantic marine boundary layer. *J. Geophys. Res. Atmos.* 114, 1–14. <https://doi.org/10.1029/2009JD011878>.
- 4) Long, C. M., Nascarella, M. A. and Valberg, P. A. 2013. Carbon black vs. black carbon and other airborne materials containing elemental carbon: Physical and chemical distinctions, *Environmental Pollution*. Elsevier Ltd, 181, 271–286. doi: 10.1016/j.envpol.2013.06.009.
- 5) Pope, R.J., Savage, N.H., Chipperfield, M.P., Arnold, S.R., Osborn, T.J., 2014. The influence of synoptic weather regimes on UK air quality: Analysis of satellite column NO<sub>2</sub>. *Atmos. Sci. Lett.* 15, 211–217. <https://doi.org/10.1002/asl2.492>.
- 6) Pope, R.J., Savage, N.H., Chipperfield, M.P., Ordóñez, C., Neal, L.S., 2015. The influence of synoptic weather regimes on UK air quality: Regional model studies of tropospheric column NO<sub>2</sub>. *Atmos. Chem. Phys. Discuss.* 15, 18577–18607. <https://doi.org/10.5194/acpd-15-18577-2015>
- 7) Sanchez-Marroquin, A., Hedges, D.H.P., Hiscock, M., Parker, S.T., Rosenberg, P.D., Trembath, J., Walshaw, R., Burke, I., McQuaid, J., Murray, B., 2019. Characterisation of the

filter inlet system on the BAE-146 research aircraft and its use for size resolved aerosol composition measurements. *Atmos. Meas. Tech.* 12, 5741–5763.

<https://doi.org/https://doi.org/10.5194/amt-12-5741-2019>.

- 8) Siddans, R., Gerber, D. and Miles, G. 2015. Optimal Estimation Method retrievals with IASI, AMSU and MHS measurements.
- 9) Stein, A.F., Draxler, R.R., Rolph, G.D., Stunder, B.J.B., Cohen, M.D., Ngan, F., 2015. Noaa's hysplit atmospheric transport and dispersion modeling system. *Bull. Am. Meteorol. Soc.* 96, 2059–2077. <https://doi.org/10.1175/BAMS-D-14-00110.1>.
- 10) Wagner, R., Jähn, M. and Schepanski, K. 2018. Wildfires as a source of airborne mineral dust - Revisiting a conceptual model using large-eddy simulation (LES), *Atmospheric Chemistry and Physics*, 18(16), 11863–11884. doi: 10.5194/acp-18-11863-2018.

# Supplementary Material: Impact on Air Quality and Health due to the Saddleworth Moor Fire in Northern England

**Graham A.M<sup>1</sup>, Pope R.J<sup>1,2</sup>, Pringle K.P<sup>1</sup>, Arnold S.<sup>1</sup>,  
Chipperfield, M.P<sup>1,2</sup>, Conibear, L.A<sup>1</sup>, Butt, E.W<sup>1</sup>, Kiely L.<sup>1</sup>,  
Knote, C.<sup>3</sup>, and McQuaid, J.B<sup>1</sup>**

<sup>1</sup> Institute for Climate and Atmospheric Science, School of Earth and Environment, University of Leeds, Leeds, LS2 9JT

<sup>2</sup> National Centre for Earth Observation, University of Leeds, Leeds, LS2 9JT

<sup>3</sup> Meteorological Institute, LMU Munich, Munich, Germany

E-mail: [ee15amg@leeds.ac.uk](mailto:ee15amg@leeds.ac.uk)

## 11.1 AURN data

Table 12. shows details of AURN sites used in model evaluation within this study.

<b>Site Name</b>	<b>Site Type</b>	<b>Latitude (°N)</b>	<b>Longitude (°E)</b>
Blackpool Marton (0)	Urban Background	53.80	-3.01
Carlisle Roadside (1)	Urban Traffic	54.89	-2.95
Hull Freetown (2)	Urban Background	53.75	-0.34
Leeds Centre (3)	Urban Background	53.80	-1.55
Leeds Headingley (4)	Urban Traffic	53.82	-1.76
Liverpool Speke (5)	Urban Industrial	53.35	-2.84
Manchester Piccadilly (6)	Urban Background	53.48	-2.24
Preston (7)	Urban Background	53.77	-2.68
Salford Eccles (8)	Urban Background	53.48	-2.33
Sheffield Centre (9)	Urban Traffic	53.41	-1.46
Sheffield Devonshire Green (10)	Urban Background	53.38	-1.48
Warrington (11)	Urban Industrial	53.39	-2.62
Wigan Centre (12)	Urban Background	53.55	-2.64
Wirral Tranmere (13)	Urban Background	53.37	-3.0
York Fishergate (14)	Urban Traffic	53.95	-1.08
York Bootham (15)	Urban Background	53.97	-1.09

## 11.2 Wildfire Emissions Scaling

Since FINNv1.5 does not include emissions from peat we scale FINN emissions over Saddleworth Moor (Figure 65) to try to account for this. We use observations of PM<sub>2.5</sub> from AURN sites and modelled surface PM<sub>2.5</sub> from WRF-Chem simulations to tune our scaling. We find that increasing scaling by a factor of 1-10 of the original FINN values throughout the fires results in the lowest root mean square error (RMSE) when the model is compared to observations (see Table 8). This is likely due to changing fuel source through the fire lifetime, from the surface vegetation (heather and grass) initially, which FINN accounts for. Once surface vegetation had been burnt the fire began to burn the peat underneath (Greater Manchester Combined Authority, 2019), which has much higher emissions per unit burnt area. Thus, later in the fire lifecycle (26<sup>th</sup> – 28<sup>th</sup>), using a larger scaling for emissions improves agreement with observations.

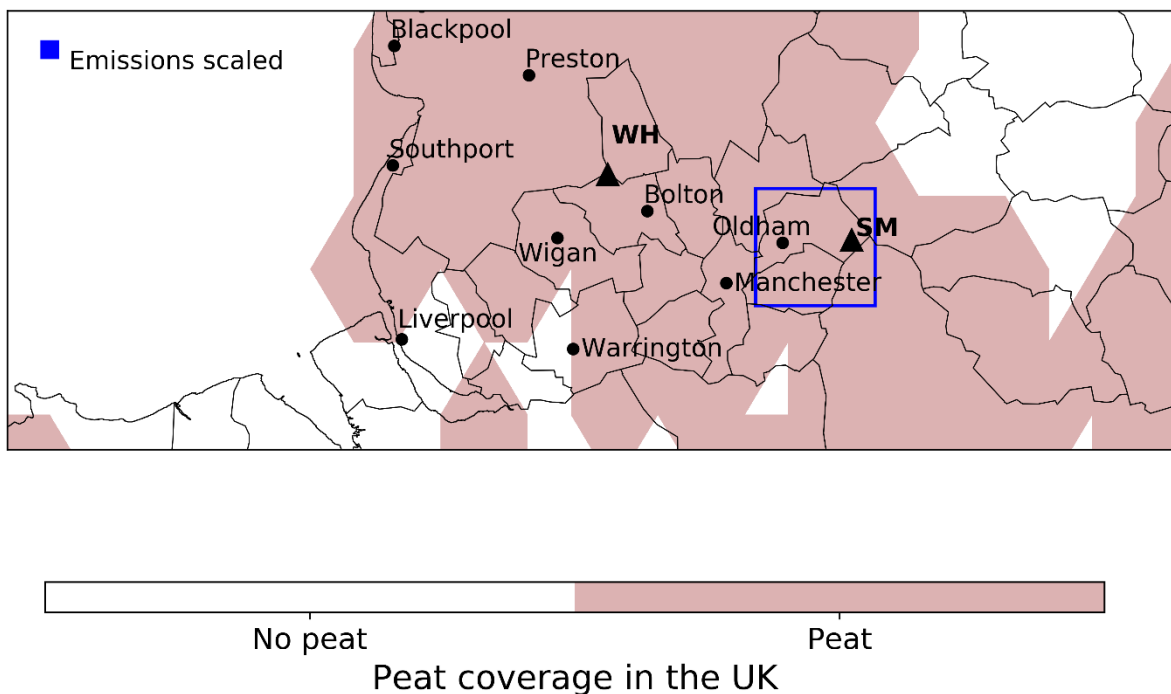


Figure 65. Area over which scaling was applied (blue) to FINNv1.5 emissions for use in WRF-Chem simulations over plotted on peat coverage in domain (Xu, et al., 2018)

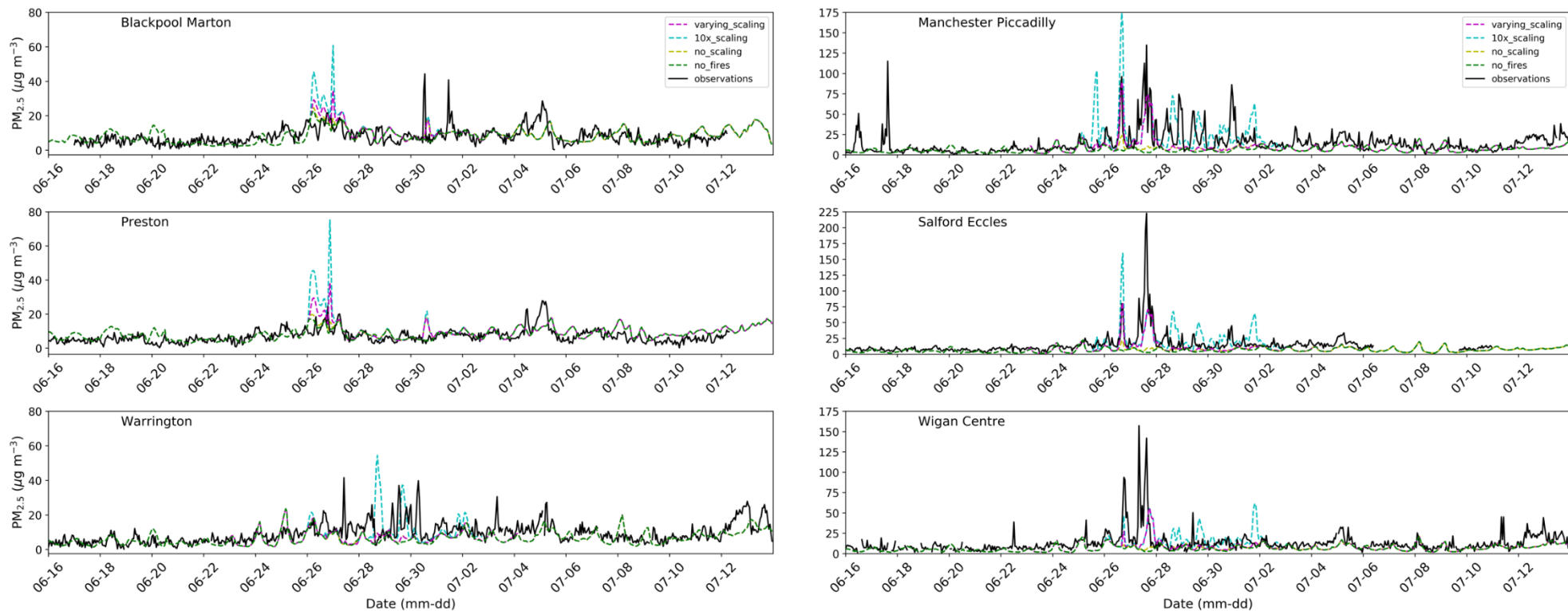


Figure 66. Hourly observed and simulated surface PM<sub>2.5</sub> between June 16<sup>th</sup> and July 14<sup>th</sup> 2018. Modelled values are from the no fires (green), no scaling (yellow), 10x scaling (cyan) and time-varying scaling simulations (magenta) (see Manuscript: Model Evaluation and Table 8). Observations from AURN sites are indicated in black.

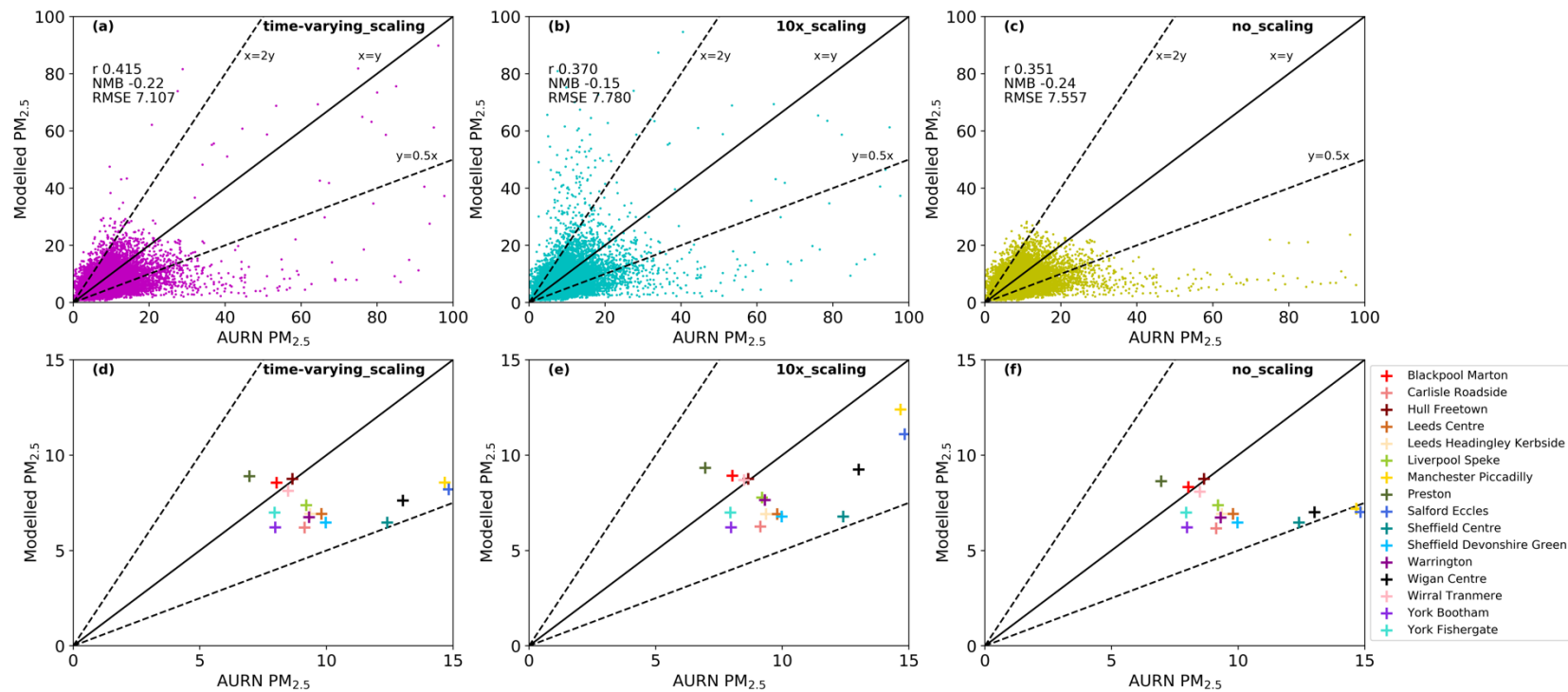


Figure 67. (a) Time-varying scaling, (b) 10x scaling and (c) no scaling simulated and observed hourly  $PM_{2.5}$  concentrations at all sites. Individual sites are shown in (d-f), with the mean for each observational site between June 16<sup>th</sup> – July 14<sup>th</sup> 2018 indicated by coloured crosses. The 1:1, 0.5:1 and 1:0.5 lines are shown for reference. The mean correlation coefficient (r), mean bias (MB), normalised mean bias (NMB) and root mean squared error (RMSE in  $\mu g m^{-3}$ ) across all sites for the simulation period (June 16<sup>th</sup> – July 14<sup>th</sup> 2018) are also indicated in (a)-(c).

## 11.3 Model set-up

### 11.3.1 Release of emissions

Although WRF-Chem is set-up to emit fire emissions using a plume-rise parameterisation by default (Freitas, et al., 2007), several studies have found that emissions from fires are released and remain in the boundary layer (BL). This scheme potentially represents an incorrect vertical distribution of the emissions (Archer-Nicholls, et al., 2015). Given the size of the Saddleworth Moor fires (8 km<sup>2</sup>) and the peak height of flames (4 m), the plume-rise parameterization is likely to overestimate the injection height of the emissions from the fires. Therefore, we release 100 % of emissions at the surface. Kiely *et al.* (2019) found that releasing emissions at the surface for WRF-Chem simulations of Indonesian fires, using a similar model set-up to this study, increased the average simulated surface PM<sub>2.5</sub> concentration by a factor of 1.34-1.36 compared with injecting 50% at the surface and 50% in the boundary layer.

### 11.3.2 Anthropogenic Emissions

Anthropogenic emissions are from EDGAR-HTAP2 (Janssens-Maenhout, et al., 2015), a compilation of different gridded inventories that give global coverage. Emissions include SO<sub>2</sub>, NO<sub>x</sub>, CO, NMVOC, NH<sub>3</sub>, PM<sub>10</sub>, PM<sub>2.5</sub>, BC and OC. European emissions are from the EMEP-TNO (MACCII) dataset, which includes all activities except international shipping and international aviation. All gaps in EDGAR-HTAP2 are filled with bottom-up emissions from EDGAR v4.3.

## 11.4 Model Evaluation

Assessing model performance at hourly resolution, without scaling FINN fire emissions (no scaling), the model performs relatively poorly across all sites. Pearson correlation score is similar to simulations without fire emissions (no fires) (0.35 and 0.32 respectively). RMSE, NMB and NMAE are also similar to the simulation with no fire emissions ( $7.56 \mu\text{g m}^{-3}$  and  $7.70 \mu\text{g m}^{-3}$ , -0.24 and -0.26, 0.47 and 0.48, respectively). Poor performance of the model is dominated by sites where fire emissions are not being captured well (see Figure 66). When a 10-times scaling (10x scaling) is applied to FINN emissions over Saddleworth Moor the correlation is improved (0.37) and NMB is substantially improved (0.16). However, the RMSE ( $7.78 \mu\text{g m}^{-3}$ ) and NMAE (0.50) worsen since the model over predicts  $\text{PM}_{2.5}$  emissions in in the early stages of the fire (Figure 66).

The improvement in model performance is also clear in Figure 67. Figure 67 (a-f) indicate much better agreement between the model and observations with the time-varying scaling (time-varying scaling) compared to (10x scaling) and no scaling (no scaling). The site averages are also much better predicted by the model with scaling applied (Figure 67 (c) & (d)). All model predictions of mean concentrations lie within the 1:0.5 and 0.5:1 range when scaling is applied (Figure 67 (d)).

## 11.5 Population Exposure to $\text{PM}_{2.5}$

We use population count data for 2015 (NASA Socioeconomic Data and Applications Center (SEDAC) Center for International Earth Science Information Network (CIESIN), and Columbia, 2018) to assess population exposure to  $\text{PM}_{2.5}$  during the period of the fires (June 23<sup>rd</sup> – June 30<sup>th</sup>).

Firstly, we calculate exposure to several PM<sub>2.5</sub> concentration bins in line with the Daily Air Quality Index (DAQI), used by the UK Government to advise the public on how to reduce the associated health effects of exposure to pollutants. We use the four bins (Table 13) for PM<sub>2.5</sub> concentrations and calculate the total number of people exposed to each concentrations bin each day within the week-long period (June 23<sup>rd</sup>-30<sup>th</sup> 2018).

Table 13. Daily Air Quality Index (DAQI) bands for PM<sub>2.5</sub> (µg m<sup>-3</sup>) and associated behaviour advised by the UK government to reduce the population’s risk. Concentrations for each band are also indicated.

<b>DAQI Band</b>	<b>Advice</b>
Low (0-35 µg m <sup>-3</sup> )	Enjoy outdoor activities as normal
Moderate (36-53 µg m <sup>-3</sup> )	Adults and children with lung problems and adults with heart problems who experience symptoms should consider reducing strenuous activity, especially outdoors
High (54-70 µg m <sup>-3</sup> )	Anyone who experience symptoms should consider reducing strenuous activity, especially outdoors, those at risk should reduce strenuous activities
Very High (>71 µg m <sup>-3</sup> )	Everyone should reduce outdoor activity – those with asthma may need to use their reliever inhaler more

Results indicate PM<sub>2.5</sub> concentrations remained within the low DAQI bin between June 23<sup>rd</sup> and June 25<sup>th</sup> and on June 29<sup>th</sup>, with no exposure to higher concentrations (Figure 68). However, during the Saddleworth Moor (June 26<sup>th</sup> and 27<sup>th</sup>) and Winter Hill (June 30<sup>th</sup>) fires air quality was substantially degraded and many were exposure to the highest DAQI values. A total of 1 million and 1.7 million people were exposed to PM<sub>2.5</sub> concentrations of >36 µg m<sup>-3</sup>

on June 26<sup>th</sup> and 27<sup>th</sup>, concentrations where the DAQI suggests behaviour alterations to reduce exposure (see Figure 68). Within this total, 0.2 million and 0.5 million were exposed to the highest DAQI values ( $71+ \mu\text{g m}^{-3}$ ) and another 0.2 and 0.6 million to high DAQI values ( $54 - 70 \mu\text{g m}^{-3}$ ). During the Winter Hill fires, another 0.06 million were exposed to  $\text{PM}_{2.5}$  above  $36 \mu\text{g m}^{-3}$  on June 29<sup>th</sup> and 30<sup>th</sup>. When this is compared to the no fires simulation (Figure 71) it becomes clear that the degradation in the DAQI seen (Figure 40 (a) and Figure 68) was dominated by the fires.

To put this into a global context we calculate exceedances of the WHO 24-hour threshold of  $25 \mu\text{g m}^{-3}$ . This also allows the impact of the fires on air quality and health to be considered (Figure 69). Over the week of the fires (June 23<sup>rd</sup> – June 30<sup>th</sup> 2018) 4.5 million people were exposed to concentrations above the WHO 24-hour  $\text{PM}_{2.5}$  safe-limit on at least one day (Figure 40 (b)). This represents 30% of the population being exposed to unhealthy  $\text{PM}_{2.5}$  concentrations. The total exposure was dominated by the Saddleworth Moor fires on 26<sup>th</sup> and 27<sup>th</sup> June, with 1.5 and 2.6 million people exposed above the WHO limit (Figure 69). Another 0.05 and 0.3 million people were exposed above the limit on the 29<sup>th</sup> and 30<sup>th</sup> June. This indicates exposure above the WHO limit over the week-long period (June 23<sup>rd</sup> and 30<sup>th</sup>) was dominated by  $\text{PM}_{2.5}$  from the fires (note totals may not add up due to rounding). These exceedances have the potential to have harmful effects on health across the region and put a large strain on medical services.

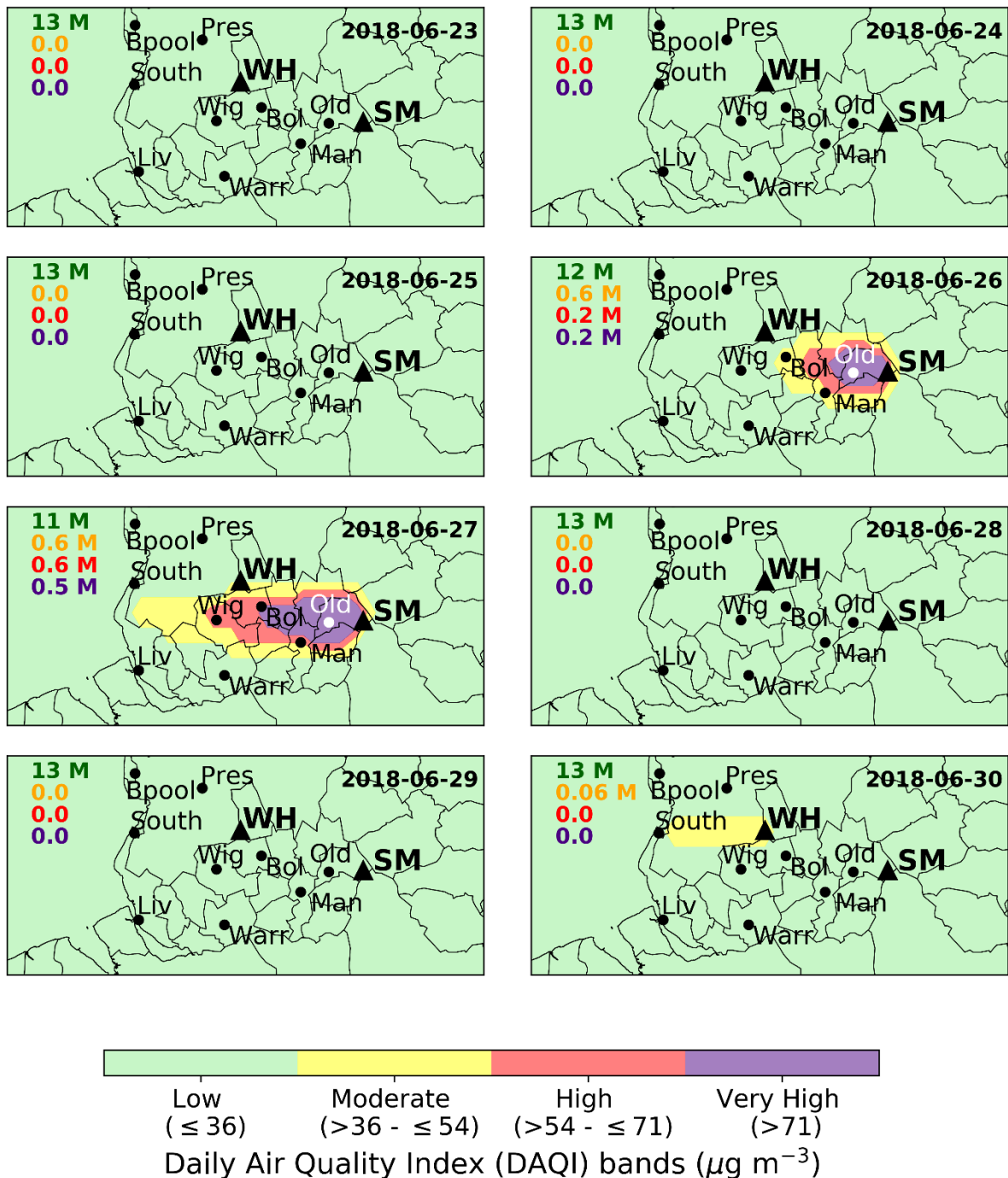
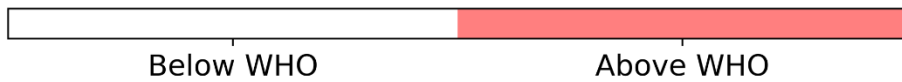
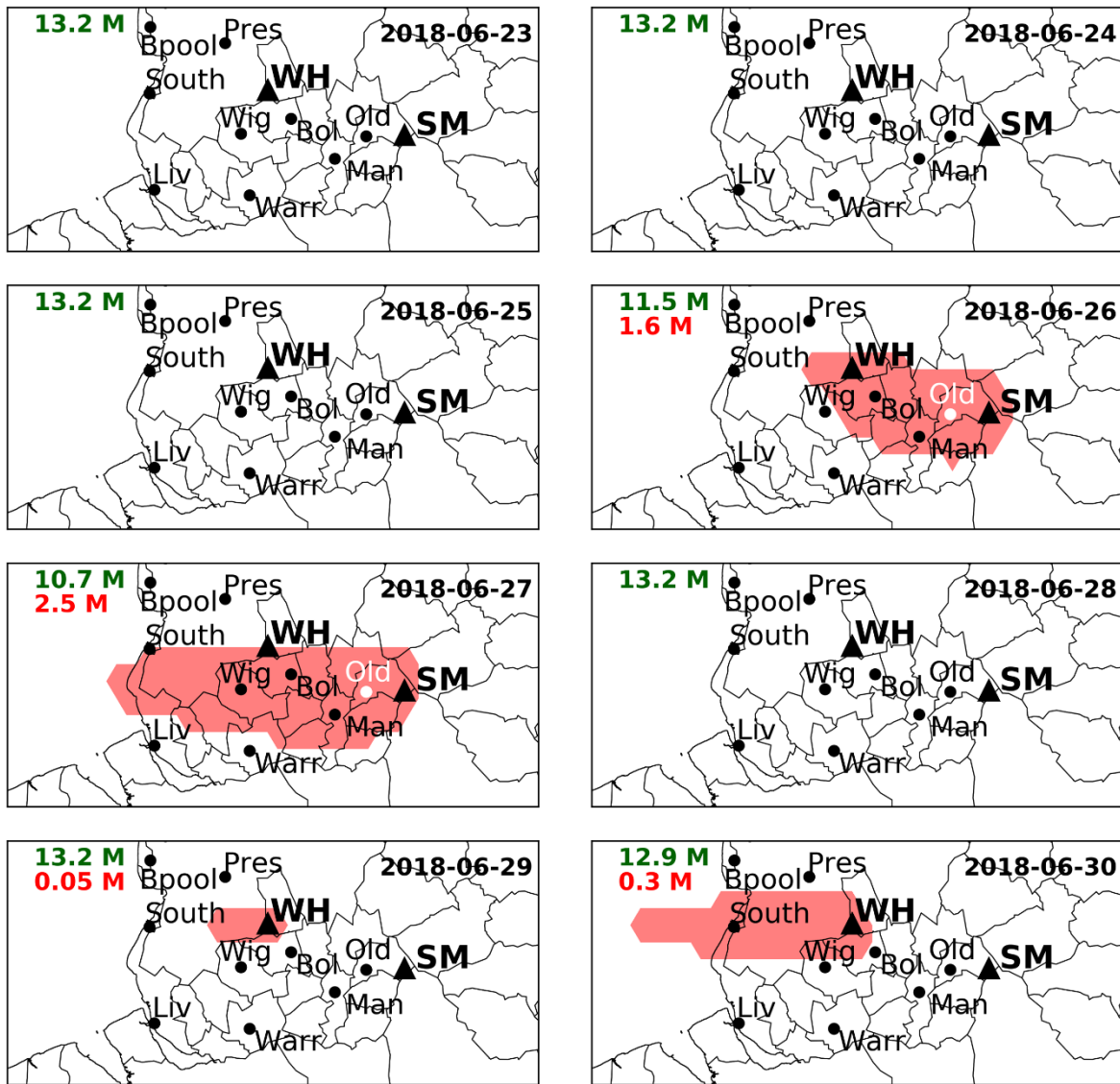


Figure 68. Areas of low ( $0-35 \mu\text{g m}^{-3}$ ), moderate ( $36-53 \mu\text{g m}^{-3}$ ), high ( $54-70 \mu\text{g m}^{-3}$ ) and very high ( $>71 \mu\text{g m}^{-3}$ )  $\text{PM}_{2.5}$ , as defined by the Daily Air Quality Index (DAQI). Coloured numbers correspond to total number of people exposed to each DAQI level on each day. Saddleworth Moor (SM) and Winter Hill (WH) are indicated by black triangles, while highly populated urban areas are indicated by black circles and abbreviated in line with definitions in Figure 65. See Table 13 for more information on the DAQI.



Exposure to PM<sub>2.5</sub> above and below WHO 24-hour safe limit ( $\mu\text{g m}^{-3}$ )

Figure 69. Areas where PM<sub>2.5</sub> is above the WHO 24-hour limit of  $25 \mu\text{g m}^{-3}$  and total population exposed to PM<sub>2.5</sub> below (green) and above (red) this threshold on each day between June 23<sup>rd</sup> and June 30<sup>th</sup> 2018. Saddleworth Moor (SM) and Winter Hill (WH) are indicated by black triangles, while highly populated urban areas are indicated by black circles and abbreviated in line with definitions in Figure 65.

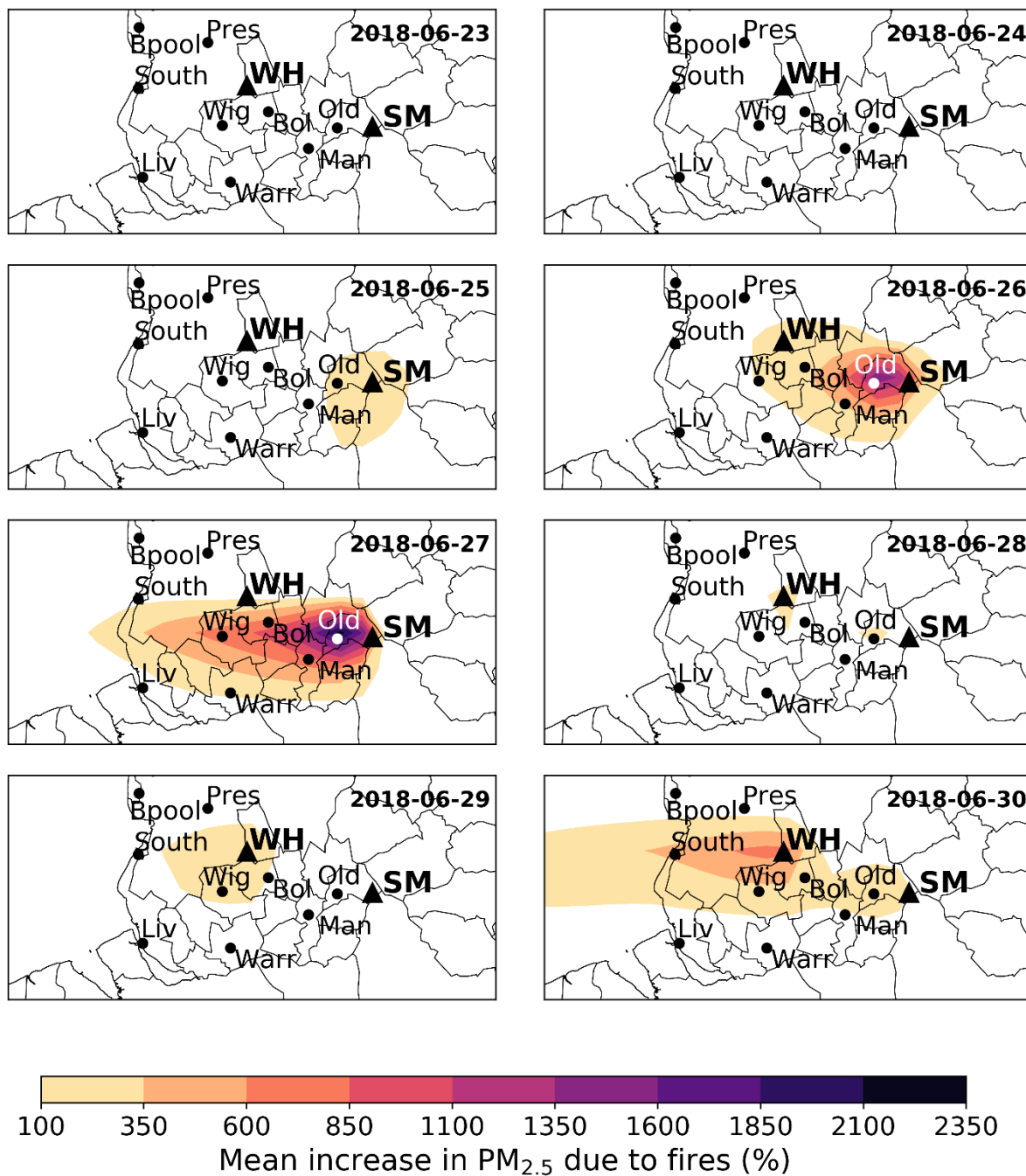


Figure 70. Daily mean percent increase in PM<sub>2.5</sub> due to fires between June 23<sup>rd</sup> and June 30<sup>th</sup> 2018. Calculated as,  $\left(\frac{PM_{2.5} \text{ Fires} - PM_{2.5} \text{ No sFires}}{PM_{2.5} \text{ No Fires}} \times 100\right)$ , where 10% represents a 10% increase in PM<sub>2.5</sub>. Saddleworth Moor (SM) and Winter Hill (WH) are indicated by black triangles, while highly populated urban areas are indicated by black circles and abbreviated in line with definitions in Figure 65.

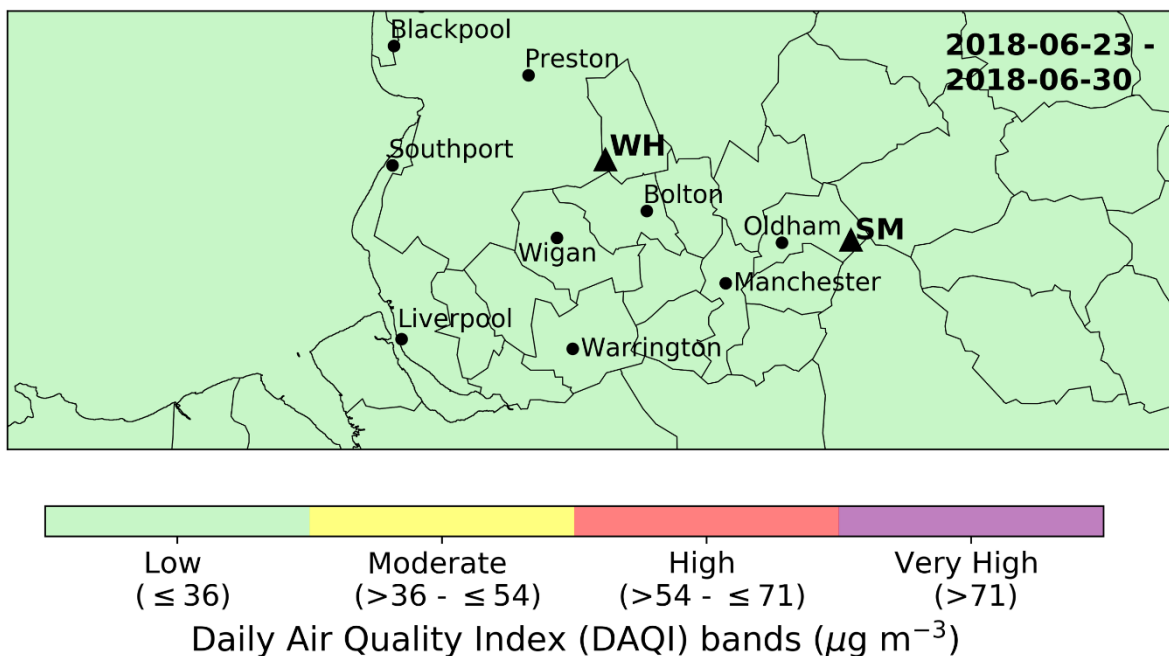


Figure 71. Areas of low ( $0-35 \mu\text{g m}^{-3}$ ), moderate ( $36-53 \mu\text{g m}^{-3}$ ), high ( $54-70 \mu\text{g m}^{-3}$ ) and very high ( $>71 \mu\text{g m}^{-3}$ )  $\text{PM}_{2.5}$  as defined by the Daily Air Quality Index (DAQI) in the no fires simulation. Saddleworth Moor (SM) and Winter Hill (WH) are indicated by black triangles, while highly populated urban areas are indicated by black circles and abbreviated in line with definitions in Figure 38. See Table 13 for more information on the DAQI.

Figure 70 can be used to further understand why the DAQI and WHO thresholds were exceeded during the week-long period. There are large increases in  $\text{PM}_{2.5}$  across the same regions where the concentrations thresholds were exceeded (Figure 68, Figure 69 and Figure 70). On 26<sup>th</sup> and 27<sup>th</sup> June the daily mean increase in  $\text{PM}_{2.5}$  reaches  $>1000\%$  and  $>1800\%$ , respectively over the fire source. This decreases steeply with distance from the fire sources but over Manchester and Bolton  $\text{PM}_{2.5}$  increases of between 100-850% are observed and increases of 100% are observed as far west as the Irish Sea. During the Winter Hill fires (29<sup>th</sup> and 30<sup>th</sup> September) increases in  $\text{PM}_{2.5}$  concentrations are also increased by 100% over a large region including Wigan, Bolton and Manchester and  $>300\%$  over Southport.

We also use this dataset to calculate the health impact of the fires due to short-term exposure to PM<sub>2.5</sub>. The impact is dependent upon several factors including the assumed safe level of exposure to PM<sub>2.5</sub> below which no negative impacts of health would occur, known as the theoretical minimum risk exposure level (TMREL). We present the findings of a 0 µg m<sup>-3</sup> limit in the main manuscript since there is little evidence to suggest a safe-level of exposure. However, we also explored the impact of the TMREL (referred to as X<sub>0</sub> in the manuscript) on our results using the lower (2.4 µg m<sup>-3</sup>) and upper (5.9 µg m<sup>-3</sup>) limits from the global burden of disease 2015 study (GBD Collaborators 2015, 2017) in Table 14.

The results indicate that the mean number of deaths brought forward between June 23rd-30th are a factor 2.5 (0.91 vs 0.37), 6.3 (0.63 vs 0.10) higher for the Fires ON and OFF simulations for a TMREL of 0.0 µg m<sup>-3</sup> compared to TMREL of 5.9 µg m<sup>-3</sup>. Despite the differences in total excess mortality calculated using the different thresholds, the number of mortalities due to the fires (i.e. Fires ON – Fires OFF) is the same for all three thresholds. Alongside this, both the mean and the maximum increase in mortality due to fires (mortality increase Fires ON – Fires OFF) are similar for all three threshold values (~1.07 excess deaths per day and ~3.85 excess deaths per day, respectively). This is likely due to the population being exposed to concentrations much above the TMRELS used (i.e. PM concentrations due to fires were much above 2.4 or 5.9 µg m<sup>-3</sup>), leading to the TMREL used having little effect on the results. However, the percentage increase in mortalities and the percentage of mortalities due to fires both vary substantially depending on the TMREL used as a result of the decreased excess mortality in the no fires simulation when using a TMREL of 2.4 and 5.9 µg m<sup>-3</sup>, compared with 0.0 µg m<sup>-3</sup>. For the 2.4 and 5.9 µg m<sup>-3</sup> thresholds the mean increase in excess mortalities is 60.9 and 260.3% (compared with 39.5% for 0.0 µg m<sup>-3</sup>). The percentage of mortalities attributable

to the fires is also higher for the 2.4 and 5.9  $\mu\text{g m}^{-3}$  limits at 28.7 and 61.3% (compared to 22.2% for 0.0  $\mu\text{g m}^{-3}$ ).

Table 14. Sensitivity of short-term exposure excess mortality results between 23<sup>rd</sup> and 30<sup>th</sup> June on theoretical minimum risk exposure level (TMREL) used. Lower confidence level (lcl), medium confidence level (mcl) and upper confidence levels (ucl) are indicated, based on the 95% confidence intervals of the exposure response function.

Safe threshold value used (X <sub>0</sub> )	mean mortality (Fires ON)			mean mortality (Fires OFF)			mean mortality (Fires ONLY)			mortality increase (Fires ON-Fires OFF)		% mortality increase (Em Fires ON – Em Fires OFF/ Em Fires ON)*100		% mortalities from fires (Em Fires ON – Em Fires OFF/Em Fires OFF)*100	
	lcl	mcl	ucl	lcl	mcl	ucl	lcl	mcl	ucl	mean	max	mean	max	mean	max
<b>0.0</b>	1.77	3.53	5.26	1.22	2.45	3.67	0.55	1.08	1.59	1.07	3.84	39.5	148.5	22.2	59.8
<b>2.4</b>	1.33	2.65	3.95	0.79	1.57	2.36	0.54	1.08	1.59	1.07	3.85	60.9	225.6	28.7	69.3
<b>5.9</b>	0.73	1.44	2.14	0.20	0.40	0.60	0.53	1.04	1.61	1.04	3.86	260.3	922.1	61.3	100.0

## 11.6 Economic Cost of the fires

The economic cost of the fires is calculated using the Department for Transport (DfT) ‘Value of Prevented Fatality’ (VPF) estimate. We choose this estimate over estimates from other UK based studies (Table 15 (a)) because it is widely used across different government sectors to value the economic impact of mortality. The DfT estimate also lies within the range of values found in other studies (see Table 15 (a)).

The DfT VPF is comprised of three parts: the ‘Willingness to Pay’ (WtP) component, medical costs and gross lost output. WtP considers what an individual would be willing to pay to reduce the risk of being killed or injured. The estimated WtP value uses a contingent valuation approach, based on a survey by Carthy *et al.* (1998), in which 167 respondents were asked how much they would be willing to pay to reduce the risk of death or injury. The gross lost output is estimated using the human capital approach, this places a monetary value on loss of health based on the loss of economic productivity due to mortality. Finally, medical costs are estimated using the average cost of a fatality in 1984/1985 based on data provided by the Department of Health for ambulance and hospital treatment. These were scaled to 2008 values by the DfT.

There are clear limitations within the DfT VPF method to estimate the economic value of prevented fatality and these should be considered within the total £5.5 M estimate. Firstly, the WtP survey sample is small and so this reduces the representativeness of the final estimate for the entire UK population. The small sample size is due to the high money and time cost of carrying out lengthy one-to-one interviews with respondents to ensure they are able to answer in a way that reflects their preferences fairly. Since the WtP survey was carried out over a long period, up to 2 years in some cases, using a large amount of evidence to support estimates we

can have some confidence that estimates are reasonable. However, within this study we introduce some uncertainty into the results by scaling 2008 estimates to 2018 using inflation from the Bank of England. This assumes that underlying values remain applicable over time, which may or may not be true and so this should be kept in mind when interpreting the economic cost results.

Table 15. a) Previous studies estimating the Value of Prevented Fatality in the UK and government estimates across the world. The value used for this study from the Department for Transport, UK is highlighted in grey. b) Detailed values of VPF used to calculate cost of mortality during fires – these values were multiplied by the excess mortality from PM<sub>2.5</sub> from fires (i.e. PM<sub>2.5</sub> Fires – PM<sub>2.5</sub> No Fires). Values are taken from Viscusi et al. (2003) and Deolitte (2009).

a) Study	Sample / Approach	Value of Statistical Life in £ M in 2000 (converted to GBP)	Value of Statistical Life in £ M in 2018 (2000 values scaled to inflation)
Marin and Psacharopoulos (1982)	General Household Survey	2.8	4.6
	<i>Human Capital</i>		
Siebert and Wei (1994)	General Household Survey	6.2 - 7.6	10.3 – 12.6
	<i>Human Capital</i>		
Sandy and Elliott (1996)	Social change and Economic Life Initiative Survey	3.4 – 45.9	5.6 – 74.4
	<i>Human Capital</i>		
Arabsheibani and Marin (2000)	General Household Survey	13.2	21.8
	<i>Human Capital</i>		
Sandy et al. (2001)	Social change and Economic Life Initiative Survey	3.8 - 49.0	6.3 – 81
	<i>Human Capital</i>		
<b>Government Reports</b>	<b>Sample / Approach</b>	<b>Value of Statistical Life in £ M in 2008/2002 (converted to GBP)</b>	<b>Value of Statistical Life in £ M in 2018 (2008 values scaled to inflation)</b>

Department for Transport, UK	Willingness to Pay Survey	1.9 (2008)	2.5
	<i>Contingent Valuation &amp; Human Capital</i>		
European Commission	Willingness to Pay Survey	0.9 (2002)	1.4
	<i>Contingent Valuation</i>		
US VPF	Willingness to Pay Survey	3.1 (2008)	4.1
	<i>Contingent Valuation</i>		

<b>b) Department for Transport, UK</b>		<b>2008 £</b>	<b>2018 £</b>
<b>Total VPF</b>		1,876,830	2,469,513
<i>Human Cost</i>		1,232,800	1,622,105
<i>Medical</i>		6,310	8,303
<i>Lost Output</i>		624,190	821,303
<i>Other costs</i>		13,540	17,816

Table 16. (a) Number of hours within each DAQI bin (0-24, 24-48, 48-71, 71+  $\mu\text{g m}^{-3}$ ) in 2018 (2018/01/01-2018/12/31), simulation period (2018/06/16 – 2018/07/14) and fire period (2018/06/23 – 2018/06/30). (b) Percentage of total annual hourly DAQI occurrences that occurred within the simulation or fire period (i.e. for 0-24  $\mu\text{g m}^{-3}$  bin: simulation period (5471/65870\*100) and fires period (1375/65870\*100)).

a)  AURN Site	Hourly Daily Air Quality Index (DAQI) occurrences											
	2018 (2018-01-01 to 2018-12-31)				Simulation period (2018-06-16 to 2018- 07-14)				Fire Period (2018-06-23 to 2018-06-30)			
	0-24	24-48	48-71	71+	0-24	24-48	48-71	71+	0-24	24-48	48-71	71+
Blackpool Marton	6847	270	23	6	621	5	-	-	168	-	-	-
Leeds Centre	7442	669	57	9	633	6	-	-	163	-	-	-
Liverpool Speke	8009	282	6	5	664	8	-	-	164	4	-	-
Manchester Piccadilly	7462	567	55	26	575	64	14	11	123	25	11	8
Preston	8004	319	26	6	625	7	-	-	167	1	-	-
Salford Eccles	6935	332	23	13	472	35	3	10	132	23	3	10
Warrington	7368	382	19	4	634	24	-	-	158	7	-	-
Wigan Centre	6239	455	33	12	587	43	5	7	139	14	5	7
Wirral Tranmere	7564	407	17	5	660	9	-	-	161	6	-	-
<b>Total hours</b>	<b>65870</b>	<b>3683</b>	<b>259</b>	<b>86</b>	<b>5471</b>	<b>201</b>	<b>22</b>	<b>28</b>	<b>1375</b>	<b>80</b>	<b>19</b>	<b>25</b>

b)  AURN Site	Percentage of Annual DAQI hourly occurrences within simulation periods (%)							
	Simulation period (2018-06-16 to 2018-07-14)				Fire Period (2018-06-23 to 2018-06-30)			
	0-24	24-48	48-71	71+	0-24	24-48	48-71	71+
<b>Blackpool Marton</b>	9.1	1.9	-	-	2.5	-	-	-
<b>Leeds Centre</b>	8.9	0.9	-	-	2.2	0.7	-	-
<b>Liverpool Speke</b>	8.3	2.8	-	-	2.0	1.4	-	-
<b>Manchester Piccadilly</b>	<b>7.7</b>	<b>11.3</b>	<b>25</b>	<b>42</b>	<b>1.6</b>	<b>4.4</b>	<b>20</b>	<b>31</b>
<b>Preston</b>	7.8	2.2	-	-	2.1	0.3	-	-
<b>Salford Eccles</b>	<b>6.8</b>	<b>10.5</b>	<b>13.0</b>	<b>76.9</b>	<b>1.9</b>	<b>6.9</b>	<b>13.0</b>	<b>76.9</b>
<b>Warrington</b>	8.6	6.3	-	-	2.1	1.8	-	-
<b>Wigan Centre</b>	<b>9.4</b>	<b>9.5</b>	<b>15.2</b>	<b>58.3</b>	<b>2.2</b>	<b>3.1</b>	<b>15.2</b>	<b>58.3</b>
<b>Wirral Tranmere</b>	8.7	2.2	-	-	2.1	1.5	-	-

## 11.7 References

- 1) Archer-Nicholls, S., Lowe, D., Darbyshire, E., Morgan, W.T., Bela, M.M., Pereira, G., Trembath, J., Kaiser, J.W., Longo, K.M., Freitas, S.R., Coe, H., McFiggans, G., 2015. Characterising Brazilian biomass burning emissions using WRF-Chem with MOSAIC sectional aerosol. *Geosci. Model Dev.* 8, 549–577. <https://doi.org/10.5194/gmd-8-549-2015>
- 2) Carthy, T., Chilton, S., Covey, J., Hopkins, L., Jones-Lee, M., Loomes, G., Pidgeon, N., Spencer, A., 1998. On the Contingent Valuation of Safety and the Safety of Contingent Valuation: Part 2 - The CV/SG “Chained” Approach. *J. Risk Uncertain.* 17, 187–214. <https://doi.org/10.1023/a:1007782800868>.
- 3) Cohen, A.J., Brauer, M., Burnett, R., Anderson, H.R., Frostad, J., Estep, K., Balakrishnan, K., Brunekreef, B., Dandona, L., Dandona, R., Feigin, V., Freedman, G., Hubbell, B., Jobling, A., Kan, H., Knibbs, L., Liu, Y., Martin, R., Morawska, L., Pope III, C.A., Shin, H., Straif, K., Shaddick, G., Thomas, M., van Dingenen, R., van Donkelaar, A., Vos, T., Murray, C.J.L., Forouzanfar, M.H., 2017. Estimates and 25-year trends of the global burden of disease attributable to ambient air pollution: an analysis of data from the Global Burden of Diseases Study 2015. *Lancet* 389, 1907–1918. [https://doi.org/10.1016/S0140-6736\(17\)30505-6](https://doi.org/10.1016/S0140-6736(17)30505-6).
- 4) Freitas, S.R., Longo, K.M., Chatfield, R., Latham, D., Silva Dias, M.A.F., Andreae, M.O., Prins, E., Santos, J.C., Gielow, R., Carvalho, J.A., 2007. Including the sub-grid scale plume rise of vegetation fires in low resolution atmospheric transport models. *Atmos. Chem. Phys.* 7, 3385–3398. <https://doi.org/10.5194/acp-7-3385-2007>.
- 5) Greater Manchester Combined Authority. 2019. Response to Freedom of Information Request 1920-057. Available at: Unpublished.

- 6) Janssens-Maenhout, G., Crippa, M., Guizzardi, D., Dentener, F., Muntean, M., Pouliot, G., Keating, T., Zhang, Q., Kurokawa, J., Wankmüller, R., Denier Van Der Gon, H., Kuenen, J.J.P., Klimont, Z., Frost, G., Darras, S., Koffi, B., Li, M., 2015. HTAP-v2.2: A mosaic of regional and global emission grid maps for 2008 and 2010 to study hemispheric transport of air pollution. *Atmos. Chem. Phys.* 15, 11411–11432. <https://doi.org/10.5194/acp-15-11411-2015>.
- 7) Kiely, L., Spracklen, D. V., Wiedinmyer, C., Conibear, L., Reddington, C.L., Archer-Nicholls, S., Lowe, D., Arnold, S.R., Knote, C., Firoz Khan, M., Talib Latif, M., Kuwata, M., Hapsari Budisulistiorini, S., Syaufina, L., 2019. New estimate of particulate emissions from Indonesian peat fires in 2015. *Atmos. Chem. Phys.* 19, 11105–11121. <https://doi.org/10.5194/acp-19-11105-2019>.
- 8) NASA Socioeconomic Data and Applications Center (SEDAC) Center for International Earth Science Information Network (CIESIN) and Columbia, U. of (2018) Gridded Population of the World, Version 4 (GPWv4): Population Count, Revision 11. <https://doi.org/10.7927/H4JW8BX5>.
- 9) Xu, J., Morris, P.J., Liu, J., Holden, J., 2018. PEATMAP: Refining estimates of global peatland distribution based on a meta-analysis. *Catena* 160, 134–140. <https://doi.org/10.1016/j.catena.2017.09.010>.

# Supplementary Material: Impact of the 2019/2020 Australian megafires on Air Quality and Health

Ailish M. Graham<sup>1</sup>, Richard J. Pope<sup>1,2</sup>, Kirsty P. Pringle<sup>1,3</sup>,  
Stephen R. Arnold<sup>1</sup>, Luke A. Conibear<sup>1</sup>, Helen Burns<sup>1</sup>, Richard  
Rigby<sup>1</sup>, Nicolás Borchers-Arriagada<sup>4</sup>, Edward W. Butt<sup>1</sup>,  
Laura Kiely<sup>1</sup>, Carly Reddington<sup>1</sup>, Dominic V. Spracklen<sup>1</sup>, Matt  
Woodhouse<sup>5</sup>, Christoph Knote<sup>6</sup>, James B. McQuaid<sup>1</sup>

<sup>1</sup> School of Earth and Environment, University of Leeds, Leeds, LS2 9JT, UK

<sup>2</sup> National Centre for Earth Observation, University of Leeds, Leeds, LS2 9JT, UK

<sup>3</sup> Edinburgh Parallel Computing Centre, Bayes Centre, Edinburgh, EH8 9BT, UK

<sup>4</sup> Menzies Institute for Medical Research, University of Tasmania, Hobart, TAS 7000

Australia

<sup>5</sup> The Commonwealth Scientific and Industrial Research Organisation, Australia

<sup>6</sup> Meteorological Institute, LMU Munich, Munich, Germany

Correspondence to: Ailish M. Graham (ee15amg@leeds.ac.uk)

## 12.1 Fire Emissions

FINN near real-time (NRT) emissions for 2019 and 2020 are used within the WRF-Chem model simulations since FINNv1.5 emissions were not yet available during the time the model simulations were run. In order to evaluate FINN NRT emissions, we compare the relationship between the annual total PM<sub>2.5</sub> emissions and annual total MODIS fire hotspots in 2018, 2019 and 2020 to the relationship in previous years (2010-2017) (Figure 72). Data for 2019 indicate

that PM<sub>2.5</sub> emissions per fire hotspot were much higher than previous years (Figure 72). This is likely due to the high levels of dry fuel availability during 2019 (van Oldenborgh, et al., 2020). Following completion of the model simulations, FINNv1.5 emissions became available for 2019 meaning FINNv1.5 and FINN NRT annual PM<sub>2.5</sub> emission totals for 2018 and 2019 could be directly compared. Generally, FINN v1.5 and NRT PM<sub>2.5</sub> emissions are in good agreement for 2018, while for 2019 FINN NRT PM<sub>2.5</sub> emissions (~1 Tg) are slightly higher than FINNv1.5 PM<sub>2.5</sub> emissions (~0.9 Tg) (Figure 72). However, the magnitude of difference between the FINN emission datasets is small given that there is such a large range in PM<sub>2.5</sub> emission estimates between the five key fire emissions datasets (~1 to >7.5 Tg) (Figure 73).

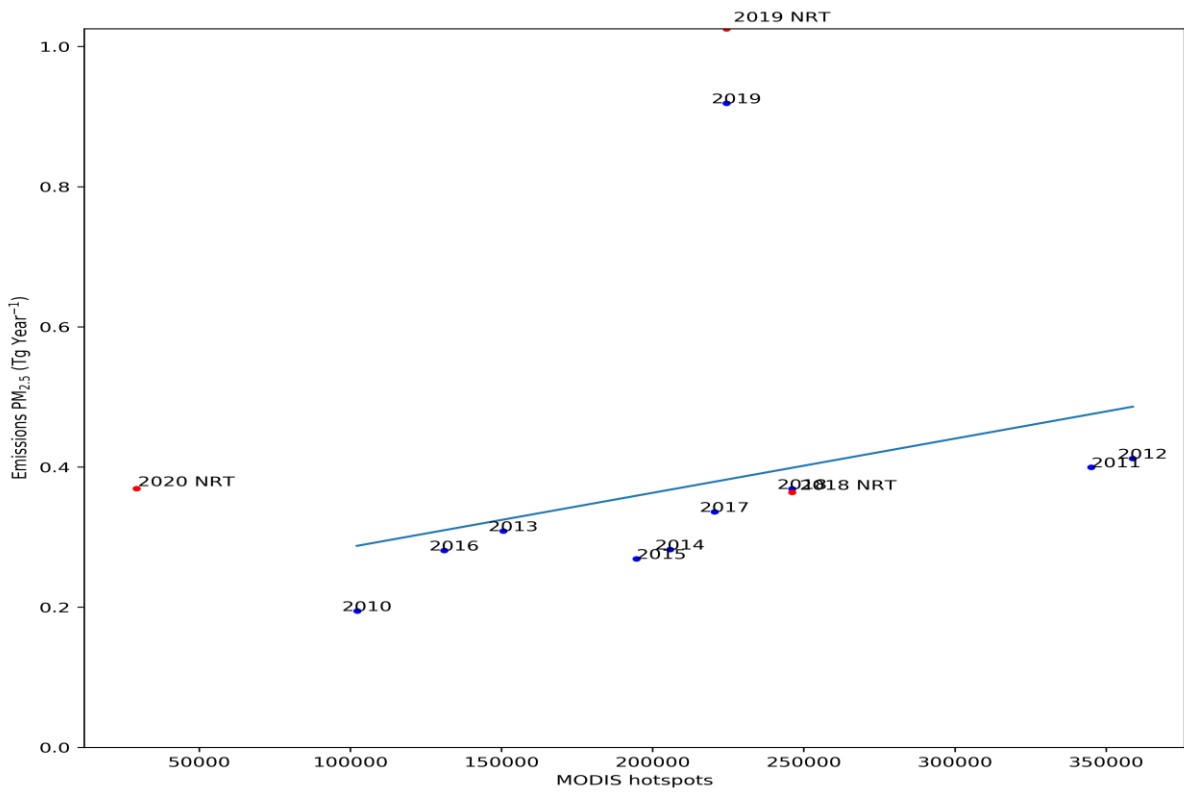


Figure 72. Comparison of FINNv1.5 and FINN near-real time (NRT). 2010-2019 FINNv1.5 PM<sub>2.5</sub> emissions (red) and 2018-2020 FINN near real time (NRT) PM<sub>2.5</sub> emissions are plotted against MODIS hotspots. The linear fit for 2010-2019 FINNv1.5 is shown in blue.

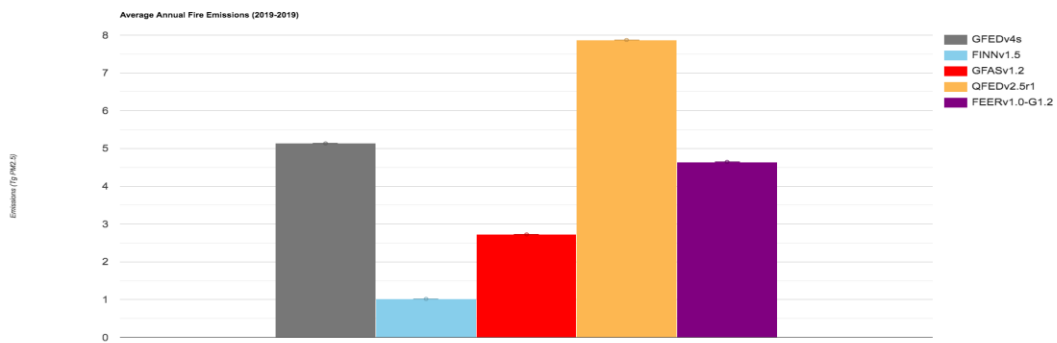
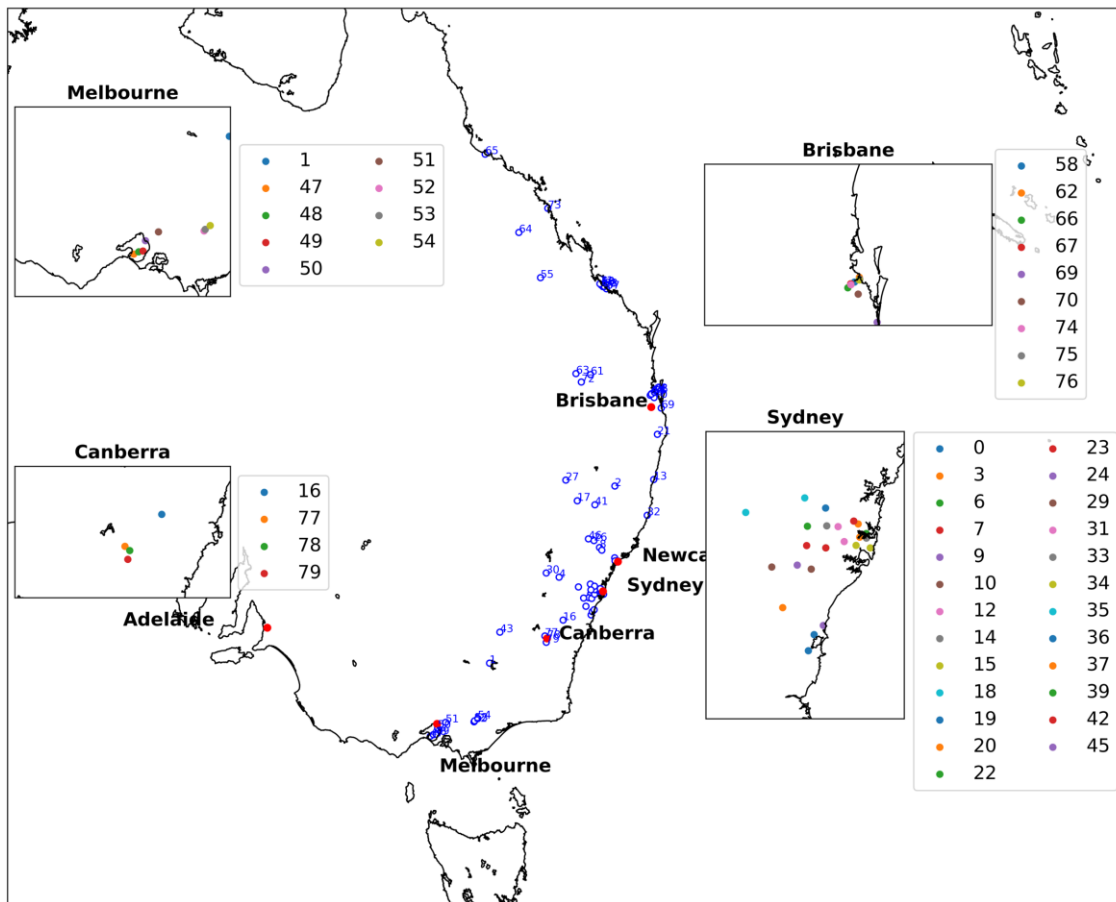


Figure 73. Annual fire PM<sub>2.5</sub> emission estimates for Australia in 2019. The five key fire emissions datasets are shown: GFED, FINN, GFAS, QFED and FEER (Liu, et al., 2020).

## 12.2 Model Evaluation

Daily mean PM<sub>2.5</sub> concentrations from ground-based observational sites across Victoria, New South Wales, Queensland and Australian Capital Territory were used to evaluate model performance between September 1<sup>st</sup> and January 31<sup>st</sup>. The locations of sites used are indicated in Figure 74.



- |                          |                         |                        |                            |
|--------------------------|-------------------------|------------------------|----------------------------|
| ○ 0 - ALBION PARK STH    | ○ 20 - LINDFIELD        | ○ 40 - STOCKTON        | ○ 60 - Fisherman's Landing |
| ○ 1 - ALBURY             | ○ 21 - LISMORE          | ○ 41 - TAMWORTH        | ○ 61 - Hopeland            |
| ○ 2 - ARMIDALE           | ○ 22 - LIVERPOOL        | ○ 42 - VINEYARD        | ○ 62 - Lytton              |
| ○ 3 - BARGO              | ○ 23 - LIVERPOOL SWAQS  | ○ 43 - WAGGA WAGGA NTH | ○ 63 - Miles Airport       |
| ○ 4 - BATHURST           | ○ 24 - MACQUARIE PARK   | ○ 44 - WALLSEND        | ○ 64 - Moranbah (Utah Dr)  |
| ○ 5 - BERESFIELD         | ○ 25 - MAYFIELD         | ○ 45 - WOLLONGONG      | ○ 65 - North Ward          |
| ○ 6 - BRADFIELD HIGHWAY  | ○ 26 - MUSWELLBROOK     | ○ 46 - WYONG           | ○ 66 - Rocklea             |
| ○ 7 - BRINGELLY          | ○ 27 - NARRABRI         | ○ 47 - Churchill       | ○ 67 - South Brisbane      |
| ○ 8 - CAMBERWELL         | ○ 28 - NEWCASTLE        | ○ 48 - Footscray       | ○ 68 - South Gladstone     |
| ○ 9 - CAMDEN             | ○ 29 - OAKDALE          | ○ 49 - Geelong South   | ○ 69 - Southport           |
| ○ 10 - CAMPBELLTOWN WEST | ○ 30 - ORANGE           | ○ 50 - Melbourne CBD   | ○ 70 - Springwood          |
| ○ 11 - CARRINGTON        | ○ 31 - PARRAMATTA NORTH | ○ 51 - Moe             | ○ 71 - Targinie            |
| ○ 12 - CHULLORA          | ○ 32 - PORT MACQUARIE   | ○ 52 - Morwell East    | ○ 72 - Upper Humbug        |
| ○ 13 - COFFS HARBOUR     | ○ 33 - PROSPECT         | ○ 53 - Morwell South   | ○ 73 - West Mackay         |
| ○ 14 - COOK AND PHILLIP  | ○ 34 - RANDWICK         | ○ 54 - Traralgon       | ○ 74 - Woolloongabba       |
| ○ 15 - EARLWOOD          | ○ 35 - RICHMOND         | ○ 55 - Blackwater      | ○ 75 - Wynnum              |
| ○ 16 - GOULBURN          | ○ 36 - ROUSE HILL       | ○ 56 - Boat Creek      | ○ 76 - Wynnum West         |
| ○ 17 - GUNNEDAH          | ○ 37 - ROZELLE          | ○ 57 - Boyne Island    | ○ 77 - Civic               |
| ○ 18 - KATOOMBA          | ○ 38 - SINGLETON        | ○ 58 - Cannon Hill     | ○ 78 - Florey              |
| ○ 19 - KEMBLA GRANGE     | ○ 39 - ST MARYS         | ○ 59 - Clinton         | ○ 79 - Monash              |

Figure 74. Ground-based observational sites used in model evaluation of daily mean PM<sub>2.5</sub> concentrations.

The performance of model simulations was compared with observations (Figure 75). Two options were tested for nudging. Firstly, potential temperature, the horizontal and vertical winds and the water vapour mixing ratio (all meteorological variables) were nudged above the boundary layer and only horizontal and vertical winds were nudged within the boundary layer, using the 6-hourly ERA5 reanalysis (fires, no fires, plume\_rise and scaled\_1.5). Secondly, nudging was performed for all meteorological variables in all vertical levels using the 6-hourly ERA5 reanalysis (nudged\_BL\_fires, nudged\_BL\_no\_fires and nudged\_BL\_scaled). In both cases, meteorology was re-initialised every two weeks using meteorological boundary conditions in order to minimise model drift. Nudging for all meteorological variables in all vertical levels improved simulated PM<sub>2.5</sub> concentrations by reducing the Root Mean Square Error (RMSE), Normalised Mean Absolute Error (NMAE) and Normalised Mean Bias (NMB) ([fires]  $r = 0.42$ , RMSE = 24.1  $\mu\text{g m}^{-3}$ , NMB = -0.49, NMAE = 0.74 compared with [nudged\_BL\_fires]  $r = 0.39$ , RMSE = 22.9  $\mu\text{g m}^{-3}$ , NMB = -0.17, NMAE = 0.72) (Table 17). Alongside this, two fire emission release options were tested, releasing emissions evenly distributed through the boundary layer [fires, nudged\_BL\_fires] and releasing emissions using the plume-rise module [plume\_rise]. When the fires and plume\_rise simulations are compared, results indicate that there is little sensitivity to the emission release option chosen ([fires]  $r = 0.42$ , RMSE = 24.1  $\mu\text{g m}^{-3}$ , NMB = -0.49, NMAE = 0.74 compared with [plume\_rise]  $r=0.41$ , RMSE = 24.2  $\mu\text{g m}^{-3}$ , NMB = -0.51, NMAE = 0.75) (Table 17). Evenly distributed emissions throughout the boundary layer was therefore chosen as the emissions release option to use. Finally, scaling FINN emissions over the model domain was also performed, since FINN emissions lie at the low-end of emission dataset estimates (Figure 73). FINN emissions for

October 1<sup>st</sup> to January 31<sup>st</sup> were scaled by 1.5 in order to match the annual total for GFED. When nudging in the boundary layer was not performed (scaled\_1.5, this led to improved correlation with observations ([scaled\_1.5] r =0.41) but a slightly worse RMSE, NMB and NMAE (Table 17). However, when scaled emissions were used for the simulation with nudging in the boundary layer (nudged\_BL\_1.5), although correlation decreased slightly ([nudged\_BL\_1.5] r =0.41) and RMSE and NMAE were worse, the NMB decreased substantially ([nudged\_BL\_1.5] NMB =-0.03) (Table 17). Overall, scaling led to overestimating peak PM<sub>2.5</sub> concentrations observed during the fires. As a result, the nudged\_BL\_fires and nudged\_BL\_no\_fires were chosen to carry out the analysis with.

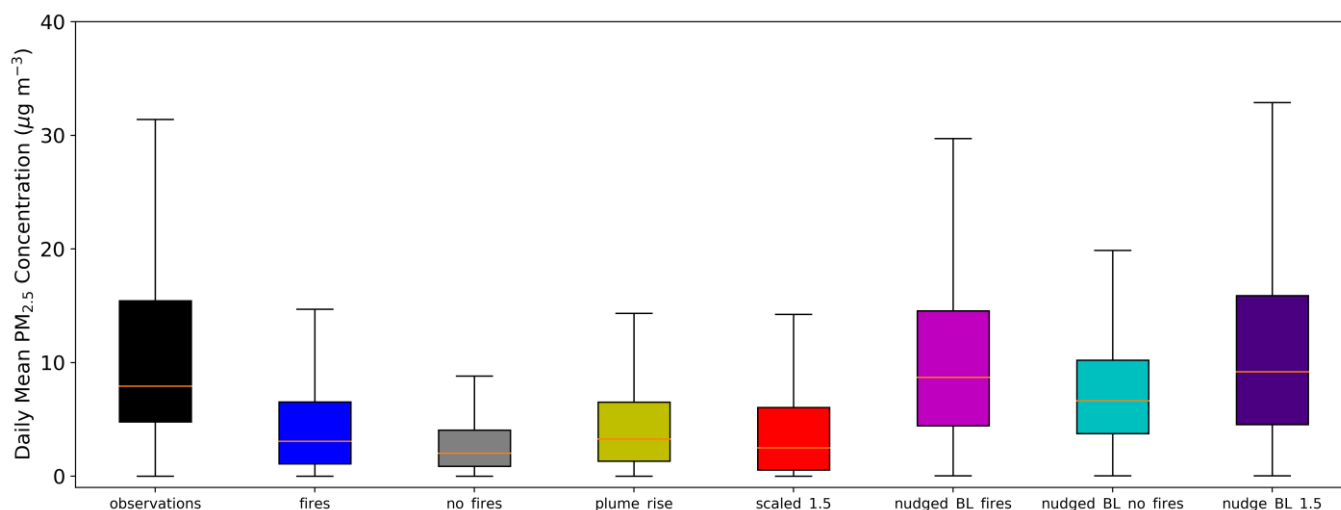


Figure 75. Comparison of PM<sub>2.5</sub> concentrations from model sensitivity simulations with PM<sub>2.5</sub> observations from 80 observational sites across eastern-Australia. The fires, no\_fires, plume\_rise and scaled\_1.5 simulations, in which all meteorological variables above the BL were nudged, while within the BL only horizontal and vertical winds were nudged. In the fires and scaled\_1.5 simulations fire emissions were released evenly through the BL, while in plume\_rise the plume rise module was used. The fires and plume\_rise simulations used FINN NRT emissions and in the scaled\_1.5 simulation these emissions were scaled by 1.5 in Australia. In the nudged\_BL, nudged\_BL\_no\_fires and nudged\_BL\_scaled\_1.5 simulations nudging was performed for all vertical levels and all meteorological variables. The nudged\_BL and nudged\_BL\_1.5 simulations used FINN NRT emissions and in the nudged\_BL\_1.5 simulation these emissions were scaled by 1.5 in Australia and fire emissions were released evenly through the BL. In both the no\_fires and nudged\_BL\_no\_fires simulations no fire emissions were released.

Table 17. Model evaluation statistics for each of the WRF-Chem simulations for daily mean PM<sub>2.5</sub>. Statistics shown are the mean value of Pearson correlation coefficient (r), root mean squared error (RMSE), normalised mean bias (NMB), and normalised mean absolute error (NMAE) at each observational site for the full simulation time period (September 1<sup>st</sup> 2019 to January 31<sup>st</sup> 2020). Simulations shown are: fires, no\_fires, plume\_rise and scaled\_1.5 simulations, in which all meteorological variables were nudged above the BL, while within the BL only horizontal and vertical winds were nudged. In the fires and scaled\_1.5 simulations fire emissions were released evenly through the BL, while in plume\_rise the plume rise module was used. The fires and plume\_rise simulations used FINN NRT emissions and in the scaled\_1.5 simulation these emissions were scaled by 1.5 in Australia. In the nudged\_BL, nudged\_BL\_no\_fires and nudged\_BL\_1.5 simulations nudging was performed for all vertical levels and all meteorological variables. The nudged\_BL and nudged\_BL\_1.5 simulations used FINN NRT emissions and in the nudged\_BL\_1.5 simulation these emissions were scaled by 1.5 in Australia, in both cases fire emissions were released evenly through the BL. In both the no\_fires and nudged\_BL\_no\_fires simulations no fire emissions were released.

<b>Simulation</b>	<b>r</b>	<b>RMSE (<math>\mu\text{g m}^{-3}</math>)</b>	<b>NMB</b>	<b>NMAE</b>
<b>Fires</b>	0.42	24.1	-0.49	0.74
<b>No_fires</b>	0.19	26.5	-0.75	0.82
<b>Plume_rise</b>	0.41	24.2	-0.51	0.75
<b>Scaled_1.5</b>	0.37	25.1	-0.49	0.78
<b>Nudged_BL_fires</b>	0.39	22.9	-0.17	0.72
<b>Nudged_BL_no_fires</b>	0.14	25.3	-0.45	0.77
<b>Nudged_BL_1.5</b>	0.41	24.3	-0.03	0.76

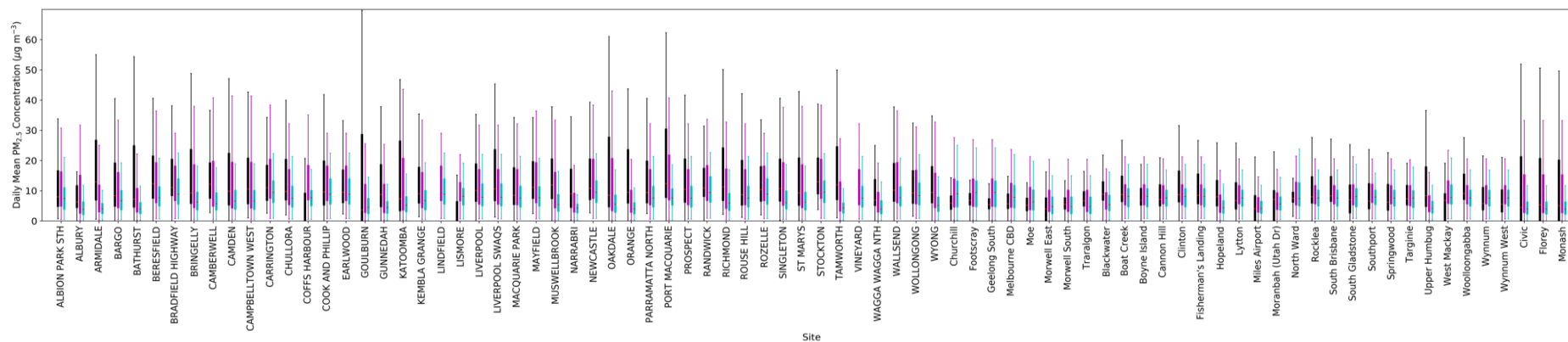


Figure 76. Comparison of daily mean  $PM_{2.5}$  concentrations from model sensitivity simulations with  $PM_{2.5}$  observations from 80 observational sites across eastern-Australia. Observations are shown in black, nudged\_BL\_fires in magenta and nudged\_BL\_no\_fires in cyan for each site.

Evaluating the performance of the model simulations by comparing the nudged\_BL\_fires and nudged\_BL\_no\_fires  $PM_{2.5}$  daily mean concentrations at each observational site between September 1<sup>st</sup> and January 31<sup>st</sup> indicates that the model performs relatively well. Generally, the model replicates the observed  $PM_{2.5}$  concentrations well, though with a negative bias, as was seen across all sites (Table 17). However, it is clear that the model under predicts observed  $PM_{2.5}$  concentrations across some sites, these are all located in NSW and ACT where the most intense fire occurred (Figure 76). Therefore, it is likely that the model is unable to capture the high concentrations observed by point measurements due to strong concentration gradients close to the fires that would not be captured at the model resolution (30 km).

### 12.3 Monthly Mean PM<sub>2.5</sub> concentrations

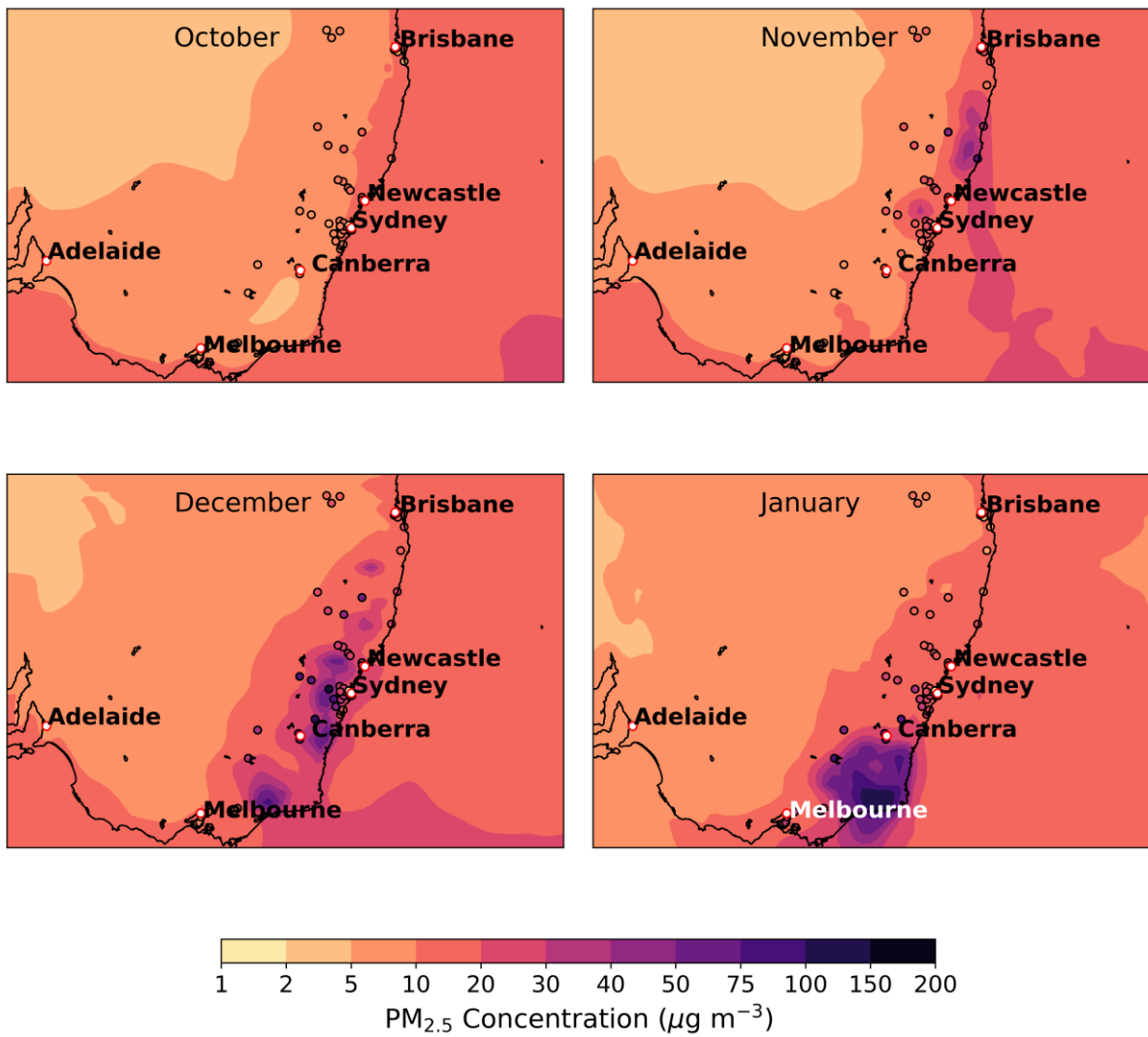


Figure 77. Monthly mean modelled PM<sub>2.5</sub> concentrations across eastern-Australia from the fires (nudged\_BL\_fires) simulation. Monthly mean observations are over plotted.

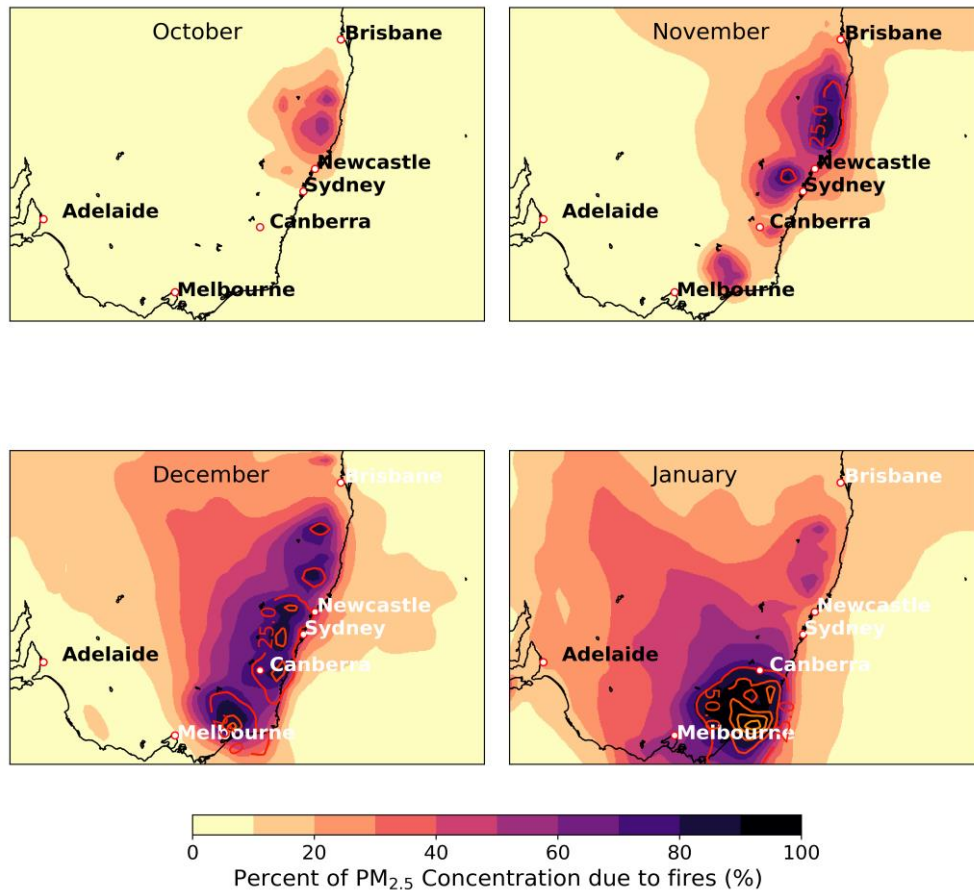


Figure 78. Monthly mean percentage of PM<sub>2.5</sub> attributable to fires, calculated as  $\frac{PM_{2.5} \text{ fires} - PM_{2.5} \text{ no fires}}{PM_{2.5} \text{ fires}}$  using the nudged\_BL\_fires and nudged\_BL\_no\_fires simulations. Monthly mean PM<sub>2.5</sub> concentrations from the nudged\_BL\_fires simulation are also overlaid in contours for reference.

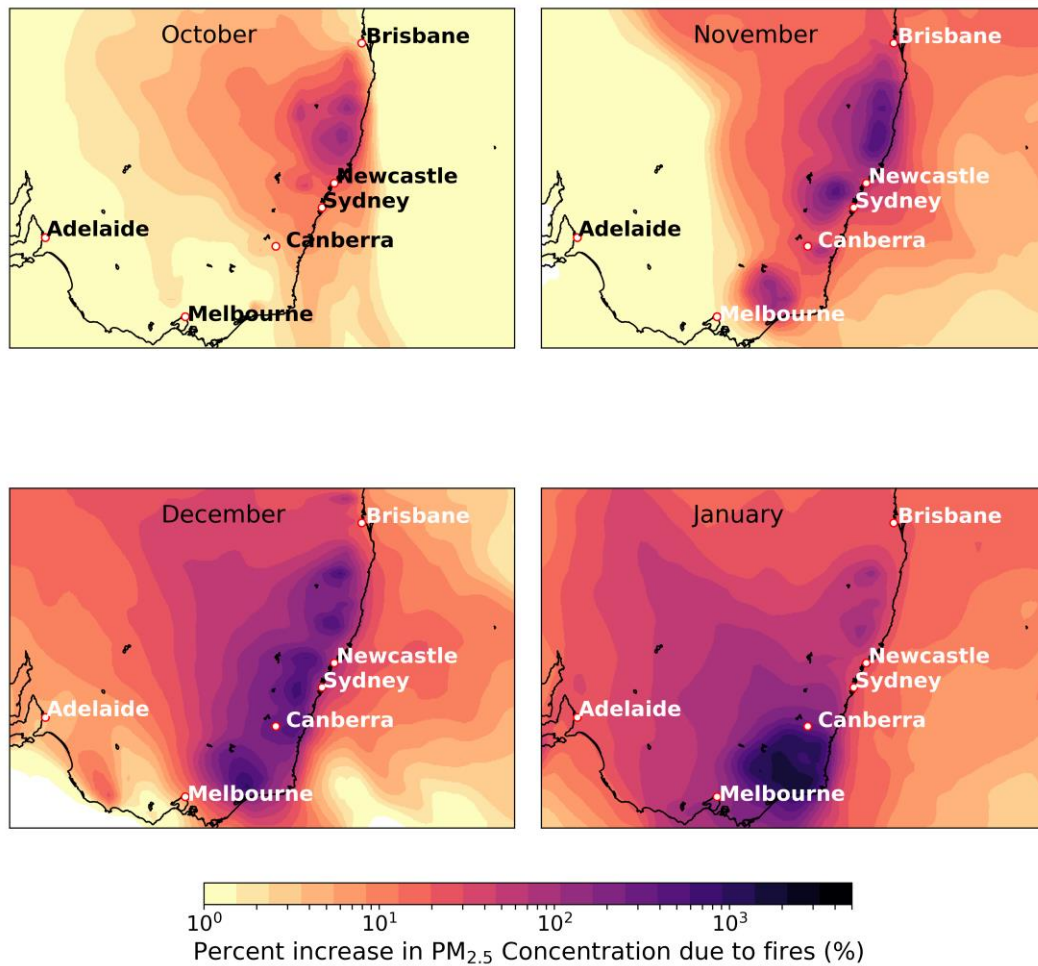


Figure 79. Monthly mean percentage increase in PM<sub>2.5</sub> attributable to fires, calculated as  $\frac{PM_{2.5} \text{ fires} - PM_{2.5} \text{ no fires}}{PM_{2.5} \text{ no fires}}$  using the nudged\_BL\_fires and nudged\_BL\_no\_fires simulations.

## 12.4 Population Exposure

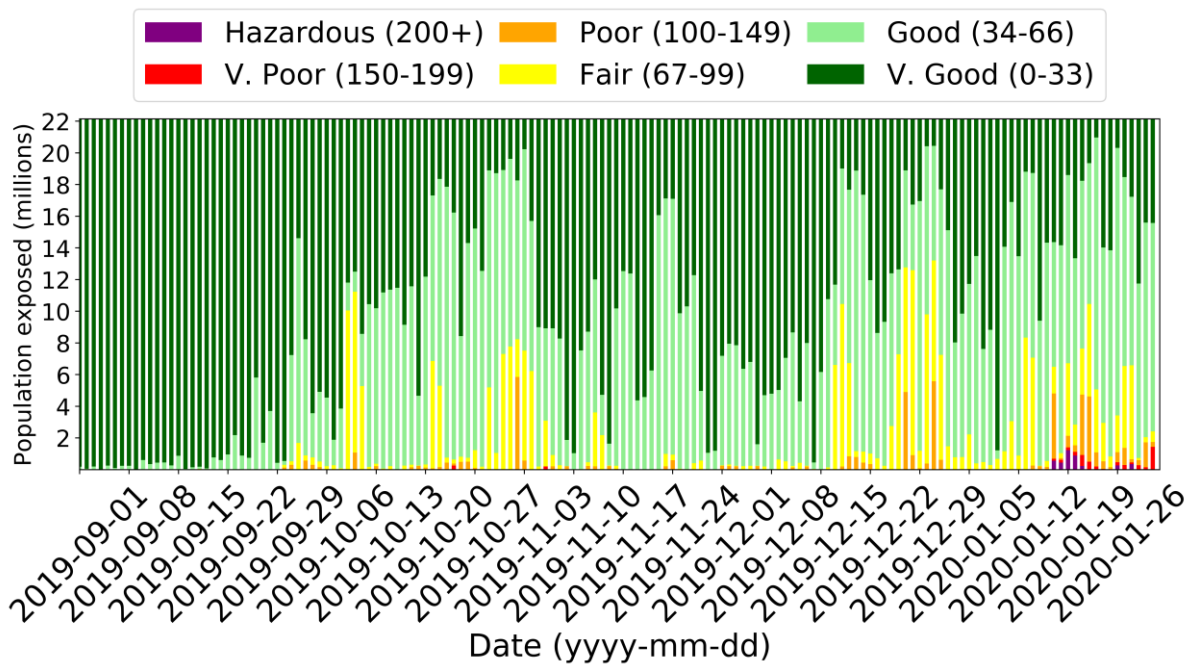


Figure 80. Daily population exposure to Air Quality Index Values across eastern-Australia between September 1<sup>st</sup> and January 31<sup>st</sup> in the nudged\_BL\_no\_fires simulation. More information on how the AQI is calculated in Table 25.

Table 18. Monthly population exposure to PM<sub>2.5</sub> AQI values in the nudged\_BL\_fires simulation (calculated as the monthly mean of daily sum population exposure). More information on how the AQI is calculated in Table 25.

<b>AQI</b>	<b>September</b>	<b>October</b>	<b>November</b>	<b>December</b>	<b>January</b>
<b>V. Good</b>	20.7 m	10.2 m	8.9 m	8.4 m	5.7 m
<b>Good</b>	726,000	9.6 m	8.6 m	9.0 m	12 m
<b>Fair</b>	13,400	2.1 m	2.4 m	3.8 m	3.2 m
<b>Poor</b>	5891	298,000	1.1 m	746,000	787,000
<b>V. Poor</b>	41	12,100	255,000	80,000	253,000
<b>Hazardous</b>	0	93	122,000	109,000	238,000

Table 19. Monthly population exposure to PM<sub>2.5</sub> AQI values in the nudged\_BL\_no\_fires simulation (calculated as the monthly mean of daily sum population exposure). More information on how the AQI is calculated in Table 25.

<b>AQI</b>	<b>September</b>	<b>October</b>	<b>November</b>	<b>December</b>	<b>January</b>
<b>V. Good</b>	20.7 m	10.8 m	12.2 m	11.5 m	7.8 m
<b>Good</b>	726,000	9.3 m	7.8 m	7.7 m	11.1 m
<b>Fair</b>	13,000	1.9 m	1.2 m	2.5 m	2.3 m
<b>Poor</b>	6,000	164,000	273,000	508,000	652,000
<b>V. Poor</b>	41	9,000	6,500	530	147,000
<b>Hazardous</b>	0	0	0	0	130,000

Table 20. Monthly population exposure to PM<sub>2.5</sub> AQI in cities (calculated as the monthly mean of daily sum population exposure). More information on how the AQI is calculated in Table 25.

**Brisbane**

<b>AQI</b>	<b>September</b>	<b>October</b>	<b>November</b>	<b>December</b>	<b>January</b>
<b>V. Good</b>	3.5 m	1.3 m	728,000	1 m	1.4 m
<b>Good</b>	150,000	2.1 m	2.2 m	2.5 m	2 m
<b>Fair</b>	0	250,000	561,000	261,000	342,000
<b>Poor</b>	0	93,000	161,000	5,300	2,000
<b>V. Poor</b>	0	0	904	144	205
<b>Hazardous</b>	0	0	0	0	0

**Sydney**

<b>AQI</b>	<b>September</b>	<b>October</b>	<b>November</b>	<b>December</b>	<b>January</b>
<b>V. Good</b>	6.2 m	2.8 m	1.1 m	155,000	1.3 m
<b>Good</b>	83,000	2.9 m	2.7 m	980,000	2.9 m
<b>Fair</b>	1,050	731,000	900,000	1.8 m	1.4 m
<b>Poor</b>	0	49,000	112,000	1.6 m	615,000
<b>V. Poor</b>	0	0	86,000	582,000	204,000
<b>Hazardous</b>	0	0	10,000	1.4 m	6,400

**Newcastle-Maitland**

<b>AQI</b>	<b>September</b>	<b>October</b>	<b>November</b>	<b>December</b>	<b>January</b>
<b>V. Good</b>	5.4 m	3.4 m	3.4 m	1.4 m	2.5 m
<b>Good</b>	39,000	1.4 m	1.1 m	1.8 m	1.9 m
<b>Fair</b>	145	677,000	578,000	719,000	677,000
<b>Poor</b>	0	162,000	235,000	769,000	272,000
<b>V. Poor</b>	0	58,000	170,000	463,000	210,000
<b>Hazardous</b>	0	0	2,500	418,000	33,000

**Canberra-Queanbeyan**

<b>AQI</b>	<b>September</b>	<b>October</b>	<b>November</b>	<b>December</b>	<b>January</b>
<b>V. Good</b>	629,000	510,000	514,000	162,000	155,000
<b>Good</b>	2,000	129,000	88,000	131,000	121,000
<b>Fair</b>	0	12,900	13,000	122,000	92,000
<b>Poor</b>	0	896	15,000	84,000	85,000
<b>V. Poor</b>	0	0	1,100	63,000	69,000
<b>Hazardous</b>	0	0	174	90,000	132,000

**Melbourne**

<b>AQI</b>	<b>September</b>	<b>October</b>	<b>November</b>	<b>December</b>	<b>January</b>
<b>V. Good</b>	5.2 m	1.8 m	1 m	1.1 m	2.5 m
<b>Good</b>	1.2 m	2.6 m	3.5 m	2.9 m	2.1 m
<b>Fair</b>	1,500	1.7 m	994,000	1.6 m	1 m
<b>Poor</b>	0	468,000	905,000	1.1 m	352,000
<b>V. Poor</b>	0	0	59,000	0	37,000
<b>Hazardous</b>	0	0	0	0	590,000

**Adelaide**

<b>AQI</b>	<b>September</b>	<b>October</b>	<b>November</b>	<b>December</b>	<b>January</b>
<b>V. Good</b>	1.2 m	424,000	530,000	495,000	910,000
<b>Good</b>	408,000	920,000	669,000	811,000	631,000
<b>Fair</b>	3,300	302,000	311,000	298,000	67,000
<b>Poor</b>	0	10,000	92,000	53,000	47,000
<b>V. Poor</b>	0	0	0	0	781
<b>Hazardous</b>	0	0	0	0	14

Table 21. Mean and maximum (September 1<sup>st</sup> – January 31<sup>st</sup>) population-weighted PM<sub>2.5</sub> concentrations for states and cities in eastern-Australia.

State	Mean Population-weighted PM <sub>2.5</sub> (µg m <sup>-3</sup> )		Maximum population-weighted PM <sub>2.5</sub> (µg m <sup>-3</sup> )	
	This Study	Borchers Arriagada <i>et al.</i> (2020)	This Study	Borchers Arriagada <i>et al.</i> (2020)
Australian Capital Territory	14.1	113.1	155.1	920.1
New South Wales	13.4	21.5	53.4	80.9
Queensland	9.7	18.9	22.9	87.2
Victoria	9.1	26.9	81.8	270.6
All domain	11.6	23.7	58.3	98.5
City	Mean Population-weighted PM <sub>2.5</sub> (µg m <sup>-3</sup> )		Maximum population-weighted PM <sub>2.5</sub> (µg m <sup>-3</sup> )	
	This Study	Borchers Arriagada <i>et al.</i> (2020)	This Study	Borchers Arriagada <i>et al.</i> (2020)
Brisbane	9.7		26.4	
Newcastle Maitland	14.3		48.7	
Sydney	13.8		58.4	
Canberra-Queanbeyan	14.2		156.2	
Melbourne	9.0		80.5	
Adelaide	7.0		26.5	

Table 22. 2018 regional all-cause, all-age mortality rates per 100,000 for Australia (Australian Bureau of Statistics, 2020).

<b>State</b>	<b>Mortality Rate</b>
Australian Capital Territory	479.142911
New South Wales	603.286756
Queensland	574.890405
South Australia	736.687279
Tasmania	772.433221
Victoria	543.519059

## 12.5 Health Impacts

Table 23. The total number of deaths brought forward between October 1<sup>st</sup> and January 31<sup>st</sup> due to short-term exposure to PM<sub>2.5</sub> in the nudged\_BL\_fires and nudged\_BL\_no\_fires simulations. Using the subtraction method, the number of deaths brought forward due to exposure to PM<sub>2.5</sub> from fires has also been estimated (fires only).

<b>Simulation</b>	<b>Deaths brought forward</b>
Fires	624 (95% CI: 229, 1008)
No Fires	444 (95% CI: 155, 714)
Fires Only	180 (95% CI: 74, 294)

Table 24. The total number of deaths brought forward due to fires (nudged\_BL\_fires-nudged\_BL\_no\_fires) between October 1<sup>st</sup> and January 31<sup>st</sup> due to short-term exposure to PM<sub>2.5</sub> in each state and the large cities. Note the entire area of the Northern Territory and South Australia states was not included in the model domain so the total for these states is not included here.

<b>Region</b>	<b>Deaths brought forward</b>
New South Wales	109 (95% CI: 41, 176)
Victoria	35 (95% CI: 13, 56)
Queensland	24 (95% CI: 15, 41)
Tasmania	2 (95% CI: 1, 2)
Australian Capital Territory	9 (95% CI: 3, 15)
<b>City</b>	<b>Deaths brought forward</b>
Brisbane	9 (95% CI: 3, 14)
Newcastle Maitland	6 (95% CI: 2, 10)
Sydney	65 (95% CI: 24, 105)
Canberra Queanbeyan	9 (95% CI: 4, 15)
Melbourne	23 (95% CI: 9, 38)
Adelaide	2 (95% CI: 1, 3)

Table 25. Australian Quality Index (AQI) values and description. The 24-hour AQI is calculated based on the relevant Air National Environment Protection Measure (NEPM) standard, or advisory standard, for each pollutant using the equation (AQI = air pollutant concentration/air pollutant standard x 100). The 24-hour standard for PM<sub>2.5</sub> is 25 µg m<sup>-3</sup>.

Category	AQI Range	Description
Very Good	0-33	Air quality is considered very good, and air pollution poses little or no risk.
Good	34-66	Air quality is considered good, and air pollution poses little or no risk.
Fair	67-99	Air quality is acceptable. However, there may be a health concern for very sensitive people.
Poor	100-149	Air quality is unhealthy for sensitive groups. The general population is not likely to be affected in this range.
Very Poor	150-199	Air quality is unhealthy, and everyone may begin to experience health effects. Sensitive people may experience more serious health effects.
Hazardous	200+	Air quality is very unhealthy. Everyone may experience more serious health effects.

## 12.6 References

- 1) Liu, T., Mickley, L.J., Marlier, M.E., DeFries, R.S., Khan, M.F., Latif, M.T., Karambelas, A., 2020. Diagnosing spatial biases and uncertainties in global fire emissions inventories: Indonesia as regional case study. *Remote Sens. Environ.* 237, 111557.  
<https://doi.org/10.1016/j.rse.2019.111557>.